

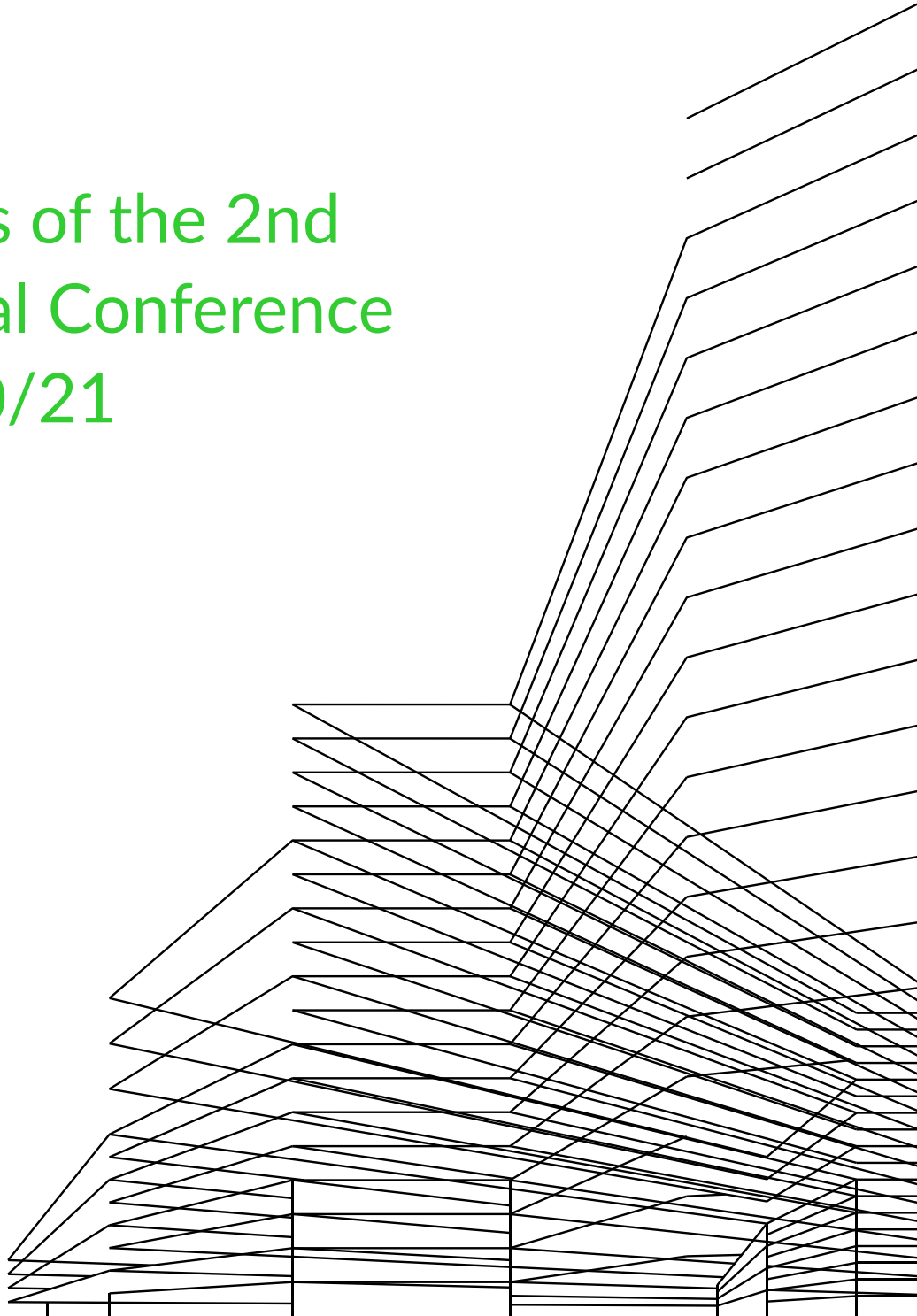
CoMS_
2020/21

**Construction Materials for
a Sustainable Future**

**Proceedings of the 2nd
International Conference
CoMS 2020/21**

Volume 1

Slovenian National
Building and Civil
Engineering Institute,
Ljubljana, 2020



Conference CoMS_2020/21, 2nd International Conference on Construction Materials for a Sustainable Future
Editors Aljoša Šajna, Andraž Legat, Sabina Jordan, Petra Horvat, Ema Kemperle, Sabina Dolenc, Metka Ljubešek, Matej Michelizza
Design Eksit ADV, d.o.o.
Published by Slovenian National Building and Civil Engineering Institute (ZAG), Ljubljana, 2020
Price Free copie

First electronic edition

Available at <http://www.zag.si/dl/coms2020-21-proceedings.pdf>

<http://www.zag.si>



© 2020 Slovenian National Building and Civil Engineering Institute

This work is licensed under the Creative Commons Attribution-NonCommercial-NoDerivs 4.0 International License.

<https://creativecommons.org/licenses/by-nc-nd/4.0/>

ISBN 978-961-94071-8-9 (pdf)

CIP - Kataložni zapis o publikaciji pripravili v Narodni in univerzitetni knjižnici v Ljubljani

COBISS.SI-ID=44042499

ISBN 978-961-94071-8-9 (pdf)

Conference Program Committee

- Andraž Legat (chair)
- Ivana Banjad Pečur
- Dubravka Bjegović
- Mirjana Malešev
- Vlastimir Radonjanin
- Wolfram Schmidt
- Andreas Rogge
- Aljoša Šajna

Scientific Committee

- Andrej Anžlin
- Boris Azinović
- Ivana Banjad Pečur
- Ana Baričević
- Dubravka Bjegović
- Uroš Bohinc
- Meri Cvetkovska
- Sabina Dolenc
- Vilma Ducman
- Roland Göttig
- Lucija Hanžič
- Miha Hren
- Ksenija Janković
- Sabina Jordan
- Friderik Knez
- Lidija Korat
- Tilmann Kuhn
- Andreja Kutnar
- Andraž Legat
- Marjana Lutman

Organizing Committee

- Aljoša Šajna (chair)
- Sabina Jordan
- Ema Kemperle
- Darko Korbar
- Sabina Dolenc
- Matej Michelizza
- Petra Horvat

- Mirjana Malešev
- Katja Malovrh Rebec
- Ksenija Marc
- Sebastjan Meža
- Kristina Mjornell
- Ana Mladenović
- Laurens Oostwegel
- Alexander Passer
- Vlastimir Radonjanin
- Wolfram Schmidt
- Marjana Serdar
- Ruben Snellings
- Irina Stipanović
- Aljoša Šajna
- Andrijana Škapin
- Goran Turk
- Rok Vezočnik
- Johan Vyncke
- Vesna Žegarac Leskovar
- Aleš Žnidarič

TABLE OF CONTENTS

1. Boris Azinović, Andreja Pondelak, Jaka Gašper Pečnik and Vaclav Sebera Flexible polymer connections for CLT structures	6
2. Natalija Bede, Silvija Mrakovčić Flexural behaviour of high strength concrete with steel and polypropylene fibres	14
3. Maurizio Bellotto, Luka Zevnik On the use of metallurgical slags alternative to blastfurnace slags in the formulation of alkali-activated binders	23
4. Filip Brleković, Tamara Fiolić, Juraj Šipušić Sustainable Insulating Composite from Almond Shell	32
5. Olivera R. Bukvić, Suzana R. Draganić, Mirjana Đ. Laban, Vlastimir S. Radonjanin Façade fire safety – legal framework in Serbia, Croatia and Slovenia	39
6. Vesna A. Bulatović, Mirjana M. Malešev, Miroslava M. Radeka, Vlastimir S. Radonjanin and Ivan M. Lukić Sulfate resistance of concrete after two years exposure to aggressive solutions	48
7. Barrie Dams, Yiwei Hei, Paul Shepherd and Richard J Ball Novel cementitious materials for extrusion-based 3D printing	56
8. Sandra Ofner, Manuel Megel, Martin Schneider and Carina Neff Electromagnetic fibre alignment to optimize the fibre utilization of ultra -high performance concrete (UHPC)	66
9. Mergim Gaši, Bojan Milovanović, Jakov Perišić and Sanjin Gumbarević Thermal bridge assessment in prefabricated ventilated façade systems with recycled aggregates	75
10. Gradisar Luka, Dolenc Matevz, Klinc Robert and Turk Ziga Designing generatively to achieve an efficient and optimised solution	84
11. Dusan Z. Grdic, Nenad S. Ristic, Gordana A. Toplicic - Curcuc, Jelena Bijeljčić, Zoran J. Grdić Resistance of concrete made with finely milled cathode ray tube glass as a supplementary cementitious materials to sulphate attack	96
12. Sanjin Gumbarević, Bojan Milovanović, Mergim Gaši and Marina Bagarić The impact of building zone elements on airtightness	106
13. Kristina Hadzievska, Toni Arangjelovski, Darko Nakov and Goran Markovski Sulfate resistance of cement with different volumes of fly ash	115
14. Ivan Hafner, Tvrtko Renić, Tomislav Kišiček and Mislav Stepinac Seismic strengthening of stone masonry structures – state of the art	124
15. Lucija Hanžič, Jurij Karlovšek, Tomaž Hozjan, Sabina Huč, Zhongyu Xu, Igor Planinc and Johnny C.M. Ho Experimental and numerical investigation of restrained shrinkage of concrete	133
16. Johannes Horvath ECOroads (Economical COncrete roads)	143
17. Ksenija Janković, Dragan Bojović, Marko Stojanović, Iva Despotović, Lana Antić Properties of concrete kerbs with recycled aggregate from precast elements	148
18. Sabina Jordan, Friderik Knez, Miha Tomšič and Marjana Šijanec Zavrl First experiences in the development of slovenian sustainable building indicators	154
19. Naser Kabashi, Enes Krasniqi and Milot Muhaxheri Influence of waste glass addition on concrete properties	163

TABLE OF CONTENTS

20. Naser Kabashi, Mihrie Bajoku Corrosion - cracking parameter in the concrete structure and impact in reinforced steel bars	172
21. Tomislav Kišiček, Nikolina Uglešić Numerical modelling of concrete beam reinforced with FRP bars subjected to bending until failure	181
22. Sanjay Korukonda and Sumedha Maharana Non-Destructive Evaluation and Monitoring Cement Concrete - An Experimental Approach	190
23. Karmen Kostanić Jurić, Nina Štirmer and Ivana Carević Sustainable pre-treatment of wood biomass ash for partial cement replacement	197
24. Paulina Krolo, Natalija Bede, Davor Grandić and Ivan Palijan Influence of density on tensile and compressive properties of polyurethane foam	208
25. Alisa Machner, Marie H. Bjørndal, Aljoša Šajna, Lucija Hanžič, Yushan Gu, Benoît Bary and Klaartje De Weerd Measurement of the chloride resistance of Environmentally friendly and Durable conCrete	216
26. Bojan Milovanović, Mergim Gaši Sanjin Gumbarević and Marina Bagarić Education for zero energy buildings using building information modelling	225
27. Tiana Milovic, Mirjana Malesev, Miroslava Radeka and Vlastimir Radonjanin Thermal compatibility of repair mortars based on fly ash as SCM according to en 13687-1	235
28. Michael Mrissa, Jan Vcelak, László Hajdu, Balázs Dávid, Miklós Krész, Jakub Sandak, Anna Sandak, Rok Kanduti, Monika Varkonji Sajn, Anja Jutraz, Katja Malovrh Rebec Extending BIM for Air Quality Monitoring	244
29. Darko Nakov, Hatim Ejupi, Goran Markovski and Toni Arangjelovski Fibre reinforcement – the key to sustainable reinforced concrete structures	251
30. Mihael Ramšak Appropriate sound insulation of facades as a measure to ensure acceptable acoustic comfort in residential buildings	259
31. Pavel Rovnaník, Cecilie Mizerová, Ivo Kusák and Pavel Schmid Self-sensing properties of the slag geopolymer composite with graphite powder under flexure	268
32. Fidan Salihu, Meri Cvetkovska, Koce Todorov, Nikola Postolov and Riste Volčev Inspection, assessment and repair of fire damaged concrete structure	276
33. Paulo Ščulac, Davor Grandić and Ivana Štimac Grandić Degradation of tension stiffening due to corrosion – an experimental study on cracked specimens	286
34. Nina Štirmer, Jelena Šantek Bajto, Ivana Carević, Ivana Hržan Mechanical properties of concrete containing wood biomass ash	295
35. Gordana G. Tanasijević, John L. Provis, Vedran N. Carević, Ivan S. Ignjatović and Miroslav M. Komljenović Effect of accelerated carbonation on the efficiency of immobilization of Cs in the alkali-activated blast furnace slag	303
36. Priscilla Teck, Ruben Snellings, Jan Elsen Characterization of the reaction degree of slag in a cement by neural networks based electron microscopy image analysis	312
37. Dejan Vasić and Marina Davidović BIM application in civil engineering projects	322

TABLE OF CONTENTS

- | | | |
|---|--|-----|
| 38. Dejan Vasić, Mehmed Batilović, Marina Davidović and Tatjana Kuzmić | Application of terrestrial laser scanning methodology in façade reconstruction and rehabilitation projects | 330 |
| 39. Luka Zevnik, Maurizio Bellotto | Industrialization of an alkali-activated slag binder: solving the issues of early strength and superplasticizer efficiency | 336 |
| 40. Lea Žibret, Martina Cvetković, Maruša Borštnar, Mojca Lončnar, Andrej Ipavec and Sabina Dolenc | Use of steel slag for the synthesis of belite sulfoaluminate clinker | 351 |

1

Boris Azinović, Andreja Pondelak, Jaka Gašper Pečnik and Vaclav Sebera

Flexible polymer connections for CLT structures

FLEXIBLE POLYMER CONNECTIONS FOR CLT STRUCTURES

Boris Azinović¹, Andreja Pondelak², Jaka Gašper Pečnik³ and Vaclav Sebera⁴

^{1,2} Slovenian National Building and Civil Engineering Institute, Department of structures
Dimičeva ul. 12, 1000 Ljubljana
e-mail: boris.azinovic@zag.si, andreja.pondelak@zag.si

^{3,4} InnoRenew CoE, Department of Materials
Livade 6, 6310 Izola
e-mail: jaka.pecnik@innorenew.eu, vaclav.sebera@innorenew.eu

SUMMARY: This paper explores the possibility of using flexible polymer adhesives to dissipate energy in CLT buildings during earthquakes. In the first series of tests, pull-off tests of various polyurethane (PUR) adhesives were performed. The connection was tested in pull-pull configuration using monotonic, tension-only loading. The tests have shown that the adhesive can resist large deformations already in tension loading and with small thicknesses of the bond-line. Based on the pull-off test results, one adhesive has been selected for further testing. Monotonic lap-shear tests were performed with the selected adhesive and thick bond-line (3 mm and 6 mm). The results show, that the standard method for lap-shear testing (EN 205) needs to be adapted for thick glue-line. It was found that the strength of 3 mm glue-line is higher than 6 mm one, which is in agreement with adhesion theory. The flexible PUR adhesives could potentially be used in CLT structures for anchoring the CLT wall with “flexible” glued-in rods or as a “flexible” vertical shear connection between the CLT walls. Such systems have a potential to dissipate energy in seismic areas.

KEY WORDS: CLT connections, flexible adhesive, polyurethane, energy dissipation, pull-off, lap-shear.

1 INTRODUCTION

Cross-laminated timber (CLT) is becoming an increasingly popular building material in Europe and across the world. The versatility of CLT has encouraged engineers to build multi-storey structures in earthquake prone areas, although there is limited experience and research about the behaviour of such structures during earthquakes.

The behaviour of CLT buildings during earthquakes depends mainly on the behaviour of the connections between adjacent panels. If the connections between the panels are strong enough these structures are able to achieve damage-free performance even during the strong earthquakes. However, if the connections are too rigid, large accelerations can occur in the upper stories. This may result in injuries to occupants and damage to property which is not acceptable in terms of serviceability. Therefore, the structural system should be modified to incorporate the dissipative behaviour. This can be achieved with dissipative connections which may be installed in different parts of the structure. Several solutions of dissipative connections have already been suggested so far to improve the ductile response of CLT buildings [1-5] but the research has been mainly focused on the mechanical connectors with concentrated plasticity. In such systems, the dissipation is concentrated in a small area which must be very carefully designed in order to prevent damage to other parts of the structure. In addition, the mechanical connectors are robust and difficult to hide inside the construction.

Therefore, the aim of this research is to investigate alternative options for energy dissipation by employing adhesive joints made of deformable polymer materials between the panels. For this purpose, elastic adhesives based on polyurethane could be used. Adhesives with good deformable properties have already been developed at the Cracow University of Technology for elastic joining of structural elements and to provide protective coating. They have already been successfully applied for the repair and seismic strengthening of cracked masonry structures [6-8]. The initial pull-off adhesion tests show that the new adhesive could also be used for gluing timber elements.

The flexible adhesive with energy dissipating properties allows for various applications in CLT structures to increase their seismic performance. The adhesives could be applied to the vertical joints between adjacent panels or they could be used in combination with glued-in rods (both options are schematically shown in Figure 1). For this purpose, the panels

should be broken up into smaller wall segments which allow panel rocking movement during the seismic event. When the rocking occurs, the energy is dissipated by the adhesive layer in vertical joints and/or glued-in rods. In this paper, experiments of pull-off and lap-shear behaviour of various polyurethane (PUR) adhesives are presented.

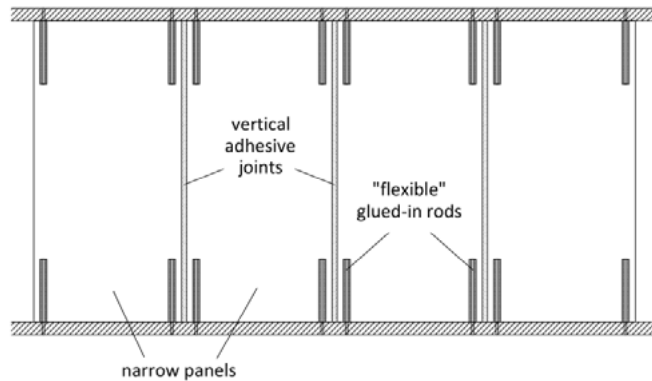


Figure 1: Possible use of flexible polymer adhesives in CLT structures

2 EXPERIMENTS

The experiments were performed at the Slovenian National Building and Civil Engineering Institute (pull-off tests) and at InnoRenew CoE (lap-shear tests). The tested pull-off specimens were composed of 2 timber pieces (dimensions 24 x 38 x 200 mm) made of spruce (*Picea abies L.*), which were glued according to the producer instruction at the cross section perpendicular to the fibre direction (Figure 2a). After sanding the surface, ZP primer was applied on the timber pieces [7]. Primer was left for an hour to dry completely. On the surface prepared with primer, 5 various adhesives were applied to connect the two timber pieces; (i) PMM, (ii) PSM, (iii) PS, (iv) PST and (v) PTS [7]. For each of the 5 adhesives, at least 7 specimens were tested. The tests were performed as displacement controlled using Universal testing machine Zwick Roell Z050 at constant rate 2 mm/min until failure of specimens was achieved.

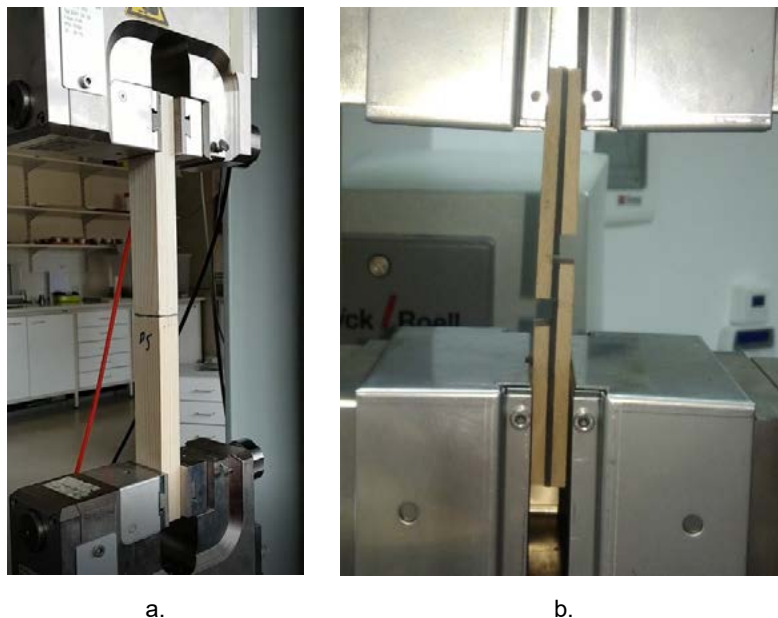


Figure 2: Configuration of: a. Pull-off tests, b. lap-shear tests.

For lap-shear tests beech (*Fagus Sylvatica L.*) boards were used as suggested in the standard EN 205. The grain direction was following longitudinal direction of the boards, which were planned and sanded to a thickness of 5 mm (+/- 0.2 mm) and cut into boards with final dimensions of 170 x 150 mm in length and width, respectively. Moisture content (MC) was measured with a dielectric measuring device for each board. ZP primer was applied, similarly as with the pull-off tests to cover the bonding surface. After primer dried out, two samples were prepared with thin 3 mm and thick 6 mm glue line. Spacers of desired thickness were glued on the edges of panel to create barriers for the enclosure where

adhesive was poured in. Two component adhesive PS was then precisely weighted in separated containers and mixed together using an electrical drill and metal fork. After 1 min of mixing both components together, adhesive was poured into the prepared wooden panels with spacers. Second panel was put on the top of the adhesive layer, to create three-layer composite of wood-adhesive-wood. No specific pressure was required, load was only applied to close the gaps between the spacers and panels. Three sandwich panel for 3 mm and two sandwich samples for 6 mm glue-line samples were prepared. Samples were dried 72 h to cure completely. After curing, samples were cut into final dimensions of 170 × 20 mm (longitudinal vs. crosswise) and put into climate chamber with standard climate conditions at 20 °C temperature and 65% relative humidity for 10 days. After conditioning, 8 specimens for 3 mm and 6 specimens for 6 mm glue-line were cut according to EN 205 standard for tensile test to determine static strength of adhesive bond. Static tensile tests were carried out using Universal testing machine Zwick Roell Z050 with testing speed of 5 mm/min.

3 RESULTS

The first sub-chapter presents the selection of adhesives for further testing, where pull-off tests were performed as a decision tool. The failed bond-line surface was additionally characterized by SEM imaging to discover the characteristic failure. In the second sub-chapter, basic behaviour of 3 mm and 6 mm thick glue line under tension shear loading is presented.

3.1 Pull-off tests

Results of pull-off strength differ according to the de-cohesion or de-adhesion effect. When the sample’s failure occurs between the adhesive and the timber part coated with primer the predominant failure mechanism was de-adhesion, while when it occurs within the adhesive then it is de-cohesion (Figure 3). Between the 5 tested adhesives the pull-off strength varies as it promotes different types of failure or their combination. Dependence of the pull-off strength on the adhesive selections is shown in Table 1. Obtained results compared to tensile strength of adhesive itself do not show direct correlation, therefore, meaning that for some adhesives de-adhesion was predominant failure mechanism.

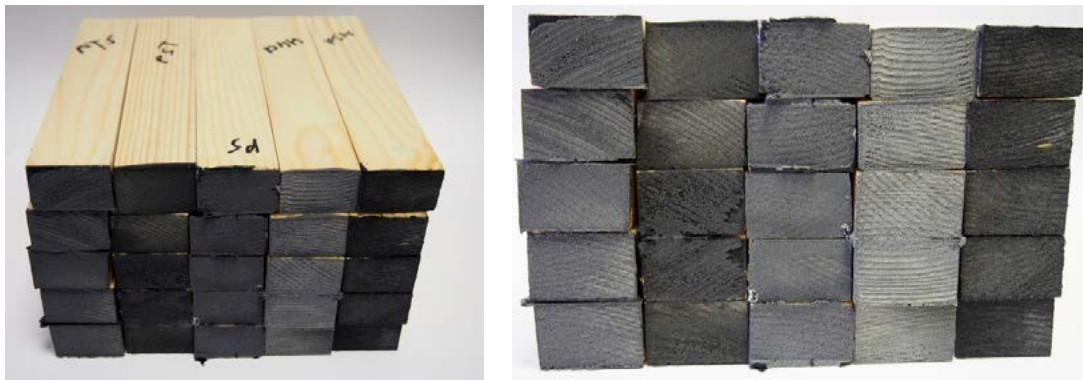


Figure 3: Damaged surface after failure under pull-off tests

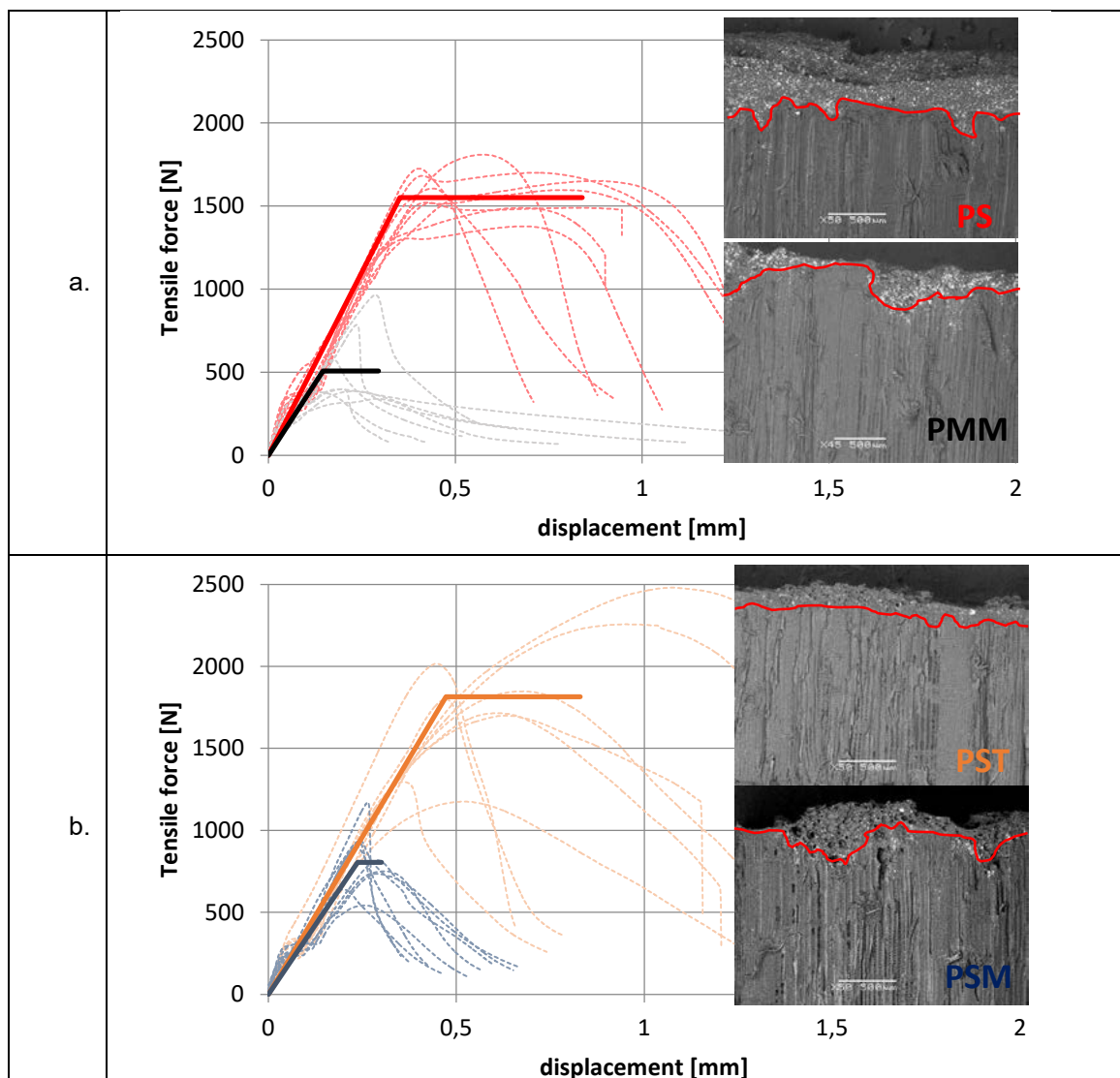
For each of the failed specimens, the force displacement diagram was idealised with a bi-linear curve according to the procedure described in [9]. From the idealised curve a sort of ductility factor was estimated as a quotient between the displacement at failure and displacement at initiation of damage (Table 1). The average ductility value for the examined adhesives was approximately 2 in all cases, proving the assumption that the bond-line doesn’t fail in brittle manner.

Table 1: Average results of pull-off experiments

Adhesive	Tensile strength of adhesive [N/mm ²]	Pull-of strength of bond-line [N/mm ²]	Average ductility of idealized curves
PTS	3.1	1.29	2.08
PST	4.0	1.99	1.76
PS	2.5	1.70	2.39
PSM	2.2	0.88	1.27
PMM	1.0	0.56	2.02

In Figure 4, all of the results are shown in the form of force displacement diagrams, where dotted curves represent each test series and thick lines the idealized bi-linear curves. In addition, a typical failed surface for each adhesive is shown. The images of failed surfaces were produced by scanning electron microscope (SEM), where magnification was approximately 50 in all cases. A cut was made from the side to observe the penetration of the adhesive into the timber part. The red line represents the boundary between adhesive and timber coated with ZP primer. The characterization of the bond-line revealed a good correlation with results of pull-off strengths. It was found, that PMM and PSM are the most prone to de-adhesion effect. This consequently proved to have a large effect on the pull-off strength, which was lower than 1 N/mm² for both adhesives. For this reason, PMM and PSM were excluded for further investigation as they seem to be inappropriate in terms of bonding on wood surface coated with ZP primer.

On the other hand, adhesives PTS, PST and PS reached mostly a cohesive failure. The difference in their response is therefore mainly due to different structure of adhesives. As it can be concluded from Table 1, PTS has the lower pull-off strength among these three adhesives. The latter can also be explained by the SEM images, since it appears that PTS has the most porous structure (Figure 4c) and is therefore easier to break under tensile load. Adhesives PS and PST proved to be the most stable and reached similar ductility and strength values (Table 1). The coefficient of variation for PST adhesive was larger than for PS adhesive. Meaning that there were also cases where PST failed in brittle manner. The objective of the research was to discover the most ductile behaviour, which was similar for both PS and PST. Since PST reached the highest pull-off strength, it was selected for further investigation.



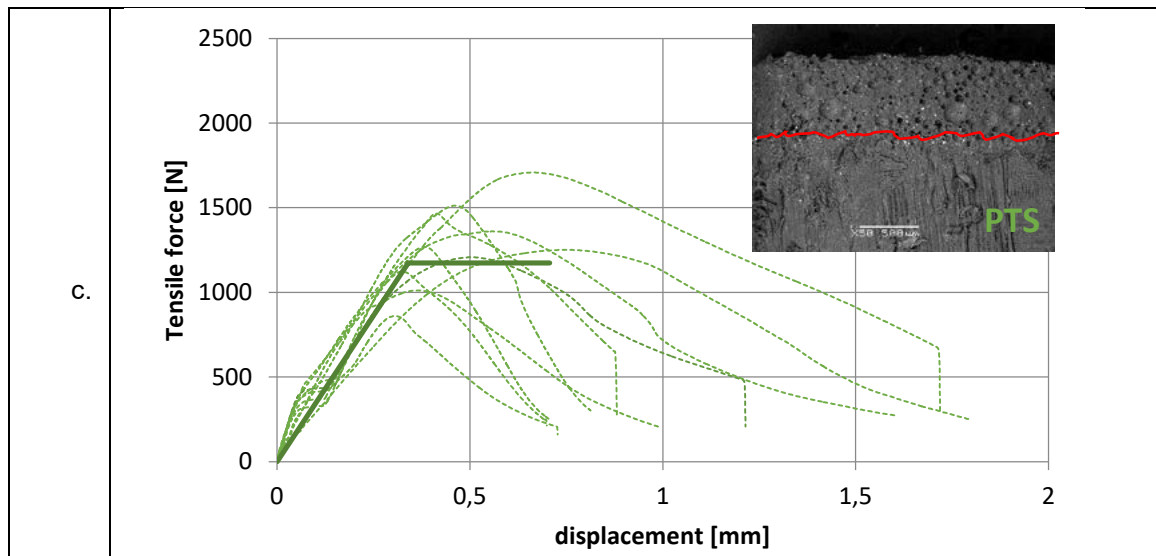


Figure 4: Results of pull-off tests with SEM characterization of adhesives: a.) PS and PMM, b.) PST and PSM and c.) PTS.

3.2 Lap-shear tests

The task of the second part of the study was to perform simple lap-shear tests on the adhesive PST, which was selected as one of the most promising candidates from the pull-off tests. A standard procedure for lap-shear tests, which is described in EN 205 was adapted to test thick glue-line. As it is marked in Figure 5, all the specimens under tensile shear load started breaking at the edge of the bond-line.

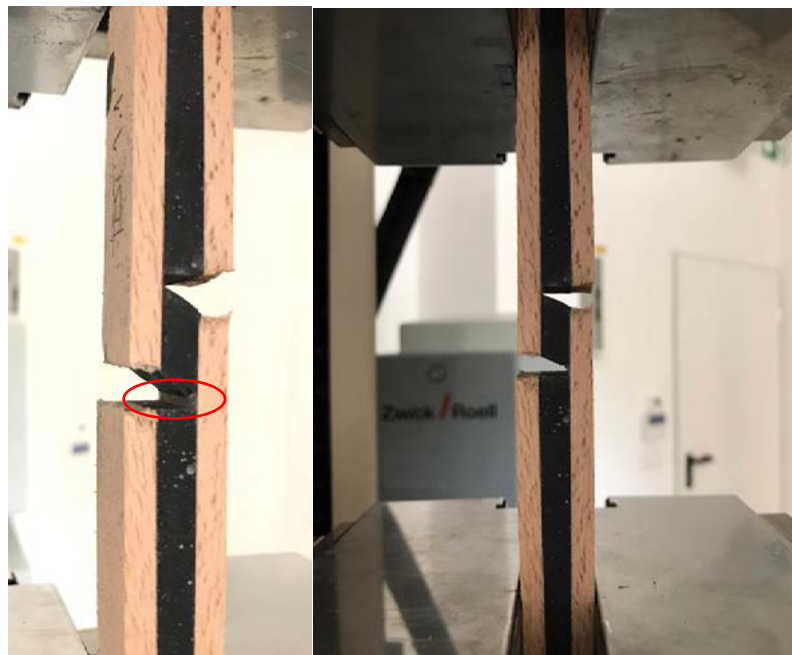


Figure 5: Point of fracture in the lap-shear test specimens.

Diagrams with force-displacement relationships for 3 mm and 6 mm bond-line are plotted in Figure 6, where orange lines represent 3 mm and black 6 mm thick bond-line. Integer numbers from Test 1 - Test 8, represents 3 mm bond line, one's with decimal numbers from Test 1.1 – Test 6.1 represents 6 mm bond line. As it seen from the diagram, 6 mm bond-line shows lower stiffness and smaller variability compared to 3 mm bond line. However, lower maximum forces were reached. The stiffness variability of 3 mm glue bonds samples may be explained by a higher variability of the bonding area (see Table 2). These preliminary tests showed that thinner glue-lines results in higher strengths, however, the displacement at initiation of failure is lower for thinner glue-line.

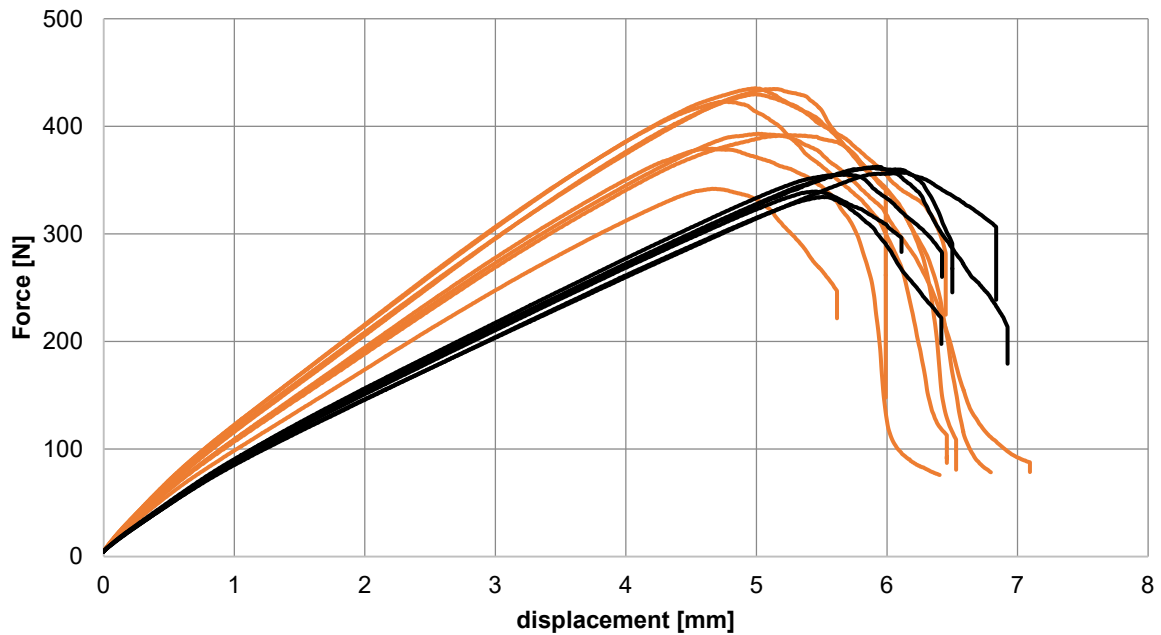


Figure 6: Force-displacement relationship for 3 mm (orange) and 6 mm (black) glue line under monotonic tensile shear test.

In Table 2, measurements of the bond line area and maximum force are presented. Glue-line of 3 mm thickness exhibits higher strength than 6 mm glue-line. F_{max} values obtained at the static tests, can be used to define amplitude cycles for cyclic evaluation, which will be a topic for further studies.

Table 2: Measurements of a bond line area for specimens dedicated to the static test with maximum force at break (F_{max}) and calculated strengths.

Sample	Specimen	Bond length [mm]	Bond width [mm]	Thickness [mm]	Bonding area [mm ²]	F_{max} [N]	Strength [N/mm ²]
3 mm	T1	12.0	20.2	13.5	242.2	391.8	1.62
3 mm	T2	11.8	20.2	13.5	238.4	379.2	1.59
3 mm	T3	11.6	20.2	13.7	233.9	393.1	1.68
3 mm	T4	12.8	20.1	13.7	257.4	434.7	1.69
3 mm	T5	12.7	20.2	13.8	256.0	435.4	1.70
3 mm	T6	12.1	20.3	13.5	245.1	423.1	1.73
3 mm	T7	12.3	19.9	13.6	245.4	430.0	1.75
3 mm	T8	10.8	20.2	13.5	218.2	342.0	1.57
median		12.1	20.2	13.6	243.7	408.1	1.69
SD		0.6	0.1	0.1	11.8	31.0	0.06
6 mm	T1.1	12.7	20.1	16.6	254.0	362.4	1.43
6 mm	T2.1	12.7	20.2	16.2	255.5	355.2	1.39
6 mm	T3.3	12.3	20.3	16.8	249.7	357.0	1.43
6 mm	T4.1	12.3	20.2	16.2	248.8	339.4	1.36
6 mm	T5.1	12.4	20.2	16.4	249.5	361.4	1.45
6 mm	T6.1	12.4	20.1	16.2	248.4	334.4	1.35
median		12.4	20.2	16.4	249.6	356.1	1.41
SD		0.2	0.1	0.2	2.8	10.8	0.04

As seen from the Figure 6, all the diagrams exhibit similar behaviour. The elastic part is nonlinear, but can be decomposed to two linear elastic parts. Such behaviour is typical for hyperelastic materials such as rubber and it seems, that bond-line is thick enough to show such behaviour. The nonlinear elastic part ends with the yield point and very small part of the plastic region. The elastic part of the deformation composes about 70-90 % of whole deformation range. From the maximal forces, the strength of the bond-line was computed for all lap shear tests. Average results are depicted in Table 3. The lower strength of thicker bond-line is in an agreement with adhesion theory.

Table 3: Descriptive statistics of lap-shear test.

specimen	Mean (MPa)	SD (MPa)	CoV (%)	Median (MPa)	<i>n</i>
Beech 3 mm	1.67	0.06	3.7	1.69	8
Beech 6 mm	1.40	0.04	2.6	1.41	6

4 CONCLUSIONS AND FURTHER WORK

The pull-off tests of flexible polyurethane adhesives applied on timber coated with ZP primer were made. The tests have demonstrated promising behaviour of the adhesives PS and PST in terms of their ductility already with thin glue-line and tensile loading. Mostly cohesive failure occurred, which indicates that the potential of high elastic deformation capability of these two adhesives could be exploited also when bonded to timber.

Results of monotonic lap-shear tests for the selected adhesive PST showed that relatively large elastic displacement can be expected in tensile shear loading. The average displacement at initiation of failure for 3 mm thick bond-line was approximately 5 mm, which proves the initial assumption of deformation capability. The tests have also shown that load-carrying resistance of the connection is proportional to the thickness of the adhesive. It was found that the strength of 3 mm glue-line is higher than 6 mm one, which is in agreement with adhesion theory.

To test the seismic behaviour of the connections with “flexible” PUR adhesives, a series of cyclic tests on larger specimens with realistic boundary conditions is necessary. For this reason, the presented research was performed as a preliminary decision tool for selecting adhesives for further evaluation. A more detailed work plan for testing glued-in rods and vertical connections with flexible adhesive PS or PST under cyclic loading is planned. Further research will provide more reliable information, whether the resistance of flexible connections with PUR adhesives is sufficient to be used for seismic resistant CLT structures. Cyclic tests are also necessary to evaluate the energy dissipation capacity, which is crucial information on whether the flexible connections can be used for seismic energy dissipation.

ACKNOWLEDGMENTS

The authors gratefully acknowledge the European Cooperation in Science and Technology for funding the InnoRenew CoE project [grant agreement #739574] under the H2020 Spreading Excellence and Widening Participation Horizon2020 Widespread-Teaming program, and Slovenian research program P2-0273; ARRS.

REFERENCES

- [1] Scotta, R., et al.: Dissipative Connector for CLT Buildings: Concept, Design and Testing. *Materials*, 9, 139, 2016.
- [2] Latour, M. and Rizzano, G. Cyclic behavior and modeling of a dissipative connector for cross-laminated timber panel buildings. *J. Earthq. Eng.*, 19, 137–171, 2015.
- [3] Loo, W.Y.; et al.: Experimental testing of a rocking timber shear wall with slip-friction connectors. *Earthq. Eng. Struct.*, 43, 1621–1639, 2014.
- [4] Hashemi, A, et al.: Seismic resistant structures with Cross Laminated Timber (CLT) walls coupled with innovative Resilient Slop Friction (RSF) joints. NZSEE 2017 conference, Wellington, New Zealand, 27-29 April 2017.
- [5] Smith, T. et al.: Seismic response of hybrid-LVL coupled walls under quasi-static and pseudo-dynamic testing. New Zealand Society for Earthquake Engineering Conf., Palmerston North, New Zealand, 2007.
- [6] Palermo, A, et al.: From theory to practice: Design, analysis and construction of dissipative timber rocking post-tensioning wall system for Carterton Events Centre, New Zealand. *Proc.*, 15th World Conf. on Earthquake Engineering, Lisbon, Portugal, 24–28, 2012.
- [7] Kwiecień A., Highly deformable polymers for repair and strengthening of cracked masonry structures. *GSTF International Journal of Engineering Technology (JET) Vol.2 No.1: 182-196, May 2013.*
- [8] Viskovic A. et al.: Quick seismic protection of weak masonry infilling in filled framed structures using flexible joints. KEM.747.628, Trans Tech Publications, Vol. 747, pp 628-637.
- [9] Yasumura, M. and Kawai, N.: Estimating seismic performance of wood-framed structures, in: *Proc. 5th World Conf Timber Eng. WCTE, Montreaux, Switzerland, 1998: pp. 564–571.*

2

Natalija Bede, Silvija Mrakovčić

Flexural behaviour of high strength concrete with steel and polypropylene fibres

FLEXURAL BEHAVIOUR OF HIGH STRENGTH CONCRETE WITH STEEL AND POLYPROPYLENE FIBRES

Natalija Bede¹, Silvija Mrakovčić¹

¹ Faculty of Civil Engineering in Rijeka, University of Rijeka, Department for Computer Modelling of Materials and Constructions, Radmile Matejčić 3, 51000 Rijeka, Croatia
e-mail: natalija.bede@uniri.hr, silvija.mrakovcic@uniri.hr

SUMMARY: High strength concrete (HSC) is very often used in structural design due to its numerous advantages in comparison to ordinary concrete. However, HSC has a major disadvantage, high brittleness. In general, addition of fibres to concrete mixture increases ductility. Hence, to overcome limitation of HSC steel fibres and combination of steel fibres with different volume fraction of polypropylene fibres (PP) were added to concrete matrix. The main purpose of this work was to investigate the effect of the addition of hybrid steel-polypropylene fibres on flexural behaviour of concrete. Based on three-point bending tests flexural strength and flexural toughness are experimentally determined. Further, load-displacement curves and typical failure mode from flexural tests are given. Moreover, standard cube specimens were tested to determine the compressive strength. All above mentioned properties are compared to referent concrete.

KEY WORDS: high strength concrete, steel fibres, polypropylene fibres, hybrid concrete, compression test, flexural test

1 INTRODUCTION

Nowadays, a high-strength concrete (HSC) is often used in structural design. By using HSC complex modern structures such as skyscrapers, high towers and long-span bridges can be constructed. HSC has numerous advantages in comparison to ordinary strength concrete (OSC) such as improved durability, higher strength and stiffness. However, it has a major disadvantage, high brittleness [1]. Concrete structures in their service life are subjected to different types of dynamic loads such as earthquakes, impact loads or blasts. Hence, toughness, ductility and high energy absorption capacity are among the most desirable properties for concrete structures.

It is well known that inclusion of fibres in concrete improves many of the engineering properties, especially ductility and toughness [2, 3]. Nowadays, various types of fibres made of steel, polymers, carbon, glass and natural materials are used for reinforcing concrete [2]. The properties of fibre reinforced concrete (FRC) depend on the type of fibres used, amount, geometry and density and their orientation and distribution in the concrete matrix. Polypropylene and steel fibres are the most commonly used and studied fibres. Recent studies have confirmed that the use of hybrid fibres, or a combination of two or more types of fibres, makes concrete that has better engineering properties than concrete with only one type of fibres [2-6].

To predict structural response, it is important to fully understand main mechanical characteristics of concrete. The compressive strength is a main property needed in the design of concrete elements. Hence, compression test on fibre reinforced HSC (FRHSC) were carried out. The structures in their service life are more often subjected to flexure than to direct tension. Consequently, the flexural properties of FRHSC are important for design of concrete structures. Hence, test on beams in flexure were carried out to investigate the effect of different fibres on flexural properties of concrete such as first peak strength, flexural strength, residual strength and flexural toughness.

The load-displacement curve until the first peak characterizes the behaviour of the FRC up to the onset of cracking in the concrete matrix. Substituting values of loads at first crack displacement in the modulus of rupture formula first peak strength can be calculated [7, 8]. FRC is characterized by a significant residual strength and enhanced flexural toughness due to crack-bridging mechanism of fibres. Residual strength provides performance of concrete in post-cracking region. According to standard ASTM C1609/C1609M [7] the substituting values of loads at specific displacements of $l/600$ and $l/150$ of the beam span length in the modulus of rupture formula residual strength can be calculated. The flexural toughness is the measure of the energy absorption capacity of a specimen. According to the standard ASTM C1609/C1609M [7] the flexural toughness can be determined by measuring the area under load-displacement curve up to displacement of $l/150$ of the specimens span.

In this paper the experimental program is given in Chapter 2 and the results are presented and discussed in Chapter 3. Finally, some relevant conclusions are drawn in Section 4.

2 EXPERIMENTAL PROGRAM

For the purpose of experimental testing 30 cubes are tested for compressive strength and 45 beams under flexure using three-point bending test setup to characterize behaviour of steel fibre HSC (SFRHSC) and hybrid fibre HSC (HyFRHSC). HyFRHSC contained fixed volume fraction (V_f) of steel fibres and varying volume fraction of polypropylene (PP) fibres. All tests were performed at the Faculty of Civil Engineering in Rijeka, Croatia.

2.1 High strength concrete mixture

For this experimental program five concrete mixtures containing different volume fractions of steel and PP fibres were designed to analyse the fibre contribution to compressive strength and flexural properties. The first mixture was the HSC control mixture made without fibres, denoted as REF in Table 1. The other four (4) mixtures are made with 1.5% of steel fibres but with different volume fraction of PP fibres (0%, 0.1%, 0.2% and 0.3%). To clearly name concrete mixture following marking was used: the letter S for steel fibres and the letters MF for monofilament PP fibres. The corresponding number assigned to letters indicates the volume percentage of fibres used in the mixture (Table 1). The density of the fresh concrete for each concrete mixture is shown in Table 1.

Table 1: Fibre content in designed concrete mixtures and density

Concrete mixture notation	Steel fibre content V_f (% vol) / (kg/m ³)	Monofilament PP fibre content V_f (% vol) / (kg/m ³)	Density (kg/m ³)
REF	0	0	2135
S 1.5	1.5 / 117	0	2282
S 1.5 - MF 0.1	1.5 / 117	0.1 / 0.91	2151
S 1.5 - MF 0.2	1.5 / 117	0.2 / 1.82	2126
S 1.5 - MF 0.3	1.5 / 117	0.3 / 2.73	2094

Notation: S-steel fibres, MF-monofilament polypropylene (PP) fibres

The materials used to cast concrete specimens were locally available cement CEM I 52.5R, crushed limestone sand with a maximum size of 2 mm, quartz sand and silica fume. To ensure good bond between concrete matrix and fibres there is no coarse aggregate in the mix composition. The water binder ratio was kept constant at 0.3. Appropriate dose of super plasticizer and stabilizer have been added for the desired workability. The quantities of materials in 1m³ of REF mixture were equal to 640 kg, 160 kg, 256 kg, 20 kg, 4.8 kg, 614 kg and 560 kg for cement, silica fume, water, superplasticizer, stabilizer, sand and quartz, respectively. Two types of straight micro fibres were used: steel fibres 13 mm long and with diameter of 0.2 mm and polypropylene monofilament fibres 12 mm long and with diameter of 0.02 mm.

Each concrete mixture was batched separately. Each batch consisted of six cubes and nine prisms. A vibrating table was used to compact the concrete in the moulds in three layers. After demoulding, the specimens are cured immersed in water tank for 28 days.

2.2 Test set-up and specimen geometry

For the compression tests a universal testing machine with a maximum load capacity of 3 MN was employed (see Figure 1a). To determine concrete compressive strength cube specimens of 150 mm edge according to testing standard HRN EN 12390-3 [9] were used. Six (6) specimens for each concrete mixture were tested.

As there is no standard methodology for testing concrete with fibres various standards have been proposed for the characterisation of flexural behaviour of the OSC with fibres however with different specimen sizes, loading rates, loading arrangement etc. [7, 8]. Moreover, standards for OSC cannot be directly transferred to HSC. Hence, to get insight into the flexural behaviour of FRHSC flexural test were performed with some modifications but under the same conditions for all concrete mixtures.

HSC specimens without a notch were tested in a three-point bending setup, with a force concentrated in the middle of the span. Specimens were prismatic beams with cross-section of 100 mm × 100 mm and a span length of 300 mm. Figure 1b shows the test setup used in flexural test. The flexural tests were carried out by means of servo-controlled hydraulic machine with a maximum capacity of 300 kN. The tests were performed with the displacement control. In total, two Linear Variable Differential Transducers (LVDT) were used for measuring central point displacement, each on the longitudinal side of the beam as shown at the Figure 1b. During testing the load-displacement history was recorded up to deflection of min 3 mm to obtain post-peak behaviour. Nine (9) specimens at each concrete mixture were tested.

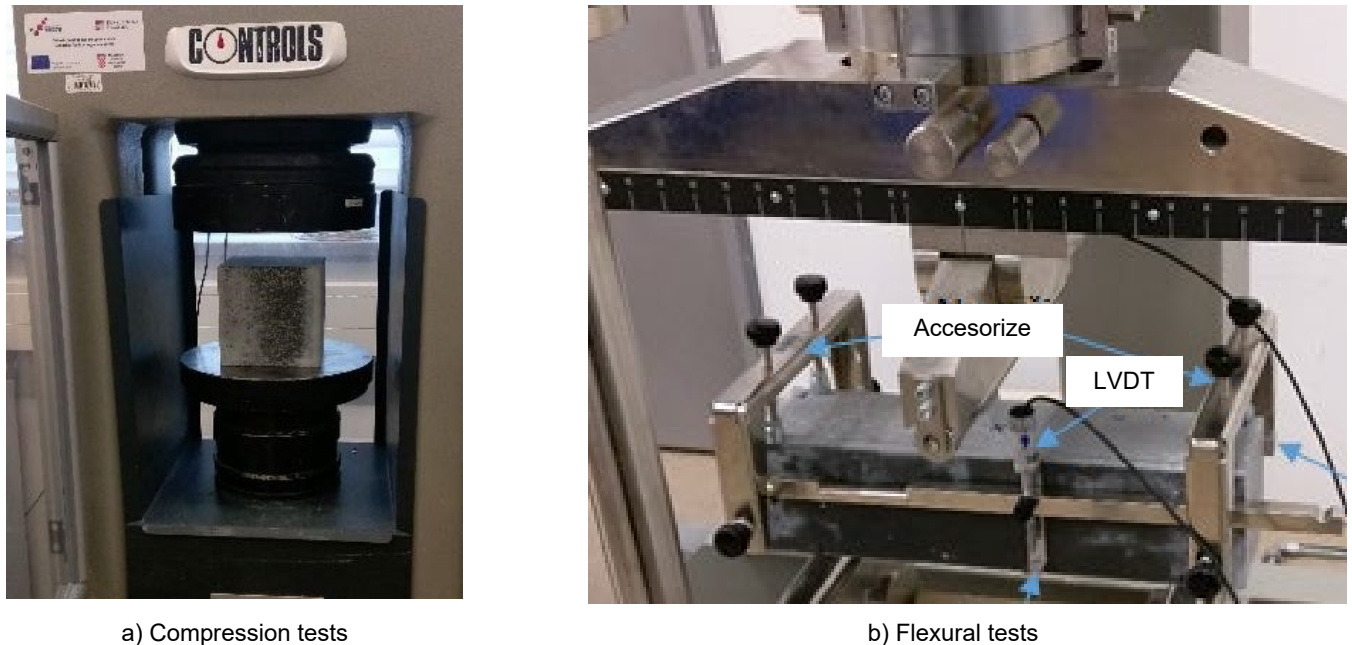


Figure 1: Test setup [11]

3 EXPERIMENTAL RESULTS

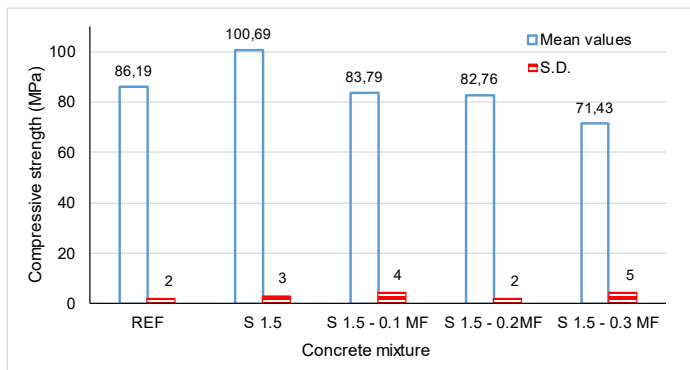
In this chapter results of the performed experiments are presented. Following material properties were tested on 28-day age concrete specimens: compressive strength, first peak strength, flexural strength, residual strength and flexural toughness. All the result obtained have been compared with REF concrete (0% of fibres).

3.1 Compressive strength

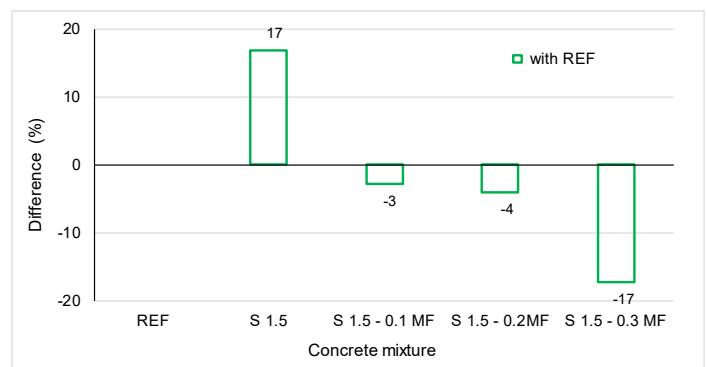
The mean values of the compressive strength together with the standard deviation for each concrete mixture are reported in Figure 2. The test results show good consistency and acceptable scatter. The mean compressive strength ranges from 71 MPa to 101 MPa, so concrete can be specified as HSC [11].

The highest compressive strength is achieved for the concrete mixture S 1.5 containing only one type of fibres - steel fibres. The percentage decrease and increase in compressive strength over REF concrete are presented in Figure 2b. Maximum increase in compressive strength is 17% compared with the values of REF mixture. It is observed that the compressive strength decrease with an inclusion of PP fibres and increase in fibre volume content. The compressive strength in mixes with 0.1, 0.2 and 0.3 % of PP fibres decreased by 3%, 4% and 17%, respectively, compared to the REF mixture. Hence, the lowest compressive strength was obtained for hybrid concrete mixture S 1.5-0.3MF with highest PP fibre volume content. Similar tendency was found in [4]. This can be attributed to the uneven distribution of fibres in concrete matrix and higher porosity of concrete matrix. More detailed information on the fresh concrete properties can be found in [11].

In general, combination of steel and PP fibres results in reduction of compressive strength. Moreover, increase of PP fibres has negative influence on the mean compressive strength of hybrid concrete. Concrete with the steel fibres achieved the highest compressive strength.



a) Mean values

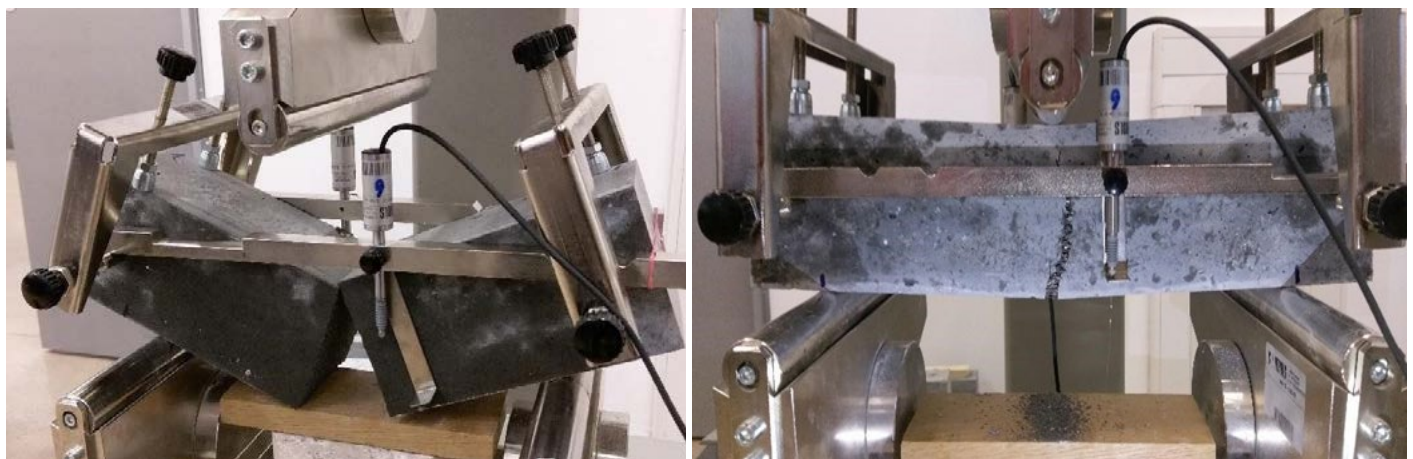


b) Compared with REF concrete (% of fibres)

Figure 2: Compressive strength of concrete mixtures with different fibre content

3.2 Flexural properties

Figure 3 shows typical failure mode obtained for the flexural test for beams without fibres and beam with fibres. As expected, REF specimen broke in extremely brittle manner into two pieces. On the other hand, for FRHSC specimens the fragmentation is prevented due to the inclusion of fibres indicating enhanced ductility over the REF specimens. Thus, it can be concluded that the effect of fibres on the brittleness of HSC is remarkable.



a) Without fibres

b) With fibres

Figure 3: Typical failure mode observed after flexural test on concrete beams [11]

Typical load-displacement curves obtained in this investigation for each concrete mixture are presented in Figure 4. Again, the results showed the typical load-displacement response for HSC without fibres (see Figure 4a). FRHSC load-displacement curves clearly showed typical multiple-peak load values under flexure (see Figure 4b). In general, it can be observed that after first peak appeared, load continue increase for all FRHSC specimens. After reaching maximum load, load started decrease slowly. Moreover, it can be clearly observed that maximum load values differ while post-peak response is very similar for all specimens. Accordingly, experimentally recorded load-deflection curves are analysed to investigate pre-peak behaviour and post-peak behaviour of tested concrete mixtures in detail.

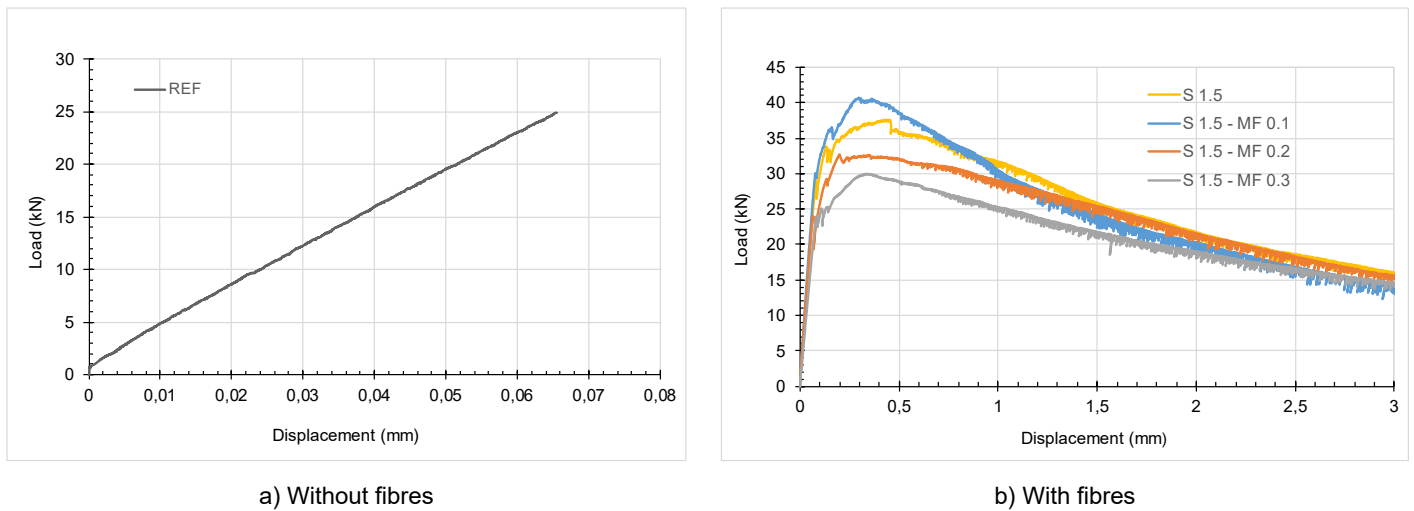


Figure 4. Typical load-deflection curves recorded in flexural test on concrete beams

3.2.1 Pre-peak response

First peak strength values together with their standard deviations are shown in Figure 5. The scatter of test results within a particular concrete mixture is relatively low. The percentage decrease or increase in first peak strength over REF concrete is presented in Figure 5b. Comparison of the given results shows that the first peak maximum strength is achieved by hybrid concrete mixture S 1.5 - MF 0.1, even 21% higher over REF concrete. In comparison with value obtained for compressive strength (see Figure 2) it can be concluded that compressive strength is not the key reason for that increase, rather combination of properties of the used hybrid fibres. Further, for concrete mixture S 1.5 the increase of 14% in the first peak strength compared to REF mixture is calculated. This time, compressive strength can be main reason for obtained increase.

It is important to note that the presence of higher volume content of PP fibres decreases the first peak strength of HyFRHSC to values even lower than REF concrete. Compared to REF mixture this decrease amounts to 4% for S 1.5 - MF 0.2 and 7% for S 1.5 - MF 0.3. It can be concluded that small reduction of first peak strength of hybrid concrete mixtures over REF concrete is related to decrease of compressive strength (see Figure 2) which represents the property of concrete matrix.

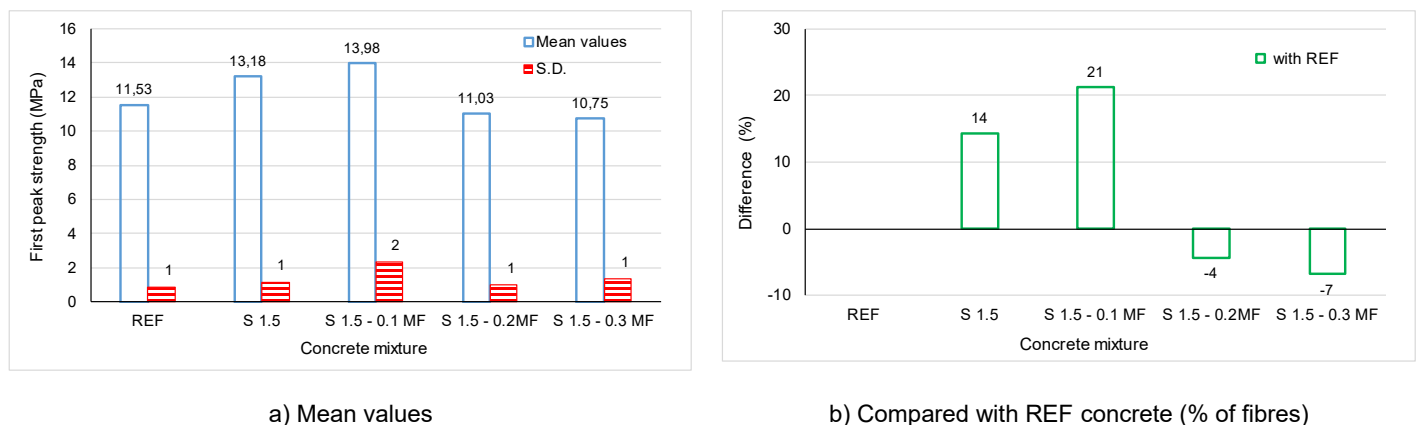
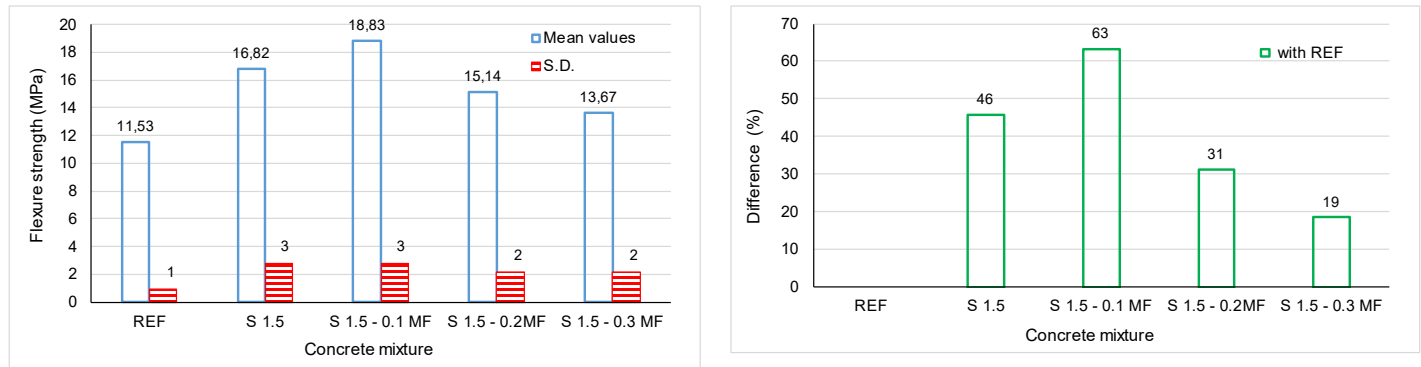


Figure 5: First peak strength of concrete mixtures with different fibre content

3.2.2 Flexural strength

Figure 6 shows mean values of flexural strength of the tested concrete mixtures together with standard deviations. The scatter of test results within concrete mixtures with fibres is found to be higher compared to REF concrete, but still relatively low. As expected, flexural strength of REF concrete mixtures is the lowest. On the other hand, increase in flexural strength is observed for all FRC mixture. The percentage of the increase in flexural strengths over REF concrete

is presented in Figure 6b. It is expected that PP fibres do not contribute to the strength [12], however, for hybrid concrete mixture S 1.5 - MF 0.1 maximum flexural strength is obtained, approximately 63% higher over REF concrete mixture. Similar results are given in [6]. Due to lower value of compressive strength (see Figure 2a) this growth is attributed to the used hybrid fibres. Further, for hybrid concrete mixture S 1.5 - MF 0.2 increase reduces to 31 % and only 19 % for S 1.5 - MF 0.3. Hence, for hybrid concrete mixtures with fibre volume fraction greater than 0.1%, again similar decreasing trend is observed. SFRHSC mixture S1.5 exhibits slightly lower flexural strength than the hybrid concrete mixture S 1.5 - MF 0.1 (see Figure 6). This small difference, however, can be attributed to the higher compressive strength of SFRHSC.



a) Mean values

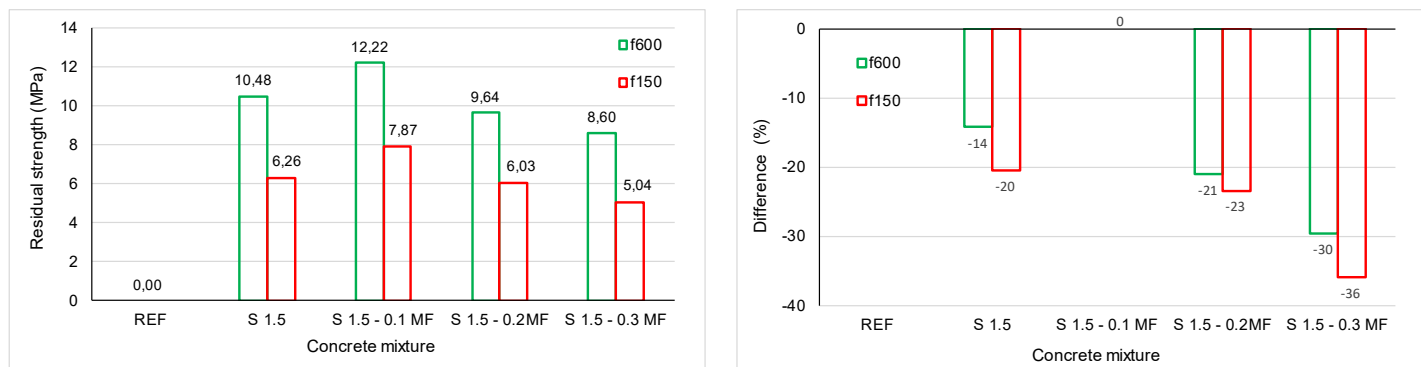
b) Compared with REF concrete (% of fibres)

Figure 6: Flexural strength of concrete mixtures with different fibre content

3.2.3 Post-peak response

Figure 7 shows residual strength values calculated at selected displacements of 0.5 mm and 2 mm which equals to displacement at $l/600$ and $l/150$, respectively. REF concrete specimens with 0% of fibres showed no residual capacity. Again, hybrid concrete mixture S 1.5 - MF 0.1 showed highest residual strength at specified displacements. With further increase of PP fibre volume fraction residual strengths decrease by 21% and 30% for displacement at 0.5 mm and by 23% and 36% for displacement at 2 mm. In SFRHSC mixture S 1.5 smaller reduction in residual strength is obtained, by 14% and 20% at 0.5 mm and 2 mm displacement, respectively.

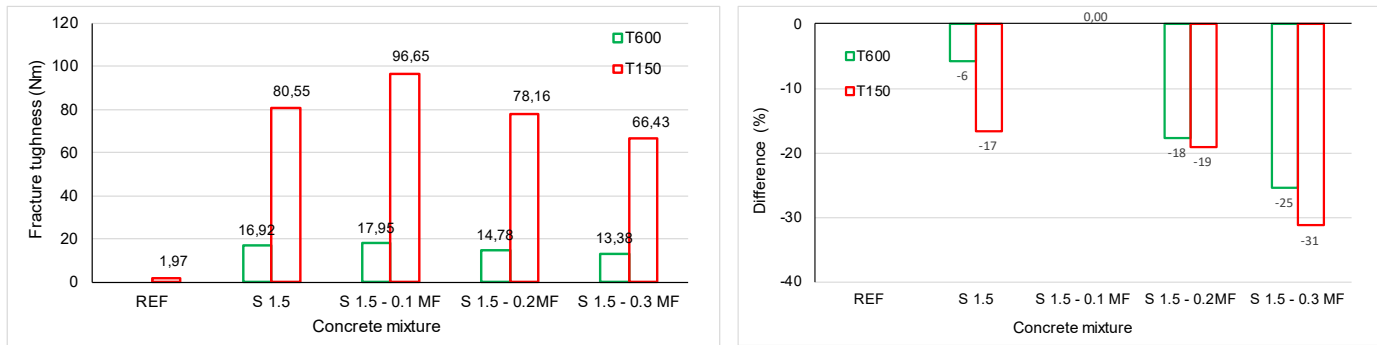
Figure 8 shows average values of flexural toughness calculated at 0.5 mm (equal to displacement at $l/600$) and 2 mm (equal to displacement at $l/150$). Flexural toughness of REF concrete mixture is calculated from the area under the load-displacement curve until complete breakdown of specimen. The fracture toughness of REF concrete mixture was found to be negligible compared to SFRHSC and HyFRHSC. Again, the same trend was observed. As expected, hybrid concrete mixture S 1.5 - MF 0.1 achieved the highest flexural toughness, 15 times higher at 0.5 mm displacement and even 50 time higher toughness value at 2 mm displacement over REF concrete. With increasing PP fibre content flexural toughness again showed decreasing trend. Compared with S 1.5 - MF 0.1 values were lower 18% and 25% at displacement of 0.5 mm and 19% and 31% at 2 mm displacement. However, concrete mixture S 1.5 showed smaller difference of 6% and 17% at 0.5 mm and 2 mm displacement, respectively.



a) Mean values

b) Compared with hybrid concrete mixture S 1.5 - MF 0.1

Figure 7: Residual strength of different concrete mixtures



a) Mean values

b) Compared with hybrid concrete mixture S 1.5 - MF 0.1

Figure 8: Flexural toughness of concrete mixtures with different fibre content

4 CONCLUSIONS

Experimental tests have been carried out on concrete mixtures prepared with fixed volume fraction of steel fibres and varying volume fraction of polypropylene fibres to study flexural properties of hybrid high strength concrete. Based on the test results obtained, following conclusions are made:

1. Inclusion of the steel fibres enhance compressive strength of concrete. Also, steel fibres positively affect on flexural properties of concrete.
2. Combination of steel and PP fibres reduce strength of hybrid concrete.
3. Combination of steel and PP fibres in volume content of 0.1% positively affected flexural properties of hybrid concrete. However, increasing PP fibre content beyond 0.1% reduced flexural properties of hybrid concrete.
4. Flexural toughness of SFRHSC and HyFRHSC showed remarkably higher values compared to REF mixture
5. Test results show that combination of steel and PP fibres improved flexural properties of hybrid concrete compared to single fibre mixture. However, to enhance properties of hybrid concrete in flexure it is important to have optimum volume fraction of used combination of fibres.
6. Further studies and statistical data analysis of concrete mixtures are required to confirm given conclusions.

ACKNOWLEDGEMENTS

This work has been supported in part by Ministry of Science, Education and Sports of the Republic of Croatia under the project Research Infrastructure for Campus-based Laboratories at the University of Rijeka (no. RC.2.2.06-0001).

REFERENCES

- [1] Abid, A.S.; Ribakov, Y.: Recent trends in steel fibered high-strength concrete. *Materials and Design*, Vol. 32 (2011), pp.4122-4151
- [2] Šahinagić-Isović, M.: *Posebne vrste betona: mikroarmirani beton*. Univerzitet "Džemal Bijedić" u Mostaru, Građevinski fakultet, Mostar, Bosna i Hercegovina (2015).
- [3] Narayanan, S.; et al.: Past investigations on mechanical and durability properties of hybrid fiber reinforced concrete, *International Journal of Civil Engineering and Technology*, Vol. 10 (2019), No.3, pp. 1-10.
- [4] Tamil Selvi, M.; Thandavamoorthy, T.S.: Mechanical and durability properties of steel and polypropylene fibre reinforced concrete. *International Journal of Earth Sciences and Engineering*, Vol. 7 (2014), No.2, pp. 696-703, ISSN: 0974-5904
- [5] Kanagavel, R.; Kalidass, A.: Mehanička svojstva hibridnog mikroarmiranog betona s miješanim cementom, *Građevinar*, Vol. 69 (2017), No. 1, pp.1-10.
- [6] Singh, S. P.; Singh, A. P.; and Bajaj, V.: Strength and flexure toughness of concrete reinforced with steel-polypropylene hybrid fibres, *Asian journal of civil engineering (Building and housing)*, Vol. 11 (2010), No.4, pp.495-507

- [7] ASTM C1609/C1609M-12. Standard test method for flexural performance of fiber-reinforced concrete (using beam with third-point loading), *ASTM Committee*, 2012.
- [8] ASTM C1018-97. Standard test method for flexural toughness and first crack strength of fiber-reinforced concrete (using beam with third-point loading), *ASTM Committee*, 1997.
- [9] HRN EN 12390-3:2009. Ispitivanje očvrstlog betona - 3. dio: Tlačna čvrstoća ispitnih uzoraka, *Hrvatski zavod za norme*, 2009.
- [10] ACI 363.2R-98: Guide to quality control and testing of high-strength concrete, *ACI Committee*, 1998.
- [11] Ušić, I.: *Prodor klorida kroz mikroarmirani beton visokih uporabnih svojstava*, Diplomski rad, Građevinski fakultet, Sveučilište u Rijeci, Rijeka, Hrvatska (2017)
- [12] Bošnjak, J.; Sharma, A.; Grauf, K.: Mechanical properties of concrete with steel and polypropylene fibers at elevated temperatures, *Fibers*, Vol. 7 (2019), No. 2, pp.1-13.

3

Maurizio Bellotto, Luka Zevnik

On the use of metallurgical slags alternative to blastfurnace slags in the formulation of alkali-activated binders



ON THE USE OF METALLURGICAL SLAGS ALTERNATIVE TO BLASTFURNACE SLAGS IN THE FORMULATION OF ALKALI-ACTIVATED BINDERS

M. Bellotto¹, L. Zevnik²

¹ Polytechnic of Milano, Department of Chemistry, Materials and Chemical Engineering "G.Natta"
Piazza Leonardo da Vinci 32, 20133 Milano, Italy
e-mail: mauriziopietro.bellotto@polimi.it

² Leonardo d.o.o.
Storžiška 4, Kranj, Slovenia
e-mail: l.zevnik2@gmail.com

SUMMARY: Alkali-activated blast furnace slags can be used for the formulation of one-part binders to produce load-bearing structures replacing conventional Portland cements. The European production of blast furnace slag sums to about 19.2 Mio Tons (Euroslag, 2018). More than 81% of it is used to produce cement and concrete. Most of the remainder is not quenched and is therefore not a suitable pozzolanic addition. Thus, no blast furnace slag is left for alkali-activated binders. Moreover, the cost of ground granulated blast furnace slag (GGBS) is higher than the one of CEM II cement, the most widespread in Europe, making alkali-activated binders not commercially attractive.

It is therefore necessary to find alternative sources of slags which may constitute additional volumes of low-priced material. The first choice is the use of foundry cupola-furnace slag, whose composition is quite similar to GGBS. Its actual composition differs according to the quality of pig-iron produced, and it may show higher Mg contents in the case of spheroidal pig iron. The observed different reactivity is due to the different pore solution chemistry and nucleation kinetics, which can be accounted for with the addition of reactive silica and/or soluble Ca^{2+} containing species.

Another important source of slag is the ladle refining of steel, which accounts for the production of 4 Million Tons of white slag in Europe, presently entirely landfilled. This slag is richer in calcium with respect to GGBS, making it difficult to quench and granulate. We have performed tests adding a silicon bearing material (silica sand, foundry sand) to the molten slag in the ladle to modify its composition and make it suitable for quenching and granulation. The material which is produced is as reactive as GGBS and is a suitable candidate for the production of alkali-activated slag binders.

KEY WORDS: One-part alkali activated slag binder; foundry slag; white steel slag; circular economy; industrial symbiosis.

1 INTRODUCTION

Alkali-activated binders are a diverse class of materials which constitute one of the members of the current and future toolkit of 'sustainable cementing binder systems' [1–4]. These binders can be formulated with a wide range of aluminosilicate precursors, with differing availability, reactivity, cost and value worldwide. Thus, alkali-activated binders need to be optimized with locally available material and will probably never constitute a worldwide standardized commodity the way Portland cement is today. On one side this diversity means that this class of materials is very versatile and locally adaptable, on the other alkali-activated binders lack the robustness of Portland cement, both as mix design latitude and as compatibility with chemical admixtures.

Among the precursors which have been proposed and used since longer times, metallurgical slags and in particular blast furnace slags are the most effective, and prone to deliver ready-to-use solutions. The first data reporting the possibility of producing a binder material from granulated blast-furnace slag and caustic soda in combination with slaked lime go back to 1895 [5]. In 1940, A. Purdon reported on the results of first extensive laboratory studies on cements without Portland cement clinker, consisting of slag and caustic alkalis produced with a base and an alkaline salt [6]. Purdon developed a slag cement with high early strength, and high slag content (> 90%). He discovered that blast-furnace slag can be activated more intensely by adding caustic alkalis such as NaOH or KOH [7] than by adding lime or Portland clinker. Caustic alkalis can be added directly to the cement or NaOH can be formed at the moment of cement batching. This is done by adding salts with alkaline hydrolysis, such as Na_2CO_3 and $\text{Ca}(\text{OH})_2$, to the cement to form

NaOH (eq. 1). Other salts such as Na₂SO₄ can also be used as a substitute for Na₂CO₃ [6]. These formulations are still being studied [8] and are still in use today, eventually including other industrial by-products like kiln bypass condensation dust [9]. These alkali-activated slag binders have the important property of being 'one-part binders' which set and harden upon the addition of water only, without the need to add caustic alkaline solutions. This allows the use of the technological batching equipment developed and in use to produce Portland cement concrete.



The development of alkali-activated slag binders was made possible by the technical improvements connected to the advanced techniques used in the steel production for the fast cooling of blast furnace slag realized in the first decades of the twentieth century. 'Le Purdociment', the binder developed by Purdon in Belgium, was cheaper in production than Portland cement because of its high percentage of blast furnace slag in comparison with traditional Belgian blast furnace slag cements ($\cong 70\%$), and because of the absence of Portland clinker. Today more than 87% of the 19.2 Mio Tons of blast furnace slags produced in Europe are quenched and vitrified [10]. All of this material (16.8 Mio Tons [10]) is used as a cement and concrete addition, leaving little margin for the production of alkali-activated binders. Moreover, the price of granulated blast furnace slag is comparable or higher than the price of Portland cement clinker making alkali-activated slag binders un-attractive from the commercial perspective. This situation, coupled with the limitations in possible use of alkali-activated binders coming from the international regulations, makes the industrial use of alkali-activated binders still a case of study. To overcome this situation, it is necessary to find an alternative abundant source of a material with similar properties than GGBS, possibly at a lower price. Also, in the short term, it is necessary to exploit the possibility provided by the international regulations to produce high slag binders with the minimum possible clinker content to fit into the limits and with activator content less than the maximum allowable undeclared addition. This in the time span needed to propose and approve regulations specifically conceived for alkali-activated binders.

2 MATERIALS AND METHODS

2.1 Analytical methods

The elemental chemical composition of the different materials was measured by X-ray fluorescence (XRF) with a wavelength dispersive spectrometer Philips PW2400.

Their phase composition was determined by X-ray diffraction (XRD), using a Panalytical X'Pert Pro diffractometer equipped with the X'Celerator detector and Cu K α radiation, adopting a Bragg-Brentano geometry, on a 2 θ range of 5-80°, step size of 0.017° 2 θ , time per step of 50s, using a flat spinner.

The foundry sand was analysed by thermogravimetry, to measure the amount of carbon black present as a result of the pyrolysis of the organic binder during casting. Thermal analysis measurements (TG-DTG) were performed using a DTA-TG SEIKO 6300 thermal analyser. The experiments were conducted under flowing air in the temperature range of 25-1000 °C. The heating rate was set at 10°C/min.

The hydration behaviour of the different formulations was tested by isoperibolic calorimetry, with a custom-built device constituted by a multi-cell calorimeter equipped with type K thermocouples. Amounts of 60.0 \pm 0.1 g of the binder paste samples were placed into 80 ml insulated containers which were then sealed. The containers were placed into an insulated chamber, and the thermocouples measured the samples' temperature and the temperature inside the insulated chamber. The heat exchange characteristics of the insulated sample containers and the sample specific heats were calibrated in order to derive heat fluxes in W/g_{binder} and cumulative hydration heat in J/g_{binder}.

2.2 Materials

The materials which have been investigated in the present work are slag from cupola-furnace foundry and white steel slag from electric arc furnace. The composition of the slag of a cupola-furnace is very similar to the one of a blast-furnace. We have used the slag coming from two production sites of a foundry (Fonderia Corrà S.p.A., Italy). In one of them there is an installation for water cooling and granulation of the slag, while in the other the slag is usually slowly air cooled. In this latter case we have arranged a pilot water cooling system to provide the material for testing. The former site works with a fortnight production cycle between reconstruction of the refractory lining, while the latter works with a daily cycle.

Both sites run a hot blast process. The foundry slag composition is significantly constant as shown in Table 1. Two types of slag are obtained, differing in the Mg content which is higher when spheroidal pig iron is produced because of the recycle of the runners and risers and if using a dolomitic carbonate fluxing charge. In Table 1 are reported the average and standard deviation of the measurement of 10 slag samplings per type of slag.

Table 1: Average foundry slag composition.

Element (oxide)	Ca-rich slag		Mg-rich slag	
	average (%)	σ (%)	average (%)	σ (%)
SiO ₂	42.6	3.8	45.7	2.8
CaO	38.9	3.4	22.0	2.7
Al ₂ O ₃	9.5	1.5	12.5	1.8
MgO	2.19	0.15	16.1	0.6
Fe ₂ O ₃	1.7	1.6	0.67	0.29
Na ₂ O	0.53	0.37	0.26	0.09
K ₂ O	0.46	0.24	0.29	0.05
TiO ₂	0.80	0.27	0.55	0.06
MnO	1.45	0.87	1.81	0.65
P ₂ O ₅	0	–	0	–

Regardless of the type of slag, Ca-rich or Mg-rich, the quenched and granulated material is completely amorphous, as shown in Figure 1.

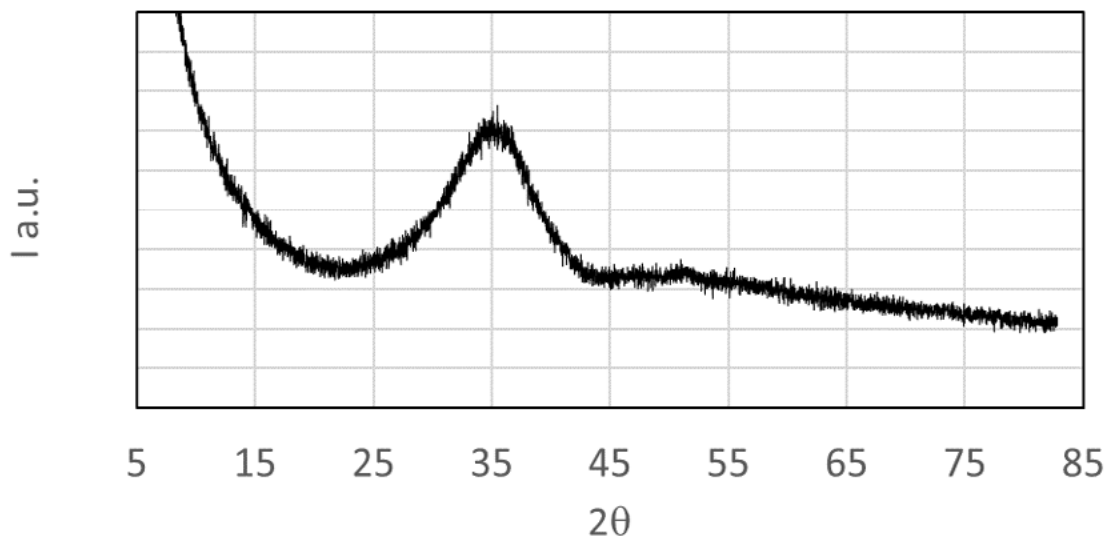


Figure 1: XRD pattern of granulated and ground foundry slag.

The white steel slag comes from an electric arc furnace (Acciaierie Beltrame S.p.A.). Its composition is richer in Ca compared to blast furnace slag, which increases the viscosity of the melt and makes water quenching and granulation more difficult, because of the risk of explosions. To obtain a material closer in composition to blast furnace slag, which is easier to quench and granulate, it is necessary to add a source of silica to the molten slag. As a source of silica we used the exhaust foundry sand, which is constituted by quartz sand, small additions of bentonite and a thermoset resin which pyrolyzes during the casting and completely burns out when the exhaust foundry sand is added to the molten steel slag.

The composition of the white steel slag is reported in Table 2.

Table 2: Steel slag composition.

Element (oxide)	Abundance
SiO ₂	20.14 (%)
CaO	51.20 (%)
Al ₂ O ₃	17.37 (%)
Fe ₂ O ₃	3.92 (%)
MgO	6.75 (%)
TiO ₂	0.42 (%)
MnO	0.49 (%)
Na ₂ O	0.11 (%)
K ₂ O	0.04 (%)
P ₂ O ₅	0 (%)
total major	100.44 (%)
S	16532 (ppm)
Cr	1013 (ppm)

The thermogravimetric analysis of the foundry sand is reported in Figure 2. The weight loss between 200°C and 600°C which may be attributed to the black carbon combustion amounts to about 4%.

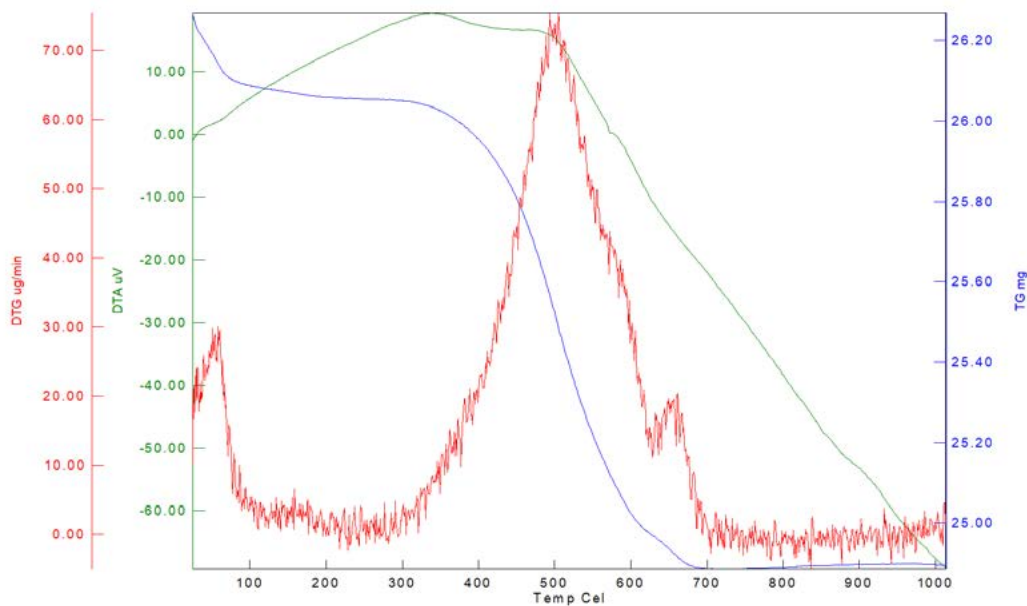


Figure 2: Thermogravimetric analysis of the foundry sand.

The XRD pattern of the foundry sand, reported in Figure 3, shows the presence of quartz with minor amounts of alkali feldspar, pyroxene, ankerite (mixed Ca-Fe carbonate) and of partially dehydroxylated montmorillonite. To bring the composition of the white steel slag closer to the one of blast furnace slag, 30% by weight of foundry sand was added to the molten steel slag and the reacted mixture was quenched and granulated with water. The composition of the blend is reported in Figure 4, and the XRD pattern of the quenched granulated and ground blend is reported in Figure 5, showing some merwinite (Ca₃Mg(SiO₄)₂) and cristobalite crystalline phases and a majority of an amorphous component.

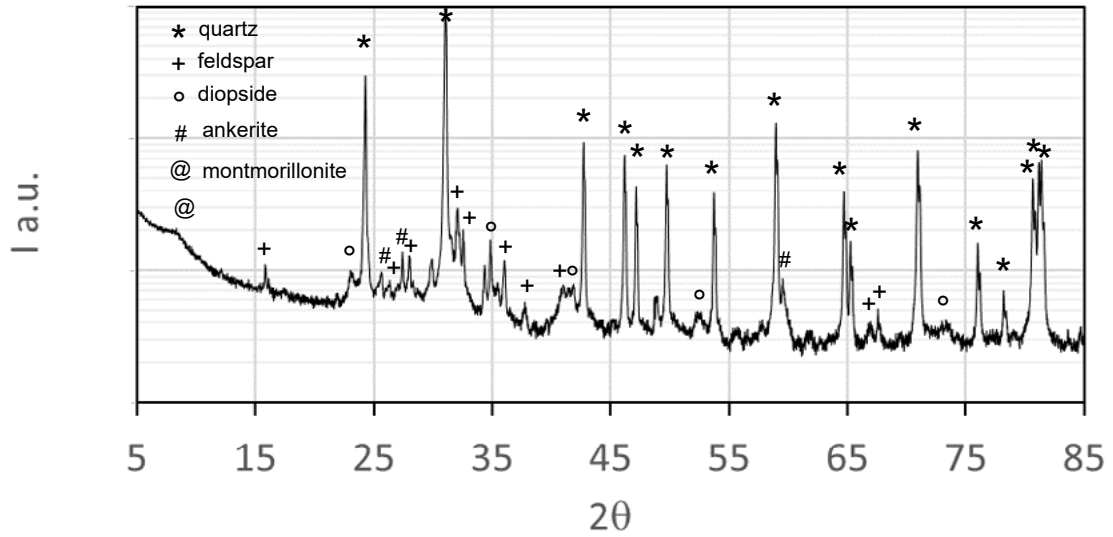


Figure 3: XRD pattern of the foundry sand. The intensity scale is logarithmic to enhance the minor phases.

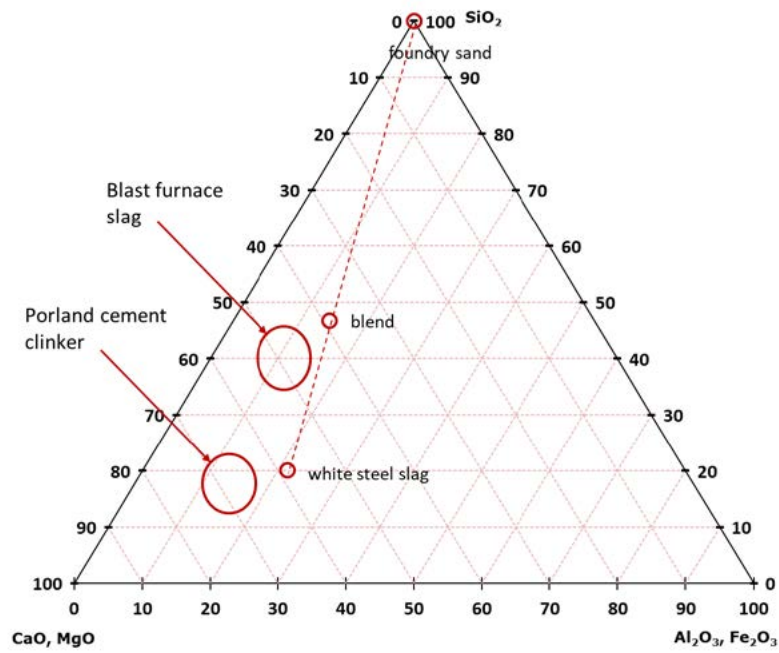


Figure 4: Composition of the white steel slag and of the reacted blend with the foundry slag.

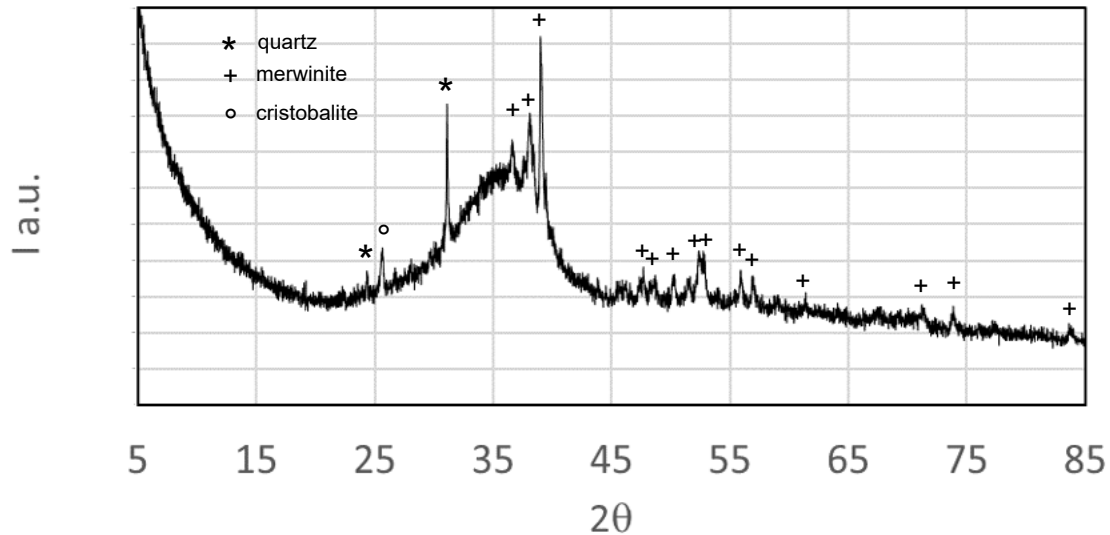


Figure 5: XRD pattern of the quenched granulated and ground reacted blend of the white steel slag and the foundry sand.

3 RESULTS

The reactivity of the Ca-rich foundry slag blended with Portland cement in a 50:50 mixture is close to the reactivity of blast furnace slag, as shown in the calorimetric curves of Figure 6. The Mg-rich foundry slag has a lower reactivity. The pozzolanic index at 7 days, measured as the fraction of reference CEM I cement which would give the same cumulative hydration heat of slag in a 50:50 cement and slag mixture after 7 days of curing, is 0.24 for blast furnace slag, 0.18 for Ca-rich foundry slag and 0.05 for Mg-rich foundry slag.

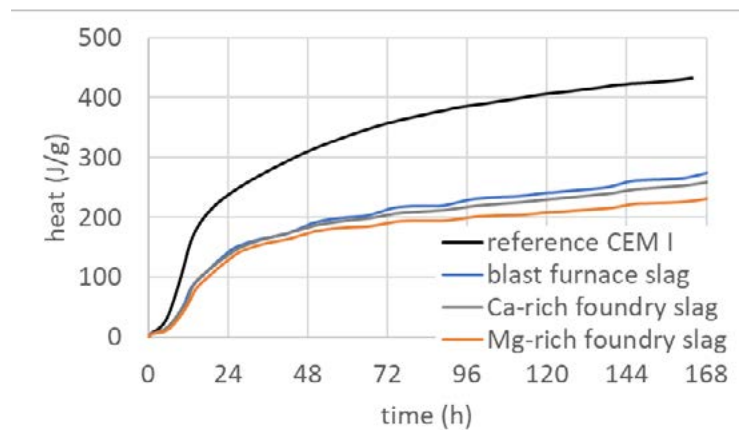


Figure 6: Calorimetric measurements of 50:50 blends of CEM I and foundry slag.

In an alkali-activated binder (ECONcrete [9]: slag activated with Na_2SO_4 and Portland cement clinker) the Mg-rich foundry slag shows an even more important lower reactivity, as shown in the calorimetric curves of Figure 7. This is probably due to the higher Mg and lower Ca concentration in the interstitial solution which hampers C-S-H precipitation [11]. The addition of Metakaolin (Argical M 1000 from Imerys) mitigates partially this phenomenon.

The reactivity of the white steel slag reacted with the foundry sand, blended with Portland cement in a 50:50 mixture is higher than the reactivity of blast furnace slag, as shown in the calorimetric data of Figure 8. The pozzolanic index at 7 days is 0.24 for blast furnace slag and 0.49 for the steel slag reacted with the foundry sand.

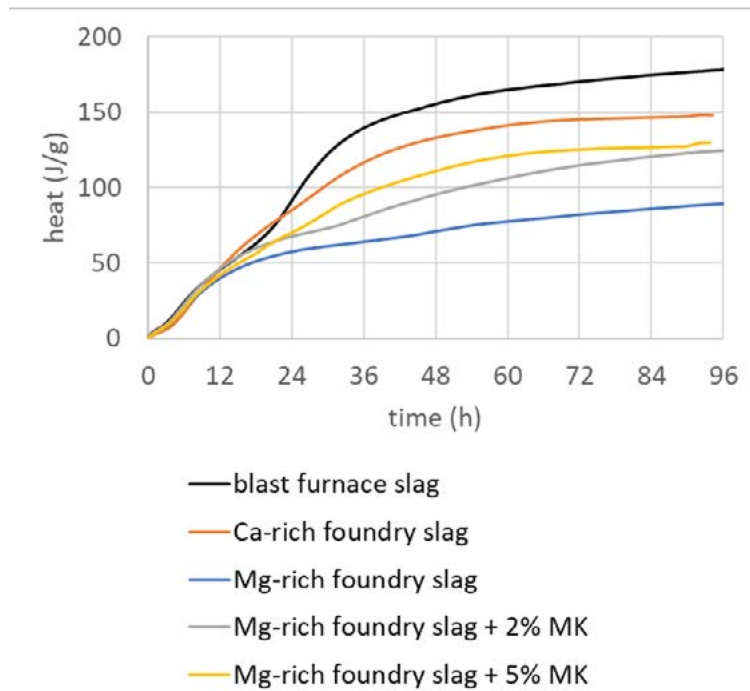


Figure 7: Calorimetric measurements of Na₂SO₄ activated foundry slag binders.

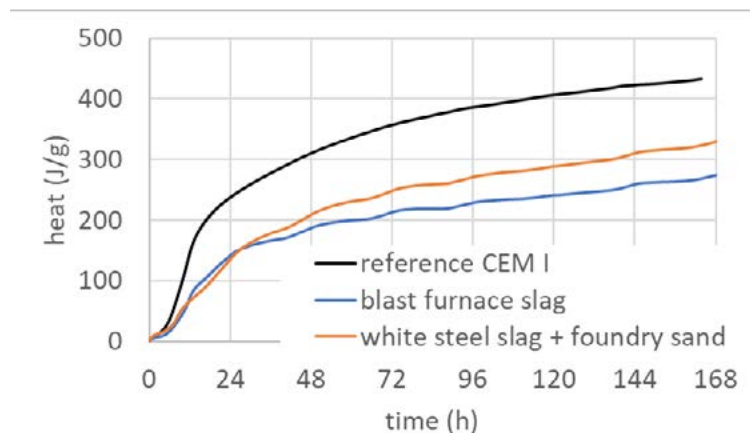


Figure 8: Calorimetric measurements of 50:50 blends of CEM I and steel slag reacted with foundry sand.

4 CONCLUSIONS

The valorisation of metallurgical slags other than blast furnace slag has the potential to provide abundant and low-cost material with good hydraulic reactivity, suitable for the formulation of alkali-activated binders. Foundry slag from cupola-furnace can be used as it is, without any chemical modification. A quenching-granulation process must be added in order to obtain a completely amorphous material with high reactivity both blended with Portland cement and formulated in an alkali-activated binder. A critical point in the use of foundry slag is its Mg content. For MgO contents higher than about 6-8% the reactivity in alkali-activated binders decreases probably because of the more difficult C-S-H precipitation from the interstitial contact solution.

White steel slag is a special waste that mostly requires landfill disposal since no real widespread technology is available to treat it. Its composition and physical properties make it unsuitable for rapid cooling and granulation. However, it is possible to use its heat content in the molten state to react it with a source of silica, so to move the composition of the reacted blend towards blast furnace slag. By doing so it is possible to obtain a material which may be quenched and

REFERENCES

- [1] J.L. Provis, J.S.J. van Deventer (Eds.), *Geopolymers Structure, processing, properties and industrial applications*, CRC Press, ISBN 978-1-84569-449-4, Woodhead Publishing Limited, Abington Hall, Granta Park, Great Abington, Cambridge CB21 6AH, UK (2009).
- [2] C. Shi, J. Qian, High performance cementing materials from industrial slags - a review, *Resour. Conserv. Recycl.* 29 (2000) 195–207.
- [3] C. Shi, A. Fernández-Jiménez, A. Palomo, New cements for the 21st century: the pursuit of an alternative to Portland cement, *Cem. Concr. Res.* 41 (2011) 750–763.
- [4] C. Shi, P.V. Krivenko, D.M. Roy, *Alkali-activated Cements and Concretes*, Taylor & Francis, Abingdon, UK, (2006).
- [5] J. Whiting, Manufacture of cement. US Patent No 544706, (1895).
- [6] A.O. Purdon, The action of alkalis on blast furnace slag, *J. Soc. Chem Ind.*, 59, (1940), 191 – 202.
- [7] A.O. Purdon, Improvements in processes of manufacturing cement, mortars and concretes, Great Britain Patent No, GB427227A (1935).
- [8] M. Bellotto, M.C. Dalconi, S. Contessi, E. Garbin, G. Artioli, Formulation, performance, hydration and rheological behavior of ‘just add water’ slag-based binders. Proceedings of the 1st International Conference on Innovation in Low-Carbon Cement and Concrete Technology, London (2019).
- [9] L. Zevnik, M. Bellotto, Industrialization of an alkali-activated slag binder: solving the issues of early strength and superplasticizer efficiency. Proceedings of CoMS 2020, Bled, Slovenia (2020).
- [10] <https://www.euroslag.com/products/statistics/statistics-2018/> Accessed 2020-02-10.
- [11] R.J. Myers, S.A. Bernal, and J.L. Provis, A thermodynamic model for C-(N-)A-S-H gel: CNASH_{ss}. Derivation and validation, *Cement and Concrete Research*, 66, (2014) 27-47.

4

Filip Brleković, Tamara Folić, Juraj Šipušić

Sustainable Insulating Composite from Almond Shell

Sustainable Insulating Composite from Almond Shell

Filip Brleković¹, Tamara Fiolić¹, Juraj Šipušić¹

¹Faculty of Chemical Engineering and Technology, University of Zagreb
Marulićev trg 19, 10000 Zagreb
e-mail: fbrlekovi@fkit.hr

SUMMARY: New generations of insulating materials are prepared as composite materials in which renewable plant fibrous material, a by-product of agricultural activity, is bonded by common inorganic binders. In addition to good mechanical properties and low density, these composite materials also possess good insulating properties. In this paper, the preparation of biocomposite material on the basis of almond shell with potential application in construction has been studied. Composites from milled and sieved almond shells and wood-wool in combination with Portland cement and sodium silicate solution have been prepared. The hydrolytic properties of prepared composites were investigated. Flexural strength of prepared composites has been tested on modified existing equipment. Thermal properties were examined on device THB-100 Linseis, GmbH. Calorific value test was carried out in IKA® Calorimeter System C 7000. Composites prepared with Portland cement didn't meet the needed criteria due to the cease of cement setting in the presence of almond shell. Further tests were carried out on composites prepared with sodium silicate solution as a binder. The most stable hydrolytic properties and optimal water glass consumption had composites prepared with almond shell particle distribution from 1.25 to 2.5 mm. Mechanical bending test on samples 160×40×33 mm showed that the stress of 0.12 MPa causes irreversible deformation and cracking with maximum deformation of 2.5 %. Measured thermal conductivity was $0.203 \pm 0.005 \text{ Wm}^{-1}\text{K}^{-1}$ and thermal diffusivity was $0.124 \pm 0.01 \text{ mm}^2\text{s}^{-1}$. Examined mechanical and thermal properties of composite material are comparable to the properties of insulating materials available on the market. The advantage of such material is so-called binding of CO₂, because production and use of this kind of material, CO₂ embedded in the plant material is bonded throughout the lifetime of the building. Overall CO₂ balance of the composite board, as a probable commercial product in the future, also includes CO₂ emissions due to the inorganic binder used, and in this preliminary stage it is not possible to express quantitatively.

KEY WORDS: composite, insulating material, almond shell, thermal conductivity, thermal diffusivity.

1 INTRODUCTION

In the wake of new ecological and environmentally friendly composite materials, more and more insulating construction materials consist of agricultural waste and inorganic binders.[1] Such composites can be classified as biocomposites due to one of the components being of natural origin. Biocomposites are used in the construction industry as structural and non-structural composites due to their numerous advantages over other materials, some of which are lower weight and lower production costs. Natural fibres (wood and non-wood) are used as reinforcers because of their structure; they give strength and rigidity to the material.[2] An example of natural fibre is wood wool, which is often used in the manufacture of cement wool boards, which are used for thermal and sound insulation and fire protection. Using agricultural waste as a constituent in biocomposite material has a numerous advantages, some of which are added value to the agricultural product and its waste and so-called binding of CO₂ due to the embedded CO₂ in the plant material which is bound throughout the lifetime of the building. Such waste material needs to be conjoined with binders which could be organic (e.g. epoxide resins) or inorganic (cement and sodium silicate solution). Epoxide resins give high strengths while cement contributes to high hydrolytic resistance as well as resistance to highly aggressive media.[3,4] With the initial idea of creating composite using a bio-waste fibre, the aim of this work was to produce a biocomposite material that could compete with other similar products in the market and possibly also to be used for thermal insulation. An example of natural fibre and agricultural waste, with primary exploitation as fuel, is almond shell which can be used in composite materials as an ecological alternative to incineration. Almond shell with its highly porous structure and low density is usually used in combination with epoxide resins for composite particle boards.[4] Less used and familiar mineral binder that could be used is water glass (sodium silicate solution), thick syrupy liquid which polymerizes.[5] During the design and manufacture of biocomposites it is important to consider all of the advantages and disadvantages of materials

used. Production costs of such biocomposite should be as low as possible while it should be easily disposable without any negative impact to the environment. Choosing materials that are compatible with the binder and predicting which combination of material and binder will give satisfactory mechanical and chemical properties of the biocomposites is of utmost importance.[6]

2 METHODS USED

Acquired almond shells were hand milled and afterwards hand sieved through a 2.5, 1.25 and 0.8 mm sieves. First type of composite was prepared by mixing largest particle fraction (≥ 2.5 mm) with Portland cement. Portland cement was premixed with water-cement ratio of 0.5 and then combined with almond shells in ratio of 1:2 by mass. After the mixing, the shells were put into the mould and pressed by a weight and left to set. Second version of composite was prepared with all four of the particle fractions by quenching the fibres in the mould with sodium silicate solution. The composites were prepared with addition of the wood wool. Wood wool was used as a base and cover for almond shell particles creating a "sandwich" structure. After few minutes the excess of water glass was drained off and shells were pressed with weight and water glass was left to polymerize for seven days. Water glass composites were weighed before and after drying and polymerization of sodium silicate to determine the fraction with optimal sodium silicate consumption. Two types of sodium silicate were used: commercial and laboratory made. Laboratory made sodium silicate was made with sodium hydroxide, silica gel and distilled water in molar ratios of $\text{NaOH}:2.6 \text{ SiO}_2:6.09 \text{ H}_2\text{O}$. The mixture was heated until all of the silica gel dissolved, usually within 30 minutes. The hydrolytic resistance of the prepared composites was tested out by placing the material into distilled water and measuring time until it completely fell apart, during which the pH of the distilled water was being measured by laboratory pH meter. Mechanical properties were tested out on tensile testing machine *Zwick 1445* with added component from flexural test device for concrete prisms to determine flexural properties of the prepared composites. Thermal conductivity of the composite materials was tested out on commercial device THB-100 Linseis, GmbH and upper and lower calorific values were determined by IKA® Calorimeter System C 7000 with Cooler C 7002. In addition to thermal properties chloride and sulphur content was measured by X-ray fluorescence spectroscopy, XRF.

3 RESULTS

Composites prepared with Portland cement as binder didn't meet the needed criteria. Portland cement didn't set in period of seven days and the particles didn't bind. Consequently, the almond shell compounds extraction was carried out. The extract of two fractions of almond shells was mixed with Portland cement and placed in semiisoperibole microcalorimeter to determine the effect of compounds that can be found in and on the surface of the shells. These compounds acted as plasticizers and retardants which prolonged setting time as can be seen on Fig.1.

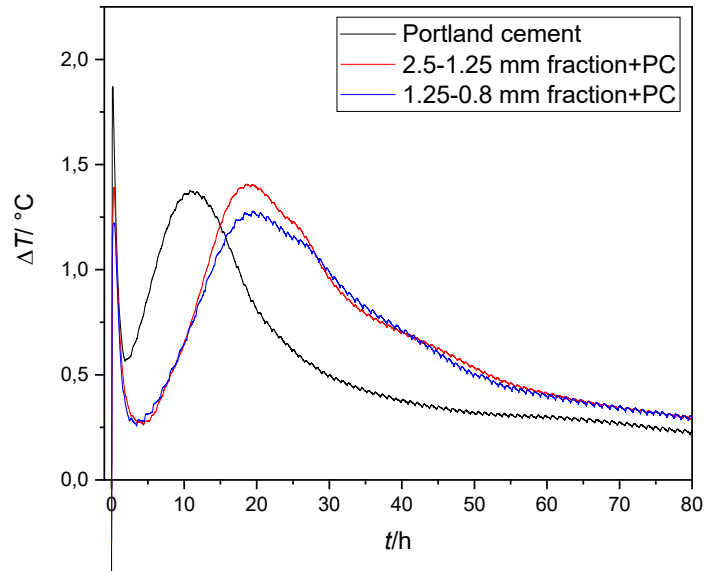


Figure 1. Microcalorimetry results of Portland cement and almond shell extracts, raw data

After the failed composite with Portland cement the sodium silicate solution was selected as a new mineral binder. The optimal consumption of water glass for individual fractions of milled and sieved shell particles was determined (Table 1.). By milling of almond shells, the following mass fractions were obtained: 23.0 %, 53.2 %, 11.6 % and 12.2 % for size fractions: ≥ 2.5 mm, 2.5-1.25 mm, 1.25-0.8 mm and ≤ 0.8 mm respectively.

Table 1. Sodium silicate solution consumption for each sieved fraction

Size fraction	≥ 2.5 mm	2.5-1.25 mm	1.25-0.8 mm	≤ 0.8 mm
Water glass consumption per gram of almond shell	1.98 g/g	1.39 g/g	1.42 g/g	1.16 g/g

As can be seen from the Table 1. the smallest particles showed the lowest water glass consumption. This result is due to the close packing of the fine particles where water glass was not able to soak and reach all of the particles, which is also one of the reasons why this composite had poor mechanical properties. The best result for water glass consumption, as well as good preliminary mechanical and visual properties, had composite prepared with particle fraction of 2.5-1.25 mm. Figure 2. shows trial composites made from all of the particle fractions.



Figure 2. Trial composites made from water glass, wood wool and milled almond shell particle size fraction a) ≥ 2.5 mm, b) 2.5-1.25 mm, c) 1.25-0.8 mm and d) ≤ 0.8 mm

Hydrolytic properties were tested out by placing composites in 400 mL of distilled water and measuring time until it completely collapsed into starting components. During the hydrolytic resistance test, pH of the water in which the composite was placed was measured. For all composites prepared with smaller and bigger particles it took approximately 40 minutes to break down in water and for composites prepared with particles from fraction 2.5-1.25 mm it took 80 minutes to collapse. The measured pH of water for every sample reached maximum of 11.0 then dropped to 10.5 and remained at that value until the total collapse of the composite. Due to the bad hydrolytic properties of commercial water glass new laboratory made sodium silicate solution was prepared. Using sodium hydroxide, silica gel and distilled water in molar ratios of $\text{NaOH}:2.6 \text{ SiO}_2:6.09 \text{ H}_2\text{O}$ new solution was made.[7, 8] Materials made with laboratory water glass did not show better hydrolytic resistance. From the properties shown so far, the composite made with particles fraction of 2.5-1.25 mm size with wood wool and commercial water glass was chosen for further investigation of mechanical and thermal properties. Using a bigger mould composite board with dimension $390 \times 270 \times 33$ mm was made. Biocomposite board was sawn into pieces of defined size and dimensions needed for different analyses. For mechanical testing three samples of $160 \times 40 \times 33$ mm were sawn and tested out on tensile testing machine with added component from flexural test device, Figure 3. shows the sample and modified equipment.



Figure 3. Modified equipment and composite sample before and after testing flexural strength

Results given by three point bending flexural test show that all 3 samples cut out of the prepared composite board

have a breaking point around 0.12 MPa. The samples were tested out with a regime of jaw speed of 10 mm/min up to the point of visible breakage in material. Deformation at maximum stress for all three samples was between 1.7 and 2.5 %. (Figure 4.)

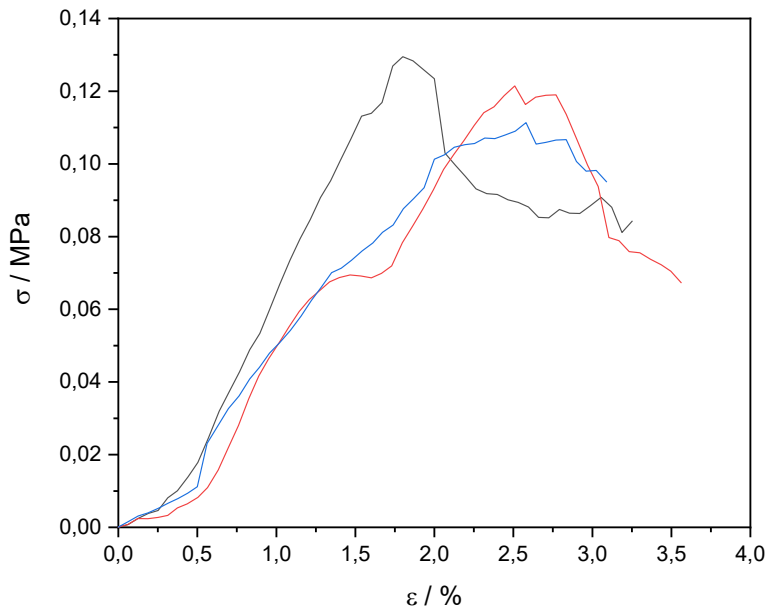


Figure 4. Stress vs. deformation of 3 samples cut out of the prepared composite board.

For the thermal conductivity and diffusivity test two pieces of composite were polished and tested. Sensor was placed between two polished surfaces and pressed with sample holder. Results show a thermal conductivity of $0.203 \pm 0.005 \text{ Wm}^{-1}\text{K}^{-1}$ and diffusivity $0.124 \pm 0.01 \text{ mm}^2\text{s}^{-1}$. In order to achieve significantly lower thermal conductivity, the composite should be prepared at even higher porosity, and this kind of composite is probably not likely to achieve such a low thermal conductivity (less than $0,060 \text{ Wm}^{-1}\text{K}^{-1}$) without significantly reducing mechanical properties. Since according to EN 13162-EN 13171 standard series material is only classified as thermal insulator if the thermal conductivity is less than $0,060 \text{ Wm}^{-1}\text{K}^{-1}$, this kind of material could not be classified as thermal insulator. Calorific values of prepared composites are 18.507 kJ/g for the higher calorific value and 17.315 kJ/g for the lower calorific value. The values are similar as one would expect for the cellulose based material. For the possible future applications of this kind of composite board, reaction to fire class should be established according to the ISO 5660-1 test. Having in mind that the full recipe is not defined nor optimized, this kind of test is not yet conducted. At present, relatively exposed/uncovered organic component could easily burn and impair poor fire resistant properties. We assume that optimal cover of organic particles with binder would increase mechanical properties and possibly even give B class fire reaction of the composite. For the chloride content, tests show less than 0.005 % chloride content and for sulphur content it was less than 0.034 %.

4 CONCLUSION

Water glass, wood wool and almond shell particles with size in range from 2.5 to 1.25 mm in a “sandwich” structure create a sustainable biocomposite with good mechanical and thermal properties for initial stage of development of a product. However, both mechanical properties and thermal properties should be further optimized, and reaction to fire class should be established. Portland cement is not a viable binder for this kind of composite due to the effect of organic soluble content of almond shells, which postpones main hydration reactions in Portland cement and impedes setting. Water glass as an alternative binder is a good choice but requires more research to reach satisfactory hydrolytic properties (for example, the addition of milled zeolite showed increase of hydrolytic resistance under the same conditions). Using commercial water glass does not produce a composite with acceptable hydrolytic resistance. Mixing

Portland cement and sodium silicate solution could result in composite with increased hydrolytic resistance. Mechanical test results are a direct consequence of the shape of tested part of composite board. Sample holder dimensions set the limitations of the composite cut tested where the wood wool fibres were too short and could not give additional strength to samples. Further test should be employed on a larger scale sample to mimic the conditions in which the real composites is employed. Biocomposite made out of waste almond shell and wood wool is a practical way of efficiently taking care of waste products as well as reducing CO₂ emissions, but actual CO₂ balance of the product is not yet possible to calculate quantitatively because it depends on the final recipe.

ACKNOWLEDGMENTS

This work has been supported by the projects PZS-2019-02-1555 in Research Cooperability Program of the Croatian Science Foundation funded by the European Union from the European Social Fund under the Operational Programme Efficient Human Resources 2014-2020 and UIP-2019-04-2367 of the Croatian Science Foundation.

REFERENCES

- [1] Osarenmwinda, J. O., & Nwachukwu, J. C., Development of Composite Material from Agricultural Wastes. *International Journal of Engineering Research in Africa*, Vol. 3 (2010), 42–48, 1663-4144.
- [2] Yatim J. M., et al., Biocomposites for the construction materials and structures, Faculty of Civil Engineering, Universiti Teknologi, Malaysia, 2003.
- [3] Johansson E., Woodwool slabs - production, properties and use. *Building Issues*. Vol. 6 (1994), 28.
- [4] Chaudhary A. K., et al., Effect of Almond Shell Particles on Tensile Property of Particleboard; *Journal of Materials and Environmental Science*, Vol. 4 (2012) 1, 109-112, 2028-2508
- [5] Campbell J. M., Method of applying sodium silicate binder, U.S. Patent 2,481,390, Patented Spet. 6, 1949
- [6] Mohanty A.K., et al., Sustainable Bio-Composites from Renewable Resources: Opportunities and Challenges in the Green Materials World, *Journal of Polymers and the Environment*, Vol. 10 (2002) ½, 19-26, 1566-2543
- [7] Vail, J.G., Soluble silicates, their properties and uses, vol. 1, American Chemical Society Monograph Series, Reinhold publishing corporation, New York, 1952.
- [8] Vail, J.G., Soluble silicates in industry, American Chemical Society Monograph Series, Reinhold publishing corporation, New York, 1928.

5

Olivera R. Bukvić, Suzana R. Draganić, Mirjana Đ. Laban, Vlastimir S. Radonjanin

Façade fire safety – legal framework in Serbia, Croatia and Slovenia

FAÇADE FIRE SAFETY – LEGAL FRAMEWORK IN SERBIA, CROATIA AND SLOVENIA

Olivera R. Bukvić¹, Suzana R. Draganić², Mirjana Đ. Laban³, Vlastimir S. Radonjanin⁴

^{1,2,3,4}University of Novi Sad, Faculty of Technical Sciences, Department of Civil Engineering and Geodesy
Trg Dositeja Obradovica 6, 21000 Novi Sad, Serbia

¹e-mail: olivera.bukvic@uns.ac.rs

²e-mail: suzanav@uns.ac.rs

³e-mail: mlaban@uns.ac.rs

⁴e-mail: radonv@uns.ac.rs

SUMMARY: Fire safety is one of the basic requirements buildings should meet during exploitation period. In recent years, façade fires took dozens of human lives and caused great material damage. In the last two years, Serbia's fire safety regulations have been significantly improved, in line with Serbia's commitments to the EU accession process. Regulation on Construction Products EU defines the minimum requirements that must be implemented into national legislation of EU member states and countries in the process of joining the EU. The performance of building materials, and especially the reaction to fire, which are part of the exterior walls of buildings may significantly affect the possibility of spreading fire on the façade of the building, as well as the transfer of fire to adjacent rooms in the building affected by the fire. According to previous research studies on fire safety regulations for housing in Europe, there is still broad variety of systems of technical requirements for buildings in the various European countries, despite the existence of the Regulation on Construction Products and the development of Euro Codes. The goals and topics are quite similar, but detailed study reveals considerable variety of functional requirements, performance requirements, and specifications, with inconsistency within the requirements of some countries. A comparative analysis of fire safety requirements for residential building façades in Serbia, Croatia and Slovenia is performed in the paper, according to the current legislation in all three countries, in order to evaluate the need for further fire safety improvements. This article focuses on the analysis of fire safety of façades, in order to identify differences in both levels of requirements and strategies that may be significant in practice.

KEY WORDS: fire, facades, residential buildings, regulations

1 INTRODUCTION

According to World Fire Statistics, in the 2017, the highest percentage of total fires were building fires (37.3%) [1]. The data on residential multi-storey building fires was collected in Finland and Sweden, for the 2004-2012 and 2004-2011 period, respectively. The results showed that out of average 508 fires per year in Finland, 10% percent of them started as external ignitions. In Sweden, the average number of fires per year was 2739, with 9% of external ignition fires. Furthermore, the statistical analysis of building fires reported in United States showed that out of 177,833 fires, 68% were residential fires. Although exterior wall fires (i.e. fires where external walls are the first ignited construction element) cause of 1.3% - 3% of total building fires and 2% of residential fires, due to the great extent of fire spread and injuries caused by combustible façade systems, in recent years, façade fires took dozens of human lives and caused great material damage [2]. The unfortunate incidents around the world confirm above stated - Tamweel Tower in Dubai, United Arab Emirates (2012), Mermoz Tower, in Roubaix, France (2010), residential building in Dijon, France (2010), residential building in Shanghai, China (2010), etc. [2]. The most recent event with disaster consequences was the Grenfell Tower fire in London, UK (2017), causing 72 fatalities [3].

The performance of building materials, especially the reaction to fire, which are part of the exterior walls of buildings, may significantly affect the possibility of spreading fire on the façade of the building, as well as the transfer of fire to

adjacent rooms in the building affected by the fire. In order to define the minimum fire safety requirements that must be implemented into national legislation of EU member states, European Union (EU) sets the Regulation on Construction Products (CPR) [4]. Serbia, Croatia and Slovenia implemented the CPR in national legislation - Croatia and Slovenia as EU member states, while Serbia did it in light of the EU accession process. Despite this fact and the fact that regulations in all three countries were the same and developed in the same manner until 1990s, the variety of fire safety requirements or even some definitions is present. Also, the same situation is in European Union. Previous research studies on EU countries regulations revealed a significant differences in functional and performance requirements in European countries as well [5,6], even after the implementation of CPR and development of Euro Codes. However, there is an initiative in EU countries to make a further step towards the harmonized regulations. Recently, the project funded by European Commission proposed a framework for European harmonized method for testing and assessing of façades [7].

This study aims at analysing the regulatory system in Serbia, Croatia and Slovenia on the example of performance requirements of residential building façades. Identification of differences should point out the “weak spots” of implementing the regulations in practice. This is of great importance, having in mind that certain design and construction companies and construction products are present in the markets of all three countries.

The structure of regulatory system in all three analysed countries is based on the same principals. The main regulations defining general principles on fire safety are the *Law on Fire Protection* (Serbia), *Fire Protection Act* (Croatia) and *Fire Protection Act* (Slovenia). Detailed requirements are regulated by bylaws, guidelines and standards [8–10]. In Croatia, the bylaw is *Ordinance on Fire Resistance and other Requirements for Buildings in Case of Fire* (hereinafter the Ordinance). Slovenian bylaw *Rules on fire safety in buildings*, prescribes *Technical guideline TSG-1-001:2019 for Fire Safety in Buildings* (hereinafter the Technical guideline), as mandatory document for fire safety design [11]. These documents combine the requirements for (among other) residential buildings and fire safety of façades [12,13]. In Serbian regulatory system, the *Regulation on Technical Requirements for Fire Protection of Residential, Business and Public Buildings* prescribes fire safety requirements for residential buildings in terms of design approach, performance requirements, etc. Fire safety of façade is regulated by separate document: *Regulation on Technical Requirements for Fire Safety of External Building Walls* (hereinafter Regulation) [14]. Additionally, while in Serbia and Slovenia fire safety of high-rise buildings is defined in separate documents (Serbia-regulation, Slovenia-guidelines), Croatian regulatory system incorporated these requirements in the Ordinance [12,14–16]. The fire classification of construction products and structural elements is based on EU standard *EN 13501-1:2010 Fire classification of construction products and building elements* in all three countries, making the basis for comparison of performance requirements. In general, national standards in each country are adopted EU standards, while the regulatory differences reflect in bylaws, adjusted to national specificities.

2 METHOD

To analyse and compare fire safety requirements from each country regulation system, the main focus was on mandatory regulations on fire safety of façades in Serbia, Croatia and Slovenia: *Regulation on Technical Requirements for Fire Safety of External Building Walls* (Serbia, Official Gazette 59/2016, 36/2017 and 6/2019), *Ordinance on Fire Resistance and other Requirements for Buildings in Case of Fire* (Croatia, Official Gazette 29/13, 87/15) and *Technical guideline TSG-1-001:2019 for Fire Safety in Buildings* (Slovenia) [12–14]. Additionally, information was extracted from other supplementary regulations and technical guidelines on fire safety (i.e. criteria for defining the high-rise buildings).

This paper includes residential buildings façade requirements, while other building purpose groups are excluded. Building design regulations in all three countries use building classification based on European Union Classification of Types of Construction (CC) [17], but additional classifications are used [13,14,18], taking into the consideration the relevant building characteristics regarding façade fire safety (e.g. building height and gross floor area). For the purpose of comparative analysis of fire safety requirements, the comparison of classifications was made. After defining the types of residential buildings as subjects of analysis, criteria for conducting the analysis were defined. In order to meet the general requirements for providing the necessary building fire safety level (e.g. to obtain the load-bearing capacity of the structure during fire, preventing the spread of fire, safe evacuation of people, etc.) a set of requirements for building materials and elements is prescribed in regulations. These include reaction to fire of applied materials, fire resistance of structure elements, horizontal and vertical façade fire barriers, separation of buildings, etc. [8,9,19]. The key aspect of each regulation that has the significant impact on of fire safety and performance of façades was detected, which resulted in

establishing reaction to fire requirements as criteria for comparative analysis [20]. Additional remarks were made regarding the horizontal and vertical façade fire barriers requirements.

3 RESULTS

The comparative analysis of fire safety regulations resulted in defining the reaction to fire requirements as main comparison criteria. The Table 1 shows building categories listed in regulations and descriptions of residential buildings in each category. The Serbian regulation classifies buildings in 5 categories, with high-rise buildings being left out and regulated with specific regulation, which is not focused only on façades, but all structure elements as well [16]. The same number of categories is recognized in Croatian Ordinance with addition of the requirements for high-rise building façades, while Slovenian Technical guideline use CC classification and additionally divide buildings by height. Despite the fact that those categories refer to other building purpose groups as well, the Table 1 shows only types of residential buildings, based on the inclusion criteria of this study.

Table 1 - Building classification in Serbian, Croatian and Slovenian regulations [12–15]

Serbia		
Category	Description	
A	no residential buildings	
B	• Residential, mixed occupancy (residential-business) with gross floor area $\leq 400\text{m}^2$	
V1	• Residential, mixed occupancy (residential-business) buildings with gross floor area $400\text{m}^2 - 2000\text{m}^2$ and height $\leq 15\text{m}$	
V2	• Residential, mixed occupancy (residential-business) buildings with gross floor area $> 2000\text{m}^2$ and height $15\text{m} - 22\text{m}$.	
G	• Residential, mixed occupancy (residential-business) buildings with height $22\text{m}-30\text{m}$	
Croatia		
ZPS 1	• Detached buildings accessible to the fire-fighters from minimum three sides for the purpose of extinguishing fires from the ground level, they have up to three above-ground floors, with the height of the highest residence floor of maximum 7 meters measured from the fire service access level or from where the evacuation of endangered people is possible, and which contain one resident unit of up to 400 m^2 gross floor area and with up to 50 occupants.	
ZPS 2	• Detached and semi-detached buildings, with up to three above-ground floors, with a 7 meter height of the residence floor measured from the outside elevation from the fire service access level and from where the evacuation of endangered people is possible, and which contain maximum three resident units of single gross floor area up to 400 m^2 and with a total of up to 100 occupants.	
ZPS 3	• Buildings with three above-ground floors with the height of the highest residence floor up to 7 meters measured from the outside elevation from the fire service access level and from where the evacuation of endangered people is possible, where fewer than 300 persons gather. These buildings are not included in subgroups 1 and 2.	
ZPS 4	• Buildings with up to four above-ground floors with the height of the highest residence floor up to 11 meters measured from the outside elevation from the fire service access level and from where the evacuation of endangered people is possible, and which include one resident unit without limitation in gross floor area or more resident units of single gross floor area up to 400 m^2 and a total of up to 300 occupants.	
ZPS 5	• Buildings with the height of the highest residence floor up to 22 m measured from the outside elevation from the fire service access level and from where the evacuation of endangered people is possible, and which do not belong to the subgroups ZPS 1, ZPS 2, ZPS 3 and ZPS 4, as well as buildings which mostly consist of underground stories, buildings where immobile persons or persons with reduced mobility reside	
ZPS 6	• High-rise buildings ($>22\text{m}$)	
Slovenia		
11	• Residential buildings	Up to 10m height; from 10m to high-rise ($>22\text{m}$)
111	• One-dwelling buildings	
112	• Two- and more dwelling buildings	
11301	• Residential buildings with service residences for	

	the elderly	
11302	• Other residences for communities	

After conducting the comparative analysis, it is concluded that regulation approach is the same in all three countries. The height of the building is recognized as important factor for determination of fire risk in each regulation, which resulted in building classification according to its height. The height is defined as the distance from ground floor approachable by fire trucks to the highest residence floor level. [12,13,16]. Slovenian Technical guidelines only refer to buildings up to 10m high and more than 10m to high-rise height, where the high-rise building is defined as building with height >22m [13]. Serbian regulation defines building categories by setting the building height limit at 15m and 30m and Croatian regulation sets this limit to 7m and 22m (see Table 1). This is in line with definition of high-rise buildings in each country (Serbian >30m, Croatia >22m) [12,16]. Single gross floor area is defined only in Croatian Ordinance, while building gross floor area is defined in Serbian regulation, and along with the building height, describes building categories. Number of residence units and floors are relevant in Slovenian and Croatian regulations. In addition, Croatian Ordinance takes into consideration the number of occupants in building and the position of other buildings (e.g. detached and semi-detached building) [12–14,18]. These kind of classification criteria are present in other Serbian regulations [21], but in regulations on façades are not listed. The findings of building classification analysis showed potential difficulties in conclusive matching the building classes from different regulations, due to the inconsistency in classification criteria.

3.1 Reaction to fire requirements

Reaction to fire is defined as material response to fire in terms of contribution to fire during the exposure by its own decomposition. In each country's regulations, material response in fire is classified according to the European Reaction to Fire Classification System (Euroclass), defined in European standard EN 13501-1: Fire classification of construction products and building elements, adopted as the national standard. There are seven reaction to fire classes - A1, A2, B, C, D, E and F describing material's combustibility, where A1 and A2 classes stand for non-combustible materials. Additionally, three smoke production classes are assigned as criteria for reaction to fire - s1, s2 and s3, where s1 stands for small amount of smoke production during fire to s3 substantial smoke production. Furthermore, criteria on flaming droplets and/or particles defines 3 classes: d0, if no flaming droplets/particles occur within 600s; d1, if no flaming droplets/particles, persisting longer than 10s, occur within 600s; d2, if no performance is declared or if the product does not comply with d0 or d1 classification criteria [22]. Detailed reaction to fire requirements for each country depending on building categories and façade types are given in Table 2, Table 3 and Table 4.

Table 2: Reaction to fire requirements for façades- Serbian regulations [14]

Type of façade	Building category			
	B	V1	V2	G
Masonry (bricks, blocks, etc.) and concrete (precast or cast-in-place) walls with thermal insulation and with external masonry, concrete or similar cladding for protection from weathering - non ventilated; pre-casted self bearing façade panels				
External wall system	C-s2, d2	B-s1, d1	A2-s1, d1	A2-s1, d1
Components of external wall				
External layer(s)	B-s2, d1	B-s2, d1	A2-s1, d1	A2-s1, d0
Thermal insulation	E-s2, d2	E-s2, d1	D-s2, d1	C-s2, d1
Masonry (bricks, blocks, etc.) and concrete (precast or cast-in-place) walls with thermal insulation and with external masonry, concrete or similar cladding for protection from weathering - ventilated				
External wall system	C-s2, d2	B-s2, d1	A2-s1, d1	A2-s1, d0
Components of external wall				
External layer(s)	C-s2, d2	B-s2, d1	A2-s1, d1	A2-s1, d0
Substructure				
Dowel type substructure	C	B	A2	A2
Dotted substructure	A2	A2	A2	A2
Thermal insulation	B-s2, d1	A2-s1, d0	A2-s1, d0	A2-s1, d0
Masonry (bricks, blocks, etc.) and concrete (precast or cast-in-place) walls with ETICS				
External wall system	D-s2, d2	B-s2, d1	B-s1, d1	A2-s1, d0

Components of external wall				
Finishing layer(s)	C-s2, d1	B-s2, d1	B-s1, d1	A2-s1,d0
Thermal insulation	E-s2, d2	B-s2, d1	A2-s1, d1	A2-s1, d0

Table 3: Reaction to fire requirements for façades - Croatia [12,18]

Construction parts	Subgroup of buildings						High-rise
	ZPS1	ZPS2	ZPS3	ZPS4		ZPS5	
Suspended ventilated elements of façades							
Classified system	E	D-d1	D-d1	C-d1		B-d1	A2-d1
Execution with the following classified elements							
Finishing layer	E	D	D	A2-d1	or	B-d1	A2-d1
Substructure							
Dowel type substructure	E	D	D	D	or	D	A2
Dotted substructure	E	D	A2	A2		A2	A2
Insulation	E	D	D	B		A2	A2
Thermal contact system of façades (ETICS)							
Classified system	E	D	D-d1	C-d1		B-d1	A2-d1
Composition of layers with the following classified components							
Finishing layer	E	D	D	C		B-d1	A2-d1
	E	D	C	B		A2	A2

Table 4: Reaction to fire requirements for façades – Slovenia [13]

Groups of (residential) buildings	Building height	
	up to 10m	from 10 to high-rise buildings
External wall claddings		
One dwelling buildings	D-s3,d2	B-d0
Two-and more dwelling buildings	D-s3,d2	B-d0
Residential buildings with service residences for the elderly	ground-floor buildings D-d0, buildings with several above-ground floors B-d0	A1 or A2
Other residences for communities	for ground-floor buildings D-d0, for buildings with several above-ground floors B-d0	A1 or A2
Sandwich panels with metal skin on both sides		
Residential buildings	A2-s1, d0	
Composite systems for external thermal insulation (ETICS) with combustible insulation		
not specified	B-d1	A1 or A2
Ventilated façades (insulation)		
not specified	A1 or A2-s1, d0	

Types of façades in Serbian and Croatian regulations are defined in the same way, considering the possibility of their use as a system or as separate classified components. While Serbian Regulation refers to non-ventilated, ventilated and ETICS façade systems, Croatian Ordinance prescribes the set of requirements for ventilated and ETICS façade systems. Although the building categories could be compared since at least one classification criteria is overlapping, different value intervals of compared characteristics leads to non-unified categorization. Therefore, the comparison is not completely transparent. Façade types in Slovenian regulation are not defined as a system and components like in Serbian and Croatian regulations, which results in inability to compare the requirements in a precise and exact way.

The use of F Euroclass materials is not allowed in any of referenced regulations. The lowest material class that can be applied is E in Serbia and Croatia and D in Slovenia. The smoke spread and the flaming droplets/particles requirements are defined in Serbian regulation for all types of façade systems and components (only d0 and d1 classes are allowed), except substructure elements. Smoke production requirements are not prescribed in Croatian regulations, and for some of the façade elements only the combustibility class is defined (see Table 4). Non-combustible materials are mandatory for thermal insulation of ventilated façades in Slovenian Technical guidance, regardless the building class and height. This criteria is prescribed for V1, V2 and G classes in Serbian Regulation, and ZPS 4,5,6 in Croatian. Furthermore, non-combustibility requirements are defined for: building height from 15m in Serbian regulation (V2 and G building category, except thermal insulation of non-ventilated façades and ETICS, when installed as external wall system), in Croatian for some elements even for buildings with 7m height (e.g. dotted substructure) (categories ZPS3, ZPS4, ZPS5 and high rise buildings) and in Slovenian mainly for the buildings higher than 10m with the exception of sandwich panels (non-combustible materials are applied in buildings with height lower than 10m).

Considering listed differences, reaction to fire requirements in Serbian, Croatian and Slovenian regulations can be compared with certain adjustments of building classifications. The consequences of differences in building classification and reaction to fire requirements as well as mutual impact of these two criteria is explained in following example (Table 5).

Table 5 - Differences in building classifications and reaction to fire requirements in Serbia, Croatia and Slovenia - example

Building description	Building 1:		Building 2:		Building 3:	
Country	<ul style="list-style-type: none"> H=9.5m four above-ground floors, 4 residential units on each floor, 64 occupants, gross floor area: 250m² gross area: 1000m² 		<ul style="list-style-type: none"> H=12.5m, five above-ground floors, 4 residential units on each floor, 80 occupants gross floor area: 250m² gross area: 1250 m² 		<ul style="list-style-type: none"> H=25m 	
Serbia	V1	system: B-s2, d1	V1	system: B-s2, d1	G	system: A2-s1, d0
		finishing layers: B-s2, d1 insulation: B-s2, d1		finishing layers: B-s2, d1 insulation: B-s2, d1		finishing layers: A2-s1, d0 insulation: A2-s1, d0
Croatia	ZPS 4	system: C	ZPS 5	system: B-d1	ZPS 6	system: A2-d1
		finishing layers: C insulation: B		finishing layers: B-d1 insulation: A2		finishing layers: A2-d1 insulation: A2-d1
Slovenia	112	system: B-d1	112	system: A1, A2	high-rise	system: A1, A2
		NA		NA		NA

In Table 5 the characteristics of three buildings are listed. The buildings are classified according to the criteria in each country's regulation. Furthermore, for each building class, the reaction to fire requirements for ETICS façade system are defined.

Table 5 shows that level of matching between reaction to fire criteria mostly depends on the building height. For the building 1, Serbian and Slovenian regulations prescribe B fire class for façade systems, although smoke production class is defined only in Serbian regulations (see Table 5). Croatian Ordinance requirements are less strict, allowing C-d1 class for façade systems. Regarding the façade components, Serbian regulation prescribes B class for both finishing and insulation layer, while C class is allowed for finishing layer and B class for insulation by Croatian Ordinance. Since building 2 is higher than building 1, it is classified differently in Croatian and Slovenian regulations due to additional



criteria defined, while it keeps the same class in Serbian regulations. This resulted in reaction to fire requirement being the same for the façade system in Serbia and Croatia (class B), while Slovenian regulations require A1 or A2 class. Regarding the façade components, Croatian regulation is more strict for the thermal insulation layer, prescribing A2 combustibility class. Finally, the complete matching is possible for building 3 (i.e. building height >22m), where all three regulations require the combustibility class A1 or A2 (non-combustible materials), with exception of Serbian regulation which prescribes both smoke production class and flaming droplets/particles class as well. This points out the variety of requirements, more in strictness of prescribed reaction to fire classes (due to the different building classification and differences in maximum height within one class), than in the general fire safety concept.

Additionally, Serbian regulation prescribes the reaction to fire of finishing (decorative) layers when they are not a component of façade system. Requirements are defined depending on the thickness of the layer and percentage of façade covered by the layer [14]. Due to the fact that this requirement does not exist in Croatian and Slovenian regulations, it was not taken into consideration.

3.2 Horizontal and vertical fire barriers - general notes

Vertical and horizontal fire barriers on façades are used for preventing the fire spread on façades [12–14,20]. Minimum requirements for horizontal and vertical barriers vary in dimensions, while the concept is the same for each country -the openings are rounded with non-combustible materials and horizontal continuous belts are built in the façade of alternating floors for preventing the vertical fire spread. Horizontal fire spread is prevented by built in non-combustible vertical barriers. Reaction to fire of barriers is defined as at least A2-s1, d0 in Slovenian technical guidance [13], while in Serbian regulation fire resistance class of barrier is prescribed depending on it's position. Class A1 is mandatory on the borders of the fire segments (part of the building consisting of two or more fire compartments) and A2 on the borders of the fire compartments [14]. Croatian Ordinance prescribes A1 and A2-s1, d0 classes for barriers preventing horizontal and vertical fire spread [11].

4 CONCLUSIONS

This paper presents the comparative analysis of fire safety requirements for residential buildings façades, considering the Serbian, Croatian and Slovenian current fire safety legislation. By reviewing the regulations, it is concluded that the general framework and approach to fire safety is based on the same general principles in all three countries. Each country has regulations adjusted to national specificities, while national standards are adopted EU standards.

The regulations were analysed by two façade performance-related criteria: reaction to fire and general requirements for horizontal and vertical fire barriers. Furthermore, differences in building classifications are recognized as the main issue in applying the regulations in practice, since it is the first step in defining the performance requirements. Although building classes from one regulation could be matched with the classes from other with certain adjustments, there is no possibility to establish the conclusive system, since the criteria for classification vary in each country's regulation. Reaction to fire requirements varies in terms of the level of requirements, depending mostly on height of the assessed building. While Serbian and Slovenian regulations prescribe the higher requirements for lower buildings, this changes with the increase of building height, where Croatian and Slovenian regulations become more strict than Serbian. Complete match in reaction to fire requirements is possible only for buildings higher than 22m. Additionally, regulations refer to different façade descriptions and types. This makes the comparison and application of different regulations non-unified and less exact. By analysing the minimum requirements for horizontal and vertical barriers in all three countries regulations, it is concluded that the concept of designing the barriers is the same. Insignificant variations occur in dimensions, but in all regulations the use of non-combustible materials for horizontal and vertical barriers is mandatory.

The study presented in this paper should be considered as an initial step towards the comparison of Serbian, Croatian and Slovenian regulations, while, for more detailed analysis, additional studies should be conducted, considering all fire safety requirements. These kinds of analysis are deemed as the basis for creating the single market in Serbia, Croatia and Slovenia with the support of implemented CPR as a tool. Although CPR prescribes harmonized rules for the construction products market, the regulations in these countries should provide the same concepts and level of fire safety requirements. In order to support the single market, a certain level of regulation transparency in interpretation should be provided as well, so the regulations could be understood and implemented more easily in design and construction practice in the region.

ACKNOWLEDGMENTS

Research in this paper is supported by the Ministry of Education, Science and Technological Development of the Republic of Serbia and realized within the project at Department of Civil Engineering and Geodesy, Faculty of Technical Sciences in Novi Sad: A comprehensive approach to improvement of interdisciplinary researches in construction education and science.

REFERENCES

- [1] Brushlinsky NN, Ahrens M, Sokolov SV, Wagner P. World Fire Statistics. Center of Fire Statistics, International Association of Fire and Rescue Services; 2019.
- [2] White N, Delichatsios M, Ahrens M, Kimball A. Fire hazards of exterior wall assemblies containing combustible components. MATEC Web Conf 2013;9:02005. <https://doi.org/10.1051/mateconf/20130902005>.
- [3] Moore-Bick M, Chairmen of the Inquiry. Grenfell Tower Inquiry: Phase 1 Report Overview. 2017.
- [4] Construction Products Regulation (CPR) - Regulation (EU) No 305/2011 of the European Parliament and of the Council of 9 March 2011 laying down harmonised conditions for the marketing of construction products and repealing Council Directive 89/106/EEC. European Parliament; 2011.
- [5] Sheridan L, Visscher HJ, Meijer FM. Building regulations in Europe, Part 2 - A comparison of technical requirements in eight European countries. vol. 24. Delft, Netherlands: DUP Science, Delft University Press; 2003.
- [6] Boström L, Hofmann-Böllinghaus A, Colwell S, Chiva R, Tóth P, Moder I, et al. Development of a European approach to assess the fire performance of facades n.d.:312.
- [7] Anderson J, Boström L, Chiva R, Guillaume E, Colwell S, Hofmann A, et al. European approach to assess the fire performance of façades. Fire Mater 2020:fam.2878. <https://doi.org/10.1002/fam.2878>.
- [8] Law on Fire Protection. Off Gaz Repub Serbia 1112009 202015 872018 872018 n.d.
- [9] Fire Protection Act. Off Gaz Repub Croat 9210 2010.
- [10] Fire Protection Act. Off Gaz Repub Slov 32007 2007.
- [11] Rules on Fire Safety in Buildings. Off Gaz Repub Slov 6117 2017.
- [12] Ordinance on Fire Resistance and other Requirements for Buildings in Case of Fire. Off Gaz Repub Croat 2913 8715 2015.
- [13] Technical Guideline TSG-1-001:2019 for Fire Safety in Buildings. Off Gaz Repub Slov 6117 7217 2019.
- [14] Regulation on Technical Requirements for Fire Safety of External Building Walls. Off Gaz Repub Serbia 592016 362017 62019 2019.
- [15] Smernice požarnovarnostnih ukrepov za visoke stavbe (h>22 m). Inženirska zbornica Slovenije, Matična sekcija inženirjev tehnologov in drugih inženirjev; 2010.
- [16] Regulation on Technical Requirements for Fire Protection of High-rise Buildings. Off Gaz Repub Serbia 802015 672017 1032018 2018.
- [17] Classification of Types of Construction - CC, final version. Eurostat 1997.
- [18] Rukavina MJ, Carević M, Pečur IB. FIRE PROTECTION OF FAÇADES - The Guidelines for Designers, Architects, Engineers and Fire Experts. Zagreb, Croatia: University of Zagreb, Faculty of Civil Engineering; 2017.
- [19] Building Act. Off Gaz Repub Slov 11205 10207 10909 3810 6017 2017.
- [20] White N, Delichatsios M. Chapter 6 - Regulations. Fire Hazards Exter. Wall Assem. Contain. Combust. Compon., New York: Springer Verlag; 2015.
- [21] Regulation on Technical Requirements for Fire Protection of Residential, Business and Public Buildings. Off Gaz Repub Serbia 222019 2019.
- [22] EN 13501-1:2010 Fire classification of construction products and building elements - Part 1: Classification using data from reaction to fire tests 2010.

6

**Vesna A. Bulatović, Mirjana M. Malešev, Miroslava M. Radeka,
Vlastimir S. Radonjanin and Ivan M. Lukić**

Sulfate resistance of concrete after two years exposure to aggressive solutions

SULFATE RESISTANCE OF CONCRETE AFTER TWO YEARS EXPOSURE TO AGGRESSIVE SOLUTIONS

Vesna A. Bulatović¹, Mirjana M. Malešev², Miroslava M. Radeka³, Vlastimir S. Radonjanin⁴ and Ivan M. Lukić⁵

^{1,2} University of Novi Sad, Department of Civil Engineering and Geodesy

Sime Miloševića 12, 21000 Novi Sad

e-mail: vesnam@uns.ac.rs, miram@uns.ac.rs, mirka@uns.ac.rs, radonv@uns.ac.rs, lookic@uns.ac.rs,

SUMMARY: The sulfate resistance of four types of concrete immersed in 5% Na₂SO₄ or 5%MgSO₄ solutions for period of 24 months was investigated. Two water to cement ratios were varied (0.38 and 0.55) and two types of common cement were used: Portland cement (CEM I 42.5R) and blastfurnace cement (CEM III 32.5N LH/SR). Control specimens were cured in lime-saturated water. Sulfate resistance was monitoring through change in compressive strength and volume change. Thermogravimetric analysis and differential scanning calorimetry (TGA–DSC) were used as an additional analysis. It is concluded that both methods (change in compressive strength and length change) show results that lead to the similar assessment of sulfate resistance. The experimental results of chosen methods showed that the effect of w/c ratio was more pronounced for the portland cement, while the blastfurnace cement was less affected by an increase in the w/c ratio. Concrete will achieve satisfactory sulfate resistance after immersion in sulfate solutions for 24 months if appropriate type of cement or water to cement ratio is chosen.

KEY WORDS: CEM III, sulfate resistance, compressive strength, length change, TGA-DSC

1 INTRODUCTION

The sulfate resistance of concrete is mainly dependent on the water/binder ratio and the composition of cement as it determines how much ettringite or gypsum form initially. The expansion of mortars/concrete containing conventional cement blended with supplementary cementitious materials (SCMs) such as blast furnace slag is lower than the expansion of plain Portland cements [1]. The hydration reaction of slag reduces the amount of calcium hydroxide (CH), produces additional C-S-H which refines the pore structures [2] and thereby lowers the availability of CaO [1]. It leads to the formation of a smaller quantity of ettringite and gypsum, as well as to lower crystallization pressures [2] and thereby increase the sulfate resistance of concrete [2]. Also, more aluminum is bound in the low Ca/Si C-S-H phases present in these binders and thereby reduces the availability of aluminium for additional ettringite formation [4].

Ground granulated blast furnace slag (GGBS) has been widely used as a supplementary cementitious material (SCM) to improve the sulfate resistance of concrete [2]. It is industrial by-product and using it in cementitious materials is environmentally beneficial as it helps in reducing carbon dioxide emissions and energy use due to cement production [5]. Namely, the manufacture of GGBS is more environmentally friendly than that of PC. Compared to PC, GGBS requires less than one fifth of the energy to produce, generates one fifteenth of carbon dioxide emissions and does not require quarrying of virgin materials [6]. The use of slag as a partial replacement of Portland cement (PC) in blended cements and in ready mixed concrete (e.g. CEM III according EN) not only consumes large amount of unused waste produced by the steel industry, but also reduces the carbon dioxide emissions arising from cement manufacture and reduces the energy required by the cement industry.

External sulfate attack is caused by the interaction between sulfate rich water or soil (most often with Na₂SO₄ and MgSO₄) and cement paste in concretes. Cracking, expansion and loss of bond between the cement paste and aggregate are common damages [7]. Testing with sodium and magnesium sulfate is reported that magnesium is more deleterious for blended cements, like slag blended CEM III/B cement with high levels of cement substitution [8]. Slag blended cements have been reported to show surface deterioration rather than expansion compared to CEM I binders. The formation of M-S-H (decalcified C-S-H) and brucite (magnesium hydroxide) have been reported for different cements exposed to magnesium sulfate solutions. Brucite precipitates in high pH environments due to a very limited solubility of this mineral. The hydroxide ions are supplied by destabilization of cement hydrates like portlandite and C-S-H. The result of this process is decalcification of the binder with precipitation of gypsum as the released calcium reacts with the sulfate

ions in solution.-The lower calcium content of the slag blended mortars means that gypsum formation leads to a stronger decalcification of C-S-H, so that M-S-H forms instead of leached C-S-H and brucite as in the case of CEM I. Surface erosion is a less significant form of deterioration for the CEM I mortars as it occurs only on the edges and corners. For the CEM III/B binder, surface erosion is the dominant deterioration mechanism. Weak zones, of predominantly M-S-H, form and fall off; exposing fresh surface to degradation. Consequently, the sulfate ions do not penetrate to any significant depth and macroscopic expansion does not occur. Any length changes observed are due to surface degradation in proximity of the gauge alignments, and would probably not be seen if the alignment pins were more deeply embedded [8].

The paper presents the results of the resistance to sulfate attack of concrete in which two types of cement and two water to cement ratios were combined. For the evaluation of sulfate resistance of these concretes, immersed in sodium and potassium sulfate solutions, a drop of compressive strength, length change and thermal analysis (TGA-DSC) were used. The results of a long-term testing (730 days) of the sulfate resistance of selected types of concrete are presented in this paper. By the analysing the literature in this field it has been concluded that there is a lack of such research, so this paper contributes to better understanding of the behaviour of the concrete with different compositions exposed to sulfate solutions over a long period of time.

2 EXPERIMENTAL

Sulfate resistance of four concretes was determined by immersing specimens in 5% Na₂SO₄ and 5% MgSO₄. Two types of cement (CEM I 42.5R and CEM III/B 32.5N LH/SR) and two w/c ratios (w/c₁=0.55 and w/c₂=0.38) were varied. In all mixtures the river aggregate was used as fine and coarse aggregate.). For the evaluation of sulfate resistance of these concretes a drop of compressive strength, length change and thermal analysis (TGA-DSC) were used.

2.1 Materials and mixture proportion

For the preparation of concrete the following component materials were used:

- Cement: Portland cement CEM I 42.5R and Low heat/sulfate-resistant cement CEM III/B 32.5N LH/SR.
- River aggregate (0/4mm, 4/8 and 8/16mm).
- Chemical admixture (HRWRA - "SikaViscoCrete 3070" and "SikaViscoCrete 5500HP", "Sika"- Switzerland).
- Tap water.

The basic physical properties of cement were tested according to standards EN 196-1, EN 196-3 and EN 196-6. Aggregate was tested according to EN 932-1. Based on the mineralogical-petrographic analysis of aggregate, the dominant mineral is quartz (75%), followed by calcite (13%), while the other minerals are present in a smaller percentage.

The concrete mix was designed based on the following conditions:

- Absolute volume of cement and water is around 0.3m³.
- Maximum grain size is 16mm.
- Two w/c ratios were used in this study: 0.38 and 0.55.
- The amount of super-plasticizer was based on the need to achieve the required consistency.
- Air content was approximately 2%.

Designed compositions of concrete mixtures and their labels are shown in Table 1.

Table 1: Mixture proportions of concrete in kg/m³

Concretes	m _c (CEM I)	m _c (CEM III)	m _v	m _{a,f}	m _{a,c}	m _{spk}	w/c
NPC1	350	-	192.5	930	858	-	0.55
NPC2	423	-	161.0	936	864	5.9	0.38
NMC1	-	338	186.0	936	864	0.7	0.55
NMC2	-	416	158.0	937	865	2.5	0.38

m_c-quantity of cement; m_v-quantity of water; m_{a,f}-quantity of fine aggregate; m_{a,c}-quantity of coarse aggregate; m_{spk}-quantity of super-plasticizer; w/c-water-cement ratio

2.2 Curing, specimen preparation and labels

All specimens were cured in lime-saturated water for 28 days. After that period, compressive strength was determined by testing three specimens from each mixture. One third of the remained specimens were transferred to containers with 5% Na₂SO₄ and another third in 5% MgSO₄ solution where they were stored until testing periods (90, 180, 365 and 730 days). The last third of specimens were submerged in lime-saturated solution for 90, 180, 365 and 730 days.

The cubic specimens of 150mm were tested for compressive strength at the age of 28 days (designated as 0) and cylindrical specimens (D=100mm, H=100mm) were tested for compressive strength at 90, 180, 365 and 730 days immersed in sulfate solutions. For each mixture and for each solution, three specimens were tested. Length change was determined on prismatic specimens (100x100x500mm) For each mixture and for each solution, three prisms were measured once a week until the above-mentioned observed periods.

Specimens from each mixture were categorized in three series and labelling with five letters in the following way: those with the first letter "E" were cured in lime-saturated water solution, those with "N" were immersed in 5% Na₂SO₄ solution and those with "M" were stored in 5% MgSO₄ solution. The second letter in the label ("N") indicates the natural aggregate. The third letter refers to the type of cement: "PC" stands for CEM I and "MC" stands for CEM III. And the last letter denotes w/c ratio: "1" is for w/c=0.55 and "2" is for w/c₂=0.38. The value of compressive strength at the age of 28 days was taken as the initial value labelled as 0, meaning that the time of exposure to different conditions (sulfate and lime-saturated solutions) started from this point.

2.3 Methods

Compressive strength was tested according to EN 12390-3 before the specimens were immersed in sulfate solutions and after storing them in these solutions for 90, 180, 365 and 730 days.

The length change was measured continuously according to the procedure given in UNI 11307.

Thermal analysis TGA-DSC was determined on all specimens for 730 days. TGA-DSC tests (Setaram, Labsys Evo) with a balance accuracy of 0.1µg, were performed on the specimens of ~30mg, crushed material, by heating in alumina crucible, 20-1000°C, at 10°C/min heating rate under argon atmosphere.

3 RESULTS AND DISCUSSION

3.1 Compressive strength

The average results of concrete compressive strength after 90, 180, 365 and 730 days of immersion in MgSO₄, Na₂SO₄ and lime-saturated water are presented in Table 2. In this table are also presented the strength values prior to the exposure to sulfate solutions at 28 days (0 days).

Table 2: Compressive strength (MPa) of specimens

Concrete series	0 days	90 days	180 days	365 days	730 days	Concrete series	0 days	90 days	180 days	365 days	730 days
ENPC1	46.3	54.4	55.1	56.3	59.3	ENMC1	31.8	45.3	46.4	49.7	46.3
NNPC1		55.8	42.9	27.6	20.8	NNMC1		43.4	46.1	45.1	48.9
MNPC1		56.3	52.3	48.8	36.4	MNMC1		43.3	42.5	44.3	43.7
ENPC2	72.5	79.3	87.9	87.0	96.5	ENMC2	52.8	70.0	71.4	71.7	71.5
NNPC2		80.7	79.7	87.6	86.4	NNMC2		62.6	64.7	69.2	67.5
MNPC2		81.1	71.5	81.4	75.1	MNMC2		76.0	74.7	80.1	72.0

From the data in the Table 2 it can be concluded that almost all concretes have an increase in compressive strength after all observed periods of exposure to Na₂SO₄ or MgSO₄ solutions (90, 180, 365 and 730 days) corresponding to 28-day reference specimens. The exception is concrete with CEM I and w/c=0.55 immersed in Na₂SO₄ and MgSO₄ solutions

for 180, 365 and 730 days. The series that were immersed in Na₂SO₄ solution showed a decrease in compressive strength of 7% (NNPC1 after 180 days), 40% (NNPC1 after 365 days) and 55% (NNPC1 after 730 days). The specimens exposed to attack of MgSO₄ solution had a decrease in compressive strength of 21% (MNPC1 after 730 days of exposure to solution).

For the better understanding, relative compressive strength values are illustrated in Figure 1. These values present the relation between the compressive strength of specimens immersed in selected sulfate solution and their corresponding reference values of the same age.

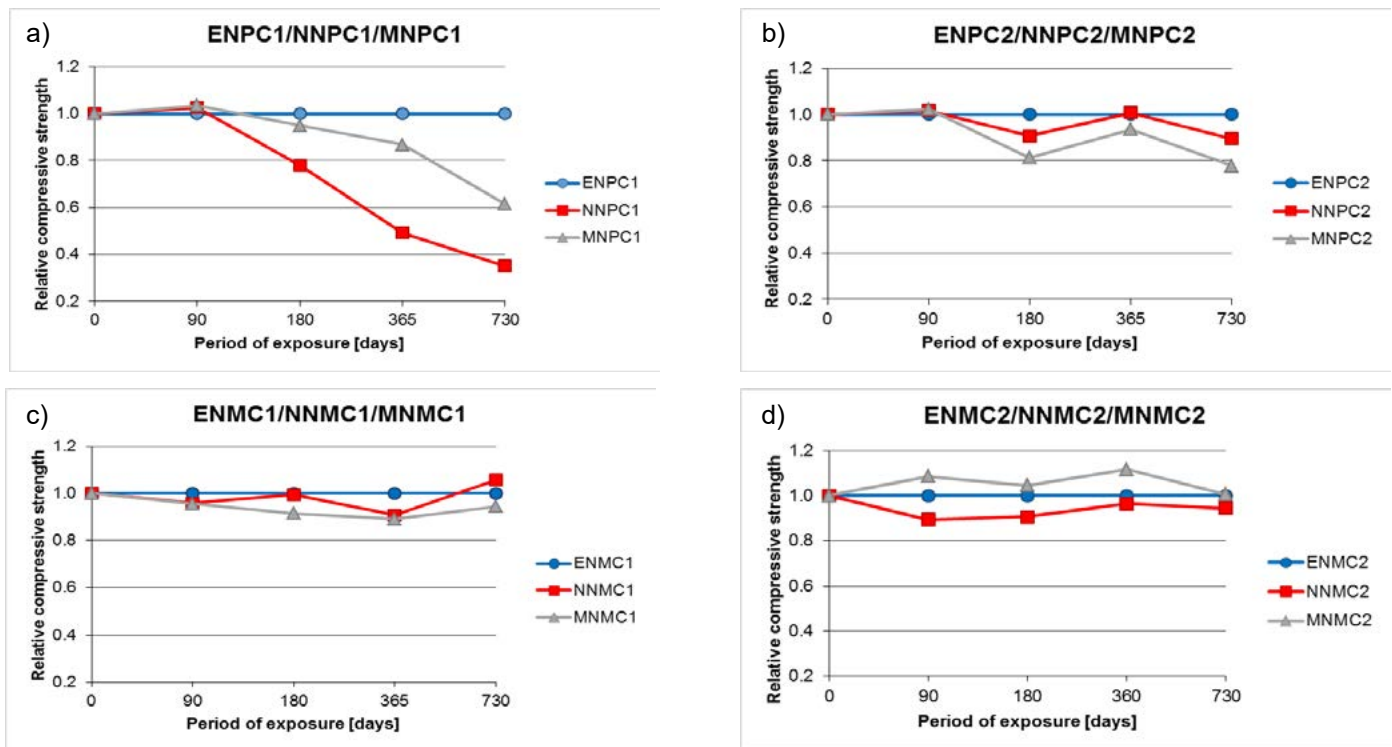


Figure 1: Changes of compressive strength of concretes exposed to sulfate solutions in relation to corresponding strength of reference specimens

After 90 days of storing in both sulfate solutions, concretes with CEM I (NNPC1, MNPC1, NNPC2, MNPC2) did not show any significant difference in compressive strength compared to reference series (ENPC1, ENPC2). Concretes with CEM III showed little change in compressive strength, up to 10%.

After 180 days of immersion in Na₂SO₄ and MgSO₄ solutions concretes with CEM I (Figure 1a, 1b) showed greater decrease of compressive strength compared to 90 days and it was about 22% for series NNPC1 and about 19% for series MNPC2. For concretes with CEM III a decrease was up to 10% for both sulfate solutions.

Concrete with CEM I and $w/c_1=0.55$, after 365 and 730 days of immersion in both sulfate solutions had the greatest decrease of compressive strength. These decreases were 51% and 65% for NNPC1 after 365 and 730 days respectively and 13% and 39% for MNPC1 for the same periods. The remarkable strength loss after 730 days of immersion in MgSO₄ solution had series with CEM I and $w/c_2=0.38$ (MNPC2) and it was about 22%. On the other hand concretes with CEM III, regardless of the type of sulfate solutions and water to cement ratio showed a change in compressive strength up to 10%, which is not so significant.

The calculated values of compressive strength decrease were compared to 25% strength loss limit for sulfate resistant concrete given by Mehta [13], to evaluate sulfate resistance of tested concretes. Based on that criterion, series with CEM I and $w/c_2=0.38$ (NNPC2, MNPC2) and all series with CEM III (NNMC1, MNMC1, NNMC2, MNMC2) have satisfactory sulfate resistance for the observed periods of time (up to 730 days). It can be noticed that series MNPC2 is very close to this limit value (22%) after 730 days of exposure to MgSO₄ solution. Series with CEM I and $w/c_1=0.55$ (NNPC1) do not fulfil the chosen criterion already for 365 days immersion in Na₂SO₄ solution.

3.2 Length change

Length change results of reference concrete specimens as well as specimens immersed to Na_2SO_4 and MgSO_4 solutions are shown in Figure 2. Every one of four diagrams presents monitoring of the length change for one concrete mixture depending on the type of solutions and the time of exposure.

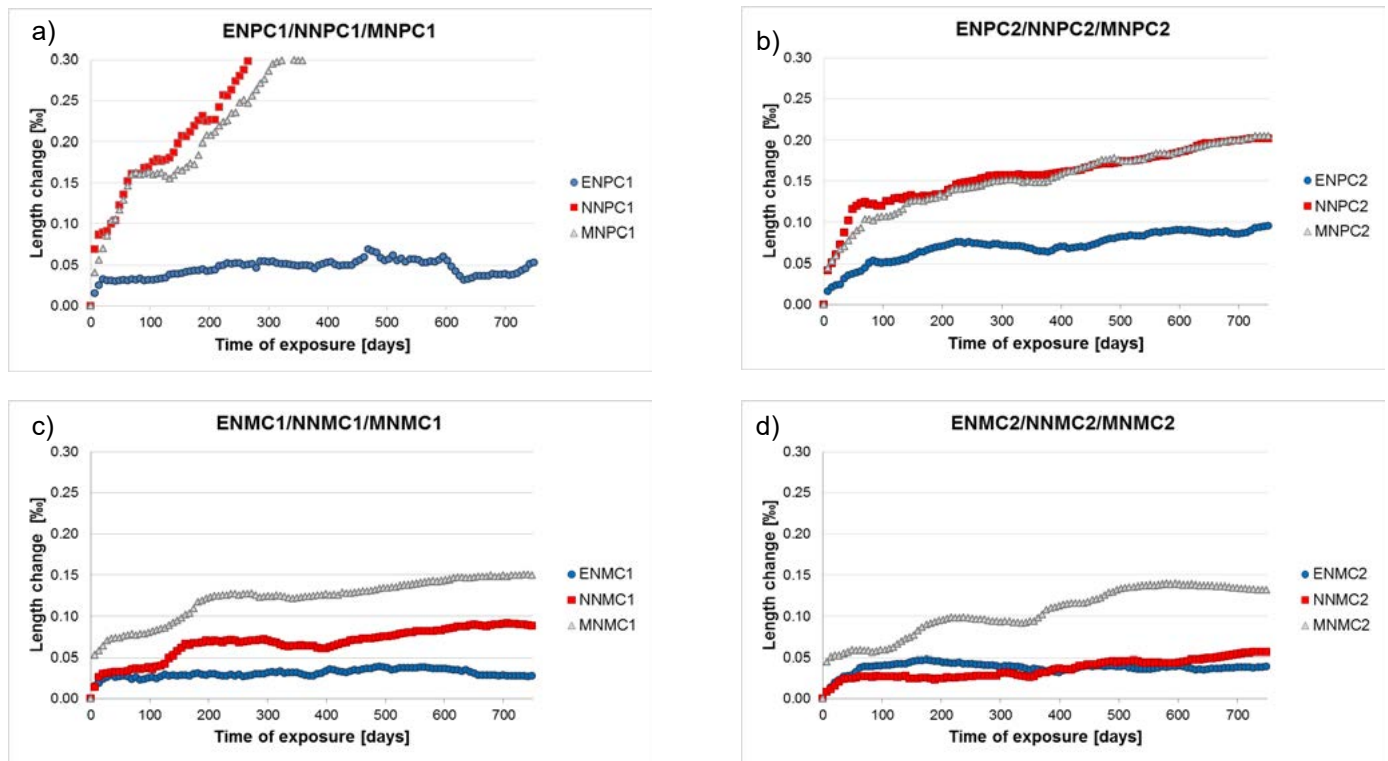


Figure 2- Length change of concretes exposed to sulfate solutions and lime - saturated water

From Figure 2 it can be observed that the lower water to cement ratio leads to significantly reduction of the linear expansion of concrete specimens with CEM I immersed in sulfate solutions (Figure 2a, 2b). However, this fact is not noticed for concretes with CEM III (Figure 2c, 2d).

Undoubtedly the largest linear expansion has concrete mixture with CEM I and $w/c_1=0.55$ for both sulfate solutions. By comparing the values of linear expansions of concrete specimens with CEM I and $w/c_1=0.55$ (Figure 2a) stored in different solutions it is seen that there are no significant differences among corresponding measured values. Concrete mixture with CEM I and $w/c_2=0.38$ show the similar behaviour but with significantly smaller values of linear expansion. The concrete specimens with CEM III have smaller values of linear expansion compare to specimens with CEM I, for both water to cement ratios. The specimens immersed in MgSO_4 solution have larger values of linear expansion compare to specimens stored in Na_2SO_4 solution for all observed period.

For evaluation of sulfate resistance of observed concrete mixtures, the calculated values of length changes were compared to expansion limit given by Miller and Manson [13]. They proposed expansion of 0.2‰ as the limit value for sulfate resistance of concrete. As can be seen, concrete with CEM I and larger water to cement ratio exceeded this limit after approximately 160 days storing in sulfate solutions, while concrete with same cement but smaller water to cement ratio reached it after 650 days. Concrete specimens with CEM III and both water to cement ratios have length expansion significantly below chosen criterion even after 730 days of expose to both sulfate solutions. Based on this criterion, all series with CEM III have satisfactory sulfate resistance for all observed periods.

3.3 TGA analysis

Figure 3 presents the TGA-DSC curves of all concrete samples stored in lime-saturated water, Na_2SO_4 and MgSO_4 for 730 days. The thermal decomposition behaviour shows several characteristic temperature ranges that can be identified according to the mass loss in TGA curves and DSC peaks. All samples present an evident mass loss with wide peak

around 100°C, attributed to the loss of physically bound water. Another significant peak is at around 460°C due to dehydration of portlandite. After exposure to sulfate attack, the mass loss corresponding to the portlandite is reduced for samples with higher water to cement ratio and both type of cement. At the same time with this decrease, the amount of lost mass is increased up to 200°C, which can be attributed to the formation of gypsum and/or ettringite. Also, the amount of portlandite is higher for samples with CEM I compare to samples with CEM III. It can be explained by the fact that the secondary hydration reactions of slag in CEM III decrease the portlandite contents. Samples exposed to the sulfate solutions have significant peak about 140°C that are believed to be due to gypsum. The amount of gypsum is greatest for samples immersed in MgSO₄ for all observed concretes. One new peak noticed at about 130°C for MNPC1. It may be assigned to ettringite. The weight loss in the range 500-920°C could be related to: the weight loss of structural OH⁻ groups from C-S-H gel (DSC at ≈570°C) and decomposition of carbonate (DSC at ≈ 770°C or 780°C). Amount of mass loss in this range is less for samples with CEM III. The mass loss that is assigned to the C-S-H gel was smaller for samples immersed in magnesium solution compare to the reference one, maybe because of transformation this gel to M-S-H. The samples MNPC1 have one additional peak about 400°C that may be assigned to brucite.

The total mass loss (from 20°C to 1000°C) for specimens with CEM I is from 11.0% to 12.7% and for specimens with CEM III is smaller, and is from 7.6% to 10.9%.

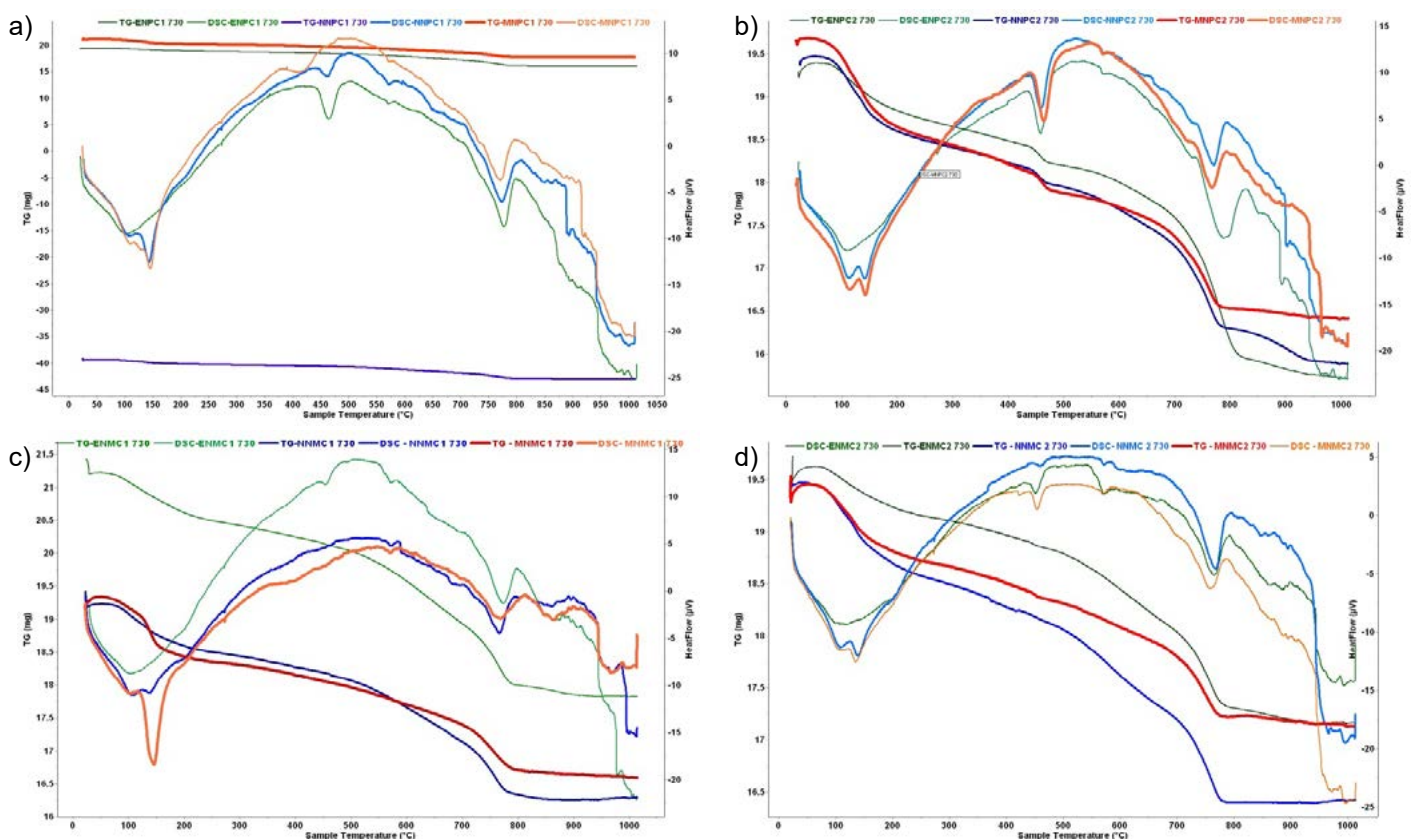


Figure 3- TGA-DSC of specimens exposed to solutions for 730 days

4 CONCLUSION

The cement type, i.e. its chemical and phase composition, has the greatest impact on concrete resistance to sulfate corrosion, while the effect of water to cement ratio depends on the type of cement and has negligible influence on sulfate resistance of concrete with CEM III. The results show that concrete with CEM I and smaller water to cement ratio and concrete with CEM III satisfy the criterion given by Mehta for compressive strength even after 730 days of exposure to sulfate solutions. The expansion limit given by Miller and Manson was satisfied in concretes with CEM III and both water to cement ratio for observed period.

TG/DSC analysis indicates on microstructure changes (i.e. formation of ettringite, gypsum and M-S-H) for the samples exposed to MgSO₄ solution. By the measuring of volume changes of tested concretes, it was noticed that concretes with

CEM III showed the highest length change values of all concrete specimens exposed to MgSO_4 solution for 730 days. This length change values can be connected with weight loss of these concretes up to 200°C (corresponding to the loss of absorbed water and water from the other calcium aluminate hydrates, decomposition of gypsum, ettringite and C-S-H) and at $\approx 570^\circ\text{C}$ (corresponding to decomposition of C-S-H) in comparison to the concretes exposed to Na_2SO_4 solution.

This investigation shows that over a long period of exposure to the aggressive solutions, MgSO_4 solution causes a little more surface damage than Na_2SO_4 solution in case of concrete with CEM III. This statement is confirmed by changes in linear expansion and by thermal analysis.

ACKNOWLEDGMENTS

Research in this paper is supported by the Ministry of Education, Science and Technological Development of the Republic of Serbia and realized within the project at Department of Civil Engineering and Geodesy, Faculty of Technical Sciences in Novi Sad: A comprehensive approach to improvement of interdisciplinary researches in construction education and science.

REFERENCES

- [1] Kunther, W; Lothenbach, B: Improved volume stability of mortar bars exposed to magnesium sulfate in the presence of bicarbonate ions, *Cement and Concrete Research*, 109 (2018), pp. 217-229
- [2] Yan, X et al.: Evaluation of sulfate resistance of slag contained concrete under steam curing, *Construction and Building Materials*, 195 (2019) 231-237
- [3] Parekh, D.N; Modhera D.C.D.: Characterization of recycled aggregate concrete, *Inter. Journal of Adv. Eng. Tech.*, October-december 2011 (Vol. II, Issue IV) 321-330
- [4] Hwang, J.P. et al.: Enhancing the durability properties of concrete containing recycled aggregate by the use of pozzolanic materials, *Journal of Civ. Eng.*, 17(1) (2013) 155-163
- [5] Atta-ur-Rehman et al.: Influence of titanium dioxide nanoparticles on the sulfate attack upon ordinary Portland cement and slag-blended mortars, *Materials*, 11 (2018) 365
- [6] Rashad, A.M. et al.: Chemical and mechanical stability of sodium sulfate activated slag after exposure to elevated temperature, *Cement and Concrete Research*, 42 (2012), pp. 333-343
- [7] Santhanam, M. et al.: Mechanism of sulfate attack: A fresh look Part1: Summary of experimental results, *Cement and Concrete Research*, 32 (2002) 915-921
- [8] Gao, X. et al.: Characterization and application of municipal solid waste incineration (MSWI) bottom ash and waste granite powder in alkali activated slag, *Journal of Cleaner Production*, 164 (2017) 410-419
- [9] SRPS EN 196-1. Methods of testing cement - Part 1: Determination of strength. Institute for standardization of Serbia; 2008
- [10] SRPS EN 196-3. Methods of testing cement - Part 3: Determination of setting times and soundness. Institute for standardization of Serbia; 2010
- [11] SRPS EN 196-6. Methods of testing cement - Part 6: Determination of fineness. Institute for standardization of Serbia; 2011
- [12] SRPS EN 932-1. Tests for general properties of aggregates - Part 1: Methods for sampling. Institute for standardization of Serbia; 2008
- [13] Ghafoori, N. et al.: Resistance to external sodium sulphate attack for early-opening-to-traffic Portland cement concrete, *Cem. Concr. Comp.* 30 (2008) 444-454

7

Barrie Dams, Yiwei Hei, Paul Shepherd and Richard J Ball

Novel cementitious materials for extrusion-based 3D printing



NOVEL CEMENTITIOUS MATERIALS FOR EXTRUSION-BASED 3D PRINTING

Barrie Dams¹, Yiwei Hei¹, Paul Shepherd² and Richard J Ball¹

¹ BRE Centre for Innovative Construction Materials,
Department of Architecture and Civil Engineering
University of Bath, UK
e-mail: bd272@bath.ac.uk

² Centre for Advanced Studies in Architecture,
Department of Architecture and Civil Engineering
University of Bath, UK

SUMMARY: 3D printing (or ‘additive manufacturing’ (AM)) systems used to manufacture cementitious structures, either in-situ or off site, utilise specialist formulations. This paper describes a new cementitious formulation which can be extruded from a syringe device without the requirement for the addition of an accelerator at the nozzle. This miniature approach brings advantages in that the system required is smaller, lighter, consumes less power and is suitable for mounting on robots which are not reliant on external power or material supplies. Applications of this smaller scale system include concrete crack repair in hard to access areas and printing of specialist conductive formulations which can be used for sensing. Cementitious pastes were successfully printed using a miniature deposition device which could be carried by a small robotic printing agent. Appropriate workability and buildability following deposition was achieved through the use of cellulose gum additions to the mix formulation. Analysis and characterisation tests carried out on fresh mixes enabled comparison of a 1:1 mix of aluminium lactate and diethanolamine with the commercially available accelerator *Master X-Seed*, and mixes with no accelerating admixture added. When compared to results featuring no accelerating agent, tests demonstrated that *Master X-Seed* was the more effective accelerator, promoting early compressive and flexural strength development, but neither accelerator made a constructive contribution to required rheological properties. *Master X-Seed* was the more effective accelerator, but rheology results suggest the difference occurs logistically too soon for a miniaturised deposition system. The retardation effect of cellulose gum and the potential role of in-situ and off-site miniaturised AM methods are evaluated.

KEY WORDS: 3D printing, cementitious material, accelerators, workability, buildability, rheology.

1 INTRODUCTION

Previous academic and industrial research into the use of cementitious-based materials in additive manufacturing (AM, which is often referred to by the term ‘3D printing’) has evolved at a considerable rate over the previous decade. It is now estimated that there are currently thirty projects worldwide investigating 3D printing with cementitious materials for building and civil use in the construction industry [1]. The vast majority of investigations are based upon the AM principal of fused deposition modelling (FDM), which involves the extrusion of a suitably viscous-like material (which could be cementitious or polymeric) through a nozzle to create an object, which may have been designed as a three-dimensional model within software and then ‘sliced’ into horizontal layers, one discreet horizontal layer at a time [2].

Deposition in the cementitious-based material projects had predominantly taken place without the use or requirement of a permanent or temporary supporting formwork. This additive approach, which only uses material specifically required for the object, starkly contrasts with traditional subtractive methods [3] which have typically been employed historically in the construction industry – a sector which can be viewed as being conservative and risk-averse [4].

Within the construction industry, AM technology is still in a relative state of infancy [5] and the technology has been relatively slow to make a significant breakthrough in terms of practice and profile, especially when compared to manufacturing-based industries such as aerospace and automotive [6].

AM offers the construction industry several advantages over traditional practise. By building layer by layer, only the material specifically required is deposited, thus significantly reducing material wastage on a construction-scale project.

Less labour is required for an automated AM process, reducing costs, delays and the risk of accidents. When an integrated approach involving services is undertaken, there are potential cost benefits to a project in the reduction of timescales, despite potentially high raw material costs [3]. Additionally, AM also offers bespoke design at little extra cost [3], as a complex, architecturally innovative design typically takes no longer to 3D print than a more straightforward rectilinear design.

The reduction of labour-related accidents, injuries and fatalities is the major justification for increased automation in an inherently dangerous industry which regularly involves working in difficult-to-access locations and at height. Between 2012 and 2017, there were 196 fatalities in the construction sector in the UK, of which 96 were due to falling from high places. Meanwhile, 11,520 injuries owing to falls from height are reported each year. The death toll in the construction sector is four times that of all other industries [7]. Automated construction systems possess the potential to substantially address this situation and promote a safer construction environment.

A cementitious-based viscous material suitable for AM construction must possess an appropriate balance between 'pumpability' (the ability of a fresh mix to move through a deposition system), 'printability' (the level of ease at which material passes through a nozzle) and 'buildability' (the ability of freshly deposited material to retain shape following extrusion and when subjected to load from subsequent layers) [8]. Within this conference paper, 'pumpability' and 'printability' are encompassed by the general term 'workability'.

A mix possessing good workability requires liquid-like behaviour and low viscosity, whereas a mix containing good buildability exhibits more solid-like behaviour and high viscosity. There is an inherent trade-off involved in the formulation of a suitable cementitious-based material for AM construction, with the aim being the realisation of a material which possesses an appropriate balance between these two crucial parameters. The formulated cementitious mix must possess sufficient buildability to enable passage through the deposition device used whilst also possessing sufficient buildability to allow the extruded material to retain its shape following deposition and resist excessive deformation which may arise from the subsequent deposition of further layers of material.

There are differing approaches employed for deposition of cementitious-based materials using FDM-based AM extrusion methods. Systems often employ a cementitious mixture containing a retarder which is easily pumped from the mixer. Just prior to the nozzle, an accelerator is then added ensuring a suitably rapid set upon printing to mitigate against sagging of the extruded filament and to allow multiple layers to be printed on top of one another within an acceptable time period.

AM extrusion equipment is often on a large, construction scale with the deposition device being mounted on a frame or gantry. Examples of this approach include concrete printing, developed at Loughborough University, UK [9], [10] and Contour Crafting, developed at the University of Southern California, USA [11]. Alternative methods involve using a large compound robotic arm with multiple degrees of freedom which is either stationary or mobile when situated on a movable platform allowing larger prints. An example of this approach is the digital construction platform project developed by the Massachusetts Institute of Technology, USA [12].

A further option involves the use of smaller, coordinated multiple mobile agents. This approach involves extra elements of complexity, as each mobile unit involved must be aware of the location and activity of the other printing agents in order to avoid collisions in movement and duplication of deposition in identical or similar locations [13]. The approach of using smaller, multiple agents inherently requires the miniaturisation of the deposition equipment involved in relation to larger, construction scale methods. The advantages of using a multiple smaller agent approach is the potential for reducing timescales due to the successful implementation of agents simultaneously printing, the possibility of greater precision due to enhanced mobility for detailed repair work of structures and the printing of conductive specimens for experimental work involving monitoring sensors.

A crucial decision in the formulation of AM cementitious-base mixes is deciding on which approach is used to control the rheology of the fresh mixes and achieve the desired balance between workability and buildability. Two main contrasting options are available. Firstly, the use of accelerating admixtures, the effects of which do not begin immediately while the material is passing through the deposition equipment, but instead take effect once the material has been deposited in order to stiffen the mix to avoid deformation following deposition of subsequent layers. This approach involves high precision with regards to timing; if the accelerator takes effect too soon, the material can stiffen within the deposition device and will not be viable to print. The second approach, as an alternative to accelerating admixtures, is to

formulate the mixes so that the fresh rheological properties do not require further acceleration. This can be achieved by adding an agent which possesses shear-thinning properties to the mix. Such materials promote a reduction in viscosity of a fresh cementitious-based material while it is under stress, for example moving through a deposition device, while also promoting an increase of viscosity once the material is deposited and retaining shape while at rest. However, extruded filaments are subsequently stressed by successive layers and need to continually resist deformation.

Here we report both material approaches in the context of a multi-agent deposition system with miniaturised deposition devices. Mixes containing accelerating admixtures and shear-thinning visco-elastic mixes, without accelerating admixtures, were investigated and the results evaluated to determine a suitable approach. A key consideration is timing – if the accelerator is to be effective for a miniaturised AM system, it must not take effect too soon as enough time must be allowed for the deposition of a complete cartridge. The miniaturised deposition device system used by the authors requires approximately 25 minutes to make the mix, load the cartridge, fully extrude the material and withdraw the deposition device. Therefore, the effectiveness of the accelerators will be judged accordingly by performance relative to this timescale.

2 METHODOLOGY

This section outlines the methodology involved in the manufacture of the mixes and the various tests carried out.

2.1 Mix specification and manufacture

Three mixes were manufactured: Mix 1 which featured no accelerating agent, Mix 2 which featured the commercially available product *Master X-Seed* 100 (supplied by BASF, UK) and Mix 3 which employed a laboratory formulated accelerating admixture of 1:1 Aluminium Lactate to Diethanolamine (individual chemicals supplied by Sigma-Aldrich, UK). Previous research demonstrated the effectiveness of aluminium lactate – diethanolamine combinations as an accelerating agent for a simple cement paste featuring CEM I [14], along with just water and plasticiser [15]. Mix proportions were determined by weight and mix constituents by percentage of weight are shown in Table 1.

Dragon Alpha CEM I 42.5R CEM I was the basis of the mixes for this study. The binder was augmented by the addition of type – ‘F’ pulverised fuel ash (PFA) (EN-450, supplied by Cemex). The ratio of CEM I:PFA in all three mixes was 65:35. The polycarboxylate-based superplasticiser Master Glenium ace 499 was added to provide extra workability to the fresh mixes whilst maintaining a water/binder ratio below 0.5 in order to promote strength in the cured material.

Hydroxyethyl methyl cellulose (HEMC) gum (Walocel VP-M-7701, supplied by Dow Chemicals) fulfilled two important functions as an admixture in the mix. Firstly, in preliminary tests it provided a high degree of water retention and ‘thickening’ of the mix which reduced constituent segregation and the potential for dead zones within material cartridges primarily via the mechanism of water sorption [16]. Secondly, it possessed shear-thinning properties, decreasing viscosity when mixes were subjected to shear stresses and increasing viscosity when the mix was at rest. It was utilised in other cementitious-based material investigations for these properties [17].

Mixes were manufactured by firstly hand-mixing the dry constituents, followed by the addition of water, plasticiser and accelerating admixture (where specified). Mechanical mixing was applied using a beater moving in planetary motion for a period of 60 seconds at 60 revolutions per minute (rpm) followed by gathering the mixture together by hand and a further period of mixing at 120 rpm for 60 seconds.

Table 1 - Mix formulation showing constituent quantity as a percentage of weight

Mix	Mix 1	Mix 2	Mix 3
CEM I % Wt.	45.6	46.2	46.2
PFA % Wt.	24.6	24.9	24.9
Hydroxyethyl methyl cellulose, HEMC % Wt.	0.61	0.62	0.62
Plasticiser % Wt.	0.74	0.72	0.72
Water % Wt.	28.5	24.4	24.4
1:1 Aluminium lactate: Diethanolamine % Wt.	-	-	3.25
<i>Master X-Seed</i> % Wt.	-	3.25	-

Total %	100	100	100
---------	-----	-----	-----

Extrusion tests were carried out utilising a miniature deposition device featuring a 60ml capacity syringe as the material cartridge suitable for a small multiple agent printing robot to carry. For a full specification and images of the device, the reader is referred to [15]. The ability to extrude circular beads of material through an 8 mm diameter nozzle was attempted at 25 minutes, 50 minutes and 75 minutes after initial mixing of the constituents.

2.2 Analysis and Characterisation

Rheology of the test mixes was assessed to quantify the effects of the accelerating solutions added. Oscillation tests were carried out on a TA Instruments DHR-2 rheometer to determine the complex modulus G^* , of the fresh mixes. This served to quantify the rigidity of the fresh mixes determined by the extent to which deformation is recoverable (elastic modulus, solid-like behaviour) or non-recoverable (viscous modulus, liquid-like flow) and summing the two components. Disposable aluminium flat plates with a 25 mm diameter upper geometry and 40 mm lower plate were used with a geometry gap of 1 mm, into which material was inserted immediately following the completion of mixing. The displacement-controlled oscillatory tests used a small angular velocity of 5.0×10^{-5} radians per second, ensuring that the material stayed within the linear viscoelastic region. A constant frequency of 1 Hz equating to an angular frequency of 6.28 radians per second and a plate temperature of 25°C was maintained.

A cone penetrometer test was used to evaluate the difference between mixes 1 and 2 while a body of freshly mixed material was at rest and exposed to the environmental temperature (the laboratory temperature was $21.5^\circ \pm 1^\circ$ for mix 1 and $17.5^\circ \pm 1^\circ$ for mix 2, with relative humidity for both tests at $72\% \pm 3\%$). 150 g batches of freshly mixed material were transferred to a circular container (as shown in Figure 1). The cone of the penetrometer device was adjusted to touch the surface of the mortar, with this initial distance reading recorded. At five-minute intervals over a period of 90 minutes, the cone was released and the depth to which the tip penetrated the material was recorded.

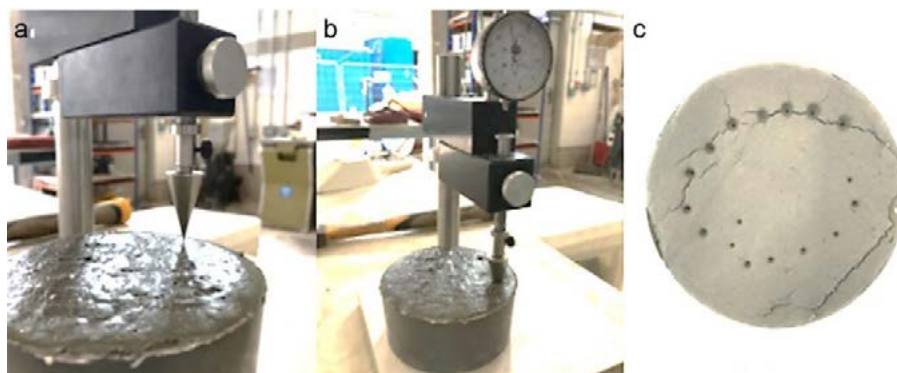


Figure 1 - Cone penetrometer tests showing (a) the lowering of the tip, (b) penetration of the fresh material and (c) the stiffening material at the conclusion of a series of tests conducted at five minute increments.

Compressive and flexural strength tests were carried out 24 hours following the formulation of mixes to ascertain the extent to which the accelerating admixtures impacted upon early strength. A 50 kN Instron Universal 2630-120/305632 testing machine was used for mechanical tests. Prismatic test specimens of the test mixes were manufactured in accordance with British Standards BS EN 12390-5:2009 (BSI, 2009) and tested in four-point bending to determine flexural strength and on 40 mm x 40 mm sections of the prisms to determine compressive strength.

Dry samples of the HEMC powder were coated in a 10 nm layer of gold to prevent charging and increase the signal-to-noise ratio prior to imaging at magnifications of x43 and x500 using a JEOL SEM6480LV Scanning Electron Microscopy (SEM).

3 RESULTS

Mixes can be considered to have an open time in excess of 75 minutes as the deposition device was still able to extrude the material in 8 mm diameter beads at this point (but could not be extruded at 120 minutes). It can be observed in Figure 2, which shows mix 2, that material experienced stiffening, with the 75-minute extrusions showing greater

precision and definition in the vertical line printed. This was similarly evident in mix 1, which was also easier to extrude than mix 2. Mix 3, which although extrudable, did not produce defined layers at the 75 minute stage.

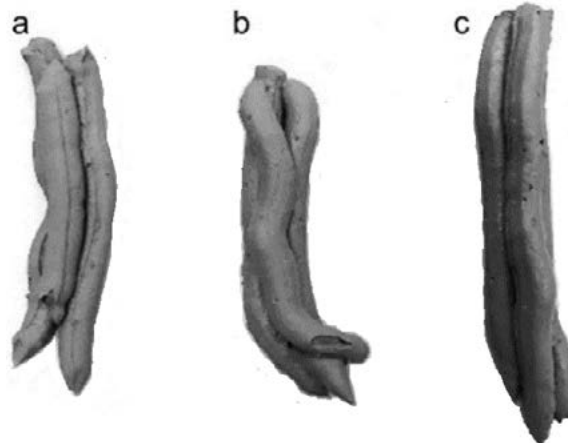


Figure 2 - Beads of mix 2 extruded by the deposition device at (a) 25 minutes, (b) 50 minutes and (c) 75 minutes after mixing.

Figure 3 shows the complex modulus G^* of mixes 1 to 3. It is important for a miniature deposition device that G^* values should be low enough to allow extrusion, but high enough for extruded material to retain shape and resist deformation. A miniature deposition device inherently requires lower G^* value material than large, powerful construction scale deposition equipment (capable of extruding stiffer material, albeit with greater energy requirements). The material of all three mixes exhibited visco-elastic behaviour, with a tendency towards elastic, solid-like properties in fresh material flow; in all mixes G^* component Elastic modulus dominated over the viscous modulus component. It can be seen that *Master X-Seed* exerts the greater influence over G^* (increasing from 3 MPa to 5 MPa at 25 minutes) in the early stages of the test. It can be surmised that given the deposition difficulties at two hours, a G^* value of between 3 – 6 MPa is suitable for a miniature deposition device; less than this value would signify a mix which was too workable for AM.

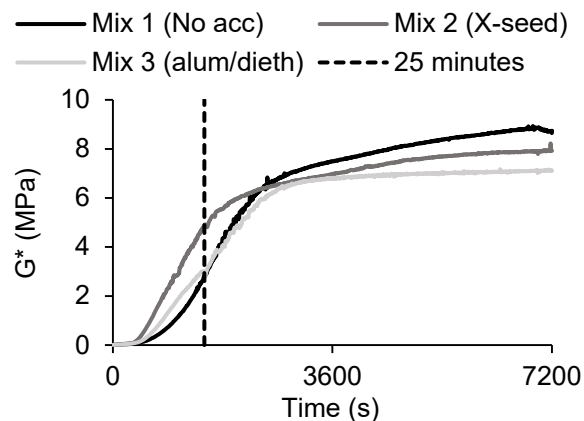


Figure 3 - Complex modulus G^* for Mixes 1-3, with the 25-minute mark indicated.

Figure 4 (left) shows the cone penetration results for mixes 1 (no accelerator) and 2 (*Master X-Seed*) with the laboratory temperature indicated. *Master X-Seed* can be observed to have had an impact on material stiffening at 90 minutes, although the cone was still able to penetrate the mix 2 material by 5 mm.

1 day compressive and flexural strength tests are shown in Figure 4 (right). *Master X-Seed* contained in Mix 2 made a significant difference to both flexural and compressive strength, with the aluminium lactate-diethanolamine combination contained in mix 3 having no discernible effect.

SEM results are shown in Figure 5. The HEMC microstructural image shows water-absorbing fibres between 10 and 50 μm in diameter. These micro-fibres wrap around water molecules, adsorbing water and expanding, reducing segregation and bleeding in the fresh mix.

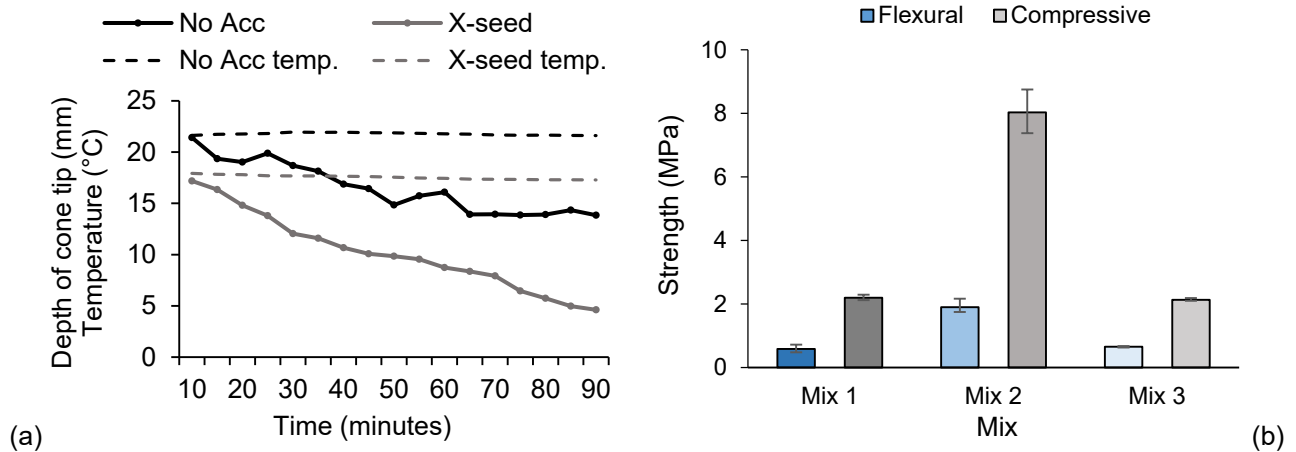


Figure 4 – (a) Cone penetrometer tests showing mix 1 (no accelerator) and mix 2 (*Master X-Seed*). (b) Flexural and compressive strength tested 1 day after mixing for mix 1 (no accelerator), mix 2 (*Master X-Seed*) and mix 3 (aluminium lactate-diethanolamine).

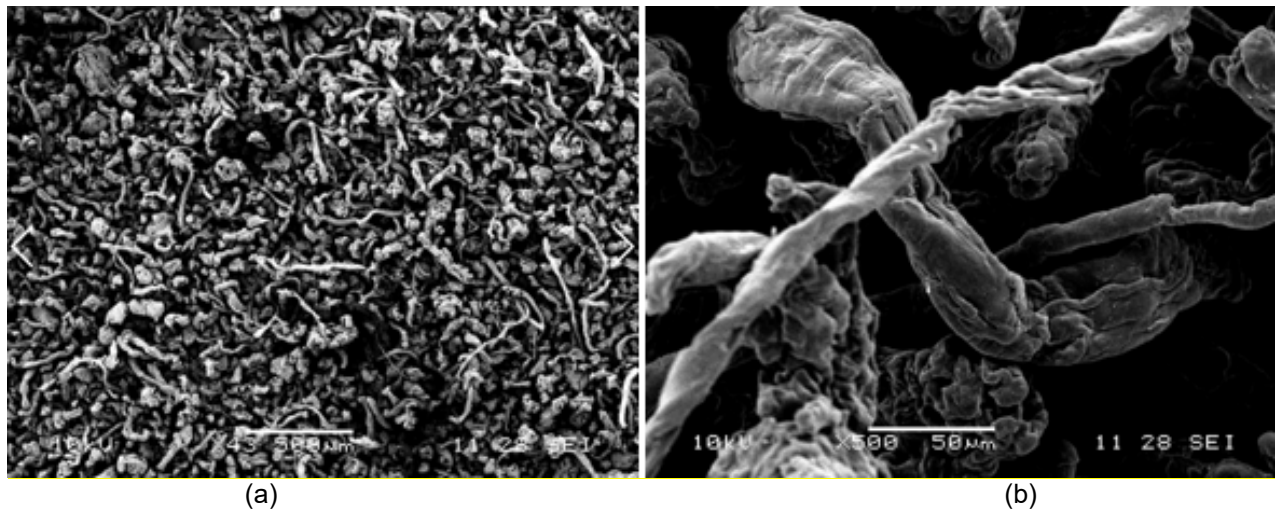


Figure 5 – Scanning Electron Microscope (SEM) images of Hydroxyethyl methyl cellulose (HEMC) particles at (a) x43 and (b) x500 magnification.

4 DISCUSSION

Master X-Seed was the more effective of the two accelerators, promoting the development of strength and stiffness and the extrusion of defined, straight layers. Aluminium lactate and diethanolamine did not prove to be an appropriate accelerating admixture for a cementitious mix containing cellulose gum.

Water-retaining cellulose ether particles adsorb on to the surface of calcium hydro-aluminates resulting from initial C_3A -water reactivity, delaying the dissolution of C_3A and effectively retarding the fresh mix. With gypsum both present and absent, cellulose ethers have been shown to retard the crystallisation of calcium hydro-aluminates [18]. Through adsorption, cellulose ethers can also reduce the nucleation and growth rate of calcium silicate hydrate (C-S-H) on the surface of C_3S particles [19].

Master X-Seed consists of a suspension of nanosized crystalline C-S-H seeds and is designed to promote the rapid nucleation and growth of C-S-H crystals, primarily targeting the reduction of the dormant period following initial C_3A reactions [20]. When using *Master X-Seed* and considering the demonstration of cellulose ethers adsorbing on to C-S-H particles, it is suggested that mixes developed in this study may have experienced retardation at this later stage, with the effectiveness of *Master X-Seed* diminished by the presence of cellulose ethers. However, in this study it is the early

stages of reactivity following mixing which are of prime interest. Although accelerators designed to target silicate hydration and benefit the development of long-term strength are not designed to have radical early effects [21], *Master X-Seed* did demonstrate an early accelerating influence with mixes showing increased G^* and strength.

A solution comprising aluminium salt and diethanolamine is an alkali-free accelerator, which are designed to act upon aluminates, introducing a larger quantity of aluminium ions into the fresh mix to achieve acceleration [22] and promoting the quick formation of needle-like ettringite particles with the intention of stiffening the mix rapidly [21]. The presence of lactic acid in cement has been shown to accelerate aluminate phases rather than silicate phases [23]. Therefore, if cellulose ether inhibits the formation of hydration products arising from initial C_3A reactivity, aluminium lactate – diethanolamine ceases to be an effective accelerating solution and is not appropriate for AM extrusion processes.

HEMC molecules increase the viscosity of the water in the mix by adsorbing on to water molecules, expanding and attracting molecules in adjacent chains. Cellulose ether molecules entangle and intertwine amongst themselves at low shear rates, but at high shear rates disentanglement and subsequent alignment parallel to flow direction occurs [24] - this pseudoplastic behaviour is desirable for a miniaturised AM deposition device suitable for a multiple agent approach. Cellulose ether molecules additionally readily absorb moisture from the air [24].

However, considering the performance of *Master X-Seed* in tests, in practical use, a period of time following the completion of mixing has to be allowed for loading the material into a cartridge, placement of the cartridge into a deposition device, attachment of the deposition device to a printing agent and allowing the printing agent to manoeuvre into position before material can start flowing through the system and the full cartridge extruded (taken as 25 minutes in this study). It can be seen in the G^* tests (Figure 3) that *Master X-Seed* affects the mix prior to this time and suggests that it may be inappropriate for AM due to the risk of excessive stiffening occurring in the material while still in the deposition device prior to extrusion. After this timescale, it is suggested by rheology results that *Master X-Seed* becomes less effective, with the mix with no accelerating agent achieving the highest complex modulus G^* value post-extrusion.

Two possible alternative options are available for miniaturised AM. Firstly, the shear-thinning properties of the fresh mix could be used to provide sufficient buildability following deposition without the need for an explicit acceleration admixture to be applied. Further admixtures known to possess shear thinning properties as an alternative to HEMC, such as Diutan gum or Welan gum [25] could be trialled in miniaturised AM mixes.

A second option would be to investigate the use of calcium aluminate cements (CAC). The addition of CAC to a cementitious binder promotes the formation of C_3A and the rapid hardening or 'flash setting' of material [26], [27]. CAC may be added into a Portland cement-rich system, in which CAC would supplement the main binding materials of CEM I and PFA. CAC may additionally be the primary binding constituent in a mix; however, it is suggested that this approach may be challenging for AM, with the risk of a flash-setting occurring while material was still within the deposition system. The aim of this approach would be to control the quantities of CAC added as a minority constituent to a CEM I-rich system to avoid a short-timescale flash-set. Furthermore, adding calcium sulphate (CS) and retarding or accelerating constituents compatible with CAC may also need to be investigated and added as appropriate to achieve this aim and avoid C_3A flash-setting.

Considering the role that multi-agent AM extrusion may take in the construction industry, there are broadly two possible contrasting applications – on-site, in-situ construction or repair of monolithic structures or off-site pre-fabrication of elements and components, which would be transported to site for assembly. Transporting prefabricated materials to site can be costly and challenging and autonomous in-situ construction can improve process control and adaptability to site conditions [12]. However, materials used in monolithic buildings created in-situ can be highly difficult to recycle or reuse in further construction following the initial design life of a building. Typically, for in-situ concrete buildings demolition is the economic and only viable process [28].

In contrast, the manufacture of prefabricated components using indirect mechanical connections to assemble promotes design for disassembly and the potential to reuse or recycle building elements following the completion of first use [29]. In-situ construction typically adheres to linear economy principals of make – use – disposal whereas off-site pre-fabrication is suitable for sustainable construction practices which adhere to circular economy principals, where at the end of design life buildings are disassembled and the elements are either rearranged into a different configuration reflecting a change of use, or recycled for further use in construction without being downgraded (such as crushed aggregate for roads in the case of concrete [28]). Research into reversible design and off-site prefabricated designs appropriate for

disassembly is taking place in Europe in research investigations such as the Circular bio-based construction industry (CBCI) [30] and Buildings as material banks (BAMB) projects [31].

5 CONCLUSIONS

These experiments have shown that in a cementitious mix with a viscosity suitable for AM with a miniaturised deposition device, *Master X-Seed* is the more potent accelerating agent. The retardation effects of HEMC within a cementitious paste reduce the effectiveness of aluminium lactate - diethanolamine. However, considering the requirement of fresh material to first pass through a deposition system in the AM process, it can be concluded that *Master X-Seed* may also not be entirely suitable. This is because the impact of the accelerator may occur while fresh material is still passing through a deposition system and high workability and low viscosity are desired at this stage. To allow for variation in the timing of deposition following the mixing of fresh material, this study suggests that using a shear-thinning rheology-modifying agent is a suitable, and time-flexible, approach to provide sufficient buildability with miniaturised AM. Alternatively, the use of CAC as a minority constituent to control the stiffening process may be investigated with a deposition system of known deposition timescales so that workability remains high pre-extrusion with the onset of rapid stiffening of the paste as soon as possible post-extrusion.

ACKNOWLEDGMENTS

The Aerial AM project is funded by the Engineering and Physical Sciences Research Council (EPSRC) [grant number EP/N018494/1]. This study was supported by the EPSRC Centre for Decarbonisation of the Built Environment (dCarb) [grant number EP/L016869/1] and a University of Bath Research Scholarship. The Circular Bio-based Construction Industry (CBCI) project is funded by the European Union Regional Development Fund Interreg 2 Seas Mers Zeeen (2S05-036). The authors express thanks to the following: William Bazeley, Neil Price, David Surgenor, Martin Naidu, (Laboratory Technical personnel, University of Bath, UK), Oscar Cano Iranzo, Robert Baumann and Igor Toutkewicz (The Dow Chemical Company - HEMC supplies).

REFERENCES

- [1] R. A. Buswell, W. R. Leal de Silva, S. Z. Jones, and J. Dirrenberger, "3D printing using concrete extrusion: A roadmap for research," *Cem. Concr. Res.*, vol. 112, no. June, pp. 37–49, 2018, doi: 10.1016/j.cemconres.2018.05.006.
- [2] U. Kalsoom, P. N. Nesterenko, and B. Paull, "Recent developments in 3D printable composite materials," *RSC Adv.*, vol. 6, 2016, doi: 10.1039/c6ra11334f.
- [3] R. A. Buswell, R. C. Soar, A. G. F. Gibb, and A. Thorpe, "Freeform Construction: Mega-scale Rapid Manufacturing for construction," vol. 16, pp. 224–231, 2007, doi: 10.1016/j.autcon.2006.05.002.
- [4] S. K. Arora, R. W. Foley, J. Youtie, P. Shapira, and A. Wiek, "Drivers of technology adoption - the case of nanomaterials in building construction," *Technol. Forecast. Soc. Change*, vol. 87, pp. 232–244, 2014, doi: 10.1016/j.techfore.2013.12.017.
- [5] F. Bos, R. Wolfs, Z. Ahmed, and T. Salet, "Additive manufacturing of concrete in construction: potentials and challenges of 3D concrete printing," *Virtual Phys. Prototyp.*, vol. 11, no. 3, pp. 209–225, 2016, doi: 10.1080/17452759.2016.1209867.
- [6] S. C. Joshi and A. A. Sheikh, "3D printing in aerospace and its long-term sustainability," vol. 2759, 2015, doi: 10.1080/17452759.2015.1111519.
- [7] S. Executive, "Fatal injuries arising from accidents at work in Great Britain 2017," Accessed: Jan. 08, 2018. [Online]. Available: www.hse.gov.uk/statistics/.
- [8] T. T. Le, S. A. Austin, S. Lim, R. A. Buswell, A. G. F. Gibb, and T. Thorpe, "Mix design and fresh properties for high-performance printing concrete," pp. 1221–1232, 2012, doi: 10.1617/s11527-012-9828-z.
- [9] T. T. Le *et al.*, "Hardened properties of high-performance printing concrete," *Cem. Concr. Res.*, vol. 42, no. 3, pp. 558–566, 2012, doi: 10.1016/j.cemconres.2011.12.003.
- [10] S. Lim, R. A. Buswell, T. T. Le, S. A. Austin, A. G. F. Gibb, and T. Thorpe, "Developments in construction-scale additive manufacturing processes," *Autom. Constr.*, vol. 21, pp. 262–268, 2012, doi: 10.1016/j.autcon.2011.06.010.
- [11] J. Zhang and B. Khoshnevis, "Optimal machine operation planning for construction by Contour Crafting," *Autom. Constr.*, vol. 29, pp. 50–67, 2013, doi: 10.1016/j.autcon.2012.08.006.
- [12] S. J. Keating, J. C. Leland, L. Cai, and N. Oxman, "Toward site-specific and self-sufficient robotic fabrication on

- architectural scales,” *Sci. Robot.*, 2017, doi: doi: 10.1126/scirobotics.aam8986.
- [13] X. Zhang *et al.*, “Large-scale 3D printing by a team of mobile robots,” *Autom. Constr.*, vol. 95, no. July, pp. 98–106, 2018, doi: 10.1016/j.autcon.2018.08.004.
- [14] British Standards Institution, “BS EN 197-1:2011 BSI Standards Publication Cement,” no. October 2015, 2019.
- [15] B. Dams, Y. Wu, P. Shepherd, and R. J. Ball, “Aerial Additive Building Manufacturing of 3D printed Cementitious Structures,” in *37th Cement and Concrete Science Conference UCL*, 2017, no. Paper 055.
- [16] D. Büllichen, J. Kainz, and J. Plank, “Working mechanism of methyl hydroxyethyl cellulose (MHEC) as water retention agent,” *Cem. Concr. Res.*, vol. 42, no. 7, pp. 953–959, 2012, doi: 10.1016/j.cemconres.2012.03.016.
- [17] G. Michaeli, “The concentration dependence of the ‘zero-shear’ specific viscosity for a commercial hydroxyethylmethylcellulose (HEMC) in water at several temperatures,” *Carbohydr. Polym.*, vol. 9, no. 4, pp. 269–275, 1988, doi: 10.1016/0144-8617(88)90045-8.
- [18] J. Pourchez, P. Grosseau, and B. Ruot, “Current understanding of cellulose ethers impact on the hydration of C3A and C3A-sulphate systems,” *Cem. Concr. Res.*, vol. 39, no. 8, pp. 664–669, 2009, doi: 10.1016/j.cemconres.2009.05.009.
- [19] J. Pourchez, P. Grosseau, and B. Ruot, “Changes in C3S hydration in the presence of cellulose ethers,” *Cem. Concr. Res.*, vol. 40, no. 2, pp. 179–188, 2010, doi: 10.1016/j.cemconres.2009.10.008.
- [20] BASF, “Master X-Seed 100 - Hardening accelerating admixture for concrete - EN 934-2: T7,” 2016.
- [21] L. Reiter, T. Wangler, N. Roussel, and R. J. Flatt, “The role of early age structural build-up in digital fabrication with concrete,” *Cem. Concr. Res.*, vol. 112, no. November 2017, pp. 86–95, 2018, doi: 10.1016/j.cemconres.2018.05.011.
- [22] R. Myrdal, “Advanced cementitious materials - controlling hydration development,” 2007.
- [23] N. B. Singh, S. Prabha, and A. K. Singh, “Effect of lactic acid on the hydration of portland cement,” *Cem. Concr. Res.*, vol. 16, no. 4, pp. 545–553, 1986, doi: 10.1016/0008-8846(86)90092-X.
- [24] K. H. Khayat, “Viscosity-enhancing admixtures for cement-based materials - an overview,” *Cem. Concr. Compos.*, vol. 20, pp. 171–188, 1998.
- [25] M. Sonebi, “Rheological properties of grouts with viscosity modifying agents as diutan gum and welan gum incorporating pulverised fly ash,” *Cem. Concr. Res.*, vol. 36, no. 9, pp. 1609–1618, 2006, doi: 10.1016/j.cemconres.2006.05.016.
- [26] J. H. Ideker and M. P. Adams, “Calcium Aluminate Cements Revisited,” 2011.
- [27] A. K. Maier, L. Dezmirean, J. Will, and P. Greil, “Three-dimensional printing of flash-setting calcium aluminate cement,” *J. Mater. Sci.*, vol. 46, no. 9, pp. 2947–2954, 2011, doi: 10.1007/s10853-010-5170-4.
- [28] W. Salama, “Design of concrete buildings for disassembly: An explorative review,” *Int. J. Sustain. Built Environ.*, vol. 6, no. 2, pp. 617–635, 2017, doi: 10.1016/j.ijbsbe.2017.03.005.
- [29] C. Morgan and F. Stevenson, “Design and detailing for deconstruction,” *Scottish Ecol. Des. Assoc.*, no. 1, pp. 1–68, 2005, [Online]. Available: http://www.bot.yildiz.edu.tr/ids09/_data/_readings/DESIGN AND DETAILING FOR DECONST.pdf.
- [30] S. Verspeek and F. Van Der Burgh, “Performance of bio-based facades,” in *3rd International Conference on Bio-Based Building Materials*, 2019, pp. 1–6.
- [31] E. Durmisevic *et al.*, *Explorations for reversible buildings*, no. 642384. 2019.

8

Sandra Ofner, Manuel Megel, Martin Schneider and Carina Neff

Electromagnetic fibre alignment to optimize the fibre utilization of ultra -high performance concrete (UHPC)

ELECTROMAGNETIC FIBRE ALIGNMENT to OPTIMIZE the FIBRE UTILIZATION of ULTRA -HIGH PERFORMANCE CONCRETE (UHPC)

Sandra Ofner¹, Manuel Megel², Martin Schneider³ and Carina Neff⁴

^{1,3} Carinthia University of Applied Sciences, Department of Civil Engineering and Architecture
Villacher Str. 1, 9800 Spittal an der Drau, Austria
e-mail: m.schneider@cuas.at, s.ofner@cuas.at

^{2,4} Kaiserslautern University of Applied Sciences, Department of Civil Engineering
Schoenstraße 11, 67659 Kaiserslautern, Germany
e-mail: mame0024@stud.hs-kl.de, carina.neff@hs-kl.de

SUMMARY: As UHPC itself is a very brittle material, steel fibres are usually used to achieve a more ductile behaviour. Because of the viscosity of the UHPC matrix in its fresh state, the steel fibres follow the direction of the filled in concrete and, as a result, they are more or less randomly oriented, which means that only a small amount of them are aligned in the required direction to absorb tension stresses. Due to that fact, it is difficult to predict the behaviour of UHPFRC components while loading because only a small amount of fibres can be taken into account for designing the structure. Furthermore, it is not efficient and, in particular, not ecological to insert more steel fibres than required to achieve the desired result. Concerning this, an existing approach is to align the steel fibres in the fresh liquid UHPC with magnetic fields. This proceeding can lead to an increasing of the material efficiency. The focus of the present case study is to align steel fibres in UHPFRC members and in subsequently added strengthening layers.

KEY WORDS: UHPFRC, fibre alignment, electromagnetic fields, subsequent strengthening

1 INTRODUCTION

Ultra- High Performance Concrete (short: UHPC) is an high- tech material which is based on a very fine grain size distribution out of cement, micro silica, quartz powder, quartz sand, water and super plasticizer. With this composition, it is possible to reach compressive strengths of more than 150 MPa after 28 days. Due to the fine matrix, UHPC has almost no capillary pores. This fact leads to a high resistance against Chloride or freeze- thaw cycles and this causes a higher durability of UHPC compared to Normal Strengths Concrete (short: NSC).

In addition to these benefits resulting from the high packing density, also some disadvantages occur by using UHPC as a structural building material: UHPC is a very brittle material, which can exhibit an almost exploding behaviour under compression. Moreover, UHPC is not able to absorb any tension stresses, which makes the structural behaviour of concrete members difficult to predict. The most common way to handle these disadvantages is to add steel fibres in the UHPC matrix.

However, problems still occur when using steel fibres in UHPC structures such as the fibre orientation, which is influenced, among other things, by the pouring mechanism and the geometry of the concrete member. Due to that fact, it is difficult to predict the behaviour of UHPFRC components while loading because only a small amount of fibres can be taken into account for designing the structure. Furthermore, it is not efficient and in particular not ecological to insert more steel fibres than required to achieve the desired result. Concerning this, an existing approach is to align the steel fibres in the fresh liquid UHPC with magnetic fields [1] [2] [3]. This proceeding can lead to an increasing of the material efficiency.

2 PRE-TESTS

According to [2] pre-tests with ultrasound gel were performed to see the effect of the magnetic alignment. Therefore, some transparent formworks (4 x 4 x 16 cm) were produced to fill them up with gel and fibres. To make the test comparable with real UHPFRC matrix, the gel fibres combination was mixed with water to get the same spread flow

measurement as the UHPFRC. After that, the magnetic alignment was performed with one permanent magnet (Neodym; SuperDym C20).



Figure 1: Pre- tests on fibre alignment with a permanent magnet

Figure 1 shows the test specimen before (left) and the specimen after the magnetic treatment with the permanent magnet (right). The movement of the magnet was in longitudinal direction of the specimen. It is obvious that the fibres are aligned in the direction of the magnetic movement and are concentrated along the surrounding surfaces of the formwork.

Unfortunately, the matrix behaviour and especially the inner viscosity couldn't be rebuilt by just using ultrasonic gel with fibres. Therefore, quartz sand was added to the mixture but with this combination, it was not possible to see the fibres anymore and so the following tests were already performed with UHPFRC matrix.

3 TESTING PROCEDURE

The current paper deals with the magnetic orientation of steel fibres in UHPC, which means Ultra-High Performance Fibre Reinforced Concrete (short: UHPFRC). The most common setting for testing the possible magnetic alignment of steel fibres is to use a coil and to adjust the formwork with the fresh concrete in the core to align the fibres in longitudinal direction of the member. The idea of the present case study is to use the magnetic alignment while applying strengthening layers on already existing concrete parts. Therefore, NSC Plates (C 50/60) were produced with the dimensions 70 x 15 x 5.5 cm (see Figure 2).

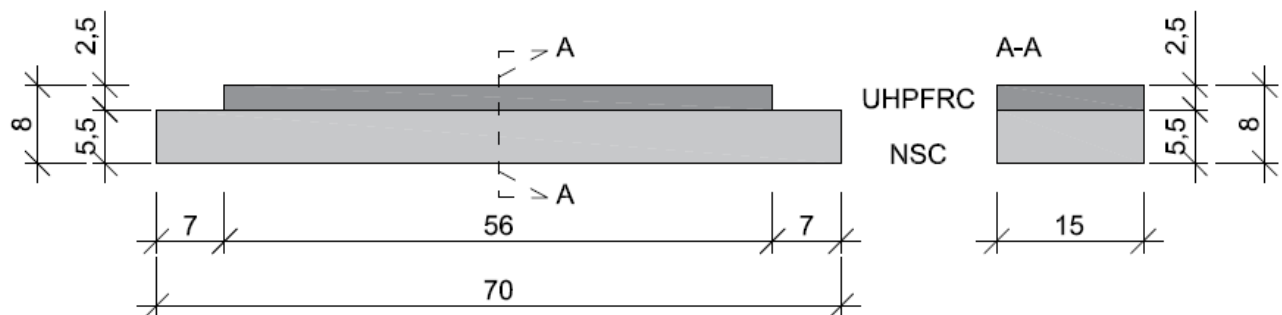


Figure 2: dimensions of the bending test specimens in cm

To investigate a real bond behaviour between the substrate and the overlay concrete, the interface layer was roughened with high pressure water jetting (HPW). A mean roughness of 2 – 2.5 mm was measured according to the sand patch method [4].



Figure 3: left: sand patch method; right: formworks for the overlay concrete

In Figure 2 and Figure 3 (on the right side) it can be seen that the overlay concrete has not been casted until the very end of the substrate. This is because of the fact that a strengthening layer in reality also cannot be produced under support.

To investigate the alignment effect of different concrete mixtures, the amount (2 and 3 Vol-%) and length of fibres (5 and 9 mm) in the mixtures were varied. For the alignment of the fibres in the matrix, so called permanent magnets (Neodym; SuperDym C20), with a quadratic shape and a side length of 2 cm were used. One magnet has an adhesive bond strength of 11.5 kg on steel.

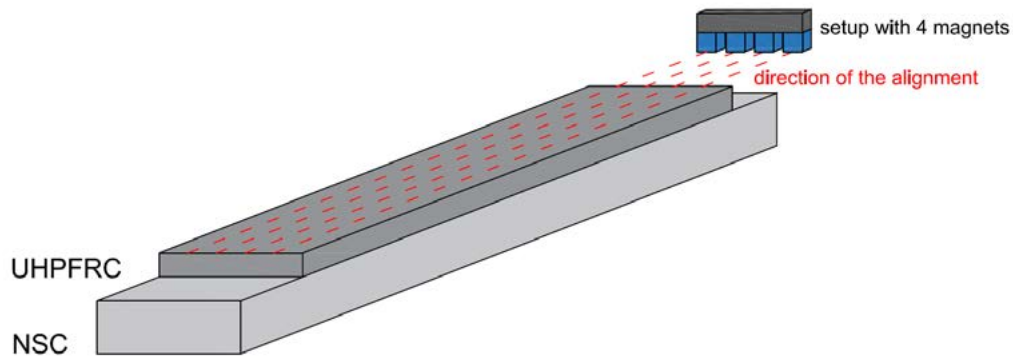


Figure 4: alignment with 4 magnets

Figure 4 schematically shows the alignment of the fibres in the UHPFRC matrix. The setup with the 4 magnets was moved in longitudinal direction of the concrete member. Here it has been varied the number of movements and the speed of moving them over the length of the specimen (slow: 0.5 m/s, fast: 1.0 m/s). To make it easier to compare the results, a labelling has been introduced that shows the number of movements and the speed (see Table 1). To compare the aligned UHPFRC overlays with ordinary poured (non-treated) ones, 2 reference plates of each test series were cast. In addition, each test series consists of two test specimens. Table 1 depicts the test setup of alignment.

Table 1: Test setup of alignment

Test series	Label	Fibre length [mm]	Fibre content [Vol-%]	Number of movements	Speed
1	B	5	2	4	Slow
2	B	5	3	4	Slow
3	B	9	2	4	Slow
	C	9	2	24	Slow
	D	9	2	4	Fast
4	B	9	3	4	Slow

To investigate the effect of the alignment, bending tests were performed according DIN EN 12390-5 for testing the bending tensile strength. Figure 5 depicts the test setup in the lab.



Figure 5: test setup for testing the strengthening with the aligned fibres in UHPFRC

The middle span between the supports was 60 cm, while the load introduction points were positioned in 20 cm distance from the supports.

The test setup was defined as a 4- point bending test but due to the higher forces, which have been reached by using 9 mm long fibres in the UHPFRC matrix, shear failure occurred in the regions of the support and therefore the setup has been changed to 3- point bending. The test was performed way controlled with 0.5 mm /min. The deflection was measured in the middle of the specimen on the bottom side. The test results are shown in the following load deflection diagrams. It has to be mentioned that subsequently strengthened plates without alignment of the fibres in the overlay are labelled with NA (no alignment) and plates which were produced with magnetic alignment are labelled with A (alignment).

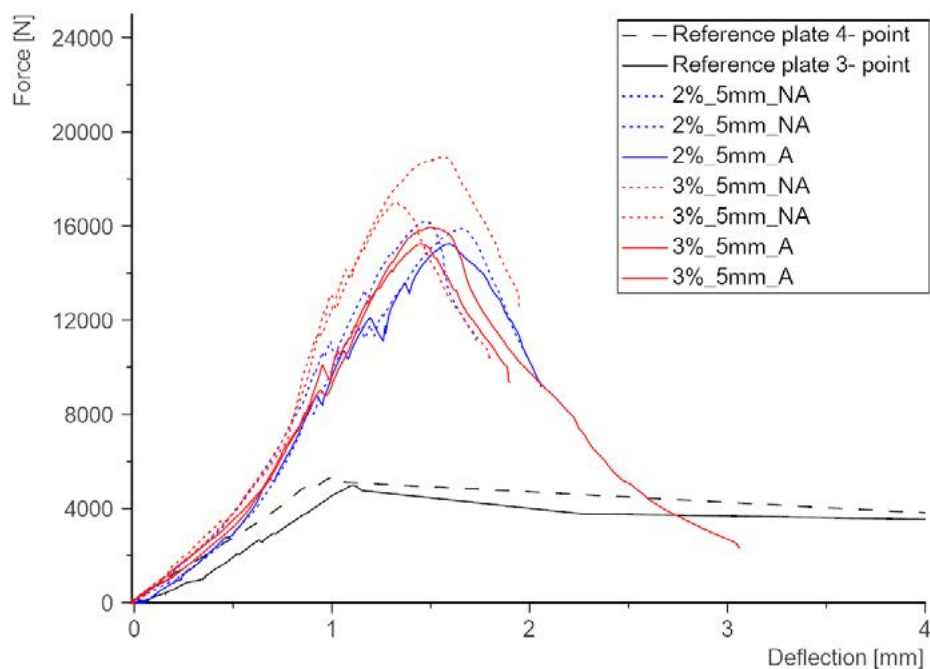


Figure 6: test results 5 mm fibres 2 and 3 Vol-%

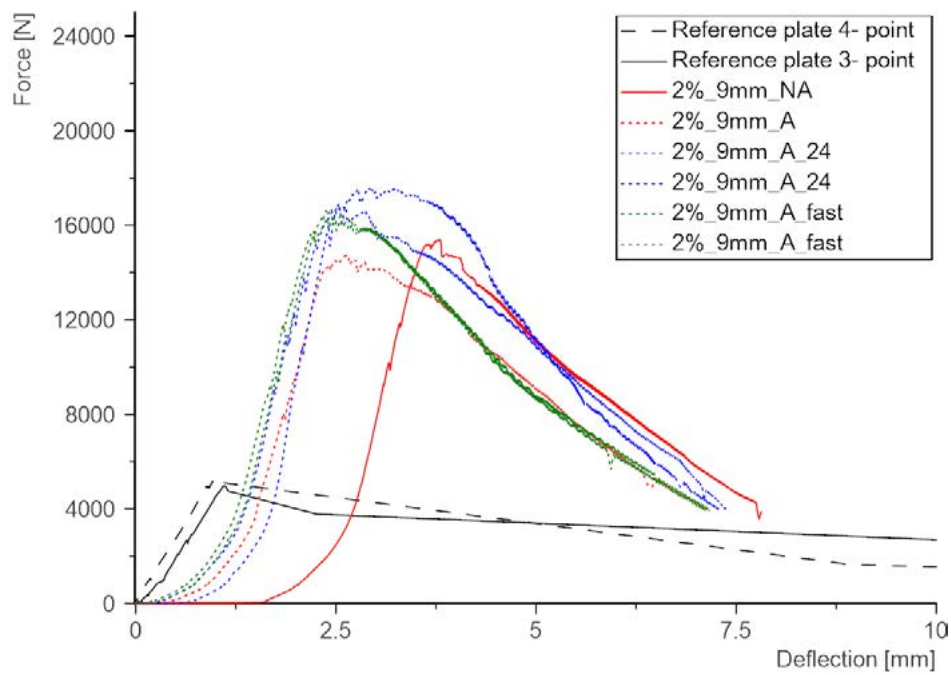


Figure 7: test results 9 mm fibres 2 Vol-%

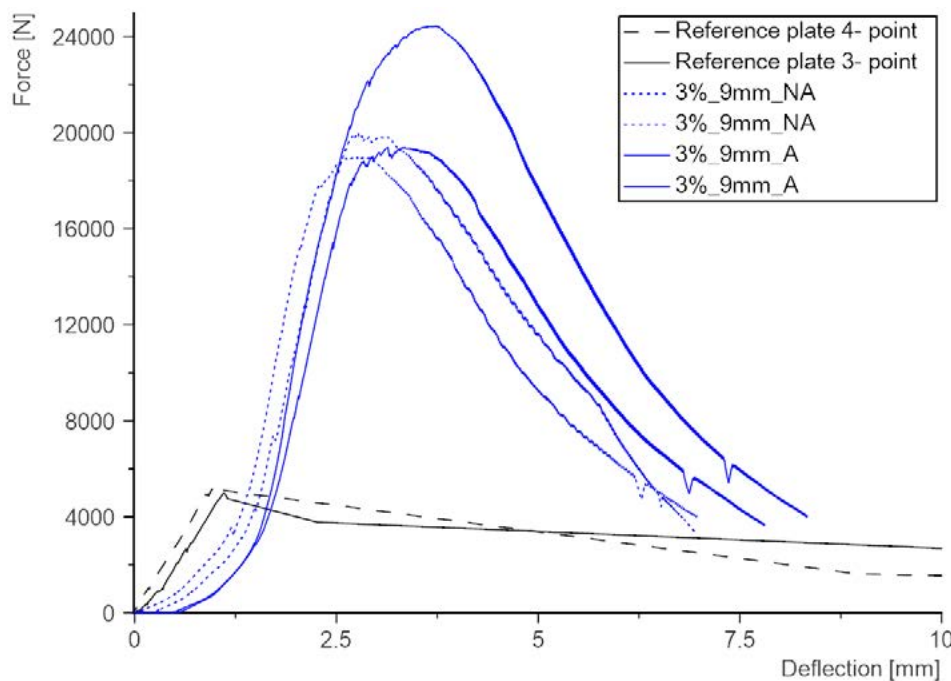


Figure 8: test results 9 mm fibres 3 Vol-%

The previous Figures 6 - 8 are showing the load deflection diagrams of the bending tests with different material and alignment setups as explained in Table 1. Obviously, the strengthening of the substrate with the subsequent added layer of UHPFRC increased the load bearing capacity of the concrete member by at least more than 150 %. It can be seen that by using a fibre length of 5 mm, the ultimate load bearing capacity is negatively influenced after the magnetic aligning process, while in case of using 9 mm long fibres the mean ultimate loads are higher than the not aligned reference plates. Especially Figure 7 depicts the influence of the number of movements of the magnets over the concrete surface because the post- peak behaviour is more pronounced. The speed of the movements had no noticeable effect on the load bearing capacity.

Table 2 shows the summarized test results of the bending tests. Label A means reference plates with overlay, but without magnetic treatment.

Table 2: results bending tests

Test series	Label	Test setup	Alignment	Mean ultimate load [kN]	Mean deflection [mm]
1	A	4- point	No	16	1.5
	B		Yes	15.5	1.5
2	A	4- point	No	18	1.5
	B		Yes	16	1.5
3	A	4- point	No	Shear failure	-
	A	3- point	No	15.5	2.5
	B	4- point	Yes	Shear failure	-
	B	3- point	Yes	15	2.5
	C		Yes	17.25	3
	D		Yes	16.75	3.5
4	A	3- point	No	19.5	3
	B		Yes	22	3.5
Reference*	-	4- point	-	5	1.3
Reference*	-	3- point	-	5	1.3

* without overlay – only substrate

The properties of the used concretes are listed in Table 3.

Table 3: material properties of the used concretes

Material	Compressive strength [MPa]*	Splitting tensile strength [MPa]*	Young's Modulus [MPa]*
NSC (C50/60)	66	5	38.000
UHPFRC 2Vol-%, 5mm	138	11	45.000
UHPFRC 3Vol-%, 5mm	150	15	46.000
UHPFRC 2Vol-%, 9mm	147	13	47.000
UHPFRC 3Vol-%, 9mm	150	16	52.000

* day of testing

4 VISUAL CONTROL OF THE ALIGNING EFFECT WITH CT- ANALYSES

To check the effect of the aligning process, small test specimens with a side length of 4 cm and a thickness according to the plates of 2.5 cm were cut out of the UHPFRC overlays and scanned with a Micro CT in cooperation with the University of Applied Sciences Wiener Neustadt in the labs of MedAustron. To demonstrate the visual analysability, pictures of the mixtures were combined with 5 mm long fibres as depicted in the following Figure 9.

It can be seen that the orientation of the fibres has been achieved with the magnetic treatment up to a depth of 2 cm from the top. As observed in the bending plates, the orientation of the 5 mm fibres is negatively affected by the aligning process because it seems that the fibres are bundled together in one direction and the effect of interaction between the different orientations is disturbed.

Moreover, it has to be mentioned that because of the viscosity of UHPFRC and the low thickness of the overlay, the fibres were already well orientated after pouring without magnetic treatment.

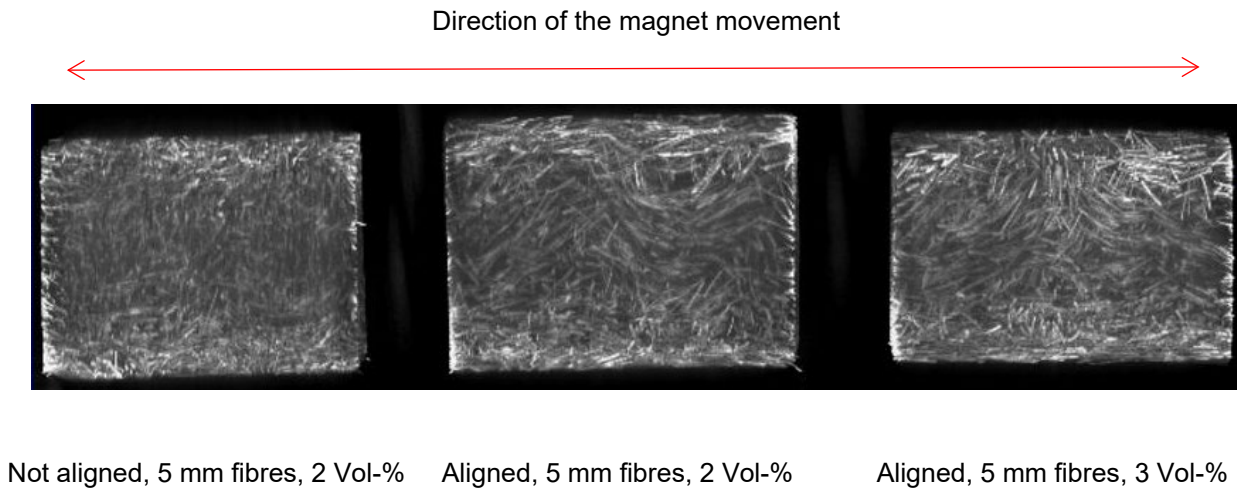


Figure 9: CT evaluation of the 5 mm fibres alignment effects

In case of using the 9 mm long fibres and the reached effect of the higher ultimate load bearing capacity, it is assumed that the inner resistance and the lever arm of the fibres in the UHPC matrix is bigger compared to the 5 mm fibres and so it is more difficult to align the fibres along the desired direction. Therefore, there were no bundles of fibres in the specimens and some fibres could be aligned as requested which led to the higher loads.

5 CONCLUSION AND PREVIEW

The present case study deals with the possibility of magnetic fibre orientation in UHPFRC. Therefore, subsequently strengthened concrete members of C 50/60 were produced and tested with 3- and 4- point bending procedures. The subsequently added strengthening UHPFRC layers differ in the amount and the length of the fibres as well as the number of movement and the speed of the magnetic aligning process.

The following observations could be made during the variation of the fibre contents: By varying the fibre content while using the 5 mm fibres, the flexural strength was found to deteriorate after the magnetic aligning process. In case of varying the 9 mm fibres content, no improvement in flexural strength was observed at a fibre content of 2 Vol-%, and even a slight deterioration. However, at a fibre content of 3 Vol-%, the performance remained the same compared to the unaligned strengthening layers, and even a slight increase in the flexural strength was observed.

Magnetic fibre orientation in UHPFRC is possible. The length of the fibres has a big influence on the positive outcome of the alignment process, as well as the number of movements. In case of using the 9 mm long fibres, it is assumed that the inner resistance and the lever arm of the fibres in the UHPC matrix is bigger compared to the 5 mm fibres and so it is more difficult to align them along the desired direction. In the present case study these facts were advantageous, because due to the dimensions of the strengthening layer, and especially the thickness, the fibres were already sufficient aligned of right after pouring because of the viscosity of the UHPFRC matrix. Therefore, by trying to align the 9 mm fibres, there were no bundles of fibres in the specimens and some fibres could be aligned as requested, which led to the higher loads. While performing the aligning process, it is important to check whether there are no fibre bundles because these are negatively affecting the interaction of the fibres next to each other over the whole width of the specimen. The speed of the alignment process had no apparent effect on the load-bearing behaviour of the strengthened plates. The increased number of movements of the magnet across the strengthening layer showed a positive effect in the case of the 9 mm fibres in one test specimen.

The next step would be to test the alignment with a big coil and the alignment with robotic support. Results of these test setups should show the possibility of using these procedures in precast fabrics among others.

ACKNOWLEDGMENTS

The authors want to thank the University of Applied Sciences Wiener Neustadt in Cooperation with MedAustron for the possibility to perform the Micro CT analyses there, as well as the internal Engineering IT department for giving important information regarding magnetic effects and influences. The test results and more activities on this topic are summarized in [5].

REFERENCES

- [1] Ru Mu et al.: Aligning steel fibers in cement mortar using electro-magnetic field. In: Construction and Building Materials 131 (2017), S. 309 – 316
- [2] Ledderose, L. et al.: Robotergestützte, magnetische Ausrichtung von Mikro-Stahldrahtfasern in dünnwandigen UHPFRC-Bauteilen. In: Beton- und Stahlbetonbau 114 (2019), Heft 1, S. 33-42
- [3] Wiffels, M.J.H et al.: Magnetic orientation of steel fibres in self-compacting concrete beams: Effect on failure behavior. In: Cement and Concrete Composites 80 (2017), S. 342–355
- [4] Kaufmann, N.: Das Sandflächenverfahren. Straßenbautechnik, Heft 3, 1971
- [5] Megel, M.: Elektromagnetische Faserausrichtung zur Optimierung des Fasernutzungsgrades von Ultrahochfestem Beton. Bachelorarbeit, Hochschule Kaiserslautern: Fachbereich Bauen und Gestalten, 2020.

9

Mergim Gaši, Bojan Milovanović, Jakov Perišić and Sanjin Gumbarević

Thermal bridge assessment in prefabricated ventilated façade systems with recycled aggregates

THERMAL BRIDGE ASSESSMENT IN PREFABRICATED VENTILATED FAÇADE SYSTEMS WITH RECYCLED AGGREGATES

Mergim Gaši¹, Bojan Milovanović², Jakov Perišić³ and Sanjin Gumbarević⁴

¹ University of Zagreb, Faculty of Civil Engineering
Fra Andrije Kačića Miošića 26, 10000 Zagreb, Croatia
e-mail: mergim.gasi@grad.unizg.hr

² University of Zagreb, Faculty of Civil Engineering
Fra Andrije Kačića Miošića 26, 10000 Zagreb, Croatia
e-mail: bojan.milovanovic@grad.unizg.hr

³ URBANE IDEJE d.o.o.
Ljudevita Gaja 26 A, 10430 Samobor, Croatia
e-mail: jakov.perisic@urbaneideje.hr

⁴ University of Zagreb, Faculty of Civil Engineering
Fra Andrije Kačića Miošića 26, 10000 Zagreb, Croatia
e-mail: sanjin.gumbarevic@grad.unizg.hr

SUMMARY: Despite numerous national regulations, it has been shown that the traditional practice when insulating building envelope is insufficient if not enough attention is given to thermal bridges. Heat losses through thermal bridges are much higher than the heat losses through the surrounding area. Because of that, the thermal bridges are accompanied by lower surface temperatures, resulting in the higher risk of water vapour condensation and the formation of mould, and ultimately building damage. Therefore, much attention should be given to the design of thermal bridges and ultimately, its construction. This paper deals with the impact of thermal bridges on the outer building envelope of the ventilated façade system of the first ECO-SANDWICH® house in Croatia. The house is built in Koprivnica as part of the Green Zone project. It is designed according to the standards for passive houses using innovative, ventilated Eco-sandwich® façade panels, designed at the Faculty of Civil Engineering, University of Zagreb. All the details in this paper are modelled as two-dimensional, according to the HRN EN ISO 10211 standard. The numerical calculation is carried out by software specialised for the heat flow and thermal bridge calculation – Flixo. The output result, linear heat transfer coefficient (Ψ), which quantifies the impact of linear thermal bridges on the one-dimensional heat flow, is analysed by variation of parameters, such as thermal insulation thickness. Finally, the numerical results are compared with the results obtained by default values of linear thermal bridges according to the standard HRN EN ISO 14683. This comparison is made to show the error between the results obtained by the numerical calculation and the default values, which are typically taken in the traditional calculation of heat losses in buildings.

KEY WORDS: Thermal bridges; Eco-sandwich; linear thermal transmittance; thermal transmittance; Flixo.

1 INTRODUCTION

Since the building sector is responsible for approximately 40% of the total energy consumption and 36% of total CO₂ emission, the European Council issued the Energy Performance of Building Directive (EPBD) in 2002. After the energy crisis, the Council has made the Directive mandatory in order to satisfy the Kyoto protocol agreement [1]. Because of the severity of the problem regarding the energy consumption and CO₂ emission, two more versions of the Directive were issued. The second version from 2010 set the goals to reduce energy consumption by 20% and increase the use of renewable energy by 20% [2]. As a result of that decision, the number of nearly zero-energy buildings and passive houses increased. Due to the high thermal insulating power of these buildings transmission heat losses through these so-called weak points of building elements (e.g. thermal bridges) became more pronounced. If thermal bridges are not adequately designed and, more importantly, adequately built on-site, then higher heat losses may occur.

Because of the change in the surface temperature between the thermal bridges and undisturbed area of the building elements, building damage such as surface condensation and mould may occur. If these problems are not adequately solved, they can have harmful effects on human health. The studies show that in approximately 70% of cases, the main reason for building damage is moisture [3]. This paper gives the analysis of thermal bridges that occur in prefabricated ventilated façade system in Flixo software [4] which is validated by EN ISO 10211 standard [5] (Thermal bridges in building construction — Heat flows and surface temperatures — Detailed calculations). Flixo uses the finite element method to calculate the temperature distribution over the cross-section of the building envelope element for stationary heat transfer. For each thermal bridge, the linear heat transfer coefficient ψ , which quantifies the impact of linear thermal bridges on the one-dimensional heat flow, and temperature factor f_{Rsi} , which quantifies the risk of surface condensation, are calculated. Numerical analysis is done in accordance with HRN EN ISO 10211 [5] standard. The numerical results are then compared with the results obtained by default values of linear thermal bridges according to the standard HRN EN ISO 14683 [6]. This comparison is made to show the error between the results obtained by the numerical calculation and the default values, which are typically taken in the traditional calculation of heat losses in buildings.

2 METHODOLOGY

Thermal bridges are characterised by two or three-dimensional heat losses through the building envelope. Because of the higher-dimensional heat transfer calculation, a numerical analysis is needed. The procedure used for the numerical analysis of thermal bridges is given by HRN EN ISO 10211 standard. That procedure is implemented in Flixo – a Finite Element Method (FEM) based software used for the calculation of heat losses through building elements. The results of the analysis are the temperature and total heat flux distribution throughout the whole building element from which the linear heat transfer coefficient ψ (ψ -value) is calculated. Since the calculation of the U-value, ψ -value and f_{Rsi} is not based on the numerical calculation, the following standards are used:

HRN EN ISO 10211	Thermal bridges in building construction – Heat flows and surface temperatures – Detailed calculations [5].
HRN EN ISO 6946	Building components and building elements – Thermal resistance and thermal transmittance – Calculation methods [7].
HRN EN ISO 10077-2	Thermal performance of windows, doors and shutters – Calculation of thermal transmittance – Part 2: Numerical method for frames [8].
HRN EN ISO 14683	Thermal bridges in building construction – Linear thermal transmittance – Simplified methods and default values [6].
TRRUETIB	Technical Regulation on Rational Use of Energy and Thermal Insulation in Buildings [9].

3 CASE STUDY

The building being analysed is the first ECO-SANDWICH® house in Croatia (Figure 1a). The house is a result of the collaboration between the University of Zagreb, Faculty of Civil Engineering, and the industry (BETON-LUČKO d.o.o., KNAUF INSULATION d.o.o. and EURCO d.d.). Apart from being the first house built from the ECO-SANDWICH® panels, it is the first passive house built from recycled materials. The house has three storeys and a flat roof. Each storey has one apartment. The main structure is made of concrete (Figure 1b), and the outer concrete layer is fixed to the load-bearing structure by metal fastenings (Figure 1c).

The thermal bridges analysed in this research are shown in Table 1 with their numerical counterparts (geometrical models). Three thermal insulation (TI) thicknesses are chosen in order to show the dependence of the impact of thermal bridges for different TI thicknesses. Façade metal fastenings can be considered as point thermal bridges since the heat flow around them cannot be described as two-dimensional. According to HRN EN ISO 10211, point thermal bridges can be neglected. Furthermore, layers with a negligible thickness (such as hydro isolation and vapour barrier) can also be neglected. In the case of ventilated façade systems, HRN EN ISO 10211 dictates that all layers after the ventilated air cavity (from the ventilated air layer to the outermost exterior layer) should not be a part of the numerical model and that the exterior boundary condition should be modelled using the internal surface resistances. However, during the construction process of the prefabricated building elements, temperature and relative humidity sensors were installed in characteristic layers of the panels [10], and they can be used to model the boundary condition inside the ventilated air

cavity.

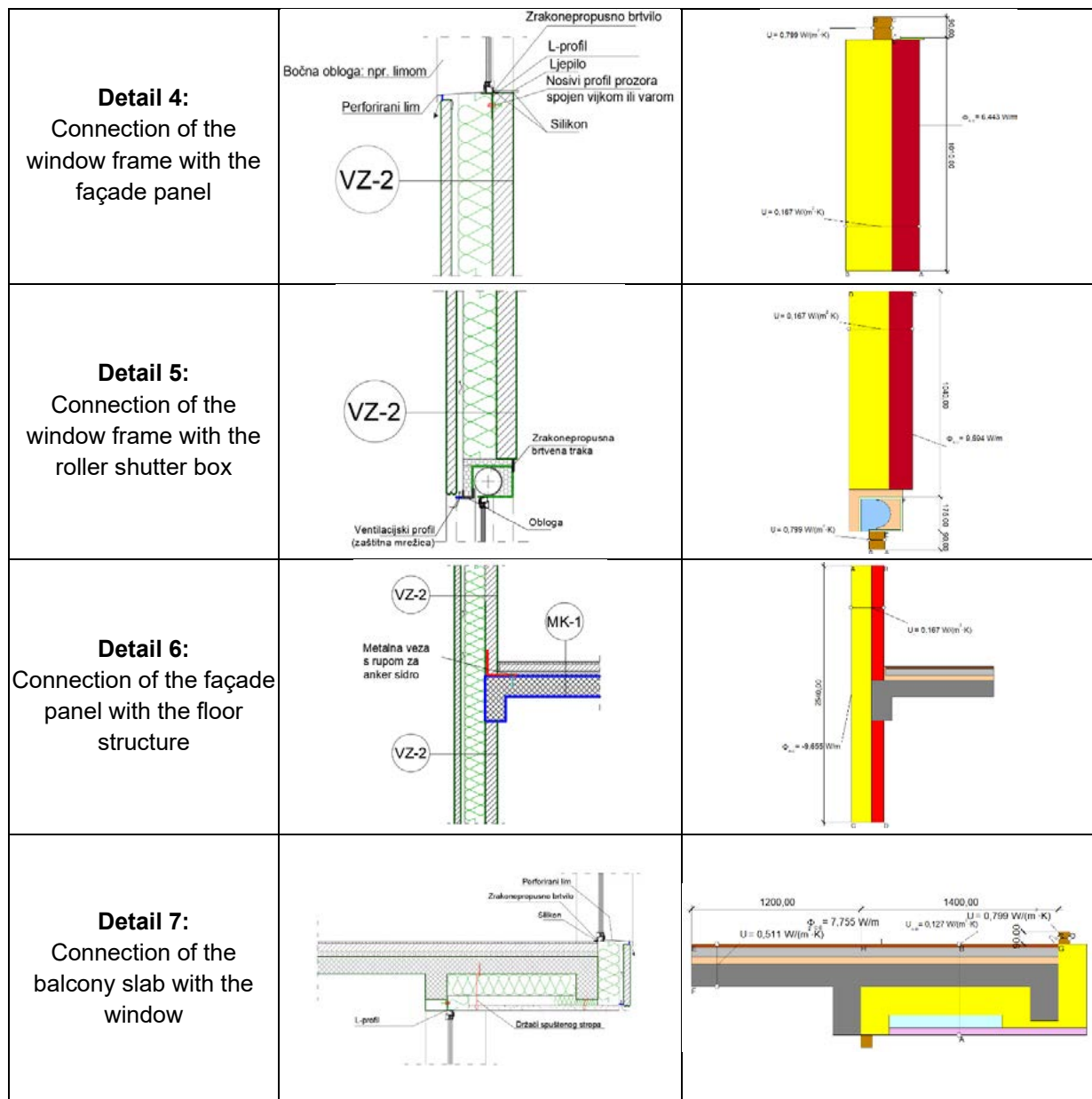
Boundary conditions are chosen from the in-situ measurements [10] as $-2,7\text{ }^{\circ}\text{C}$ for the surface temperature of the element bordering the air cavity, with the surface resistance $R_{si} = 0\text{ W}/(\text{m}^2\text{ K})$. Internal boundary conditions are modelled with the internal air temperature of $20\text{ }^{\circ}\text{C}$ and the internal surface resistance according to HRN EN ISO 6946 [7]. The roller shutter box is modelled according to HRN EN ISO 10077-2 standard as a separate submodel, and the result of the submodel is the U-value and it is used for the calculation of one-dimensional heat losses through the roller shutter box.



Figure 1: ECO-SANDWICH® house

Table 1: Thermal bridge details (taken from [11])

Description	Designed	Numerical model
Detail 1: Connection of the roof with the façade		
Detail 2: Connection of the base slab with the façade		
Detail 3: Connection of the two façade panels		



4 RESULTS

In Table 2, U-values and ψ -values of all seven thermal bridge details are shown for TI thickness of 10, 15 and 20 cm. The ψ -values are calculated using external (ψ_e), overall internal (ψ_{oi}), and internal (ψ_i) dimensions of the corresponding thermal bridges according to [5]. These results are compared with the default values given in [6] (Table 3) and are shown in Figure 2.

Table 2: U-values and ψ -values of thermal bridge details for TI thickness of 10, 15 and 20 cm according to the numerical analysis

		Detail 1	Detail 2	Detail 3	Detail 4	Detail 5	Detail 6	Detail 7
TI thickness ZU cm	$U_1 \text{ [W/(m}^2 \text{ K)]}$	0,167	0,105	0,167	0,167	0,167	0,167	0,511
	$U_2 \text{ [W/(m}^2 \text{ K)]}$	0,166	0,167	0,167	0,080	0,094	0,518	0,127
	$U_3 \text{ [W/(m}^2 \text{ K)]}$	–	0,167	0,167	–	0,080	–	–
	$\psi_e \text{ [W/(m K)]}$	0,019	0,122	-0,051	0,017	0,066	0,001	0,172
	$\psi_{oi} \text{ [W/(m K)]}$	0,166	0,185	0,083	0,017	0,066	0,001	–

	Ψ_i [W/(m K)]	0,166	0,185	0,083	0,017	0,066	0,052	–
TI thickness 15 cm	U_1 [W/(m ² K)]	0,217	0,124	0,220	0,220	0,220	0,220	0,511
	U_2 [W/(m ² K)]	0,220	0,220	0,220	0,080	0,094	0,518	0,155
	U_3 [W/(m ² K)]	–	0,220	0,220	–	0,080	–	–
	Ψ_e [W/(m K)]	0,012	0,139	-0,052	0,013	0,077	0,001	0,187
	Ψ_{oi} [W/(m K)]	0,184	0,201	0,102	0,013	0,077	0,001	–
	Ψ_i [W/(m K)]	0,184	0,201	0,102	0,013	0,077	0,067	–

Table 2 continued

TI thickness 10 cm	U_1 [W/(m ² K)]	0,314	0,150	0,320	0,320	0,320	0,320	0,511
	U_2 [W/(m ² K)]	0,320	0,320	0,320	0,080	0,094	0,518	0,198
	U_3 [W/(m ² K)]	–	0,320	0,320	–	0,080	–	–
	Ψ_e [W/(m K)]	-0,010	0,159	-0,054	0,007	0,090	0,003	0,229
	Ψ_{oi} [W/(m K)]	0,211	0,218	0,138	0,007	0,090	0,003	–
	Ψ_i [W/(m K)]	0,211	0,218	0,138	0,007	0,090	0,099	–

Table 3: ψ -values of thermal bridge details for TI thickness of 10, 15 and 20 cm according to HRN EN ISO 14683

	HRN EN ISO 14683						
	Detail 1	Detail 2	Detail 3	Detail 4	Detail 5	Detail 6	Detail 7
Ψ_e [W/(m K)]	0,6	0,6	-0,05	0	NA	0	NA
Ψ_{oi} [W/(m K)]	0,8	0,75	0,15	0	NA	0	NA
Ψ_i [W/(m K)]	0,8	0,75	0,15	0	NA	0,1	NA

Minimal surface temperatures on the internal surface and their corresponding temperature factors are calculated to determine the risk of surface condensation on the internal surface (Table 4). The temperature factors are calculated for the internal air temperature of 20 °C and the external air temperature of -2,7 °C (Table 4).

Table 4: Minimal surface temperatures and temperature factors

	Detail 1	Detail 2	Detail 3	Detail 4	Detail 5	Detail 6	Detail 7
	TI thickness 20 cm						
$\theta_{si,min}$ [°C]	18,56	15,88	18,99	17,81	14,42	19,38	17,54
f_{Rsi} [-]	0,94	0,82	0,96	0,90	0,75	0,97	0,91
TI thickness 15 cm							
$\theta_{si,min}$ [°C]	18,31	15,49	18,72	17,89	14,47	19,18	17,44
f_{Rsi} [-]	0,93	0,80	0,94	0,91	0,76	0,96	0,91
TI thickness 10 cm							
$\theta_{si,min}$ [°C]	17,86	14,96	18,21	17,43	14,57	18,80	17,24
f_{Rsi} [-]	0,91	0,78	0,92	0,89	0,76	0,95	0,90

Detail 1:

As can be seen in Figure 2a, ψ -values calculated using a numerical model are much lower than those given in [6]. For the thermal insulation thickness of 20 cm, the ψ -value given in [6] is 60 times higher than the ψ -value calculated from the numerical analysis results if external dimensions are used for the calculation of the ψ -value and 4,8 times higher if internal (or overall internal) dimensions are used. The change in the thermal insulation thickness affects the ψ -value significantly.

If the thermal insulation thickness is reduced from 20 cm to 15 cm, then the ψ -value calculated using the external dimensions (ψ_e) is reduced by 58%. If the thickness is reduced from 15 cm to 10 cm, then that difference is 108%, and for the reduction of thickness from 20 cm to 10 cm that difference is as high as 152%. For the ψ -value calculated using the internal dimensions (ψ_i), the change in the TI thickness does not affect the ψ -values as significantly. If the TI thickness is reduced from 20 cm to 15 cm, the difference is 10,8%; 14,7% for the reduction from 15 cm to 10 cm and 27% for 20 cm to 10 cm reduction. The simplified analysis of the surface condensation on the internal surface shows that there is no risk for the surface condensation (Table 4).

Detail 2:

As it can be seen in Figure 2b, the ψ -values calculated using a numerical model are much lower than those given in HRN EN ISO 14683. For the thermal insulation thickness of 20 cm the ψ -value given in [6] is 4,92 times higher if external dimensions are used for the calculation of the ψ -value and 4,05 times higher if internal (or overall internal) dimensions are used. In Figure 2b, a linear increase in the ψ -value can be seen for the increase in the TI thickness from 10 cm to 15 cm and 15 cm to 20 cm. The simplified analysis of the surface condensation on the internal surface shows that there is no risk for the surface condensation (Table 4).

Detail 3:

As it can be seen in Figure 2c, ψ -values calculated using a numerical model are similar to those given in HRN EN ISO 14683. Numerical analysis shows that the ψ -value calculated using the external dimensions is not affected by the change in the TI thickness. For the ψ -value calculated using the internal dimensions, the difference is 22,9% for the change in the thickness from 20 cm to 15 cm, 35,3% for 15 cm to 10 cm change and 66,0% for 20 cm to 10 cm change. There is no risk of surface condensation in this case (Table 4).

Detail 4:

According to HRN EN ISO 14683, all three ψ -values (ψ_e , ψ_{oi} and ψ_i) are zero (Figure 2d). However, numerical analysis shows that is not the case. Due to the geometry of the numerical model ψ -values calculated using external, overall internal and internal dimensions are equal. The difference in the ψ -values is 23,5% for the change in the thickness from 20 cm to 15 cm, 46,15% for 15 cm to 10 cm change and 36,4% for 20 cm to 10 cm change. There is no risk of surface condensation in this case (Table 4).

Detail 5:

HRN EN ISO 14683 does not give the ψ -value for this case. Due to the geometry of the numerical model ψ -values calculated using external, overall internal and internal dimensions are equal in this case too (Figure 2e). The difference in the ψ -values is 16,7% for the change in the thickness from 20 cm to 15 cm, 16,9% for 15 cm to 10 cm change and 58,8% for 20 cm to 10 cm change. There is no risk of surface condensation in this case (Table 4).

Detail 6:

In the case of the ψ -values calculated using the external (and overall internal) dimensions, the HRN EN ISO 14683 gives good agreement with the numerically calculated values (Figure 2f). However, in the case of the ψ -value calculated using the internal dimensions, the difference between the values given in HRN EN ISO 14683 and the numerical analysis is 1,92 times higher for 20 cm TI thickness and, 1,49 times higher for 15 cm TI thickness and for the 10 cm TI thickness the values are identical. For the ψ -value calculated using the internal dimensions, the difference is 28,9% for the change in the thickness from 20 cm to 15 cm, 47,8% for 15 cm to 10 cm change and 90,4% for 20 cm to 10 cm change. There is no risk of surface condensation in this case (Table 4).

Detail 7:

HRN EN ISO 14683 does not give the ψ -value for this case. This detail has two thermal bridges that have a combined effect on the overall heat losses through the observed building element. The calculation of the ψ -value of each thermal bridge is done separately, and then their ψ -values are added together (Figure 2g). Numerical analysis showed the reduction of the ψ -value by 8,7% for the change in the TI thickness from 20 cm to 15 cm, 22,5% for the change from 15

cm to 10 cm and 33,4% for 20 cm to 10 cm change in the TI thickness. There is no risk of surface condensation in this case (Table 4).

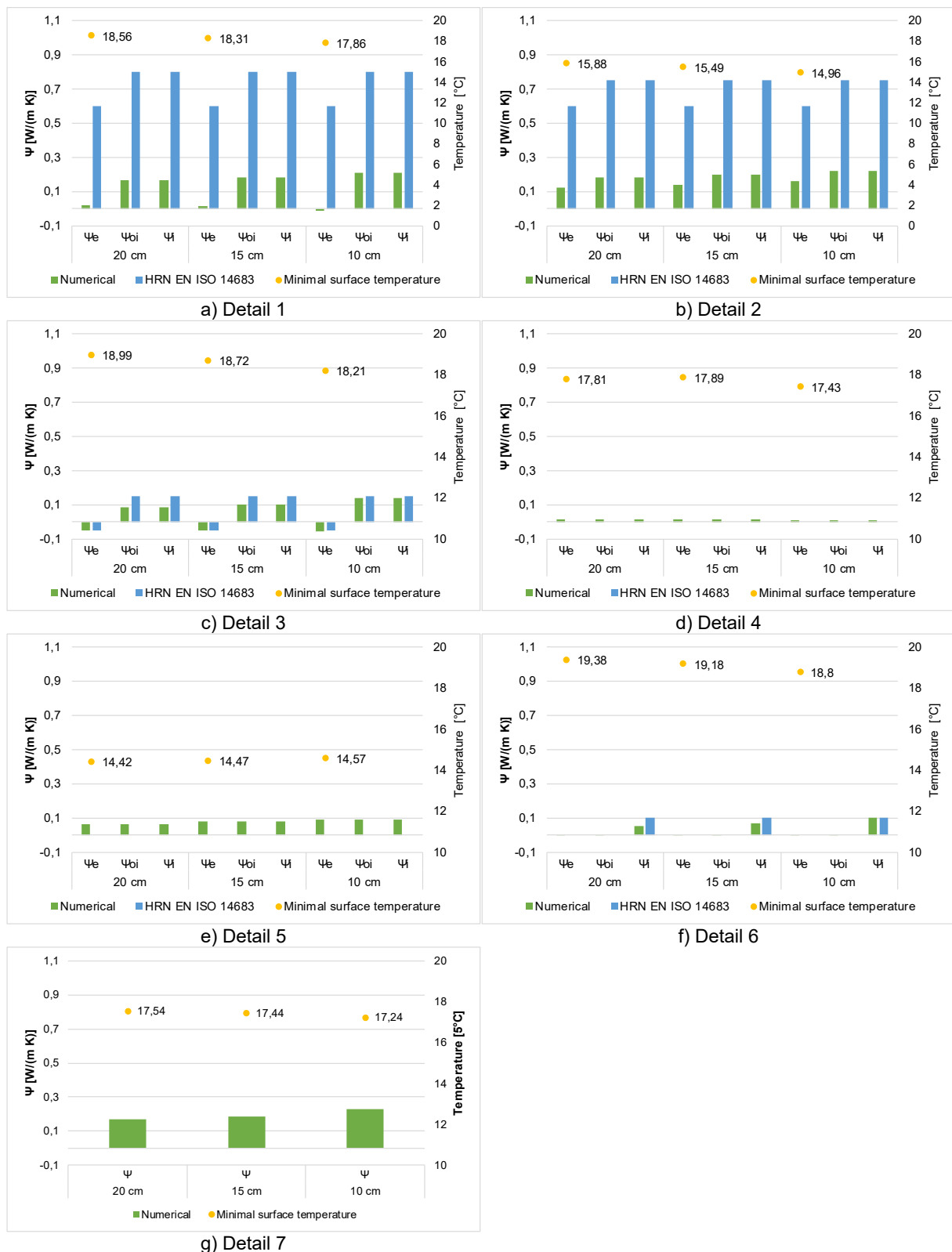


Figure 2: Comparison of the results for different thermal insulation thicknesses

5 CONCLUSIONS

Nearly zero-energy buildings (NZEBs) are becoming the standard in building high-performance energy buildings. One

of the key aspects in achieving better energy efficiency of buildings is through quality design and construction. One of the most overlooked problems in the design phase is the thermal bridges and not only for the calculation of the energy consumption but also due to the building damage caused by surface condensation in the operation phase. Eco-sandwich® house analysed in this research proved as an excellent example for the analysis of the thermal bridges. Numerical models analysed in this research are carried out according to the HRN EN ISO 10211 standard, and the results are compared to the default values given by the HRN EN ISO 14683 standard. Except for the comparison of the results according to beforementioned standards, the effect of the thermal insulation thickness on the ψ -value is also analysed.

The analysis of the results showed that the default values given by HRN EN ISO 14683 gave several times higher values than those calculated from the results of the numerical analysis, which initially predicts higher energy consumption in the building's operation phase. It must be noted that these simplified values given in HRN EN ISO 14683 are not applicable for only a small number of cases since they are calculated for only one TI thickness and simplified geometries. These simplified values are implemented in software that architects and engineers use in everyday practice when calculating building energy consumptions without knowing the error they make. ψ -values are chosen for elements that best describe the thermal bridge or part of a building. Moreover, some of the details (like 5 or 7) are not given in the HRN EN ISO 14683, and the only way to compensate for the heat losses due to the presence of the thermal bridges is by the numerical analysis.

Even though the two-dimensional numerical analysis is superior to the values given in standards such as HRN EN ISO 14683, it has some disadvantages. One of the main disadvantages is that two-dimensional analysis cannot capture heat flux deviations caused by point thermal bridges such as façade metal fastenings, dowels, and penetration of structural elements (beams or columns) through the building envelope. In order to achieve more realistic energy consumption, a three-dimensional numerical analysis is needed.

ACKNOWLEDGMENTS

This research was done as a part of a master thesis by Jakov Perišić under the title "Numerical Analysis of Thermal Bridges". One of the authors (Sanjin Gumbarević) would like to acknowledge the Croatian Science Foundation and the European Social Fund for the support under the project ESF DOK-01-2018.

REFERENCES

- [1] Chou, J.S.; Bui, D.K.: Modeling heating and cooling loads by artificial intelligence for energy-efficient building design. *Energy Build* 82(2014):437–46, (2014). Doi: 10.1016/j.enbuild.2014.07.036
- [2] EPBD: Energy performance of buildings directive 2010/31/EU (recast). *Off J Eur Union*, (2010). Doi: doi:10.3000/17252555.L_2010.153.eng
- [3] Milovanović, B.: Toplinska ovojnica zgrade – problemi i rješenja u praksi:37–44, (2012)
- [4] Infomind GmbH: Flixo, (2019)
- [5] EN ISO 10211: Thermal bridges in building construction — Heat flows and surface temperatures — Detailed calculations. *CEN*, (2017)
- [6] EN ISO 14683: Thermal bridges in building construction — Linear thermal transmittance — Simplified methods and default values, (2017)
- [7] EN ISO 6946: Building components and building elements — Thermal resistance and thermal transmittance — Calculation methods, (2017)
- [8] EN ISO 10077-2: Thermal performance of windows, doors and shutters -- Calculation of thermal transmittance -- Part 2: Numerical method for frames, (2017)
- [9] Republic of Croatia, Ministry of Construction and Physical Planning: Technical Regulation on Rational Use of Energy and Thermal Insulation in Buildings, (2017)
- [10] Bagarić, M.; Banjad Pečur, I.; Milovanović, B.: Hygrothermal performance of ventilated prefabricated sandwich wall panel from recycled construction and demolition waste – A case study. *Energy Build* 206, (2020). Doi: 10.1016/j.enbuild.2019.109573
- [11] Perišić, J.: *Numerička analiza toplinskih mostova*. University of Zagreb, Faculty of Civil Engineering, (2018)

10

Gradisar Luka, Dolenc Matevz, Klinc Robert and Turk Ziga

Designing generatively to achieve an efficient and optimised solution



DESIGNING GENERATIVELY TO ACHIEVE AN EFFICIENT AND OPTIMISED SOLUTION

Gradisar Luka¹, Dolenc Matevz¹, Klinc Robert¹ and Turk Ziga¹

¹ University of Ljubljana, Faculty of Civil and Geodetic Engineering, Jamova 2, 1000 Ljubljana, Slovenia

e-mail: luka.gradisar@fgg.uni-lj.si

e-mail: matevz.dolenc@fgg.uni-lj.si

e-mail: robert.klinc@fgg.uni-lj.si

e-mail: ziga.turk@fgg.uni-lj.si

SUMMARY:

Recent developments in the field of artificial intelligence and related areas have opened up new possibilities for computers to generate solutions independently. One such approach is generative design. Generative design is proving to be an efficient alternative design approach to the traditional processes. In this paper we present the framework for generative design, which is characterised by three main features: computational model, generator and design evaluation. This framework was applied to the practical example of the search for an efficient passive shading system with complex geometry. Here we used BIM models from Revit and Dynamo environment to build a computational model. For the generation and evaluation of the design alternatives Project Refinery was used together with Python. We have learned that this approach can be beneficial to us by automating the search for design solutions, creating complex designs we wouldn't think of and generating more design options from which we can find the efficient design more quickly. The same approach can be applied to any real-world design problem which we can translate to the computational model.

KEY WORDS: Generative design, optimisation, computational design, parametric modelling, BIM, automation.

1 INTRODUCTION

In recent years, technological development has accelerated drastically. Computers are becoming more powerful and intelligent. This is reflected in the increasing use of digital tools being introduced in the construction industry. The work of designers over time already changed by replacing pen and paper with CAD tools and now with BIM. Current approach to the building design still involves a lot of manual work. The designer creates designs based on his experience, previous projects, and creativity under the given conditions. The designer is the one who proposes the solution to the problem and computers are to help with presentation, documentation and analysis, but they do not help with the solving process. This opens up new possibilities and approaches.

One such approach is the generative design. The main idea of this approach is the collaboration between the designer and the machine, which has complementary capabilities, such as: sorting large amounts of data, generating and analysing large number of results, finding optimal solutions and iterative improvement of the solution [1]. In this process, we shift the focus from the creation of the design to the definition of the design problem with its conditions and goals. A well-defined problem can then be analysed with different algorithms to generate a large set of results from which the designer selects the optimal solution. Such concept was already introduced in 2002 by Caldas and Norford [2], where they searched for the optimal sizing of windows in a building. In 2010, author Krish [3] used the generative design approach in integration with CAD, to design an MP3 player and a coffee table. Authors Johan et al. [4] used it in structural design to explore different planar space truss systems, and authors Lohan et al. [5] searched for an optimal thermal path with topology optimisation. Recent research has focused on using artificial intelligence methods to generate designs, as shown by authors Oh et al. [6], where they used neural networks to create different designs of a 2D wheel.

The paper will introduce and explain generative design methods and how can they be integrated into the design process. The process will be demonstrated on a specific use-case where the analysis and comparison of the approach was carried out. The approach is general and can be used to help with the design in other areas of construction.

2 WHAT IS GENERATIVE DESIGN

Generative design is an iterative design process in which the designer defines the computational model with its design goals. Next the computer automates the generation of a variety of design alternatives. These results are to help a designer to better understand the design and the relationships between parameters and objectives. This helps to further develop the design or to find the final design solution [3].

This process changes the focus from result to a problem-oriented. Usually the designer does not know which design solution best fits the given conditions. The designer proposes a design and then analyses it with various tools to determine whether the proposed solution is suitable or not. This works for well-known problems, but fails for new problems due to lack of experience. We also do not know whether the design solution found is the best or whether it can be improved. With iterations we can produce a small sample that we can use to compare different design solutions, but this takes time that we sometimes cannot afford. In the generative design approach, we shift the focus to the definition of the problem and its objectives, from which the computers generate several design alternatives with different solvers. This automates the process of creating and analysing design solutions, resulting in a wider range of optimised results. Using a larger sample, we can identify patterns and relationships between the design parameters and its outputs. By understanding the problem, we can now adjust the design and more easily find the most suitable design solution.

Generative design framework has three characteristic features: computational model, generator and design evaluation as shown in Figure 1. A computational model is required so that the generator can produce and analyse different design alternatives. Building a computational model is a difficult step, given that the problem has to be described with a set of rules and equations. The model is also parametric, with parameters that change the design, resulting in different alternatives, each given a fitness score for different design objectives [7]. By ranking the alternatives, we can see how each design performs in different design goals. The generator represents different solvers that are used to generate multiple designs. The solvers differ depending on the problem we are trying to solve. One of these solvers are evolutionary algorithms, which are common for solving multi-objective optimisations [8]. When we generate a large number of designs, it is difficult to review all of them. When evaluating results, tools such as Pareto front, parallel coordinate coordinates plot and visual comparison are being used to additionally filter the results to a smaller sample that meets our boundaries and conditions to find design solution.

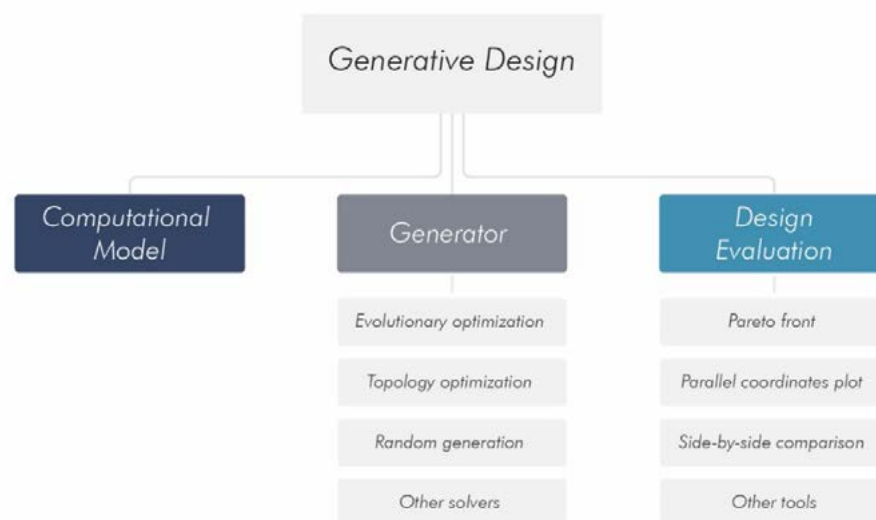


Figure 1: Generative design framework

2.1 Computational model

In generative design, we will refer to the computational model as the geometric model on which a computer can operate. Usually used are two different computational models: a model consisting of finite elements and a model created from a script. Both consist of a set of rules or instructions on how the model should behave or be constructed [7]. In order for the generator to produce different designs, the models should also contain input and output variables that describe the properties of a particular design solution. By changing the input variables, the design changes. Each design solution has different output values that are used to evaluate and compare them [2]. Output values like cost, volume, efficiency, capacity and other positive or negative characteristics that we want to either maximise or minimise.

2.2 Generator

Generator is a part of generative design that takes over the generation of multiple design alternatives. It automates the process of changing various design parameters and testing different solutions instead of the designer. It uses a computational model to create different design solutions by changing input variables to meet the design goals. The generator works by utilizing different solvers to create design alternatives. Since there are usually a large number of possible combinations of input variables, therefore design alternatives, the most commonly used solvers are optimisation algorithms, such as topology optimisation [9] and evolutionary algorithms [4]. However, there are also other solvers that generate designs by selecting different input variables based on specific rules.

2.3 Design evaluation

In this part of the process we analyse and compare the generated results. The generator produces many possible design solutions, each with associated input and output values. This way we can compare them between each other and see which one performs better. Since this generates a considerable number of results, it is beneficial to use appropriate tools for their analysis.

When using generative design, we are often dealing with more than one design goal. If we want to optimise the design, this translates to multi objective optimisation. If the objectives oppose, a design can only be improved in one objective at the expense of the other. This means that we cannot find a single solution that is the best, but that we get more than one optimal result, the so-called Pareto optimal solutions. Between them we cannot say which one is better than the other. They are all optimal. Some of them are better in one objective and worse in the others. By plotting the output values as a loss or gain function, as shown in Figure 7, we can find a Pareto front. The values on the Pareto front are the optimal Pareto results [8]. They can either help us find the final optimal solution or give us a reference to how close we are to the optimal design.

Another suitable tool is a parallel coordinates plot. With it we show all variables next to each other. This helps us to understand how the design behaves by changing these variables and what connections exist between them. We are also able to add additional boundaries to the variables and limit the design solutions to a selected sample. With a smaller sample, it is easier to inspect the selected designs individually. In addition, we can compare them visually by displaying them side by side.

By evaluating different design alternatives, we gain a better understanding of how the input variables affect the design and its performance. This knowledge helps us to further develop the computational model and find the solution to the design problem [1].

3 CASE STUDY

Generative design was applied to a case study building with a large glazed surface. As energy efficiency is an important part of the building design, a shading solution was required to reduce energy consumption. In order to reduce it, the design idea was to create shading elements that would illustrate the natural appearance of the wood grain texture and thus complement the timber design of the building. Subsequently, a generative approach was used to find an optimal shape of the shading elements to satisfy identified design goals while maintaining the visual complexity of the design.

We want to create a computational model of the shading elements. The elements will be horizontal and in the form of wood grains. With this we wanted to achieve three main design goals. First, we wanted to create efficient shading for the building, secondly, we wanted to reduce the material needed to construct the elements and finally, we wanted to give the building an interesting appearance. To develop a good generative design, it is important to clearly define a design problem and its design goals. Illustrations like in Figure 2 and 6 are recommended for this purpose.

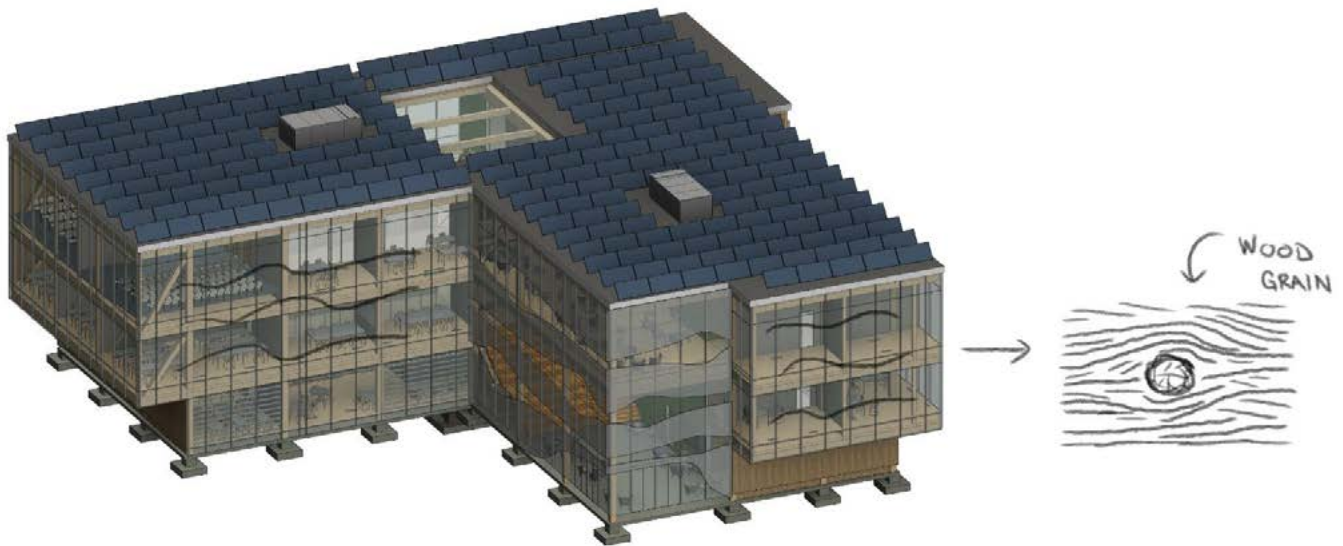


Figure 2: Illustration of the design problem.

For the generative design we needed an environment to build a computational model, a generator to generate design alternatives and an interface to evaluate the design results. The software applications used for the presented use case were Autodesk Revit, Dynamo, Project Refinery and a code editor for the Python programming language. In Revit we had a BIM model to which we wanted to add an optimised shading system. Complex geometries like the discussed shading elements cannot be modelled by hand, or it would take too much time. Therefore, the modelling was done with Dynamo, a software for computational design [10]. In Dynamo we used visual programming to build the computational model and manipulate with data. To generate different design alternatives, Project Refinery was used, which is an add-on for Dynamo. It has various solvers for generating and an interface for examining the results [11]. It is also included in the Revit 2021 version under the name Generative Design [12]. For the additional design evaluation, Python was used to organise the results using Pareto front, parallel coordinates plot and additional plots to better understand the relationships between variables and their impact on the design. This helped us to further develop the model and refine the overall design of the shading elements, since the process of creating the computational model and evaluating different designs was iterative as shown in Figure 3. Once the final design parameters were found, the geometry was then exported back to Revit and added to the BIM model.

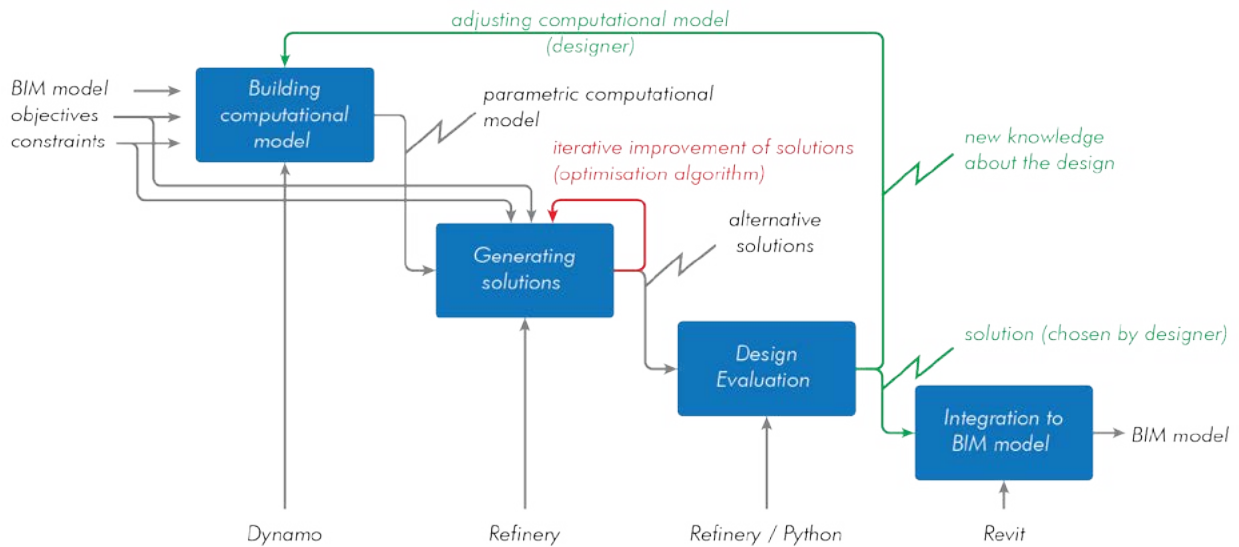


Figure 3: IDEF0 diagram of generative design for the case study problem.

3.1 Computational model

The starting point was a BIM model of the case study building. From the model, the façade surfaces, their orientation and position were extracted into the Dynamo environment. They were baselines on which the computational model of the shading elements was built. To create a computational model, we connected different Dynamo nodes between them. These are specific functions that describe how the model looks like [13]. The model of the shading elements was created by dividing the façade surface into horizontal elements. A more complex geometry was derived from the horizontal elements by incorporating shape curves, trigonometric functions and the addition of smaller openings. Figure 4 illustrates the process of building the computational model in Dynamo.

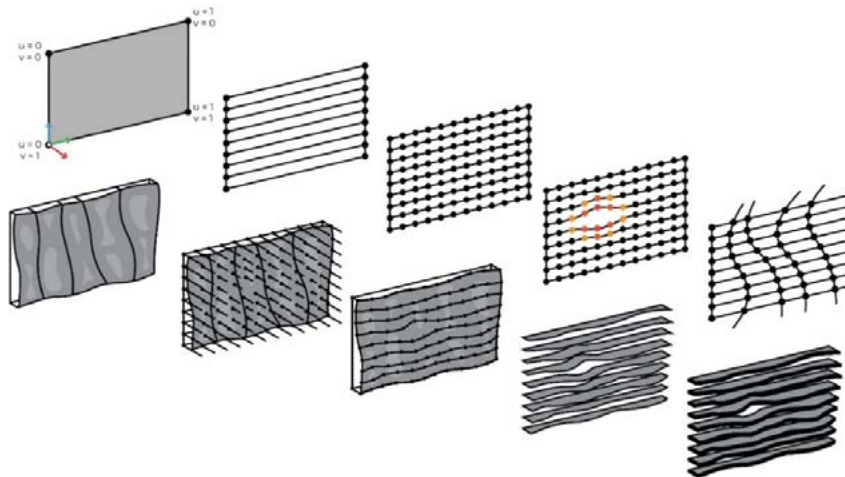


Figure 4: Build process illustration of the computational model in Dynamo.

Parameters that change the design have been simplified to the number of horizontal divisions and the offset multiplier that represents the width of the elements. To evaluate the design alternatives, the sunlight analysis was programmed. Here we simulated the sun rays in the sun vector direction at the different times and counted the number of sun rays that were either blocked by the geometry or transmitted through as shown with different colours in Figure 5. In addition, the total volume was extracted from the model geometry for the cost evaluation.

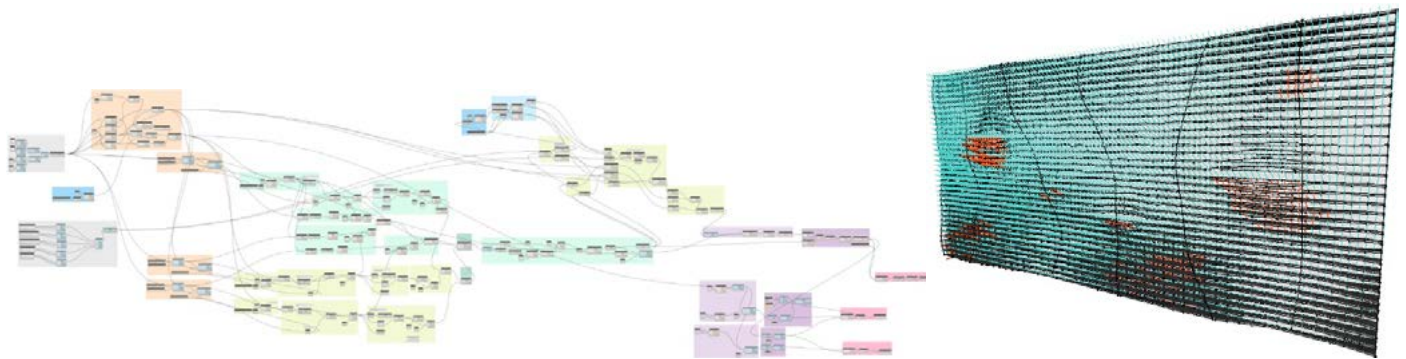


Figure 5: Dynamo script and sunlight analysis of generated geometry.

3.2 Generator

In the next step of the generative design, we determined what type of generator we will use and matched it with a compatible computational model. For the presented problem we wanted to perform a multi-objective optimisation with a solver using the evolutionary algorithms. To evaluate the different possible shapes, we defined output variables that represented the objectives we wanted to maximize and minimize. Based on the design goals, three targets were selected for optimisation: 1) the total material usage that we wanted to minimize, 2) the shading efficiency in summer and 3) in winter. We wanted to block direct sunlight in the summer and not block it in the winter in order to warm the interiors. The following objectives were defined in the computational model as numerical values, by which we were able to compare and rank different design alternatives. Figure 6 shows the input and output variables, which were as follows:

Input variables:

- Number of horizontal elements
- Width of the elements

Output variables:

- Total volume
- Number of sunrays passing through the shading elements in summertime
- Number of sunrays blocked by shading elements in wintertime

Project Refinery then used the computational model and created different design solutions with associated output variables by changing the input variables in order to find optimum output values.

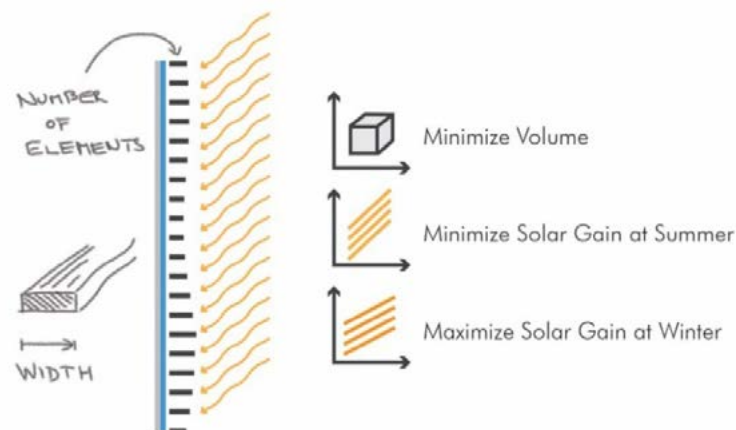


Figure 6: Objectives of the design optimisation.

3.3 Design evaluation

From the very beginning, we decided to have as few design variables as possible. If the problem had many design parameters and goals, the best approach would be to break the problem down into smaller ones and solve them step by step. This way we could focus on the whole problem with the aim to find input variables that created an efficient design and met the design goals. By analysing the output variables, we were able to compare different designs and their performance. This helped us understand how the overall design behaves and how efficient it can be.

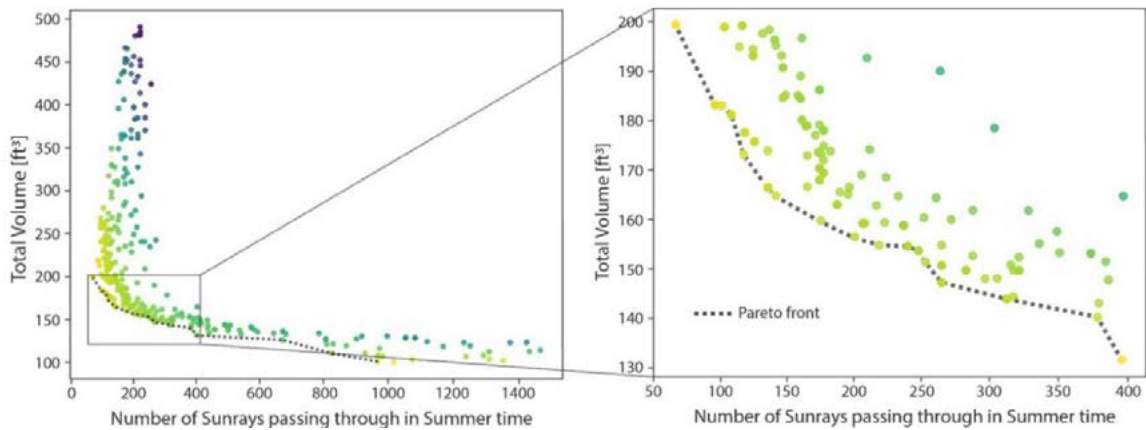


Figure 7: Pareto Front constructed from the analysis results.

From the generated results and their output values, we plotted the Pareto front, as shown in Figure 7. The Pareto front gave us an indication of which design alternatives were optimal. This allowed us to see how close we were to the optimal design when we examined alternatives in other design goals, such as visual appearance. We also decided that instead of the total volume, i.e. the initial cost of the elements, we should focus more on efficiency, which would be important over time. Here, the use of an interactive parallel coordinates plot in Figure 8 and the visual comparison in Figure 9 helped in the additional evaluation of the solutions.

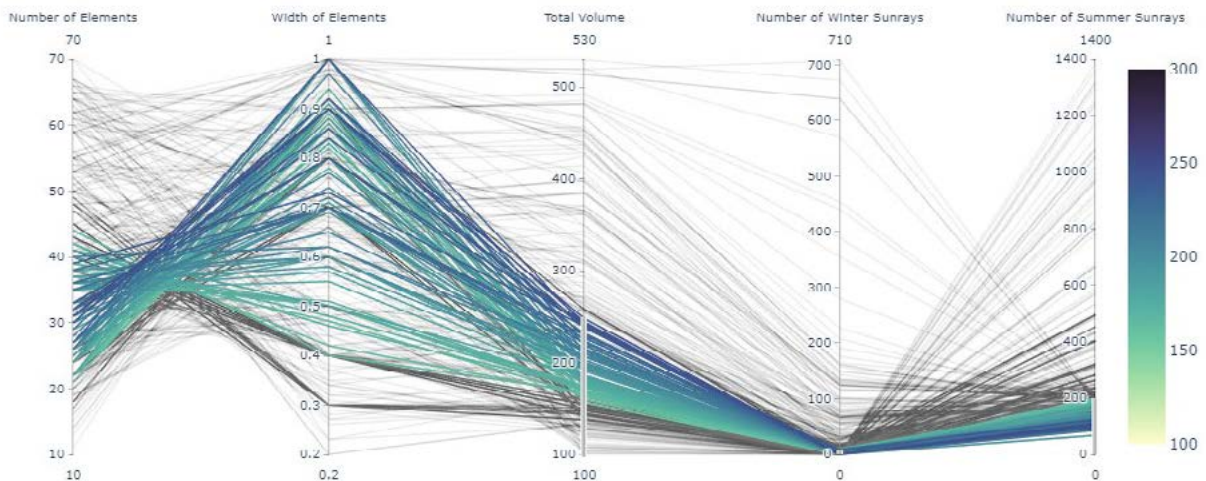


Figure 8: Parallel coordinates graph for filtering results.

With the parallel coordinates plot we filtered the results. Here we added additional constraints for each variable to limit the result pool. This helped us to understand the relationships between the variables. One of these relationships showed that the width of the elements had a greater influence on the efficiency than the number of elements, while the total volume of elements was still not significantly affected compared to a higher number of elements and a smaller width. This helped us in the design process, as we focused more on the width than on the number of the elements in the next

iterations of adjusting computational model. This helped us to evolve the design based on the initial design evaluation. By comparing and exploring different design alternatives, we were now prepared to find a final design solution.

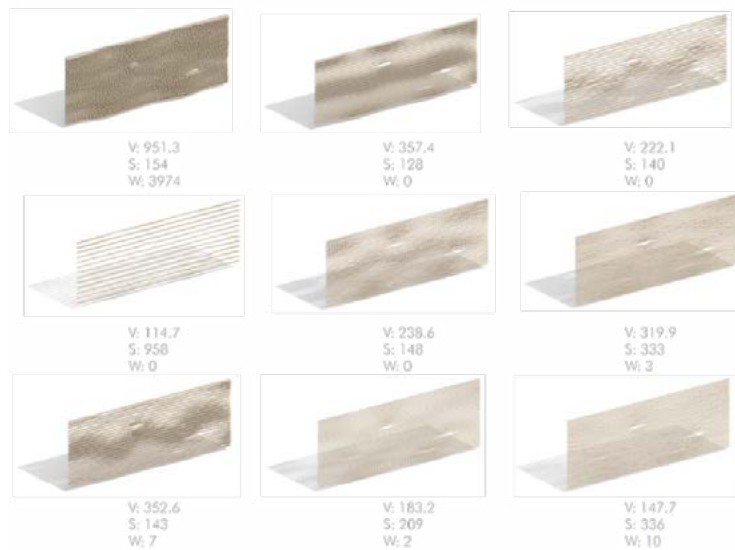


Figure 9: Visual comparison between the design alternatives.

3.4 Design solution

The design was based on a simple idea of horizontal louvres for passive shading. This idea was developed by adding various complexities to the design to create an interesting shape in the form of a wood grain. We added depth to the elements by using equations to create a wavy surface. Small openings and additional curvatures were introduced to the elements to simulate the irregularities in nature. Since we built the computational model, it is also easy to change the design later if it comes to any changes to the building.

Through the development and research of design alternatives, we were now ready to find a final design and integrate it into the building. This step depended heavily on us, the designers. As we had several design goals, there was not just one, but multiple possible solutions. Design is also subjective, either from the designer's point of view or from the investor's point of view. It was therefore up to us to evaluate different options and choose the one that, in our expert opinion, best met the design goals. In order to find the final design parameters for the shape to integrate it into the building, we used the knowledge gained from the design evaluation process. We found out what values of the input parameters would give us optimal results, and so we had a threshold above which we could adjust to see which overall design solution would fit us better. In search for the design solution, we also had to consider the visual appearance of the building. After we determined the values of the input variables, additional details were added to complete the final design, which was then integrated into the building as shown in Figures 10 and 11. In the end, the final design was not one of the Pareto optimal solutions, but it was the one we decided would best fit all design goals, including the look of the facade. This solution was still close to the optimum, so we can say that it is an efficient solution overall. When we first approached this problem without the generative design process, it was difficult to consider all design goals at once. We tried a few different solutions and picked one that we thought had a good appearance and would perform well for shading in the summer, but we did not know if it was optimal or if it could be improved upon in other design goals. It was difficult to compare different design solutions because we had no reference values to see how our design performed, and it would be too time-consuming to manually check all the possibilities. When we compared the solutions before and after using generative design, we found that the total material required for the design was reduced by 307%, while the shading was still efficient. In the initial design, we placed too much emphasis on the overall appearance of the façade and summer efficiency, and less on the other goals. With the generative design process, we were able to clearly see the design behaviour for all design goals and chose one which fit all of them according to our own assessment.

This process raises the question whether generative design replaces the human component in design. The current answer is no. The designer is still responsible for the two out of three components from the generative design framework. Firstly, the creation of the computational model and secondly, the evaluation of the results. The computer only generates and analyses various design alternatives. Generative design is a process that combines a designer with an intelligent tool to complete a designer in the weaker areas: analysis of large amounts of data, analysis of repetitive tasks, automation. We also know that it is almost impossible to find the perfect concept in the beginning. We have to iterate to find the best solution. This is especially difficult when we have to meet with multiple design goals. This is where generative design can help us a lot in concept development. We can define the problem and let the algorithms find a solution that takes multiple design goals into account. In this way, we can also find a concept that we never thought of and from which we can now continue to build our design.

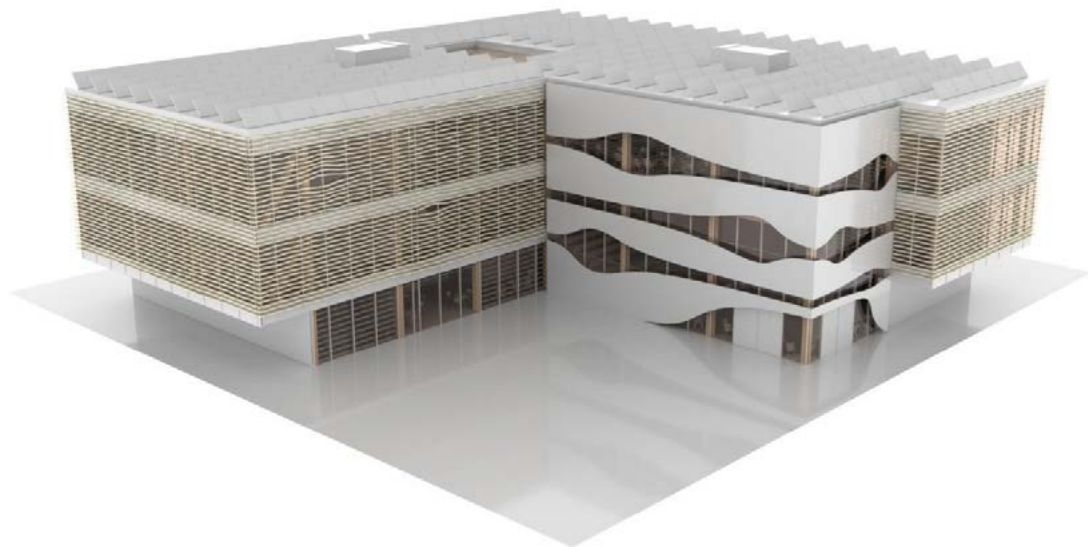


Figure 10: Render of the shading elements integrated into the building design.

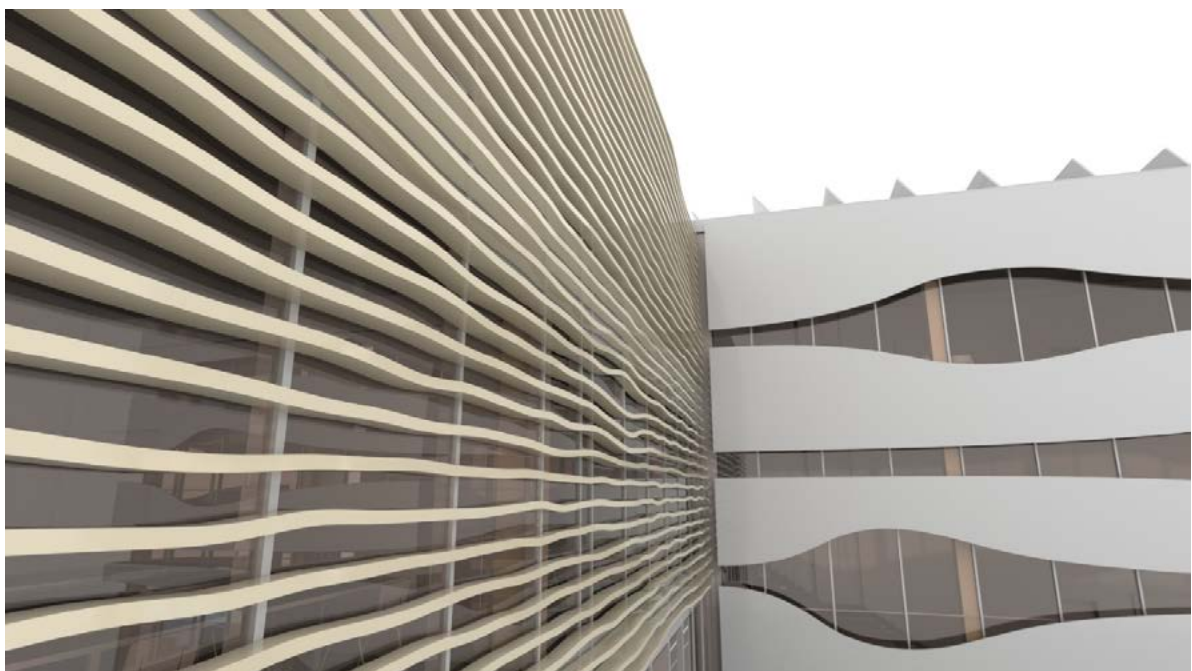


Figure 11: Close-up render of the integrated design solution.

4 CONCLUSIONS

Generative design is an efficient approach to solve design problems. Here, the time spent on the creation and analysis of the individual solution is used to define the computational model, from which multiple solutions are generated. By automating the generation of multiple design alternatives, we save a lot of time. Time that would be spent on iterating a single solution. Instead, we have to invest a lot of time to describe a real-world problem as a set of rules and equations from which algorithms can generate a variety of solutions. By analysing these solutions, the designer can better understand the problem and find the efficient design faster.

With the generative process, we have designed an optimal and aesthetic shading for a building façade. We created computational model of the shading elements and generated different design alternatives with the help of optimisation solvers. This helped us to find a solution that increased the shading efficiency and reduced the overall material requirements by 307% from our initial design. This process is general and can be applied to any problem that can be described as a computational model. It can be used in different design stages or in combination. It can be used in a conceptual stage to find starter design and then continue with the detailed analysis. Or it can be used from start to end, by breaking down a complex design problem to smaller parts. In each part we can then involve generative design.

The generative design is still reliable on the designer, it does not intend to replace one. The advantages of this process are that it complements human capabilities. Using various algorithms, we automate the generation and analysis of a large number of possible design outcomes. The designer then examines these results to learn more about the design problem. With this knowledge and his experience, he selects a final solution. This also paves the way for future work involving various artificial intelligence technologies such as machine learning to further develop generative design. The main advantages of generative design compared to the traditional design process, which were found in the course of the work, are:

- With this process we can produce results that we would never think of or that are too complex to produce manually,
- We can find more possible design solutions,
- We save time by automating the creation and analysis of a variety of design alternatives,
- By evaluation large number of results, we can better understand the design problem.

REFERENCES

- [1] Generative Design. Generative Design Primer, Available from https://www.generativedesign.org/01-introduction/01-02_generative-design Accessed: 2020-05-07
- [2] Caldas, L. G. & Norford, L. K.: A design optimization tool based on a genetic algorithm, *Automation in Construction*, (2002) No. 11 (2): 173-184. doi: 10.1016/s0926-5805(00)00096-0.
- [3] Krish, S.: A practical generative design method, *Computer-Aided Design*, (2011) No. 43 (1): 88-100. doi: 10.1016/j.cad.2010.09.009.
- [4] Johan, R., Chernyavsky, M., Fabbri, A., et al.: Building intelligence through generative design, Proceedings of the 24th International Conference of the Association for Computer-Aided Architectural Design Research in Asia (CAADRIA), Wellington, New Zealand, April 2019, CAADRIA, Hong Kong, (2019)
- [5] Lohan, D. J., Dede, E. M., Allison, J. T.: Topology for heat conduction using generative design algorithms, *Structural and Multidisciplinary Optimization*, (2016) No. 55, 1063-1077. doi: 10.1007/s00158-016-1563-6
- [6] Oh, S., Jung, Y., Kim, S., Lee, I., Kang, N.: Deep Generative Design: Integration of Topology Optimization and Generative Models, *Journal of Mechanical Design*, (2019) No. 141 (11): 1. doi: 10.1115/1.4044229
- [7] Stasiuk, D.: Design Modeling Terminology, Available from <https://archinate.files.wordpress.com/2018/06/dstasiuk-design-modeling-terminology1.pdf> Accessed: 2020-05-15
- [8] Eckart, Z. & Lothar T.: Multiobjective Evolutionary Algorithms: A Comparative Case Study and the Strength Pareto Approach, *IEEE Transactions on Evolutionary Computation*, (1999) No. 3 (4): 257-271. doi: 10.1109/4235.797969.
- [9] Ravi, A.: What Generative Design Is and Why It's the Future of Manufacturing, Available from: <https://www.newequipment.com/research-and-development/article/22059780/what-generative-design-is-and-why-its-the-future-of-manufacturing> Accessed: 2020-05-15

- [10] What is Dynamo. The Dynamo Primer, Available from https://primer.dynamobim.org/01_Introduction/1-2_what_is_dynamo.html Accessed: 2020-04-20
- [11] Generative Design for Revit and Dynamo. Generative Design Primer, Available from https://www.generativedesign.org/01-introduction/01-05_gd-for-revit Accessed: 2020-05-07
- [12] Generative Design in Revit now available. Autodesk, Available from <https://blogs.autodesk.com/revit/2020/04/08/generative-design-in-revit/> Accessed: 2020-05-13
- [13] Nodes. The Dynamo Primer, Available from: https://primer.dynamobim.org/03_Anatomy-of-a-Dynamo-Definition/3-1_dynamo_nodes.html Accessed: 2020-05-15

11

**Dusan Z. Grdic, Nenad S. Ristic, Gordana A. Toplicic - Curcuc, Jelena Bijeljić,
Zoran J. Grdić**

Resistance of concrete made with finely milled cathode ray tube glass as a supplementary cementitious materials to sulphate attack

RESISTANCE OF CONCRETE MADE WITH FINELY MILLED CATHODE RAY TUBE GLASS AS A SUPPLEMENTARY CEMENTITIOUS MATERIALS TO SULPHATE ATTACK

Dusan Z. Grdic¹, Nenad S. Ristic², Gordana A. Toplicic - Curcuc³, Jelena Bijeljic⁴, Zoran J. Grdic⁵

^{1,2,3,4,5} University of Nis, Faculty of Civil Engineering and Architecture, Aleksandra Medvedeva 14, 18000 Nis, Serbia
e-mail: dusan.grdic@gaf.ni.ac.rs, nenad.ristic@gaf.ni.ac.rs, gordana.toplicic.curcuc@gaf.ni.ac.rs, jelena.bijeljic@vtsnis.edu.rs, zoran.grdic@gaf.ni.ac.rs

SUMMARY: Sustainable building is one of the key requirements in contemporary civil engineering aimed at reducing the harmful impact on the environment. Since the turn of the twenty first century, it has been insisted on usage of recycled materials which could, at least in part, substitute traditional materials. Even though the TV sets with cathode ray tubes are no longer being produced, the amount of cathode ray tube glass (CRT) on the waste disposal sites has still been increasing. The goal of experimental research was determining potential for usage of finely milled CRT glass as a supplementary cementitious material and checking resistance of such concretes on the sulphate action. Six experimental batches of concrete were made. The replacement percentage of cement with CRT was: 5%, 10%, 15%, 20% and 35%, by cement mass. Each batch consisted of 18 cylindrical specimens with a diameter of 100 mm and height of 100 mm. A half of specimens was cured in saturated solution of calcium-hydroxide until the test. The second half of specimens was kept for the first 28 days in the saturated solution of calcium-hydroxide, after which they were exposed to action of 5% solution of sodium-sulphate. Assessment of durability of concrete to sulphate action was performed by the visual evaluation of concrete appearance and by testing the variation of compressive strength of treated concrete specimens at the age of 3, 6 and 12 months.

KEY WORDS: cathode ray tube glass; sustainable building, recycling; environment, sulphate action, durability.

1 INTRODUCTION

1.1 Cathode ray tube glass disposal and recycling problem

Electronic industry is one of the most important and fast growing industries in the world. Its growth and development in the recent decades created numerous jobs, accelerated technological development and simultaneously contributed to generation of considerable e-waste due to phasing out of electronic devices. Computer monitors and TV sets with cathode ray tubes have not been sold in Europe since 2011. However, these devices are still present in the households, and it is estimated that the landfills in Europe annually receive between 50.000 tons and 150.000 tons of obsolete CRT screens. It is anticipated that the quantity of collected CRT glass at the annual level will not be reduced in the future period (Andreola F. et al. 2007). The CRT waste recycling process is very important, in environmental terms. There are two possible systems of cathode tube recycling – open and close loop recycling. The close loop recycling comprises recycling of old screens and production of new CRT devices. Regarding that in Europe there are no more factories producing new screens with cathode tubes, most often the CRT waste is exported to the countries where CRT screen factories still exist. The open loop recycling uses old CRT screens for production of new and different products (Singh N. et al. 2016). There is a large number of scientific papers studying the potential of application of CRT glass in production of: ceramic tiles, artificial marble, glass jewelry, decorative crystals, etc.

One of the possible directions of cathode glass usage considers the civil engineering industry, whereby glass would be used for making of cement composites in two ways. The first option is to use it as a fine aggregate, which would replace a certain amount of natural aggregate. The other option is to use finely milled waste glass as a replacement for a share of cement when making mortar and concrete. One of the problems which can occur when using recycled glass aggregate for making of cement composites is the emergence of alkali-silicate reaction (ASR). Recycled glass has a high percentage of amorphous silicon dioxide (a glass bottle has around 70%) which has a potential of reacting with alkali from

cement, creating an ASR gel (Rajabipour F. et al. 2010). This gel in the presence of moisture during a prolonged period of time has a tendency to expand, which can initially cause cracks, and later on, a complete destruction of hardened concrete. The research indicated that glass grain size has a considerable impact on the ASR reactivity of glass (Idir R et al. 2011; Shayan A et al. 2006). It was found that the size of cracks inside glass grains, occurring due to crushing and pulverization processes, determines the ASR reactivity (Maraghechi H et al. 2014; Rajabipour F et al. 2010, Matos A. et al. 2012). Where the internal cracks are larger, ASR occurs more readily. On the other hand, very finely milled powder does not cause the alkali – silicate reaction considering the presence of a small number of micro-cracks. The experimental research is focused on testing the impact of finely milled glass as a replacement for a portion of cement when making concrete, and on the concretes modified in this way resistance to the sulphate effects.

1.2 Sulphate action mechanism

The sulphate salts dissolved in water can have extremely adverse effects on concrete. Most common sulphates are those of calcium, magnesium, potassium and sodium. Sulphates are present both in soil and in ground waters. Also, acidic rain and seawater contain dissolved sulphates which is an aggressive environment for concrete structures exposed to their action. Industrial waste disposal is recognized as locations with potentially very high sulphate concentration. Sulphate corrosion can most often be first detected on the edges and periphery of concrete elements, and after a long lasting exposure there occur cracks and decline of strength. This type of corrosion is a very complex process in chemical terms.

The basic products of sulphate ions reaction with the products of cement hydration are: ettringite, gypsum and thaumasite (Bjegović D. et al. 2015; Bulatović V. 2017; Grdić Z. 2011; Neville A. M. 2001). Numerous researches of the sulphate attack development mechanism showed that there is a correlation between the content of celita mineral $\cdot\text{Al}_2\text{O}_3$ (tricalcium aluminate) content in Portland cement and onset of sulphate attack. Cement, and by this, concrete, with high content of celita will cause emergence of sulphate reaction whose product will be ettringite, which can be described by the chemical equation:



Occurrence of ettringite increases the volume of solid matter up to 55% which gives rise to occurrence of considerable stresses in cement rock which causes onset of cracks. Ettringite is capable of absorbing water when found in microcrystalline form, and solid matter volume can be increased as much as 120%. Sulphates can also react with calcium hydroxide ($\text{Ca}(\text{OH})_2$), which also causes increase of volume and decline in bearing capacity of a structure. The following relation describes the action of sodium sulphate:



The mentioned reaction is also called the gypsum corrosion, considering that the reaction product is gypsum ($\text{CaSO}_4 \cdot 2\text{H}_2\text{O}$). In the case of concrete exposed to a long-lasting action of sulphate, during the first ten years, the sulphate corrosion is caused by the reaction (1), while after the mentioned period, the primary role in concrete deterioration is caused the by the reaction (2). The onset of cracks due to the increase of solid matter volume is not always the only manifestation of sulphate corrosion. Actually, in a large number of cases, the cement rock “softens” and disintegrates. There is also decalcification of C-S-H gel whereby the cement rock is softened and exhibits properties like putty (Grdić Z. 2011; Neville A. M. 2001).

Thaumasite is a very rare mineral which can occur in nature in some basic types of rocks, such as limestone. Thaumasite consists of calcium silicates, carbonates and sulphates $\text{CaSiO}_3 \cdot \text{CaCO}_3 \cdot \text{CaSO}_4 \cdot 15\text{H}_2\text{O}$. It is necessary that several conditions are met to cause occurrence of thaumasite in concrete. Damp environment, temperature below 15 °C, source of sulphate ions, most commonly from ground waters or soil, presence of carbonates in the aggregate used from making concrete and of calcium silicate which is present in hydrated PC. Similar to other products of sulphate corrosion, thaumasite can cause concrete devastation after a protracted period, too. Thaumasite can occur in the existing cracks and voids in concrete, however it needs not cause concrete degradation. Devastation occurs when thaumasite replaces a portion of or entire hardened cement matrix (Bjegović D. et al. 2015).

1.3 Testing of sulphate resistance of cement composites modified with waste glass

In the previous period, various sulfate resistance tests were performed on mortars and concretes wherein a portion of cement or fine aggregate was replaced with different varieties of waste glass. For instance, comprehensive testing of concretes properties containing various waste E-glass particle contents was conducted (Chen H. et al. 2006). The size distribution of cylindrical E-glass particles was from 38 to 300 μm and about 40% of particles was less than 150 μm . Sulphate-immersion test was performed with reference to ASTM C 267. The volume expansion of chemical reaction induces internal stresses, which may generate internal cracks and ultimately lead to failure. After five cyclic wet-and-dry exposures, significant weight loss and strength reduction were recorded, which exhibited strong sulphate attack on specimens. An increase in E-glass content significantly decreases weight and strength loss, particularly of the specimens with lower water/binder ratio. Based on the properties of hardened concrete, optimum E-glass content is found to be 40–50 wt.% in this study. The surface defects of tested specimens also show a qualitative evidence of sulphate attack.

Crushed waste glass from windshields and commercial glass containers were also the subject of research (Matos A. et al. 2012). Researches tested mechanical strength and durability of mortar using glass powder as a partial cement replacement (0%, 10% and 20%) material to ascertain applicability in concrete. Resistance to external sulphate attack was evaluated according to the Portuguese standard E – 462. Blended Portland cement with 10% replacement with WGP showed an impressive resistance to sulphate attack, far higher than SF marginally within the limit of 0.10%. The pozzolanic activity of WGP and SF binds portlandite (CH) released in the hydration of calcium silicates (C_3S and C_2S) so CH is no longer available for reaction with sulphates. This prevents the formation of gypsum. Pozzolanic reaction produces a secondary C–S–H that also decreases the capillary porosity of mortar and enhances significantly the paste - aggregate interface.

The features, compressive strength, sulphate and chloride resistance and expansions related to alkali – silica reaction (ASR) were examined on cement - based mortars produced with cement containing waste glass (WG) and industrial by-products (Ozkan O. et al. 2007). Resistance to sulphates was tested by comparing compressive strength of specimens exposed to 4% Na_2SO_4 with the strength of reference specimens. These results show that replacement of cement by waste glass alone increased the durability of mortars to sulphate attack. If waste glass is used combined with granulated blast-furnace slag or fly ash then sulphate resistance is more increased. Especially the waste glass and blast-furnace slag combination provides the best results.

The comparative analysis of waste glass powders behaviour of different fineness with that of natural pozzolana, coal fly ash and silica fume was also studied (Carsana M. et al. 2014). Seven mortars mixtures were made with glass powders and other mineral additions in which the share of replacement of cement was 30%, except for silica fume used at 10%. One of durability tests was expansion due to sulphate attack in according to ASTM C1012 standard. Mortars with ground glass showed a negligible expansion (0.04%) even after more than 1 year of immersion in the sulphate solution (when tests were interrupted). Only the mortar with silica fume showed lower values. On the other hand, mortars with ground quartz sand reached an expansion of 0.1% just after two months of tests and the reference mortar (OPC) after about eight months.

The methodology of mentioned research was used as a basis for the choice of fineness of the waste CRT glass so that its pozzolanic activity could be activated. Two criteria used by the cited authors were used for the evaluation of own experimental research, those being: visual inspection of the sample surface and variation of compressive strength.

2 MATERIALS AND METHODES

2.1 Used materials

Ordinary Portland cement CEM I 52.5R manufactured by "CRH" Novi Popovac, satisfying all the quality requirements stipulated by the standards SRPS EN 196-1:2018, SRPS EN 196-3:2017, SRPS EN 196-6:2011 and SRPS EN 197-1:2013 was used for making of concrete mixtures. Three fractions (0/4 mm, 4/8 mm i 8/16 mm) of the river aggregate from the South Morava river were used. The CRT glass came from the recycling center "Jugo - Impex E.E.R." d.o.o. from Niš. Large shards of CRT glass granted by the recycling center were milled using a laboratory ball mill so that glass could pass the sieve opening of 0.063 mm with no residue. For making of concrete mixes, tap water from the municipal water supply system was used, as well as the chemical superplasticizer admixture Sika[®] ViscoCrete[®] 4000 BP.

2.2 Concrete mixtures composition

Reference concrete (E) is produced with 400 kg of pure PC and 1800 kg of three-fraction aggregate. Water/cement ratio was constant in all experimental batches, and amounted to 0,438. The share of replacement of cement with CRT glass was: 5%, 10%, 15%, 20% and 35%, in respect to the mass of cement. Designations of concrete mixes were made according to the share of replacement, whereby WG is an abbreviation of - waste glass. For instance, in the case of 20% of replacement of cement with CRT glass, the batch mark is WG20. The complete composition of concrete mixes is presented in table 1.

Table 1: Compositions of the concrete mixtures used in the experiment

Concrete	Aggregate			Cement	CRT glass	Water	water - binder ratio	Admixture
	0/4mm	4/8 mm	8/16 mm	CEM I 52,5R	<0,063 mm	water supply	$m_v / (m_c + m_{wg})$	Sika Viscocrete 4000 BP
	kg/m ³	kg/m ³	kg/m ³	kg/m ³	kg/m ³	kg/m ³	-	kg/m ³
E	774	414	612	400	0	175.3	0.438	2.40
WG5	774	414	612	380	20	175.3	0.438	2.40
WG10	774	414	612	360	40	175.3	0.438	2.40
WG15	774	414	612	340	60	175.3	0.438	2.40
WG20	774	414	612	320	80	175.3	0.438	2.40
WG35	774	414	612	260	140	175.3	0.438	2.40

2.3 Testing program and procedure of concrete samples production

2.3.1 Program of testing

Program of testing can be divided in two phases. In the first phase, physical characteristics of component materials were tested. In the experimental part of the paper are presented the most important characteristics of powdered CRT glass, chemical composition and particle size distribution. In this phase, the glass pozzolanic activity was tested (SRPS B.C1.018:2015) as well as the FTIR spectrum and XRD diffractogram of CRT glass. Alkali - silicate reactivity was tested according to the ASTM C227-10 standard on mortar series.

In the second phase, numerous tests of physical and mechanical characteristics were performed on the hardened concrete. This paper features only the results of the sulphate resistance test in accordance with the procedure described in the following text.

2.3.2 Concrete samples production

Prior to making each concrete batch, special attention was paid to the homogenization of cement with an appropriate quantity of milled CRT glass. For that purpose, an adequately sized vessel with a lid was used, and a mixer fitted with a special attachment. During the mixing process, which lasted 5 minutes, the special attachment revolved at 850 rev/min. Three precisely measured fractions of dried aggregate, from the coarsest to the finest, were added into the wetted mixing drum. After that, a half of the planned amount of water was added into the mixer, and it was mixed for 30 seconds in order to wet the aggregate grains evenly. Then, cement mixed with milled CRT glass and the remaining water were poured into the mixer. From that moment, a calibrated stop-watch measured the mixing time of these component materials. After 60 seconds from the start of mixing, the superplasticizer was added, with the total mixing time amounting to 5 minutes.

Currently, there is no standard in Serbia which defines the procedure of testing of concrete resistance to sulphate attack but a very thorough and comprehensive testing of sulphate resistance of concrete based on the recycled aggregate was conducted (Bulatović V. 2017).

In this paper, each experimental concrete batch was composed of 18 cylinder shaped specimens, having diameter 100 mm and height of 100 mm (a total of 108 specimens). Concrete is cast into metal moulds, and placed using a vibrating table. Half of all specimens comprised of "reference" specimens which were cured in saturated lime water up to the testing. The other half of specimens, after the necessary preparations, at the age of 28 days was immersed and cured in a 5% solution of NaSO₄ up to the testing. The procedure of preparation and curing of experimental samples looked like this:

- Making of concrete and keeping in hermetically closed moulds for 7 days at the temperature 20 ± 2 °C;
- Demoulding, reduction the basis of the cylinder to be parallel by cutting and curing for 14 days in saturated lime water (solution of 1,8 g Ca(OH)₂ to 1 dm³ of water). "Reference" specimens of all batches (half of specimens) remained in lime water up to the moment of testing;
- 21 days after making, half of the samples intended for exposure to sodium sulphate were taken out of the lime water. Considering the expected degradation of samples after the long term presence of sulphate solution, bases of the extracted specimens were coated with Sikadur - 31 CF epoxy to prevent occurrence of stress concentration on the occasion of compressive strength testing;
- Half of the extracted specimens, after coating with epoxy was cured in the air in laboratory for 7 days; (Figure 1,a)
- At the age of 28 days, the specimens coated with epoxy were immersed in 5% solution of Na₂SO₄ (solution of 50 g of sodium sulphate to 1 dm³ of water);
- Replacement of total 5% solution of Na₂SO₄ in specimen curing vessels after 3, 6 and 12 months with regular checks of pH value (Figure 1, b);
- Comparative testing of compressive strength of samples cured in Ca(OH)₂ and Na₂SO₄ solutions at 3, 6 and 12 months.

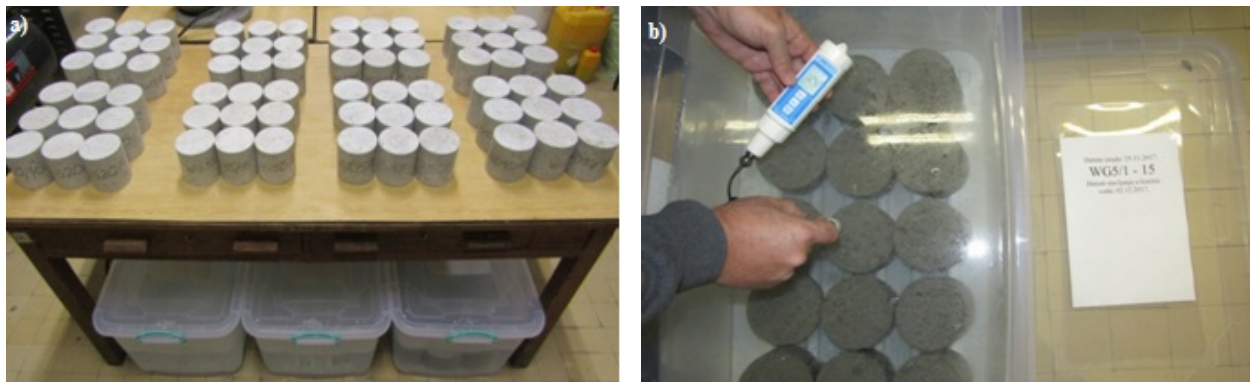


Figure 1: Curing of specimens in air, in the laboratory for 7 days (a) and Na₂SO₄ solution pH value checks (b)

Anhydrous sodium sulfate by the distributor DOO "Top Star" Zrenjanin was used. Dissolving of calcium hydroxide and sodium sulfate was done in warm water at temperature 28 - 32 °C. Only after cooling of the solution the specimens were immersed and kept in suitable containers. Solution pH value and lime water value in containers were performed using pH meter PH-220 with a range from 0 to 14 pH and measuring resolution of 0,01 pH. The pH solution value of Na₂SO₄ was ~7,5, i.e. ~12,5 u in the case of saturated lime water.

3 EXPERIMENTAL RESULTS AND DISCUSSION

3.1 Phase I

Finely milled CRT glass had a density of 2.84 g/cm³ and specific surface area by Blaine of 2450 cm²/g. Chemical composition of glass is presented in Table 2. Figure 2a shows particle size distribution of CEM I 52.5R, while in Figure 2b particle size distribution of the examined glass is displayed. More than 63% of glass grains were finer than 36 µm, while 42% were finer than 20 µm. Around 25% of cathode glass particles were finer than 10 µm.

Table 2: Chemical composition of CTR glass

Chemical compound	SiO ₂	Al ₂ O ₃	Fe ₂ O ₃	CaO	MgO	K ₂ O	Na ₂ O
Share [%]	60.61	2.88	0.58	1.31	0.53	6.45	7.61

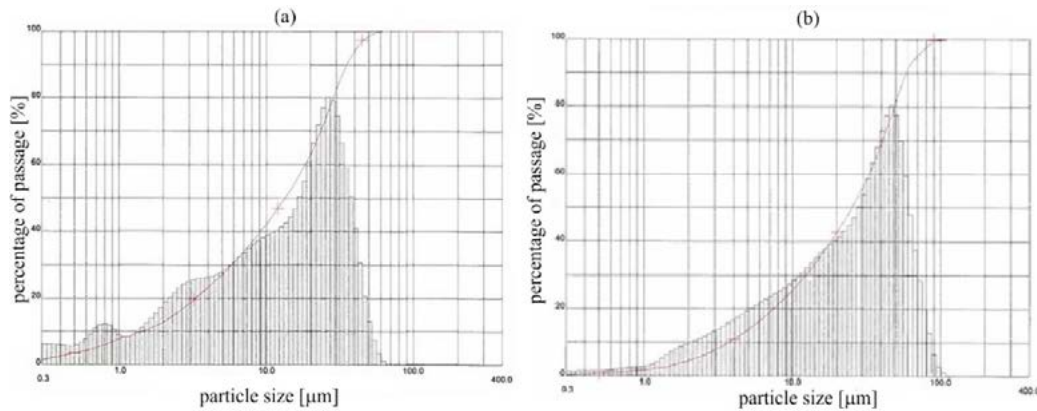


Figure 2: Particle size distribution of CEM I 52.5R (a) and CRT glass (b)

Pozzolanic activity of the glass was tested according to the standard SRPS B.C1.018:2001. The used standard classifies the pozzolanic material in three ways: according to the content of reactive silica (SiO₂), according to the particle size distribution and according to the mechanical properties. Glass pozzolanic activity was examined on the basis of the tested mechanical properties of mortar. The glass must have grains finer than 0,063 mm and be dried at the temperature of 98 °C. For preparation of mortar were used, 1350 g standard sand composed of three fractions, 300 g of fine CRT glass, 150 g of standard hydrated lime and 270 cm³ of water. Mechanical strengths are tested on the test specimens having dimensions 40 mm x 40 mm x 160 mm. The test specimens are hermetically enclosed in tin boxes, where after the first 24 h spent in laboratory conditions they continue to be cured at the temperature of 55 °C for additional six days. The results of the obtained mechanical properties of mortar are presented in table 3.

Table 3: Results of mechanical properties of mortar

Test specimen	Flexural strength [MPa]	Compressive strength [MPa]
1	2.36	5.76
		5.82
2	2.28	5.76
		5.82
3	2.43	5.95
		5.82

The material is considered to be pozzolanicly active and it is ranked to have no less than class 5, if at the age of seven days the minimum flexural strength is 2 MPa and compressive strength 5 MPa, which was proved with this test (Grđić D et al. 2015).

The FTIR analysis of the samples was made in the areas 4000 to 400 cm⁻¹, at a resolution of 2 cm⁻¹, on the BOMEM Michelson Hartman & Braun Series MB spectrometer. The absorption band at about 3400 cm⁻¹ and 1650 cm⁻¹, showing that only a small amount of water is present in the glass, can be attributed to the stretching and bending vibration of either free OH groups or free H₂O molecules. The water has no substantial effect on the structure of the glass. It is also often reported that bands within the range from 900 to 1100 cm⁻¹ are composite features of Si-OH species. The strong band at the frequency of ~800 cm⁻¹, therefore, is assigned to stretching vibration of Si-OH. The peak near 450 cm⁻¹ and a low frequency peak near 700 cm⁻¹ is assigned to Si-O-Si out of plane bending and Si-O-Si stretching modes respectively

(Figure 3a).

The XRD method was used for determination of mineral composition of investigated samples by the apparatus GNR Explorer, with scintillating counter at a voltage of 40 kV and electric current of 30 mA. Peak 2θ degree positions at about 19.0496, 29.6040, 40.7237 and 50.1789, with the maximum relative intensity at 29.6040 clearly show the presence of SiO₂ (quartz) in samples. Peaks from the XRD diffractogram indicate the presence of amorphous SiO₂, whereby the prominent peak at 40 indicates the presence of SiO₂ in the crystal form, too (Figure 3b).

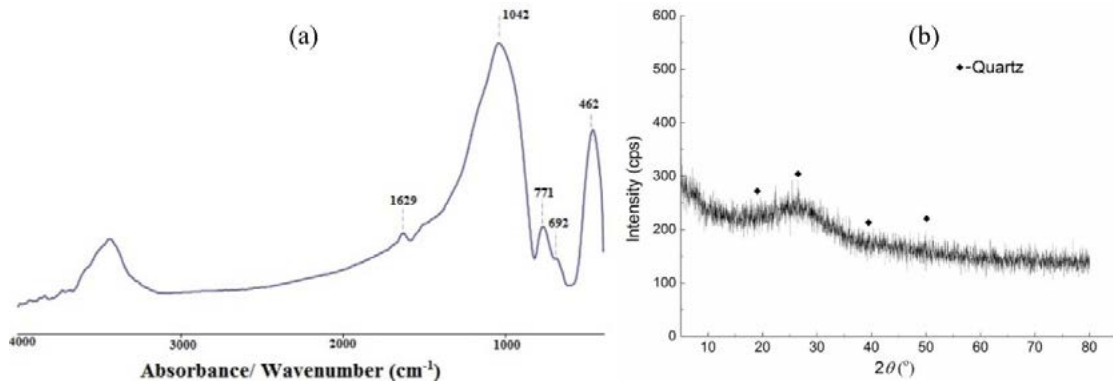


Figure 3: FTIR spectra of the CRT glass (a) and XRD diffractogram of CRT glass (b)

3.2 Phase II - Resistance of concrete made with CRT glass on sulphate attack

The level of sulfate resistance of concrete batches with CRT glass added was determined by comparing the compressive strength of reference specimens for each batch and of the specimens exposed to sulphate attack, table 4. Comparative testing of mechanical strengths was performed after exposing concrete to sulphate solution for 3, 6 and 12 months. Testing of compressive strength was conducted according to the standard ASTM C1231. In addition to strength variation, a visual inspection of potential damage of the specimens kept in the sulphate solution was performed.

Concrete	Reference specimens cured in solution of Ca(OH) ₂			Specimens cured in 5% solution of Na ₂ SO ₄			Strength variation $\Delta f_{p,n}$ [%]		
	f_{E3} [MPa]	f_{E6} [MPa]	f_{E12} [MPa]	f_{NS3} [MPa]	f_{NS6} [MPa]	f_{NS12} [MPa]	$\Delta f_{p,3}$ [%]	$\Delta f_{p,6}$ [%]	$\Delta f_{p,12}$ [%]
E	67.76	71.14	72.71	66.33	69.07	71.27	2.16	2.92	1.98
WG5	63.83	67.02	71.54	58.95	62.64	67.22	7.64	6.54	6.04
WG10	62.30	69.27	73.51	61.57	63.72	66.15	1.17	8.01	10.01
WG15	65.08	71.83	74.70	60.71	64.96	68.59	6.72	9.56	8.18
WG20	58.37	62.96	68.26	57.54	60.33	64.38	1.42	4.18	5.69
WG35	46.81	52.98	58.58	44.75	50.02	56.60	4.39	5.59	3.39

Strength variation was calculated according to the following formula:

$$\Delta f_{p,i} = \frac{f_{E,i} - f_{NS,i}}{f_{E,i}} \cdot 100 = [\%] \quad (3)$$

Where:

f_{Ei} - compressive strength of reference specimens after 3, 6 and 12 months of curing in Ca(OH)₂ solution in MPa;

f_{NSi} - compressive strength of specimens in 5% Na₂SO₄ solution after 3, 6 and 12 months in MPa;

$\Delta f_{p,i}$ – concrete compressive strength variation in %;

If the results of compressive tests of reference specimens cured in calcium hydroxide solution at the tests after 3 months ($f_{E,3}$) are firstly observed, it can be concluded that with the increase of share of finely milled CRT glass, compressive strength declines. Concrete mixes WG20 and WG35 have 13,9% and 30,9% lower strength than the reference batch E, respectively. At the tests after 6 months ($f_{E,6}$), the initial difference in compressive strength of the reference batch and sample up to the level of replacement of 15% of glass is reduced, while at the test after 12 months ($f_{E,12}$) the concrete mixture WG15 has 2,7% higher strength than E concrete. At the final test of concrete reference mixes after one year, WG20 and WG35 still have lower strengths than the reference batch, but this difference is now lower - 6,1% and 19,7%, respectively. Explanation for such increase of strength of concrete mixes with addition of CRT glass can be found in the process of pozzolanic reaction of glass. The nature of pozzolanic reaction of CRT glass is such that it occurs later than the process of cement hydration and that it is most intensive after 28 days which can explain the reduction of difference in the measured values of compressive strengths of the reference batch and batches with added glass.

After the impact of the presence of CRT glass on the compressive strength of concrete has been defined, one can observe sulphate resistance of experimental concretes. After curing the specimens in 5% solution of Na_2SO_4 for 12 months, no decline of compressive strength higher than 10% was found in comparison to the samples cured in calcium hydroxide. More important, the visual inspection of these specimens did not find any damage such as cracks or flaking. i.e. loss of mass. The tests are still underway, so after the curing period of 2 and 3 years in the presented conditions, the resistance to sulphate attack will be assessed. Generally speaking, it can be concluded that all the experimental mixes are resistant to action of sodium sulphate. At this moment, after one year of testing, it cannot be stated, with any degree of certainty, what the impact of present CRT glass on this kind of concrete resistance is.

4 CONCLUSIONS

After the impact of the presence of CRT glass on the compressive strength of concrete has been defined, one can observe sulphate resistance of experimental concretes. After curing the specimens in 5% solution of Na_2SO_4 for 12 months, no decline of compressive strength higher than 10% was found in comparison to the samples cured in calcium

Based on the obtained experimental results, a number of conclusions can be drawn:

- Based on the results of testing of pozzolanic activity of finely milled glass on lime mortar according to the SRPS B.C1.018:2015, the average value of compressive strength of 5,82 MPa was obtained. It can be concluded that the experimental glass is pozzolanically active, and it is class 5.
- The peak near 450 cm^{-1} and a low frequency peak near 700 cm^{-1} of FTIR analysis are assigned to Si-O-Si out of plane bending and Si-O-Si stretching modes, respectively.
- Peaks from an XRD diffractogram indicate the presence of amorphous SiO_2 , whereby a prominent peak at $40 \text{ } 2\theta$ indicates the presence of SiO_2 in the crystal form.
- Replacement of cement with CRT glass finer than $63 \text{ }\mu\text{m}$ the amount of 35% by mass does not cause occurrence of alkali - silicate reaction. Free silicon in glass powder, which is amorphous material, will be quickly consumed during the pozzolanic reaction, and it will react with other compounds to form a mineral phase. In this way, the dissolved silicon dioxide will be included in the crystal grid of cement gel and it will not be available for the process of alkali-silicate reaction which would normally occur quite later than the pozzolanic reaction.
- By measuring the compressive strength of concrete specimens where a portion of cement was replaced with CRT glass, cured in calcium hydroxide, it was found in time, the difference of compressive strengths in comparison to the reference batch E declines. At the tests after 12 months, the batches where cement was replaced with up to 15% of CRT glass have the same or higher compressive strengths than the reference batch.
- After curing the specimens in 5% solution of Na_2SO_4 for 12 months, no decline of compressive strength higher than 10% was found in comparison to the samples cured in calcium hydroxide. Generally speaking, it can be concluded that all the experimental mixes are resistant to action of sodium sulphate.

- The visual inspection of these specimens did not reveal any damage such as cracks or flaking. i.e. loss of mass after exposing the samples to sulphate attack.
- The testing is underway, so after the curing period of 2 and 3 the resistance to sulphate attack will be reassessed.

ACKNOWLEDGEMENTS

The work reported in this paper is a part of investigation within the research project TR 36017 „Utilization of by – products and recycled waste materials in concrete composites in the scope of sustainable construction development in Serbia: investigation and environmental assessment of possible applications“ supported by Ministry for Science and Technology, Republic of Serbia. This support is gratefully acknowledged.

REFERENCES

- [1] Andreola, F.; Barbieri, L.; Corradi, A.; Lancellotti, I.: CRT glass state of the art: A case study: Recycling in ceramic glazes., *Journal of the European Ceramic Society* (2007), Volume 27, Issues 2–3, pp 1623-1629.
- [2] Bjegović, D.; Štirmer, N.: *Theory and concrete technology*. Book (2015), Faculty of Civil Engineering, University of Zagreb.
- [3] Bulatović, V.: *Sulphate resistance of concrete with recycled aggregate concrete*, Doctoral Thesis (2017), Faculty of Technical Sciences, University of Novi Sad.
- [4] Carsana, M.; Frassoni, M.; Bertolini, L.: Comparison of ground waste glass with other supplementary cementitious materials, *Cement and Concrete Composites* (2014), Volume 45, pp 39-45.
- [5] Chen, H.; Huang, R.; Wu, K.; Yang, C.: Waste E-glass particles used in cementitious mixtures. *Cement and Concrete Research* (2006), Volume 36, pp 449 - 456.
- [6] Grdić, D.; Ristić, N.; Topličić - Čurčić, G.: Effects of Addition of Finely Milled Cathode Tube Glass Powder on Concrete Properties. Proceedings 13th International Scientific Conference INDIS 2015 – Planning, Design, Construction and Renewal in the Civil Engineering, University of Novi Sad, Faculty of Technical Sciences.
- [7] Grdić, Z.: *Concrete technology*, Book (2011), Faculty of Civil Engineering and Architecture.
- [8] Idir, R.; Cyr, M.; Tagnit, A.: Pozzolanic properties of fine and coarse color – mixed glass cullet, *Cement and Concrete Composites* (2011), Volume 33, pp 19-29.
- [9] Maraghechi, H.; Maraghechi, M.; Rajabipour, F.; Pantano, C.: Pozzolanic reactivity of recycled glass powder at elevated temperatures: Reaction stoichiometry, reaction products and effect of alkali activation, *Cement and Concrete Composites* (2014), Volume 53, pp 105-114.
- [10] Matos, A.; Sousa-Coutinho, J.: Durability of mortar using waste glass powder as cement replacement, *Construction and Building materials* (2012), Volume 36, pp 205-215.
- [11] Neville, A. M.; Brooks, J.J.: *Concrete Technology*, Book (2001), Produced by Pearson Education Asia Pte Ltd, Printed in Singapore, pp 431.
- [12] Ozkan, O.; Yuksel, I.: Studies on mortars containing waste bottle glass and industrial by-products, *Construction and Building materials* (2007), Volume 22, pp 1288-1298.
- [13] Rajabipour, F.; Maraghechi, H.; Fisher, G.: Investigating the Alkali – Silica Reaction of Recycled Glass Aggregates in Concrete Materials, *Journal of Materials in Civil Engineering* (2010), Volume 22, pp 1201-1208.
- [14] Singh, N.; Li, J.; Zeng, X.: Global responses for recycling waste CRTs in e- waste, *Waste Management* (2016), Volume 57, pp 187-197.
- [15] Shayan, A.; Xu, A.: Performance of glass powder as a pozzolanic material in concrete: A field trial on concrete slabs,

12

Sanjin Gumbarević, Bojan Milovanović, Mergim Gaši and Marina Bagarić

The impact of building zone elements on airtightness



THE IMPACT OF BUILDING ZONE ELEMENTS ON AIRTIGHTNESS

Sanjin Gumbarević¹, Bojan Milovanović², Mergim Gaši³ and Marina Bagarić⁴

^{1,2,3,4} University of Zagreb, Faculty of Civil Engineering, Department of Materials

Fra Andrije Kačića Miošića 26, 10000 Zagreb, Croatia

e-mail: sgumbarevic@grad.unizg.hr, bmilovanovic@grad.unizg.hr, mgasi@grad.unizg.hr, mbagaric@grad.unizg.hr

SUMMARY: To achieve the goals set by the European Union (EU) in terms of energy savings and decrease of the greenhouse gas emissions, the member states of the EU obliged that they would increase the number of the Nearly Zero-Energy Buildings (NZEB). That increase has to be accomplished not only by building new NZEBs but also by deep energy renovations of old ones. One of the criteria to fulfil NZEB demands is to ensure the airtightness of the building, which is usually tested by an air pressurisation test. As there will be a great number of buildings which must undergo the testing in the near future, it is important to find a way to speed up the testing for the multizone buildings. This paper presents research based on the results of building zone airtightness estimations based on a fan pressurisation test by the so-called Blower Door system. It is a part of research whose goal is to develop a predictive model of the air-change-rate for a multizone building based on randomly tested zones. The paper describes a connection between the airtightness of tested building zones and elements which make up these zones. This research is crucial as a starting point for the development of the predictive model in order to define the parameters that affect these measurements. Statistical analysis was performed not only for the analysed results but also for an exploration of the connection between the zone elements and the zone's airtightness as well. The paper presents a hypothesis based on the abovementioned research and proposes further research for the future development of the model.

KEY WORDS: Airtightness, Fan Pressurisation Testing, Statistical Analysis, Nearly Zero-Energy Buildings, Blower Door

1 INTRODUCTION

In order to achieve energy savings and to decrease the greenhouse gas emissions most efficiently, the European Union declared the building sector as crucial if the energy targets are to be reached [1]. For that reason, European Commission adopted directives ([2–5]) that mandate that not only all the new buildings must have the performance of Nearly Zero-Energy Buildings (NZEB) but also the old buildings must undergo deep energy renovation for the same reason. The savings can be achieved by building and retrofitting certain buildings with adequate heat resistant materials and constructions.. In this way, the transmission heat losses are reduced. In order to reduce the heat losses due to infiltration, it is essential to minimise the infiltration of air through the building envelope because air leakage (infiltration) through unintentional cracks on the building envelope has a large impact on energy demand for heating. The key thing for reducing the infiltration heat losses can essentially be set in one sentence – “Build tight, ventilate right” [6]. The airtightness of building envelope can be tested by the procedure described in ISO 9972:2015 standard. The standard introduces a fan pressurisation method for determination of air permeability of buildings. The method is described in more detail in subsection 2.1 *Air pressurisation test*. The result of the test is an assessment of air leakage through the building envelope based on the air changes per hour for a pressure difference of 50 Pa (n_{50}) between the air on both sides of the fan. One of the criteria to fulfil NZEB demands is by measuring the airtightness of buildings described by the results of this testing.

Infiltration through the building envelope is a physical phenomenon which happens due to pressure difference between the interior and exterior environment. This action takes place through unintentional cracks in the envelope, and it depends on the wind velocity, temperature difference and crack position on the envelope [7]. Infiltration losses in modern residential buildings are near 0,1 1/h whereas the minimum overall air change rate (sum of infiltration air change rate and natural and/or mechanical air change rate) must be at least at 0,5 1/h because of hygienic minimum requirements. The infiltration can be directly measured with “tracer gas” method as described in ISO 12569:2017, where a concentration of certain gas in the tested zone is observed at day-to-day occupancy, so the results must be interpreted in that way. The

gas which is used for this purpose must satisfy criteria defined in [8]: safety (should not pose a hazard to people), non-reactivity (should not react chemically or physically with any part of the system under study), insensibility (should in no way affect the processes that are being studied), uniqueness (should be able to be recognised from all other constituents of air), measurability (concentration of it must be quantifiable through some instrumentation).

For the reasons stated in the first passus of this section, it can be concluded that there will be a great number of buildings which must undergo the air pressurisation testing in the near future, so it is important to find a way to speed up the procedure of testing for multizone buildings. For the development of such a procedure, it is important to observe all the parameters influencing the infiltration. Which parameters were analysed and ranked as significant, highly significant, not enough discussed and not directly linked to infiltration phenomenon are taken from [9]. This paper analyses a set of parameters (described in section 2. Methodology) based on data from past air pressurisation tests and its correlation to resulting n_{50} . When exploring the previous works from the literature, two types of predictive models that are commonly used for estimating the airtightness were chosen – predictions based on statistical analysis ([10–12]) and predictions based on artificial neural network ([13–15]). Prediction models based on statistical analysis from large databases use multiple linear regression models. On the contrary, the artificial neural network models are based on significantly smaller databases and lack validation. Both types of models could be improved by experimental and numerical exploring of the airflow through cracks on the building envelope so the impact of the certain parameter on airtightness could be specified in more detail. Similarly, the group of authors (Fernández-Agüera et al.) in [9] state that future work should focus on the standardisation of data presentation and the development of a new airtightness predictive model. They state that it is essential to draw an appropriate classification of “air paths” on the building envelope to develop such a model.

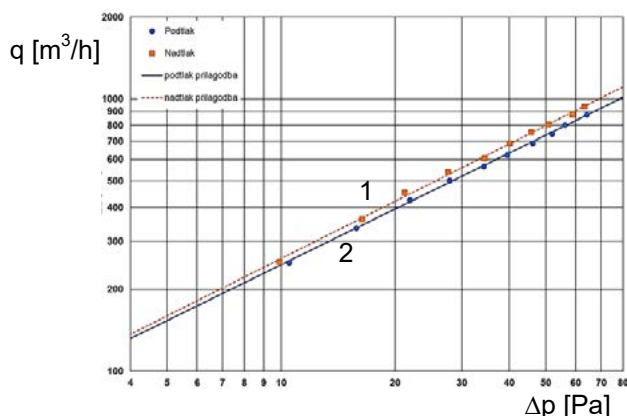
The classification described in [9] should be supported by computational fluid dynamics simulations of air flows for various types of cracks with experimental validation of numerical models as stated before. As a starting point for research for developing the procedure which will speed up the testing of multizone buildings, this paper shows causality of envelope elements on tested zone airtightness based on raw results and data from air pressurisation tests.

2 METHODOLOGY

In order to observe the phenomena defined in the introduction, more specifically the impact of chosen parameters on the building airtightness, a study on 23 air pressurisation tests were carried out. Observed parameters were zone volume, envelope area, envelope area - zone envelope ratio, envelope area which is a boundary to the exterior in m^2 as a percentage of overall envelope area, area of transparent elements in m^2 and as a percentage of overall envelope area, and zone height. These parameters were derived from the air pressurisation tests and are then compared with resulting n_{50} from each test.

2.1 Air pressurisation test

In order to observe the only physical phenomenon of airtightness that is of interest (more specifically airflow through tested zone envelope), certain air pressure differences have to be realised. For that reason, test equipment consists of a fan that is able to pressurise or depressurise the tested zone. The fan is connected to a pressure-measuring device and airflow rate measuring system so that the controlled airflow (in or out of zone) can be ensured to satisfy predetermined pressure differences between the indoor and outdoor environment. Testing equipment and the resulting graph can be seen in Figure 1.



a) b)

Figure 1. a) Resulting graph (1- pressurisation, 2 - depressurisation). b) Test equipment as defined in ISO 9972:2015.

The law that the results from air pressurisation test follow is defined by the exponential equation (1) and can be seen in Figure 1 a):

$$q_{pr} = C_L (\Delta p_r)^n, \tag{1}$$

where q_{pr} is air leakage rate at a specific reference pressure difference, C_L is air leakage coefficient, Δp_r is reference pressure and n is airflow exponent. This exponential law for estimating the airtightness is introduced in [16] in 1980, and it is still in use today. After the parameters from equation (1) are defined based on the experimental results, the air change rate at a pressure difference of 50 Pa can be determined as a ratio between the air leakage rate at 50 Pa (q_{50}) and the zone volume (V):

$$q_{50} = C_L (50)^n \tag{2} \qquad n_{50} = \frac{q_{50}}{V}, \tag{3}$$

The results of n_{50} and analysed parameters can be seen in Figure 2 – Figure 10.

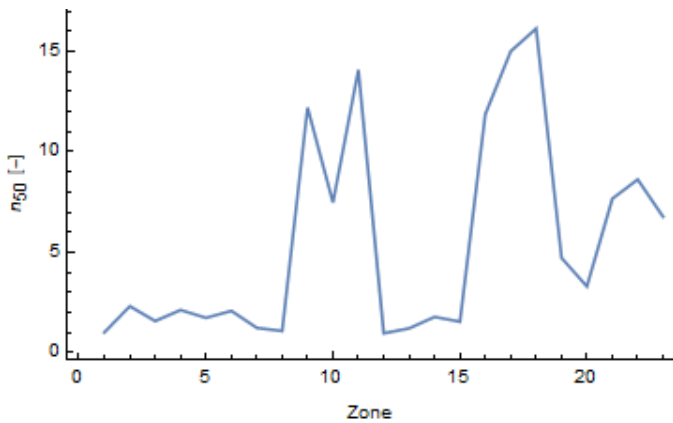


Figure 2. Results for n_{50} .

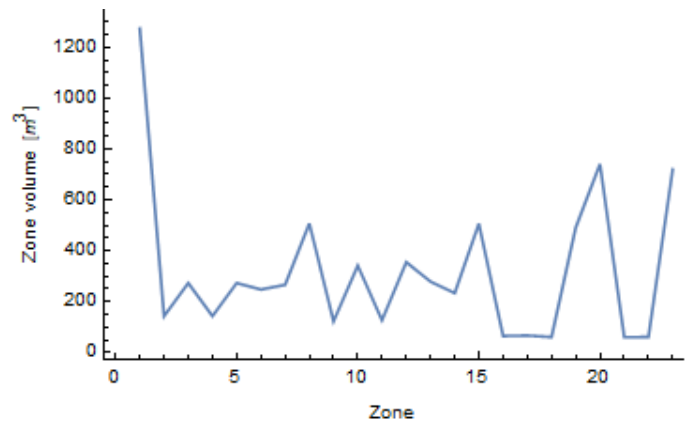


Figure 3. Zone volume in m^3 .

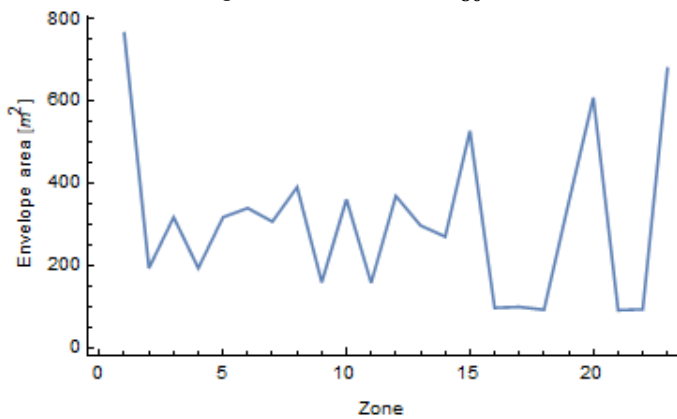


Figure 4. Envelope area in m^2 .

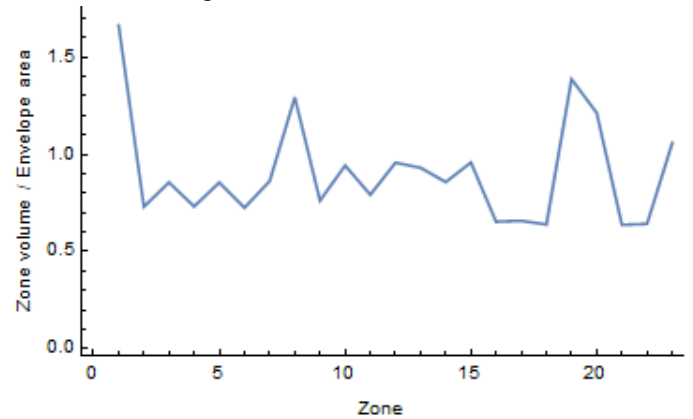


Figure 5. Volume to envelope area ratio.



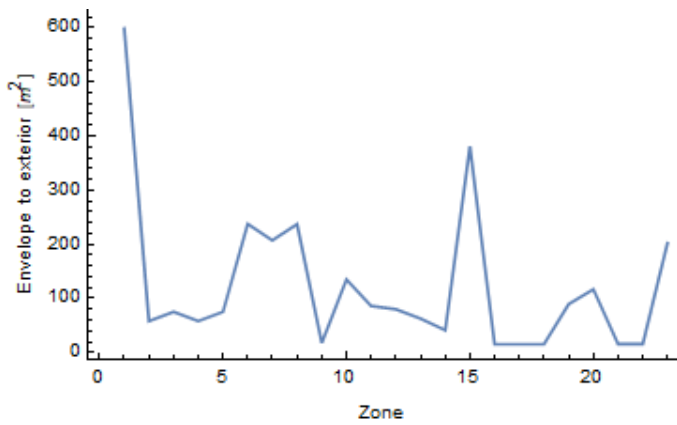


Figure 6. Envelope as a boundary to the exterior in m^2 .

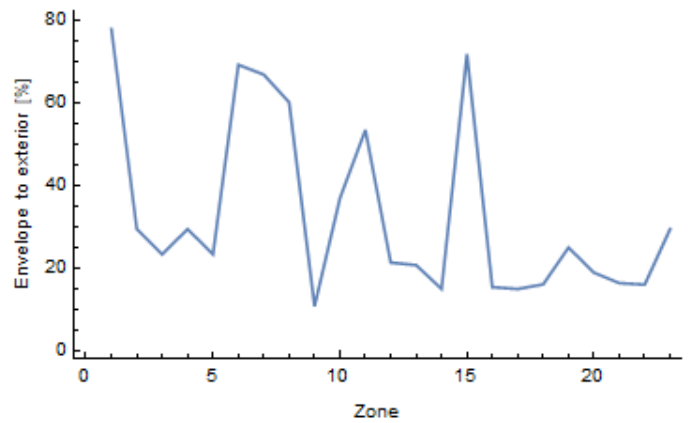


Figure 7. Envelope as a boundary to the exterior in %.

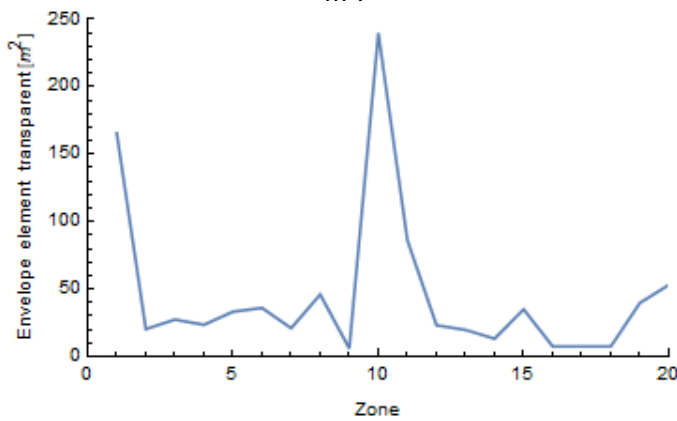


Figure 8. Transparent envelope elements in m^2 .

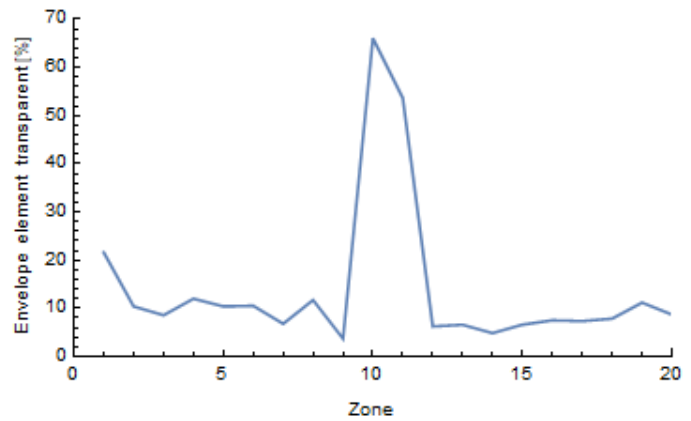


Figure 9. Transparent envelope elements in %.

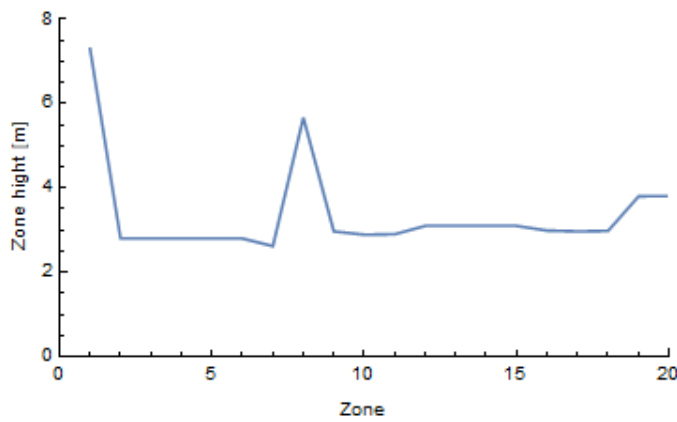


Figure 10. Tested zone height in m.

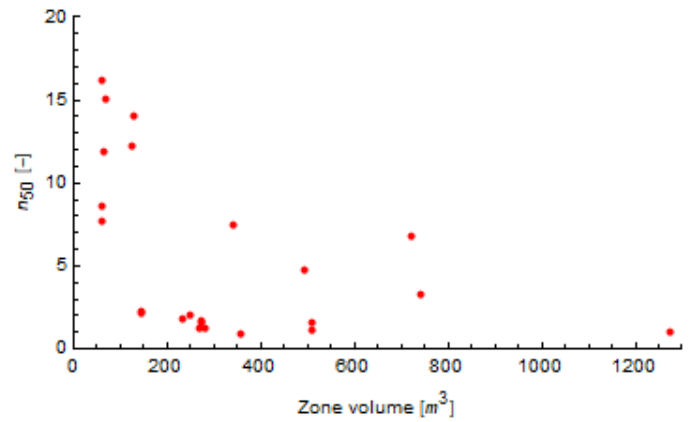


Figure 11. Relation n_{50} to zone volume.

Figure 11 shows the relationship between the resulting n_{50} and the tested zone volumes. It can be seen that the data from Figure 11 follows a nonlinear trend. All the other parameters behave similarly, so this is taken into account when observing the results. For that case, the results were presented on a graph with a logarithmic scale of both axes. Table 1 shows the statistical description of the data on which the study was conducted (parameters that are shown in Figure 2 – Figure 10).

Table 1. Statistical data description (count – number of samples, mean – mean value, std – standard deviation, min – minimal value, 25% – lower quartile, 50% – middle quartile, 75% – upper quartile, max – maximal value).

	Zone volume	Envelope area	Ae/Vo	Envelope to exterior		Envelope transparent		Zone height	n_{50}
	[m^3]	[m^2]	[m^{-1}]	[m^2]	%	[m^2]	%	[m]	-
mean	320.22	310.1	1,105	123.4	33.4	43.2	13.4	3.34	5.50

std	289.08	190.4	0.2657	139.6	21.6	55.5	15.2	1.06	5.13
min	60.03	94.2	0.601	15.5	11.0	6.0	3.7	2.62	0.96
25%	125.20	161.1	1,044	29.6	16.4	10.4	7.1	2.85	1.56
50%	266.43	309.0	1,169	75.4	23.6	23.5	8.6	2.99	2.31
75%	423.82	367.2	1,373	168.5	45.4	42.9	10.9	3.10	8.15
max	1273.66	766.0	1,568	598.5	78.1	240.0	66.1	7.30	16.15

2.2 Analysis method

For exploring the possible relations between selected parameters and n_{50} , a nonlinear fit of the experimental data was carried out. The analysis was done with Wolfram Mathematica [17], more specifically with function NonlinearModelFit. The function fits a nonlinear model of a predefined shape with parameters defined by the least-squares method. When observing the graphs of the relationship between all the analysed parameter and n_{50} (e.g. Figure 11) it can be seen that the best function that describes these relations is $a x^b$. In this function, x is variable and a and b are the parameters estimated by the least-squares method to describe the analysed dataset with a minimal deviation from all the values by comparing them to the function. Also, for each model fit, the adjusted R^2 value was introduced to observe the strength of the relationship between the selected parameters and n_{50} .

3 RESULTS

In order to present data and non-linear models more clearly, they are displayed on a log-log plot. The graphs also include the equation which describes data the best and adjusted R^2 that tells how well the data fit the nonlinear model. Relations between the selected parameters and the n_{50} are shown in Figure 12–Figure 19. As the analysis was done on 23 measurements (which is not a sufficient number to state the predictions with great certainty), the results will be interpreted by taking this into account – focusing rather on certain phenomena than on describing the nonlinear models to develop the predictive model from just 23 measurements. From the resulting graphs, it can be seen that data can be classified based on adjusted R^2 in three groups $R^2 > 0.75$ (Figure 12, Figure 13 and Figure 15), $0.6 < R^2 < 0.7$ (Figure 14, Figure 16 and Figure 17) and $R^2 \approx 0.5$ (Figure 18 and Figure 19). The interpretations of the graphs are presented alongside with conclusions in section 4. *Conclusion.*

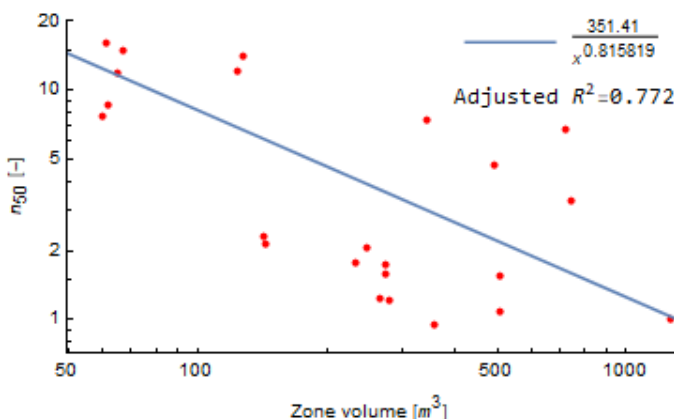


Figure 12. The relation between the zone volume and n_{50} .

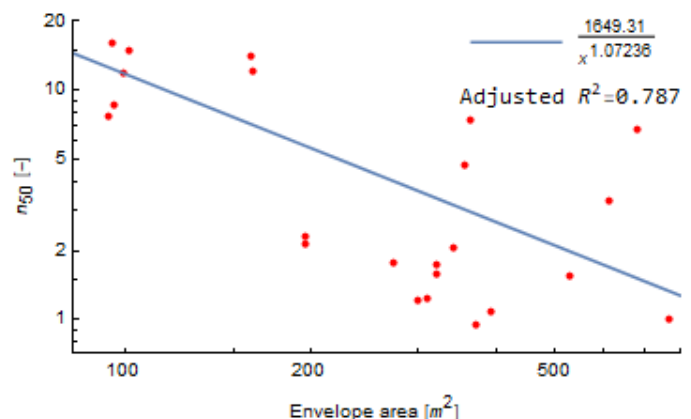


Figure 13. The relation between the envelope area and n_{50} .

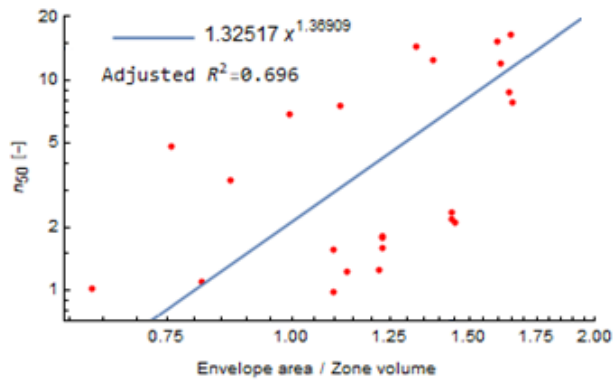


Figure 14. The relation between the envelope area/zone volume ratio and n_{50} .

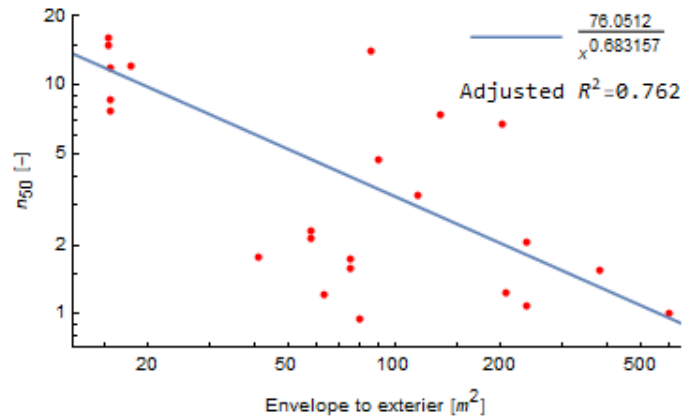


Figure 15. The relation between the area of the envelope that is a boundary to the exterior and n_{50} .

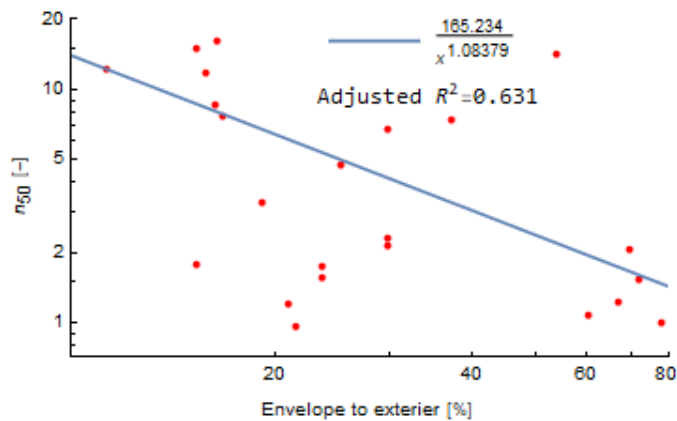


Figure 16. The relation between the percentage of the envelope that is a boundary to exterior and n_{50} .

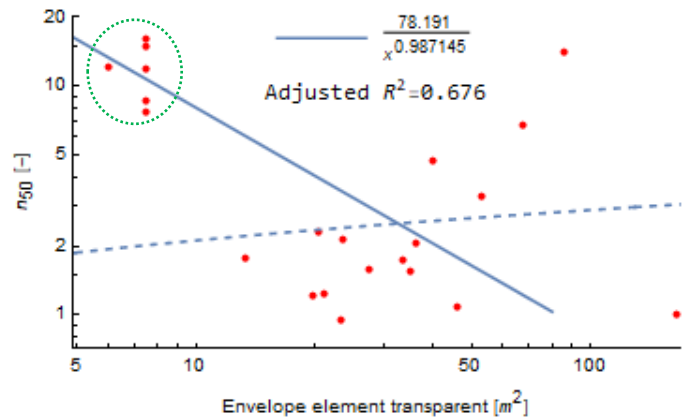


Figure 17. The relation between the area of transparent elements on envelope and n_{50} . Dashed-blue trend ($R^2 = 0.555$) is for data when neglecting the circled data.

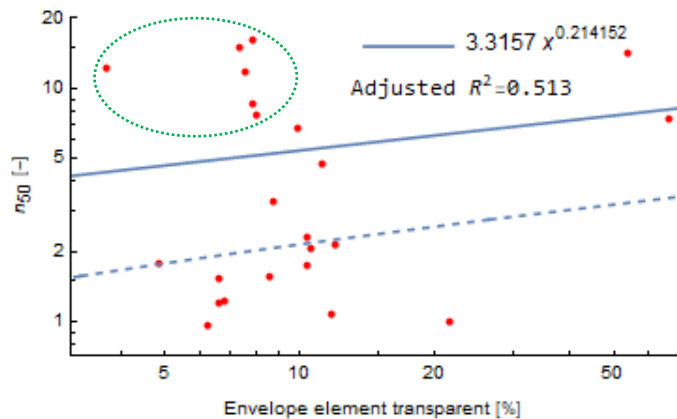


Figure 18. The relation between the percentage of the envelope that is transparent and n_{50} . Dashed-blue trend ($R^2 = 0.759$) is for data when neglecting the circled data.

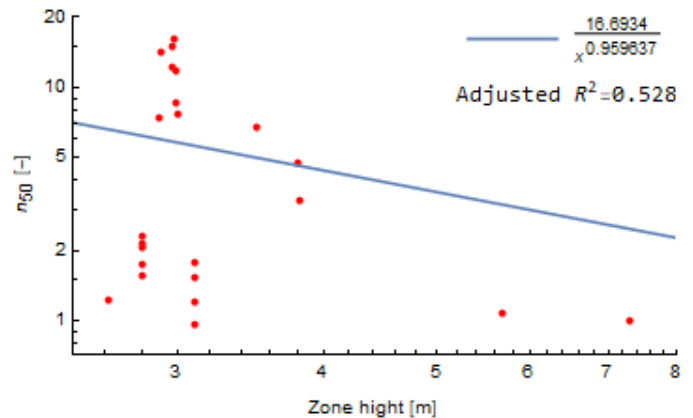


Figure 19. The relation between zone height and n_{50} .

4 CONCLUSION

The graphs from *Section 3. Results* show a few quite interesting facts. As can be seen in Figure 12 and Figure 13, the results show that the smaller the zones are, the greater n_{50} is. Also, the result database contains two research studies in which a multi-zone part was tested by testing it as a whole and then by testing subzones that are forming it. For both studies, n_{50} had a lower value for multi-zone part than expected. For one of these two studies, the recorded result of n_{50} was even smaller when testing all zones together than in the case when each subzone was tested separately. Therefore, it could be concluded that smaller zones could have greater “sensitivity” on envelope defects, probably due to more equally distributed pressure on the envelope surface than in the case of the bigger zones (especially when observing the

envelope area). For the same reason, it could be explained that with the increase of the zone height, n_{50} decreases (Figure 19).

It can be concluded that with the increase of the envelope area/zone volume ratio n_{50} decreases which can be due to more complex geometry that envelopes the zone volume so there are more spots where deficiency or crack can occur. From Figure 15 and Figure 16, one worrying phenomenon can be seen. With the increase of the envelope area, which is exposed to the exterior, n_{50} is decreasing. The reason could be poor airtightness between the interior zones which should be ensured amongst fire protection measures.

When analysing the percentage of transparent parts on the envelope, it can be seen in Figure 18 that if the percentage of transparent parts increases, the n_{50} also increases. The reason could be the increasing of the windows' frame length (a boundary between opaque and transparent parts) as that is a place where the most often the leakages occur. If we neglect the data which represents buildings with worn-out windows (circled dashed-green data in Figure 17), the same behaviour can be seen as in Figure 18 (dashed blue model). The analysis also showed that these are the only two parameters which change the behaviour of the model drastically when the data from worn-out windows is neglected. For other models the behaviour is similar to the one which includes data from new and old windows (the difference between blue and dashed-blue line) and does not affect the interpretations and conclusions.

Although this study presents research on a relatively small number of test results, some promising conclusions were presented. For future research, it is necessary to develop a grading system for assessing the quality of construction of the elements forming the building envelope because they impact the airtightness the most. After that, it is essential to perform a much more detailed analysis that will show the dependency of n_{50} on each new parameter and old ones, amended with new observations based on the grading system.

ACKNOWLEDGMENTS

One of the authors (Sanjin Gumbarević) would like to acknowledge the Croatian Science Foundation and the European Social Fund for the support under the project ESF DOK-01-2018.

REFERENCES

- [1] European Commission: *Energy Efficiency Plan 2011*. Brussels
- [2] European Parliament and the Council of the European Union: *Directive 2010/31/EU of the European Parliament and of the Council of 19 May 2010 on the energy performance of buildings (recast)*. European Parliament
- [3] European Parliament and the Council of the European Union: *Directive (EU) 2018/844 of the European Parliament and of the Council of 30 May 2018 amending Directive 2010/31/EU on the energy performance of buildings and Directive 2012/27/EU on energy efficiency*
- [4] European Parliament and the Council of the European Union: *Directive 2012/27/EU of the European Parliament and of the Council of 25 October 2012 on energy efficiency*
- [5] European Parliament and the Council of the European Union: *Directive (EU) 2018/2002 of the European Parliament and of the Council of 11 December 2018 amending Directive 2012/27/EU on energy efficiency*
- [6] Perera, M.D.A.E.S.; Marshal, S.G.; Solomon, E.W.: *Ventilation for Energy Efficiency and Optimum Indoor Air Quality. 13th AIVC Conference "Ventilation for Energy Efficiency and Optimum Indoor Air Quality,"* Nice, France, (1992)
- [7] Sherman, M.H.; Chan, R.: *Building Airtightness: Research and Practice*
- [8] Sherman, M.H.: *Tracer-gas techniques for measuring ventilation in a single zone. Build Environ 25(4):365–74, (1990). Doi: 10.1016/0360-1323(90)90010-O*
- [9] Prignon, M.; Van Moeseke, G.: *Factors influencing airtightness and airtightness predictive models: A literature review. Energy Build 146:87–97, (2017). Doi: 10.1016/j.enbuild.2017.04.062*
- [10] Fernández-Agüera, J.; Domínguez-Amarillo, S.; Sendra, J.J.; Suarez, R.: *Predictive models for airtightness in social housing in a Mediterranean region. Sustain Cities Soc 51(July):101695, (2019). Doi: 10.1016/j.scs.2019.101695*
- [11] Montoya, M.I.; Pastor, E.; Carrié, F.R.; Guyot, G.; Planas, E.: *Air leakage in Catalan dwellings: Developing an airtightness model and leakage airflow predictions. Build Environ 45(6):1458–69, (2010). Doi: 10.1016/j.buildenv.2009.12.009*
- [12] Khemet, B.; Richman, R.: *A univariate and multiple linear regression analysis on a national fan (de)Pressurization testing database to predict airtightness in houses. Build Environ 146:88–97, (2018). Doi:*

- 10.1016/j.buildenv.2018.09.030
- [13] Krstić, H.; Koški, Ž.; Otković, I.I.; Španić, M.: Application of neural networks in predicting airtightness of residential units. *Energy Build*:160–8, (2014). Doi: 10.1016/j.enbuild.2014.08.007
- [14] Krstic, H.; Otkovic, I.I.; Todorovic, G.: Validation of a Model for Predicting Airtightness of Residential Units. *Energy Procedia* 78:1525–30, (2015). Doi: 10.1016/j.egypro.2015.11.182
- [15] Krstić, H.; Otković, I.I.; Kosiński, P.; Wójcik, R.: Validation of neural network model for predicting airtightness of residential and non-residential units in Poland. *Energy Build* 133:423–32, (2016). Doi: 10.1016/j.enbuild.2016.10.011
- [16] Sherman, M.R.; Grimsrud, D.T.: *Measurement of infiltration using fan pressurization and weather data*. Berkeley
- [17] Wolfram Research Inc.: *Mathematica*, Version 12.0. Champaign, Illinois, (2019)

13

Kristina Hadzievska, Toni Arangjelovski, Darko Nakov and Goran Markovski

Sulfate resistance of cement with different volumes of fly ash



SULFATE RESISTANCE OF CEMENT WITH DIFFERENT VOLUMES OF FLY ASH

Kristina Hadzievska¹, Toni Arangelovski², Darko Nakov² and Goran Markovski²

¹ DIU Urban Engineering DOOEL Skopje
France Preshern Str. 64 B-5, 1000 Skopje, Republic of North Macedonia
e-mail: hadzievskak@gmail.com

² University "Ss. Cyril and Methodius", Faculty of Civil Engineering - Skopje, Department of concrete and timber structures
Blvd "Partizanski Odredi" No 24, 1000 Skopje, Republic of North Macedonia
e-mail: arangelovskitoni@gf.ukim.edu.mk, nakov@gf.ukim.edu.mk, markovski@gf.ukim.edu.mk

SUMMARY: Sulfate attack is a complex severe set of chemical and physical processes that have great influence on concrete durability by changing the microstructure of the cement paste and concrete. Sulfate resistance of concrete should be obtained including requirements for low-permeability concrete, use of sulfate resistance cement and proper production of concrete. In this paper an extensive experimental research is presented on the possibility of using fly ash as a partial replacement of OPC clinker and its influence on the sulfate resistance of cement. For that purpose, four samples of fly ash from the TPP Bitola were taken in the time period of two weeks. All cement components including fly ash were completely tested from the aspect of chemical composition and physical properties. Two samples of fly ash which showed the biggest difference in their fineness were chosen for further investigations and preparation of cements. Laboratory cements were prepared by varying the quantity of fly ash as replacement of OPC clinker, from 0% to 50%. For all laboratory produced cements complete chemical analysis and determination of the physical and mechanical properties have been carried out. The method of Koch & Steinegger and the recommendations of the Technical Committee of Cement given in CEN/TR 15697 were used for determination of sulfate resistance of the laboratory cements. According to this method, small specimens (prisms with dimensions 10/10/60mm) were prepared and then cured in deionized water and aggressive solution – 4.4% Na₂SO₄. The corrosion coefficient calculated on the basis of flexural strength of the specimens tested after 56 days in aggressive solution was used as indicator of sulfate resistance of the cements. On the basis of the test results, it is determined that the fly ash and all laboratory cements fulfil the quality criteria defined in the standards. It is also concluded that the cements with 30% fly ash show the best results from the aspect of sulfate resistance.

KEY WORDS: fly ash, sulfate resistance, aggressive sodium sulfate solution, Koch & Steinegger method

1 INTRODUCTION

Sulfate attack is the term used to describe a series of chemical reactions between sulfate ions and the components of hardened concrete, principally the cement paste, caused by exposure of concrete to sulfates and moisture. As is the case with other aggressive chemicals, sulfates are potentially most deleterious to concrete when present in gaseous or liquid form, the latter situation being the most common; attack by solid sulfate-containing chemicals is rare [1].

Some accepted facts about sulfate attack are: sulfate attack is not a single or a simple chemical reaction; it is a complex sequence of physical and chemical processes resulting in chemical and physical (micro-structural) modifications of the cement paste matrix; restructuring of the matrix is eventually evidenced by several possible modes of deterioration and leads to loss of mechanical and physical properties expected of any particular concrete structure; sulfate attack is not fully characterized by any one of the many possible reactions between the sulfate and cement paste components (e.g., presence of ettringite, formation of gypsum, dissolution of calcium hydroxide or decalcification of calcium silicate hydrate); relationships between the degree of chemical, physical or microstructural change caused by sulfate attack reactions and the degree of mechanical damage are complex and non-linear [2].

The resistance that a cement matrix provides to sulfate attack depends on a number of factors included: nature of the reaction products formed with the sulfate solution and in particular, whether their formation results in disruptive expansion; impermeability of the matrix (including the important paste-aggregate interfacial zone) which provides a barrier against penetration of sulfate ions; concentration of sulfate ions (g/l SO₄); mobility of the sulfate containing groundwater; nature of

accompanying cation e.g. Na^+ , Mg^{2+} , Ca^{2+} etc.; pH of the sulfate bearing ground water/solution; presence of other dissolved salts such as chlorides; temperature of the exposure; degree of pre-curing before exposure, although in the field this is only likely to affect the performance of the concrete surface; presence of finely divided limestone (calcium carbonate) in the aggregate, or carbonate ions dissolved in the groundwater, which may promote the formation of thaumasite under low temperature conditions [3].

In the standard EN 206 sulfate corrosion is defined under the chemical attack according to the exposure classes XA2 and XA3 for which use of sulfate resistance Portland cement conforming to EN 197-1:2011 [4] is mandatory (Annex F Recommendation for limiting values of concrete composition from EN 206:2013+A1:2016 [5]).

Current sulfate resisting cements standardised in CEN members' countries can be divided into two categories: Portland cements (CEM I) with a maximum permitted C_3A content and Portland composite cements containing appropriate levels of glassy blast furnace slag, fly ash or natural pozzolana. Portland composite cements (i.e. CEM II, III, IV and V types) provide resistance to sulfate attack which is predominantly micro-structural in nature [3].

Use of mineral additives such as fly ash in the cements is most promising to control sulfate attack to concrete, but so far there is no sulfate resistance Portland fly ash cement approved by the EN 197-1:2011 [4]. The problem of defining sulfate resistance of Portland cement is because there are many different mortar test procedures: standardised ASTM C1012, GOST 4798, round robin as a draft EN standard under activities of WG12/TG1 and methods used in Germany such as Wittekindt, SVA and Koch Steinegger. The test procedures share the following characteristics: specimens have a high surface to volume ratio; with the exception of the GOST test procedure the use of highly concentrated Na_2SO_4 solutions (16 g/l SO_4^{2-} to 34 g/l SO_4^{2-}); replacement of the Na_2SO_4 solution at monthly intervals (apart from the ASTM C1012 timings which vary according to age); use of nationally (or European) standardised test sand; assessment of sulfate resistance at an early age e.g. 56 days in the Wittekindt test and rather poor reproducibility [3].

To determine the influence of mineral addition of fly ash to the sulfate resistance of Portland cement, a laboratory cements were produced with different percentage of fly ash ranging from 11% to 50% from the weight of OPC clinker. Following types of cement were used: C1-Portland cement CEM I, C1-11 Portland fly ash cement with addition of 11% of siliceous fly ash which simulate the properties of commercially available cement CEM II/A-V 42.5R from USJE factory TITAN Group, C1-20 Portland fly ash cement with addition of 20% of siliceous fly ash, C1-30 Portland fly ash cement with addition of 30% of siliceous fly ash, C1-40 Portland fly ash cement with addition of 40% of siliceous fly ash and C1-50 Portland fly ash cement with addition of 50% of siliceous fly ash.

Sulfate resistance of the cements was tested using the Koch &Steinegger method given in CEN/TR 15697:2008 [3] Cement – Performance testing for sulfate resistance – State of the art report. A 4.4% sodium sulfate solution Na_2SO_4 with solution concentration of 29.8 g/l SO_4^{2-} , was used for immersion of specimens for a certain time of period 21+56 days. Small size specimen prisms 10/10/60mm were used with surface/volume ratio of $0.43\text{mm}^2/\text{mm}^3$. For 21 days the specimens first were cured in ionized water. Then certain number of specimens were immersed in sodium sulfate solution. The specimens were tested at age of 21+28, 21+56 and 21+90 days to determine the flexural strength and the compressive strength. Results from testing flexural strength were used to determine the sulfate resistance coefficient S_r at age of 21+56 days.

2 EXPERIMENTAL PROGRAM

2.1 Testing of components for preparation of laboratory cements

2.1.1 OPC clinker

OPC clinker is the main component used for preparation of laboratory cements. The same is taken from the regular production of Cement Factory TITAN Skopje. After crushing in laboratory crusher, the sieve analysis of the OPC clinker has been carried out. Complete phase composition was done using the XRD method (X-ray diffraction analysis) and it is concluded that the main component of the OPC clinker is calcium oxide (CaO) with content of more than 60% [6]. The content of C_3A is 13% which indicates that this OPC clinker is not resistant to sulfate attack.

The phase composition of the OPC clinker is carried out using the method of X-ray diffraction. The results are

presented in Table 1. It is obvious that dominate mineral phase in the OPC clinker is C_3S phase with 60.7% followed by C_2S phase with 11.5%, C_3A phase with 13% and C_4AF phase with 7.7%.

Table 1: Phase composition of OPC clinker

Phase name	Mass.%
C_3S	60.7
C_2S	11.5
C_3A	13.0
C_4AF	7.7
Portlandite	1.7
Periclase	1.9
Arcanite	0.7
Lime	0.1
Quartz	0.9
Anorthite	1.6
Σ	100.0

2.1.2 Gypsum

Gypsum which was used for preparation of the cements is a product of Factory Knauf Radika from Debar. After drying, the gypsum was tested from the aspect of its grain size composition. The data for humidity, chemical and mineralogical composition of gypsum are taken from the regular periodic tests done in Cement Factory TITAN.

2.1.3 Fly ash

The siliceous fly ash from Thermal Power Plant Bitola was used as a mineral additive for the purpose of this experimental research. The samples for testing of fly ash were previously prepared using standard procedures. Complete chemical analysis according to EN 196-2:2013 [7] was carried out and the results are presented in Table 2 [6,8].

Table 2: Chemical composition of the fly ash

Chemical component	Mass.%
SiO_2	55.51
Al_2O_3	22.06
Fe_2O_3	8.25
CaO	5.20
SO_3	0.91
MgO	2.19
Na_2O	0.59
K_2O	2.80
Loss of ignition	1.41
Σ	98.92

From the aspect of chemical composition, the main component of the fly ash is SiO_2 with 55.51%. The content of CaO is 5.20%. According to the criteria for classification of fly ash given in EN 450-1:2012 [9], the fly ash used in this research is siliceous fly ash (V).

One factor that have positive influence on the sulfate resistance is the content of 0.91% SO_3 in the chemical composition of fly ash. Higher level of SO_3 in a range between 1% to 4% provide greater resistance to sulfate attack.

The improved resistance can be attributed to the increased level of sulfated phases, such as ettringite, formed during initial hydration, which are stable in the presence of an elevated sulfate level [3].

Morphology of the particles of fly ash is determined using SEM analysis. SE images of fly ash are presented below in Figure 1. It is evident that the fly ash contains agglomerates with different sizes mainly containing primary particles less than 10µm.

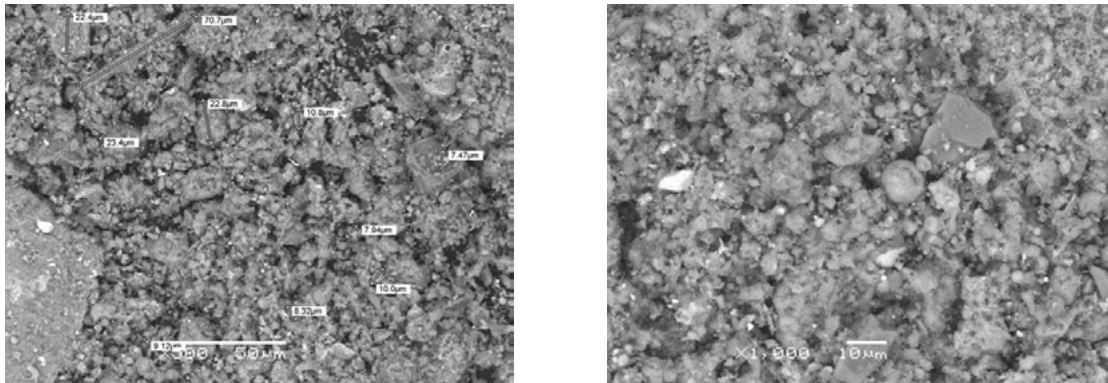


Figure 1: SE images of fly ash

The following tests are additionally carried out: determination of physical properties, mineralogical analysis and trace elements analysis as well.

2.2 Preparation and classification of laboratory cements

Laboratory cements were prepared by milling the constituents (OPC clinker, gypsum and fly ash). The capacity of the milling machine is 5kg with milling time of 35min. In order to achieve more efficient milling, special additive in amount of 2ml has been added.

For the purpose of this research, six laboratory cements were prepared by varying the quantity of fly ash as partial replacement of the OPC clinker from 0% to 50%. In Table 3 below, marking of all laboratory produced cements, as well as content of the constituents is presented [6,8].

Table 3: Laboratory produced cements

Cement type	Content of constituents (%)		
	OPC clinker	Gypsum	Fly ash
C	95	5	0
C-11	84	5	11
C-20	75	5	20
C-30	65	5	30
C-40	55	5	40
C-50	45	5	50

In accordance with the criteria for cement composition and marking given in EN 197-1:2011 [4], the laboratory cements can be classified as follows:

- Cement "C" – CEM I (Portland cement)
- Cement "C-11" and "C-20" – CEM II A/V (Portland cement with siliceous fly ash content between 6% and 20%)
- Cement "C-30" – CEM II B/V (Portland cement with siliceous fly ash content between 21% and 30%)
- Cement "C-40" and "C-50" – CEM IV/B (Pozzolanic cement with siliceous fly ash content between 36% and 55%)

All laboratory cements were tested from the aspect of their chemical composition and physical-mechanical properties. Additionally, the influence of content of fly ash in the cements on different parameters was analysed and certain conclusions were made. It is important to mention that the standard consistency increases with addition of fly ash in the cement in the range of 27.6% for Portland cement CEM I to 47% for cement C1-50. Standard consistency for the cements

C1-11, C1-20, C1-30, C1-40 and C1-50 are 31.6%, 32.0%, 38.4% and 46.0% respectively according to EN 196-3:2016 [10].

Determination of the cement compressive strength was performed using the EN Standard EN 196-1:2016 [11]. Results from the testing of compressive strength of cements is shown in Figure 2.

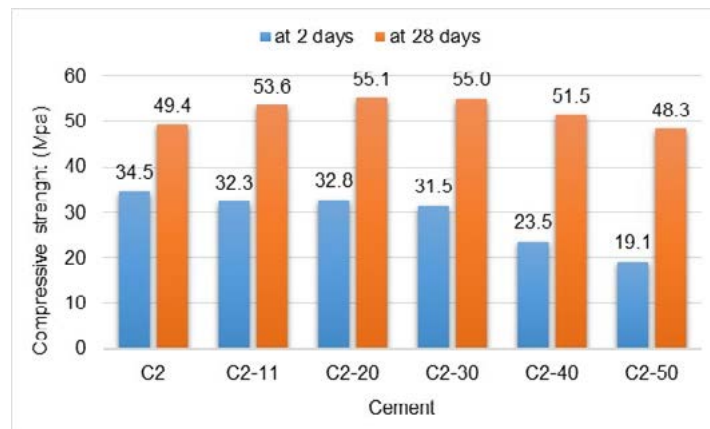


Figure 2: Compressive strength of cements at 2 and 28 days

According to the criteria given in EN 197-1:2011 [4], it can be concluded that all cements belong to the class of standard strength 42.5. The compressive strength of the cements at age of 28 days is within the limits of 42.5MPa and 62.5MPa. The pure cement and cements with 11%, 20%, 30% and 40% content of fly ash belong to the class of cement with high early strength 42.5R (compressive strength at age of 2 days higher than 20MPa). Only the cement with content of 50% fly ash belongs to the class of cement with normal early strength 42.5N (compressive strength R_c at age of 2 days < 20MPa).

2.3 Testing of influence of fly ash on the sulfate resistance of laboratory cements

The sulfate resistance of cements was tested and determined using the Koch & Steinegger method and the recommendations of the Technical Committee for Cement given in CEN/TR 15697:2008 [3]. According to this method, small specimens-prisms with dimensions 10/10/60mm were prepared. Specimens were made of mortar with cement/sand ratio 1:3 and water-cement factor $w/c=0.6$.

The specimens were cured in the mould for 24h in laboratory conditions (temperature $20\pm 2^\circ\text{C}$ and humidity higher than 80%). Then, the prisms were kept immersed in deionized water for 21 days. After that, half of the specimens were immersed in aggressive solution (4.4% Na_2SO_4) and the other half stayed immersed in deionized water for the whole testing period. The flexural and compressive strength of the prisms were tested at the age of 28, 56 and 90 days after immersing in aggressive solution and deionized water. The indicator of sulfate corrosion is the coefficient of sulfate resistance S_r , calculated as a ratio between flexural strength of the prisms cured in aggressive solution and the ones cured in deionized water at the age of 21+56 days. According to the Koch & Steinegger method, the cements are sulfate resistant if the value of this coefficient is higher than 0.7 [3]. Sulfate resistance coefficient is given by the following equation [3]:

$$S_r = \frac{\text{flexural strength of specimens cured in aggressive solution}}{\text{flexural strength of specimens cured in deionized water}} \geq 0.7$$

Figure 3. shows the way of curing the specimens in plastic containers.



Figure 3: Curing of specimens

Testing of the mechanical properties of the small specimens was carried out using hydraulic testing machine type “Controls 50kN”. Due to the small dimensions of the specimens, additional elements for supporting and load application were made. The speed of load application was 0.5mm/min for testing of flexural strength and 10mm/min for testing of compressive strength. Figure 4. shows the way of testing the mechanical properties of the specimens.



Figure 4: Testing of flexural and compressive strength

It should be noted that during the testing period, some of the specimens cured in aggressive solution suffered deformation and degradation. The specimens made of pure cement were deformed 18 days after immersion in 4.4% Na_2SO_4 solution. Development of such deformation and degradation, as well as change in specimens shape were regularly followed and registered up to the end of testing period. The deformed specimens made of pure cement are presented in Figure 5 [6].



Figure 5: Deformed prisms made of pure cement 18 and 90 days after immersion in 4.4% Na_2SO_4

Deformation and degradation of the specimens made of cement with 11% and 20% fly ash were also noticed later during the testing period. For example, the prisms with 20% fly ash suffered initial deformation and change in the shape 50 days after immersion in aggressive solution, which is shown in Figure 6 below.



Figure 6: Deformed prisms made of cement with 20% fly ash

The corrosion coefficient was calculated only for the cements with 30%, 40% and 50% fly ash as partial replacement of OPC clinker, i.e., the cements with higher content of fly ash. The reason for this is the fact that during the experimental research some of the specimens treated in aggressive solution were destroyed before reaching the expected age (21+56 days). The corrosion coefficient for these cements is presented in Table 4 [6,8].

Table 4: Values of the corrosion coefficient

Cement type	S_r coefficient
C-30	1.63
C-40	1.17
C-50	1.18

From the results presented above, it is obvious that the corrosion coefficient for the cements with higher content of fly ash is higher than the minimum value ($S_r=0.7$). In other words, according to the criteria given in Koch & Steinegger method, cements C-30, C-40 and C-50 are sulfate resistant cements.

The cement C-30 has the highest value for the corrosion coefficient which is for about 38.7% higher than values of the coefficient for cements with 40% and 50% fly ash. On the other hand, S_r for C-30 is for about 2.3 times, for C-40 and C-50 1.7 times higher than the minimal value of the corrosion coefficient ($S_r=0.7$) respectively.

3 CONCLUSIONS

On the basis of the performed tests of sulfate resistance of laboratory produced Portland-fly ash cement, the following conclusions have been reached:

- Laboratory produced Portland cements CEM I, Portland-siliceous fly ash cements noted as CEM II/A-V and CEM II/B-V fulfil the quality criteria defined in EN 197-1:2011 [4].

- Fly ash fulfil the quality requirements in terms of chemical composition and physical properties given in EN 450-1:2012 [9].

- Phase composition of the tested OPC clinker, used for laboratory produced cements, shows that the content of calcium aluminate is approximately 13%. This value is greater than the permitted 5% for sulfate-resisting Portland cement CEM I/SR 5 defined in EN 197-1:2011 [4].

- In terms of sulfate resistance, best behaviour in 4.4% sodium sulfate solution (Na_2SO_4) shows cement with 30% fly ash replacement of OPC clinker with sulfate resistance coefficient $S_r=1.63>0.7$. Cements which have a higher addition of fly ash (40% and 50%) are also sulfate resistant but with lower values of sulfate resistance coefficient $S_r=1.17$ and $S_r=1.18$ respectively. Use of mineral additives such as siliceous fly ash generally improves permeability of the Portland fly ash cement but higher content of siliceous fly ash also put more alumina (Al_2O_3) in the system which decreases sulfate resistance of the Portland-fly ash cement.

- The Koch & Steinegger method is just a one of many different methods for sulfate resistance test of cement defined in MKTI CEN/TR 15697:2008 [3] to be able to conclude that Portland-fly ash cement is sulfate-resistant. It is necessary to perform tests by other methods and applications of various sulfate solutions.

ACKNOWLEDGMENTS

The authors would like to express their gratitude to the following laboratories where the laboratory tests and investigations necessary for this research were carried out: Cement Factory "Usje" AD Skopje especially to Vladichevska Ljupka; Institute for Testing of Materials and Development of New Technologies "Skopje" AD Skopje; Department for Research, Development and Quality (R&D and Quality Department) of TITAN Group in Athens, Greece; Slovenian National Building and Civil Engineering Institute ZAG in Ljubljana, Slovenia; Institute for testing of materials IMS in Belgrade, Serbia and Fluxana GmbH & Co.KG in Bedburg-Hau, Germany.

REFERENCES

- [1] Skalny, J., Marchand, J., Odler, I.: Sulfate attack on concrete, SPON PRESS a Taylor & Francis Group, ISBN 0-419-24550-2 (Print Edition), London 2002
- [2] Skalny J.; Pierce S. J.: Sulfate attack: An Overview, Materials Science of Concrete: Sulfate Attack Mechanisms, The American Ceramic Society, ISBN 1-57498-074-2, Westerville, 1999, pp.49-63
- [3] CEN (Comité Européen de Normalisation) CEN/TR 15697:2008 Cement – Performance testing for sulfate resistance – State of the art report, Brussels, Belgium (provided by ISRSM-Standardization Institute of the Republic of North Macedonia)
- [4] CEN (Comité Européen de Normalisation) EN 197-1:2011 Method of testing cement – Part 1: Composition, specifications and conformity criteria for common cements, Brussels, Belgium (provided by ISRSM-Standardization Institute of the Republic of North Macedonia)
- [5] CEN (Comité Européen de Normalisation) EN 206:2013+A1:2016 Concrete-Specification, performance, production and conformity, Brussels, Belgium (provided by ISRSM-Standardization Institute of the Republic of North Macedonia)
- [6] Hadzievska K., Sulfate resistance of cement with fly ash, University "Ss Cyril and Methodius", Faculty of Civil Engineering – Skopje, February 2019, master thesis
- [7] CEN (Comité Européen de Normalisation) EN 196-2:2013 Method of testing cement - Part 2: Chemical analysis of cement, Brussels, Belgium (provided by ISRSM-Standardization Institute of the Republic of North Macedonia)
- [8] Hadzievska, K., Arangjelovski, T., Fidanchevska, E., Vladichevska, Lj., Popovska, M.: Influence of fly ash on sulfate resistance of cement, Proceedings of 18th International Symposium of Macedonian Association of Structural Engineers, Cvetkovska., M. (Ed.), pp. 1387-1396, ISBN: 978-608-4510-36-9, Ohrid, October 2019, Jofi-Sken, Skopje, 2019
- [9] CEN (Comité Européen de Normalisation) EN 450-1:2012 Fly ash for concrete - Part 1: Definition, specifications and conformity criteria, Brussels, Belgium (provided by ISRSM-Standardization Institute of the Republic of North Macedonia)
- [10] CEN (Comité Européen de Normalisation) EN 196-3:2016 Method of testing cement - Part 3: Determination of setting times and soundness, Brussels, Belgium (provided by ISRSM-Standardization Institute of the Republic of North Macedonia)
- [11] CEN (Comité Européen de Normalisation) EN 196-1:2016 Methods of testing cement - Part 1: Determination of strength, Brussels, Belgium (provided by ISRSM-Standardization Institute of the Republic of North Macedonia)
- [12] CEN (Comité Européen de Normalisation) EN 196-5:2011 Method of testing cement – Part 5: Pozzolanicity test for pozzolanic cement, Brussels, Belgium (provided by ISRSM-Standardization Institute of the Republic of North Macedonia)
- [13] CEN (Comité Européen de Normalisation) EN 196-6:2018 Method of testing cement – Part 6: Determination of fineness, Brussels, Belgium (provided by ISRSM-Standardization Institute of the Republic of North Macedonia)
- [14] CEN (Comité Européen de Normalisation) EN 196-7:2007 Method of testing cement – Part 7: Methods of taking and preparing samples of cement, Brussels, Belgium (provided by ISRSM-Standardization Institute of the Republic of North Macedonia)
- [15] CEN (Comité Européen de Normalisation) EN 450-2:2005 Fly ash for concrete - Part 2: Conformity evaluation, Brussels, Belgium (provided by ISRSM-Standardization Institute of the Republic of North Macedonia)
- [16] CEN (Comité Européen de Normalisation) EN 451-1:2017 Method of testing fly ash. Determination of free calcium oxide content, Brussels (provided by ISRSM-Standardization Institute of the Republic of North Macedonia)
- [17] CEN (Comité Européen de Normalisation) EN 451-2:2017 Method of testing fly ash. Determination of fineness by wet sieving, Brussels, Belgium (provided by ISRSM-Standardization Institute of the Republic of North Macedonia)

14

Ivan Hafner, Tvrtko Renić, Tomislav Kišiček and Mislav Stepinac

Seismic strengthening of stone masonry structures – state of the art



SEISMIC STRENGTHENING OF STONE MASONRY STRUCTURES – STATE OF THE ART

Ivan Hafner¹, Tvrtko Renić², Tomislav Kišiček³ and Mislav Stepinac⁴

¹ University of Zagreb Faculty of Civil Engineering, Department of Structural Engineering
Fra Andrije Kačića-Miošića 26, 10000 Zagreb
e-mail: ivan.hafner@grad.unizg.hr

² University of Zagreb Faculty of Civil Engineering, Department of Structural Engineering
Fra Andrije Kačića-Miošića 26, 10000 Zagreb
e-mail: tvrtko.renic@grad.unizg.hr

³ University of Zagreb Faculty of Civil Engineering, Department of Structural Engineering
Fra Andrije Kačića-Miošića 26, 10000 Zagreb
e-mail: tomlav.kisicek@grad.unizg.hr

⁴ University of Zagreb Faculty of Civil Engineering, Department of Structural Engineering
Fra Andrije Kačića-Miošića 26, 10000 Zagreb
e-mail: mislav.stepinac@grad.unizg.hr

SUMMARY: In Croatia, a great amount of buildings are built in masonry. The majority of them were built before the development of seismic codes and a lot of them are vernacular, unreinforced structures. As a result, many of these buildings need to be evaluated and, if needed, strengthened. Today, codes and guidelines for the evaluation and retrofitting of existing masonry structures do exist but are not very comprehensive and require a lot of engineering subjective judgement to implement. Furthermore, the problem lies in the complexity of implementing retrofitting methods since most of the masonry buildings are in use (private or public) during the strengthening. Besides that, a great number of buildings in Croatia (i.e. City of Dubrovnik) and around the world built in stone masonry have a great heritage value so the requirements made by conservators play a part in the methods used as well. An overview of the most commonly used methods of seismic analysis and strengthening are presented in this paper. The main objective of this paper is to comprehend, gather and compare different state-of-the-art principles of seismic retrofitting of structures focusing on stone masonry. Different approaches are analysed and compared in order to get closer to a unified method of evaluation and strengthening of existing structures.

KEY WORDS: stone masonry, buildings, seismic capacity, strengthening methods, retrofitting methods

1 INTRODUCTION

Masonry is one of the pioneers in the field of civil engineering, as a material and as a construction system. Also, it is well established that masonry is one of the most commonly used materials in the world due to its construction simplicity and characteristics like fire resistance, sound and heat insulation and economic considerations. It is estimated that roughly 70% of the world's building stock is built in masonry [1]. A similar estimation is valid for Croatia. In addition, Croatia is very famous for the great number of stone masonry buildings that have immense cultural significance and high historical importance (i.e. Split, Dubrovnik). That alone is the reason why the assessment and rehabilitation of existing masonry structures must be conducted on a very high level [2], [3]. Most of these masonry buildings are vernacular, unreinforced structures built before the seismic codes were developed (1970's) and the data available about their material characteristics are quite scarce. So, a seismic evaluation and retrofitting are usually needed. The best indication of that is the fact that in the building sector in Croatia, it is recognized that up to 40% of the expenses are spent for the rehabilitation, modification and demolition of existing structures (see Figure 1) [4]. However, this issue is much more layered than this. In the last decade enormous sums of money were spent on the energy renovation of the EU building stock [5]. The same period was filled with very strong earthquakes throughout Europe that resulted in loss of human lives, severe damage of masonry and concrete structures and great economic losses. Moreover, structural damage was identified on a number of buildings which had already undertaken energy efficiency upgrades [5]. Therefore, it is clear that

seismic retrofitting should be a priority in the renovation and modification of existing masonry structures. It should also be mentioned that the problem lies in the complexity of implementing retrofitting methods for masonry buildings since most of them are in use (public or private) during the strengthening. Finally, as has already been stated, a fair amount of these buildings are built in stone masonry with great cultural value so requirements made by conservators should be fully met [6], [7]. In the following chapters an overview of the most commonly used methods of seismic retrofitting of masonry structures shall be presented, with an insight into some new and attractive methods and ideas. It should be noted that the seismic strengthening methods are connected to the area in which they are used and that the state of the art is usually done on a regional level. The methods will be compared and discussed throughout the paper with the main objective of getting closer to a unified method of evaluation and strengthening of existing masonry structures.

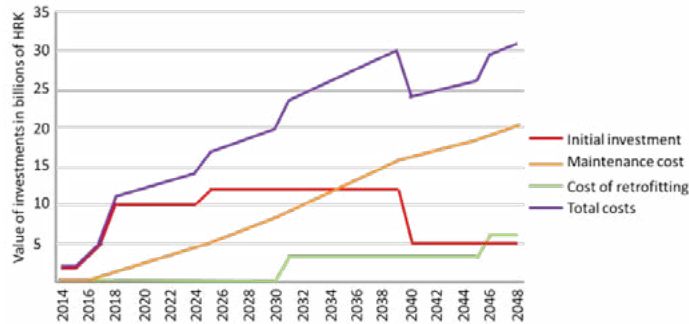


Figure 1: Investment in the renovation of Croatian national building stock [4]

2 RETROFITTING METHODS WITH METAL (STEEL) ELEMENTS

As a material, stainless steel has been used in the field of reinforcement and stabilizing of structures since the 1920's [8]. In recent years, the engineering community has paid more attention to FRP reinforcement than to steel reinforcement even though the latter has been in the market for quite some time and had a great number of applications. The initial cost of steel and the stronger commercialization of FRP are the strongest reasons for this problem [8]. However, great mechanical properties, reversibility of the methods and the limited mass addition of retrofitting interventions using stainless steel are very positive arguments that are making stainless steel a subject of great interest in the construction community, especially in the field of cultural heritage preservation [6]. If you also take into account that the use of steel elements largely increases the resistance and the ductility of the building during earthquakes, it is quite clear why stainless steel is the number one choice on most occasions. The first methods that are going to be shown are based on the different use of stainless-steel profiles (bars). The simplest earthquake resistant technique is the installation of stainless-steel profiles in the corners of stone masonry structures where two walls meet. The edges of the steel profiles are bent at the end and inserted into pre-drilled holes (Figure 2 a)) [9]. The second method known as the "Reticulatus system" consists of the insertion of stainless-steel cords in the mortar joints that have been stripped to a depth of 40-60 mm. After that the cords are embedded with new mortar and connected with transverse stainless-steel solid bars (5-8 mm diameter) in both vertical and horizontal direction forming a mesh of sorts (Figure 2 b)) [8]. Since the "Reticulatus method" can be performed from the outside of the building it should be recognized that this method can have a very good application in the reinforcement of stone masonry structures with high cultural and historical value that are in private or public use during the strengthening.

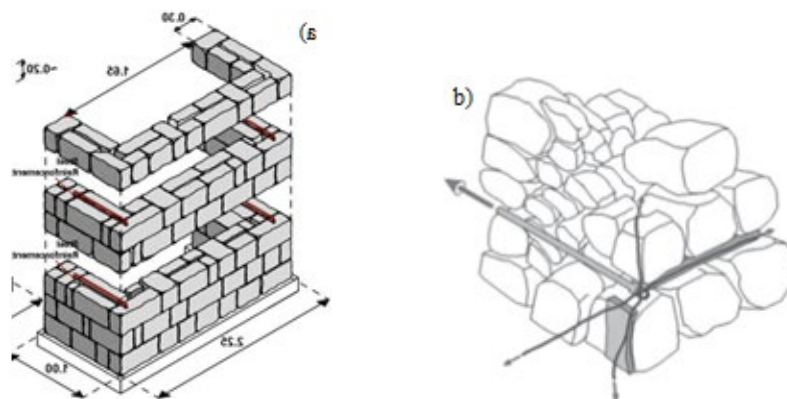


Figure 2: a) Bent stainless steel profiles [9]; b) “Reticulatus system” [8]

A similar method to the “Reticulatus system” is the “CAM” system (Active Confinement of Masonry) that is formed from stainless-steel ribbons distributed in a mesh pattern that are used as tie rods opposing to the deformation and disconnection of wall panels. The application of these ribbons requires drilling of small transverse holes in the wall (Figure 3) [8], [10]. Besides ribbons, an actual stainless-steel mesh can be used as well. On each face of the wall a steel mesh is placed, linked through transverse connectors with additional steel plates that are used in corners or openings. The plates are connected by screwed rods to provide an effective link between crossing walls (Figure 4) [11], [12].



Figure 3: Stainless-steel system using ribbons, plates and angular elements [10]

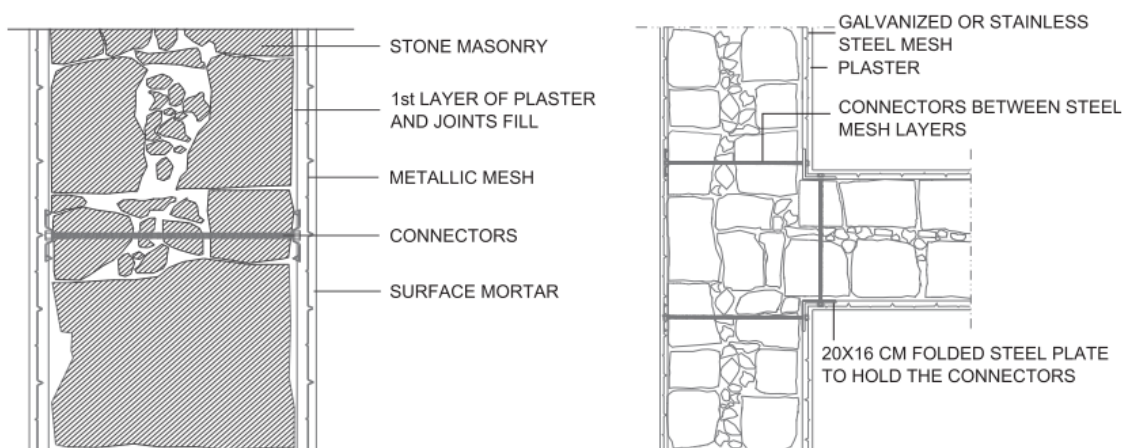


Figure 4: Stainless-steel mesh with corner reinforcement [11]

After the “mesh pattern” systems, some different methods using steel must be mentioned. One of the most commonly used methods that could almost be categorized as traditional is the use of metallic tie rods in a diagonal pattern [13]. This method is quite a suitable alternative since it is very cost effective and produces an increase in ductility capacity and energy dissipation. A similar, more up to date method, consists of stainless-steel strips that are placed in a diagonal pattern from the outside of the building. The method is conducted in a number of steps with the first being the removal of existing plaster. After that, the mortar joints are striped and repointed with new mortar and holes are drilled. The next step is to apply the stainless strips which are then fixed with steel nuts (Figure 5) [6]. Both of these methods can be applied from the outside of the building which is a great pro but on the other hand the façade will not stay intact because the reinforcement is quite visible. A fairly less known method is the use of stainless-steel cords that are embedded in either epoxy or mortar. The method is very simple and elegant and can be used for historic masonry structures. The method is shown in the picture (see Figure 6) [14]. In the end, specifically for stone masonry buildings with cultural value, different types of metal anchors (Figure 7) [15] and steel clamps and bolts (Figure 8) [16] can be used.



Figure 5: Stainless-steel strips [6]

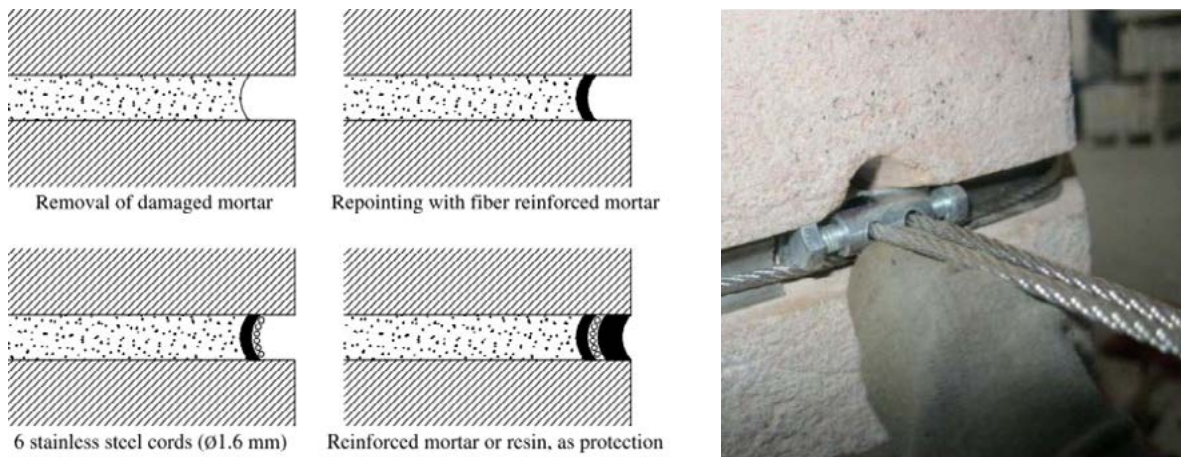


Figure 6: The application of stainless-steel cords [14]

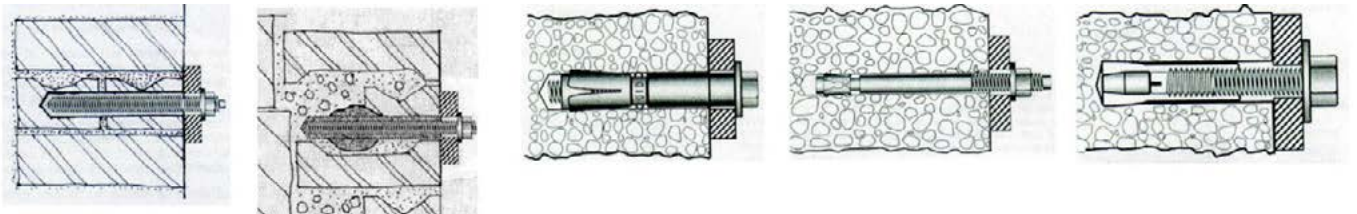


Figure 7: Different types of bonded anchors [15]

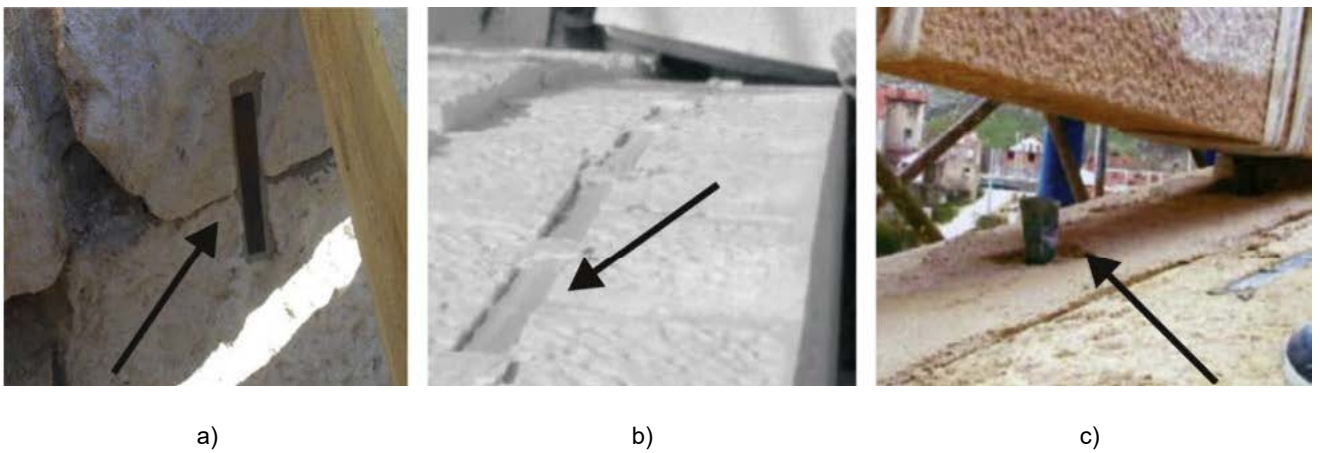


Figure 8: a),b) Steel clamps [15] c) Steel bolts [16]

3 RETROFITTING METHODS USING DIFFERENT TYPES OF MORTAR

As an infill and a binding element for stones, bricks and concrete masonry, mortar was already used in the ancient times when it was usually made from clay or mud. Throughout the years a great number of different variants of this binding material were invented (ordinary Portland cement mortar, polymer cement mortar, lime mortar etc.). Today, there are different types of mortar with high quality characteristics that can be used in the field of retrofitting and strengthening of masonry structures. Therefore, the focus is set on some new and different methods that are used for this purpose. Most commonly known as ECC, engineered cementitious composites are used as a retrofitting technique for improving the performance of unreinforced masonry structures. They can be defined as a type of cement composite reinforced with synthetic fibres (usually polymer fibres). When loaded by a tensile force, they exhibit a strain-hardening characteristic which significantly enhances the behaviour of structures under seismic loads adding both high tensile strength and ductility [17], [18]. Besides ECC, a similar type of mortar is available in today's market. FRCM or Fibre Reinforced Cementitious Matrix combines a high performance sprayable mortar with a fibre grid that create a thin layered system [19]. The biggest upside of this system is the lack of additional weight or volume to the existing structure. The two most frequently used types of FRCM should be differentiated depending on the type of fibre used in the system. Glass [20][21] (Figure 9 a)) and carbon [22] (Figure 9 b)) FRCM are the ones mostly associated with masonry structures. FRCMs are actually a particular part of Textile Reinforced Mortars or TRMs [22]. TRM consists of textile fibre reinforcement (with open-mesh configuration) combined with inorganic matrices (i.e. cementitious mortars) [5]. It is used as a strengthening and a retrofitting material for masonry structures based on high strength-to-weight ratio, minimal invasiveness, applicability at low temperatures, resistance at high temperatures, vapor permeability, easy and safe application for workers and most importantly chemical and mechanical compatibility with various masonry substrates and reversibility for heritage structures [23]. The use of TRM in masonry structures provides strengthening for axial loads, in-plane shear or flexure and out-of-plane flexure [23].

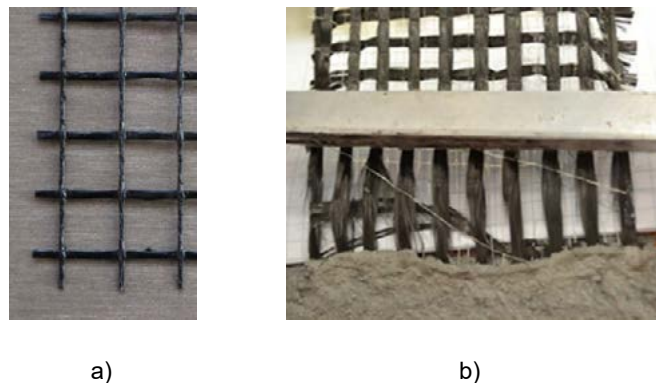


Figure 9: a) Glass fibre mesh [21] b) Carbon fibre mesh [22]

4 RETROFITTING METHODS USING FRP

In Fibre-Reinforced Polymers or FRPs a polymeric matrix of organized long fibres (one- or multi-directional) are arranged to create a composite material [24]. A sufficient bond with a masonry substrate is achieved through an organic, commonly epoxy agent [23]. The fibres provide high tensile strength while the agent (matrix) provides a dual role of protecting the fibres against the environment and transferring the stresses from the masonry to the fibres [24]. It should be stated that FRP, as a strengthening technique for buildings with cultural and historical value, is very appropriate since it is reversible, low weight, not time consuming and does not affect the aesthetics of buildings [25]. The greatest downside in the use of FRP products is the potential of brittle debonding which may decrease the effectiveness of strengthening. FRP products used for strengthening and retrofitting that are commercially available come in different forms like bars (rods), laminates (strips), meshes and tendons [1]. The differentiation between basic types of FRP is the material from which the fibres are made [1]. The three basic types are Glass (GFRP) [24]–[28], Aramid [24] and Carbon [24], [25], [27], [29], [30] fibres. When we talk about different methods of FRP reinforcement one of the most commonly used methods is based on using FRP strips (Figure 10 a)) [25], [28]–[30]. The basic idea is to polish the surface with a brush or high-pressure air on which the strips will be applied. The fabric of the strips is then soaked up with the epoxy resin and applied to the panel surfaces which were previously impregnated with the same resin [29]. The second method is based on reinforcing meshes made from FRP wires and epoxy resin (Figure 10 b)) [7], [26], [28]. The structural interaction between

the masonry wall and the mesh is guaranteed by specific connectors (Figure 10 c)) [26].

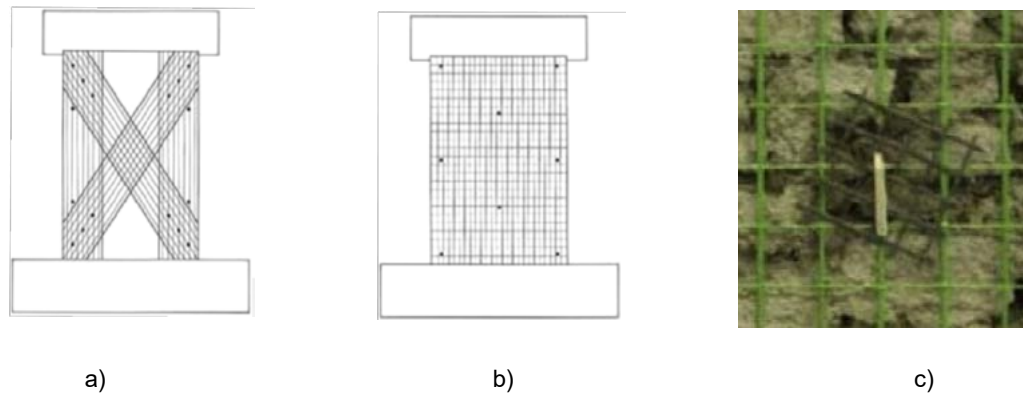


Figure 10: a) FRP strips [28] b) FRP mesh [28] c) L shaped connectors inserted in the wall [28]

A similar method to the mesh is the use of FRP sheets which are usually used for column confinement [24]. Also, a few very specific methods do exist. The use of carbon fibre rope is a technique very similar to the Near Surface Mounted Reinforcement (NSMR) technique used in RC structures. In this technique a braided carbon fibre rope is impregnated with an epoxy saturant and installed in prepared paths[31]. These pathways are created by cutting straight grooves running vertically through head joints and brick units (Figure 11 a)) and horizontally at bed joints (Figure 11 b)). After cutting and cleaning the grooves with compressed air, epoxy primer is applied. After installing the reinforcement, another layer of epoxy adhesive is applied to fully surround the FRP carbon fibre rope [31]. Last but not least is the sprayed-FRP method that has showed great promise in the field of seismic strengthening of both masonry and RC structures [32].

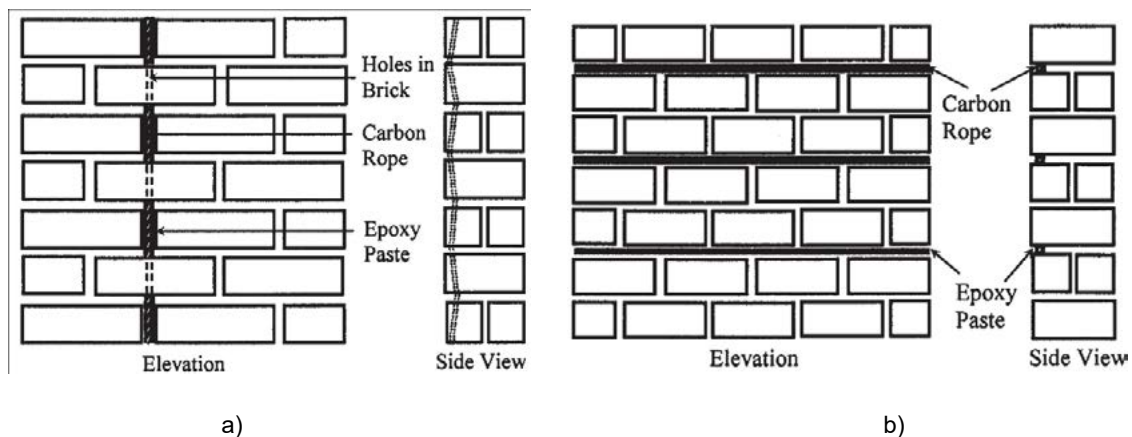


Figure 11: a) Installation of Carbon Fibre Rope as Vertical Reinforcement [31] b) Installation of Carbon Fibre Rope in Bed Joints [31]

5 SPECIFIC RETROFITTING METHODS

In this section a couple of specific methods, that haven't been classified before, will be dissected. The first method is very simple. It is based on building a wall that is parallel to an existing single-leaf wall. The two walls are then bonded with each other using a mortar joint merging them into a unified double-leaf wall [33]. The second method is similar to the "Reticulatus method" that was described in section 2 of this paper. Hybrid "Reticulatus" technique is a combination of the previously mentioned "Reticulatus method" and GFRM jacketing [26]. The technique is consisted of a continuous mesh made from stainless steel cords inserted into the mortar. The cords are arranged in the vertical and horizontal directions to form a mesh whose size typically depends on the dimensions of the stone elements. The intersecting nodes of these cords are then connected to the opposite face of the masonry wall by means of transverse stainless steel bars that are able to provide a full interaction between the cords and the specimen (see Figure 12) [26]. In the end, a series of traditional methods are shown in [34], [35] as well as various materials that are used in forming a mesh that is suitable as an effective strengthening technique [36].

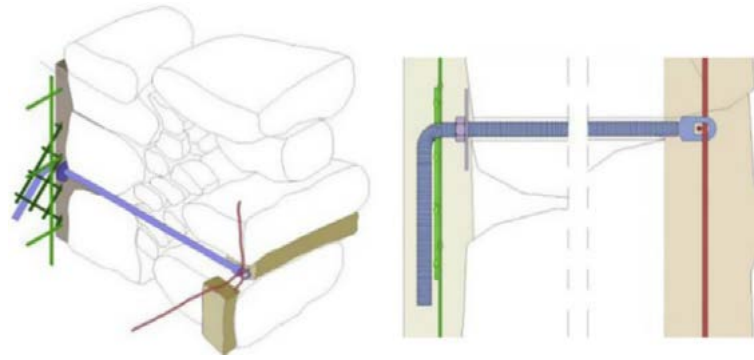


Figure 12: Hybrid "Reticulatus" strengthening technique [26]

6 CONCLUSION

As it was already stated, it is quite complicated to fulfil all the requirements that are set for the seismic retrofitting of existing masonry structures, especially for those that are built in stone. The first criterion is of course the financial aspect. The stainless-steel retrofitting methods and the ones using simple mortar still have an edge over FRP and FRCM methods even though it should be mentioned that the price of these products has severely dropped in the last few decades. On the other hand, if future costs are taken into consideration, corrosion does not affect FRP products which is very important when talking about future renovations and restoration. Also, the lower weight of FRP products and the easier manoeuvring at the construction site are great pros for these types of retrofitting methods. The possibility of conducting a retrofitting method while a building is in use should also be taken into consideration. With all of this said it is quite difficult to say which type of method should be used in seismic retrofitting of existing stone masonry structures, but a couple of them should be highlighted. The application of stainless-steel cords is quite interesting because no invasion in the interior of the building is needed, it is quite elegant and simple, and the financial aspect is satisfactory. A similar method is the use of Carbon Fibre Rope as a reinforcement with the possibility of retrofitting in vertical and horizontal direction as its best characteristic. Both methods are not that invasive with the façade practically staying the same which is extremely positive especially for buildings with high cultural value. For simple stone masonry structures the Hybrid "Reticulatus" technique should also be considered. In the end, it should be established that the field itself is going in the right direction, with more and more of new and inspiring methods being invented and tested that are slowly but surely replacing the traditional methods in seismic retrofitting.

ACKNOWLEDGMENT

The authors wish to acknowledge that this paper was made as a part of the ARES project, an Installation Research Project granted by HRZZ- Croatian Science Foundation.

REFERENCES

- [1] Babatunde, S. A.: "Review of strengthening techniques for masonry using fiber reinforced polymers," *Compos. Struct.*, Vol. 161 (2017), pp. 246–255.
- [2] Stepinac, M. et al.: "Methods for the assessment of critical properties in existing masonry structures under seismic loads-the ARES project," *Appl. Sci.*, Vol. 10 (2020), No. 5.
- [3] Stepinac, M.; Gašparović, M.: "A review of emerging technologies for an assessment of safety and seismic vulnerability and damage detection of existing masonry structures," *Appl. Sci.*, Vol. 10 (2020), No. 15.
- [4] Republic: "Proposal of the Long-Term Strategy for Mobilising Investment in the Renovation of the National Building Stock of the Republic of Croatia," Vol. (2014), No. April.
- [5] Bournas, D. A.: "Concurrent seismic and energy retrofitting of RC and masonry building envelopes using inorganic textile-based composites combined with insulation materials: A new concept," *Compos. Part B Eng.*, Vol. 148 (2018), pp. 166–179.
- [6] Borri, A. et al.: "Stainless steel strip – A proposed shear reinforcement for masonry wall panels," *Constr. Build. Mater.*, Vol. 211 (2019), pp. 594–604.

- [7] Juhássová, E. et al.: "Stone masonry in historical buildings - Ways to increase their resistance and durability," *Eng. Struct.*, Vol. 30 (2008), No. 8, pp. 2194–2205.
- [8] Corradi, M. et al.: "A review of the use of stainless steel for masonry repair and reinforcement," *Constr. Build. Mater.*, Vol. 181 (2018), pp. 335–346.
- [9] Murano, A. et al.: "Influence of traditional earthquake-resistant techniques on the out-of-plane behaviour of stone masonry walls: Experimental and numerical assessment," *Eng. Struct.*, Vol. 201 (2019), No. February, p. 109815.
- [10] Spinella, N. et al.: "Experimental in situ behaviour of unreinforced masonry elements retrofitted by pre-tensioned stainless steel ribbons," *Constr. Build. Mater.*, Vol. 73 (2014), pp. 740–753.
- [11] Diz, S. et al.: "Efficiency of strengthening techniques assessed for existing masonry buildings," *Eng. Struct.*, Vol. 101 (2015), pp. 205–215.
- [12] Branco, M.; Guerreiro, L. M.: "Seismic rehabilitation of historical masonry buildings," *Eng. Struct.*, Vol. 33 (2011), No. 5, pp. 1626–1634.
- [13] Rinaldin, G. et al.: "Cyclic behavior of masonry walls strengthened by tie rods," *Eng. Struct.*, Vol. 184 (2019), No. January, pp. 287–300.
- [14] Borri, A. et al.: "Masonry confinement using steel cords," *J. Mater. Civ. Eng.*, Vol. 25 (2013), No. 12, pp. 1910–1919.
- [15] Muñoz, R. et al.: "Experimental results on mechanical behaviour of metal anchors in historic stone masonry," *Constr. Build. Mater.*, Vol. 163 (2018), pp. 643–655.
- [16] Smoljanović, H. et al.: "A finite-discrete element model for dry stone masonry structures strengthened with steel clamps and bolts," *Eng. Struct.*, Vol. 90 (2015), pp. 117–129.
- [17] Deng, M.; Yang, S.: "Cyclic testing of unreinforced masonry walls retrofitted with engineered cementitious composites," *Constr. Build. Mater.*, Vol. 177 (2018), pp. 395–408.
- [18] Li, V. C.: "On Engineered Cementitious Composites (ECC)," *J. Adv. Concr. Technol.*, Vol. 1 (2003), No. 3, pp. 215–230.
- [19] Maddaloni, G. et al.: "Dynamic assessment of innovative retrofit techniques for masonry buildings," *Compos. Part B Eng.*, Vol. 147 (2018), pp. 147–161.
- [20] Feo, L. et al.: "Irregular stone masonries: Analysis and strengthening with glass fibre reinforced composites," *Compos. Part B Eng.*, Vol. 92 (2016), pp. 84–93.
- [21] Estevan, L. et al.: "Stone masonry confinement with FRP and FRCM composites," *Constr. Build. Mater.*, Vol. 237 (2020), p. 117612.
- [22] Carozzi, F. G. et al.: "Experimental investigation of tensile and bond properties of Carbon-FRCM composites for strengthening masonry elements," *Compos. Part B Eng.*, Vol. 128 (2017), pp. 100–119.
- [23] Kouris, L. A. S.; Triantafyllou, T. C.: "State-of-the-art on strengthening of masonry structures with textile reinforced mortar (TRM)," *Constr. Build. Mater.*, Vol. 188 (2018), pp. 1221–1233.
- [24] Cascardi, A. et al.: "Reversible techniques for FRP-confinement of masonry columns," *Constr. Build. Mater.*, Vol. 225 (2019), pp. 415–428.
- [25] Simonič, M. J. et al.: "Ispitivanje i analiza nosivosti na posmik zidova ojačanih s FRP-om," *Gradjevinar*, Vol. 66 (2014), No. 6, pp. 533–548.
- [26] Gattesco, N. et al.: "Experimental and numerical study on the shear behavior of stone masonry walls strengthened with GFRP reinforced mortar coating and steel-cord reinforced repointing," *Eng. Struct.*, Vol. 90 (2015), pp. 143–157.
- [27] Zampieri, P. et al.: "A review of methods for strengthening of masonry arches with composite materials," *Eng. Struct.*, Vol. 171 (2018), No. May, pp. 154–169.
- [28] Triller, P. et al.: "Seismic Behavior of Strengthened URM Masonry - An Overview of Research at ZAG," *Procedia Eng.*, Vol. 193 (2017), pp. 66–73.
- [29] Luccioni, B.; Rougier, V. C.: "In-plane retrofitting of masonry panels with fibre reinforced composite materials," *Constr. Build. Mater.*, Vol. 25 (2011), No. 4, pp. 1772–1788.
- [30] Hamdy, G. et al.: "Plane and vaulted masonry elements strengthened by different techniques – Testing, numerical modeling and nonlinear analysis," *J. Build. Eng.*, Vol. 15 (2018), pp. 203–217.
- [31] Korany, Y.; Drysdale, R.: "Enhancing Flexural Resistance of Historic Masonry Walls Using Carbon Fibre Ropes," *Mason. Soc. J.*, Vol. 22 (2004), No. 1, pp. 27–38.
- [32] Parghi, A.; Alam, M. S.: "A review on the application of sprayed-FRP composites for strengthening of concrete and masonry structures in the construction sector," *Compos. Struct.*, Vol. 187 (2018), pp. 518–534.
- [33] Wang, C. et al.: "Retrofitting of masonry walls by using a mortar joint technique; experiments and numerical validation," *Eng. Struct.*, Vol. 117 (2016), pp. 58–70.
- [34] Maio, R. et al.: "The seismic performance of stone masonry buildings in Faial island and the relevance of implementing effective seismic strengthening policies," *Eng. Struct.*, Vol. 141 (2017), pp. 41–58.
- [35] Bhattacharya, S. et al.: "A critical review of retrofitting methods for unreinforced masonry structures," *Int. J. Disaster Risk Reduct.*, Vol. 7 (2014), pp. 51–67.
- [36] Chourasia, A. et al.: "Experimental investigation of seismic strengthening technique for confined masonry buildings," *J. Build. Eng.*, Vol. 25 (2019), No. June, p. 100834.

15

**Lucija Hanžič, Jurij Karlovšek, Tomaž Hozjan, Sabina Huč, Zhongyu Xu,
Igor Planinc and Johnny C.M. Ho**

Experimental and numerical investigation of restrained shrinkage of concrete



EXPERIMENTAL AND NUMERICAL INVESTIGATION OF RESTRAINED SHRINKAGE OF CONCRETE

Lucija Hanžič^{1,2*}, Jurij Karlovšek², Tomaž Hozjan³, Sabina Huč^{3,1}, Zhongyu Xu², Igor Planinc³ and Johnny C.M. Ho⁵

¹ Slovenian National Building and Civil Engineering Institute (ZAG)
Dimičeva ulica 12, 1000 Ljubljana, Slovenia
e-mail: info@zag.si, * lucija.hanzic@zag.si

² The University of Queensland, School of Civil Engineering
Bldg. 49, Staff Rd, St Lucia QLD 4072, Australia
e-mail: enquiries@civil.uq.edu.au

³ University of Ljubljana, Faculty of Civil and Geodetic Engineering
Jamova cesta 2, 1000 Ljubljana, Slovenia
e-mail: tajnistvo@fgg.uni-lj.si

⁴ University of Ljubljana, Faculty of Chemistry and Chemical Technology
Večna pot 13, 1000 Ljubljana, Slovenia
e-mail: info@fkkt.uni-lj.si

⁵ Guangzhou University, School of Civil Engineering
Guangzhou 510006, China

SUMMARY: To promote the understanding of shrinkage related behaviour of concrete used for tunnel linings the experimental and theoretical investigation including numerical and analytical approach was performed on ring-shaped specimens. Overall one analytical (an.) and two numerical models, namely (i) and (ii) were also developed. Models (an.) and (i) considered the restraining steel ring to be rigid, thus not exhibiting any deformation. Numerical model (ii) considered the steel ring to be deformable. The experimental set-up consisted of a large concrete ring with an inner diameter of 120 cm, an outer diameter of 160 cm and 20 cm in height. The restraining steel ring was 5.5 cm thick. Two concrete rings were made, namely R1 with a low compressive strength of ~26 MPa and the other, R2, with medium compressive strength of ~40 MPa. The strain was measured in the hoop direction on the inner circumference of the steel ring and on the outer circumference of the concrete ring. Concrete rings were subjected to circumferential drying. Numerical model (ii) predicted critical time to the formation of the first crack to be between 13 and 14 days. The experimentally determined critical time is found to be 11 to 13 days with cracks gradually opening over several days. This was indicated by changes in measured concrete and steel strain. Modelled concrete strain just before cracking was between -20 and $-30 \times 10^{-6} \text{ m m}^{-1}$ however, measured concrete strain was $\sim 150 \times 10^{-6} \text{ m m}^{-1}$. Modelled steel strain was between -30 and $-40 \times 10^{-6} \text{ m m}^{-1}$ while measured steel strain was between -10 and $20 \times 10^{-6} \text{ m m}^{-1}$. These discrepancies, in particular the positive steel strain obtained in experiments, require further investigation and improvements of the experimental set-up.

KEY WORDS: Concrete; tunnel lining; restrained shrinkage; Reissner beam theory; modelling.

1 INTRODUCTION

The concrete lining is applied in tunnels to resist the ground and water pressure. The lining is either cast-in-situ or constructed from the precast segments. It is important to apply the lining immediately after the excavation of a tunnel section to protect workers and equipment from the cave-ins or collapse of the unstable ground. The first protective lining is often applied by spraying concrete directly onto the walls of the excavated cavity where concrete sets and hardens, thus creating a protective layer. During the hardening process concrete shrinks due to chemical reactions and water evaporation. Shrinkage is restrained by the underlying rock or soil leading to stress gradients and cracking of the concrete layer. To further the understanding of the restrained shrinkage an analytical model based on the Reissner's beam theory has been proposed and presented by Hozjan et al [1]. The next milestone in this study is data collection via an experimental set-up and model verification.

The common method for measuring concrete shrinkage utilises a non-restrained beam. This method is implemented in standards like Australian standard AS 1012.13 [2] and European norm EN 12390-16 [3]. However, as stated by the *Concrete Institute of Australia*, relations between unrestrained and restrained shrinkage are complex with restrained shrinkage being less than unrestrained [4, p.25]. Therefore, various experimental configurations, summarized by Carlswärd [5], have been proposed to simulate concrete cracking under restrained shrinkage conditions, each with their own set of limitations and drawbacks. However, as can be seen from the work conducted by Weiss and his associates [6]–[8] the restrained shrinkage ring is being recognized as a good value-for-money test, owing to its simplicity, versatility and quantity of derived information.

Standard test implementing this method is American standard ASTM C 1581 [9] which is suitable for mortar and concrete with a maximum aggregate size of 13 mm. The ring specimen used in this test is rather small with the inner diameter, height and wall thickness being 33, 15 and 3.8 cm respectively. These dimensions are too small for sprayed concrete and therefore, a large shrinkage ring set-up is adopted in this study, with the inner diameter of the concrete ring being 120 cm and the outer diameter being 160 cm, yielding wall thickness of 20 cm [10]. The restraining element in this set-up is a steel ring located inside the concrete specimen. Strain measurements were taken on the inside of the steel ring and on the perimeter of the concrete ring, both in the hoop direction.

The main aim of this paper is to present the experimental results of the restrained shrinkage test carried out on two concrete rings, one with low and the other with medium strength concrete. Additionally, the analytical model reported in [1] is summarized and compared to a recently developed numerical model. Experimental results are assessed in terms of their suitability for model verification and the need for further improvements is discussed. Development of the presented shrinkage models aims to enhance the understanding of problems related to the cracking of concrete lining in tunnels.

2 EXPERIMENTAL

The large restrained shrinkage ring consists of a pedestal with push-up hydraulic supports. Plywood sections are placed onto the pedestal so that together with the supports in a retracted position they constitute the base part of the formwork. Steel ring with an outer diameter of 120 cm, the height of 20 cm and the wall thickness of 5.5 cm is placed onto the pedestal. A metal strip, folded into a circle with a diameter of 160 cm, is laid concentrically around the steel ring with spacers keeping the metal strip 20 cm from the steel ring at any point. Metal strip and steel ring thus constitute the vertical part of the formwork into which the concrete is cast. Once concrete sets and gains enough strength to support its own weight it is possible to use the push-up supports to lift the concrete and steel ring from the base and expose the bottom surface to drying. In this experiment, the concrete ring was exposed to circumferential drying only. Main parts of the restrained shrinkage test set-up are shown in a labelled photograph in Fig. 1a.

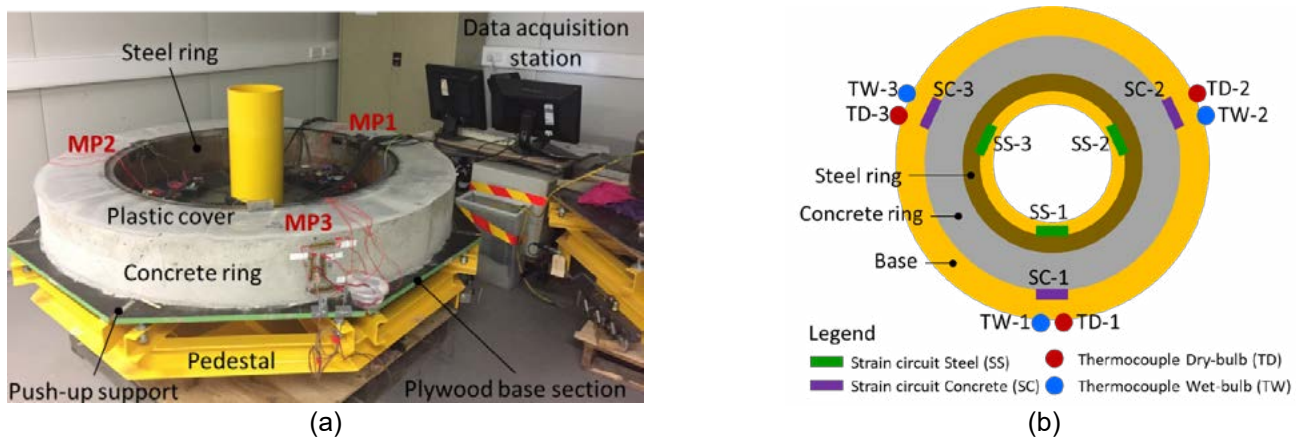


Figure 1: Experimental setup showing (a) photograph of the station with its parts labelled, and (b) schematics of measurement positions and instrumentation arrangement. “MP” stands for Measurement Point.

There are three measurement positions (MP) located circumferentially with 120° angle between adjacent points. Each MP consists of (1) a pair of thermocouples, (2) steel strain-gauge circuit, and (3) concrete strain-gauge circuit. Instrumentation arrangement is schematically presented in Fig. 1b. Thermocouples are attached to the base with a tip

situated half-height of the concrete ring. One serves as a dry-bulb and the other as a wet-bulb temperature gauge allowing for temperature and relative humidity measurements. Both, steel and concrete strain-gauge circuits are wired in a Wheatstone half-bridge configuration. The active arm of the circuit consists of two strain-gauges wired in a series and attached in the hoop direction. Two dummy strain-gauges are wired in a series onto the adjacent arm of the Wheatstone bridge. Such a configuration allows for temperature compensation. In the case of concrete, dummy strain gauges were attached vertically onto the concrete ring while in the case of steel they were attached on a separate steel plate which was placed in thermal contact with the steel ring. Wheatstone bridge was completed with resistors so that resistance of each arm was 240 Ω. All instruments were connected to a data logger *dataTaker DT800* programmed with *DeLogger* [11] software. Data were recorded every 30 s where each recorded value was an average of 30 measurements taken at 1 s intervals.

The experiment was set up in an air-conditioned room with a constant temperature of 20 ± 2 °C and relative humidity ranging between 60 and 80 %. Concrete was manually placed into the formwork and compacted by the means of poker vibrators. Spacers, holding the metal strip in place, were gradually removed and the gaps were filled with concrete. The surface was trowelled and covered with plastic to prevent evaporation. In addition, accompanying cylindrical specimens with a nominal diameter of 10 cm and a nominal height of 20 cm were cast as per AS 1012.8.1 [12]. These specimens were demoulded ~24 h after casting, wrapped in plastic and stored next to the shrinkage ring. They were used for determination of compressive strength and modulus of elasticity preferably on the day the first crack was observed.

The external circumference of the steel ring was lined with plastic to prevent adhesion of concrete to steel and therefore friction-related strain was assumed negligible. The metal sheet, which was removed ~24 h after casting, was coated with formwork lubricant. The concrete ring thus produced had an inner diameter of 120 cm while its thickness and height were 20 cm. In this experiment, the concrete ring was not lifted. Formwork base prevented drying through the bottom and plastic sheet prevented drying through the top. Hence, the concrete ring was exposed to circumferential drying only. Concrete strain-gauges were attached after demoulding. First, a hand-held grinder was used to remove the mortar layer locally at the three MP locations. Next, compressed air was used to blow off the dust particles and dry the surface. Finally, the surface was cleaned with ethanol and strain-gauges applied using CN-E adhesive from *Tokyo Measuring Instruments Lab*.

Two concrete rings, namely R1 and R2, each with its own mix design, were tested. Concrete mix design and properties of the constituent materials are given in Table 1. Concrete was prepared in a laboratory concrete pan mixer in two 110 L batches for each specimen. Cement was General Purpose (GP) type as defined by AS 3972 [13] and fly ash was Grade 1 according to AS 3582.1 [14]. Manufactured sand and coarse aggregate particles had angular grains while the grains of the river and fine sand were round. The aggregate composition was optimised using the particle size distribution data. All aggregates were dried before use.

Table 1: Properties of concrete components mix design for concrete rings R1 and R2 used in the restrained shrinkage test. Mix design is given as mass of components required for 1 m³ of concrete.

Concrete components and their properties					Concrete mix design (kg per 1 m ³ of concrete)	
Material		Symbol	Density (kg m ⁻³)	Water absorption (wt%)	R1	R2
Powders	Cement	C	3.12	---	214	315
	Fly Ash	FA	2.35	---	92	105
Aggregates	Crushed 10 mm	CA10	2.89	0.28	775	751
	Manufactured Sand	MS	2.91	0.56	388	376
	River Sand	RS	2.66	1.78	485	470
	Fine Sand	FS	2.65	0.67	291	282
Water		W	1.00	---	199	174
Superplasticizer		SP	1.07	---	---	4.2

The idea underlying the concrete mix selection was to design two workable mixes with approximately the same volumetric fraction of paste, one mix with high water content and low strength (R1) and the other with lower water content and higher strength (R2). Namely, in a concrete system, it is the hardened paste that undergoes drying shrinkage while the aggregate is considered dimensionally stable. As can be seen in Table 2, R2 contained 2 vol% more paste than R1

however, R1 paste contained more water per unit of powder material with effective water-powder ratio (WP-eff) being 0.60 for R1 and 0.38 for R2.

Table 2: Concrete mix parameters. Dosage of powders (DP) gives a total mass of active powders per 1 m³ of concrete. Absolute water-powder ratio (WP-abs) accounts for all water added to the mix while effective water-powder ratio (WP-eff) disregards water absorbed by the aggregates. Designed compressive strength is the strength expected at 28 days on specimens subjected to standard curing.

Attributes	Symbol	Unit	R1	R2
Dosage of powders	DP	kg	306	420
Water-powder ratio Absolute	WP-abs	kg kg ⁻¹	0.65	0.41
Water-powder ratio Effective	WP-eff	kg kg ⁻¹	0.60	0.38
Paste content	f _p	vol%	31	33
Designed 28-day compressive strength	σ _N	MPa	30	60

3 MODELLING

To understand the measured properties and their relation to geometric and material characteristics of the experimental set-up, two mathematical models – one analytical and the other numerical, were developed.

3.1 Analytical model

The analytical method based on the Reissner's geometrically exact beam theory [15] is applied to solve the steel-concrete ring problem. The analytical method, including a system of ten governing equations, namely the equilibrium, kinematic and constitutive equations, and the corresponding boundary conditions, is derived and explained in detail in [1] and [16]. The analytical method assumes a rigid and non-deformable steel ring, no shear strain in the concrete ring and no separation of the concrete and steel rings, enabling only an interlayer slip. The total strain in the concrete ring in the tangential direction ε_c is determined as a sum of the mechanical strain ε_m and the strain due to the shrinkage of concrete ε_{cs} as

$$\varepsilon_c = \varepsilon_m + \varepsilon_{cs} \quad (1).$$

Time development of the strain due to shrinkage of concrete is applied in accordance with Eurocode 2 (EN 1992-1-1 [17]). Since the concrete ring does not deform until the first crack is formed, the analytical method yields the following equation

$$\sigma = E \varepsilon_m = -E \varepsilon_{cs} \quad (2),$$

where σ denotes the tangential stress in the concrete ring and E the elastic modulus of concrete. Since the strain due to the shrinkage of concrete, ε_{cs} in Eq. (2), is a negative quantity, the stress in the concrete ring, σ, is tensile and the first crack forms when the tensile stress in the concrete ring is larger than the tensile strength of concrete f_{ct}

$$\sigma_{cr} = -E \varepsilon_{cs,cr} \geq f_{ct} \quad (3),$$

where σ_{cr} and ε_{cs,cr} denote the critical stress and the critical strain due to the shrinkage of concrete, respectively. The corresponding critical time is denoted t_{cr}. The location of the first crack is arbitrary since a geometrically and materially perfect concrete ring is considered. Stiffness of the contact between the concrete and the steel ring does not influence the stress in the concrete ring until the formation of the first crack. At any given time, the stress and strain fields are uniform across the concrete and the steel ring, however, they change over time.

3.2 Numerical model

The problem of the restrained shrinkage of the concrete ring is numerically solved using the finite element software COMSOL Multiphysics [18]. Two models were devised to separately solve (i) the problem of the restrained shrinkage of concrete by a rigid and non-deformable steel ring, and (ii) the problem of restrained shrinkage of concrete by a deformable steel ring. Model (i) is directly comparable to the analytical model. The influence of the deformable steel ring on the shrinkage of the concrete ring is studied in model (ii). Both problems are modelled in two dimensions (2D) since

the lateral deformations are small compared to the total axial (tangential) deformations of the concrete ring, ε_c . Symmetry is applied and therefore only half of the concrete and the steel ring is modelled. Both materials are considered isotropic and linearly elastic. Measured material parameters were used for modelling. These were determined experimentally as explained in ch. 2 and results are stated in ch. 4. The solution is obtained by the constant Newton method. A generalized alpha method is used for time discretization. A 2D numerical domain was meshed to 1450 triangular second-order (quadratic) isoparametric Lagrangian elements. The stress in the concrete ring, σ , as well as the strain in concrete, ε_c , and steel rings, ε_s , are calculated at time steps of 0.1 day.

3.3 Analytical and numerical model forecast

Stress development in the concrete ring, σ , over time, t , determined by the analytical method (an.) and numerical models (i) and (ii) is presented in Fig. 2. Figure 2a compares the analytical model (an.) and the numerical results of model (i) for concrete mixes R1 and R2. It can be seen that the numerical results agree well with the results of a relatively simple, but accurate, analytical model. Figure 2b shows the numerical results of stress development over time for model (ii) where shrinkage of the concrete ring is restrained by the deformable steel ring. The horizontal solid lines in Figs. 2a and 2b denote the estimated tensile strength of concrete, namely $f_{ct} = 1.8$ MPa for R1 (blue lines) and $f_{ct} = 2.3$ MPa for R2 (red lines). Tensile strength was estimated based on measured compressive strength using the equation given in AS 3600 [19]. The corresponding critical time, t_{cr} , at which the first crack forms, is marked with vertical dashed black lines. Analytical method (an.) and model (i) show the critical time to be 9 and 8 days for R1 and R2, respectively while model (ii) yields 14 days for R1 and 13 days for R2 which is 5 days more than models (an.) and (i).

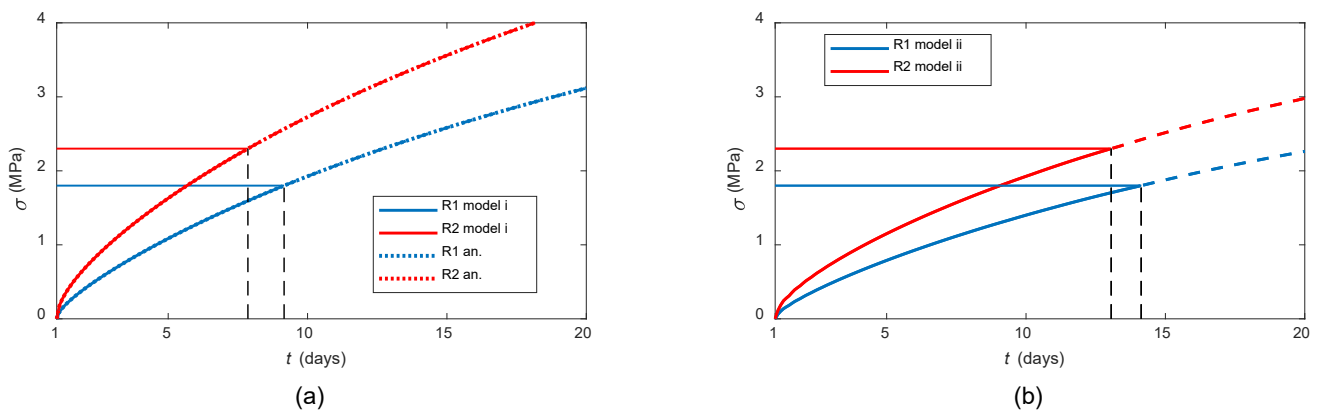


Figure 2: Time development of the stress in the concrete ring, σ , determined by (a) numerical model (i) and the analytical method (an.), and (b) the numerical model (ii) for R1 and R2 concrete. The horizontal solid lines denote the tensile strength of concrete, $f_{ct} = 1.8$ MPa for R1 (blue line) and $f_{ct} = 2.3$ MPa for R2 (red line). Vertical black dashed lines denote the corresponding critical time, t_{cr} .

Strain development in the concrete ring, ε_c , and steel ring, ε_s , over time, t , determined by the model (ii) is presented in Fig. 3. Vertical dashed black lines denote critical time as found by model (ii) in Fig. 2b. The corresponding strain is marked by the horizontal solid lines, namely blue line for R1 and red line for R2. The strain in the concrete ring, ε_c , just before the formation of the first crack, is found in Fig. 3a with values of $-22 \times 10^{-6} \text{ m m}^{-1}$ for R1 and $-27 \cdot 10^{-6} \times 10^{-6} \text{ m m}^{-1}$ for R2. The resulting strain in the steel ring, ε_s , is shown in Fig. 3b and its values are roughly in the same range, namely $-30 \times 10^{-6} \text{ m m}^{-1}$ for R1 and $\varepsilon_s = -38 \times 10^{-6} \text{ m m}^{-1}$ for R2.

Note that the stress and strain in Figs. 2 and 3 are plotted as dashed lines for $t > t_{cr}$ to potentially enable a determination of t_{cr} for different values of f_{ct} , however, the stress instantly reduces to zero and the strain relaxes to a smaller value at the formation of the first crack. The analytical method and the numerical modelling also give equal lengths of the first crack that are 0.11 and 0.12 mm for the concrete mixes R1 and R2, respectively, when a smooth sliding between the concrete and the steel rings is considered.

4 RESULTS AND DISCUSSION

Time of the first sighting of the crack and concrete properties measured on cylinders are summarized in Table 3. Measured compressive strength and modulus of elasticity were used in analytical and numerical modelling. Crack on R1

was observed rather late which was due to concrete having low strength and thus soft failure which resulted in a small width of the crack. Therefore, time to the first sighting of the crack in R1 is most likely longer than the actual appearance of the crack. For R2, daily visual inspection was carried out with a magnifying glass and a torch therefore time to the first sighting of the crack more accurately presents the time of the cracking.

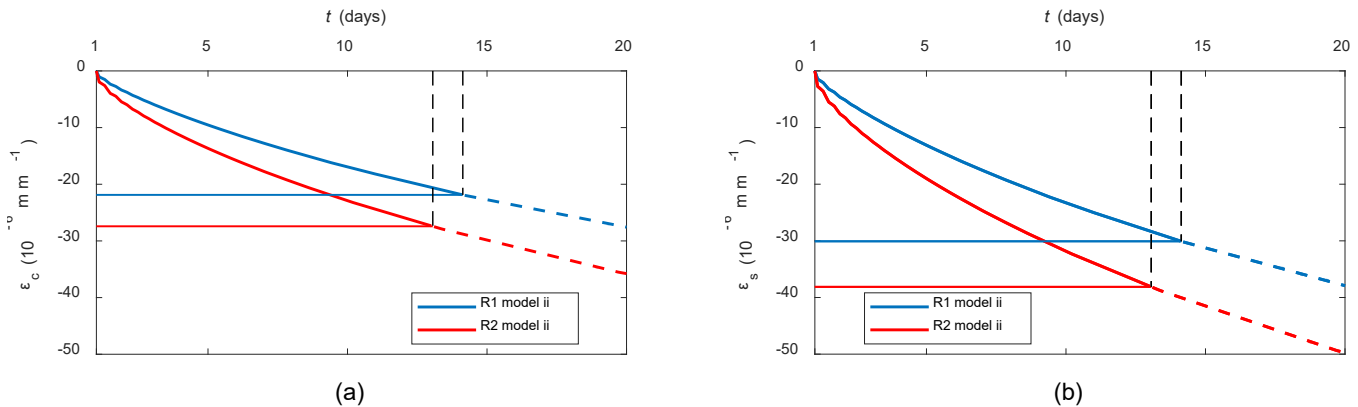


Figure 3: Time development of the strain in a) concrete ring, ϵ_c , and b) steel ring ϵ_s , determined by the numerical model (ii) for R1 and R2 concrete. The vertical black dashed lines denote the critical time, t_{cr} . The corresponding strain in the concrete, ϵ_c , and the steel, ϵ_s , rings are marked with the horizontal solid lines for the mixes R1 (blue line) and R2 (red line).

Table 3: Properties of concrete R1 and R2 at the time when the crack on restrained shrinkage ring was observed. The average value and sample standard deviation are stated. Sighting of the crack refers to the time the crack was visually spotted on the concrete ring and does not necessarily correspond to the first formation of the crack.

Concrete property	Symbol	Unit	R1	R2
Time to the first sighting of the crack	t	days	14	11
Time of tests on cylinders	t_c	days	20	11
Density	ρ_c	kg m ⁻³	2370 ± 20	2440 ± 10
Compressive strength	σ_c	MPa	26 ± 2	40 ± 5
Modulus of elasticity	E_c	GPa	31 ± 4	35 ± 5

Strain measured on steel ring for R1 and R2 is shown in Fig. 4 (a-b). Strain measurements on concrete were not successful for R1 due to problems with strain-gauge adhesion and data acquisition system. These problems were resolved for R2 by using compressed air not only to clean but also to locally dry the surface and by reprogramming the data acquisition system. Therefore, strain development in R2 concrete is shown in Fig. 4 (c).

Steel strain vs time diagrams in Fig. 4 (a-b) show a drop of strain, which indicates the formation of cracks, between 11 and 12 days after casting for R1 and between 13 and 17 days for R2. This is in agreement with the observations in Fig. 4 (c) showing a drop of concrete strain for R2 between 14 and 17 days. While the critical time, t_{cr} , predicted by the numerical model (ii) is within the same range as the actual measurements, the model predicted a shorter critical time for R2 than for R1. In this respect it should be noted, that development of macro crack on such a large ring is gradual and it happens over several days which is not accounted for by modelling.

The concrete strain measured on R2 at the time the cracking started, was negative, indicating contraction, with values being between $\sim(-180$ to $-130) \times 10^{-6}$ m m⁻¹. These values are ~ 5 -times the values predicted with the numerical model (ii). The steel strain, on the other hand, was measured to be between $\sim(10$ to $20) \times 10^{-6}$ m m⁻¹ which in absolute terms is approximately half of the predicted value. However, steel strain is positive, indicating extension, which is an unexpected outcome of the test. In this respect, it is important to note that in both experiments steel strain SS-1 is negative for the first two days dropping to a value of $\sim(-7 \times 10^{-6}$ m m⁻¹) before starting to increase. Furthermore, three discontinuities are observed in SS-1 curve on R2 (Fig. 4b) which may indicate slippage.

Temperature and relative humidity measurements obtained by dry and wet-bulb thermocouple are summarized in Fig. 5. Peaks observed in temperature measurements in R1 experiment (Fig. 5a) are due to the influx of air when the door opened, however, the temperature stabilized promptly and was fairly constant between 19 and 21 °C. This is within the room parameters of 20 ± 2 °C. A protective screen placed in front of the door resolved this issue in experiment R2, thus

temperature peaks in Fig. 5b are smaller. Humidity measurements encountered additional problems in R1 experiment since the wet-bulb thermocouple dried out frequently. This is observed in Fig. 5c as relative humidity curve plateauing at 100 %. This problem was resolved in R2 experiment and therefore such anomalies are not found in Fig. 5d. Nevertheless, the relative humidity was found to fluctuate between 40 and 80 % which is somewhat outside the room set parameters of 60 to 80 %. When comparing graphs in Figs. 4 and 5 no direct link between temperature and relative humidity fluctuations and strain measurements is found. Still, narrowing down the range of relative humidity fluctuations needs to be considered in future experiments.

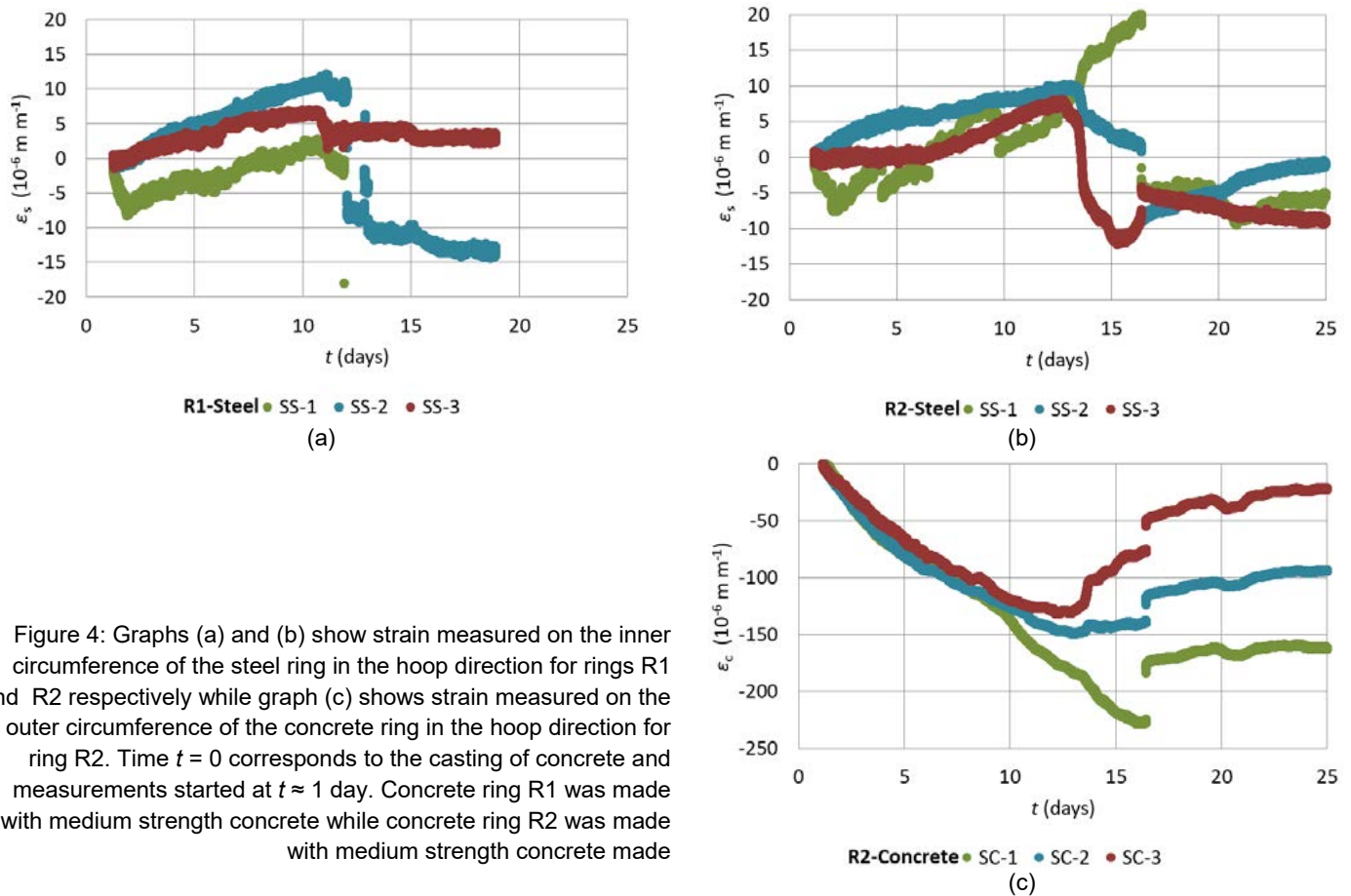


Figure 4: Graphs (a) and (b) show strain measured on the inner circumference of the steel ring in the hoop direction for rings R1 and R2 respectively while graph (c) shows strain measured on the outer circumference of the concrete ring in the hoop direction for ring R2. Time $t = 0$ corresponds to the casting of concrete and measurements started at $t \approx 1$ day. Concrete ring R1 was made with medium strength concrete while concrete ring R2 was made with medium strength concrete made

While the experimental results are promising they clearly show the need for further refinements of the test set-up. The configuration of the strain-gauges could be improved by installing independent strain-gauge circuits at the bottom, middle and at the top of the ring. This would enable capturing the variability in the vertical stain profiles due to pressure gradients which arise from drying as shown by Moon [8]. Steel strain gauge measurements should be validated by applying equal pressure on the whole circumference and by checking the quality of Wheatstone bridge thermal compensation. Furthermore, the interface between steel and concrete should be investigated for any friction and additional measures should be taken to reduce it. Sealing of the top surface could be improved by using paraffin vax or silicon cover instead of plastic. While the relative humidity measured in the vicinity of the concrete ring fluctuated between 40 and 80 %, no direct correlation was observed with fluctuations in strain measurements. Nevertheless, the experimental set-up should be moved to a humidity-controlled room.

5 CONCLUSIONS

An experiment was conducted in conjunction with the proposed analytical and numerical models aiming to enhance the understanding of restrained shrinkage of concrete. Based on the ring geometry, properties of concrete and steel and by using the equation provided by Moon [8, p.48, Eq.3.6], the degree of restraint was estimated to be ~70 %. Two concrete rings, R1 and R2, were made. Their compressive strength was ~26 MPa and ~40 MPa respectively at the time of the crack sighting. Concrete rings were subjected to circumferential drying. The resulting strain was measured in the hoop direction on the inner circumference of the steel ring and on the outer circumference of the concrete ring. While

experimental data is promising, several issues need to be resolved. Most important is the positive strain measured on the steel ring. It is recommended to instal three independent Wheatstone bridges at each MP, namely one at the bottom, one at the middle and one at the top of the steel ring. Measurements on these strain gauges should be validated by applying controlled uniform pressure on the whole circumference of the steel, for example by using a pneumatic airbag system. Unrestrained shrinkage should be measured on companion specimens to provide additional data for modelling. It might be beneficial to use mature concrete blocks, whose moisture content is in equilibrium with the test room, for dummy strain-gauges in concrete Wheatstone bridges. Further measures should be taken to prevent any slippage between steel and concrete ring and to prevent top and bottom drying.

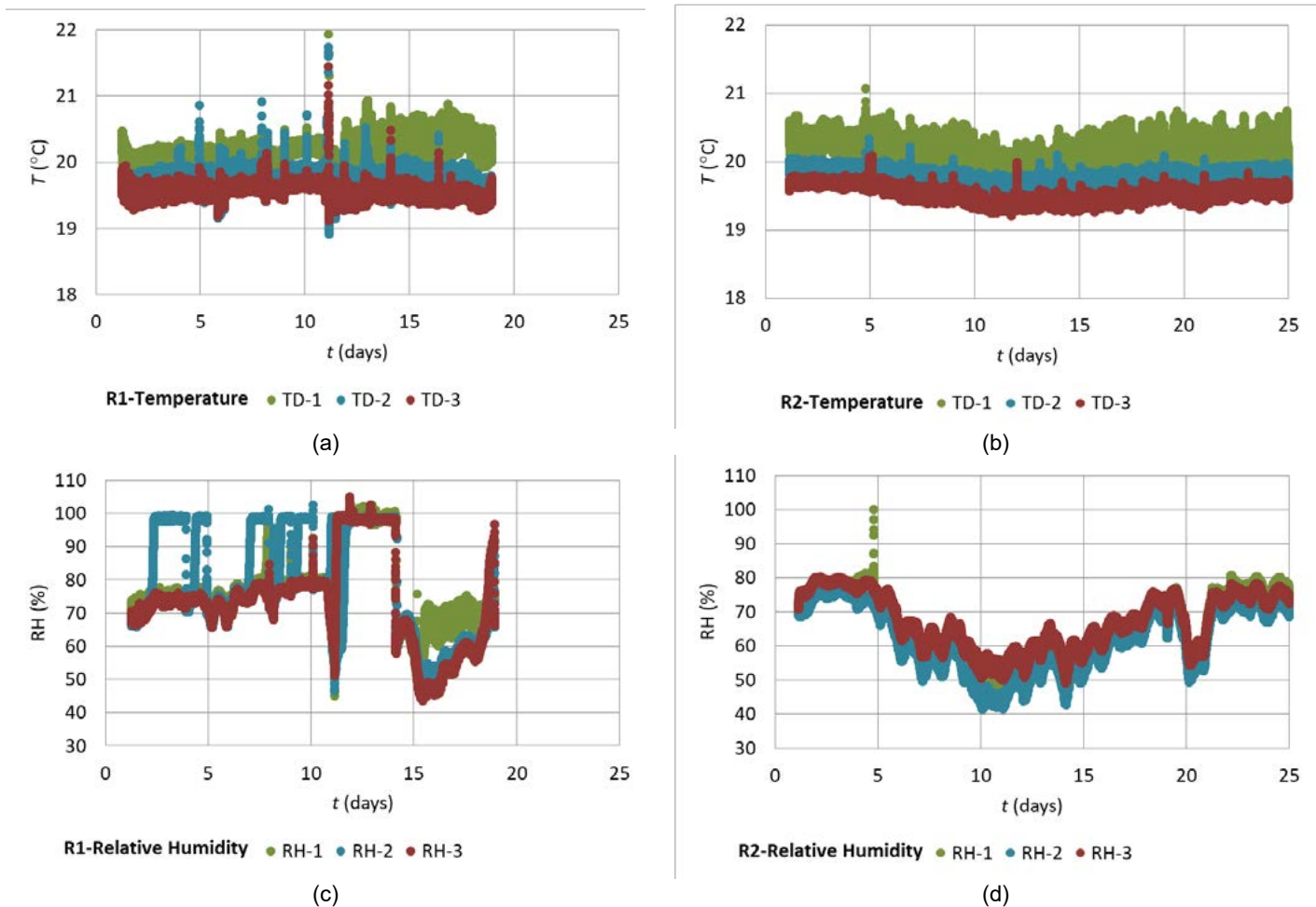


Figure 5: Graphs (a) and (b) present temperature measurements and graphs (c) and (d) present relative humidity measurements carried out at the three measuring points for rings R1 and R2 respectively. Ring R1 was made with low strength concrete while ring R2 made with medium strength concrete. Time $t = 0$ corresponds to the casting of concrete while measurements started at $t \approx 1$ day.

ACKNOWLEDGEMENTS

The authors would like to acknowledge the contribution of Mr Adrian Chau for initial equipment performance tests conducted in the scope of his bachelor's thesis at *The University of Queensland* (UQ). Technical support of Mr Jason Van Der Gevel, Mr Stewart Matthews and Mr Shane Walker (all School of Civil Engineering, UQ), as well as consultancy provided by Mr Peter Bleakley (instrumentation Workshop, UQ), are greatly appreciated. T. Hozjan and I. Planinc acknowledge the supported by the *Slovenian Research Agency* through the research core funding No. P2-0260.

REFERENCES

- [1] Hozjan T.; Karlovšek, J.; Hanžič, L.; Huč, S.; Planinc, I.: Analytical method for determination of crack development in concrete ring due to restrained shrinkage, in *Advancements in Civil Engineering and Architecture*, 2019, vol. 1: Civil Engineering, pp. 1381–1389.

- [2] AS 1012.13 Methods of testing concrete. Determination of the drying shrinkage of concrete for samples prepared in the field or in the laboratory. *Standards Australia*, 2015.
- [3] EN 12390-16 Testing hardened concrete. Determination of the shrinkage of concrete. *European Committee for Standardization (CEN)*, 2019.
- [4] Shotcreting in Australia: recommended practice. *Concrete Institute of Australia*, 2010.
- [5] Carlswärd, J.: Shrinkage cracking of steel fibre reinforced self compacting concrete overlays - Test methods and theoretical modelling, PhD thesis. *Luleå University of Technology*, Luleå, Sweden, 2006.
- [6] Weiss, W. J.; Yang, W.; Shah, S. P.: Influence of specimen size/geometry on shrinkage cracking of rings, *Journal of Engineering Mechanics*, 126 (2000)1, pp. 93–101.
- [7] Hossain, A. B.; Weiss, J.: Assessing residual stress development and stress relaxation in restrained concrete ring specimens, *Cement and Concrete Composites*, 26 (2004) 5, pp. 531–540.
- [8] Moon J. H.: Shrinkage, Residual Stress and Cracking in Heterogenous Materials, PhD thesis. *Purdue University*, West Lafayette, Indiana, 2006.
- [9] ASTM C1581 Standard test method for determining age at cracking and induced tensile stress characteristics of mortar and concrete under restrained shrinkage. *ASTM*, 2009.
- [10] Raoufi, K.; Bernard, E. S.; Weiss, W. J.: Shrinkage cracking behavior of fiber reinforced concrete: as assessed using the restrained ring test, *Journal of ASTM International*, 7 (2010) 7, pp. 1–15.
- [11] *DeLogger 5.0*, dataTaker, Industrial Temperature Sensors Ltd, 2012.
- [12] AS 1012.8.1 Methods of testing concrete. Method for making and curing concrete. Compression and indirect tensile test specimens. *Standards Australia*, 2014.
- [13] AS 3972 General purpose and blended cements. *Standards Australia*, 2010.
- [14] AS 3582.1 Supplementary cementitious materials. Fly ash. *Standards Australia*, 2016.
- [15] Reissner, E.: On one-dimensional finite-strain beam theory: The plane problem, *Journal of Applied Mathematics and Physics*, 23 (1972), pp. 795–804.
- [16] Hozjan, T.; Saje, M.; Srpčič, S.; Planinc, I.: Geometrically and materially non-linear analysis of planar composite structures with an interlayer slip, *Computers and Structures*, 114 (2013), pp. 1–17.
- [17] EN 1992-1-1 Eurocode 2: Design of concrete structures General rules and rules for buildings. *European Committee for Standardization (CEN)*, 2014.
- [18] *COMSOL Multiphysics 5.5*, COMSOL, 2019.
- [19] AS 3600 Concrete structures. *Standards Australia*, 2018.

16

Johannes Horvath

ECORoads (Economical Concrete roads)



ECORoads (Economical CONcrete roads)

Johannes Horvath

LAFARGE Zementwerke GmbH

Trabrennstraße 2A

A-1020 Wien

johannes.horvath@lafargeholcim.com

SUMMARY: Roads play a very important part in any nation's infrastructure. Their construction and maintenance, and the vehicles that travel over them, consume large amounts of energy. This energy use results in atmospheric emissions, the reduction of a non-renewable resource, and other environmental impacts. Any reduction of the lifetime energy use, even if only by a small percentage, will have significantly positive implications for sustainable development. Concrete roads are durable and safe without defects like rutting, cracking, stripping, loss of texture, and potholes, etc. This low maintenance requirement is one of the principal advantages of concrete pavements. There are well-designed concrete pavements that have required little maintenance well beyond their designed 30-year design lives. Concrete pavements are well developed at Austrian Highways and Expressways, Rural Roads predominated by asphalt. Our objective in this new branch project is to transfer the technology from H&E to rural roads. Goal of this programme is to achieve more quality, improve value for money and provide a boost to innovation in road construction in Austria.

KEY WORDS: Long design life, low maintenance, fuel saving, RCC

1 INTRODUCTION

The roads of the future can play the role of a driver of innovation. They will be designed, built, operated and maintained on the basis of modern economic instruments. Full account is to be taken of the requirements of sustainable life-cycle management, the increasing use of alternative construction materials and the application of appropriately optimized construction processes. Since the implementation of the in Construction Products Regulation CPR on July 2013 concrete and especially concrete constructions get an occasion for showing the excellent properties regarding the new approaches.

The new CPR consists now of seven claims. Especially those points which are the dominated modifications to the Construction Production Directive (CPD) are very characteristic for concrete constructions, namely long service life (point 3) and mineral genesis from a local stock (point 7) without long distances of transport.

Consequence of those requirements the branch committed to develop methods of placing rural or provincial concrete roads.

1. Mechanical resistance and stability
2. Safety in the case of fire
3. Hygiene, health and the environment
New: Considering the entire costs during life-cycle-time!
4. Safety in use
5. Protection against noise
6. Energy economy and heat retention
7. New: Sustainable use of natural resources
Use of environmental compatible raw and secondary materials in the construction works

2 ARGUMENTATIONS

Before launching the project a brainstorming regarding general properties of roads will be done. The result of pros are shown in figure 1.

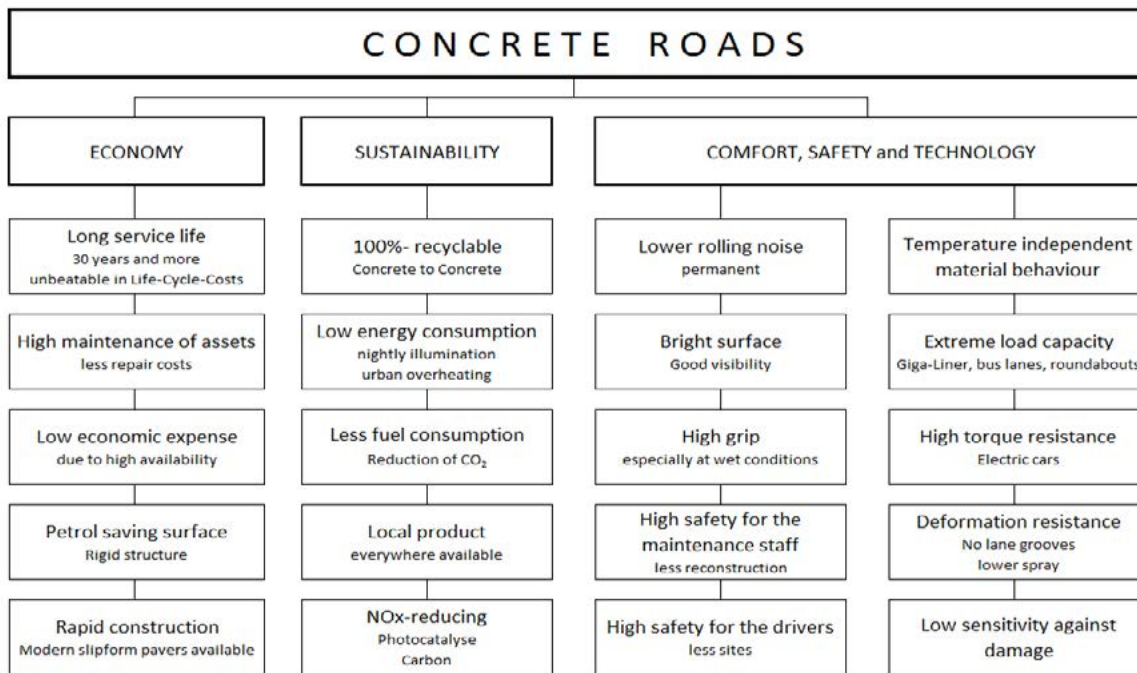
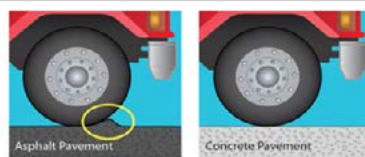


Figure 3: Pros of concrete roads

A high potential for future are the fuel saving and ongoing reduction of CO₂. In Table 1 you can see the volume of saving diesel. For instance one truck with a yearly performance of 100.000 km is saving 450 l diesel (like 1200 kg CO₂) by using a rigid surface (concrete) in comparison to a flexible (asphalt) one.

Saving potential - Fuel and CO₂



Arguments for the road owners:

	Input			NRC			DAY			YEAR			30 YEARS		
	Street-length [km]	Number of trucks per day	directions	Diesel-saving [(l/100km) ²¹	Diesel price [€/l]	CO ₂ -emission [(kg/l) ²¹	Diesel-saving [l/day]	Cost saving [€/day]	CO ₂ saving [t/day]	Diesel-saving [l/year]	Cost saving [€/year]	CO ₂ saving [t/year]	Diesel-saving [(l/30 years)]	Cost saving [€/30 years]	CO ₂ saving [t/30 years]
Etalon	100	5.000	2	0,45	1,02	2,7	4.500	4.590	12,2	1.642.500	1.675.350	4.435	49.275.000	90.260.500	133.043
A23 km ^{9,068} ²¹	17,754	9.173	2	0,45	1,02	2,7	1.466	1.495	4,0	534.987	545.686	1.444	16.049.601	16.370.593	43.334
A5 - Ausbau ²¹	35,6	2.747	2	0,45	1,02	2,7	880	898	2,4	321.251	327.676	867	9.637.520	9.830.270	26.021

Legende: ²¹NRC - National Research Council von Kanada ²²www.asfmag.at/unterwegs/dauerzaehlstellen (Durchschnitt 2014) ²³www.asfmag.at/unterwegs/dauerzaehlstellen (Durchschnitt 2014, Schrick km 22,078)

Arguments for the haulier:

Number Trucks	Input		NRC			DAY			YEAR		
	km/year/Truck	Total km/year	Diesel-saving [(l/100km)]	Diesel price [€/l]	CO ₂ -emission [(kg/l)]	Diesel-saving [l/day]	Cost saving [€/day]	CO ₂ saving [t/day]	Diesel-saving [l/year]	Cost saving [€/year]	CO ₂ saving [t/year]
1	100.000	100.000	0,45	1,02	2,7	1,2	1,3	3,3	450	459	1,2
5	100.000	500.000				6,2	6,3	16,6	2.250	2.295	6,1
10	100.000	1.000.000				12,3	12,6	33,3	4.500	4.590	12,2
50	100.000	5.000.000				61,6	62,9	166,4	22.500	22.950	60,8

Table 1: Potential of fuel and CO₂ savings



3 PROJECT

The project is scheduled over four years and comprises six work packages. Main topics are placing technologies, optimization of material and surface, dimensioning, refurbishing, life-cycle analysis and ASR.

Pilot Project – Small Slipform Paver (PCC Paver compacted concrete)

Precondition for developing of placing methods for rural roads was to consider the closed placing condition. The scenario is one lane for work and one as loop road for the traffic (see Figure 1 and 2). This situation is often given at rural roads during refurbishing. The consequence is that ordinary slipway pavers could not use because of the constrained place conditions. A new concept for a paver was necessary to fulfil these circumstances. The paver must be low weighted and flexible in track width.

Therefore a prototype was developed and tested for the first time in a pilot project in Retznei – Austria.

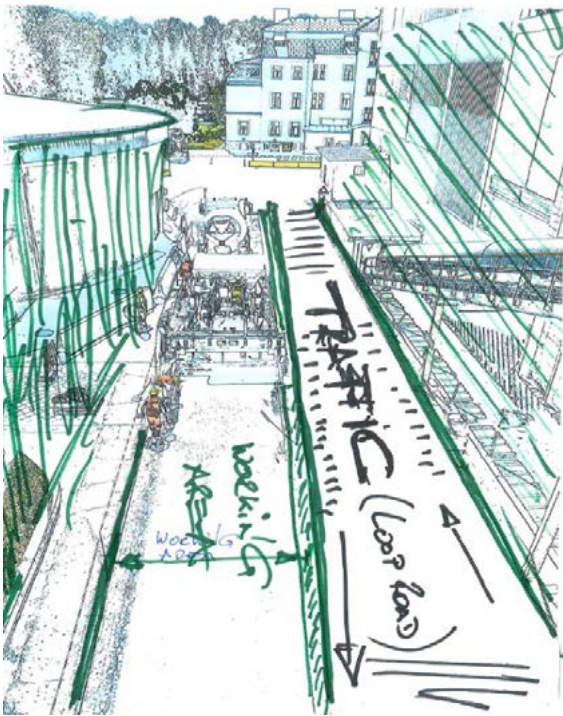


Figure 2: Working Area

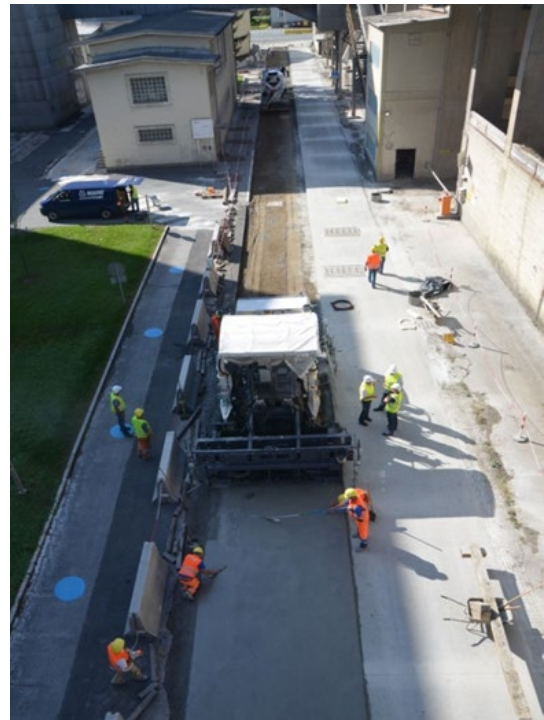


Figure 2: Working Area

Pilot Project: RCC - Roller compacted concrete

The second methodology is the placing with conventionally asphalt pavers with high performance vibration unit. This technique is compared to PCC cheaper and can be done like asphalt placing. Interested fields are rural roads and industrial areas (see fig. 4 and fig. 5).



Figure 4: Placing concrete with asphalt paver



Figure 5: Rolling

ACKNOWLEDGMENTS

Within this project, PCC- and RCC- Technology became perfection for rural roads and industrial areas. Considering the environmental arguments, concrete is a marvellous option for the future. All materials to produce concrete are regionally. No far transportations and therefore a support for the local economy. We drive concrete!

17

Ksenija Janković, Dragan Bojović, Marko Stojanović, Iva Despotović, Lana Antić

Properties of concrete kerbs with recycled aggregate from precast elements

PROPERTIES OF CONCRETE KERBS WITH RECYCLED AGGREGATE FROM PRECAST ELEMENTS

Ksenija Janković¹, Dragan Bojović², Marko Stojanović³, Iva Despotović⁴, Lana Antić⁵

^{1,2,3,5} Institute for testing of materials-IMS Institute
Bulevar vojvode Mišića 43, 1100 Belgrade
e-mail: ksenija.jankovic@institutims.rs

⁴ Belgrade University College of Applied Studies in Civil Engineering and Geodesy
Hajduk Stankova 2, 1100 Belgrade
e-mail: ivickad@gmail.com

SUMMARY: The paper presents the possibility of using recycled aggregate from precast concrete paving elements and kerbs in the production of concrete kerb units. Experimental work included several types of concrete consistency class S1, made with different amounts of cement and coarse recycled concrete aggregate. The influence of percentage and grain size of recycled concrete aggregate on concrete compressive strength at different ages was observed. Based on the experimental results, it can be concluded that the use of recycled concrete as an aggregate creates a new composite material that can be used for the production of precast elements. The results show that the replacement of the coarse natural aggregate with aggregate from crushed concrete is possible to produce concrete curbs that meet the requirements of EN 1340, but the class depends on the replacement percentage of the natural aggregate with recycled ones. In this way, the production waste is turned back to process, and the newly created concrete is certainly ecological material.

KEY WORDS: recycled concrete aggregate, concrete, kerbs, precast elements.

1 INTRODUCTION

One of the common ways to achieve more environmentally friendly concrete is crushing concrete to obtain coarse aggregate for the production of new concrete. In this way the consumption of natural resources as well as the disposal of waste concrete in landfills is reduced. As the matter of fact, the use of recycled-aggregate concrete is becoming increasingly interesting in civil construction as regards to sustainable development. Many studies show that it is possible to use crushed concrete as coarse aggregate, which has already been accounted for in the regulations of many countries [1].

Research showed that up to 30% coarse or 20% fine recycled concrete-derived aggregate had no effect on the concrete strength [2]. Concrete made with recycled aggregate (RA) or recycled concrete aggregate (RCA) also needs to be tested in order to confirm that it has adequate freeze-thaw and sulphate resistance for its intended use. The maximum strength class of concrete made with RCA should not be more than C50 [2].

Results of the investigation of Poon et al. show that the production of non-structural precast concrete blocks is possible with low grade recycled aggregate [3]. By combining recycled aggregate of brick and concrete (50:50%) it is possible to produce concrete for paving for pedestrian areas and (25:75%) for traffic [4].

In the production of precast concrete elements there are some mistakes in production which result in products that do not have certain required properties. Such products cannot be used and they most often end up at the landfill. One of the ways to reduce the formation of landfills is recycling. By crushing concrete aggregate from the concretes obtained, which can be used as a component material in the production of concrete after being fractionated.

It has been shown that it is possible to produce single-layer curbs with up to 50% replacement of natural recycled aggregate without any negative effects on their mechanical properties [5].

The possibilities of using concrete with recycled aggregate in the industrial production of various concrete products,

such as concrete pipes, paving elements and curbs, were examined. The results of testing the compressive strength of concrete pipes according to EN 1916 showed that pipes made from recycled aggregates had a strength reduction of 12% for unreinforced and 7.5% for reinforced compared to the corresponding reference pipes. For concrete paving blocks, if the natural aggregate is replaced by 40% recycled, the tensile splitting strength determined by EN 1338 is reduced by 43%. Water absorption is higher for products with recycled aggregate than for reference products. The use of recycled aggregates produces kerbs that meet the criteria of the standard in terms of bending strength according to EN 1340, but are classified as lower than the reference samples. In terms of weather resistance, products with recycled aggregate are satisfactory, as their water absorption was $\leq 6\%$ [6].

The following non-structural elements were tested: terrazzo flags for internal use, kerb units and paving blocks to the appropriate standards were also performed at 360 days of age. The obtained results confirmed the possibility of using recycled aggregate for the production of these elements. However, the surface of the terrazzo flags is not as good as that of samples produced with natural aggregate [7]. Application of concrete with recycled aggregate is not recommended for the facing (visible) layer [8].

Comparing previous test results of concrete kerbs made of ordinary concrete and properties of concrete with recycled concrete as aggregate it can be concluded that this kind of concrete can be used for the production of elements for pedestrian areas [9].

The aim of this paper is application of recycled aggregate concrete in the production of kerb units. Some properties of concrete made with different replacement level of natural aggregate by recycled concrete aggregate (25, 50, 75 and 100%), such as compressive strength, water absorption, density, were done. Testing results of kerbs with two types of recycled aggregate concrete (25 and 100% of recycled concrete aggregate) according to EN 1340 were presented.

2 EXPERIMENTAL WORK

Two reference concrete with crushed aggregate from quarries Dobrnja near Banja Luka were prepared. Concrete with aggregate from recycled concrete were designed in such a way that coarse aggregate (fractions 4/8 and 8/16 mm) was replaced with 25, 50, 75 and 100% recycled aggregate.

All the concrete mixtures tested within the experimental research were made using CEM II/B-S 42.5 N cement, manufactured by CEMEX.

The recycled aggregate was obtained by crushing damaged prefabricated elements made of concrete consistency S1, a class of strength C 35/45. After the crushing, concrete was separated into fractions 0/4 mm, 4/8 mm and 8/16 mm.

Composition of two reference concrete is showed in Table 1.

Table 1: Mix design of reference concrete

Concrete mixture	C2	C3
Cement [kg/m ³]	320	360
Water-cement ratio W/C	0.40	0.40
Aggregate-cement mix ratio A/C	6.0469	5.2778

For good quality mix design with the recycled aggregate, it is necessary to know the amount of water absorbed by the recycled aggregate, since it is always higher in comparison with the same fraction of the crushed aggregate. The higher water absorption is the consequence of the presence of residual cement stone on the grains of recycled aggregate.

Workability is not important for precast elements, so required consistency measured by slump test was 1.0 cm. Water to cement ratio depends on percentage and fractions which were replaced by recycled concrete aggregate.

The effective water-cement ratio is the same for all concrete types, but due to the increased absorption of water in the recycled aggregate, the amount of water increased from 3-15% depending on the mixtures used and the amount of recycled aggregate.

Concrete kerb units were produced in two layers. Facing layer was consist of quartz sand and cement. For base layer concrete mixture C3 was used. Recycled aggregate concrete were designed in such a way that coarse aggregate (fractions 4/8 and 8/16 mm) were replaced with 25 and 100% recycled concrete aggregate. Dimensions of kerbs were 18x24x100 cm.

3 RESULTS AND DISCUSSION

3.1 Concrete properties

The consistency of the fresh concrete was class S1 according to standard SRPS ISO 4103/1997.

The samples for testing concrete compressive strength were made. Concrete was compacted with vibration in metal cube-shaped molds with an edge length of $d = 150 \text{ mm}$, and the samples were cured in water at a temperature of $+ 20 \text{ }^\circ \text{C}$ until they were tested according to SRPS EN 12390-2 standard.

Testing of concrete compressive strength at the age of 3, 7, 14 and 28 days was carried out according to SRPS EN 12390-3 standard. Bulk density of hardened concrete was tested according to SRPS EN 12390-7 standard and ranged from 2350 to 2400 kg/m^3 . The results of the testing are shown in Figures 1-2.

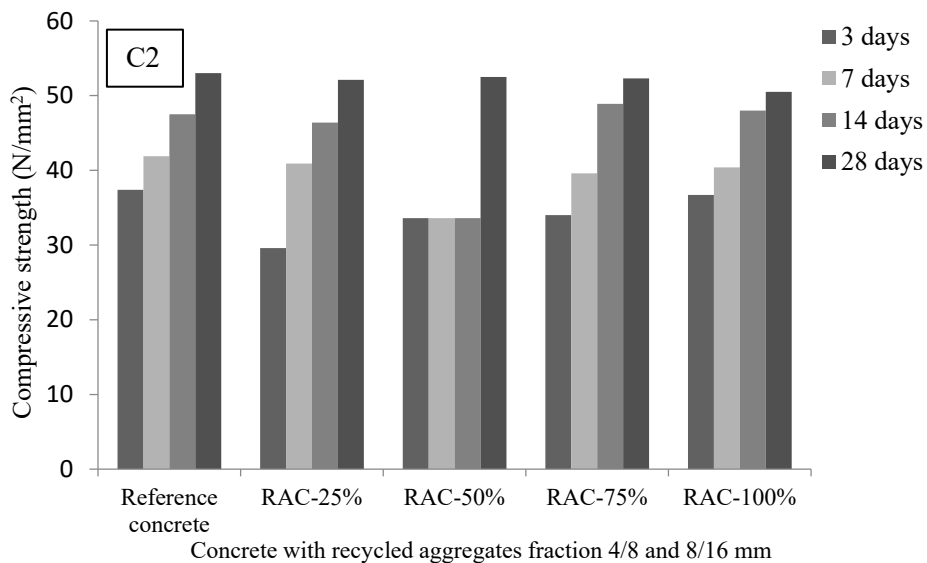


Figure 1: Compressive strength of concrete C2

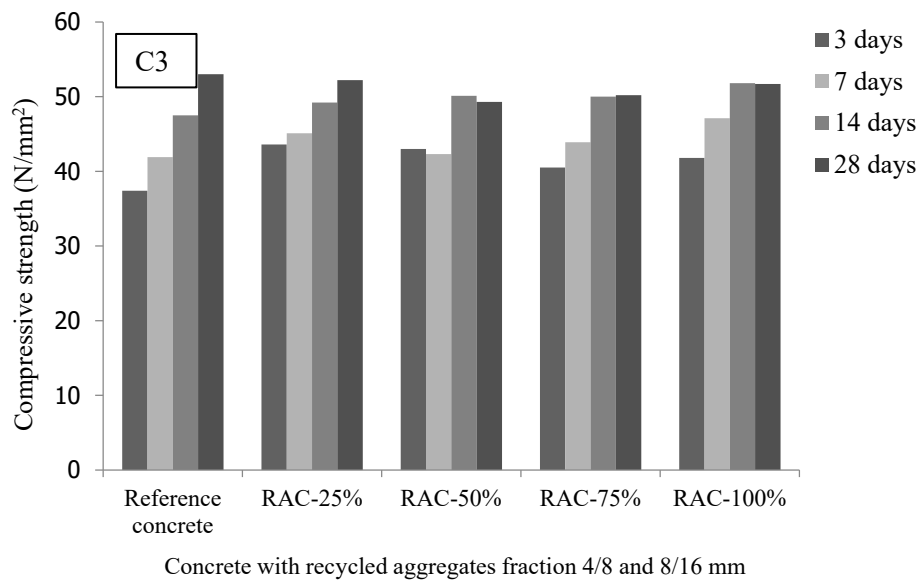


Figure 2: Compressive strength of concrete C2

Water absorption of aggregate reflects to amount of water necessary to provide concrete with same consistency, i.e. for concrete with greater amount of recycled aggregate the required amount of water is greater. Properties of concrete depend of the quality of recycled aggregate. In this case, concrete which was used for the production of recycled aggregate had compressive strength class C 35/45. That is the reason why concrete with recycled aggregate had compressive strength which is not significantly different compared to reference concrete. All concrete types also satisfied compressive strength class C 35/45. For samples with 100% recycled coarse aggregate decrease of strength was 4%, while for samples with 25% recycled coarse aggregate decrease was only 2%.

3.1.1 Concrete kerbs

Concrete paving blocks and flags were tested in terms of the following properties:

- Weather resistance,
- Bending strength,
- Abrasion resistance.

Weather resistance is determined by tests for freeze – thaw resistance with de-icing salt and for water absorption. Abrasion resistance is determined by the Wide Wheel Abrasion test, or as an alternative by the Böhme test.

All types of concrete products had a water absorption of less than 6% and a loss of mass after the freeze / thaw cycle $\leq 1.0 \text{ kg/m}^2$ and meet the requirements for both Class 2 and Class 3 resistance to weather resistance.

For all types of concrete elements, the volume loss was $\leq 18 \text{ cm}^3/50 \text{ cm}^2$ per Bohme test and met the wear resistance class 4.

Minimum bending strengths of concrete kerbs 18x24x100 cm according to EN 1340: 2003 / AC: 2006 were 4.9 MPa and 5.5 MPa, and the characteristic bending strengths were 5.3 and 5.6 MPa depending on which percentage of the natural aggregate was replaced by the recycled concrete aggregate, 100% or 25 %. Therefore, all types of kerbs met the criteria for Class 2 for bending strength classes according to EN 1340: 2003 / AC: 2006 because their minimum strengths were greater than 4.0 MPa and the characteristic strengths were greater than 5.0 MPa.

4 CONCLUSIONS

The possibilities of using recycled concrete as aggregate for production concrete kerb units were presented in this

paper. From the investigation results the following can be concluded:

The concrete density decreased as the percent of recycled aggregate increased.

The bending strength of kerbs decreased as the percent of recycled brick aggregate increased.

Water absorption of the kerbs not exceeded the limit of 6%.

Mass loss for all type of concrete kerbs after freeze/thaw test was $\leq 1.0 \text{ kg/m}^2$, so it satisfied the requirements for the best class for weather resistance according to the European standard (EN 1340).

Abrasion resistance of kerbs satisfied the requirements of the EN 1340.

It was possible to use up to 100% of recycled concrete as coarse aggregate to prepare concrete kerbs which meet the requirements of EN 1340 for bending strength Class 2.

Based on the obtained results it can be concluded that the use of aggregate from recycled concrete is possible. Concrete made with this type of aggregate can be used for the production of kerb units. In this way, the environment is protected, and the waste produced in its own production is re-used as a component material for concrete.

ACKNOWLEDGMENTS

We thank the company "BINIS", Banja Luka, which has enabled the realization of the experimental part of the paper.

The work reported in this paper is a part of the investigation supported by the Ministry of Education, Science and Technological Development, Republic of Serbia. This support is gratefully acknowledged.

REFERENCES

- [1] V. Corinaldesi, Mechanical and elastic behaviour of concretes made of recycled-concrete coarse aggregates, *Construction and Building Materials* 2010; 24: 1616–1620.
- [2] Soutsos M. N., Tang K., Millard S.G. Concrete building blocks made with recycled demolition aggregate, *Construction and Building Materials* 2011; 25: 726-735.
- [3] Poon C.S., Kou S.C., Wan H.W., Etxeberria, Properties of concrete blocks prepared with low grade recycled aggregate, *Waste Management* 2009; 29: 2369-2377.
- [4] Poon C.S., Chan D. Paving blocks made with recycled concrete aggregate and crushed clay brick, *Construction and Building Materials* 2006; 20: 69-577.
- [5] F. L. Gayarre, J. G. Perez, C. L.C. Perez, M. S. Lopez, A. L. Martínez, Life cycle assessment for concrete kerbs manufactured with recycled aggregates *Journal of Cleaner Production* 113 (2016) 41e53
- [6] F. Özalp, H. D. Yilmaz, M. Kara, Ö. Kaya, A. Sahin, Effects of recycled aggregates from construction and demolition wastes on mechanical and permeability properties of paving stone, kerb and concrete pipes, *Construction and Building Materials* 110 (2016) 17–23
- [7] C. Rodríguez, C. Parra, G. Casado, I. Minano, F. Albaladejo, F. Benito, I. Sanchez, The incorporation of construction and demolition wastes as recycled mixed aggregates in non-structural concrete precast pieces, *Journal of Cleaner Production* (2016), <http://dx.doi.org/10.1016/j.jclepro.2016.03.137>
- [8] F. L. Gayarre, C. López-Colina, M.A. Serrano, A. López-Martínez, Manufacture of concrete kerbs and floor blocks with recycled aggregate from C&DW, *Construction and Building Materials* 40 (2013) 1193–1199
- [9] Jankovic K., Loncar Lj., Kacarevic Z., Romakov Z., Bojovic, D. Some experience of testing concrete blocks and kerbs according to EN and JUS, *Proceedings of the international scientific-professional meeting "Civil engineering – science and practice"*, Žabljak, Serbia and Montenegro, 2006., Vol. 2, p. 539-544
- [10] EN 1340:2003, EN 1340:2003/AC:2006 Concrete kerb units – Requirements and test methods, CEN

18

Sabina Jordan, Friderik Knez, Miha Tomšič and Marjana Šijanec Zavrl

First experiences in the development of slovenian sustainable building indicators

FIRST EXPERIENCES IN THE DEVELOPMENT OF SLOVENIAN SUSTAINABLE BUILDING INDICATORS

Sabina Jordan¹, Friderik Knez¹, Miha Tomšič² and Marjana Šijanec Zavri²

¹ Slovenian National Building and Civil Engineering Institute, Department of Building Physics
Dimičeva ulica 12, 1000 Ljubljana
e-mail: sabina.jordan@zag.si

² Building and Civil Engineering Institute ZRMK, Centre for Indoor Environment, Building Physics and Energy
Dimičeva ulica 12, 1000 Ljubljana

SUMMARY: The construction sector is recognised as having a key impact on the life on Earth. Consequently, the EU has set clear environmental goals for 2030 and 2050, and is developing policies and tools to achieve them. One of the tools for achieving these goals is to establish a system for the evaluation of the environmental performance of buildings, with the priorities of reducing GHG emissions, saving with natural resources and preserving the environment, while maintaining sustainable development and ensuring a healthy living environment. Slovenia has joined in achieving this goal with a study on the state-of-play, commissioned a few years ago by the Ministry of the Environment and Spatial Planning, as the starting point for the development of sustainable building indicators (SBIs). The research, which included an analysis of the Slovenian legislation, commercial certification systems for sustainable buildings and development in the field of green public procurement, exposed complementary but rather different goals and views. It further showed that the Level(s), which provides a common EU approach in assessing the environmental performance of buildings, seems to be the most appropriate framework and the basis for the development of the Slovenian system of SBIs. The development of the Slovenian SBIs is currently underway within the project LIFE IP CARE4CLIMATE with the preparation of guidelines, data sources and procedures for determining the value of individual indicators for the assessment of buildings. Initial research with key construction stakeholders has shown that the solution must be linked to the national building legislation, computational methods and software tools, and also to the established planning procedures. The analyses have also shown that, parallel to developing such a system, it is essential to provide a functional supporting environment and a specific, purposely designed information platform to connect the stakeholders with the developers of the sustainable building indicators system.

KEY WORDS: sustainable building indicators, evaluation, assessment, Level(s), CARE4CLIMATE.

1 INTRODUCTION

One of the key factors for the sustainable development of society is the establishment of a sustainable approach in construction. The sustainable approach addresses a holistic view of the built environment and the building itself, which must be user friendly and environmentally friendly. Therefore, the holistic view must include the assessment and the evaluation of buildings according to sustainability criteria, i.e. environmental, economic and social aspects, as well as technical and functional aspects. In order to achieve this high quality in the process of construction of new buildings and/or their renovation, an evaluation system needs to be developed and adopted. The assessment should include a comprehensive system for the evaluation of sustainable buildings and should be based on the criteria for the assessment of individual indicators and their integration into a balanced scheme.

In the field of the evaluation of sustainable construction and certification of buildings, commercial systems already exist. Among them, the most widespread and recognisable are LEED, BREEAM and DGNB. However, they are very complex to use and are not uniform or mutually comparable to each other. The European Commission (EC) is therefore trying to establish a common framework for the evaluation of sustainable buildings, Level(s), covering the whole life cycle of a building and thus able to address their great potential for reducing greenhouse gas emissions, resource efficiency and material flow, and the health and well-being of building users [1]. The key challenge of the EC is to ensure that the uniform metric of sustainable construction is widely used throughout the value chain of the construction sector in the Europe [2].

Level(s) is a framework system of sustainable building indicators, based on the standards of the CEN/TC 350 group,

and is not designed as a certification scheme with a final evaluation score for classification. Level(s) mainly provides guidelines for the planning and construction of buildings according to sustainable principles. The system is still evolving at a European level, both in structural and functional terms, but nevertheless already provides the basis for future adaptation to national conditions. Level(s) implementation will have a significant impact on the introduction of a circular economy system, which is in line with the European Green Deal's plan to make Europe the first climate-neutral continent by 2050 [3, 4]. In fact, Level(s) is strongly related to the statement of a new Action Plan for the circular economy, which for 2021 announces a new “comprehensive strategy for a sustainable built environment”. The document also mentions the involvement of Level(s) in life cycle assessments in public procurement and European sustainable financing schemes [5].

Slovenia is aware of its commitments to the EU's goals regarding climate change and the exploitation of raw materials and natural resources. In addition, we are conscious of the importance of Slovenia's transition to a sustainable society, so we recognise the need for developing and implementing criteria for sustainable buildings. At various segments and levels, quite a few attempts have already been made to switch from energy efficiency to environmental efficiency in buildings as well, and to introduce the principle of life cycle consideration into planning. Attempts at market initiatives, incentive programmes for the implementation of state policies, as well as attempts at legal requirements in the field of construction and change in the framework of green public procurement are known. However, all these did not lead to significant progress yet. It is therefore quite obvious that Slovenia also needs a convincing professional base in this area for raising the level of the necessary professional knowledge, collection and editing of required data and for selecting the tools. In particular, Slovenia needs a methodology that will adequately cover the sustainability aspects of buildings.

The development of the Slovenian system for the evaluation of sustainable buildings was therefore proposed as an important research task in Action C4.4 within the research project LIFE17IPC/SI/00007 – LIFE IP CARE4CLIMATE (2019–2026). The activity is carried out by two institutes, GI ZRMK and ZAG, together with the Ministry of the Environment and Spatial Planning. The main aim of the Action C4.4 in the project is to create Slovenian sustainable building indicators (SBI), the comprehensive system for sustainable assessment and evaluation of buildings. The aim is also the establishment of a supportive e-environment in the form of knowledge, accessible databases and tools useful for general use. This national SBI system will be conceptually harmonised with the European system Level(s) and the content will be adjusted to the national specifics of the construction sector.

The aim of this paper is to highlight the basis for the development of Slovenian sustainable building indicators, SBI, and to provide the currently identified main obstacles and shortcomings to their implementation, which were perceived in the first phase of system development.

2 THE BASIS FOR SBI

The starting point for the development of the Slovenian SBI was the study of the current situation in Slovenia, “Review of the system of sustainability criteria with a transfer proposal” [6], which was prepared in 2017 by GI ZRMK and ZAG on behalf of the Ministry of the Environment and Spatial Planning. Based on the results of comparing existing international schemes for assessing sustainable buildings, and evaluating the possibility of transferring individual systems to the Slovenian legislative environment, the researchers prepared an initial suggestion for a set of criteria. They also proposed an action plan for the introduction of a system of sustainable building indicators (SBI). The concept was in line with current trends in sustainable construction in the EU, with the emerging Level(s). The Slovenian concept also supported the implementation of priority policies in the field of reducing greenhouse gas emissions in the life cycle of the building. Furthermore, it promoted efficient use of water, raw materials, healthy and comfortable living conditions, and addressed the adaptation to climate change.

The basis for the development of the Slovenian system is the aforementioned European framework Level(s), prepared by the Joint Research Centre – JRC in 2015-2017 [7]. Level(s) is a common EU framework of core sustainability indicators for the evaluation of office and residential buildings. The system is structured into six macro objectives and provides a set of individual indicators, scenarios and tools for assessing the environmental performance in a building's life cycle. In addition to environmental characteristics, it also includes an assessment of other important properties of buildings that affect healthy and comfortable living, as well as an assessment of life-cycle costs and the management of potential future risks for the operation of the buildings.

The common EU Framework of core sustainability indicators, presented in the JRC publication [7], provides:

- Macro objectives, defined in the areas of energy, materials and waste use, water and indoor air quality, which contribute to the set European and national policy orientations in the field of sustainable construction.
- A set of nine core indicators (and sub-indicators) and common metrics for measuring the properties of buildings that contribute to each macro objective. The system is designed to promote the use of the Life Cycle Assessment (LCA) and Life Cycle Costing (LCC) methods.
- Lifecycle-based scenario tools: a set of four scenario tools and one data collection tool, together with a simplified LCA analysis that supports a comprehensive analysis of building properties taking into account the entire life cycle.
- Property valuation influence and reliability rating, which can assess the potential positive effect on the valuation of the property and demonstrate the reliability of the performance appraisal in the valuation using the Level(s) framework.

Depending on the complexity, the method provides for three levels of assessment (hence the name of the method: Level(s)):

- Level 1: Common performance assessment – determination of indicators based on a common methodology, the simplest and most accessible type of use for each indicator.
- Level 2: Comparative performance assessment – comparison between functionally equivalent buildings, at the national level or within the portfolio of buildings of one investor (need for laying down the rules to support the comparability of results).
- Level 3: Performance optimisation assessment – advanced use of indicators, for professionals to perform complex analyses (which may include accurate simulations, modelling, anticipating future costs, risks and life cycle opportunities) and determine the optimal design of the building.

The Level(s) framework is not yet finalised at this time; its Beta version was available for testing from autumn 2017 to September 2019, which, according to the analysis [2], included 136 construction projects from 21 countries, including 2 from Slovenia. Detailed analysis [8] of the response of experts revealed the general expectations of the profession regarding Level(s). It showed that due to the complexity of the system, only indicators at Level 1 were mostly tested. It also highlighted methodological gaps, especially in the life cycle aspect and in the use of results in the decision-making process, as Level(s) does not provide reference values.

The European Commission continues with the development of the Level(s) framework, with great emphasis in the future on integration into digitised planning through BIM tools and on the realisation of the idea of a building passport.

3 DEVELOPMENT AND CONCEPT OF SBI

3.1 Action plan of SBI

In the next phase of the development of Slovenian sustainable buildings indicators (SBI) the research work became part of the project LIFE IP CARE4CLIMATE (2019-2026), Action 4.4. The first two years were dedicated to stakeholder consultations and the preparation of the initial Alpha version of SBIs. Stakeholders were consulted through several workshops: workshop with the public sector, construction industry, architects and engineers, researchers, professional organisations, the Eco Fund, ministries, etc. Designing of the Alpha version of SBI took place in an inclusive process with key decision makers, users and developers.

Like Level(s), the Alpha version of the SBI will undergo a testing process, which will involve interested users. The purpose of this first testing is to verify the applicability of individual, nationally adapted indicators and to define the content of everything that is needed at the national level when adapting Level(s) (e.g. knowledge, tools, databases, criteria). Testing of the Alpha version will take 12 months and will go on interactively through a "supporting environment and e-platform", including online training. Both the SBI supporting environment and the e-platform are essential for the development of the indicator system (Figure 1). The process of formation, improvement and upgrading of the SBI supporting environment and the e-platform will take place gradually. It will be created in close cooperation with external

experts in various fields in order to provide information and data to assess the selected indicator, and to share the necessary knowledge about methods, tools, standardisation and about the progress in a particular field [9].

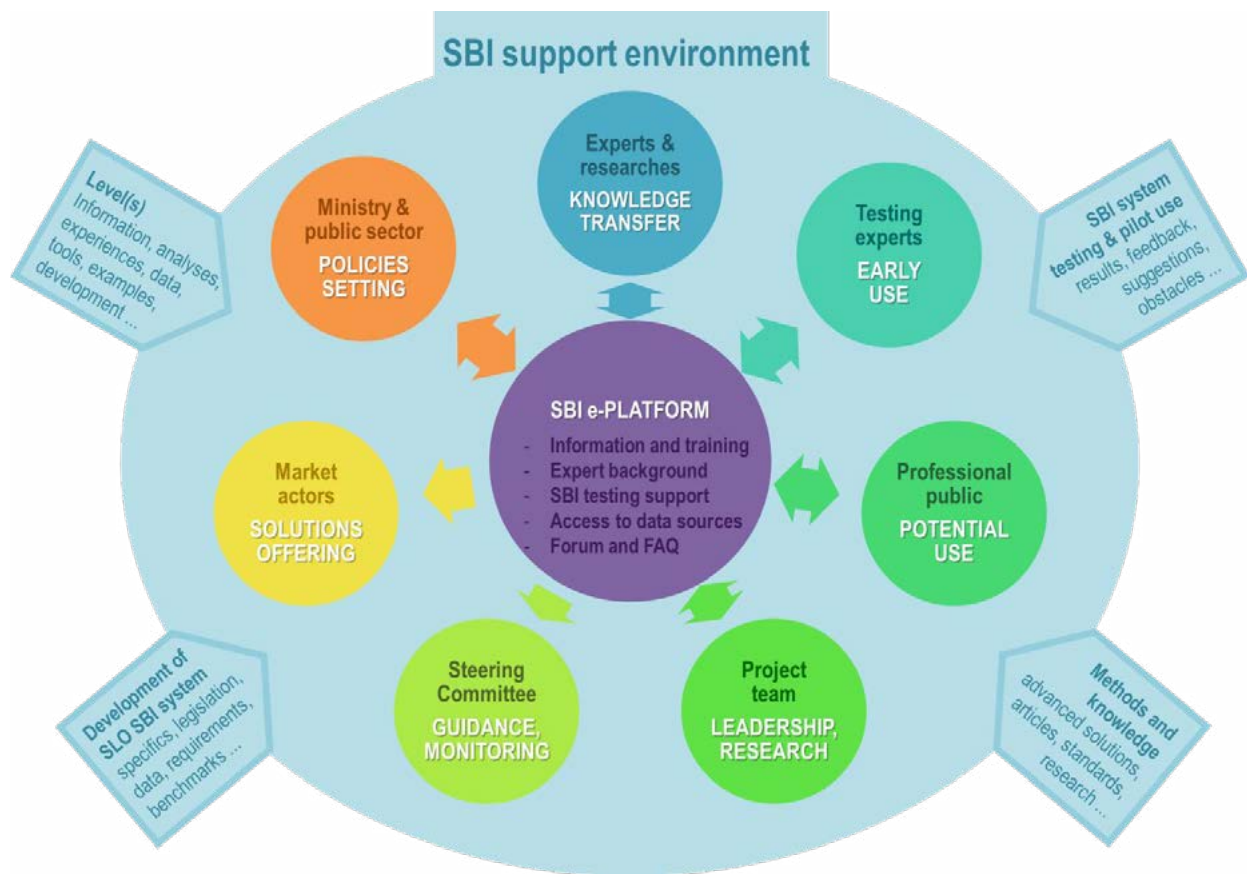


Figure 1: Structure of supporting the environment and the e-platform for Slovenian sustainable building indicators.

The second part of the project is planned for the development of the SBIs upgrade. The SBI will be integrated into a comprehensive evaluation system called the Beta version. This will be followed by the phase of balancing the indicators and testing them on the selected projects. Thus, by 2026, the plan is to prepare a functioning system for the evaluation of sustainable buildings, nationally adapted and in line with the updated Level(s) framework.

3.2 Concept of SBI

The Alpha version of the SBI contains the same structure of the six macro objectives of the Level(s) framework, and the corresponding set of indicators and tools. Already in this first version, some preliminary values of indicators are envisaged, which are harmonised with Slovenian legislation, building regulations and rules of good practice. Identified gaps in the criteria, software tools and databases have been added; as well as gaps in the knowledge required to carry out the assessment and in established construction procedures and legal bases. In this way, the general harmonisation of the Slovenian SBI and circular economy in the construction sector with European guidelines will be ensured. The proposed structure of the Alpha version of the SBI is presented by the individual macro-objectives below along with key findings and comments.

Macro-objective 1: Greenhouse gas emissions during a buildings life cycle

For indicator 1.1, *Use stage energy performance*, the procedures for determining energy use in a building are methodologically supported with the building regulation, the Rules on the efficient use of energy in buildings [10], the corresponding technical guideline and with the EN EPB family of standards. Through all the analyses, ambiguities were found, such as the determination of renewable and non-renewable parts of primary energy. But they are expected to be eliminated with the adoption of a new regulation that will consistently build the calculation methodology on the standards of the EN EPB. The various software used in Slovenia to calculate energy consumption are mainly suitable for determining the indicator. In particular, when using simpler programmes with a monthly calculation method, it is taken into

account that the reporting of energy flows is allowed in a slightly aggregated way.

Indicator 1.2, *Life cycle Global Warming Potential*, is more complex and its gradual introduction into practice can be expected. In order to define the indicator, it is necessary to make a LCA of building from cradle to cradle in accordance with SIST EN 15978. LCA analysis at this level is still very demanding for real implementation in the Slovenian environment, and a number of input data is missing. However, it is possible to apply simplifications based on the treatment of an incomplete life cycle, such as life cycle stages, described in modules in EN 15978 “A1-3, B4, B5, B6” or “A1-3, B6, C3-4, D”. These are primarily phases that demonstrate the environmental impact of the materials used and the impact of the use of the building, but may also include the impact of the end of the life cycle of the building and the burdens and benefits across system boundaries. Among the key input data for the implementation of LCA analyses are EPDs, so it will be necessary to provide a EPD database for products on the Slovenian market. Another option is to lay down rules for the use of generic data for building products and materials.

Macro-objective 2: Resource efficient and circular material life cycles

The first tool, 2.1, *Bill of Materials (BoM)*, is based on an inventory of individual materials. Inventory must include all materials that are installed in an existing building (or in case of planning, materials that will be installed) and also the materials that are expected to be available upon demolition of the building in question. For this indicator, an overview of the building components is first made, which is approximately similar to the so-called “inventory of construction works” that is a required part of Slovenian construction documentation. An overview of the materials contained in the components is then prepared and finally classified into four groups according to Eurostat: metal materials, non-metallic mineral materials, biomass-based materials and fossil energy materials. As the “inventory of construction works” in Slovenia has not yet been standardised, the preparation of the BoM will require quite a bit of effort. It can be expected that the practical use of BIM tools, which will enable the systematic provision of the necessary data from the early project phases in the design of buildings, will simplify the preparation of the BoM.

The BoM is an important starting point for the determination of some other SBIs and for the use of the group of 2.2 *Scenarios for building lifespan, adaptability and deconstruction*. These address three aspects: the planning aspect of the building and elements lifespan, the planning aspect for the adaptability and renovation of the building, and the planning aspect for decommissioning, reuse and recycling. The result is information about the building in terms of scenarios for building lifespan, its adaptability and deconstruction.

The indicator 2.3, *Construction and demolition waste and materials*, is the only indicator from Macro-objective 2 in Slovenia, which is already regulated by the construction waste management plan during construction and must be harmonised with the Decree on the management of waste generated during construction works.

The tool 2.4, *Cradle to grave Life Cycle Assessment analysis*, performed in accordance with SIST EN ISO 14040/44 and SIST EN 15978 requires in practice the use of specialised software and, above all, access to a wide range of databases. Generic data in various databases are available, but for fine optimisation at level 3, specific data on individual products and materials related to the Slovenian construction sector – production and market – is needed. Supporting software packages that meet the requirements for the implementation of the LCA are available and are already used in Slovenia. However, due to the relatively high complexity and required knowledge of the software operators, the use of these tools requires a suitably qualified user and additional resources on the part of the project team, as well as a well-informed client.

Macro-objective 3: Efficient use of water resources

This macro-objective contains only one indicator: 3.1, *Total water consumption*, which refers to the efficient use of water in the use phase of the building. The indicator assesses the use of water per occupant per year, with the exception of the use of water for the manufacture of products for the building and for the construction of the building. The Slovenian SBI has adopted the Level(s) tool for this indicator, which offers Excel tables with default values that can be used for estimations when data are not available.

The indicator is suitable for use in the Slovenian construction sector and is methodologically sufficiently supported. However, real data for the water use factor per user and for microclimatic factors (in the case of assessing the need for water for irrigation) are missing for Slovenia. But in the first step, these values can be defaulted from the Level(s) system.

Macro-objective 4: Healthy and comfortable spaces

The first of the two indicators in macro-objective 4, 4.1, deals with *Indoor air quality*. One of the building ventilation simulation tools should be used for the assessment at the planning stage, and the entire building should be included in the calculation. All parameters predicted by the method, ventilation rate, CO₂ concentration, relative humidity, benzene concentration and particulate matter (PM_{2.5/10.0}), must be classified according to the prescribed standards. In accordance with the standards, it is also possible to assess the presence of mould.

From the point of view of controlling emissions of harmful substances into the indoor environment, the method is also based on a systematic inventory of all key materials that will be installed in the building and on the indication of their emissions. Emissions of harmful pollutants for each material must be determined on the basis of standard test methods. However, the challenge in Slovenia is the availability of these data. An assessment based on measurements is performed after the completion of construction, with mandatory testing of the operation of the ventilation system, and optional measurement of radon concentrations.

The second indicator, 4.2, *Time outside of thermal comfort range*, is assessed with two sub-indicators, the operating temperature or PMV and PPD index, and the criteria for local thermal comfort. The assessment is carried out during the design of the building by means of simulations of the thermal response of the building by switching heating and cooling on and off. Any computational tool (e.g. PHPP, EnergyPlus, IDA ICE, TRNSYS) can be used for simulations. The method does not prescribe the use of dynamic simulations, but gives them an advantage. It is also possible to perform a simplified determination of the indicator with an estimate of overheating.

Macro-objective 5: Adaptation and resilience to climate change

Macro-objective 5 with one indicator, 5.1, *Scenarios for projected future climate conditions*, which refers to the climatic conditions in 2030 and 2050, has the same methodological procedure. Here, with the help of the scenario tool "Protection of occupier health and thermal comfort", the possible medium- and long-term effects of climate change on the user's health and thermal comfort in the building are examined. The analysis can be carried out with one of the proposed climate change scenarios and relevant climate data for the future. In addition to the original design of the building, simulations on the model can predict more efficient designs using advanced materials with a number of passive and active measures to reduce the effects of extreme summer temperatures caused by climate change.

Macro-objective 6: Optimised life cycle cost and value

The indicator 6.1, *Life Cycle Costs (LCC)*, is used to estimate the costs and values in the life cycle of a building. The standardised procedure covers the initial costs of building construction and the costs of operating the building, including energy, water, the maintenance, repair and/or replacement of building parts and components, and end-of-life costs. Land costs and costs for activities taking place in the building are not included in the assessment.

The LCC analysis determines the net present value (NPV) of the total discounted costs over the estimated useful life-span of the building. The use of special computer programs for this purpose is neither necessary nor common in practice. At the beginning of the introduction of the method, a simplified LCC analysis can also be used, covering only selected life cycle phases. This reduces the complexity of the analysis and brings the LCC closer to the user of the sustainable building evaluation. Selected phases can be, for example, the product phase (A1-3) and the application phase – energy and water (B6-7) or the product phase (A1-3) and the application phase – maintenance, replacement, repair, energy (B2-4, B6).

DISCUSSION

The analysis has shown that experts in Slovenia are very likely to master the Macro-objective 1 well, but they will have significantly more problems with the Macro-objective 2, as they have practically no experience with its particular indicators and tools. From its group of criteria, Building bill of materials (BoM), unified scenarios for building lifespan, adaptability and deconstruction and Cradle to grave Life Cycle Assessment, only the treatment of the indicator Construction and demolition waste and materials is already established. In addition, indicator 3.1, Total water consumption, is suitable for use in the Slovenian construction sector. It is methodologically sufficiently supported, assuming that it will be supplemented with missing data on real water use. The study further revealed that evaluating a building according to

indicators 4.1, Indoor air quality, and 4.2, Time outside of thermal comfort range, means that it is necessary to master more demanding software tools. On the other hand, the implementation of BIM and the development of plug-ins for BIM software, which will enable simpler modelling of energy flows and thermal comfort parameters in the building, are expected to facilitate and automate the process and enable its control. As this is a methodologically identical principle, a similar finding applies to indicator 5.1, Scenarios for projected future climate conditions. Additionally, it can be established that for preparing the analyses for this indicator, it will be necessary to select one of the proposed climate change scenarios at the national level and then use data from one of the climate atlases (e.g. Meteonorm) or prepare the necessary national data. And finally, the study showed that indicator 6.1, Life Cycle Costs (LCC), is manageable; nevertheless, the biggest challenge in LCC analysis will be to provide input data and boundary conditions for analysis.

Investors are currently not yet acknowledging the slightly higher planning input due to the digitisation of the process and the evaluation of sustainability aspects in buildings [10]. In the public sector, incentives and pilot projects are typically needed to highlight public procurement processes in the field of sustainable buildings. It is clear that the faster the digitisation of the construction process, especially the implementation of BIM, also means great opportunities for implementing the sustainability evaluation. But it also brings with it the need to establish system support – to provide, for example, harmonised unified databases for products and systems. Last but not least, it also brings the need to set legislative requirements for environmental product declarations (EPDs), which are gradually gaining importance on the Slovenian market [11].

With the Level(s) upgrade, the EC grasps great potential for expanding the method, including integration with national building policies and in public procurement of buildings. On the other hand, the results of testing the Level(s) framework showed a relatively low level of maturity of the system. Therefore, radical changes can be expected in the new version, which will also affect the development of the SBI in Slovenia.

CONCLUSION

The importance of sustainable buildings in Slovenia is gradually being recognised on several levels of the construction sector, including in the design profession. However, there are still many obstacles for their actual use in practice. In most cases, organisational, technical and procedural constraints, a lack of knowledge for planning and skills, gaps in the digitisation of sustainable building design and a deficiency of databases emerged. But most importantly, there is no metric for sustainable buildings in Slovenia. This shortcoming is intended to be remedied by developing the national sustainable building indicators SBI, the task currently being performed in the LIFE IP CARE4CLIMATE project in accordance with the EU Level(s) framework.

Based on initial research with key construction stakeholders, it can be concluded that the SBI solution must be strongly linked to the national building legislation, computational methods and available software tools, as well as to established planning procedures. In parallel with the development of the SBI system, it is also essential to provide a functional supporting SBI environment and e-platform.

Above all, it can be concluded that the development of Slovenian indicators of sustainable construction in Slovenia is taking place at just the right time to catch the European development wave in the introduction of common metrics for sustainable buildings.

ACKNOWLEDGMENTS

This article was created within the Action C4.4 of LIFE IP CARE4CLIMATE project (LIFE17 IPC/SI/000007), which is an integrated project co-financed by the European LIFE programme, The Climate Change Fund and the project partners.

REFERENCES

- [1] European Commission (b. d.), Available from <https://ec.europa.eu/environment/eussd/buildings.htm> Accessed: 2020-07-08

- [2] *Level(s): Taking action on the TOTAL impact of the construction sector*, Publications Office of the European Union, Luxembourg (2019) Available from https://ec.europa.eu/info/sites/info/files/levels_conference_report.pdf Accessed: 2020-07-08
- [3] COM(2019) 640 final. *The European Green Deal*, Brussels European Commission (2019) Available from <https://eur-lex.europa.eu/legal-content/SL/TXT/DOC/?uri=CELEX:52019DC0640&from=EN> Accessed: 2020-07-08
- [4] COM(2019) 640 final ANNEX. *Annex to the European Green Deal*, Brussels European Commission (2019) Available from <https://eur-lex.europa.eu/legal-content/EN/TXT/DOC/?uri=CELEX:52019DC0640&from=EN> Accessed: 2020-07-08
- [5] COM(2020) 98 final. *A new Circular Economy Action Plan For a cleaner and more competitive Europe*, Brussels European Commission (2020) Available from <https://op.europa.eu/sl/publication-detail/-/publication/6e6be661-6414-11ea-b735-01aa75ed71a1> Accessed: 2020-07-08
- [6] *Pregled sistemov trajnostnih kriterijev s predlogom prenosa*, GI ZRMK and ZAG (2017) Available from https://www.gov.si/assets/ministrstva/MOP/Dokumenti/Graditev/sistem_trajnostnih_kriterijev_porocilo1.pdf Accessed: 2020-07-08
- [7] Dodd, N.; Cordella, M. et al: *Level(s) – A common EU framework of core sustainability indicators for office and residential buildings*, Part 3, EC JRC (2017) Available from [https://susproc.jrc.ec.europa.eu/Efficient_Buildings/docs/20200204_Level\(s\)_test_phase_EU_Survey_findings_Final.pdf](https://susproc.jrc.ec.europa.eu/Efficient_Buildings/docs/20200204_Level(s)_test_phase_EU_Survey_findings_Final.pdf) Accessed: 2020-07-10
- [8] Dodd, N., Cordella, M. et al: *Level(s) test phase analysis Annex 1: Results of the EU survey*, Draft consultation version, EC JRC (2020) Available from [https://susproc.jrc.ec.europa.eu/Efficient_Buildings/docs/20200204_Level\(s\)_test_phase_EU_Survey_findings_Final.pdf](https://susproc.jrc.ec.europa.eu/Efficient_Buildings/docs/20200204_Level(s)_test_phase_EU_Survey_findings_Final.pdf) Accessed: 2020-07-10
- [9] *D7-1 Razvijajoče se letno poročilo o razvoju podpornega okolja in platforme za trajnostno gradnjo*, GI ZRMK and ZAG (2019) Available from <https://www.care4climate.si/sl/o-projektu/podrocja-aktivnosti-projekta/trajnostna-gradnja-in-ucinkovita-raba-energije-v-stavbah-in-podjetjih> Accessed: 2020-07-12
- [10] *Pravilnik o učinkoviti rabi energije v stavbah* (Rules on the efficient use of energy in buildings), Uradni list RS, št. 52/10 in 61/17 – GZ (2010) Available from <http://www.pisrs.si/Pis.web/pregledPredpisa?id=PRAV10043> Accessed: 2010-06-30
- [11] *D1 Poročilo o posvetovalnih delavnicah z deležniki o kazalnikih trajnostne gradnje*, GI ZRMK and ZAG (2019) Available from <https://www.care4climate.si/sl/o-projektu/podrocja-aktivnosti-projekta/trajnostna-gradnja-in-ucinkovita-raba-energije-v-stavbah-in-podjetjih>, Accessed: 2020-07-12

19

Naser Kabashi, Enes Krasniqi and Milot Muhaxheri

Influence of waste glass addition on concrete properties



INFLUENCE OF WASTE GLASS ADDITION ON CONCRETE PROPERTIES

Naser Kabashi¹, Enes Krasniqi² and Milot Muhaxheri³

^{1,2,3}, University of Prishtina, Faculty of Civil Engineering, Department of Materials and Structures
Sunny Hill p.n, 10 000 Prishtina, Kosovo
e-mail: naser.kabashi@uni-pr.edu, enes.krasniqi@uni-pr.edu, milot.muhaxheri@uni-pr.edu

SUMMARY: In order to address environmental effects associated with cement production, there is a need to develop alternative binders to make concrete. Crushed waste glass accumulated at some extent has a negative environmental impact, moreover likewise there is a propensity of cement production manufactures toward using supplementary cementitious materials that result on less emissions in terms of the environmental pollution. In this paper are highlighted the key findings of milled/crushed waste glass as a substitution of cement content for concrete production. The study is tackled at two different levels. Firstly, the interaction of cement and milled waste glass is established through fresh (flow test and setting times) and solid state (mortar bending and compression tests). These findings lead on optimal substitution content of waste glass with respect to cement. At the second level a correlation between crushed waste glass and aggregate grading curves is established through series of tests at fresh (slump test) and solid state (compression and bending tests). In the same time the chemical analysis of waste glass are presented and interaction with cement will be discussed. This paper gives an overview of the current progress and recycling situation of waste glass and points out the direction for the proper use of waste glass as replacement of cement. The role of glass powder as replacement of cement provides considerable value-added utilization and meaningfully affects the output of greenhouse gases from cement industry. This paper presents the feasibility of the substitution of waste glass powder for cement to achieve economical and environmentally friendly construction material. Glass powder (GP) with determined nature and fineness module used in this study had minor effect on flow results and in relevant way increases the setting time and duration of the setting. In concrete samples, the use of 10% GP as cement replacement enhances concrete compressive strength and the contribution of GP is negligible compared to the cement even when using the highest emission rate. The benefit is not only on the reuse of waste glass but also tents to create a greener environment.

KEY WORDS: Recycling glass, waste glass, supplementary cementitious materials, environment.

1 INTRODUCTION

Cement production is an energy-intensive and highly polluting process, contributing about 5–8% to global CO₂ emissions [1]. But this is oddly low considering that it makes about 50% of all solid materials we produce. Still supplementary waste additions in cement can have real impact on environmental footprint. Being that the cement is the most polluting component of concrete, the use of solid waste materials or industrial by-products as partial replacement for cement in concrete is a viable strategy for reducing the environmental and energy impacts of concrete production [2]. Since the first manufactured glass in ancient Mesopotamia [1] its production has increased since then to reach massive capacities, which inevitably involves major waste rates. In spite of the lack of information; in 2012 it was estimated that a high-income country produces 602 million tons of solid waste per year, 7% of which is glass [3]. Waste glass due to its non-compatibility of being bio-degradable in nature requires coherent considerations for alternative utilizations away from disposal sites [4].

Glass powder appears to be consonant with cement because it contains silica (SiO₂) in amounts greater than 70%. Glass can be produced with high specific surface area and is amorphous in nature, which allows it to react with portlandite [5]. Most of the studies have shown that glass powder pozzolanic reaction could be triggered at a particle size below 300µm [6]. The synergy between cement and glass powder can be advantageous to reduce the percentage of cement in concrete and manage waste glass generation, while maintain non-alterable properties of concrete. According to the previous studies in the use of glass powder in concrete production as cement replacement, there were contradictions in the available test results. Variations on results are subject to numerous factors involved such as source of recycled glass, glass chemical properties, fineness module etc. These factors considerably affect the fresh and hardened proprieties of cement mortar and concrete modified with glass powder.[8].

The influence of the amount of GP as a cement substitution has been widely studied [7,8,9], it is noted that optimal results be achieved between 10–30% [3,7], and even amounts up to 15% have shown enhancement on the compressive strength [10]. Moreover, the hydration of cement may be improved due to the particle size and the pozzolanic performance of GP [11]. Indeed, according to the physical and chemical criteria of ASTM C 618 [12] and EN 450-1 [13], glass can be considered a pozzolanic cementitious material [14].

2 MATERIALS AND METHODS

2.1 Portland Cement and Waste Glass

Samples of cement and glass powder have been examined and results are presented in table below. In this study the pozzolanic cement employed was CEM I 52.5N.

Table 1. Chemical composition of cement and Glass powder (GP).

Chemical Composition	Cement (%)	Glass powder (%)
Al ₂ O ₃	5.78	1.04
CaO	62.9	9.32
Fe ₂ O ₃	3.66	0.07
K ₂ O	0.58	0.18
MgO	2.47	4.27
Na ₂ O	0.41	13.64
SiO ₂	20.82	71.38
SO ₃	2.49	0.22

The typical soda water lime glass used in this study is obtained from cleaned glass bottles and from the glass factories. The GP is obtained through crushing and dry grinding process. Thereafter the particles are separated according to the size required. In this case glass powder is obtained by sieving the grinded glass with a passing grading curve presented in Figure 1. The chemical composition of GP determined from laboratory is compared with cement and according to EN 450-1 [13], and ASTM C 618 [12], SiO₂ + Al₂O₃ + FeO₃ minimum requirement for a standard pozzolana is 70% the results obtained from waste glass samples exceed this condition. Compounds such as BaO, TiO, MnO were present in glass powder sample, the amount of each individual component was not more than 0.3%.

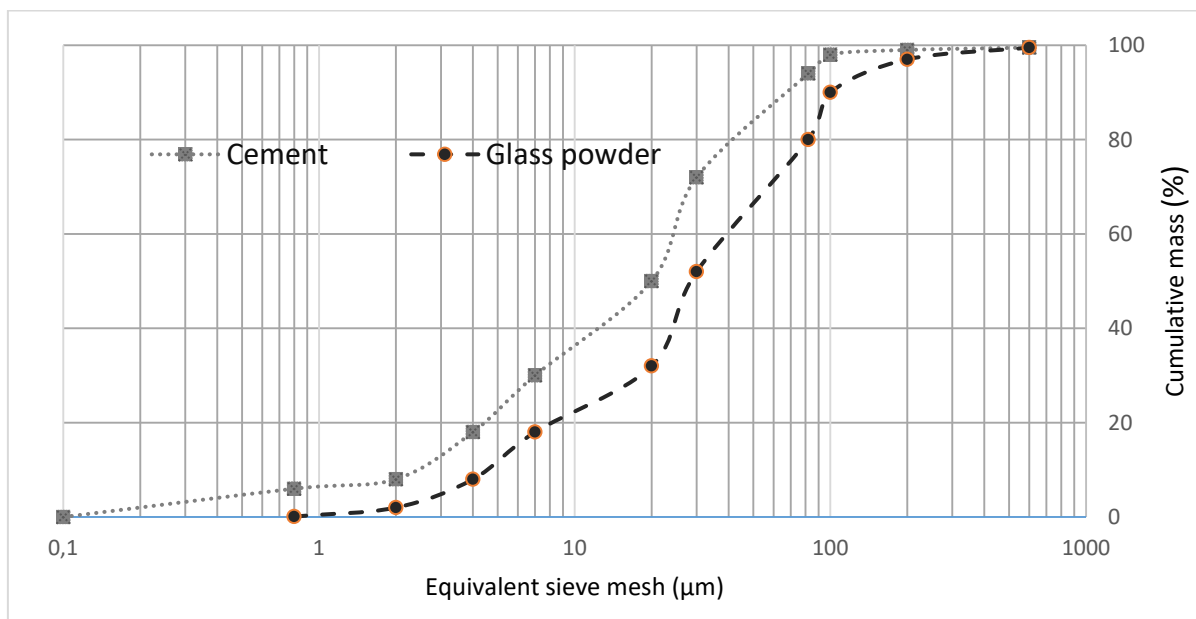


Figure 1. Cement vs glass powder particle size distribution

2.2 Cement mortar and Concrete Mix design

Ordinary Portland Cement (CEM I 52.5 N) was replaced by different amounts of glass powder. The proportions of the mortar mixture for a set of standard samples are provided in Table 2 according to EN 196-1 [15]. The influence of different quantities of glass powder is investigated, apart from reference samples, the three other mortar mixtures were prepared with 10%, 20% and 30% GP content as replacement of cement. They were prepared with a water to cement ratio of 0.5 and cement to sand ratio of 1:3.

Table 2. Mortar mixture proportions.

	Sand (g)	Cement (g)	Water (g)	GP (g)
CM	1350	450	270	-
CM-GP1	1350	405	270	45
CM-GP2	1350	360	270	90
CM-GP3	1350	315	270	135

Regarding the curing of specimens, all of them were stored in a humidity chamber, where the temperature was maintained constant at 20°C and the relative humidity (RH) was at 95%, during the first 24h after setting. Thereafter, the specimens were de-molded and kept immersed in water in optimum laboratory conditions (20°C and 100% RH), up to the corresponding testing age.

The concrete consisted of the combined grading of four fractions (0-31.5mm) at the ratio of size 0-4mm 52%; 4-8mm 16% 8-16mm 14% and 16-31.5mm 18% respectively. Similar to cement mortar samples the design mix of concrete is conducted by including glass powder as cement replacement with ratios of 10%, 20% and 30%. The detailed mix design is provided in Table 3.

Table 3. Mix proportion of concrete

	Coarse aggregate (kg)	Fine aggregate (kg)	Cement (kg)	GP (kg)	Water (kg)
CM	602.3	1280	350	-	157.5
CM-GP1	602.3	1280	315	35	157.5
CM-GP2	602.3	1280	280	70	157.5
CM-GP3	602.3	1280	245	105	157.5

2.3 Experimental methodology

The flow was measured according to EN 1015-3 [16] with a mini slump cone common for mortar examinations, the cone internal diameter was 100 mm, on a 250 mm flow table disc. The procedure was as follows: the mold was first filled with fresh mortar, then the flow table was jolted 15 times at a constant rate. Two perpendicular diameters of the mortar were then measured and recorded.

Concrete slump test or slump cone test is used to determine the workability or consistency of concrete mix prepared at the laboratory during the testing progress. Concrete slump test is carried out from batch to batch to check the influence of glass powder in workability. The slump is carried out as per procedures in EN 12350-2 [17].

Complying with EN 196-1 [15], three different prism specimens measuring (4×4×16 cm) were tested for each series at 2 and 28 curing days, from which the compressive and flexural strengths were obtained and tested Figure 2. In relation to cement specimens a set of three cubes (150 x150 x 150 cm) and prisms (150 x 150 x 600) in each case are tested for compressive and flexural strength in accordance with EN 206-1 [18]. In total nine samples were prepared including the control sample. The samples had glass powder included at various percentages (10%, 20% and 30%). During batching process, precaution was taken to ensure that the glass powders were blended homogeneously in the concrete mixer. The detailed mix design is provided in Table 3.



Figure 2. Cement mortar preparation and testing

2.3.1 Alkali-silica reaction (ASR)

The Mortar prismatic bars were prepared according to ASTM C 1260 [19] in order to measure mortar expansion. This test method provides means of detecting the potentially deleterious internal expansion cause by alkali-silica reaction (ASR)[20]. The expansion or the length change of the mortar bars due to ASR was measured at certain intervals. The method prescribed in ASTM C 1260 [19] Figure 3, was followed as it is a quick way of determining the potential reactivity of the aggregates in the mortar mix.



Figure 3. Prismatic samples for ASR testing and expansion measurement

To determine the expansion due to ASR, the length of the mortar bars is measured and recorded at the end of 3, 7, and 14 days of exposure in 1M sodium hydroxide solution, which is a mixture of 40 grams of sodium hydroxide and 900 ml of water. The container is placed in a water bath maintained at 80°C. After 24 hours, the length of the specimens is measured, and then placed back into the container with 1M NaOH maintained at 80°C. The specimens are removed briefly from the containers periodically and measured before significant cooling occurs. The average expansion of the three mortar bars, after 14 days of immersion in the hydroxide solution, is used to estimate the reactivity of the aggregate. As illustrated in Table 4, 0.0 to 0.1 percent expansion means that the specific aggregate tested is not reactive, 0.1 to 0.2 percent is considered to be inconclusive and require further testing, and greater than 0.2 percent is considered to be reactive. Afterwards, the ASR expansion of cement mortar bars is calculated by Equation (3). In this experiment, three duplicated cement mortar bars are used to obtain the average ASR expansion.

$$E_{ASR} = \frac{L_t - L_0}{L_0} 100\% \quad (3)$$

where E_{asr} (%) is the ASR expansion of cement mortar bars at the age of T (day); the L_t (mm) is the length of the mortar bars excluding both ends of the length of copper head at the curing age of T (day); the L_0 (mm) is the initial length of cement mortar bars excluding both ends of the length of metal head.

2.4 Environmental consideration-Greenhouse Gases (GHG) Analysis

In order to estimate CO₂ the values referent models [20] are used to determine the glass particle size corresponding to the 25th, 50th, 75th and 90th percentiles of the particle size, respectively, depending on the grinding time. A relation is done between the production of GP with determined fineness module of glass sample used in this research. Equation (1) (which presents R² = 0.963) is used inversely to calculate the approximate grinding time taken to obtain particles of the size used in this study.

$$D_{90} = -360\lg(\lg(t)) + 137.1 \quad (1)$$

where D₇₅ is the size (µm) of the opening of the sieve, through which 75% of the sample mass passes, and t is the grinding time in minutes. Inversion is proposed to obtain the ratio showed in Equation (2).

$$t = 10^{10 \frac{D_{75} - 137.1}{-360}} \quad (2)$$

The electricity consumption in the process of grinding and segregating the glass is from 3 to 15 kWh per ton [21]. In order to determine the influence of CO₂ emissions on electricity production, a comparison was made between the amount of CO₂ per ton of GP depending on their emissions per kWh (kgCO₂/kWh) and cement where the CO₂ emission recorded in the ICE Database is considered [22].

For determined cement used in this research, it was considered a factor of 0.912 kgCO₂/kg and an embodied energy of 4.6 MJ/kg (1277 kWh/ton) [23] in comparison to GP where an estimation was made of the energy consumption and the average CO₂ emissions provided by the OECD [16] per kWh associated with the generation of electricity (0.444 kg CO₂/kWh). In terms of the GHG and energy consumption, the contribution of GP is negligible compared to the cement.

3 RESULTS AND DISCUSIONS

3.1 Flow Test

Previous studies [14] indicated that flow ability is increased by addition of glass powder. The increase of mortar flow is related to nature of glass and fineness module, cleaner and finer GP have shown influence on flowability. In Table 4 it is demonstrated, that the GP utilised in this study had contrary effect in flow ability, as there was minor difference between the flow results at different glass replacements levels with 9, 8 and 9 percent corresponding to 10, 20 and 30% GP respectively.

Table 4. Mix proportion of concrete

	Spread (mm)
CM	160
CM-GP1	165
CM-GP2	155
CM-GP3	150

3.2. ASR measurements

The main criticism of ASTM C 1260 [19] is that the high temperature combined with the high concentration of free hydroxides creates a very harsh condition that may not give results representative of what actually happens under field conditions. Figure 4 shows the relationship between waste GP and ASR expansion of cementitious composite bars when the cement was partially replaced using waste glass powder by 10, 20 and 30%, respectively. It can be observed in Figure 4, that the ASR expansion of all cementitious composite bars increases linearly by increasing the amount of GP although even after 14 days there is no indication of samples in ASR expansions.

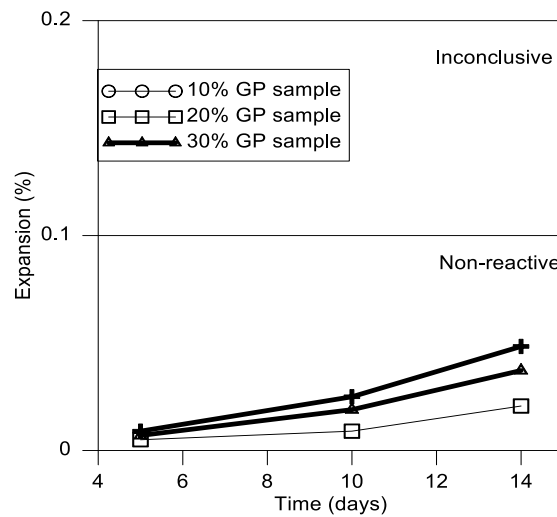


Figure 4. Alkali-silica expansion of mortar bars containing different levels of GP

3.3. Setting time

Vicat apparatus is used to determine the initial and final setting time of binder paste. Complying with EN 196-3 [24], the mould is placed in Vicat instrument where the distance from the edge of the needle and base plate is measured. As shown in Figure 5 replacing cement with GP increases the setting time and duration of the setting. With regards to workability, GP serves as a retarder increasing the period of hardening process. This property is also related to pozzolanic effect of GP and the mechanical behaviour as yielding effect.

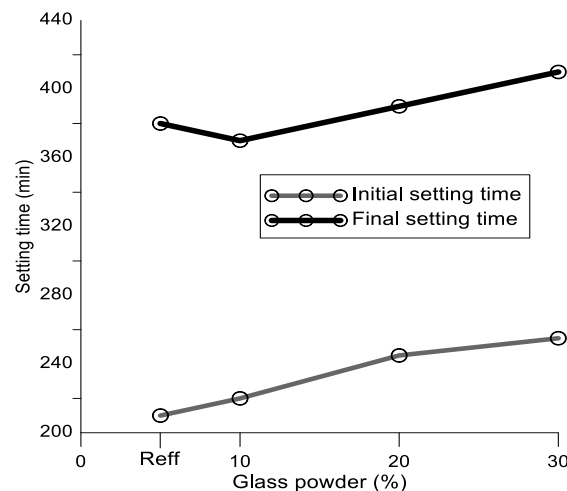


Figure 5. Initial and final setting time for different GP-cement replacements

3.4. Compressive and flexural strength of cement mortar and concrete

According EN 196-1 [15], mortar specimens are used to evaluate the compressive strength performance of cement. The testing results consists of mortar compressive strength for individual samples, mean strength, and standard deviation. In Figure 6 are presented the test results of standard mortar modified with 0%, 10%, 20% and 30% GP cement replacement after 2 and 28 days of curing. As represented below, it is obvious that the use of GP as cement replacement decreases slightly the mortar compressive and flexure strength at the considered ages. Also, relating with limits of EN 196-1 [15], only mortar mixes with 10% GP have achieved the minimum requirements of mortar compressive strength as per determined cement class. The effect of using glass powder as cement replacement on cube concrete compressive strength (f_{ck}) at 7, 14 and 28 days is shown in Figure 7 where we can observe that the use 10% GP as cement replacement enhances slightly concrete compressive strength and GP greater than 10% indicate opposite effects in sense of mechanical properties.

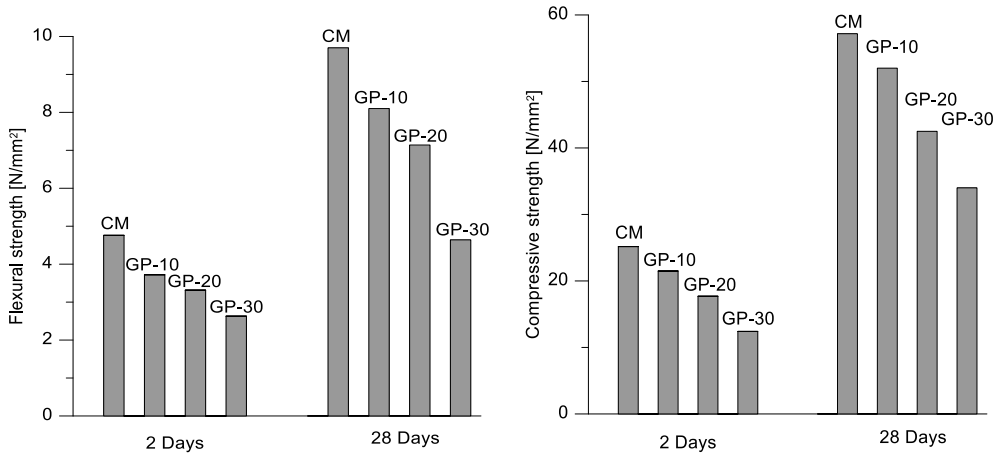


Figure 6. Flexural and compressive strength of various cement compositions

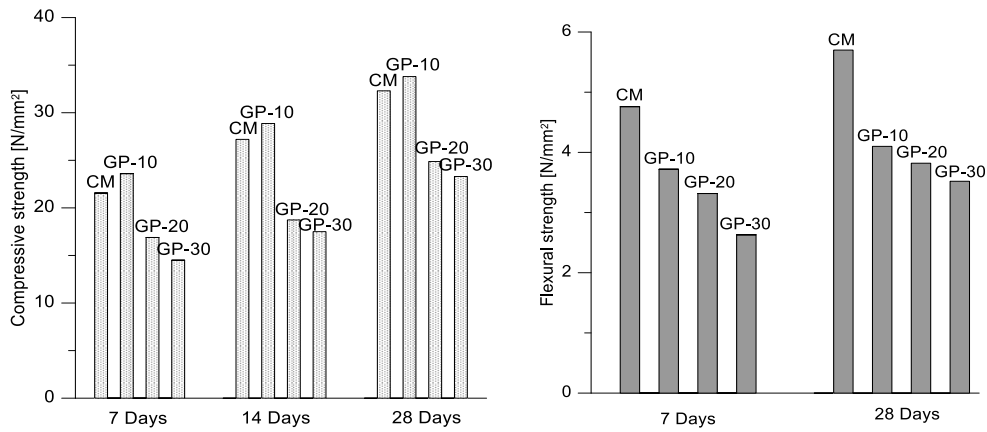


Figure 7. Flexural and compressive strength of various concrete compositions

3.5. Greenhouse Gas (GHG) Assessment

Main national source of electricity (Kosova B) is chosen for comparison with the average of 0.444 kg CO₂/kWh; and based in various countries OECD, Norway with the lowest CO₂ emission per kWh (0.008 CO₂/kWh), South Africa as the country with the highest CO₂ emissions per kWh (0.926 CO₂/kWh), and Kosovo as the object of study in the context of this investigation (0.444 CO₂/kWh). A consumption of 15 kWh per ton of GP is considered [16].

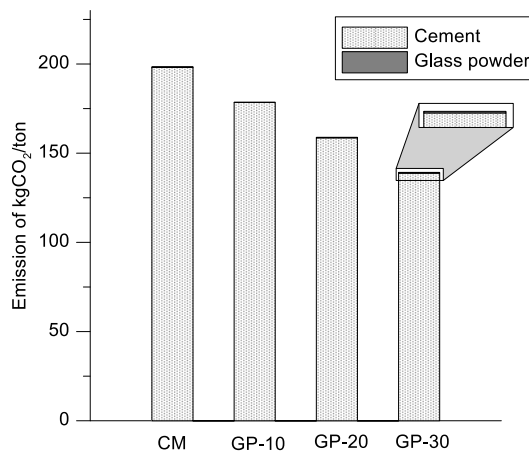


Figure 8. Comparative approach of CO₂ emission

The CO₂ associated with GP grinding is very small compared to the CO₂ associated with the cement that is replaced. The GP part is minor and ranges between 0.16% (for GP-10) and 0.32% (for GP-30) in comparison to cement (kgCO₂/ton) associated with the control sample. The greatest reduction occurs for the GP-30 sample (29.78%) compared to control sample as shown in Figure 8.

4 CONCLUSIONS

GP with determined nature and fineness module used in this study had minor effect as there was minor difference between the flow results at different glass replacements levels. In relevant way, GP increases the setting time and duration of the setting. With regards to workability, GP serves as a retarder increasing the period of hardening process. The ASR expansion of all cementitious composite bars increases linearly by increasing the amount of GP although even after 14 days there is no indication of samples in ASR expansions.

In terms of the Greenhouse Gases (GHG) and energy consumption, the contribution of GP is negligible compared to the cement even when using the highest CO₂ rate per kWh within the OECD.

The use of GP as cement replacement at determined levels decreases slightly the mortar compressive and flexure strength at the considered ages. In concrete the use 10% GP as cement replacement enhances concrete compressive strength while GP greater than 10% has a negative impact in sense of mechanical properties.

REFERENCES

1. C. Pade, M. Guimaraes The CO₂ uptake of concrete in a 100 year perspective *Cem. Concr. Res.*, 37 (9) (2007), pp. 1348-1356
2. R. Gopalakrishnan, D. Govindarajan Compressive strength and electron paramagnetic resonance studies on waste glass admixed cement *New J. Glass Ceram.*, 1 (03) (2011), p. 119
3. Jani, Y.; Hogland, W. Waste glass in the production of cement and concrete—A review. *J. Environ. Chem. Eng.* 2014, 2, 1767–1775.
4. Hoornweg, D.; Bhada-Tata, P. What a Waste. Available online: <https://openknowledge.worldbank.org/handle/10986/17388> (accessed on 5 January 2019).
5. Heriyanto; Pahlevani, F.; Sahajwalla, V. From waste glass to building materials—An innovative sustainable solution for waste glass. *J. Clean. Prod.* 2018, 191, 192–206.
6. Omran, A.; Tagnit-Hamou, A. Performance of glass-powder concrete in field applications. *Constr. Build. Mater.* 2016, 109, 84–95. [CrossRef]
7. 12.Federico, L.M.; Chidiac, S.E. Waste glass as a supplementary cementitious material in concrete—Critical review of treatment methods. *Cem. Concr. Compos.* 2009, 31, 606–610.
8. Kamali, M.; Ghahremaninezhad, A. Effect of glass powders on the mechanical and durability properties of cementitious materials. *Constr. Build. Mater.* 2015, 98, 407–416.
9. Sobolev, K.; Türker, P.; Soboleva, S.; Iscioglu, G. Utilization of waste glass in ECO-cement: Strength properties and microstructural observations. *Waste Manag.* 2007, 27, 971–976. [PubMed]
10. Aliabdo, A.A.; Abd Elmoaty, A.E.M.; Aboshama, A.Y. Utilization of waste glass powder in the production of cement and concrete. *Constr. Build. Mater.* 2016, 124, 866–877.
11. Kamali, M.; Ghahremaninezhad, A. An investigation into the hydration and microstructure of cement pastes modified with glass powders. *Constr. Build. Mater.* 2016, 112, 915–924.
12. ASTM C618 - 19 Standard Specification for Coal Fly Ash and Raw or Calcined Natural Pozzolan for Use in Concrete
13. EN 450-1:2012 Fly ash for concrete. Definition, specifications and conformity criteria
14. Matos, A.M.; Sousa-Coutinho, J. Durability of mortar using waste glass powder as cement replacement. *Constr. Build. Mater.* 2012, 36, 205–215.
15. EN 196-1:2016 Methods of testing cement. Determination of strength
16. EN 1015-3 Methods of test for mortar for masonry - Part 3: Determination of consistence of fresh mortar (by flow table)
17. BS EN 12350-2:2019 Testing fresh concrete. Slump test
18. EN 206-1:2000 Concrete. Specification, performance, production and conformity
19. ASTM C 1260-01 Standard Test Method for Potential Alkali Reactivity of Aggregates (Mortar-Bar Method); ASTM International: West Conshohocken, PA, USA, 2002.
20. Liu, S.; Li, Q.; Xie, G.; Li, L.; Xiao, H. Effect of grinding time on the particle characteristics of glass powder. *Powder Technol.* 2016, 295, 133–141.
21. British Glass Glass Recycling. Available online: <http://www.gpi.org/recycling/glass-recycling-facts> (accessed on 25 January 2019).
22. Hammond, G.P.; Jones, C.I. Embodied energy and carbon in construction materials. *Proc. Inst. Civ. Eng. Energy* 2008, 161, 87–98. [CrossRef]

20

Naser Kabashi, Mihrie Bajoku

Corrosion - cracking parameter in the concrete structure and impact in reinforced steel bars



CORROSION- CRACKING PARAMETER IN THE CONCRETE STRUCTURE AND IMPACT IN REINFORCED STEEL BARS

Naser Kabashi¹, Mihrie Bajoku²

^{1,2} University of Prishtina, Faculty of Civil Engineering, Department of Materials Sunny Hill n,n, 10 000 Prishtina, Kosovo.

e-mail: naser.kabashi@uni-pr.edu, bajokumihrie@gmail.com

ABSTRACT

Concrete structures are under the different environmental conditions, which phenomena will lead to the damages of structure in the time factor. The bridge structures are more attacked, focused on corrosion of steel bars, and with damages of structure elements. Corrosion is caused by many factors of the external environment which, through the protective layer of concrete, reaches the reinforced steel bars in the process caused by the degradation of the concrete in general. The presence of permanent humidity is the permanent factor that involves in the process many other factors from the aggressiveness of environment substances: chlorine, oxygen, carbon dioxide, sulfates, during the penetration process in concrete. The case study analyzing in this paper is a bridge structure, located in village Drelaj, the region of Rugova, mountains in Kosova. The bridge is at an altitude above 2000m and is under the constant influence of extreme temperature conditions. The methods to be applied in this case are analytical and experimental methods. The analytical method is based on measurements and calculate the depth of corrosion according to ASTM code and calculate the percentage of corrosion according to ACI code. The experimental laboratory method we will determine the corrosion rate with the Corrosion meter instrument. In the end, we will make a comparison between the results achieved, and the proposal for repairing, to increase the bearing capacity.

KEY WORDS: corrosion, environment aggressivity, cracking, concrete, reinforces steel bars.

1. INTRODUCTION

The temperature changed in region Rugova, village of Drelaj, has a major impact on the reinforced concrete structures. In this case study, we are focused in reinforced concrete bridge and behavior under the longtime of constructed and without the maintenance and under the aggressive environmental factors. The study is focused in testing the elements of concrete bridge structures which are more affected by environmental factors. The bridge was built 50 years ago, and in visual inspection are evidenced the damages and degradation of the structure in high level. The geometrical parameters of bridge are: length $L = 25.0\text{m}$ ', width $B = 7.0\text{m}$ ' and span $L_0 = 18.0\text{m}$ '. The edge elements of structures are with stone materials, presented in fig.1



Figure 1. Reinforced Concrete Bridge in Drelaj-Peja –photo (25.12.2018)

2. GENERAL CONDITIONS AND DAMAGES OF BRIDGE STRUCTURES

The bridge structure is located in a place where the altitude is very high (over 2000m), and the freeze-thaw cycles, rainfall and water level are main affected factors in degradation process the structures. The level of degradations will lead to the unused structure in very short time, because in many cases is very critical to pass the structures, especially during the winter season. The level of corrosion is very visible and presented in fig.2.



Figure 2. Corrosion process in down part of concrete slab

The concrete protective layer is completely removed and the reinforced steel are completely under environmental aggressive conditions. The structure has been long time under the influence of water, which can be aggressive, acting on the material structure causing harmful effects, such as the impact of aggressive substances in the structure concrete. From the data obtained for the last 10 years from the Ministry of Environment and Spatial Planning, the relative temperature and humidity are presented in table 1, 2 and tab. 3.

Table 1: Maximum temperature (0C) in Peja area

Months	I	II	III	IV	V	VI	VII	VIII	IX	X	XI	XII
Tem.Min(°C)	-8	-2	5	88	17	14	17	18	12	9	2	-1
Tem.Max(°C)	15	22	24	23	32	35	33	35	30	24	24	14

Table 2: Minimum temperature (0C) in Peja area

Months	I	II	III	IV	V	VI	VII	VIII	IX	X	XI	XII
Tem.Min(°C)	-17	-3	-2	0.3	4	7	13	13	4	-2	-2	-9
Tem.Max(°C)	2	14	9	13	17	23	20	21	16	15	11	5

Table 3: Relative humidity (%) max, min, and the average for 10 years in Peja-Drelaj region.

Months	I	II	III	IV	V	VI	VII	VIII	IX	X	XI	XII
Hum. Min.	82	58	48	42	60	78	54	74	71	62	54	66
Hum.max	100	84	90	96	96	92	97	100	100	96	97	98
Hum.aver.	95	73	75	78	73	85	7	86	86	81	81	87

According to the Kosovo Hydro meteorological Institute data, the minimum temperature for ten years in this area is -17°C during the January, while the maximum temperature reaches August 35.2°C . As temperatures, in this case, can change more, freeze-thaw cycles more to offer any possibility, this question in the construction where we have a loss of mass as well as maintenance is to low and will affected directly in concrete durability [1]. The most affected parts of elements are edge concrete walls and concrete slab I down part or in connection with walls, presented on fig.3.



Figure 3: Degradation concrete elements

This process during which amorphous silicon reacts with the alkali present in the cement, which later in contact with moisture increases its volume. For this reason large internal strains, cracks, diminishing durability characteristics, and also can lead to the Alkalo-Silicate reaction which has degraded the elements of the structure (the soffit part is more damaged).Prerequisites for the formation of alkali-silicate reaction in concrete are:

- Presence of alkali-containing aggregate
- Possibility of alkali content in pores filled with water in concrete.
- Moisture penetration into the concrete.

Another important parameter is carbonation in concrete which is on function of many parameters:

mix Design , Casting the concrete, maintenance ,environment aggressively and other parameters.

Due to the heavy rainfall, the wet concrete has been carbonized for a long time, the penetration of moisture deep into the concrete structure has greatly increased the carbonization of the concrete. During the carbonization process, calcium hydroxide ($\text{Ca}(\text{OH})_2$) reacts with CO_2 from the atmosphere and under the action of pH in the atmosphere where the reaction takes place.[2][3]

3. CORROSION MEASUREMENT OF REINFORCEMENT IN CONCRETE WITH CORROSION METER-EXAMINATION OF BRIDGE SECTIONS

In the study case, we are fused in identify the weak points of degradations of concrete, were through the inspections are evidenced the corrosion of reinforced bars in more damages part the concrete. Concept and next step is done using the measurements using the equipment: Corrosion Meter for positions in which the reinforcement is not exposed (separated from the concrete), we have made the measurement with the Corrosion Meter device to identify the most corroded parts of the reinforcement inside the concrete. The testing procedure is based on the colors for rate of the corrosion in display of equipment. For testing procedure it's create the closed electrical circuit by connecting the electrode to reinforced steel and the other fluid-filled electrode to the Corrosion meter. The testing of concrete elements of bridge structures we have created a map for typical measurement points. The grids for measurements are sign at a distance of 15 cm from one point to another. The following positions are evaluate using the measures, presented in fig.4.

1. The inner part of the bridge abutment
2. Section of soffit bridge
3. Front part abutment of the bridge
4. Lateral part abutment of the bridge

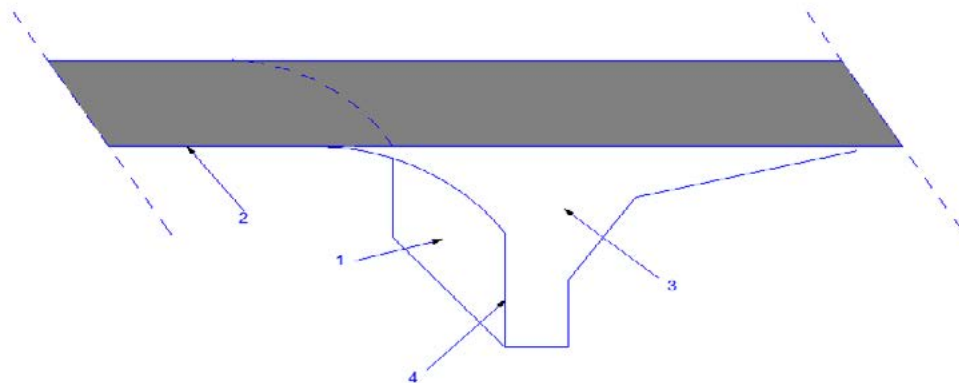


Figure 4. Measurement Positions

3.1. Review Results

The results of the bridge survey are presented in 4 forms:

- a) Corrosion Scan
- b) Cumulative Distribution

The results of the measurements are presented in 2 forms: Below we present the 2 forms of results at the most critical point in the lateral part abutment of the bridge.



Fig 5 -values of corrosion a function of potential max

The measurements for weak positions in colored form, based on the procedure are presented in fig.6

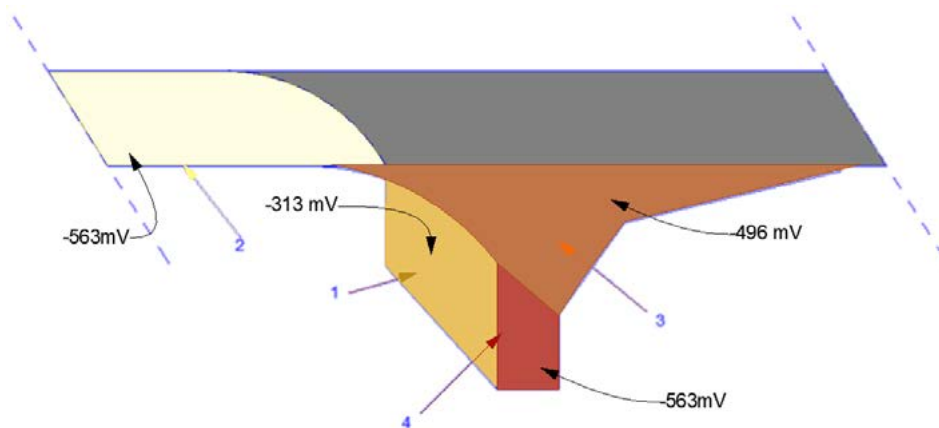


Figure 6. Values of corrosion a function of average values (%)

3.2. Calculation of the reduction of the cross-section of the steel from field measurements

Due to extreme environmental impacts, the structure is in with very high level of degraded and the reinforcement steel is under the influence of aggressive substances In time process the corrosion is increasing process and potentially increased the volume caused numerous cracks which lead to the damages the concrete layer and damages of element of structures. The reinforced steel bars being under the constant influence of the environment and corrosion has reduced its cross-section. From the observations we can see that the concrete layer of the reinforcement has been completely degraded, and the direct measurements of the diameter of reinforced steel bars \varnothing 22 mm. Evaluation

of the reinforcement that is on the outside of the damaged structure results in a high presence of corrosion and with this reduction of the diameter from the reinforcement 22mm to 2.2mm, evaluating the direct measurement method.[4] The reduction of the cross section of the reinforcement is presented in figure 7.



Figure 7. Reduction of armature cross-section caused by corrosion from direct contact with the external environment.

3.2.1. Corrosion rate measurement-ASTM Standard G31 and G1

Based on the ASTM standard for calculating steel bars corroded part is presented in expression (1.0).

$$CR \left(\frac{\mu\text{m}}{\text{years}} \right) = \frac{K \cdot 10^7 (W_i - W_f)(g)}{A(\text{cm}^2) \cdot t(\text{h}) \cdot \rho(\text{gr} \cdot \text{cm}^{-3})}, \text{ or} \quad (1.0)$$

$$CR (\text{mm}/\text{years}) = K \cdot \frac{W}{\rho A t} \quad (1.1)$$

Were the parameters are:

K-constant with values: K = 534 if CPR is in (mpy) or K = 87.6 if CPR is in mm / years

W-Weight Loss Armor (milligrams)

ρ- density of rebar (gr / cm³)

A-reinforced steel bars surface (cm²)

t-exposure time (hours)[5]

The reduced value from direct measurements using the expression (1.0) results with the reducing the diameter 2.042 mm/50 years.

The reduced value or loss of mass of reinforced steel bars is expressed in table 4, and categorizations based on the EN 12944-2.

Table 4: Corrosion Level Categorization Based on Environmental Impact (EN ISO 12944-2)

Corrosion level categorization	The loss of thickness (cross-sectional reinforcement)/ μm	Examples of the impact of environment
		The impact of outside environment
C1 (Very low)		
C2 (Low)	>1.3-25	Low level of pollution: mainly in rural areas.
C3 (Medium)	>25-50	Urban areas, sulfur dioxide pollution, coastal areas with low salt levels.

C4 (High)	>50-80	Industrial and coastal areas with medium salt levels.
C5 (Very High)	>80-200	Industrial area with high relative humidity, aggressive environment and coastal areas with high salt levels.
CX (Extreme)	>200-700	High-impact coastal areas of salt and industrial areas with extreme humidity and highly aggressive environment.

According to field measurements done in the steel bar, corrosion has been achieved a reduction of cross section up to 2.2mm or 2200µm based on the above table of EN ISO 12944-2 , than we conclude that our case study belongs to the level of CX corrosion (Level Extreme). While the calculations according to ASTM standard G31 and G1 reduction of cross-sectional reaches 2.04mm or 2200 µm based on the above EN ISO 12944-2 table can conclude that our case study of the level of corroding is CX (level EXTREME).[6]

3.2.2. Calculation of Corrosion Percentage according to ACI-408

The determine of the loss of mass (corrosion mass) is calculate according the ACI-408

The expression for calculating the percentage of steel corrosion is:

$$\%loss\ of\ mass = \frac{w}{\rho A_s l_{corr}} * 100\% \quad [7] \quad (2.1)$$

Ku:

w-is the mass loss

As-is the area of steel

l_{corr}-is the total length of steel that is to be corroded

ρ-is the density of the steel

From the calculations made according to ASTM Standard the percentage of steel corrosion is:
%loss of mass = 33.5% per 50 years.

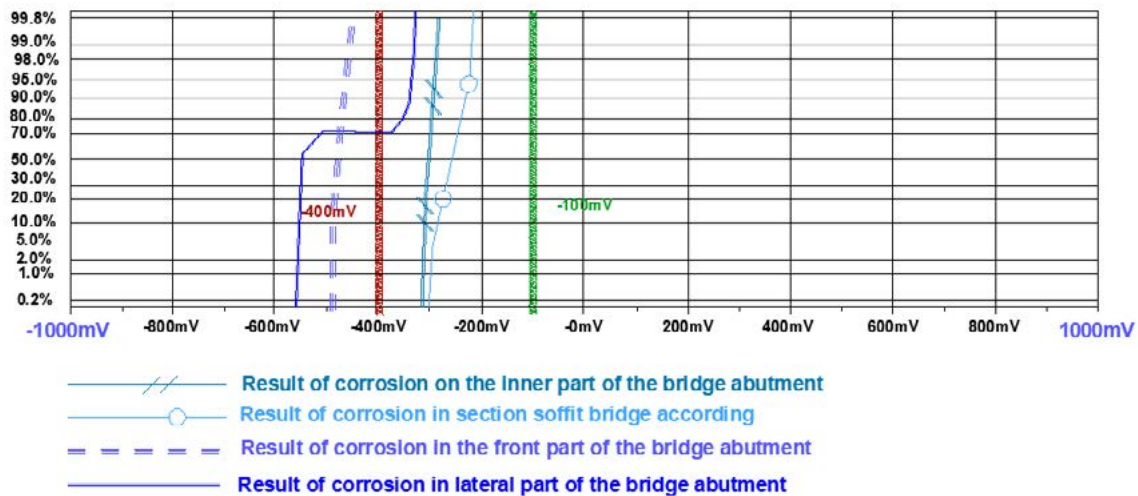
Results from direct "in situ" evaluations presented the loss of mass the percentage of steel corrosion is: **%of loss of mass = 31.063% per 50 years. (presented in Table 5)**

Table 5: Calculations and comparison between the ASTM and direct measurements (ENISO 12944-2)

	ASTM Standard	Direct "in situ" evaluations measurements
Rate of corrosion ($\frac{mm}{50vite}$)	2.04	2.2
Percentages of Corrosion ACI-408	33.5%	31.063%

Results and comparison

Below we present the comparison of the results of the measurements performed with the Corrosion Meter equipment in the field at different positions is presented in Figure 8.



4. CONCLUSIONS

From the analysis of the study case, we can conclude:

- Corrosion as a parameter is a function of aggressive parameters resulting in varying degrees of corrosion in different parts.
- The north-facing front results in higher corrosion than the lower-south, the north corrosion values reach > -500mV, while in the southern part the corrosion values are -300mV.
- The north side of the soffit is completely degraded and there is reinforcement detection, whereas in parts where we still have a protective layer the corrosion rate reaches up to -300mV, the south side is very degraded and the protective layer is reduced which has reduced the degree of corrosion (-300mV).
- From field measurements, the steel corrosion rate is 2.2 mm, while according to ASTM calculations the corrosion rate is 2.04 mm.
- According to ACI Standard 408, the corrosion rate for the measured bar (from the same bar we have determined the corrosion rate) the corrosion rate reaches (30-40) %.
- The usability of the bridge structure is directly dependent on the corrosion rate and longevity. In our case, it is questionable, since we have at certain points exceeding the corrosion limits.

Recommendations:

Immediately repairing and retrofitting the bridge structure

REFERENCES

- [1] Ministry of Environment and Spatial Planning-Pristina (2019)
- [2]. Thoft-Christensen "Corrosion and Cracking of Reinforced Concrete"-Danimark (March 2003)
- [3] C.M.Hansson, A. Poursaee, S.J.Jaffer "Corrosion of Reinforcing Bars in Concrete"(December 2012)
- [4] Lana L. Wong, Sue I. Martin, Raul B. Rebak "Methods to Calculate Corrosion Rates for Alloy 22 from Polarization Resistance Experiments"-Canada (April 3, 2006).
- [5] Designation: G1-90 (Reapproved 1999)"Standard Practice for Preparing, Cleaning, and Evaluating Corrosion Test Specimens"
- [6] N.Kabashi, "Mirëmbajtja dhe sanimi i strukturave egzistuese"- Prishtina (October 2016).
- [7] Kyle Stanish "Corrosion Effects on Bond Strength in Reinforced Concrete" National Library of Canada, Canada, (September, 1997).

21

Tomislav Kišiček, Nikolina Uglešić

Numerical modelling of concrete beam reinforced with FRP bars subjected to bending until failure

NUMERICAL MODELLING OF CONCRETE BEAM REINFORCED WITH FRP BARS SUBJECTED TO BENDING UNTIL FAILURE

Tomislav Kišiček¹, Nikolina Uglešić²

¹ University of Zagreb Faculty of Civil Engineering, Department of Structural Engineering
Fra Andrije Kačića Miošića 26, 10 000 Zagreb
e-mail: tomlav.kisicek@grad.hr

² D&Z d.o.o.
Jerolima Vidulića 7, 23000 Zadar
e-mail: nikolina@d-and-z.hr

SUMMARY: The topic of this paper is numerical modelling of concrete beams reinforced with FRP reinforcement and comparison of the results with experimental ones. Numerical models of concrete beams subjected to bending until failure, reinforced with steel, GFRP or CFRP reinforcement have been made. The finite element method was used, and the models were made in Midas FEA software. Concrete is modelled by the total strain crack theory. A smeared cracks model was used. Steel is modelled as Von Mises material, while FRP behaviour is linear elastic. The interface between the reinforcement and the concrete was also modelled, as bond – slip function. The goal is to compare the results obtained by numerical models with the results obtained by experiments, which were elaborated in previous work of first author. Experimental results contain material properties of used materials: concrete, steel and FRP reinforcement and bond slip behaviour between reinforcement and concrete. The results showed that it is possible to obtain similar results obtained by experimental research, but very important is knowledge of material behaviour and modelling of it.

KEY WORDS: reinforced concrete, FRP, bending, experimental results, numerical analysis

1 INTRODUCTION

Concrete reinforced with steel reinforcement is, today, still most common material in building structures. Due to corrosion of steel reinforcement in reinforced concrete structures, placed in aggressive environment a lot of attention has been given to fiber reinforced polymers (FRP) as replacement material for steel reinforcement. FRP materials could be produced from glass (G), aramid (A), carbon (C) or basalt (B) fibers which are connected with epoxy resin, polyester or vinyl-ester, and therefore they can be distinguished as GFRP, AFRP, CFRP or BFRP products. Beside its resistance to corrosion, FRP have other good characteristics such as: high tensile strength, good behavior under dynamic loadings, little relaxation, moisture resistance, low weight and it is magnetic resistant and electric isolator. FRP deficiencies are elastic behavior until failure (non-ductile behaviour), big differences between longitudinal and transversal mechanical characteristics and between tensile and compressive stresses and creep rupture (failure due to loss of bearing capacity under long term loadings). FRP materials have lower modulus of elasticity than steel reinforcement, and lower longitudinal coefficient of thermal expansion. FRP reinforcement is sensitive to ultraviolet exposure. Bending FRP bars made of thermoset resin should be carried out before the resin is fully cured due to inflexibility or rigid nature of cured FRP bar. GFRP is also sensitive to alkaline environment.

This paper presents finite elements modelling of concrete beams reinforced with steel or FRP bars loaded to bending, until failure which was made as a diploma thesis under first authors supervision [1]. Numerical models are made in software called Midas FEA which purpose is linear and nonlinear analysis for civil and structural engineering applications. The FEM results are compared with experimental results conducted at University of Zagreb, Civil Engineering Faculty ([2] to [6]). The goal of this work was to investigate the influence of modelling parameters on FEM results. Comparison with experimental results was also additional value to previous experimental research, because at that time the experimental results weren't compared with FEM analysis. The analytical procedures were made, and that analysis was published in papers [4], [5] and [6].

2 FINITE ELEMENT MODELLING

During this work the modelling of elements and material parameters had to be done. First the characteristics of materials (concrete, steel and FRP) were defined.

Concrete is modelled by total strain crack theory. Cracks in concrete could be modelled as discrete or smeared cracks. Midas FEA [7] uses smeared crack model which has two types, fixed crack model and rotated crack model (figure 1). In this analysis both types were used.

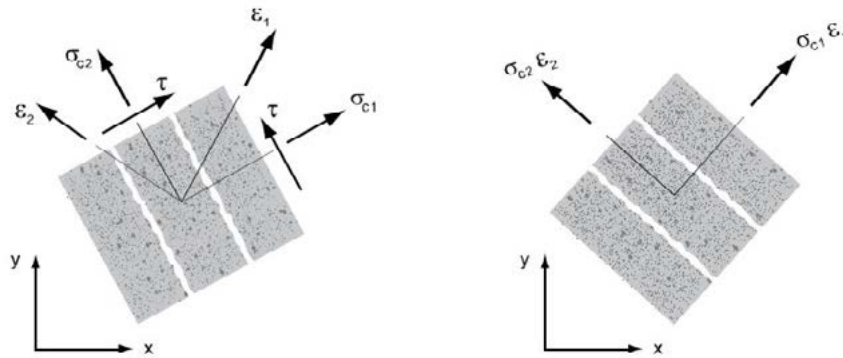
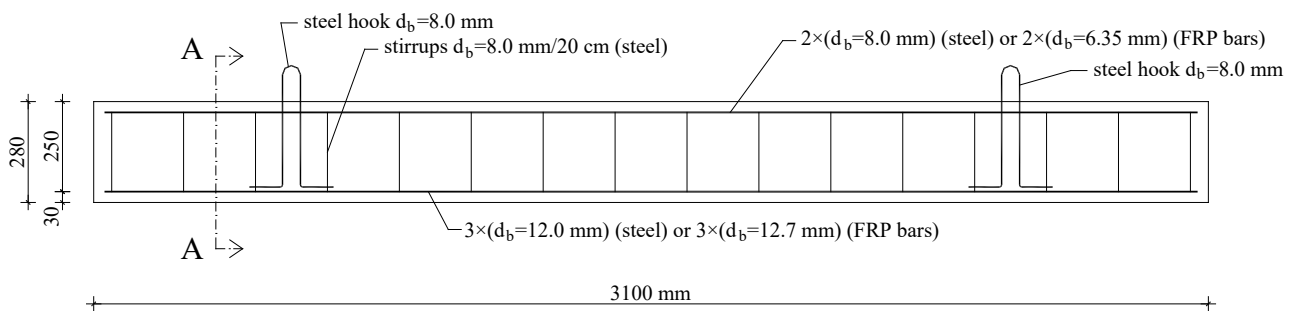


Figure 1: Fixed and rotated crack model [7]

Because of its ductile behaviour Von Mises model of material is used to model a steel reinforcement. Idealistic behaviour of steel reinforcement is bilinear which is used according to EN 1992-1-1 [8], [9]. Behavior of FRP reinforcement is taken as linear elastic until failure. The interface between concrete and reinforcement is defined as the bond-slip relationship between concrete and reinforcement which was taken according to experimental results from [2].

The dimensions of the beam elements, their cross section and reinforcement are shown in figure 2 [6]. These parameters were chosen due to length of FRP bars which was available for transportation from USA (300 cm), capabilities of the testing machine and ease of manipulation in our laboratory. The amount of reinforcement were chosen by preliminary calculations.

Longitudinal cross section of beam specimen



Cross section A-A

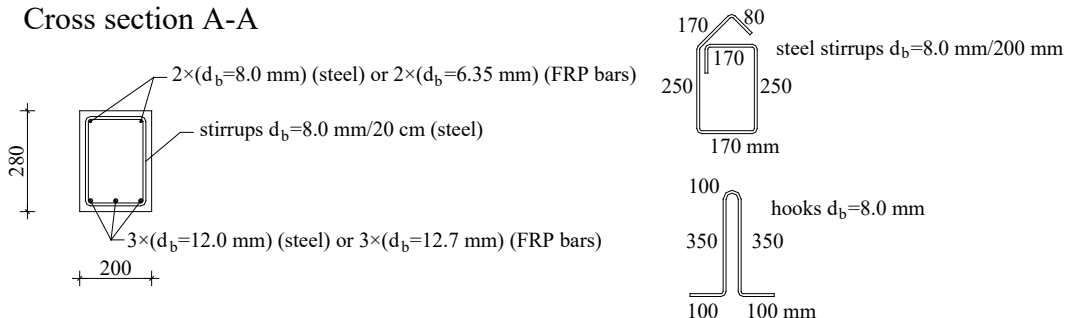


Figure 2: Dimensions and reinforcement of concrete beam specimen [6]

Three beam specimens of each type were tested by displacement control. Zwick/Roell testing machine has maximum displacement of 250 mm. Scheme of loading and LVDT setup is shown in figure 3 [6].

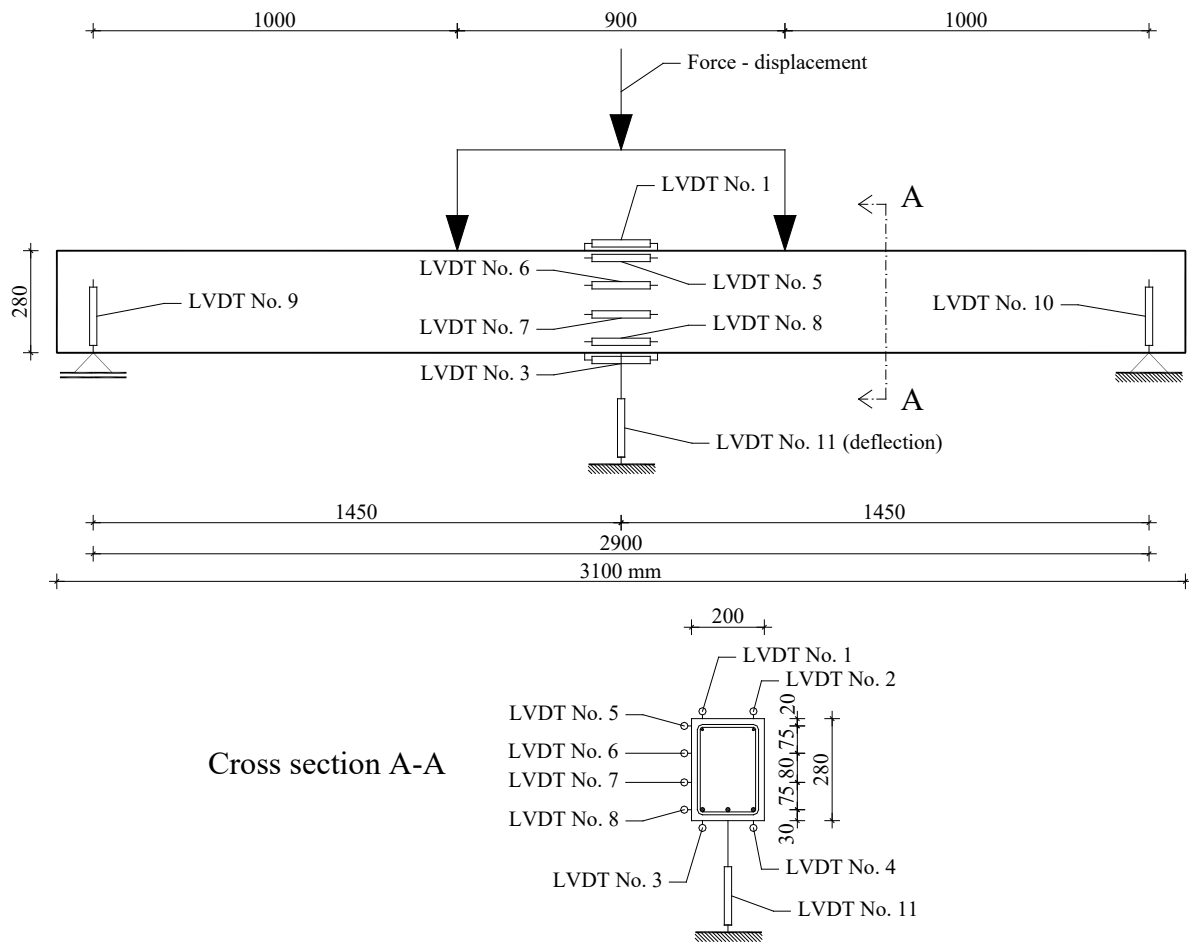


Figure 3: LVDTs setup for beam specimen [6]

FEM model of the beam element is shown on the figure 4. Concrete and reinforcement are modelled with tetrahedral solid elements while the interface between concrete and reinforcement is defined with plane elements.

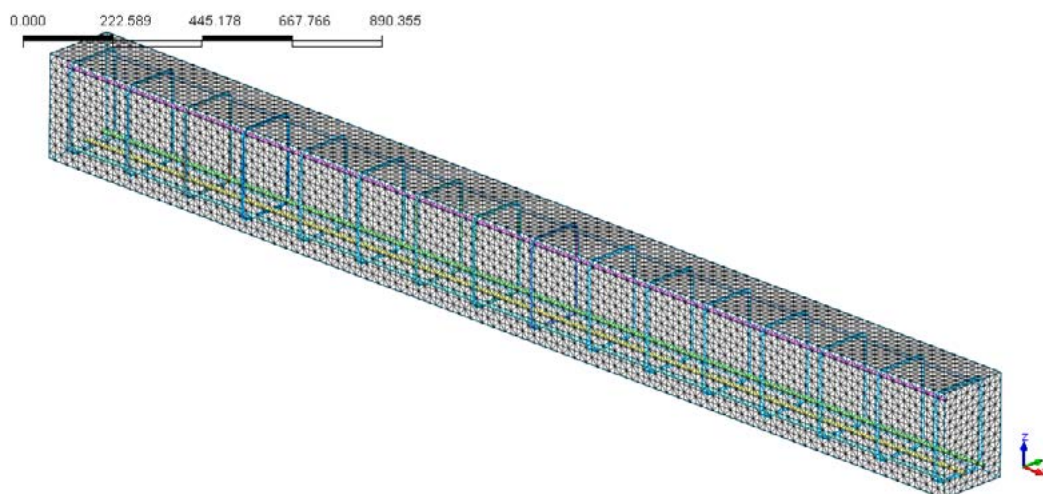


Figure 4: Beam element 3D model

Cross section of the model and part of the beam are shown on figure 5. The largest dimension of 3D elements is 20 mm and they are placed on the edges and in the middle of the beam cross section. The density of mesh is greater near

reinforcement. The size of the elements of lower reinforcement is 6 mm, and upper reinforcement and for stirrups is 4 mm.

Supports are modelled with supports in nodes of finite element mesh. One support is fixed in both horizontal directions, while second support is free in direction of the beam span. Both supports are free for rotation. Also, to avoid a stress concentration on the supports, the 30 mm thick bearing plates are placed. For the same reason the load is transferred also through the bearing plates. The dimensions of plates were 10×20 cm and 15×15 cm respectively.

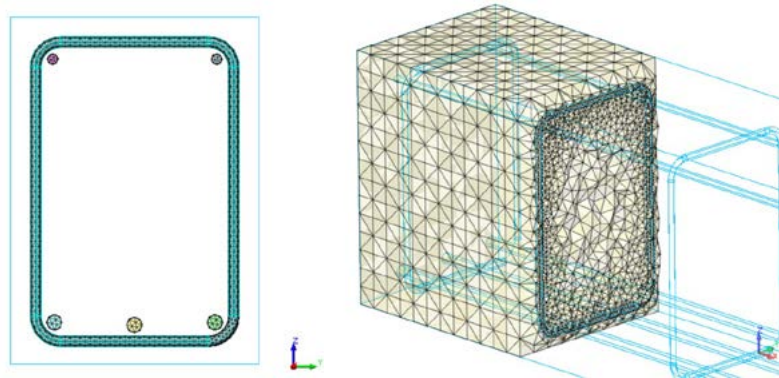


Figure 5: Cross section and part of the beam model

Bond-slip function between steel reinforcement and concrete is defined by cubical function according to Midas manual [7]. For bond-slip behaviour between FRP reinforcement and concrete, test results from [2] were taken and they were smoothed according to equation (1) from [10]:

$$\frac{\tau}{\tau_m} = (1 - e^{-4s})^{0.5} \tag{1}$$

These curves are shown on figure 6.

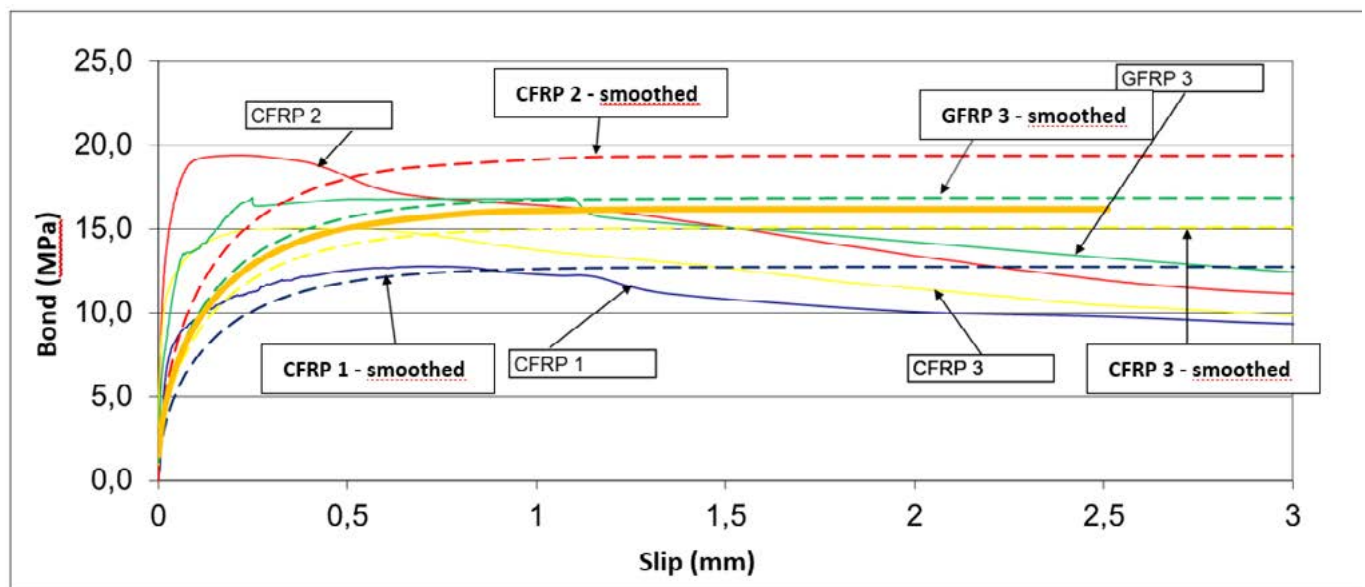


Figure 6: Smoothed and bond-slip curves from experimental work

Characteristics for steel and FRP reinforcement are taken from [2] and [6]. Steel reinforcement is modelled as bilinear material with strain hardening while FRP is defined as linear elastic material. Material characteristics are shown in table 1 [2], [6].

It must be mentioned that both types of FRP bars (GFRP and CFRP) had the same sand coating type so the results of bond-slip testing are similar. The thick orange line represents average bond-slip relationship which is taken into FEM.

Concrete is class C35/45 but the material characteristics of concrete were taken from [2]. Concrete is modelled by Total Strain Crack Theory. Stress-strain relationship of concrete in compression was taken, according to EN 1992-1-1 [8], as parabolic-rectangle diagram. Although it is better to use nonlinear stress-strain of concrete diagrams, this diagram was used because it is also used in preliminary calculations to compare them with FEM analysis. These comparisons are beyond the scope of this paper. Also, the concrete in tension was considered according to [7]. Tensile strength of concrete was taken from [2], energy G_f is defined by software for chosen concrete class.

Table 1: Average values of tensile testing results [2], [6]

Material	E (GPa)	σ_{02} (MPa)	σ_{yu} (MPa)	σ_{yl} (MPa)	ϵ_{yu} (%)	σ_{max} (MPa)	$\sigma_{failure}$ (MPa)	ϵ_{max} (%)	$\epsilon_{failure}$ (%)
Steel	211.3	590.17	606.22	585.76	3.217	672.05	462.73	10.26	12.8
GFRP	41.6	-	-	-	-	722.58	722.58	1.74	1.74
CFRP	133.7	-	-	-	-	1269.79	1269.79	0.95	0.95

Shear in concrete is also considered via shear stiffness which must be reduced with coefficient β . Total shear stiffness βG gives ratio between main stresses and strains in crack model. If the fixed crack model is used, then shear in concrete must be defined because of the shear stresses on crack surfaces. That kind of shear stiffness reduction is complicated for analysis because it causes rotation of main stress axis. Due to that rotation main stress axis don't coincide with axis of main strains. Some experimental work proves that the value of coefficient β should be close to zero. In such case the main stress axis is fixed or nearly fixed after cracking occurs [11]. In this work coefficient β was taken with values between 0.001 and 0.1, while recommended value from Midas FEA software is 0.05. In case of rotating crack model, shear has not to be defined or coefficient β can be equal to 1.0. within that kind of models there's any shear stresses at the crack surface.

3 RESULTS OF ANALYSIS AND COMPARISON WITH EXPERIMENTAL RESULTS

Several models of beams with steel, GFRP and CFRP reinforcement were analysed. Beams with steel reinforcement were used as a sample beams for testing of some options during process of modelling and they won't be shown in this paper. Some types of analysed models with FRP reinforcement are shown below.

Models with GFRP reinforcement:

Model „GFRP1“: Concrete was defined according to CEB-FIP class C30 which has lower characteristics than C35/45 and that affected the results.

Model „GFRP2“: Rotating crack model has been used and shear was defined with coefficient $\beta = 1.0$.

Model „GFRP3“: In this model fixed crack model has been used. Shear was defined with coefficient $\beta = 0.1$ but the results of calculation wasn't applicable, so the calculation was repeated with value $\beta = 0.001$. the calculation was stopped after 50 iterations due to divergence of process. The resulting force – deflection curve is shown in figure 6.

Model „GFRP4“: In this model fixed crack model has been used. Shear was defined with coefficient $\beta = 0.05$.

If we compare the test results with FEM results (figure 7), the stiffnesses of uncracked beams are similar. Cracking moment isn't the same as it should be, but the differences are not very big. Model „GFRP3“ which have highest value of shear stiffness show good compatibility with test results at the beginning of loading. After deflection of approx. 20 mm better compatibility is shown from model „GFRP4“. In general, stiffnesses of modelled beams are slightly lower than ones of tested beams and modelled beams shows greater ultimate moment than tested ones. Figures 8 and 9 show crack pattern and width for models “GFRP2” and “GFRP4”. First one is modelled with rotating crack model and second one with fixed crack model. For the same load, cracks are wider for rotating crack model. Crack patterns are similar, the cracks are concentrated in tensile area and around the stirrups, which was also the case in tested beams, and it was observed during experimental investigation described in [2].

Force – deflection diagrams

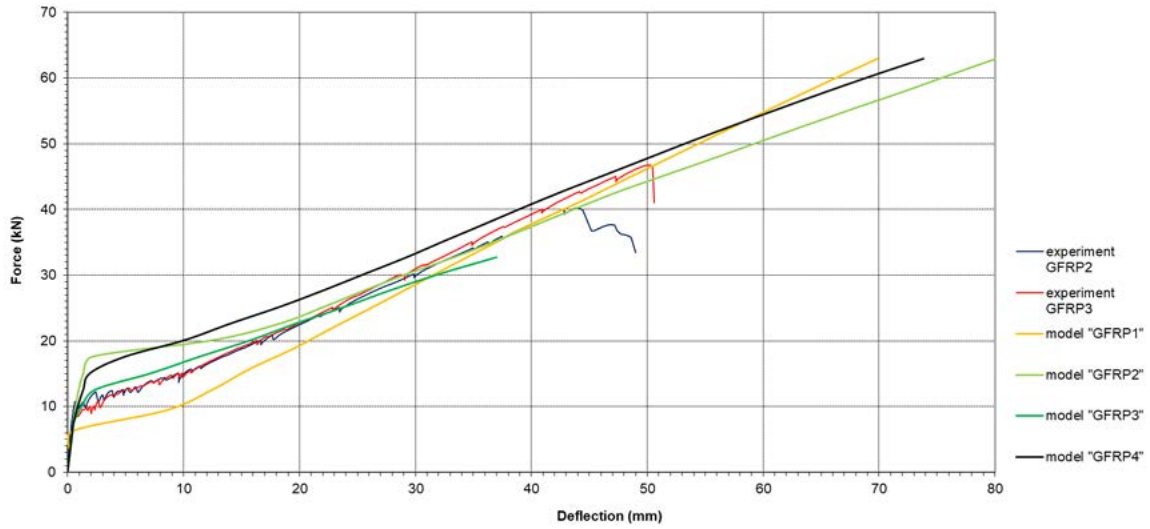


Figure 7: Force – deflection diagrams for beams reinforced with GFRP

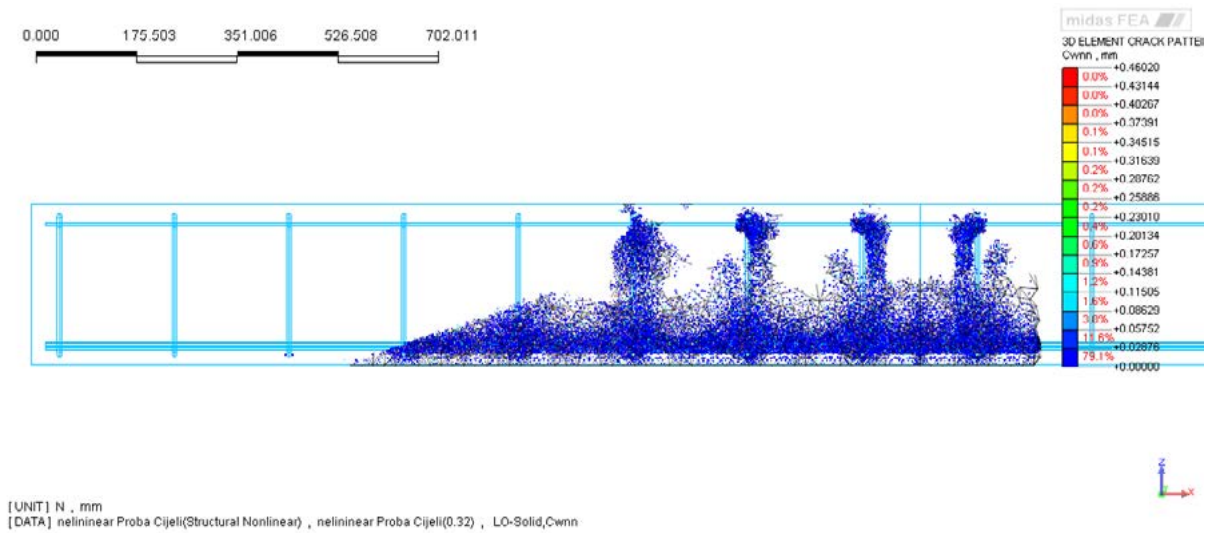


Figure 8: Crack pattern for beam model "GRFP2"

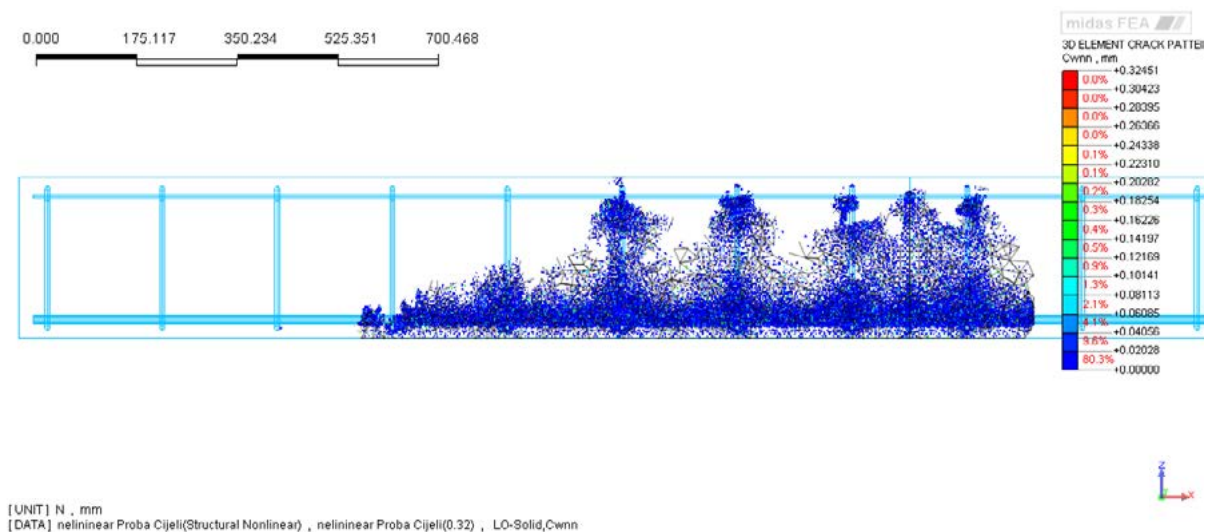


Figure 9: Crack pattern for beam model "GRFP4"

Figure 10 show crack pattern for beam reinforced with GFRP reinforcement at failure. The failure was due to concrete crushing followed by FRP rupture. Although the crack pattern from figures 8 and 9 is not for the same load level as the one at figure 10 the main cracks appear at the same distance in FEM model and in the experiment, which is the stirrup spacing of 20 cm.

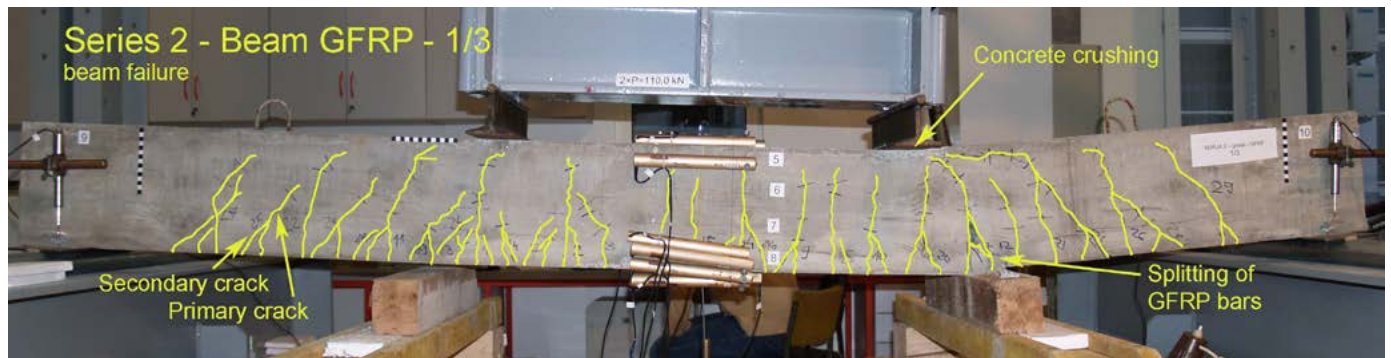


Figure 10: Crack pattern for beam reinforced with GFRP at failure

Models with CFRP reinforcement:

Model „CFRP1“: In this model fixed crack model has been used. Shear wasn't defined which was wrong and it can be seen at the results.

Model „CFRP2“: Rotating crack model has been used and shear was defined with coefficient $\beta = 1.0$.

Model „CFRP3“: In this model fixed crack model has been used. Shear was defined with coefficient $\beta = 0.05$.

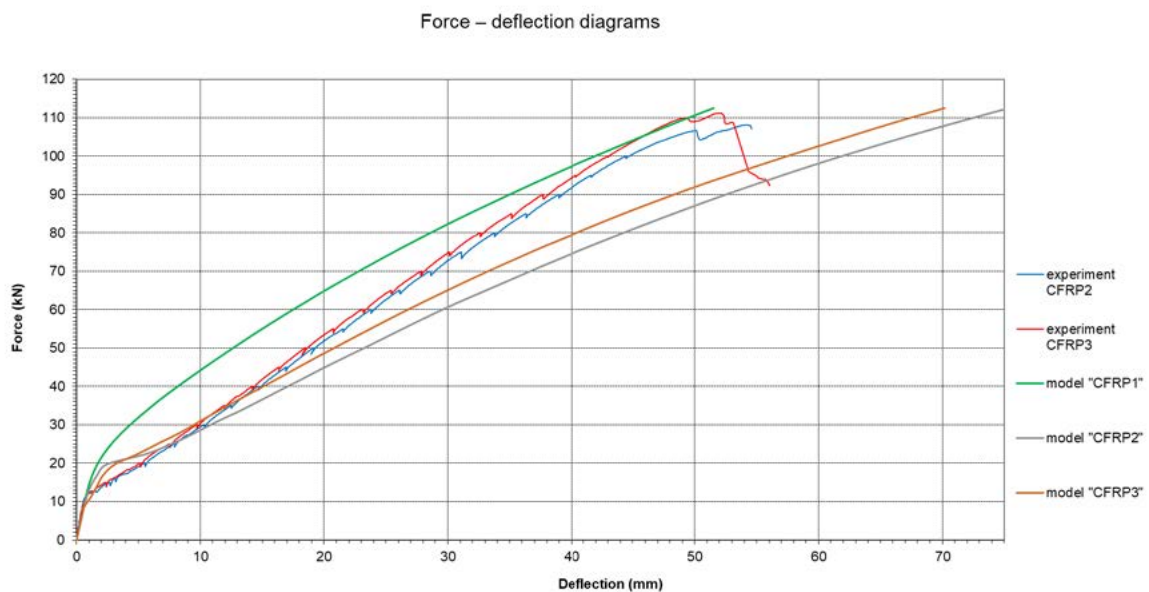


Figure 10: Force – deflection diagrams for beams reinforced with CFRP

The same as for beams reinforced with GFRP, if the test results are compared with FEM ones (figure 10), it can be seen that the stiffnesses of uncracked beams are similar. Cracking moment isn't the same as it should be, but the differences are not too big. After appearance of first cracks stiffnesses of modelled beams are lower than tested ones. Models “CFRP2” and “CFRP3” have the same behaviour, but, model “CFRP1” show greater differences. The reason is that shear wasn't defined in that model.

4 CONCLUSIONS

The goal of this work was to compare results of FEM with test results of concrete beams reinforced with GFRP or CFRP reinforcement. Three basic models were done. Models with steel reinforcement (for comparison of parameters and for calibration of other models) and models with GFRP or CFRP reinforcement.

In each group of basic models, material parameters for concrete have been changed and the results were compared with test results. It's concluded that it's very important to know exact characteristics of material, its behavior and the way how the software make the analysis.

It was shown that, beside basic characteristics of concrete, shear behavior is very important due to usage of crack models in calculations. The differences affected by shear characteristics could be very big. Coefficient of shear reduction β is very important. For fixed crack model it should be around zero (optimal value is 0.05), while, for rotating crack model it should be equal to 1.0.

Crack widths are different depending on used crack model. Rotating crack model gives wider cracks than fixed crack model.

In general, stiffness of beams before appearances of first cracks depends only on concrete characteristics, but after that point, the stiffness of modelled beams is little lower than tested ones. That's on the safe side if we consider serviceability limit states.

With numerical modelling, the results like ones from tests could be obtained but they are sensitive to input parameters, settings and software calculation procedures. That kind of calculations could be very time consuming, depending on the power of computer and especially on the size of finite elements.

ACKNOWLEDGMENTS

The authors wish to acknowledge financial support granted in the scope of short-term scientific support from University of Zagreb.

REFERENCES

- [1] Uglešić, N.: "Bending of concrete beam reinforced with FRP reinforcement - numerical model", diploma thesis, University of Zagreb, Civil Engineering Faculty, 2019.
- [2] Kišiček, T.: "Progibi betonskih greda s FRP armaturom", Ph D thesis, Zagreb, 2006.
- [3] Kišiček, T., et al: "Ispitivanje greda i ploča armiranih šipkama od PAV-a", Građevinar 59 (2007) 7. str. 581-595.
- [4] Kišiček, T., et al: "Određivanje progiba betonskih nosača s armaturom od polimera armiranih vlaknima", Građevinar 60 (2008) 6. str. 499-511.
- [5] Kišiček, T., et al: "Stress and Strain Distribution in Concrete Beams Reinforced with FRP Bars", Proceednigs of the 9th International Symposium on Fiber – Reinforced Polymer Reinforcement for Concrete Structures. Sydney, Australia, 13.-15. July 2009. The book of Abstracts, pp. 265. Editors: D.J. Oehlers, M.C. Griffith, R. Seracino.
- [6] Sorić, Z., et al: "Deflections Of Concrete Beams Reinforced With FRP Bars", Materials and Structures (2010) 43:73-90, Springer Netherlands
- [7] Analysis and Algorithm, Midas FEA, Manual
- [8] HRN EN 1992-1-1:2013, Eurocode 2: Design of concrete structures – Part 1-1: General rules and rules for buildings, European Committee for Standardization, Bruxelles
- [9] Sorić, Z., Kišiček, T.: "Betonske konstrukcije 1", Sveučilišni udžbenik, Sveučilište u Zagrebu, Građevinski fakultet, Zagreb, 2014.
- [10] Tighiouart, B., et al: "Investigation of bond in concrete member with fibre reinforced polymer FRP bars", Construction and Building Materials 12 (1998) 453- 462
- [11] Rots, J. G., Blaauwendraad, J.: "Crack models for concrete: discrete or smeared? Fixed, multi-directional or rotating?", HERON, vol. 34, 1989., no.1

22

Sanjay Korukonda and Sumedha Maharana

Non-Destructive Evaluation and Monitoring Cement Concrete - An Experimental Approach



NON-DESTRUCTIVE EVALUATION AND MONITORING CEMENT CONCRETE-AN EXPERIMENTAL APPROACH

Sanjay Korukonda¹ and Sumedha Maharana²

^{1,2} Department of civil engineering, Shiv Nadar University, Dadri-201314, Email-sumedha.maharana@snu.edu.in

SUMMARY:

From last few decades, the non-destructive evaluation and structural health monitoring (SHM) of civil infrastructures has gained popularity with advent of smart material and better sensor integration with structural system. Cement concrete system is heterogeneous nature and its strength development is very complex. Therefore, this paper studied the continuous monitoring of the concrete strength using two NDT & E method (UPV and Rebound Hammer) and Piezo-impedance based structural health monitoring (PISHM). The embedded piezo sensor (epoxy coated piezo sensor) is used for this study. Lab based concrete samples are casted along embedded sensor and monitored for 30 days of air curing. The continuous strength monitoring concrete specimen is done for 30 days using both NDE techniques and smart materials (Piezo Sensor) based evaluation. The overall results obtained from the three tests were compared for better evaluation for robust technique.

KEY WORDS: Non-destructive evaluation, Smart aggregates, ultrasonic pulse velocity method, structural health monitoring, Concrete Strength

1 INTRODUCTION

The safe and quality assessment of concrete to monitor and improve the durability and reliability of concrete structures has been the most challenging and burgeoning task in construction engineering [1]. Traditional methods like destructive evaluations of structures to evaluate the mechanical properties of concrete such as compressive strength and tensile strength has always been tedious and restrict the function of structure. The focus on direct application and implementation of advanced testing methods has heightened the need for efficient and economical evaluation of structural health monitoring, thereby paving its way towards research on non-destructive methods [2]. Non-destructive evaluation methods such as ultrasonic pulse velocity and rebound hammer have been pivotal in calculating the compressive strength of concrete. The application of stress propagation in UPV method helps to make concrete strength/hardness interpretation several parameters and properties such as material composition, mechanical and surface properties of the specimen. The pulse velocity can be directly related to modulus of elasticity, Poisson's ratio and mass density. Although various factors such as cement types, water/cement ratio affect the relationship between pulse velocity and compressive strength, compressive wave velocity has been measured as it is used in the calculation of elastic properties of concrete through which physical properties of concrete such as strength can be interpreted [4]. The stress wave propagation in UPV method is more indicative towards some critical parameter such as material composition, mechanical and surface properties of the specimen.

The other non-destructive method is Schmidt Rebound hammer test. The rebound of an elastic mass depends on the hardness of the surface against which its mass strikes. When the plunger of the rebound hammer pressed against the surface of the concrete, the spring-controlled mass rebounds and the extent of such a rebound depends upon the surface hardness of the concrete. The surface hardness and therefore the rebound taken to be related to the compressive strength of the concrete. The rebound value is read from a graduated scale and designated as the rebound number or rebound index [5]. The drawbacks of the rebound hammer test based on surface irregularities and roughness limits the reliability of this method [6].

The introduction of smart materials in non-destructive evaluation methods has been crucial in the process of eliminating specific boundary conditions that have been prevalent in traditional methods [6]. Their ability to modify their

geometric shape and material properties under the application of electric, thermal or magnetic fields help in transducing energy, which makes them as potential candidate for SHM. Piezo electric patches are also called as mechatronic transducer as they can be used not only as an actuator but also as a sensor. The Piezo-impedance based structural health monitoring is a local SHM method which operates in high frequency range (30-400kHz). Because of the direct and the converse piezoelectric effects, any change in the mechanical impedance of the structure caused by damage modifies the electrical admittance of the PZT transducer bonded to it [7].

Bhalla and Soh (2004a, b) [10] developed A two dimensional piezo-impedance approach based on the concept of effective impedance was developed to model the PZT-structure interaction manifesting active and passive part of coupled admittance signature. Any damage to the structure will cause these characteristics to change and hence changes the structural impedance ($Z_{s,eff}$), which in turn alters the admittance (\bar{Y}) as given by the following expression

$$\bar{Y} = \frac{\bar{I}}{\bar{V}} = G + Bj = 4\omega j \frac{l^2}{h} \left[\frac{\bar{\epsilon}_{33}^T}{\epsilon_{33}} - \frac{2d_{31}^2 \bar{Y}^E}{(1-\nu)} + \frac{2d_{31}^2 \bar{Y}^E}{(1-\nu)} \left(\frac{Z_{a,eff}}{Z_{s,eff} + Z_{a,eff}} \right) \left(\frac{\tan kl}{kl} \right) \right] \quad (2)$$

where ω is the angular frequency, l the half-length and h the thickness of the patch, $\bar{\epsilon}_{33}^T = \epsilon_{33}(1-\delta j)$ the complex piezoelectric permittivity (δ being the dielectric loss factor), $\bar{Y}^E = Y^E(1+\eta j)$ the complex Young's modulus (η being the mechanical loss factor), $Z_{s,eff}$ and $Z_{a,eff}$ respectively the effective impedances of the structure and the PZT patch and k the wave number. This equation couples the mechanical impedance of the structure with the electrical admittance \bar{Y} which means that any damage to the structure (change of $Z_{s,eff}$) will reflect itself as change in \bar{Y} Furthermore,

This paper aims to investigate the suitability of Non-destructive evaluation methods (UPV/RH/PISHM) for assessment of the compressive strength of concrete for 28 days continuously, which could be used for in-situ timely strength assessment for enhancing performance during the curing and the early service life.

2 EXPERIMENTAL PROCEDURE

The nine concrete cube specimen (Fig. 1) were prepared by using M30 mix design with cement, sand and aggregate ratio of 1:0.75:1.5 in accordance with IS 10262:2009 [20]. A water-cement ratio of 0.5 was maintained. Three control concrete cubes were water cured for 30 days. Other three samples were kept for air curing for 30 days and strength monitoring was done by conventional NDT (UPV and Rebound Hammer method). Another three samples were instrumented with piezo sensor. For PISHM, Piezo electric patches of dimensions 10×10×0.1 mm was used to develop epoxy encapsulated piezo sensor as embedded smart aggregates (Fig. 2). The embedded sensor was integrated into the lab based concrete sample during casting [14]. embedded sensors. PCC-VS) a proprietary product of IIT-Delhi (Bhalla and Gupta, 2007), were directly used. The embedded PZT patches kept in to the structures during casting 30mm from top surface.



Fig.1 Freshly casted cubes

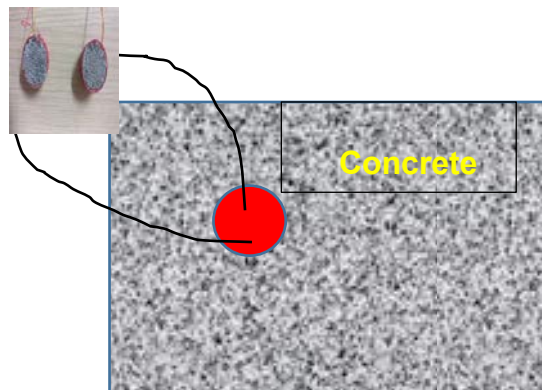


Fig.2 Piezo Encapsulated Smart Aggregates

Compressive strength of concrete increases with maturity and the values of the cube strength has obtained by finding out the pulse velocity PROCEQ from Pundit lab+.



Fig.3 UPV measurement using Pundit lab+

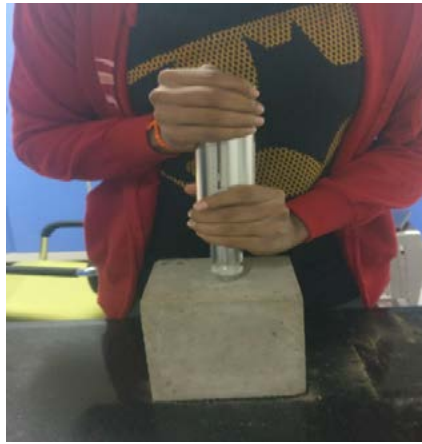


Fig.4 UPV Rebound Hammer test on lab specimen

For PISHM method, the signatures (Electro-mechanical admittance signature) were obtained from embedded smart aggregates through Keysight E4980A LCR meter for 30-300kHz for 30 days Air curing (Fig. 5 (b)).



Fig 5 (a) Concrete specimen with embedded smart aggregate (b) Data acquisition through LCR

3 RESULTS AND DISCUSSION

The compressive strength values measured from UPV method for 30 days is shown in fig. 6. It can be concluded that compressive strength/ uniform mass strength gain increased with time. As the pulse velocity increases with curing time, the concrete strength increases [16]. The average compressive strength of the concrete cube was found out to be 29.03 MPa using ultrasonic pulse velocity method.

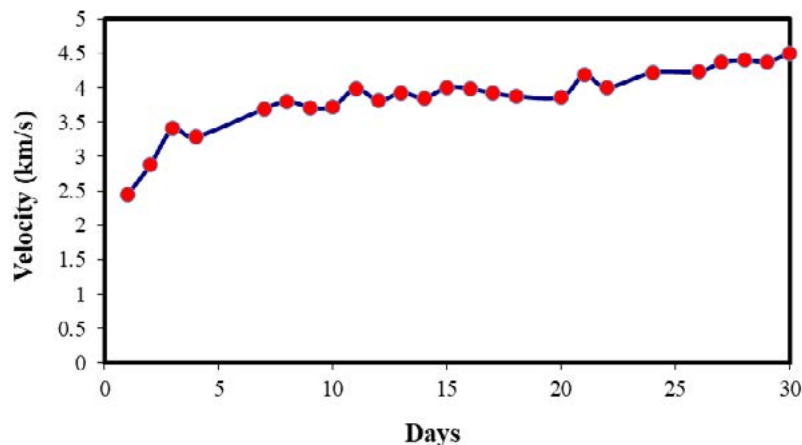


Fig 6. Concrete maturity gain with time

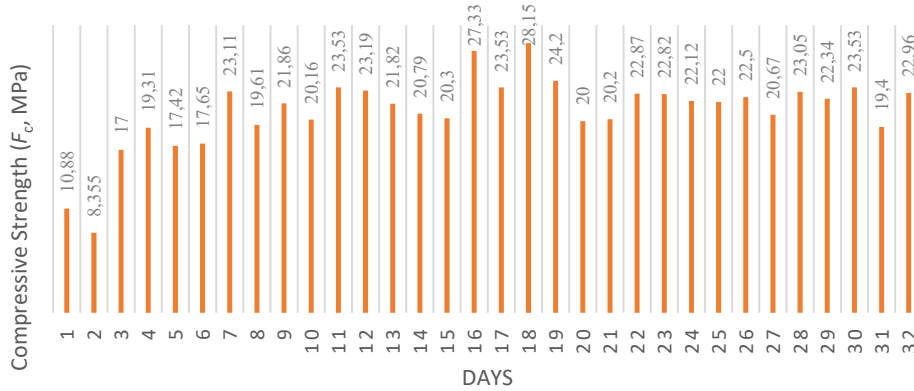


Fig 7 Variation of compressive strength (indirectly obtained from UPV) with time

The principle behind rebound hammer test is the combination of impact loading and stress wave propagation [17]. The test has been used to assess the integrity of the concrete specimen. The rebound hammer values along with compressive strength (correlated with calibrated strength curve) is shown in fig 8.

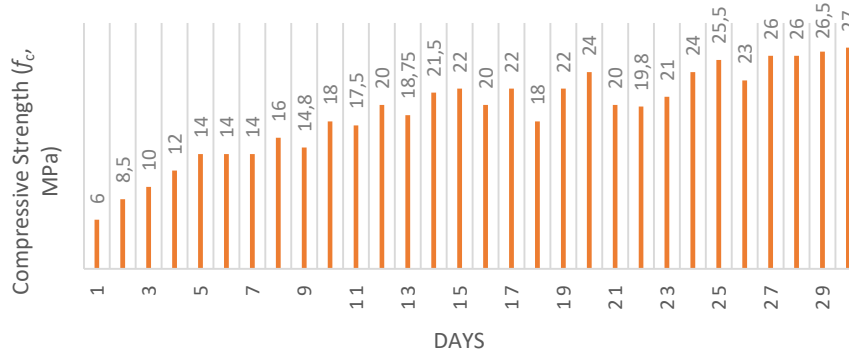


Fig 8 Variation of compressive strength (obtained from Rebound hammer) with time

The average compressive strength from the rebound hammer test has been found out to be 24.07 MPa. The average compressive strength attained from the standard destructive (crushing) evaluation through CTM for three control concrete samples experimentally obtained as 28.25 MPa. The increase in the precision and reliability in the estimation of compressive strength has been always linked with the combination of two or more non-destructive evaluation or testing methods [18]. To find a better correlation between ultrasonic pulse velocity and rebound hammer method, the strength data obtained from both NDT techniques are plotted and compared to show the overall strength gain process (indicated indirectly though velocity and hardness) has similar trend as in Fig 9.

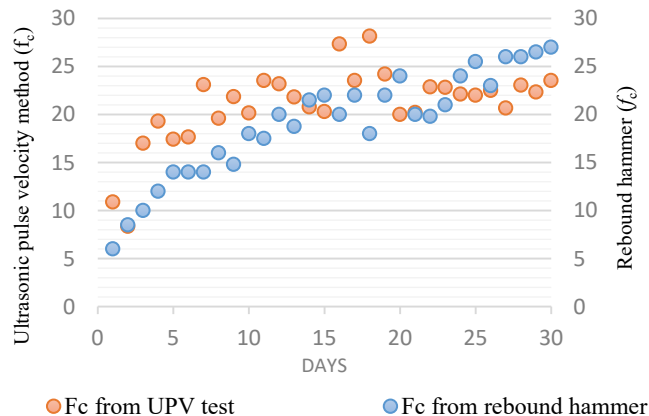


Fig.9 Multiple linear regression model between strength of rebound hammer, UPV and days

Electromechanical admittance signatures comprises of real (conductance) and imaginary (Susceptance) part, which was also recorded from day of casting till 30 days. The conductance signatures for PISHM shown that with increasing maturity days, the peak amplitude shifting to right which indicates the increasing hardness and complete strength attainment of concrete sample.

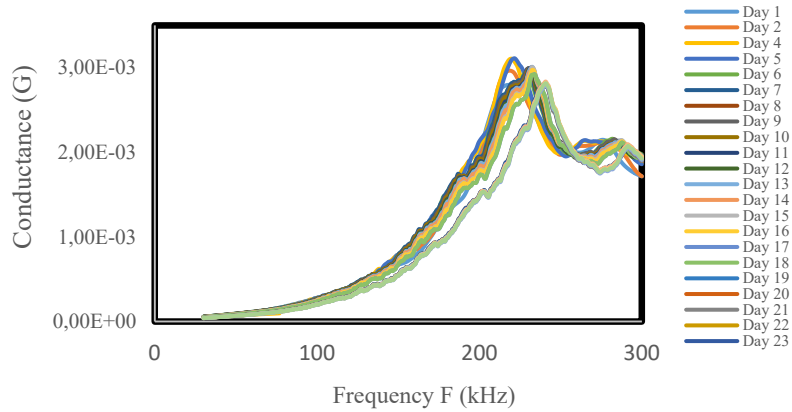


Fig 10 Conductance signature of concrete specimen

Further more, The root mean square deviation were polotted (see Fig. 11) for quantitative feature of conductance signature and can be expressed as [19].

$$RMSD (\%) = \sqrt{\frac{\sum_{i=1}^N (G_i^1 - G_i^0)^2}{(\sum_{i=1}^N G_i^0)^2}} \times 100 \quad (3)$$

where G_0 is the baseline conductance value and G_i the corresponding current conductance at the i th measurement point. The RMSD variations is lies with in 6%, which indicate significant physio-chemical change in concrete with gradual increment, indicated increase in stifnees in overall.

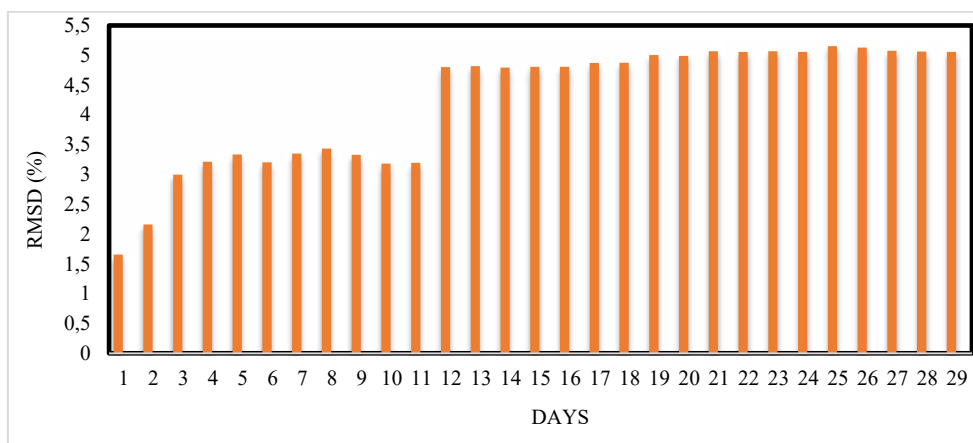


Fig 11 RMSD metrics concrete specimen

4. Conclusion

This paper discuss the the overall stregth development in concrete specimen, measured through both destructive and non-destructive test. The measurements were taken from Ultrasonic pulse velocity, rebound hammer and piezo sensor based SHM method. The compressive strength found out from UPV method, rebound hammer method and destructive

testing has found the similar range of strength value, which indicate the conventional NDT methods i.e. UPV and RH can be used as pre-emptive method to assess the strength of concrete casted during early stage of construction. Finally, Piezo impedance based strength monitoring of concrete sample has done using EMI technique. The RMSD variation of piezo signature for 30 days of curing has more similar trend as that of UPV and rebound hammer, assisting to understand concrete strength gain.

5. Reference

- 1) Petro JT and Kim J (2012) Detection of delamination in concrete using ultrasonic pulse velocity test. *Construction and Building Materials*. DOI: 10.1016/j.conbuildmat.2011.06.060.
- 2) ACI 228.1R-03 (2003) In-Place Methods to Estimate Concrete Strength Reported. ACI Committee Reports.
- 3) Malhotra VM and Carino NJ (2003) Handbook on Nondestructive Testing of Concrete, Second Edition. Handbook on Nondestructive Testing of Concrete, Second Edition. DOI: 10.1201/9781420040050.
- 4) Krautkrãmer J, Krautkrãmer H and Sachse W (1984) Ultrasonic Testing of Materials. *Journal of Applied Mechanics*. DOI: 10.1115/1.3167589.
- 5) Anon (1999) ##Introduction to non-destructive testing techniques. *Materials Evaluation*. DOI: 10.9773/sosei.53.631.
- 6) Sabbağ N and Uyanik O (2017) Prediction of reinforced concrete strength by ultrasonic velocities. *Journal of Applied Geophysics*. DOI: 10.1016/j.jappgeo.2017.04.005.
- 7) McCann DM and Forde MC (2001) Review of NDT methods in the assessment of concrete and masonry structures. *NDT and E International*. DOI: 10.1016/S0963-8695(00)00032-3.
- 8) Karaiskos G, Deraemaeker A, Aggelis DG, et al. (2015) Monitoring of concrete structures using the ultrasonic pulse velocity method. *Smart Materials and Structures*. DOI: 10.1088/0964-1726/24/11/113001.
- 9) Architectural Institute of Japan. Manual of Nondestructive Test Methods for the Evaluation of Concrete Strength; Architectural Institute of Japan: Tokyo, Japan, 1983.
- 10) Soh CK and Bhalla S (2005) Calibration of piezo-impedance transducers for strength prediction and damage assessment of concrete. *Smart Materials and Structures*. DOI: 10.1088/0964-1726/14/4/026.
- 11) Yan W, Cai JB and Chen WQ (2011) An electro-mechanical impedance model of a cracked composite beam with adhesively bonded piezoelectric patches. *Journal of Sound and Vibration*. DOI: 10.1016/j.jsv.2010.08.013.
- 12) Yan W, Chen WQ, Lim CW, et al. (2008) Application of EMI technique for crack detection in continuous beams adhesively bonded with multiple piezoelectric patches. *Mechanics of Advanced Materials and Structures*. DOI: 10.1080/15376490701410513.
- 13) Trtnik G, Kavčič F and Turk G (2009) Prediction of concrete strength using ultrasonic pulse velocity and artificial neural networks. *Ultrasonics*. DOI: 10.1016/j.ultras.2008.05.001.
- 14) Sbartai ZM, Laurens S, Elachachi SM, et al. (2012) Concrete properties evaluation by statistical fusion of NDT techniques. *Construction and Building Materials*. DOI: 10.1016/j.conbuildmat.2012.09.064.
- 15) Lorenzi A and Da Silva Filho LCP (2004) Using an Artificial Neural Network for interpreting ultrasonic pulse velocity of concrete. In: 5th International PhD Symposium in Civil Engineering - Proceedings of the 5th International PhD Symposium in Civil Engineering, 2004.
- 16) Pucinotti R (2015) Reinforced concrete structure: Non destructive in situ strength assessment of concrete. *Construction and Building Materials*. DOI: 10.1016/j.conbuildmat.2014.11.023.
- 17) Cook JE, Akers DJ, Barringer WL, et al. (2003) Guide for Obtaining Cores and Interpreting Compressive Strength Results. Society.
- 18) Silva RNF, Tsuruta KM, Rabelo DDS, et al. (2016) The use of electromechanical impedance based structural health monitoring technique in concrete structure. In: 8th European Workshop on Structural Health Monitoring, EWSHM 2016, 2016.
- 19) Park G, Cudney HH and Inman DJ (2000) An integrated health monitoring technique using structural impedance sensors. *Journal of Intelligent Material Systems and Structures*. DOI: 10.1106/QXMV-R3GC-VXXG-W3AQ.
- 20) Bureau of Indian Standards (BIS), Concrete Mix Proportioning-Guidelines. IS: 10262-2009, New Delhi, India.

23

Karmen Kostanić Jurić, Nina Štirmer and Ivana Carević

Sustainable pre-treatment of wood biomass ash for partial cement replacement

SUSTAINABLE PRE-TREATMENT OF WOOD BIOMASS ASH FOR PARTIAL CEMENT REPLACEMENT

K. Kostanić Jurić¹, N. Štirmer² and I. Carević³

^{1,2,3} University of Zagreb, Faculty of Civil Engineering, University of Zagreb
Fra Andrije Kačića Miošića 26, 1000 Zagreb
e-mail: kostanic.karmen@gmail.com

SUMMARY: In July 2019, Croatian energy market operator had 38 contracts for electricity from renewable energy sources (RES) with power plants under construction. 50% of these were for biomass power plants and represented 19% of planned install power. While the increasing number of plants creates more wood biomass ash (WBA) to manage, landfilling prices are rising and although this research is done locally, the problem is global. In 1882 the first coal fired power plant was built in London as a project by Thomas Edison. The first high-volume coal fly ash recycles in concrete was done to repair a part of the Hoover Dam in 1942. In the 80s, with first legal guidelines and construction expansion, recycling of coal ash in concrete become routine. Biomass has been used as heat energy since people learned to control fire, but when speaking about RES, we refer to modern biomass combustion systems that started to sprout in developed countries during the 90s. Extensive research on the characterization of WBA and its influence on concrete properties has been going on during the last few years. Research has also been done on the impact of recycling for other fields trying to find a quicker solution for ash disposal this time. For now, we know that WBA can be used as an active (replacement of cement) or inactive (filler, sand substitute) concrete component. Fly WBA is usually compared with coal fly ash, but ash properties vary depending on many factors - from type and growth conditions, through the combustion system, to ash management on site. The link between power plants and the concrete industry should be established through consistency and quality control. This could be achievable by establishing ash pre-treatments. Treated ashes could be a more reliable material for larger scale cement replacement.

KEY WORDS: wood biomass ash, fly ash, cementitious materials, concrete, pre-treatment, grinding, milling

1 INTRODUCTION

Solid biofuels are the oldest power source humans used for heating and cooking. The energy progress of developed countries has gone through several phases from that first energy source. Today, on energy stage, leading role belongs to renewable energy sources and bioenergy has its important part in it. However, bioenergy processes in developed countries are different than first firing processes used in poor regions of the world. When there are no options, open flame is good enough for heating and cooking, but generated smoke endangers the respiratory system of inhabitants. Providing access to electrical energy through RES is may foundations action in third world countries. Biomass used locally in this type of households is part of bioenergy as RES world statistics and we need to take it in account when dealing with ash production data. These WBAs generated in a small household in undeveloped countries quantities cannot be considered when observing ash recycling in the concrete industry.

Fossil fuels exploitation for industrial growth in economy leading countries seriously disturbed our ecosystem and caused climate changes. Humans influence in greenhouse gases content in atmosphere helped these changes. Atmosphere is mainly consisting of vapor water on which cycles humans don't have big influence. On the other hand, fossil fuels combustion and forest exploitation caused carbon dioxide (CO₂) increase, waste decomposition and animal farming contributed methane (CH₄) content in atmosphere, higher nitrous oxide (N₂O) content is result of nitrogen-based fertilizers and it is proved that chlorofluorocarbons (CFCs) helped ozone depletion. Humans influence on climate changes cannot be neglected, and between greenhouse gases our emission leader is CO₂. Most of CO₂ emission is result of energy sector. This major human influence on the Earth's atmosphere caused sets of legislation that trying to cut consumption of fossil fuels. Sweden showed some positive examples with plans to completely cut fossil fuels consumption by 2040. Many other countries like Scotland and Denmark are already produce high share of energy from RES.

International Energy Agency (IEA) reported that over 40% of global 32.840 Mt CO₂ in 2017. was emitted by electricity and heat producers and relations are given in Figure 1 [1]. According to data from 2017., 13.603 Mt of CO₂ emissions come from energy sector, and 9.761 Mt of CO₂ is a consequence of coal combustion, so it can conclude that RES can significantly contribute to reduced CO₂ [1]. There is also growing cement industry with high atmosphere impact. Production of cement with 4 billion tons annually causes emission of 5 to 7 % worlds CO₂ [2]. In cement production 40% CO₂ emission comes from production process and energy consumption and 60% is a result of a calcination of limestone [3]. Greenhouse gases reduction in the cement production can be reached in the industrial process or with replacement of raw material. While energy and heat used for processes is highly optimized, many scientific researches take places limestone decomposition field. There are two ways to reduce CO₂ from this chemical reaction, first partial clinker replacement in production process, and second cement replacement with supplementary cementitious material (SCM). Silica fume, coal fly ash and granulated blast furnace slag (GBFS) mixed with cement are already commonly used binders. These SCMs usage in commercial production is regulated with standards.

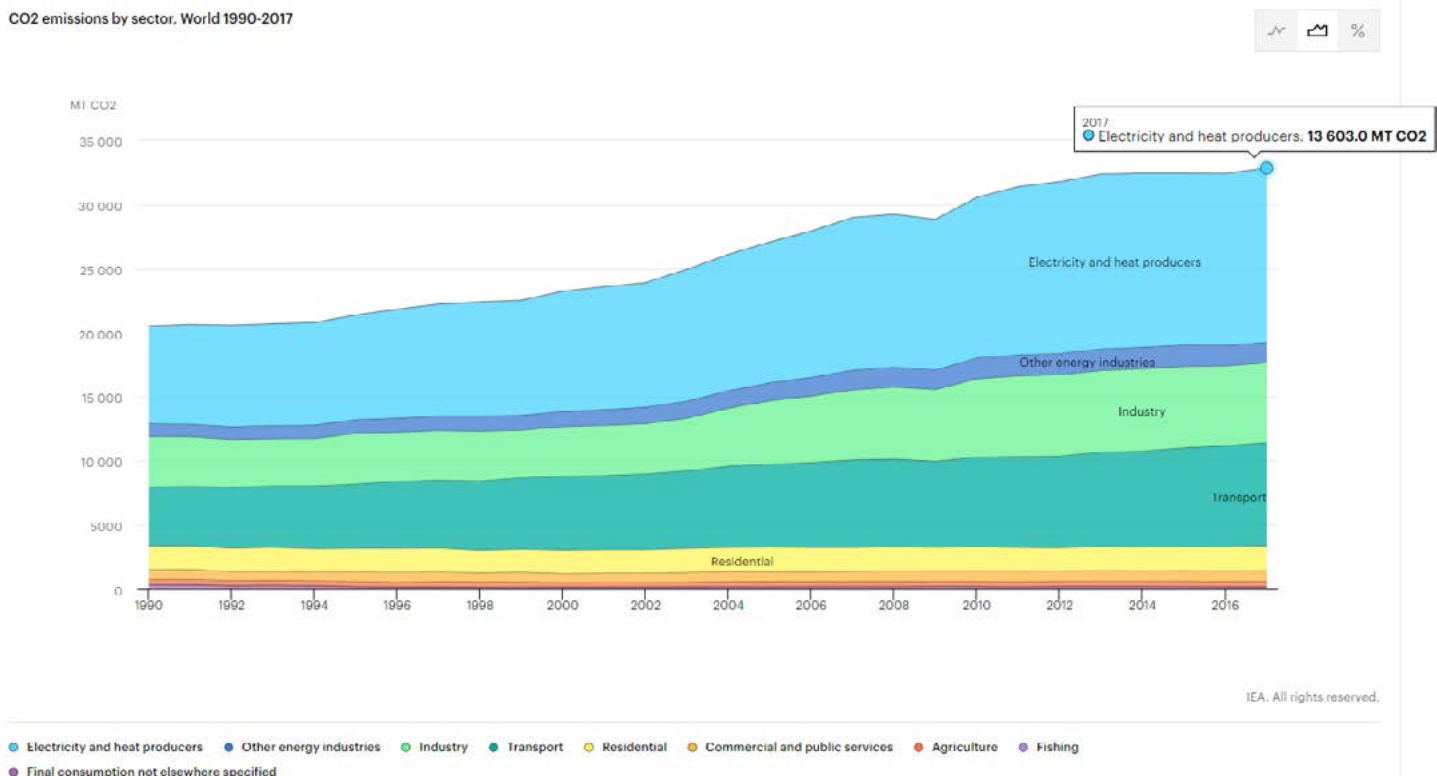


Figure 1: International Energy Agency data and statistics: World CO₂ production by sector [1]

Today many researches trying to enable different SCMs application in concrete. Various materials with hydraulic and/or pozzolanic activity are examining. Besides raw materials recycled industrial waste and by-products are testing for partial cement replacement. Very popular and worldwide used SCM is coal fly ash whose application is regulated with ASTM C618 and EN 450 standards [4],[5]. In USA 44% of coal fly ash is recycled, and 38% of total recycled ash is applied as SCM [6]. Coal fly ash application improves concrete durability performance and delay hydration process which is why is used for massive concrete structures. Coal ash is generated as bottom and fly ash, and as pozzolanic SCM only fly ash is used. High content of amorphous silicon dioxide and aluminum oxide react with portlandite and produce C-S-H gel. Standards regulate classes of ash for concrete application because different conditions under which coal ash is formed result in variable ash characteristics. Loss on ignition (≤ 9.0 % by mass), chloride ($\text{Cl}^- \leq 0.10$ % by mass), sulphate ($\text{SO}_3 \leq 3.0$ % by mass), free calcium oxide ($\text{CaO (free)} \leq 1.5$ % by mass), reactive calcium oxide ($\text{CaO (reactive)} \geq 10.0$ % by mass), reactive silicon dioxide ($\text{SiO}_2 \geq 25$ % by mass), sum of pozzolanic oxides ($\text{SiO}_2 + \text{Fe}_2\text{O}_3 + \text{Al}_2\text{O}_3 \geq 70$ % by mass), total content of alkalis ($\text{Na}_2\text{O}_{\text{eq}} \leq 5.0$ % by mass), magnesium oxide ($\text{MgO} \leq 4.0$ % by mass) and content of total phosphate ($\text{P}_2\text{O}_5 \leq 5.0$ % by mass) are chemical requirements for fly ashes specified in EN 450-1 [4]. Physical limitation is given for fineness (particles sieved on 0,045 mm sieve ≤ 40 % by mass (category N) or ≤ 12 % by mass (category S), activity index, soundness ≤ 10 mm, particle density, initial setting and water requirement [4]. Despite coal fly ash

commercial usage high volume cement replacement studies are still conducted. Chemical characteristics limit values for fly ash for concrete comparison by ASTM C618 and EN 450-1 are given in Table 1.

Table 1: Limit values for chemical characteristics of coal fly ash for concrete [4], [5]

General chemical requirements	ASTM C618	EN 450-1
Loss on ignition (Lol)	max. 6%	Category A < 5.0 % mass Category B < 7.0 % mass Category C < 9.0 % mass
Pozzolanic oxides (SiO ₂ + Al ₂ O ₃ + Fe ₂ O ₃)	Class N and F > 70 % mass Class C > 50 % mass	> 70 % mass
Reactive silicon dioxide	-	> 25 % mass
Reactive calcium oxide	-	> 10 % mass
Free calcium oxide	-	< 1.5 % mass
Magnesium oxide (MgO)	-	< 4.0 % mass
Chloride content (Cl ⁻)	-	< 0.10 % mass
Sulphate content (SO ₃)	-	< 3.0 % mass
Total content of alkali (Na ₂ O _{eq})	max. 5%	< 5.0 % mass
Soluble phosphate (P ₂ O ₅)	-	< 100 mg/kg
Total phosphate (P ₂ O ₅)	-	< 5.0 % mass

Fly WBA has similarity with coal fly ash which is extensively studied for construction materials application. Different effects in wood biomass production outcome various chemical and physical behaviour. Wood type, combustion technology and temperature, and location of ash collection, bottom or fly ash, make big difference in material characteristics. Beside main distinguishing parameters, growth and cutting conditions, material moisture and shape before combustion, collect – transport - storage process and aging also affect important WBA parameters for concrete application. Figure 2 presents fly WBAs as delivered from different power plants in Croatia. Differences between them can be seen in Figure 2. Many researches show that delivered ashes from power plants do not meet specified criteria [7], [8], [9]. Regulations are first barrier for WBA usage in concrete. WBA described by standards will be able to use commercially, which will reap benefits in the concrete industry and circular ash management.



Figure 2: Fly WBA samples from different wood biomass power plants in Croatia

Considering today growing trends in renewable energy production, it could be predicted WBA generation around 15.5 million tons per year in EU until now [10]. By the literature review wood biomass combustion generates from 0.2 to 15% ash which 70% is landfilling [11]. Through the research project “Transformation of Wood Biomass Ash into Resilient Construction Composites – TAREC²” power plants representatives reported an average 3.1% generated WBA [11]. Prices for landfilling are growing as consequence of deposit fees and stricter ecology legislation. Growing ash quantities and rising landfilling costs are motives for power plant management to look after greener and cheaper solution for ash disposal. Beside concrete industry, WBA is extensively tested for fertilizing and soil enrichment. WBA recycling for agriculture is limited with heavy metal content, especially cadmium (Cd) that is limited for fertilizers in the EU. Hazardous elements in WBA can determine waste type classification what can lead to increasing disposal expenses. Hazardous materials require stabilization treatments to prevent heavy metal reaching to the soil what increases waste management costs even when materials are not recycled. This fact could be used as extra financial support for ash treatments before using them as SCM. This paper contains review of WBA characteristics that are required for ash application in the concrete and present proposed methods of mechanical treatments for controlling that values. Purpose is to find simple,

cost efficient and applicable methods for WBA management as SCM in the cement composites.

2 WOOD BIOMASS ASH CHARACTERISTICS

WBA chemical composition varies depending on biomass source and combustion, transport and storage of ash [12]. The overall biomass yield is between 0.1 and 46% with mean value 6.8%, which is lower than the average coal fly ash yield value of 21% and range from 6 to 52% [12]. Ash yield from wood biomass drops with increase of combustion temperature [13]. Biomass fly ash particle size is usually between 10 – 100 µm [14]. Particle size varies more than with coal fly ash and shape is usually more irregular as can be seen in micrographs in Figure 3. Higher value of bulk density indicates better particle packing or finer particles. This property is also very variable in WBA and researchers report various average bulk density [8],[13],[15]. WBA particles collected on electrostatic filters are more irregular than coal fly ash from these filters. The assumption is that such forms occur due to parts of unburned wood [16]. Vasiliev et al. after extensive overview showed how large is variations in chemical, mineral and phase composition, ash yield from biomass, organic content and pH values, hence it is necessary to separately determine properties for each source of WBA and how it could be properly recycled [12]. When ash is evaluated as applicable for construction material, it is important to ensure properties constant. This is done through continuously periodically quality testing.

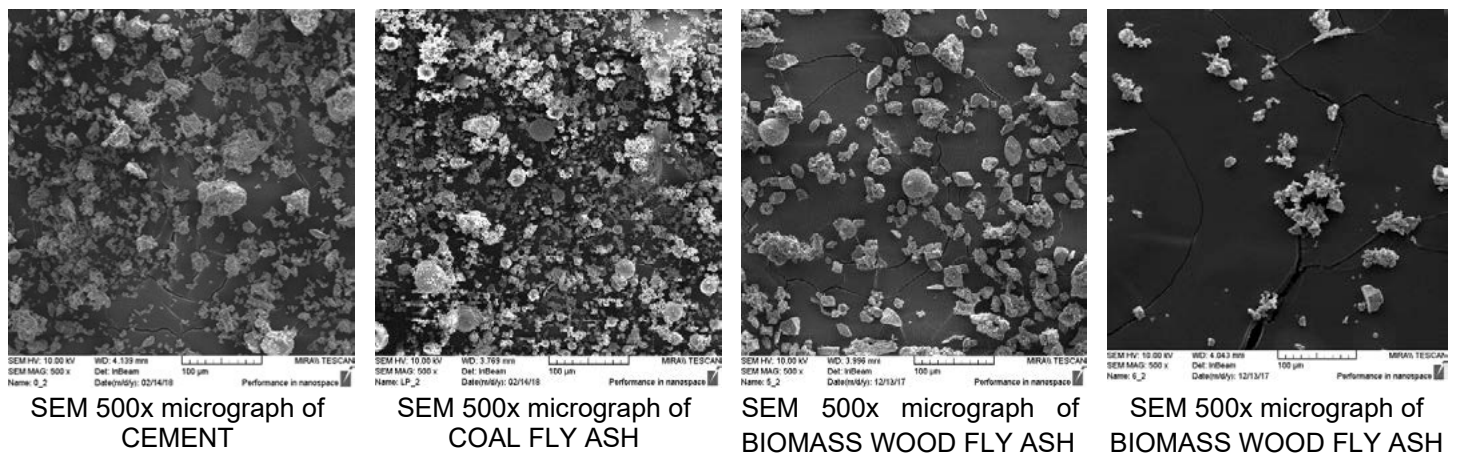


Figure 3: SCM 500x micrographs of cement, coal fly ash and two different WBAs

In order to enable the full-scale utilization of WBAs as partial resource replacements in cementitious materials, the industrial sector requires standard methods to evaluate the suitability of locally available WBAs. As said before, the starting point for such developments is the current coal ash standard and its requirements given in Table 1. Based on detailed physical and chemical analysis of 21 samples of WBA from 10 different locations in the Republic of Croatia done through the research project TAREC², Table 2 was made [14].

Table 2: Chemical characteristics of 21 tested WBA samples [14]

Content		Fly WBA			Bottom WBA		
		Min. Value	Max. value	Average	Min. Value	Max. value	Average
P ₂ O ₅	% mass	1.82	4.03	2.97	0.68	3.46	2.29
CaO	% mass	14.65	67.85	47.10	20.15	63.75	51.12
MgO	% mass	0.17	8.26	4.62	0.17	10.60	4.80
TiO ₂	% mass	0.00	0.71	0.17	0.05	0.60	0.20
SO ₃	% mass	0.44	12.35	3.90	0.12	2.25	0.93
Pozzolanic oxides	% mass	2.85	29.79	13.03	6.19	61.75	20.66
LOI	% mass	3.80	36.30	16.72	1.00	26.70	12.49
Na ₂ O _{eq}	% mass	2.92	23.33	8.12	2.10	9.71	5.45

Free CaO	% mass	0.5	23.5	9.31	0	16.9	6.17
----------	--------	-----	------	------	---	------	------

Comparing different WBAs (fly and bottom) tested through TAREC² with limit values for coal fly ash for concrete [4], [5], it was concluded and published by Carević et al. [14]:

- The average loss of ignition (LOI) of fly WBA and bottom WBA samples is 16.72% and 12.49% respectively, which is significantly higher than the maximum value allowed by EN 450-1.
- According to EN 450, if the total calcium oxide content is not greater than 10.0%, the proportion of reactive calcium oxide is satisfactory. Since in all tested WBA samples CaO content is higher, free CaO was detrimental. In both types of WBA average values for free CaO content do not meet requirement (9.31% for fly WBA and 6.17% for bottom WBA).
- Based on detailed discussion in [14], most of the WBA samples contain greater amounts of MgO and do not meet the maximum allowed content of magnesium oxide, ($MgO < 4.0\%$ by weight).
- The total alkali content expressed as the equivalent of Na_2O (Na_2O_{eq}), whose total amount was calculated as $Na_2O + 0.658 K_2O$. The total alkali content is in general higher for WBA samples; furthermore, the total alkali content is higher in fly WBA (average 8.12%) than in bottom WBA (average 5.45%).
- If we compare average sulphate values for fly and bottom WBA, it can be said that all the WBA samples satisfy the requirement of a maximum SO_3 content of 3%. But it can be noticed higher variability of results in fly WBAs where most of fly WBAs does not meet the SO_3 requirements.
- All tested WBA samples meet the requirement of a maximum allowed P_2O_5 content of 5% according to EN 450-1 standard.

From detailed preliminary characterization of collected WBAs, it can be seen deviations of WBA if comparing with the main chemical characteristics set by standards. This could lead to lower mechanical and durability properties of cement composites where WBA is used.

Research data show that WBA could be used up to 20% [17] depending on the properties of used WBA. Higher WBA content usually results in decreasing of compressive strength [7], [13], [18]. However, compressive strength is not the only important property of concrete. There are many concrete products that need to satisfy durability parameters, volume stability, and specific hydration processes. Mixtures with WBA tested on drying shrinkage exhibit lower results than control OPC mixtures, especially for cement replacement up to 10% [13]. According to [13], it cannot be stated that WBA have some effect on freezing and thawing cycles. If w/b ratio is maintained, ashes with high siliceous oxides content and evaluated pozzolanic activity prevent chloride ions penetration in concrete [19]. Many alternatives can be used as an addition or substitution of cement for up to 5 - 10%, with limited or insignificant influence on concrete properties [20]. Going beyond 10% is possible when SCM limitation, like ones stated below, are controlled.

Loss on ignition: Previous research showed that higher values of loss on ignition (LoI) decrease compressive strength [7]. Unburnt parts in ash are not reactive due to that greater LoI means lower ash reactivity [21]. Unburnt parts should be removed from SCM or material could be used as filler or aggregate but not binder. There is not enough compressive strength contribution when LoI exhibit high values [7]. Unburnt parts in ash are not reactive due to that greater LoI means lower ash reactivity [21].

Moisture content: Various or high water content in delivered ash can be a problem for usage as SCM [7]. Average 13% moisture is found in delivered fly ash [13]. Moisture in ashes causes several problems for the concrete industry, increases transport costs because of delivered water, varies delivered ash characteristics, water content in concrete components affects w/b ratio, in contact with water hydraulic materials react and form portlandite so ash is unusable later as cement replacement, cement industry uses dry or relatively dry materials [22]. These reasons indicate that moisture shall be controlled after production. Bottom and fly ash should be handled separately because of different characteristics and water content. After measuring moisture and regulating it, ashes should be sealed in containers or bags that prevent contact with moisture from the environment. Because ash reactivity with moisture and CO_2 from the environment it is important to analyse ash changes over time or find a way of storage that is not influenced by environmental factors.

Soluble salts: High water solubility (18 – 28%) are caused by soluble salts (chlorides and sulphates) content [7]. High chloride (Cl⁻) content can cause corrosion problems in reinforced concrete [7]. Chlorides in WBA are related to unburnt

carbon particles, so beside direct methods for reducing chlorides, resolving carbon particles is also an option. High sulphate content can have destructive effects on concrete. Ottosen et al. exhibit high values of soluble sulphate (S) in WBA [7]. Soluble salts cause leaching why some ashes are not suitable for forestry and agriculture what is why their potential for recycling is limited to other industries. High leaching must be prevented with chemical treatment, stabilization with binders or with washing techniques.

High carbon content: Carbon in ash has porous particles and negatively affect water requirement and other affected properties like workability and compressive strength. High carbon (C) content limits WBA application only for lower strength concrete products [13]. Unburned carbon presents most of the mass loss on ignition. These particles are not reactive and if their share in ash is high it affects strength development and cause durability problems [23]. Combustion technology at lower temperatures (e.g., 800°C) causes higher unburned carbon content than biomass combustion at temperatures above 1000°C [23]. In addition to not contributing to the strength, the increased demand for water affects the water to binder ratio, one of the starting points in designing the concrete properties. LOI increased and/or the water demand not only mean the content of unburned carbon, but unburnt carbon cause both these occurrences. In addition to the increased temperatures in the boiler that cause reduced amount of carbon, research has shown that sieving on sieves between 125 and 500 µm removes a large part of these particles [24].

High free calcium oxide (CaO) or free lime: It could increase the risk of volume instability (swelling and cracking) once it is mixed water and durability properties of concrete. Free calcium oxide in fly ash is limited in EN 450-1 for application in concrete. Volume stability must be proven if ashes with high free calcium oxides are used.

Workability reduces with increasing percent of WBA that replaces cement [13]. Low workability as consequence has higher water to binder ratio (w/b) because proper concrete placing must be enabled. Increasing w/b is in direct correlation with compressive strength drop.

Alkali content: Naik et al. reported that high alkali content in fly WBA can have positive and negative effect on concrete [22]. They can accelerate formation of hydrates. On the other hand, alkali contribute alkali silica reaction (ASR) and may lead to chemical reaction with sulphates and leaching. Alkaline salts, K₂O and MgO, has negative effect on durability of concrete [25]. A higher amount of alkali can lead to an alkali-aggregate reaction, resulting in a deterioration in the durability of the cementitious composites. For coal fly ashes total alkalis content is limit to Na₂O_{eq} < 5% [4]. While high alkali content concern mostly because of alkali aggregate reaction, some research offers another perspective. Matalkan et al. suggested taking advantage of high alkali content in biomass ash (not from wood biomass) for alkali-activated aluminosilicate binders production [26]. Washing treatments with deionized water proved to reduce chlorides, sulphates and alkalis content in wood biomass ash [27]. Berra et al. [27] exhibit higher activity index with washed ash then non-treated, but this could be due to filler effect surpasses the negative effect of soluble salts content.

Fast carbonization: Newly formed WBA is very alkali and tends to react with CO₂ from the air. Rich with CaO, WBA stored in the air, reacts with CO₂ and forms CaCO₃ and the process are called carbonatization. This reaction changes the chemical and physical properties of WBA. Ash also reacts with H₂O (added on purpose or from moisture) and forms Ca(OH)₂ in the process of self-hardening. While these processes stabilize WBA and make it suitable for forestry and agriculture, they reduce ashes reactivity and must be considered when valorising WBA for potential partial cement replacement.

Understanding the mechanisms of degradation brings us to the point of seeking solutions to reduce this impact. This means that ash pre-treatments could insure moving beyond 10% of cement replacement.

3 PRE-TREATMENTS OVERVIEW

SCM reactivity is the most important characteristic for usage as binder. If material does not exhibit pozzolan and/or latent hydraulic reaction it can be used as aggregate replacement or filler. Beneficial pre-treatments convert undesirable compounds to harmless ones or remove them. In case of WBA, these compounds are mainly alkali, moisture, unburnt content that causes high LOI, soluble salts, free CaO and MgO, irregular particles and heavy metals. Pre-treatments can reduce impurities to upgrade ashes for suitable as SCM or other application in concrete or even meet criteria in standards. It is important to detect limitation of ash, find suitable treatments, and optimise treatments parameter (time of treatment, temperature, etc.). Pre-treatment methods for upgrading WBAs and their impact on ash properties are mentioned below.

Thermal treatment: Combustion of WBA effects on lowering organic content which directly effects compressive strength of mortar/concrete. Rosales et al. with thermal treatment reduce organic matter content, water absorption and increase compressive and flexural strength [25]. Justification of energy consumption for thermal treatments of SCMs can be find in fact that clinker is produced in temperatures between 1450 and 1600°C. Many studies on coal fly ash correlate Lol and carbon which can be removed in laboratory oven treatment on 740° for 2 hours [28].

Drying: Small particles of WBA during transport can be blown away by wind and handling and can cause dusting which is why they are usually sprayed with water. Water content in concrete components has influence on w/b ratio which directly affects physical concrete characteristics. To evaporate extra water from WBA, standard procedure in laboratory testing is drying at 105°C. This method could be also applicable in industry.

Grinding and milling: Grinding and milling are mechanical treatments that improves physical properties of powder material, such as fly ash, by increasing particle fineness [29]. That treatment changes morphology and smoothness surface. Irregularly shaped WBA particles are highly porous. High porosity demands higher w/b ratio which negatively effects on compressive strength. Research conducted on grinding coal fly ash showed particles maintain same shape and reduce size, and it is concluded that workability is inversely proportional to mean particle diameter and/or specific surface area [30]. Smaller fly ash particles more easily take places between Portland cement and have filler effect. Ohenoja et al. tested three different milling methods on biomass fly ashes which led to conclusion that wider particle distribution resulted with lower w/b ratio and have positive effect on compressive strength [31]. They conclude increase WBA self-hardening (property of material to react with water and form solid structure like OPC) after 60 minutes ball milling due to better particles packing [31]. Grinding effect depends on treatment duration in a way that extended grinding time results with decreasing particle size, and after 3 hours all ash types has similar mean particle size [29]. Particle size reduction can improve pozzolanic reactivity due to correlation between particle size and specific surface area and SCMs reactivity [32]. Fly ashes generally postpone hydration process. Increasing fly ash content in binder extends setting time, but it is significantly reduced when binder is finely ground [29]. Grinding has positive effect on reduction of water requirement [29], [31], [33]. Grinding could be standard procedure for enhancement WBAs workability that usually negative affected in higher cement replacement ratios.

Extraction of light particle: Very light organic and carbon particle can excessively demand water. Ridding of light particles improves compressive strength and increase density [25]. One way to remove light particles is flotation. Ash and water are mixed in addition of soap in system shown in Figure 4. Undesirable organic and carbon particles that have multiple negative effect on WBA application in concrete are separated on the surface as residue layer. This treatment, like others that involve water, eliminates potential natural hydraulic and/or properties of ash.

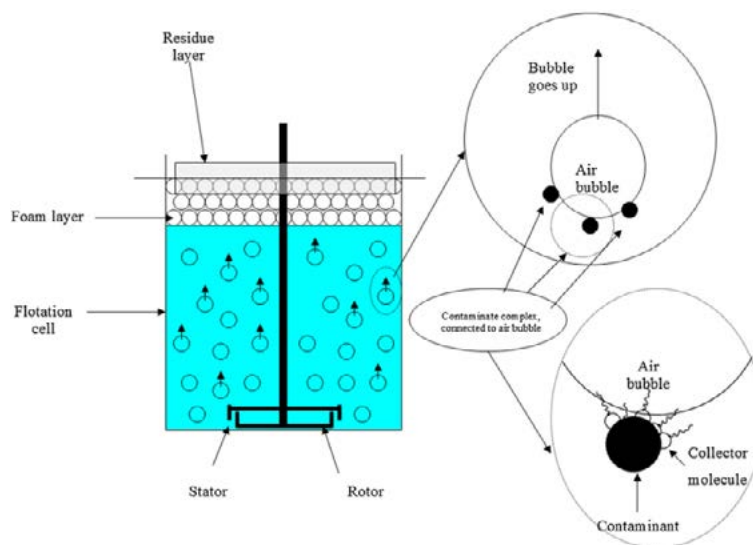


Figure 4: Flotation scheme for extraction of light particles [24]

Sieving: This method is used for removal of undesirable content like carbon and unburnt particles form WBA, but also for particle size distribution control. Doudart de la Gree et al. used sieves of 500 µm to remove carbon content and result was Lol reduction and lowering chloride content [24]. Sieving reduces chloride content because soluble chloride particles

are attached to carbon, which is why washing after sieving does not have big influence on lowering chloride content [24]. It is easily applicable in combination with other treatments. Around 50% of large organic carbon particles with significant internal porosity are removed from coal and co-combusting coal and biomass fly ash on 177 µm sieve [6].

Elutriation or water washing: WBA is washed in water to eliminate soluble salts like chlorides and sulphates. Washing with water can reduce about 71% of chloride content, as it turned out washed ashes with high Cl⁻ content can be placed within the limits of standard EN 450-1 for fly ashes application in concrete [24]. Berra et al. with washing treatment significantly lowered alkali content and increased sum of pozzolanic oxides, values after treatment meet criteria for American and European Standard [27]. Solubility also drops by lowering sulphate and chloride content, but not enough to satisfy EN 450-1 [27]. Water washing treatment improves WBA physical and chemical characteristics but not guarantee positive evaluation by standard for fly ashes in concrete. Another problem is ash exposure to water, and exploitation of all possibly present hydraulic activity. Usually, ash reacts with water and form solid boulders of material which then must be crushed and treated to produce powder material. After the whole procedure, ash reactivity is questionable. This ash could be used as sand replacement in concrete.

Crushing: Crushing is sometimes necessary for maintain powder structure of ash, but it is usually combined with other treatments like washing and sieving. Crushed WBA performed separately or after other treatments (floatation and combustion) exhibit lower water absorption then untreated ashes or treated without crushing [25].

4 CONCLUSION

After reviewing WBA properties and its possible impact on concrete properties from the literature, mechanical pre-treatments that can easily be applied in powerplants or concrete industry are listed in Table 3. In Rosales et al. research 20% cement replaced with bottom WBA, thermal treatment in combination with crushing results in 80% increase of compressive strength then non-treated bottom ash replacement [25]. This shows that with proper treatment, WBA effect on concrete can be optimized. Negative side of these methods is increasing the cost. Doudart et al. [24] analysed the effect of pre-treatments costs in countries where waste management is regulated through taxes and disposal costs. The cost of waste landfilling can only rise due to increasing environmental awareness. Many types of WBAs in its original form cannot be used in higher dosage in concrete. Therefore, pre-treatment can be considered. According to [24], combination of pre-treatments in long term can cause ash management price rise from 2.5 to 15.0 %. It is important to find optimal treatment scheme for every cooperation between power plant and construction material produces, so experimental research is the subject of future work. Cost-efficient and sustainable pre-treatment of WBA can ensure quality SCM and/or material for reduction raw materials in construction industry.

Table 3: Proposed pre-treatment to minimize negative of undesirable WBA characteristics

WBA characteristic	Limit EN 450-1	Limit ASTM C618	Proposed pre-treatment
LOI	Category A < 5.0 % mass Category B < 7.0 % mass Category C < 9.0 % mass	max. 6%	Thermal treatment Sieving
Carbon (C)	-	-	Thermal treatment Sieving
Moisture	-	-	Drying
Soluble salts (Cl, S)	Cl ⁻ < 0.10 % mass	-	Washing Sieving Cl attached on carbon particles
CaO	> 10 % mass	-	Washing Grinding
Workability	-	-	Grinding and milling
Alkali	max. 5%		Washing Chemical treatment

ACKNOWLEDGMENTS

This research was performed within research project: IP-2016-06-7701 “Transformation of Wood Biomass Ash into Resilient Construction Composites”, funded by Croatian Science Foundation.

REFERENCES

- [1] “www.iea.org,” 2010. [Online]. Available: [https://www.iea.org/data-and-statistics?country=WORLD&fuel=CO2 emissions&indicator=CO2 emissions by sector](https://www.iea.org/data-and-statistics?country=WORLD&fuel=CO2&emissions&indicator=CO2%20emissions%20by%20sector).
- [2] N. Ukrainczyk, N. Vrbos, and E. A. B. Koenders, “Reuse of woody biomass ash waste in cementitious materials,” *Chemical and Biochemical Engineering Quarterly*, vol. 30, no. 2, pp. 137–148, 2016.
- [3] K. L. Scrivener, “Options for the future of cement,” *The Indian Concrete Journal*, vol. 88, no. 7, pp. 11–21, 2014.
- [4] European Committee for Standardization, “EN 450-1:2013 Fly ash for concrete – Part 1: Definition, specification and conformity criteria.”
- [5] American society for testing and materials, *ASTM C618 Standard specification for coal fly ash and raw or calcined natural pozzolan or use in concrete*, no. 0. West Conshohocken, PA, USA: ASTM International, 2003.
- [6] N. N. N. Yeboah, C. R. Shearer, S. E. Burns, and K. E. Kurtis, “Characterization of biomass and high carbon content coal ash for productive reuse applications,” *FUEL*, vol. 116, no. X, pp. 438–447, 2014.
- [7] L. M. Ottosen, E. Ø. Hansen, P. E. Jensen, G. M. Kirkelund, and P. Golterman, “Wood ash used as partly sand and/or cement replacement in mortar,” *International Journal of Sustainable Development and Planning*, vol. 11, no. 5, pp. 781–791, 2016.
- [8] I. Carević, M. Serdar, N. Štirmer, and N. Ukrainczyk, “Preliminary screening of wood biomass ashes for partial resources replacements in cementitious materials,” *Journal of Cleaner Production*, vol. 229, pp. 1045–1064, 2019.
- [9] S. Kramar and V. Ducman, “Evaluation of Ash Pozzolanic Activity by Means of the Strength Activity Index Test , Frattini Test and DTA / TG Analysis,” vol. 3651, pp. 1746–1752, 2018.
- [10] I. Obernberger and K. Supancic, “Possibilities of ash utilisation from biomass combustion plants,” in *Proceedings of 17th European Biomass Conference & Exhibition*, 2009, no. July.
- [11] B. Milovanović, N. Štirmer, I. Carević, and A. Baričević, “Wood biomass ash as a raw material in concrete industry,” *Gradjevinar*, vol. 71, no. 6, pp. 505–514, 2019.
- [12] S. V. Vassilev, D. Baxter, L. K. Andersen, and C. G. Vassileva, “An overview of the composition and application of biomass ash. Part 1. Phase-mineral and chemical composition and classification,” *Fuel*, vol. 105, pp. 40–76, 2013.
- [13] R. Siddique, “Utilization of wood ash in concrete manufacturing,” *Resources, Conservation and Recycling*, vol. 67, pp. 27–33, 2012.
- [14] I. Carević, M. Serdar, N. Štirmer, and N. Ukrainczyk, “Preliminary screening of wood biomass ashes for partial resources replacements in cementitious materials,” *Journal of Cleaner Production*, vol. 229, pp. 1045–1064, 2019.
- [15] S. V. Vassilev, D. Baxter, L. K. Andersen, and C. G. Vassileva, “An overview of the composition and application of biomass ash.: Part 2. Potential utilisation, technological and ecological advantages and challenges,” *Fuel*, vol. 105, pp. 19–39, 2013.
- [16] A. Jaworek, T. Czech, A. T. Sobczyk, and A. Krupa, “Properties of biomass vs . coal fl y ashes deposited in electrostatic precipitator,” *Journal of Electrostatics*, vol. 71, no. 2, pp. 165–175, 2013.
- [17] L. Tosti, A. van Zomeren, J. R. Pels, and R. N. J. Comans, “Technical and environmental performance of lower carbon footprint cement mortars containing biomass fly ash as a secondary cementitious material,” *Resources, Conservation and Recycling*, vol. 134, no. March, pp. 25–33, 2018.
- [18] C. B. Cheah and M. Ramli, “Mechanical strength, durability and drying shrinkage of structural mortar containing HCWA as partial replacement of cement,” *Construction and Building Materials*, vol. 30, pp. 320–329, 2012.
- [19] S. Wang, E. Llamazos, L. Baxter, and F. Fonseca, “Durability of biomass fly ash concrete: Freezing and thawing and rapid chloride permeability tests,” *Fuel*, vol. 87, no. 3, pp. 359–364, 2008.
- [20] M. Serdar, D. Bjegovic, N. Stirmer, and I. Banjad Pecur, “Alternative binders for concrete: opportunities and challenges,” in *Future Trends in Civil Engineering*, 2019, pp. 199–218.
- [21] M. Abdullahi, “Characteristics of Wood ASH / OPC Concrete,” *Leonardo Electronic journal of Praczics and Technologies*, no. 8, pp. 9–16, 2006.
- [22] T. R. Naik, “Tests of Wood Ash as a Potential Source for Construction Materials,” 1999.
- [23] S. Demis, J. G. Tapali, and V. G. Papadakis, “An investigation of the effectiveness of the utilization of biomass ashes as pozzolanic materials,” *Construction and Building Materials*, vol. 68, pp. 291–300, 2014.
- [24] G. C. H. Doudart de la Grée, M. V. A. Florea, A. Keulen, and H. J. H. Brouwers, “Contaminated biomass fly ashes - Characterization and treatment optimization for reuse as building materials,” *Waste Management*, vol. 49, pp. 96–109, 2016.
- [25] J. Rosales, M. Cabrera, M. G. Beltrán, M. López, and F. Agrela, “Effects of treatments on biomass bottom ash applied to the manufacture od cement mortara,” *Journal of Cleaner Production*, vol. 154, pp. 424–435, 2017.
- [26] F. Matalkah, P. Soroushian, S. Ul Abideen, and A. Peyvandi, “Use of non-wood biomass combustion ash in development of alkali-activated concrete,” *Construction and Building Materials*, vol. 121, pp. 491–500, 2016.
- [27] M. Berra, T. Mangialardi, and A. E. Paolini, “Reuse of woody biomass fly ash in cement-based materials,”

- Construction and Building Materials*, vol. 76, pp. 286–296, 2015.
- [28] K. H. Pedersen and A. D. Å. Jensen, “A review of the interference of carbon containing fly ash with air entrainment in concrete,” *Progress in Energy and Combustion Science*, vol. 34, pp. 135–154, 2008.
- [29] P. Jidrada, G. Sua-iam, B. Chatveera, and N. Makul, “Recycling of combined coal-biomass ash from electric power plant waste as a cementitious material : characteristics and improvement,” *Journal of Material Cycles and Waste Management*, vol. 18, no. 3, pp. 527–540, 2016.
- [30] J. Paya, J. Monzo, M. V. Borrachero, E. Peris-Mora, and E. Gonzalez-Lopez, “Mechanical Treatment of Fly Ashes Part II: Particle Morphologies in Ground Fly Ash (GFA) and Workability of GRA-Cement mortars,” *Cement and Concrete Research*, vol. 26, no. 2, pp. 225–235, 1996.
- [31] K. Ohenoja, P. Tanskanen, O. Peltosaari, V. Wigren, J. Österbacka, and M. Illikainen, “Effect of particle size distribution on the self-hardening property of biomass-peat fly ash from a bubbling fluidized bed combustion,” *Fuel Processing Technology*, vol. 148, pp. 60–66, 2016.
- [32] M. C. G. Juenger and R. Siddique, “Recent advances in understanding the role of supplementary cementitious materials in concrete,” *Cement and Concrete Research*, vol. 78, pp. 71–80, 2015.
- [33] J. Rissanen, K. Ohenoja, P. Kinnunen, M. Romagnoli, and M. Illikainen, “Milling of peat-wood fly ash: Effect on water demand of mortar and rheology of cement paste,” *Construction and Building Materials*, vol. 180, pp. 143–153, 2018.

24

Paulina Krolo, Natalija Bede, Davor Grandić and Ivan Palijan

Influence of density on tensile and compressive properties of polyurethane foam

INFLUENCE OF DENSITY ON TENSILE AND COMPRESSIVE PROPERTIES OF POLYURETHANE FOAM

Paulina Krolo¹, Natalija Bede², Davor Grandić³ and Ivan Palijan⁴

^{1,3} Faculty of Civil Engineering University of Rijeka, Department of Structural Engineering and Technical Mechanics, Radmile Matejčić 3, Rijeka-CROATIA
e-mail: paulina.krolo@uniri.hr, dgrandic@uniri.hr

² Faculty of Civil Engineering University of Rijeka, Department of Computer Modelling of Materials and Structures, Radmile Matejčić 3, Rijeka-CROATIA
e-mail: natalija.bede@gradri.uniri.hr

⁴ Palijan d.o.o., for design and development of steel and composite structures, Diljska 1, Zagreb-CROATIA
e-mail: ipalijan@palijan.hr

SUMMARY: Polyurethane (PU) foams are widely used in building structures. Due to their good thermal and sound insulation properties, PU foams are often applied in the production of façade systems as a non-structural component. In addition, they are commonly used in structural load-bearing components, e.g. as a core material in composite sandwich panels. In order to be used in load-bearing structures, it is necessary to know their mechanical properties. The main mechanical properties of PU foams are influenced by many parameters such as density, temperature, anisotropy, loading condition, etc. In this paper, the influence of density on tensile and compressive properties of PU foam is presented. Therefore, the uniaxial tension and compression tests according to the International Standards for six different densities were performed. Based on the test results, the influence of density on tensile and compressive strength as well as compressive modulus of elasticity is reported.

KEYWORDS: polyurethane foam, density, experimental test, tension, compression, compressive modulus of elasticity

1 INTRODUCTION

The polyurethane (PU) foam is one of the most commonly used type of polymer products. This material has a wide range of application such as automotive, electronics, production of furniture, clothing, and building structures. In the field of building structures, its application may be as a non-structural component and structural load-bearing components. One of the largest application of PU foams in building construction as non-structural components are insulation panels, including wall and roof insulation, and gap fillers for spaces around the doors and windows. Energy efficiency, good thermal and sound performance and environmental benefits are the advantages of using PU foams as insulation material. As a load-bearing component, PU foams are used in various types of composite structural systems. In the last few decades, PU foams have been used with other materials to obtain composites that have low density, high toughness and ductility, high impact resistance, efficient sound and thermal insulation, and excellent mechanical properties [1]. Lightweight sandwich composite structures with PU foam core have been used for more than 60 years. These composite elements are bonded together by a PU foam core with two or more layers of structural skins made of metal, plywood, fibbers, cement, and other types of boards. All of these materials act as a single integrated system, which is used as exterior walls, partition walls, floors, roofs, and structural framing [2, 3].

In order to use PU foams in load-bearing structures, it is necessary to know their mechanical properties. The main mechanical properties of PU foams are influenced by many parameters such as density, temperature, anisotropy, loading condition, etc. [4-7]. A hybrid polyurethane (PU) foam core with foams of three different densities was applied in novel composite sandwich panel with upper and lower GFRP skins [8]. PU foams of the same density may have different mechanical properties, which depend on the foam installation process. In other words, in the same cross-section of composite elements may occur the variation of foam density, resulting from the uncontrolled foam expansion which finally affects the mechanical properties.

The main aim of this research was to investigate the influence of density on compressive and tensile strength of PU foam. Therefore, only one type of polyurethane foam but with three different nominal densities was used. In addition, the influence of the foam expansion on the density as well as mechanical properties was also investigated.

2 EXPERIMENTAL RESEARCH

In this experimental research, a total of 60 tests were performed at the Faculty of Civil Engineering in Rijeka, Croatia. Laboratory tests include uniaxial tensile and compressive tests performed according to international ISO standards and measurement of apparent density.

2.1 Material and specimen geometry

Laboratory tests have been performed on polyurethane foam for three different densities with a nominal value of 40, 45 and 50 kg/m³. To perform a tensile test according to ISO 1926:2009 standard [9] and compression tests according to ISO 844:2014 standard [6], two different specimen geometries were prepared. For uniaxial tension test, standard specimens whose nominal dimensions and shape are shown in Figure 1a were used, whereas standard prisms of size 100 mm × 100 mm × 50 mm used for uniaxial compression test are shown in Figure 1b. Tensile test specimens/compression test specimens are marked as T40-1/C40-1, where the first mark defines the type of test (T for tensile test, and C for compression test), the second mark defines the nominal density of PU foam, and the last mark defines the number of specimens.

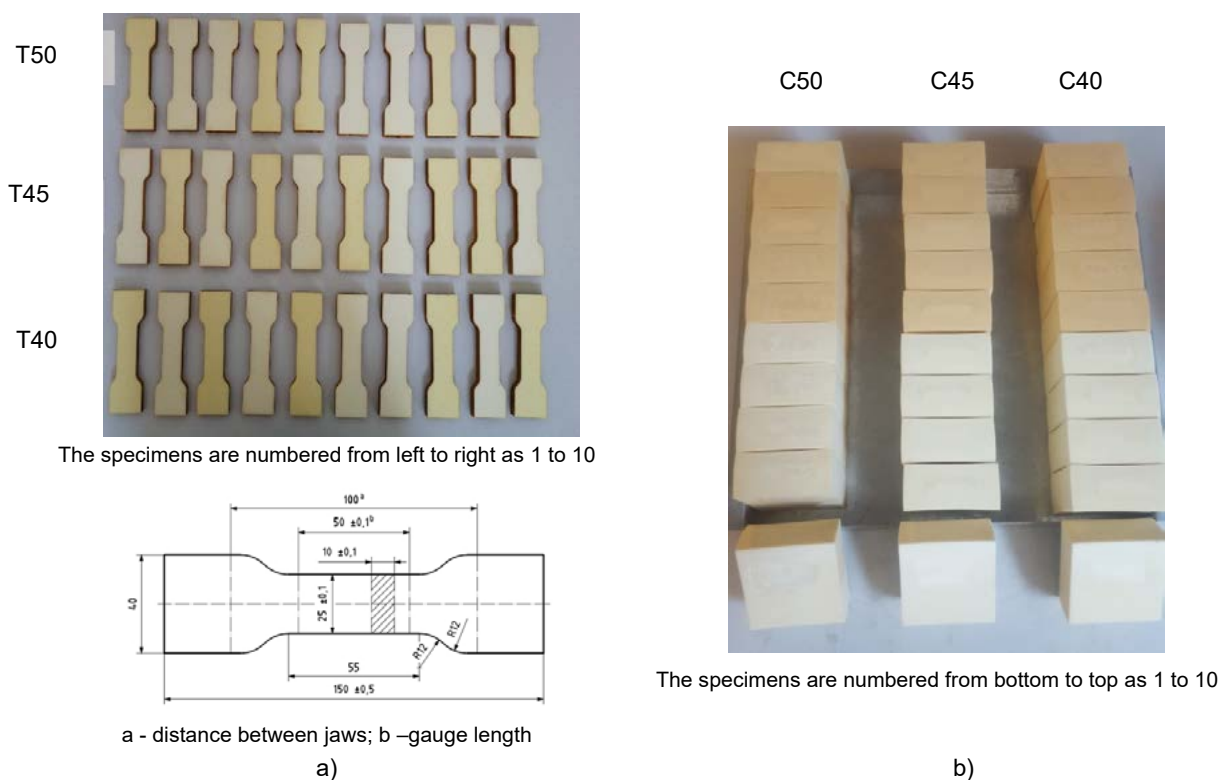


Figure 1: Test specimen geometry for a) tensile test, according to ISO 1926:2009 [9] and b) compressive test according to ISO 844:2014 [6]

For experimental research, 10 specimens per each nominal density were prepared, in total 30 specimens per each laboratory test type. However, visual inspection revealed a colour difference between the specimens of equal nominal density. Five specimens were dark-yellow while the other five were bright-yellow (see Figure 1). Accordingly, the specimens within equal nominal density were additionally classified into two groups such as specimens “D” for dark-yellow and specimens “B” for bright-yellow colour. This is most probably related to the foam expansion in a mould during processing time (see Figure 2).

Thus, the apparent density is measured for each specimen and individual values are shown in Figure 3. This values are based on the average of five specimens “B” and five specimens “D” from same nominal density, e.g. average density of five “B” tensile test specimens T40-B amounts 43.99 kg/m³, while the average value of five “D” tensile specimen T40-D amounts 34.84 kg/m³ (see Figure 3a). The percentage decrease in the density of “D” specimens over “B” is presented in Figure 4. The density difference between specimen T40-D and specimen T40-B is 20.8%, marked as T40. Density differences for other specimens were calculated in the same way, and the following values are obtained: 18.7% as the

difference between T45-D and T45-B (marked as T45), and 24.4% as the difference between T50-D and T50-B (marked as T50). Further, density values of specimens "D" were lower than density value of specimens "B" by 15.5 %, 14.9% and 17.9% for C40, C45 and C50, respectively. Comparison of the results shows that maximum density difference is obtained at nominal density of 50 kg/m³ for both tension and compression specimens. The last two columns of each diagram in Figure 3 represent the average (Avg) densities for specimens "B" and "D". In general, from given results, it can be observed that for each nominal density specimens "D" show the same trend i.e. lower density than reported nominal value while for all specimens "B" values are higher. Consequently, based on these results it is shown that uncontrolled foam expansion strongly affects density even in the same cross-section of the foam.

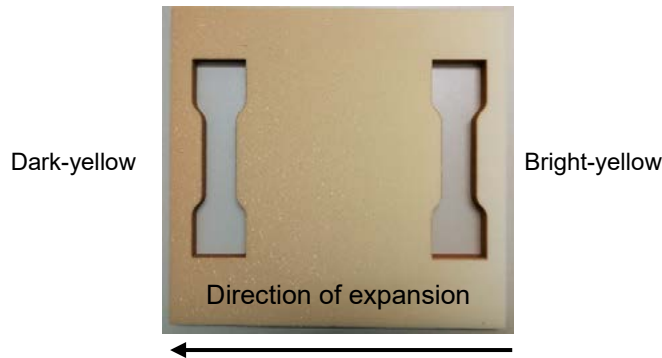


Figure 2: Foam expansion in a mould during processing time

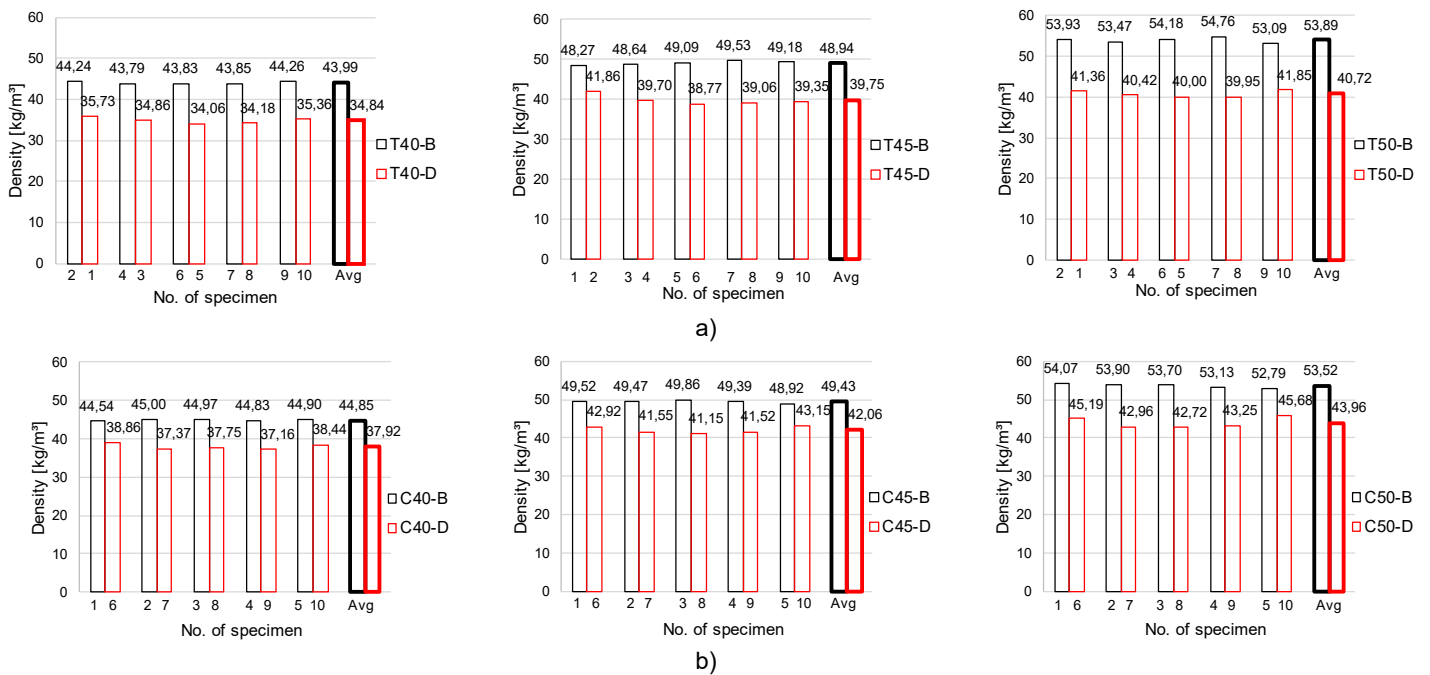


Figure 3: Polyurethane foam density for a) Tensile test specimens and b) Compression test specimens

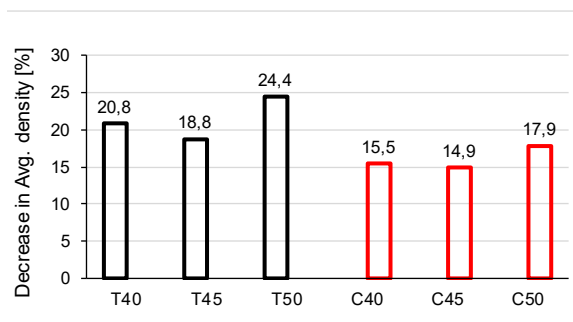


Figure 4: Percentage decrease of specimens "D" over specimens "B"

2.2 Test set-up and equipment

The laboratory tests were performed on the universal tension-compression test machine Zwick/Roell Z600. Test management and registration of the data were conducted using TestXpert II software.

The uniaxial tensile tests were performed according to ISO 1926 Standard [9]. Specimens were tested using mechanical jaws with capacities up to 10 kN, and test set-up is shown in Figure 5a. The tension in the specimen is simulated using displacement control of moving crosshead, with a test speed of 5 mm/min. The strains were measured by the extensometer on the gauge length of 50 mm. During the test, the axial force in the moving crosshead was recorded. Based on the obtained forces, the stresses at a tapered part of the specimen were calculated. End of testing is defined when the tensile strength is reduced to 50%.

Compression tests were performed according to ISO 844:2014 standard [6]. The typical test set-up used for this test is shown in Figure 4b. To ensure the fix position of the compression plates during testing, special steel equipment was designed and mounted as shown in Figure 5b. The load was applied by controlling displacement of the testing machine with a constant rate of 5mm/min until the specimen thickness is reduced to 85% of the original thickness. In other words, the test was terminated at a displacement value of 7.5 mm. During each test, force and vertical displacement in the direction of the applied compression loading were measured until the prescribed reduction in thickness. The compressive force was measured with 50 kN load cell.

A total of 60 specimens were tested, 30 specimens in tension and 30 specimens in compression. In a group of 30 tensile/compression specimens, 10 specimens were selected for each nominal PU foam density (five specimens "D" and five specimens "B"). Testing of a group of five specimens represents one series of tests. A total of six test series was conducted for tensile test and six test series for compression test. The first and second series of tensile tests include testing of five specimens "B" and five specimens "D" with a nominal density of 40 kg/m³. The third and fourth series refers to five specimens "B" and five specimens "D", with a nominal density of 45 kg/m³. The fifth and sixth series of tests refer to five specimens "B" and five specimens "D", with a nominal density of 50 kg/m³. The same procedure was performed for the compression test.

Before the start of laboratory testing, all specimens were conditioned for at least 6 hours at a relative humidity of 41 percent and an air temperature of 27.5°C.

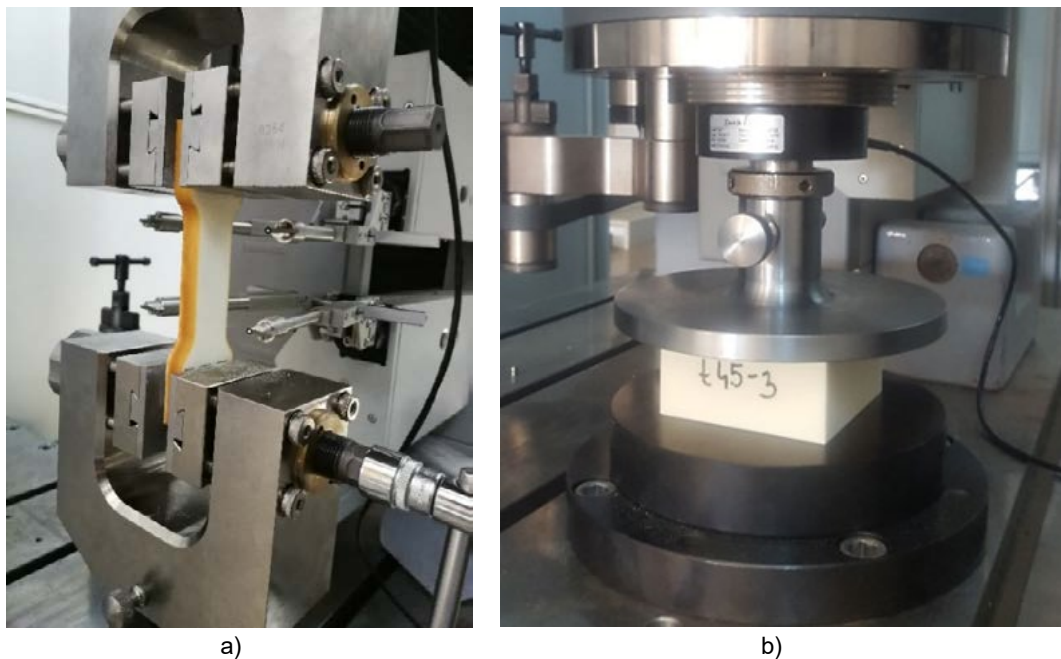


Figure 5: Test set-up for a) tensile test according to ISO 1926:2009 [9] and b) compression test according to ISO 844:2014 standard [9]

3 RESULTS

In this section are given test results with respect to the estimated six different densities: 40-D, 45-D, 50-D, 40-B, 45-B and 50-B. Labels are ordered in such a way that the first one denotes the lowest density and the last one the highest density.

The tension behaviour of PU foam is typically represented by stress-strain curves, which is shown in Figure 6a. The stress-strain curves show the test results of 10 specimens with a nominal density of 45 kg/m³. As expected, after the reaching maximum strength all specimens showed a brittle fracture. However, the difference between specimens "B" and specimens "D" is obvious. From Figure 6a, it is obvious that specimens "B" reach higher tensile strength than strength in specimens "D". It is important to note that specimens "B" reach lower strains at ultimate tensile strength than strains in specimen "D". Hence, increasing the PU foam density increases the ultimate tensile strength but decreases the total strain of the specimen.

The typical force-displacement curves obtained from the compression tests of specimens with a nominal density of 45 kg/m³ are plotted in Figure 6b. The load-displacement curves for tested foam display relatively straight pre-peak line, well-defined peak and gradual post-peak softening typically associated with the compressive behaviour of foams [6]. The compressive modulus of elasticity was determined as a tangent to the steepest part of the pre-peak line of load-displacement curve. For all 10 specimens, the load-displacement curves showed the same shape however, specimens "D" reached lower maximum force and modulus of elasticity. It is interesting to observe that both types of specimens (five specimens "D" and five specimens "B") show maximum force at approximately the same displacement.

In general, it can be observed that specimens "B" show the same trend for tensile and compressive force, and the specimens "B" have higher maximum load than specimens "D".

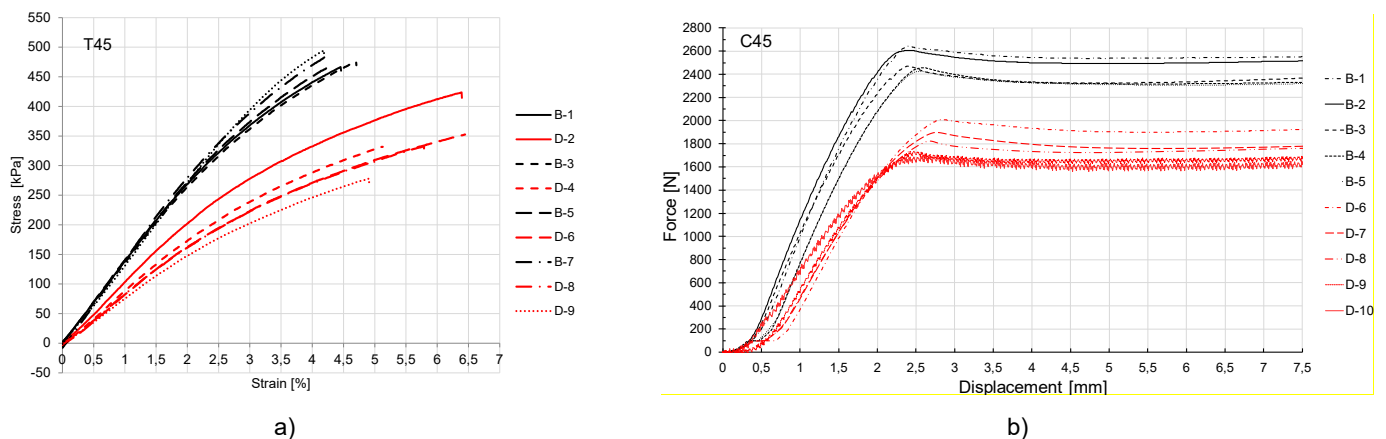


Figure 6: a) Typical stress-strain curve for tension test and b) Typical force-displacement curve for compression test

The influence of density on compressive and tensile strength of PU foams are shown in Figure 7. Each column represents the average strength for one series of testing with five specimens as detailed described above in test set-up and equipment. Average values of tensile strength are shown in Figure 7a, while the average values of compressive strength are shown in Figure 7b. The variation of the tensile and compressive strength with an average density of specimens "B" and "D" for all three nominal densities follows the same trend. It can be seen that the tensile and compressive strength increases linearly with density. Moreover, it is interesting to observe that all three specimens marked "D" with different nominal densities show lower values compared to specimens "B". The percentage decrease in tensile and compressive strength of specimens "D" with respect to specimens "B" is presented in Figure 8. The difference of tensile strength between dark and bright specimens of same nominal density amounts 31.5%, 28.13% and 36.72% which relate to T40 (decrease of T40-D over T40-B), T45 (decrease of T45-D over T45-B), and T50 (decrease of T50-D over T50-B), respectively. Also, the difference of compressive strength between dark and bright specimens amounts 25.76%, 26.88% and 34.42% which relate to C40, C45 and C50, respectively. As expected, maximum difference of strength between specimens "D" and "B" was achieved at nominal density of 50 kg/m³.

Comparison between tensile and compressive strength for six different densities are shown in Figure 9. These results

lead to the conclusion that the value of the tensile strength is approximately two times higher than compressive strength for the same density. Further, as expected, the influence of the density on the compressive modulus of elasticity shows the same trend as on strength (see Figure 10)

Therefore, the test results show that higher foam density increases the tensile strength and compressive strength as well as compressive modulus of elasticity, but decreases the total strain of specimen under tension loading.

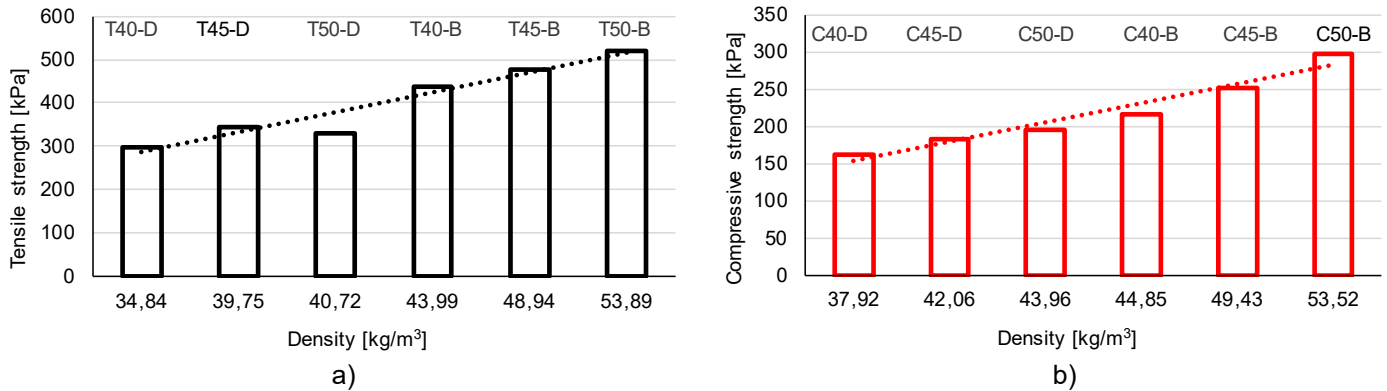


Figure 7. Influence of density on a) tensile strength and b) compressive strength

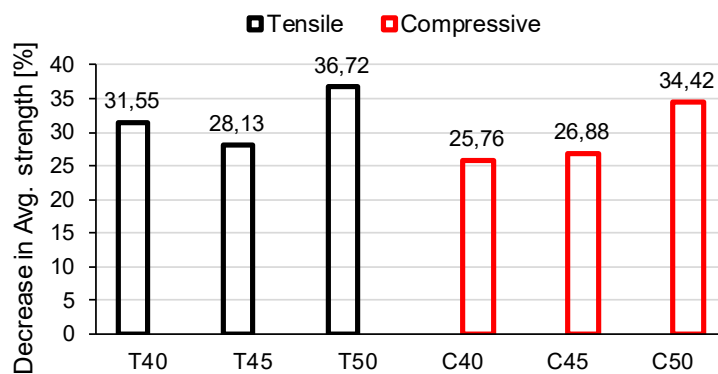


Figure 8: Percentage decrease of specimens "D" in strength over the specimens "B"

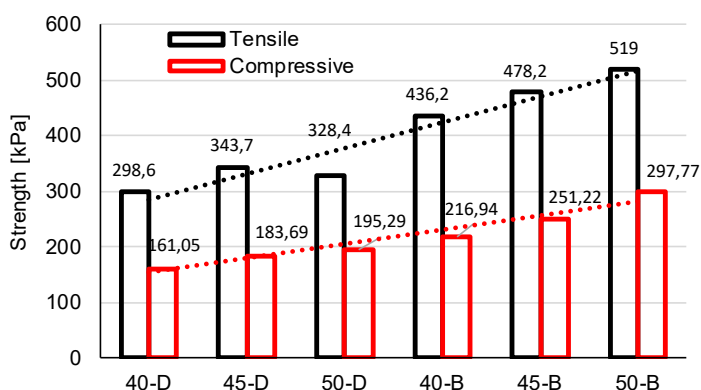


Figure 9: Comparison between tensile and compressive strength

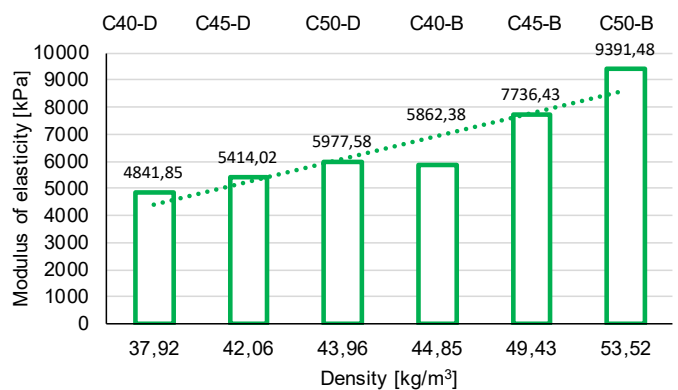


Figure 10: Influence of density on the compressive modulus of elasticity

4 CONCLUSIONS

The research presented in this paper summarizes the results of the experimental investigation on tensile and compressive properties of PU foams with three different nominal densities. Based on the test results obtained, the following conclusions can be made:

1. In order to produce foam with uniform density, uncontrolled foam expansion must be eliminated. Therefore, the mechanical properties of the same foam material can be notably improved by better control of foam expansion.
2. Test results show that the tensile strength, as well as compressive strength, increase linearly with the increase of the foam density. At the same density, tensile strength was two times higher than compressive strength for all six densities.
3. The compressive modulus of elasticity follows the linear trend as strength. It shows gradually increase with increasing density.
5. It has been shown experimentally that density is the most important parameter that affects mechanical properties of foams.

ACKNOWLEDGEMENTS

This work has been supported in part by Ministry of Science, Education and Sports of the Republic of Croatia under the project Research Infrastructure for Campus-based Laboratories at the University of Rijeka (no. RC.2.2.06-0001). The research presented in this work was done within the scientific project "Investigation of behaviour of composite panel components with integrated steel core" (ZIP-UNIRI-1500-2-20).

REFERENCES

- [1] Somarathna, H. M. C. C. et al.: The use of polyurethane for structural and infrastructural engineering application: A state-of-the-art review, *Construction and Building Materials*, vol. 190, (2018), pp. 955-1014, ISSN: 0950-0618
- [2] Sharaf, T. & Fam, A.: Analysis of large scale cladding sandwich panels composed of GFRP skins and ribs and polyurethane foam core, *Thin-Walled Structures*, vol. 71, (2013), pp. 91-101, ISSN: 0263-8231
- [3] Yuen, S. C. K. Y.; Cunliffe, G. & du Plessis, M.: Blast response of cladding sandwich panels with tubular cores, *International Journal of Impact Engineering*, vol. 110, (2017), pp. 266-278, ISSN: 0734-743X
- [4] Linul, E. et al: Study of factors influencing the mechanical properties of polyurethane foams under dynamic compression, *Journal of Physics: Conference Series*, vol. 451, (2013), pp.1-6, ISSN: 1742-6588 (print); 1742-6596 (web)
- [5] Wiyuno, P. et al.: Characterization of physical and mechanical properties of rigid polyurethane foam, *ARPJ Journal of Engineering and Applied Sciences*, vol. 11, no. 24, (2016), pp. 14398-14405, 2, ISSN: 1819-6608
- [6] Ramsteiner, F. & Forster, N. F. S.: Testing the deformation behaviour of polymer foams, *Polymer Testing*, vol. 20, (2001), pp. 661-670, ISSN: 0142-9418
- [7] Saint-Michel, F. et al.: Mechanical properties of high density polyurethane foams: I. Effect of the density, *Composites Science and Technology*, vol. 66, (2006), pp. 2700-2708, ISSN: 0266-3538
- [8] Zhao X., Tan L. and Zhang F., Mechanical Behavior of Sandwich Panels with Hybrid PU Foam Core, *Advances in Civil Engineering*, 2020, 2020.
- [9] ISO 1926:2009: Rigid cellular plastics - Determination of tensile properties, *Technical Committee ISO/TC 61, SC 10*, Switzerland, 2009
- [10] ISO 844:ISO 2014: Rigid cellular plastics - Determination of compression properties, *Technical Committee ISO/TC 61, SC 10*, Switzerland, 2014

25

Alisa Machner, Marie H. Bjørndal, Aljoša Šajna, Lucija Hanžič, Yushan Gu, Benoît Bary and Klaartje De Weerd

Measurement of the chloride resistance of Environmentally friendly and Durable conCrete

Measurement of the chloride resistance of Environmentally friendly and Durable conCrete

Alisa Machner¹, Marie H. Bjørndal¹, Aljoša Šajna², Lucija Hanžič², Yushan Gu³, Benoît Bary³ and Klaartje De Weerd¹

¹ NTNU, Norwegian University of Science and Technology, Department of Structural Engineering
Richard Birkelandsvei 1A, 7491 Trondheim, Norway
e-mail: alisa.machner@ntnu.no

² Slovenian National Building and Civil Engineering Institute, Department of Materials
Dimiceva ul. 12, 1000 Ljubljana

³ Université Paris-Saclay, CEA, Service d'Étude du Comportement des Radionucléides, 91191, Gif-sur-Yvette, France

SUMMARY: The increasing demand for concrete and thereby Portland cement, creates the need for novel low-clinker Portland composite cements. Concretes prepared with such novel composite cements need to show similar or even improved durability compared to concrete prepared with commonly used Portland composite cements. This study represents a part of the EnDurCrete project that focuses on the durability of concrete produced with novel low-clinker cements, containing high-value industrial by-products. More specifically, we investigated the chloride ingress resistance of such concrete. Concrete cylinders were submitted to chloride ingress by bulk diffusion. The chloride ingress resistance was investigated on concrete samples by μ XRF scanning and chloride titration. In addition, the chloride binding capacity of these novel binders was investigated on paste samples by determining chloride binding isotherms for both binders. In the next step of the project, these experimental results will be matched with an advanced model, which is being developed within the project. By combining modelling with experimental verification, we aim to reach a better understanding of the fundamental chloride ingress mechanisms acting on novel types of concrete. The overall goal of the work is to produce a concrete with lower cost, lower environmental footprint and with verified similar or improved durability.

KEY WORDS: chloride ingress, durability, novel binders, low CO₂, sustainability, concrete.

1 INTRODUCTION

The main goal of the Horizon 2020 project “EnDurCrete” is to develop a New Environmentally friendly and Durable conCrete, integrating industrial by-products and hybrid systems, for civil, industrial and offshore applications. This study represents a part of the EnDurCrete project that focuses on the durability of concrete produced with novel low-clinker cements, developed within the project, containing high-value industrial by-products. The study was performed as a collaboration between several EnDurCrete project partners, namely the Slovenian National Building and Civil engineering Institute ZAG (Slovenia), the Norwegian University of Science and Technology NTNU (Norway), SINTEF (Norway) and the French Alternative Energies and Atomic Energy Commission CEA (France). The novel composite cement was provided by HeidelbergCement (Germany) and the concrete samples by Acciona (Spain).

In the study presented here, we investigated the chloride ingress resistance of concrete samples prepared with novel composite cements developed within the EnDurCrete project. Chloride ingress resistance of the concrete is of major importance with regard to the durability of reinforced concrete structures exposed to seawater or de-icing salts. The concrete cover functions as a barrier for external chlorides to reach the steel reinforcement. If chlorides reach a critical level at the surface of the reinforcement, they can cause pitting corrosion [1]. Corrosion of the reinforcement steel is one of the most common deterioration mechanisms and causes for the end of service life for reinforced concrete structures exposed to seawater or de-icing salts.

Total chloride ingress profiles in concrete prepared with novel composite cements and the chloride binding isotherm for the cements were determined. These experimental results will be used to develop an advanced multi-ion transport model for chloride ingress to understand the underlying mechanisms of chloride ingress and ensure accurate service life

prediction.

To determine how far the chlorides have penetrated the concrete cover, and to determine the remaining service life of existing concrete structures, total chloride profiles are commonly obtained. Such total chloride profiles are also determined for laboratory performance tests, to determine the chloride resistance of various concretes and to predict their performance in the field, e.g. according to EN 12390-11 [2]. Total chloride profiles depict the total chloride content in each section analysed as a function of the distance from the exposed surface. For that purpose, the concrete powders from consecutive layers inwards from the exposed surface are analysed for their total chloride content.

When chlorides penetrate the concrete during the exposure to a chloride solution, part of the chlorides determined in total chloride profiles is present in the pore solution, commonly referred to as “free chlorides”, and part of the chlorides interact with the hydrates, commonly referred to as “bound chlorides”. Bound chlorides can either be chemically bound in AFm phases such as Friedel’s salt ($3\text{CaO}\cdot\text{Al}_2\text{O}_3\cdot\text{CaCl}_2\cdot 10\text{H}_2\text{O}$) or physically bound by their accumulation in the Stern layer of the C-S-H phase [3]. Therefore, the shape of the total chloride profile is determined not only by the chloride ingress depth but also by the chloride binding of the cement paste in the concrete [4–6].

Concrete cylinders prepared with the novel composite cements were submitted to chloride ingress by bulk diffusion and their chloride ingress resistance was investigated after 90 days of exposure by μXRF scanning of cut discs and chloride titration of the profile ground powders from consecutive layers from the exposed surface. In addition, the chloride binding capacity of these novel binders is investigated on paste samples prepared with two different novel composite cements. In the next step, the experimental results will be matched with an advanced multi-ion transport model, which is being developed within the project, considering chloride ingress and leaching phenomena. Therefore, all experiments performed within this study were designed in close communication with the project partners involved, in order to ensure the use of the results as input for the chloride ingress model, which is currently under development.

2 MATERIALS & METHODS

In this study, two novel composite cements, namely CEM II/C-M (S-LL) and CEM VI (S-V), developed [7] and supplied by HeidelbergCement, were used. The composition of the two cements used is shown in Table 1. Both cements are low-clinker cements, containing only 47 wt% or 50 wt% CEM I. The supplementary cementitious materials used in the two composite cements are ground granulated blast furnace slag (GGBFS) and limestone or coarse GGBFS and fly ash.

Table 1: Composition [wt%] of the novel Portland composite cements used in this study developed within the EnDurCrete project.

Novel binder	CEM I 52.5 R	GGBFS	Limestone filler	CEM I 42.5 R	Coarse GGBFS	Fly ash
CEM II/C-M (S-LL)	50	40	10	-	-	-
CEM VI (S-V)	-	-	-	47	43	10

The chemical composition as determined with XRF for both binders is shown in Table 2.

Table 2: Chemical composition of the two novel Portland composite cements used in this study developed within the EnDurCrete project, determined with XRF [wt%].

Novel binder	LOI	SiO ₂	Al ₂ O ₃	TiO ₂	MnO	Fe ₂ O ₃	CaO	MgO	K ₂ O	Na ₂ O	SO ₃	P ₂ O ₅
CEM II/C-M (S-LL)	4.36	24.18	7.16	0.56	0.10	1.39	53.67	3.23	0.71	0.18	4.08	0.07
CEM VI (S-V)	0.79	31.79	8.36	0.37	0.09	2.05	48.72	3.56	0.90	0.29	2.43	0.09

From these binders, concrete cylinders (nominal height: 20cm, nominal diameter: 10cm) were prepared according to EN 12390-2 [8] with a water-to-binder (w/b) ratio of 0.45. The sample preparation was carried out at the EnDurCrete project partner Acciona (Spain). The concrete mix design was developed by the EnDurCrete project partner HeidelbergCement and is given in mass of the component [kg] required for 1 m³ of concrete in Table 3.

Table 3: Concrete mix designs used for this study.

Sample name	Concrete components [kg/m ³]				Water
	CEM II/C-M (S-LL)	CEM VI (S-V)	SUM Aggregates	SUM Superplasticizer	
CEM II	360	-	1933	4.8	162
CEM VI	-	360	1912	2.9	162

The samples were sealed in plastic foil cured for 56 days at 20 °C. After 56 days of sealed curing, test specimens of >75 mm in height were sawn from each cylinder as illustrated in Figure 1.

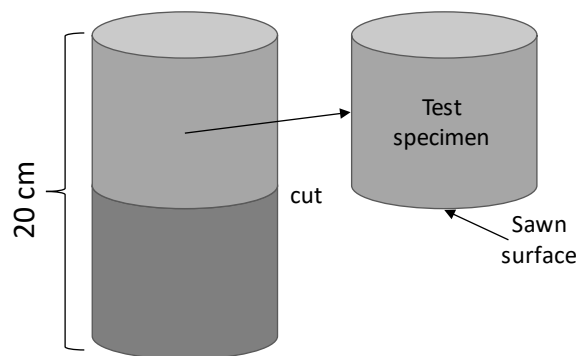


Figure 1: Schematic illustration of cutting the cylinder samples after 56 days of sealed curing.

The test specimens were saturated before exposure and all sides, except the sawn surface, were epoxy coated according to EN 12390-11 [2]. After sealing, the samples were exposed by immersion to a 3% NaCl solution according to EN 12390-11 [2] (see Figure 2). The exposure solution was prepared by mixing 30 g of laboratory-grade NaCl with 970 g deionized water. The exposure solution was exchanged weekly while keeping the surface to exposure solution ratio constant over the whole exposure time (12.5 mL/cm²).

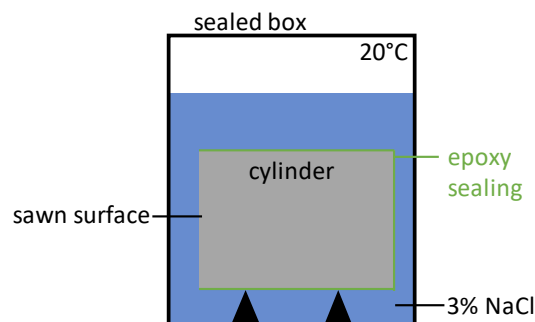


Figure 2: Schematic illustration of the chloride exposure of the test specimens by immersion.

For each binder, two twin cylinders were prepared and exposed in exactly the same way. After 90 days of exposure to the 3% NaCl solution, the cylinders were taken out of the solutions. One cylinder of each binder (test specimen 1) was profile ground by avoiding the outer rim, and the obtained powders from consecutive layers were analysed by chloride titration. This allows us to determine the total chloride content as a function of depth from the exposed surface. The other exposed cylinder of each binder (test specimen 2), was used for μ XRF scanning. For that purpose, a 2 cm disc was cut from the centre along the revolution axis of test specimen 2 of each binder. Figure 3 gives an overview of the two different types of concrete samples (test specimen 1 and test specimen 2) obtained for each binder in this study.

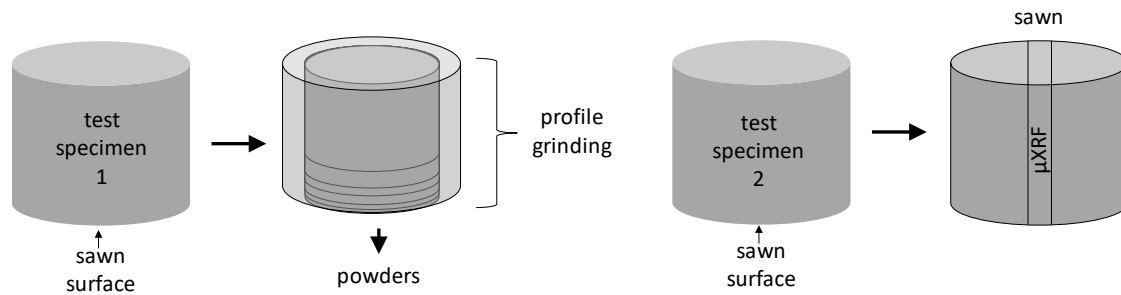


Figure 3: Schematic illustration of how the exposed cylinders (test specimen 1 and test specimen 2) of each binder were prepared for the analyses.

For the chloride analyses, 5 g of the powder extracted from each layer was dried at 105 °C overnight in an aerated oven. The dried powders were then dissolved in 50 mL HNO₃ (65% HNO₃, diluted 1:10, heated up to 80 °C). The slurry was filtered through a cellulose filter and titrated against a 0.01 mol/L AgNO₃ solution with a Titrand 905 titrator from Metrohm. The chloride content in [wt% Cl per gram dried mortar] of each section was calculated using Eq. 1,

$$Cl\ wt\% = \frac{V_{AgNO_3} \cdot c_{AgNO_3} \cdot M(Cl) \cdot V_{HNO_3} \cdot 0.001}{V_{sample} \cdot m_{mortar,dried}} \cdot 100 \quad (1)$$

where V_{AgNO_3} is the volume of the silver nitrate used for titration, c_{AgNO_3} is the concentration of the silver nitrate (0.01 mol/L), $M(Cl)$ is the molar mass of chlorine (35.5 g/mol), V_{HNO_3} is the volume of diluted HNO₃ used to dissolve the ground samples (50 mL), V_{sample} is the volume of the dissolved and filtered sample used for titration (0.1-1 mL, depending on chloride content), $m_{mortar,dried}$ is the mass of the profile ground sample after drying at 105 °C.

For the μ XRF scanning the cut discs from test specimen 2 were analysed with a Bruker M4 Tornado μ XRF equipped with an Ag X-ray tube and an SDD detector. The scans were performed with a spot size of 20 μ m, a 25 μ m step size and a counting time of 3 ms/pixel. The two samples exposed to the two different exposure solutions were measured in parallel in order to be able to compare the chloride content in them. The obtained chlorine maps are illustrated as semi-quantitative heat maps.

In addition to the concrete samples, paste samples were prepared for both binders by mixing 200 g cement (CEM VI (S-V) or CEM II/C-M (S-LL)) with 90 g of deionized water with an overhead mixer from IKA at 1600 rpm. The mixing procedure was: mixing for 1 minute, 1 minute pause, mixing again for 1 minute. After mixing, the pastes were cast in 100 mL bottles, which were sealed and cured immersed up to their bottleneck in water at 20 °C for three months. For each binder, at least three batches were mixed to obtain a sufficient amount of sample. After three months, the paste samples were crushed to a particle size < 1 mm. After the crushing, the sand like samples of all batches were homogenized and filled into 1 L plastic bottles together with 30 % additional deionized water. The ground and re-hydrated samples were then further cured at 20 °C for 3 months before exposure started. The sample preparation procedure described here was applied in order to ensure a high degree of reaction of the paste samples before exposing them to the chloride solutions.

For the exposure, 30 g of the well-hydrated cement paste samples were filled into 50 mL centrifuge tubes together with 15 mL of NaCl solution, which had different chloride concentrations ranging from 0 – 1.5 mol/L. The samples exposed to the chloride solutions were left to reach equilibrium for 1 month, while being shaken once a week. After the samples reached equilibrium, the amount of free chlorides at equilibrium ($C_{Cl,free}$) was determined with potentiometric titration of the exposure solution against 0.1 mol/L AgNO₃ using a Titrand 905 titrator from Metrohm and the amount of bound chlorides ($N_{Cl,bound}$) was calculated using Eq. 2 [9–11],

$$N_{Cl,bound} = \frac{(C_{Cl,free} - C_{Cl,eq}) \times (V_{H_2O} + V_{Cl,added}) / 100 \times M_{Cl}}{m_{sample} - m_{H_2O}} \quad (2)$$

where $C_{Cl,free}$ is the actual concentration of the free chlorides present at the beginning of the exposure in [mol/L], $C_{Cl,eq}$ is the chloride concentration measured at equilibrium in [mol/L], V_{H_2O} is the volume of free water in the 30 g well-hydrated cement paste before exposure in [mL], $V_{Cl,added}$ is the volume of exposure solution added (15 mL), and M_{Cl} is the molar mass of chlorine (35.453 g/mol), m_{sample} is the mass of the well-hydrated paste sample (30 g), and m_{H_2O} is the mass of free water in this 30 g cement paste in [g]. m_{H_2O} was determined by drying the well-hydrated but unexposed cement paste samples in the TGA at 40 °C until they reach a stable weight. V_{H_2O} was determined from m_{H_2O} assuming the density of water to be 1 g/mL.

3 RESULTS & DISCUSSION

Figure 4 shows the chlorine heat maps obtained by μ XRF scanning of the concrete samples prepared with the two different binders after exposing them to a 3% NaCl solution for 90 days. In both images, the uncoated and exposed surface is located at the bottom of the image.

Both samples show clear ingress of chlorides from the exposed surface inwards. The chlorides were detected to a depth of ~1 cm in both samples after 90 days of exposure. For the CEM II sample, higher chlorine signals were detected in the outermost sections compared to the CEM VI sample.

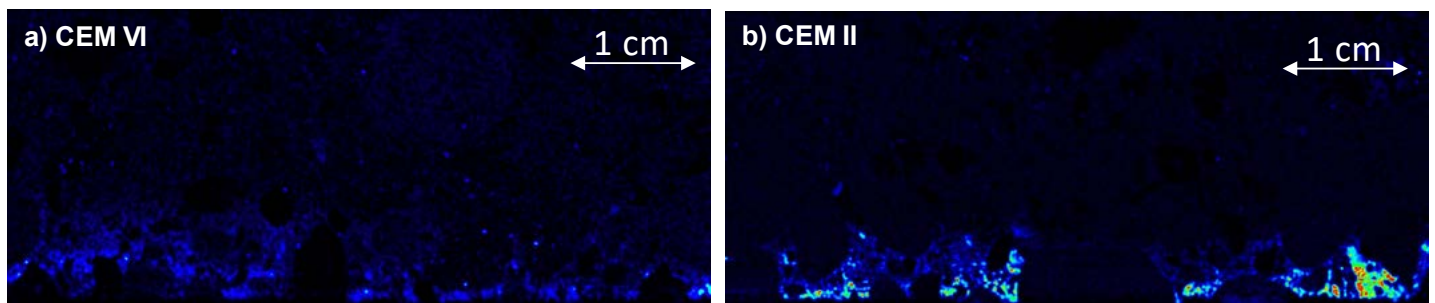


Figure 4: Chlorine heat maps obtained by μ XRF scanning of the a) CEM VI and b) CEM II concrete samples exposed for 90 days to a 3% NaCl solution. In both images the bottom surface was exposed to the chloride solutions.

In order to investigate the chloride ingress in both samples in more detail, total chloride profiles were determined on twin samples (see Figure 3) by titration against an $AgNO_3$ solution. Figure 5 shows the total chloride profiles of the samples CEM VI and the CEM II as a function of the depth from the exposed surface (depth = 0 mm).

As expected from the semi-quantitative μ XRF scanning (Figure 4), the sample CEM II shows a higher total chloride content towards the exposed surface compared to the sample CEM VI. The curves of the total chloride profiles of both samples are very similar from 5 mm on and inwards.

To understand the underlying mechanisms of the chloride ingress in concrete, chloride binding in the cement paste needs to be taken into account. Therefore, we determined the chloride binding-isotherms on paste samples for the CEM II/C-M (S-LL) and the CEM VI (S-V) (Figure 6). For the same free chloride concentration, the CEM VI shows a higher chloride binding than the CEM II. This might be due to the higher aluminium content in the CEM VI (S-V) binder compared to the CEM II/C-M (S-LL) binder (see Table 2), which potentially allows the formation of higher amounts of Friedel's salt during the exposure to the chloride solutions [12,13]. However, these results are in contrast with the results from μ XRF scanning (Figure 4) and the total chloride profiles (Figure 5), where in both cases the CEM II sample showed the highest maximum total chloride content. Therefore, the chloride binding isotherms as determined in this study do not directly explain the difference in the total chloride content between the two binders in the respective concrete samples.

There are several possible explanations for that discrepancy. The two concrete samples probably have different porosities, meaning a different amount of pore volume can be filled with chloride-containing pore solution. However, the contribution of the chloride solution filled porosity to the total chloride profiles is rather low compared to the contribution from the bound chlorides [4], and can therefore not explain the difference in the chloride profiles.

In addition, it should be noted that the chloride binding isotherms were determined on well-hydrated paste samples that are in equilibrium with the chloride exposure solutions, whereas the concrete samples of the ingress experiments are

not in equilibrium with the weekly exchanged chloride exposure solution. For the determination of the chloride binding isotherms on the paste samples, 15 mL of the chloride solution was added to the well-hydrated paste samples, which were then kept sealed until investigation. In the case of the concrete samples, the NaCl exposure solution was exchanged weekly. The 3% NaCl (= 0.9 mol/L) exposure solution initially has a pH close to neutral and did not contain calcium. This, in addition to the weekly exchange of the exposure solution, promotes leaching of e.g. calcium from the concrete samples into the exposure solution.

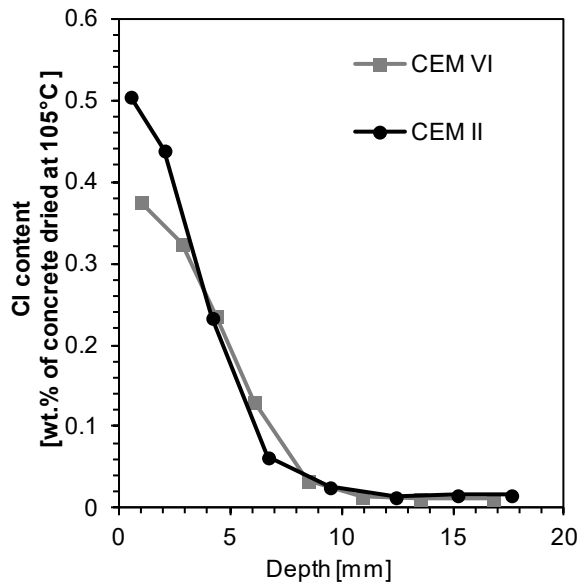


Figure 5: Total chloride profiles obtained from titration of the samples CEM VI and CEM II after 90 days of exposure as a function of the depth from the exposed surface.

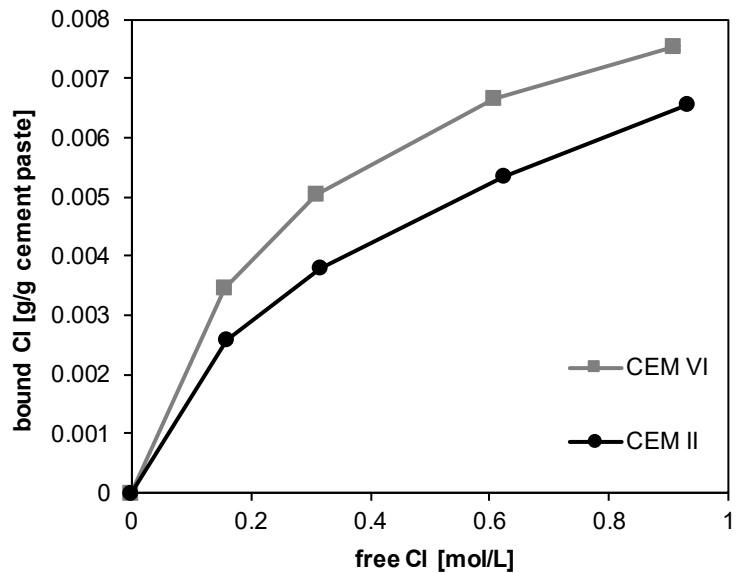


Figure 6: Chloride binding isotherms of paste samples prepared with the CEM VI (S-V) and CEM II/C-M (S-LL) binder.

In a previous study, it was shown that artificial leaching of a hydrated cement paste increased its chloride binding in an interval of decreasing pH down to pH 12 [6]. It was shown that the decreasing pH due to the artificial leaching affects the hydration phases and thereby their chloride binding capacity [6]. As leaching can have a considerable impact on the chloride binding of the cement paste, it might also alter the shape of the total chloride profile.

Total chloride ingress profiles are commonly used to predict the service life of existing concrete structures or to estimate the chloride resistance of concrete based on laboratory performance tests. For this, chloride profiles are fitted with the error function solution of Fick's second law, yielding an apparent non-steady state diffusion coefficient and a surface concentration as fitting parameters [14]. These parameters can be used to predict the service life of structures. Recently these models have been questioned as they are mainly based on laboratory testing and experience. The predicted service life is strongly dependent on parameters such as ageing coefficients which are unknown for these novel cements.

Service life modelling by fitting the total chloride profiles with the error function solution of Fick's second law would rank the two binders (CEM VI (S-V) or CEM II/C-M (S-LL)) differently as they show different maximum chloride contents in total chloride profiles, indicating a difference in potential for diffusion. Whereas, when looking just at the chloride ingress depth, the type of binder used (CEM VI (S-V) or CEM II/C-M (S-LL)) does not seem to affect the ingress depth after 90 days of exposure. Extrapolation based on total chloride profiles seems meaningless as at the end it is really the chloride ingress depth of the critical chloride content that is determining the service life of a reinforced concrete structure.

This demonstrates that there is a need for an advanced multi-ion transport model for chloride ingress based on the understanding of the fundamental mechanisms acting during chloride ingress and chloride binding in order to accurately determine the service life of new or existing concrete structures. The experimental results obtained within this study will be used to develop an advanced multi-ion transport model for chloride ingress within the EnDurCrete project. Within the multi-ion transport approach of the model, leaching will be considered, and we will therefore be able to link the binding isotherms to the total chloride ingress profiles.

This is especially important considering the increasing demand for novel composite cements. It is not possible to set up an extensive long-term testing program for every possible composition of novel cements. The fundamental multi-ion transport model would allow further variations in the composition of the cements and would allow the modelling of chloride ingress of various novel composite cements.

The experimental matrix of the study presented here does not include a reference concrete prepared with commercially available cement. However, in a parallel set of tests within the EnDurCrete project, standard performance testing was performed on the concrete samples prepared with the same concrete mix design as given in Table 3 and CEM II/C-M (S-LL) cement, and a reference concrete prepared with a similar mix design and a commercial CEM II/A 42.5 N cement. The chloride migration coefficient was determined according to NT BUILD 492 [15] by the EnDurCrete project partner Acciona (Spain). In these tests, the obtained chloride migration coefficient of the CEM II EnDurCrete concrete was considerably lower ($2.2 \cdot 10^{-12} \text{ m}^2 \text{ s}^{-1}$) compared to the reference concrete ($8.1 \cdot 10^{-12} \text{ m}^2 \text{ s}^{-1}$). Non-steady state diffusion coefficient tests on the CEM II and reference concrete according to EN 12390-11 and EN 14629 [2,16] are currently ongoing. These experimental results will be used in addition to the experimental results presented here as input for the advanced multi-ion transport model currently being developed within the EnDurCrete project.

4 CONCLUSIONS

The chloride resistance of concrete samples prepared with two novel Portland composite cements, namely CEM VI (S-V) and CEM II/C-M (S-LL), was investigated in this study. In addition, the chloride binding isotherms were determined on paste samples prepared with these novel binders. The results of the μ XRF scanning and the total chloride profiles obtained on chloride-exposed concrete samples agreed well with each other. However, the results of this study showed that total chloride profiles obtained on profile ground concrete samples and chloride binding isotherms obtained on well-hydrated paste samples do not directly match. The exposure to a 3% NaCl solution, which was exchanged weekly, possibly altered the chloride binding of the hydration phases in the concrete samples compared to the paste samples, which were exposed sealed under equilibrium conditions. The chloride ingress depth was not affected by the two different binders investigated in this study. The results of this study demonstrate the need for an advanced multi-ion transport model for chloride ingress which can be used for different composition of novel composite cements and would take into account the impact of leaching.

ACKNOWLEDGMENTS

The authors would like to thank the EnDurCrete project partners HeidelbergCement for developing the concrete mix designs and Acciona for preparing the samples for this study. In addition, we would like to thank Siri Hofstad Trapnes (SINTEF), Tone H. Nilsen (NTNU), Andreas Markali (NTNU), Oda Tjetland (NTNU) and Petter Hemstad (NTNU) for assistance, training and help with various experimental techniques. This project has received funding from the European Union's Horizon 2020 research and innovation programme under grant agreement No 760639. This publication reflects only the authors' view and the Commission is not responsible for any use that may be made of the information it contains.



REFERENCES

- [1] U. Angst, B. Elsener, C.K. Larsen, Ø. Vennesland, Critical chloride content in reinforced concrete — A review, *Cem Concr Res* 39 (2009) 1122–1138.
- [2] EN 12390-11, Testing hardened concrete - Part 11: Determination of the chloride resistance of concrete, unidirectional diffusion, European Committee for Standardization, Brussels, 2015.
- [3] C. Labbez, A. Nonat, I. Pochard, B. Jönsson, Experimental and theoretical evidence of overcharging of calcium silicate hydrate, *Journal of Colloid and Interface Science* 309 (2007) 303–307.

- [4] K. De Weerd, S.G. Ytterdal, M.R. Geiker, On the impact of phase changes on chloride profiles in concrete, in: The Nordic Concrete Federation (Ed.), Proceedings of the XXII Nordic Concrete Research Symposia, Norsk Betongforening, 2014, pp. 369–372.
- [5] K. De Weerd, D. Orsáková, A.C.A. Muller, C.K. Larsen, B. Pedersen, M.R. Geiker, Towards the understanding of chloride profiles in marine exposed concrete, impact of leaching and moisture content, *Constr Build Mater* 120 (2016) 418–431.
- [6] P. Hemstad, A. Machner, K. De Weerd, The effect of artificial leaching with HCl on chloride binding in ordinary Portland cement paste, *Cem Concr Res* 130 (2020) 105976.
- [7] G. Bolte, M. Zajac, J. Skocek, M. Ben Haha, Development of composite cements characterized by low environmental footprint, *Journal of Cleaner Production* 226 (2019) 503–514.
- [8] EN 12390-2, Testing hardened concrete - Part 2: Making and curing specimens for strength tests, European Committee for Standardization, Brussels, 2001.
- [9] K. De Weerd, D. Orsáková, M.R. Geiker, The impact of sulphate and magnesium on chloride binding in Portland cement paste, *Cem Concr Res* 65 (2014) 30–40.
- [10] A. Machner, M. Zajac, M. Ben Haha, K.O. Kjellsen, M.R. Geiker, K. De Weerd, Chloride-binding capacity of hydrotalcite in cement pastes containing dolomite and metakaolin, *Cem Concr Res* 107C (2018) 163–181.
- [11] K. De Weerd, A. Colombo, L. Coppola, H. Justnes, M.R. Geiker, Impact of the associated cation on chloride binding of Portland cement paste, *Cem Concr Res* 68 (2015) 196–202.
- [12] Z. Shi, M.R. Geiker, K. De Weerd, T.A. Østnor, B. Lothenbach, F. Winnefeld, J. Skibsted, Role of calcium on chloride binding in hydrated Portland cement–metakaolin–limestone blends, *Cem Concr Res* 95 (2017) 205–216.
- [13] M.D.A. Thomas, R.D. Hooton, A. Scott, H. Zibara, The effect of supplementary cementitious materials on chloride binding in hardened cement paste, *Cem Concr Res* 42 (2012) 1–7.
- [14] International Federation for Structural concrete (fib), Model Code for Service Life Design: Model code prepared by Task group 5.6, fib, Lausanne, 2006.
- [15] NT BUILD 492, Concrete, mortar and cement-based repair materials. Materials: Chloride migration coefficient from non-steady state migration experiments, 1999.
- [16] EN 14629, Products and systems for the protection and repair of concrete structures. Test methods. Determination of chloride content in hardened concrete, European Committee for Standardization, Brussels, 2007.

26

Bojan Milovanović, Mergim Gaši Sanjin Gumbarević and Marina Bagarić

Education for zero energy buildings using building information modelling



EDUCATION FOR ZERO ENERGY BUILDINGS USING BUILDING INFORMATION MODELLING

Bojan Milovanović¹, Mergim Gašić² Sanjin Gumbarević³ and Marina Bagarić⁴

^{1,2,3,4} University of Zagreb, Faculty of Civil Engineering, Department of Materials

Fra Andrije Kačića Miošića 26, 10000 Zagreb, Croatia

e-mail: bmilovanovic@grad.unizg.hr, mgasic@grad.unizg.hr, sgumbarevic@grad.unizg.hr, mbagaric@grad.unizg.hr

SUMMARY: The construction industry across Europe is facing major challenges in achieving energy efficiency targets, in particular for Near Zero Energy Building (NZEB), but they are also experiencing a digital revolution, with Building Information Modelling (BIM). The Fit-to-NZEB, Net-UBIEP (Horizon 2020) and BIMzeED (Erasmus+) projects intend to improve the human-capital basis of the construction sector, which is identified as a strategic initiative by the European Commission, acting on Higher Education Institutions (HEIs) and Vocational Education and Training (VET) systems in Europe. These projects support the construction industry, through education and training to upskill on technical innovation and digitalization. Not only is digitalisation trainings an important focus for the progression of the construction sector, but providing a low carbon efficient economy requires the integration of BIM with nZEB design and development approaches. At EU level, the challenge remains to introduce relevant standardised environmental and energy efficient learning topics into mainstream training and degree courses at HEIs & VETs. This paper analyses the current situation in the Architecture, Engineering and Construction (AEC) industry in several EU countries and provides a possible solution for the abovementioned problems in the field of NZEBs and BIM. The analysis of current formal and informal educational programs in the AEC industry revealed that topics related to the deep energy renovation (DER) and NZEBs are not adequately covered, or not covered at all, resulting with a lack of qualified workers and professionals. Another major problem detected in the conventional project delivering is an absence of integrated or interdisciplinary approach between all the stakeholders. This paper will show how the competences of construction stakeholders in the field of NZEBs and BIM can be increased.

KEY WORDS: Competences; NZEB; Net-UBIEP; Fit-to-NZEB; BIMzeED; BIM.

1 INTRODUCTION

The construction industry presents a major opportunity to not only reduce energy demand, but also to improve process efficiency and reduce carbon emissions; but it is also traditionally highly fragmented and often portrayed as involving a culture of “adversarial relationships”, “risk avoidance”, exacerbated by a “linear workflow”, which often leads to low efficiency, delays and construction waste [1]. Original culture and practices of the construction sector is widely perceived as a “low-tech” area with a significant proportion of “blue collar” workers but the construction industry is experiencing its digital revolution, with an intensification of digital support in all stages of building design and construction. The process of designing, re-purposing, constructing and operating a building or facility involves not only the traditional disciplines, but also many new professions in areas such as energy and environment; also there is an increasing alignment of interest between those who design and construct a facility and those who subsequently occupy and manage it, and that demands dedicated skills and competencies to address multi-objective sustainability (including energy) requirements. In this context, it is evident that building information modelling (BIM) integrated with energy performance requirements (NZEB) will facilitate the improvement of energy performance in a more effective and efficient manner. Computer generated BIM models are increasingly needed to simulate the planning, design, construction and operational phases of a NZEB project in order to reduce so called energy performance gap and to improve the quality of NZEBs.

This paper analyses the current situation in the Architecture, Engineering and Construction (AEC) industry in several EU countries as identified during the authors’ work within the consortia of the following three EU projects Fit-to-NZEB, Net-UBIEP (Horizon 2020) and BIMzeED (Erasmus+). These projects have a common denominator and that is to improve the human-capital basis of the construction sector, which is identified as a strategic initiative by the European Commission, acting on Higher Education Institutions (HEIs) and Vocational Education and Training (VET) systems in

Europe. The main aim of the paper is to establish outcomes of skill shortages in NZEB and BIM.

1.1 Nearly zero energy buildings

According to the International Energy Agency (IEA), the buildings and buildings construction sectors combined are responsible for over one-third of global final energy consumption and nearly 40% of total direct and indirect CO₂ emissions. Energy demand from buildings and buildings construction continues to rise, and to get on track with the Sustainable Development Scenario, IEA suggests that annual drops in energy intensity per square meter globally need to return quickly to at least 2.5% – the rates of the early 2000s [2]. This has resulted in a growing urgency to address energy and emissions from buildings and construction, to meet restrictive 2030 targets as specified by the European Union (EU). The EU Energy Roadmap 2050 [3] has rigorous demands and ambitious targets for the building sector. Buildings are deemed as a source of enormous untapped efficiency potential and obligatory construction of nearly zero energy buildings (NZEBs) and deep energy renovation (DER) of existing buildings is a definite direction to exploit this potential.

European Energy Performance of Buildings Directive (EPBD, 2010/31/EC) (EPBD II) [4] sets out the definition for a building with nearly zero energy consumption (NZEB) at the European level. NZEB is defined by the EPBD II as “a building that has a very high energy performance” where “the nearly zero or very low amount of energy required should be covered to a very significant extent by energy from renewable sources, including energy from renewable sources produced on-site or nearby” [4]. Article 9(1) of the EPBD II [4] requires Member States to “ensure that by 31 December 2020, all new buildings are nearly zero-energy buildings; and after 31 December 2018, new buildings occupied and owned by public authorities are nearly zero-energy buildings.”

However, if we are to achieve 2030 and 2050 targets, an increase in competences (knowledge, skills, responsibility and autonomy) from across the sector, AEC professionals, policy makers, citizens, is paramount. Additionally, it has become clear that better management of the information during the whole life cycle of the NZEB is absolutely necessary in order to avoid mistakes and have trustful information at any time / when an intervention is necessary. Furthermore, according to Yang et al. [5], an advanced NZEB design requires effective and efficient sharing of information among members from different disciplines in an Integrated Design Group (IDG) in order to make wise decisions about selecting the right set of energy retrofit design options. This could be achieved by introducing Integrated Product Design (IPD) into the NZEB design process [6]. This can be achieved by using BIM approach.

1.2 Building information modelling

Digitalisation of the AEC industry is a reality, the next revolution, is with Building Information Modelling (BIM) in the centre of it. BIM is improving methods of design, delivery and management of building assets, as it increases efficiency in how construction industry collaborates, communicates and interacts. BIM can act hand in hand with energy skills, it can provide a great opportunity to reduce the environmental impact of construction projects [7]. The acronym stands for both the building information modelling (the process) and building information model (the artefact), and the attention of the research community and software developers, alternates between the two. Initially, the challenge was the representation of buildings. As the representation matured, the attention shifted towards the processes in which these representations can be created, developed and used [8]. BIM is the pillar of the new way of working in the building sector (with all the information at hand), initiated and targeted by digitisation to optimise and manage the energy consumption of an NZEB. The BIM model of a building, when properly enriched with the correct data, and using appropriate BIM tools (software) can be used to simulate and test optimum design options; and to help deliver a more efficient building while at the same time having costs and time under control, and also reducing waste, CO₂ emissions and energy spent during construction. In use, BIM as built model with the same and even enriched data, can continue to be used to properly manage building assets.

The EU Energy Roadmap 2050 points out that an increasingly important feature of the required technology shifts with 2050 goals in sight is the use of information and communication technologies (ICT) in energy and transport and for smart urban applications [3]. BIM is the most effective supportive ICT technology for: sustainable energy, reducing carbon footprint and increasing the energy efficiency in construction sector.

2 CURRENT CONSTRUCTION MARKET IN EU WITH RESPECT TO NZEB AND BIM

The EU's building sector is responsible for 9% of the EU GDP [9] and providing 18 million direct jobs. It has to be said that out of these, specialised construction activities that include renovation work and energy retrofits account for two thirds of the overall employment in the sector. These activities are dominantly provided by SMEs.

An interesting perspective of the European NZEB construction market is the architects' one. The Architects' Council of Europe undertakes a biennial survey, the so-called ACE Sector Study [10], which collects and analyses statistical, sociological and economic data on the European Architects, the architectural market and the architectural practices and is based on responses from 30,000 Architects in 30 European countries. Surprisingly responses to this survey suggest that less work is being designed to NZEB standard than in previous years. In the previous surveys, 12 - 14% of respondents said that at least 50% of the total number of projects they had worked on in the previous 12 months were being designed as NZEBs; the 2018 figure is 11%. More work in Luxembourg and Austria than anywhere else is being designed to NZEB standards (Figure 1).

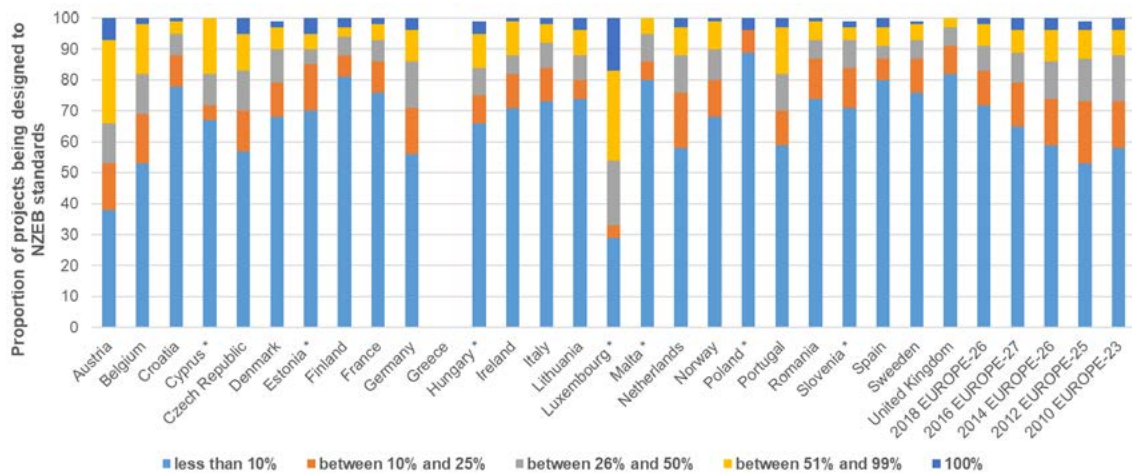


Figure 1: Proportion of projects architects are designing to nearly zero energy standards analysed by country

SMEs usually have a limited ability to follow the massive flow of information and knowledge now available and needed to design and construct NZEBs. Since the energy refurbishment works were mostly subsidised by the public funds there were a lot of interested investors and thus many companies enrolled in the field of energy efficiency who have a lot of self-confidence but realistically don't possess sufficient competences who are now also starting to deal with NZEBs. The lack of qualified workers is more than evident due to migration of workers to western European countries as well as booming publicly and privately funded energy renovation projects and the lack of students enrolled into professional high schools (VETs) related to energy efficiency. One of the most significant problems of the construction market in most EU countries (all participants in construction projects) is the lack of competencies since educational system is not currently producing experts who could enter the construction market and have sufficient competences with respect to NZEB and BIM [11]. This claim is backed by the fact that the BUILD UP Skills initiative continued via the construction skills strand of the European Horizon 2020 research and innovation programme (H2020 EE4 Construction Skills). Aiming to support and further develop multi-country qualification and training schemes, and by the fact that the 2016 H2020 call approved five projects which started in 2017 out of which three projects are focussed on Building Information Modeling (BIM). [12].

The existing skills' shortages in both main contractors and specialist sub-contractors are also a significant factor driving increased costs. In some EU countries, there are a number of emerging occupations developed from the evolution of sustainable needs and the enforcement of energy efficient building regulation. In Ireland, the newest emerging occupations are within the NZEB areas, where a number of courses to train consultants and tradespeople in NZEB construction are underway. These include *NZEB professional consultant*, *NZEB professional design consultant*, *NZEB craftworkers and operatives*, *NZEB for craftworkers*, *NZEB for construction workers*, *Environmental Certificate for Professionals*.

From the existing experience of the authors of this paper that both construction of NZEBs and DER proved to be a complex process for construction industry in general. It demands a change of business as usual procedures of everybody

involved, including architects, civil and mechanical engineers, site managers as well as construction workers (craftsmen).

Looking at the construction sector, experience has shown that a number of challenges still exist and endanger the policy goals of the EC. The construction industry needs to be able to deliver DER as well as newly build NZEBs using innovative technologies which are key in addressing new approaches for energy efficient buildings [13]. On the other hand, there is a lack of qualified and skilled workforce, which would deliver high quality NZEBs in which occupants would have healthy living conditions [13], without any construction faults occurring in use, and delivering designed energy consumption. Improving the competences of middle- and senior-level building professionals, including various trade professionals (construction workers), in sustainable energy efficient construction is therefore of key importance. It is envisioned that increasing the knowledge and skills of craftsmen about new technologies, cross-crafting good practices as well as worst practices will result with a higher level of energy performance in buildings, as well as avoiding inadequacies caused by poor practices [14]. Additionally, objectives and consequently up-skilling is regarded as an upstream measure, as outlined by a respective recent European study [15]

Digitalisation of the construction sector is increasingly recognised as a potential game changer for the sector, which could contribute significantly to sustainable development and the EU 2020 Strategy [16]. For instance, it is estimated that full-scale digitalisation in non-residential construction would lead to annual global cost savings of EUR 0.6 trillion to EUR 1.0 trillion (13% to 21%) in the engineering and construction phases and EUR 0.3 trillion to EUR 0.4 trillion (10% to 17%) in the operations phase [17]. The European Commission (EC) has thus supported, promoted and developed several policies and initiatives aiming to foster the digitalisation in the construction sector. These include inter alia the Strategy for the sustainable competitiveness of the construction sector and its enterprises (2012) [16], the EU BIM Task Group [18] and the upcoming EU Digital Construction platform which is intended to serve the purpose of facing the main challenges related to the uptake of digital tools in support of the digital evolution of the sector. In 2014, the EU commission issued directive 2014/24/EU [19], which recommends member states use building information electronic modelling tools in public construction projects. This clearly suggests a trend towards a unique construction market in the EU enhanced by BIM-based methodologies. As a result, the construction industry in EU Member States, has gradually adopted digital innovations, with BIM being a frontrunner [20]. However, there are significant differences in BIM acceptance levels across the EU, clearly demonstrated by the fact that BIM has been mandatory in some EU countries (such as UK, France, Denmark, Austria, Spain, Norway, Finland) for almost a decade whereas the legislative framework for BIM is still a matter of discussions and pilot projects in other nations [21]. The works of various BIM organizations and initiatives, standardizations, and expert groups aiming to carry out the EU directive indicate that BIM is becoming an important national issue in the EU. According to International BIM Report 2016 [22], the usage of BIM is increasing and within five years it is expected that its usage in design professions in most world countries will be over 80% [22]. In 2016, the usage of BIM in different countries was: UK 50% (74% in 2018 [23]), Canada 71%, Denmark 81%, Czech Republic 30% and Japan 49%. It was expected in [22] that by 2021 that the usage will be as follows: UK 95%; Canada 71%; Denmark 93%; Czech Republic 90% and Japan 88%. In BIM frontrunner countries BIM standard has been introduced, while in other ones BIM is yet to be defined as a standard regardless of its implementation level. There are several reasons for these variations of BIM maturity across regions. Some researchers suggest that these differences are associated and influenced by the institutional forces and national policies and mandates in different countries. However, it is important to acknowledge that differences are influenced by the socio-technical factors and the cultural and social contexts in each region as well as team experiences. Differences can also be impacted by the type of project, its scale, income, the level of complexity and the requirements of clients [24]. However, it is possible to conclude that BIM will inevitably be used in the future of all construction sectors (e.g. education, practice, legislation, public procurement process, contracting, etc.) [21].

However, there are still challenges in achieving a fully integrated collaborative multidisciplinary mode of operation. A change in working processes and an integration of BIM with individual business processes is needed [25] to achieve greater collaboration and communication across disciplines [26]. Fostering collaboration in BIMbased construction networks is a top priority for construction project managers [27]. The current adoption of BIM in the construction industry does not exploit the technology's functions to its full potential [28]. The slow pace of BIM adoption can be ascribed to the lack of clarity on how BIM can be integrated with the current business practice [26]. The ACE Sector Study [10] has determined that only a small minority, 14%, of practices are not aware of BIM, while around 2/3 of practices are aware of BIM but do not use it.

It can be concluded from [20] that government policies and initiatives aiming to foster BIM implementation should be comprehensive, including public procurement, education and development, and standardisation. By doing so,

governments are combining a top down and bottom-up approach: on the one hand they adopted public procurement amendments/regulations requiring BIM for public infrastructure projects. On the other hand, they provided downstream investments to foster research and development around BIM, which come to support companies' efforts to implement it. This way, governments managed to ensure a balance between additional requirements and incentives for the industry [20].

3 ESTABLISHED OUTCOMES OF SKILL SHORTAGES IN NZEB AND BIM

In most European countries, gaps exist in official educational programmes for professional education of EQF 3-7 levels in the field of NZEB, resulting in skill shortages of construction professionals constructing NZEBs. The mismatch is being created between learning outcomes and competences gained by students in educational institutions (both HEI and VET) and competences needed by the construction sector in the field of NZEB. This means that in many EU countries educational institutions often provide obsolete training related to BIM.

Due to the fact that there is a significant variety of approaches to NZEB definition in the different EU countries, it can be concluded that such widely different approaches will likely have a significant effect in determining the focus placed in different countries and even regions on specific topics relating to NZEB.

When employers are looking to hire additional construction staff they are mostly interested in the practical skills of the interviewee and less interested in their qualifications. Employers see little value in pure theoretical training and often practical training is a requirement, but this practical training should be as short as possible and as cheap as possible in order to drive significant numbers of workers to education. This produces a mismatch in the requirements for the increase of construction quality by the investors and the interest of design and construction company who often do not value upskilling and competences required to build NZEBs. Professionals concerned with advancing their skills seek for flexible, company specific, training which should preferably be practical on-site training.

There are no examples of a nationally coordinated approach to training construction workers, designers and other stakeholders concerning NZEBs or DER. Several training providers in different countries offer courses on energy efficiency, but few and scarce training is available on NZEB.

Regarding skills shortages, there is very little reference to airtightness training which could in turn have profound implications on achieving the construction quality and functioning of NZEBs due to the fact that airtightness is one of the benchmark quality indicators of a deep retrofit project and yet legislation in most EU countries does not require a high standard in this regard.

Moreover, the shortage of competences in the area of internal insulation is significant and since there is a great risk of creating mould in NZEB and DER projects if insulation application is not carried out in accordance with building science recommendations – the probability of occurrence of construction damage is high.

Since the definition of competences except knowledge and skills comprises also responsibility, it seems that a module on 'understanding the consequences of poor workmanship' should be a crucial element in any NZEB or DER training. It seems that there is a gap in competences of significant number of stakeholders working in the field of NZEB on their responsibility, i.e. what consequences could result from their actions.

Whilst many of the energy efficiency training programmes intended to architects (designers, supervisors) and civil engineers (designers, construction managers, supervisors) focus on improving the performance of the building envelope, there is often little mention of mechanical systems such as domestic hot water generation, storage and circulation as well as heat recovery ventilation (MVHR). Off-course these stakeholders do not have to become experts in the mentioned topics but have to have basic competences in the field. This can also be identified as skill shortage and a gap in the competences of stakeholders in many EU countries. Furthermore, the overlap between different trades (cross-crafting) is rarely covered in NZEB and/or DER training programmes.

Crucially, the gap and shortage of competences of many designers, construction managers and workers are connected to the comfort of the inhabitants and building users. The focus of trainings should extend from 'just' energy efficiency to include comfort, indoor air quality and risk of mould and condensation.

Lack of knowledge, trust, and communication between various stakeholders of the lifecycle stages of a building have also been identified as a barrier for full NZEB implementation or as one of the reasons for the underperformance of NZEBs and sustainable buildings. The optimisation of building’s energy use requires an integrated design approach and cross-disciplinary teamwork, which then leads to the high quality of indoor environments and satisfying the occupants’ needs. It is evident from this that introducing BIM would be beneficiary to NZEB design, construction and facility management process, since BIM is actually a process for creating and managing all of the information about a project, leading to an output known as a Building Information Model, which contains digital descriptions for every aspect of the physical project. Another advantage of BIM is that it supports an integrated design process, but some gaps were identified in the competencies of various stakeholders.

The gap in BIM is that integrated design courses (especially those which include specific skills to cope with NZEB challenges in cross-disciplinary teams) are scarce throughout EU educational institutions, and there are a lot of experts having little or no knowledge on integrated design. Construction companies need a single integrated platform to optimize performance across the complete lifecycle of their assets. One platform that comprises all elements from design, procurement, and implementation, through to the commissioning, operation, and maintenance of smart services. In many EU countries, and among many stakeholders there is still a large knowledge gap around BIM processes and data and its importance to the future of the construction industry. It has to be said that BIM also poses a challenge, because making it work requires a considerable upfront effort not just to adopt the technology but also to acquire relevant know-how, set standards, find the right strategic positioning, and align stakeholders.

Collaboration between designer and operator at handover is limited to the seasonal commissioning and exchange of basic information, building on documentation created without the needs of the end-user fully considered. Widespread application of BIM for purposes outside design development is unlikely to happen without corresponding and reliable standards for information management, in the areas to which it’s applied. Addressing the barriers identified here would simplify this process and enable more effective utilisation of design and operational data in ongoing performance management.

It is evident that in the case of many early adopting countries the following happened, BIM implementation succeeded at the design, engineering and construction phases, while its use is limited when it comes to the operation and maintenance phases. Reinforcing the capacities of public and private sector actors and their understanding of BIM is of crucial importance, but it has to be said that BIM education is not only a technical issue. It is not only about training workers to use BIM software, but also changing the working methods and process in a company. BIM education is hence about management change, stakeholder’s awareness and their real need has to be tackled.

A research was performed within the project BIMzeED which quantified existing competences in NZEB and BIM by surveying stakeholders. In the surveys that were distributed to educators and construction stakeholders, respondents needed to assess their knowledge and skills and also knowledge provided by existing education programs according to the scale provided in Figure 2. The educators that completed the surveys are mainly HEI professors and VET teachers who have some experience teaching energy efficiency and BIM related topics, the survey was conducted on 60 educators. In total, there were 237 respondents from construction industry where 63.7% of respondents have more than 5 years of work experience. The 47 responders in the educational provision were not administration staff but the teachers from existing HEIs and VETs in the partner countries, and this was important in order to receive better quality data.

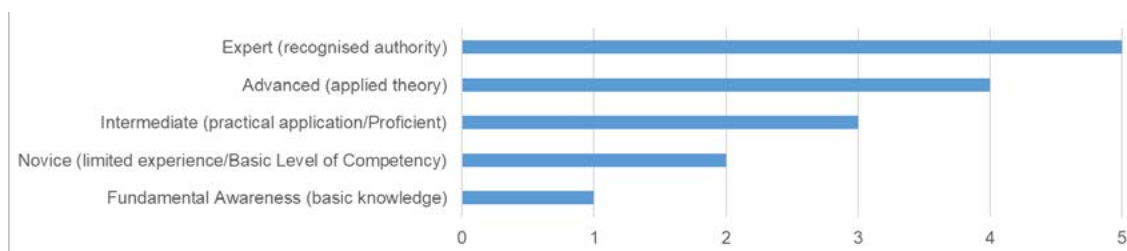


Figure 2 The scale of grading competences

Table 1: Overall score in the fields of NZEB and BIM

Questionnaire	NZEB			BIM		
	Average	Min	Max	Average	Min	Max
Education provision	2.65	2.11	3.17	3.12	2.33	3.94
Educators	2.53	1.79	3.39	2.29	1.94	2.87
Construction stakeholders	2.57	2.06	3.26	1.84	1.60	2.25

Even though the difference is not significant, in the NZEB field, education provision is offering more knowledge and skills than educators and construction industry stakeholders actually declare they possess (Table 1). As it can be seen from the scale above, this score is just little higher than basic level of competence with limited experience. It is deemed that for general improvement the competence level needs to be at least 3.5 on average. That would mean that we need to raise all competence in education provision up to the “Intermediate” or “Advanced” level. In the field of BIM, the difference between competences offered by education programs and competences of educators and construction industry stakeholders, is significant. (Table 1) The education programs offer competences which are a level higher than competences possessed by educators and construction stakeholders which is in turn just little higher than basic level of competence with limited experience. It was established that BIM competence level threshold should be at least 3.5 on average. BIM education almost meets that threshold, but educators and construction industry stakeholders need to raise up to the “Intermediate” or “Advance” level.

Table 2 shows that currently among the NZEB educators there is the largest gap in NZEB competences connected to Use and maintaining, and tendering and contracting. When we come to all participants there is the largest gap in pre-design group of NZEB competences. Table 2 shows that currently among the BIM educators, the biggest gap is in the BIM competence group “Initiation – Integration and communication” and the smallest is in the BIM competence group “Monitoring and controlling”. Looking at all participants in all groups the gap is significant but again the biggest and the smallest is in the same BIM competence groups as for BIM educators.

Table 2: Current gap in the fields of NZEB and BIM

	Groups of competences	Education provision	Educators	Educators training gap	All participants	Training gap
NZEB group of competences	General NZEB	2,89	3,05	0,16	2,96	0,07
	Pre-design	2,77	2,64	-0,13	2,45	-0,32
	Design	2,61	2,50	-0,11	2,40	-0,21
	Tendering/contracting	2,46	2,13	-0,33	2,39	-0,07
	Realization and Commissioning	2,45	2,23	-0,22	2,47	0,02
	Use and maintaining	2,38	1,95	-0,43	2,38	0,00
BIM group of competences	Introduction to BIM	3,53	2,66	-0,88	2,13	-1,40
	Project start-up	3,38	2,45	-0,93	1,95	-1,43
	Tendering	3,11	2,33	-0,79	1,83	-1,28
	Initiation (Integration and Communication)	3,51	2,27	-1,25	1,94	-1,58
	Planning (Integration)	3,17	2,21	-0,96	1,80	-1,38
	Planning (Scope, Time, Cost, Quality, Risks)	2,85	2,11	-0,74	1,74	-1,11
	Monitoring and Controlling	2,48	2,13	-0,35	1,66	-0,83
	Execution/Operation	2,85	2,11	-0,73	1,65	-1,20

The reader can use this data to get an idea of the real situation in the BIMzeED project countries and to create a remediation measures and targeted training activities as was done in the BIMzeED project in the partner countries.

4 CONCLUSIONS

BIM has a number of socio-technological advantages not only at the technological level, but also the process level, and can complement the way that architectural design artefacts are created, but also can profoundly change the collaborative process associated with the act of building. It is also clear that the design process regarding NZEB needs to be a collaborative effort between all stakeholders. There is a substantial need for professionals, such as architects and

engineers as well as other stakeholders, to be specifically educated in an integrated design approach and trained to work in cross-disciplinary teams using BIM approach. Moreover, it is essential that educational institutions bring up professionals with such competences. New technologies require talent with substantially different skills from those the AEC workforce possesses today. BIM requires experts with skills in artificial intelligence, data analysis and programming. New job profiles and sought-after skills could help to bring more women and young people (new talents) into the industry and to close the talent gap. In some countries (i.e. Ireland) new occupations are emerging within the NZEB areas. This paper analyses the current situation in the AEC industry in several EU countries and several EU projects and provides a possible solution for the training problems in the field of NZEBs and BIM. The analysis of current formal and informal educational programs in the AEC industry revealed that topics related to the DER and NZEBs are not adequately covered, or not covered at all, resulting with a lack of qualified workers and professionals. This paper shows which groups of competences of construction stakeholders in the field of NZEBs and BIM should be increased as a solution to the identified gaps.

BIMzeED training programmes are going to be designed with intention to strike a balance between theory and practice. In short, all players need to know not only the 'how' but also the 'why' and the 'what if'. Whilst the incorporation of practical training is important, it must not be introduced to the detriment of a poor theoretical basis. Studying on the examples full scale demo models and practical models, real equipment and practical walls, where trainees can implement a practical solution, or visits of construction sites with NZEBs under construction, is the most valuable. BIMzeED structured the training material and content using common learning units (LUs) with flexible standardised delivery (in class, on-line and on-site) suitable for HEI and VET training. The initial training content will include nZEB related subjects with BIM maturity. The training content will be developed and delivered in a Blended Learning format supported by a E-Learning portal, and once finalised the LUs will be made available as Toolkits to potential students, HEIs, VETs and SMEs.

ACKNOWLEDGMENTS

The Authors would like to acknowledge the Horizon 2020 projects Net-UBIEP and Fit-to-NZEB, and the Erasmus+ project BIMzeED. One of the authors (Sanjin Gumbarević) would like to acknowledge the Croatian Science Foundation and the European Social Fund for the support under the project ESF DOK-01-2018.

REFERENCES

- [1] Cardiff University: *BIMEET D2.1-BIM for energy efficiency requirements capture*
- [2] International Energy Agency: Tracking buildings. IEA. Available at: <https://www.iea.org/reports/tracking-buildings> [Date accessed: February 8, 2020]
- [3] European Commission: *Energy roadmap 2050*
- [4] European Parliament and the Council of the European Union: *Directive 2010/31/EU of the European Parliament and of the Council of 19 May 2010 on the energy performance of buildings (recast)*. European Parliament
- [5] Yang, X.; Ergan, S.; Knox, K.: Requirements of Integrated Design Teams While Evaluating Advanced Energy Retrofit Design Options in Immersive Virtual Environments. *Buildings* 5(4):1302–20, (2015). Doi: 10.3390/buildings5041302
- [6] Cromwijk, J.; Mateo-Cecilia, C.; Jareño-Escudero, C.; Schröpfer, V.; Op't Veld, P.: An Introduction to a Novel and Rapid nZEB Skill-Mapping and Qualification Framework Methodology. *Buildings* 7(4):107, (2017). Doi: 10.3390/buildings7040107
- [7] BIMcert Team: BIMcert: Answers to the European audience. BUILD UP The European Portal for Energy Efficiency in Buildings. Available at: <https://www.buildup.eu/en/news/bimcert-answers-european-audience> [Date accessed: February 8, 2020]
- [8] Turk, Ž.: Ten questions concerning building information modelling. *Build Environ* 107:274–84, (2016). Doi: 10.1016/J.BUILDENV.2016.08.001
- [9] European Commission; Internal Market Industry Entrepreneurship and SMEs Directorate General; Energy Directorate General; Joint Research Centre (JRC): *The European construction sector - A global partner:16*, (2016)
- [10] The Architects' Council of Europe: *The architectural profession in Europe 2018 - a sectoral study*
- [11] European Commission: *CORDIS results pack on construction skills*. Brussels, Belgium
- [12] Trinomics: *Final report on the assessment of the BUILD UP Skills Pillar II*
- [13] Lindkvist, C.; Karlsson, A.; Sørnes, K.; Wyckmans, A.: Barriers and Challenges in nZEB Projects in Sweden and Norway. *Energy Procedia* 58:199–206, (2014). Doi: 10.1016/J.EGYPRO.2014.10.429
- [14] Bean, F.; De Groote, M.; Volt, J.: *Opening the door to smart buildings, Driving the transition with EU directives*

- [15] Concerted Action - Energy Performance of Buildings: *Implementing the EPBD – Featuring Country Reports*. Lisbon
- [16] European Commission: *Strategy for the sustainable competitiveness of the construction sector and its enterprises*. Brussels
- [17] Boston Consulting Group: Digital in Engineering and Construction. Available at: <https://www.bcg.com/industries/engineered-products-infrastructure/digital-engineering-construction.aspx> [Date accessed: April 27, 2019]
- [18] EUBIM: EU BIM Task Group. Available at: <http://www.eubim.eu/> [Date accessed: April 27, 2019]
- [19] European Parliament Council of Europe: *Directive 2014/24/EU of the European Parliament and of the Council of 26 February 2014 on public procurement and repealing Directive 2004/18/EC*
- [20] European Commission: *European Construction Sector Observatory Building Information Modelling in the EU construction sector*
- [21] Galić, M.; Venkrbec, V.; Chmelik, F.; Feine, I.; Pučko, Z.; Klanšek, U.: Survey of accomplishments in BIM implementation in Croatia, the Czech Republic, Germany, and Slovenia. *Number 15*, (2017). Doi: 10.13167/2017.15.3
- [22] Malleon, A.; Kato, H.; Popíšílová, B.; Watson, D.; Friberg, G.: *NBS International BIM Report*
- [23] NBS: *National BIM Report 2018*
- [24] Azzouz, A.; Hill, P.; Papadonikolaki, E.: Which countries have the highest levels of BIM adoption in Europe? | BIM+. Available at: <http://www.bimplus.co.uk/people/which-country-most-bim-mature-europe/> [Date accessed: February 10, 2019]
- [25] Arayici, Y.; Egbu, C.; Coates, P.: Building information modelling (BIM) implementation and remote construction projects: issues, challenges, and critiques. Title Building information modelling (BIM) implementation and remote construction projects: issues, challenges, and critiques. *J Inf Technol Constr* 17:75–92, (2012)
- [26] Gu, N.; London, K.: Understanding and facilitating BIM adoption in the AEC industry. *Autom Constr* 19(8):988–99, (2010). Doi: 10.1016/J.AUTCON.2010.09.002
- [27] Oraee, M.; Hosseini, M.R.; Papadonikolaki, E.; Palliyaguru, R.; Arashpour, M.: Collaboration in BIM-based construction networks: A bibliometric-qualitative literature review. *Int J Proj Manag* 35(7):1288–301, (2017). Doi: 10.1016/j.ijproman.2017.07.001
- [28] Eastman, C.M.; Teicholz, P.; Sacks, R.; Liston, K.: *BIM handbook: a guide to building information modeling for owners, managers, designers, engineers and contractors*. Second edition. Hoboken: John Wiley & Sons.

27

Tiana Milovic, Mirjana Malesev, Miroslava Radeka and Vlastimir Radonjanin

Thermal compatibility of repair mortars based on fly ash as SCM according to en 13687-1

THERMAL COMPATIBILITY OF REPAIR MORTARS BASED ON FLY ASH AS SCM ACCORDING TO EN 13687-1

Tiana Milovic¹, Mirjana Malesev², Miroslava Radeka³ and Vlastimir Radonjanin⁴

^{1,2,3,4} University of Novi Sad, Faculty of Technical Sciences, Department of Civil Engineering and Geodesy
Dr. Sime Milosevica 12, 21000 Novi Sad, Serbia

e-mail: tiana.milovic@uns.ac.rs¹, miram@uns.ac.rs², mirka@uns.ac.rs³, radonv@uns.ac.rs⁴

SUMMARY: This paper presents the results of the experimental study on thermal compatibility of repair mortars based on fly ash as supplementary cementitious material (SCM) applied to the concrete substrate, determined according to EN 13687-1. Chemical composition of fly ash from a Serbian coal power plant was determined by XRF analysis. Repair mortar specimens were prepared with two “water-to-binder” ratios (0.4 and 0.5), Portland cement with 0%, 10% and 20% of fly ash as SCM and CEN standard sand. At the age of 28 days, the specially prepared specimens were exposed to 50 freeze-thaw cycles. The effect of fly ash on repair mortar tensile bond strengths after freeze-thaw cycling with exposure of specimen test surface to saturated de-icing salt solution was investigated. Afterwards, the tensile bond strengths of repair mortars were determined by pull-off test. Based on the obtained results it is concluded that all mortars met the requirement for class R4 according to EN 1504-3.

KEY WORDS: Fly ash, repair mortar, freeze-thaw cycling, de-icing salt, bond strength, XRF analysis.

1 INTRODUCTION

Despite the fact that concrete is the most widely used construction material and a fundamental component of modern infrastructure, the durability of concrete structures has become a major issue, especially in an aggressive environment [1]. For the repair and rehabilitation of concrete structures, the sustainable development of concrete industry proposes the application of repair materials which together with concrete substrates form composite concrete repair systems. The durability aspects of those repair systems should be ensured through complex measures including appropriate material selection and quality control. Standard EN 1504-9 [2] covers general principles and methods for the use of products and systems for the protection and repair of concrete structures.

In accordance with standard EN 1504-9 [2], testing of thermal compatibility of the composite material containing potential repair mortar and concrete substrate, should be done following the instructions given in standard EN 1504-3 [3]. The method described in this standard is based on freeze-thaw cycling with de-icing salt solution applied on the top surface (test surface) during freezing. The requirements for structural (classes R4 and R3) and non-structural (classes R2 and R1) repair mortars are also given in standard EN 1504-3 [3].

Beside the durability and economic issues due to repair costs, there is also an environmental issue considering that the cement industry is responsible for 5-8 % of the global CO₂ emission [4] because of the production of cement – the main binder material in concrete. One of the possible solutions for reducing the environmental impact of concrete industry represents the application of supplementary cementitious materials (SCM) such as fly ash from coal power plants. In Serbia, there are five coal burning power plants and about 6 million tons of fly ash are produced per year, while about 200 million tons of fly ash are already landfilled [5].

Generally, a very few studies have been performed dealing with the effects of freeze-thaw cycling on bond strength between repair material and concrete substrate, while the thermal compatibility of repair mortars based on fly ash as SCM applied to the concrete substrate, in accordance with EN 13687-1 [6], has not been studied yet. For example, Lee et al. [7] had evaluated reactive powder concrete (contains a type II cement, silica fume, silica sand, quartz powder, steel fiber, a superplasticizer and water) as a new repair material by the change of slant shear strength of repair material and substrate after freeze-thaw cycling up to 1000 cycles, according to the ASTM C666 (1997) [8]. Also, Qian et al. [9] had

determined splitting tensile strength and failure modes of composite specimens (three kinds of substrate concrete were casted and repaired by two types of Ordinary Portland cement mortars and one type of polymer-modified cement mortar) after freeze-thaw cycling up to 150 cycles, in accordance with ASTM C666-03 (2008) procedure A [10].

In order to determine the effect of fly ash as SCM on durability of repair cement mortars an extensive experimental research was realized. This paper deals with thermal compatibility between cement/cement-based mortars containing fly ash, and concrete substrate after 50 freeze-thaw cycles with de-icing salt solution applied on the top surface (test surface) during freezing.

2 MATERIALS AND METHODS

2.1 Mortar and concrete constituents

In order to examine the effect of fly ash as SCM in cement mortars on thermal compatibility between mortar and concrete substrate after 50 freeze-thaw cycles with de-icing salt “immersion” (in accordance with EN 13687-1 [6]), the following component materials were used:

- Ordinary Portland cement CEM I 42.5R (Lafarge-BFC Serbia),
- Fly ash from thermal power plant Nikola Tesla B,
- CEN standard sand in accordance with EN 196-1 [11],
- Natural fractionated aggregate of river origin (fractions: 0-4mm and 4-8mm),
- Superplasticizer (HRWRA) (SikaViscoCrete 3070, Sika Switzerland),
- Superplasticizer (HRWRA) (SikaViscoCrete 4000BP, Sika Switzerland),
- Deionized water for mortars preparation,
- Tap water for concrete preparation,
- Rapid hardening two component epoxy adhesive (Sikadur 31 EF).

The chemical composition of Ordinary Portland cement (CEM I 42.5R) and fly ash were determined by X-ray fluorescence (XRF) spectroscopy. The instrument used for the XRF analysis is an ED-XRF spectrometers, manufacturer Spectro Xepos from Germany. The system uses a Silicon Drift Detector (SDD), band-pass filter and focuses the X-rays from a binary Co/Pd alloy thicktarget anode (50 W/60 kV) combining polarized/direct excitation. Sample tray used for these measurements was with rotating positions for pellets. Measurements were carried out in vacuum atmosphere and Spectro XRF Analyzer Pro software was used. The samples for ED-XRF analysis were prepared in accordance with the pressed powder method. Tested materials (5 g) and binding agent (Cereox wax, Fluxana) were mixed (1 g) and the 32 mm diameter pellets were formed. The pellets were formed under 10 tones load applied via a laboratory hydraulic press. The obtained results are shown in Table 1.

Table 1: Chemical composition of CEM I 42.5R and fly ash

Sample	Chemical composition, (%)								
CEM I 42.5R	Na₂O	MgO	Al₂O₃	SiO₂	P₂O₅	SO₃	Cl	K₂O	2.2
	0.318	2.754	5.103	21.399	0.137	3.470	0.023	0.765	
	CaO	TiO₂	Cr₂O₃	Mn₂O₃	Fe₂O₃	ZnO	SrO	BaO	
	66.665	0.231	0.019	0.091	2.645	0.053	0.101	0.039	
Fly ash	Na₂O	MgO	Al₂O₃	SiO₂	P₂O₅	SO₃	Cl	K₂O	2.3
	0.329	2.941	22.256	45.255	0.084	3.113	0.000	1.130	
	CaO	TiO₂	Cr₂O₃	Mn₂O₃	Fe₂O₃	ZnO	SrO	BaO	
	10.464	1.442	0.080	0.234	10.073	0.116	0.087	0.140	

*Loss on ignition

2.2 Concrete substrate

For the purpose of evaluation the thermal compatibility between potential repair mortar and concrete substrate, at first, the concrete substrates with reproducible surface texture and appropriate strength had to be made and properly cured in

accordance with EN 1766 [12]. In this case, standard EN 1504-3 [3] prescribes the usage of concrete substrate, type MC (0.40). Recommendations for concrete mix composition, type MC (0.40) and required properties for hardened concrete, in accordance with EN 1766 [12], as well as adopted concrete mix proportion are given in Table 2.

Table 2: Recommendations for concrete composition with required properties [12] and adopted concrete mix proportion

Required properties [12]		Adopted concrete mix proportion	
Concrete type	MC(0.40)	Mix proportion, 1 m ³	
Maximum aggregate size, (mm)	8	Aggregate, (kg) Fractions 0-4mm & 4-8mm	1650
Water/cement ratio	0.40	Tap water, (kg)	179
Cement content, (kg/m ³)	455	Cement, (kg)	455
28 day mean compressive strength	to satisfy class C 50/60	Superplasticizer (HRWRA) SikaViscoCrete 4000BP, (g)	4.55
Minimum required surface tensile strength, (MPa)	3.0		

Total of ten concrete substrates (350x350x50mm) and three standard cubes (150x150x150mm) were prepared and cured in moulds under polyethylene sheeting for 24 h after casting, at (20 ± 2)°C. After that, they were demoulded and cured for 27 days underwater at (20 ± 2)°C, in accordance with standard EN 1766 [12].

After 28 days, the cubes were used for determination of concrete compressive strength. The obtained mean value of 67.95 MPa satisfied required class C 50/60 according to EN 206-1 [13].

At the age of 28 days, the bottom face of concrete specimens were, at first, prepared by sand-blasting, and then the specimens were stored under normal laboratory conditions, at (21 ± 2)°C and (60 ± 10)% relative humidity, until the age of 3 months. One concrete substrate was used for the determination of surface tensile strength by pull-off test (Fig. 1) according to EN 1542 [14], immediately before application of mortars on the remaining substrates. The achieved mean value of 5.82 MPa, met the requirement for minimum surface tensile strength of 3.0 MPa.



Figure 1: Determination of surface tensile strength of concrete substrate by pull-off test

Six concrete substrates were used for application of different types of repair mortar (signed with M at the end of specimen's name). The specimens prepared in this way, were exposed to freeze-thaw cycling. Remaining three concrete substrates were used for preparation of etalon specimens (signed with ME at the end of specimen's name) for six types of repair mortars (two types of mortars per concrete substrate).

2.3 Repair mortars

Six different cement/cement-based mortar types were made for the purpose of evaluation the thermal compatibility (freeze-thaw) between them and concrete substrates. In potential repair mortars, Portland cement was substituted with 0%, 10% and 20% of fly ash as SCM, by mass. Mortar mixtures were prepared with two water-to-binder ratios, 0.4 and 0.5 according to EN 12190 [15]. Composition of mortar mixtures, which were placed on concrete substrates, is shown in Table 3. Superplasticizer (HRWRA) SikaViscoCrete 3070 was added in all mortar mixtures with lower water-to-binder

ratio (FA20bM(E) required larger amount of superplasticizer than PCbM(E) and FA10bM(E)). In the case of mortar mixtures with higher water-to-binder ratio, a small amount of superplasticizer was added only in FA20aM(E).

Table 3: Composition of mortar mixtures

Mix proportions						
	PCaM(E)	FA10aM(E)	FA20aM(E)	PCbM(E)	FA10bM(E)	FA20bM(E)
CEM I 42.5 R, (g)	450	405	360	450	405	360
Fly ash, (g)	-	45	90	-	45	90
Standard sand, (g)	1350	1350	1350	1350	1350	1350
Deionized water, (g)	225	225	225	180	180	180
Superplasticizer, (% by mass of binder)	-	-	0.35	0.6	0.6	1.0
w/b ratio	0.5	0.5	0.5	0.4	0.4	0.4

The used signs: PC – Ordinary Portland cement; FA – fly ash; a – w/cm=0.5; b – w/cm=0.4

Mortar mixtures were applied on prepared concrete substrates, in a layer with thickness of 25 mm. These specially prepared specimens (Fig. 2) were cured as it is recommended in EN 13687-1 [6], 24 h in moulds, 6 days underwater and 21 days in the standard laboratory climate.



Figure 2: Placed mortars on concrete substrates: Test specimens for freeze-thaw testing (left) and etalon specimens (right)

2.4 Methods

Thermal compatibility between potential repair mortars and concrete substrate, after 50 freeze-thaw cycles with de-icing salt solution applied on the top surface (test surface) during freezing, in accordance with [3, 6], was estimated by measuring the tensile bond strength according to [14].

After 28 days of recommended curing regime, six test specimens were hydro and thermally insulated at all sides except the testing one, which was covered with tap water for 24 h before starting the freeze-thaw cycling in accordance with [6]. All test specimens were exposed to one freeze-thaw cycle per a day. The cycle consists of two phases:

- 2 h in climate chamber covered with pre-cooled saturated NaCl solution at -15°C (Fig. 3 - left),
- 22 h, at standard laboratory conditions covered with tap water at temperature of (21±2)°C, (Fig. 3 - right).



Figure 3: Test specimens in climate chamber covered with pre-cooled saturated NaCl solution at -15°C (left) and thawing of test specimens at standard laboratory conditions (right)

After every 10 cycles, the test surface of test specimens was visually inspected.

During the first 25 cycles, etalon specimens were cured in the standard laboratory conditions, while during last 25 cycles they were put back into the water. After the end of cycling, both, test and etalon specimens were conditioned at the standard laboratory climate for 7 days, and then the bond strength of repair mortars was determined according to [14].

3 RESULTS AND DISCUSSION

The results of presented experimental investigation were analysed regarding:







- the fulfillment of the requirements for repair mortars in a term of thermal compatibility between examined mortars and concrete substrate after 50 freeze-thaw cycles with de-icing salt solution applied on the top surface during freezing according to [3],
- the effect of fly ash as SCM on bond strength and surface alterations of potential repair mortar, and
- the effect of different water-to-binder ratios on bond strength and surface alterations of potential repair mortars.

3.1 Visual inspection of test surface

After every 10 freeze-thaw cycles, test surface of test specimens was visually inspected. The appearance of these surfaces after the end of cycling, is shown in Table 4.

The delamination of mortar layer from concrete substrate or/and delamination in mortar layer were not noticed. The analyses of obtained results of visual inspection indicated that all mortars met the requirement for repair mortars in a term of thermal compatibility (freeze-thaw) according to [3].

Table 4: Test surface appearance of the test specimens after 50 freeze-thaw cycles






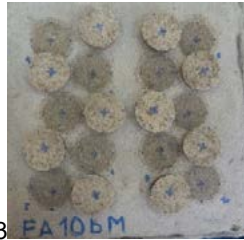


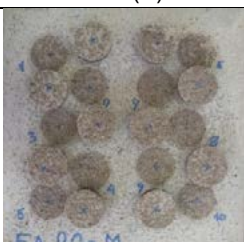
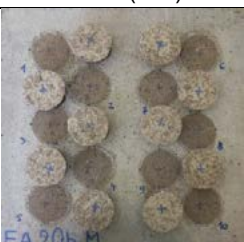


Surface look of the test specimens after 50 freeze-thaw cycles	
Mortars prepared with w/cm=0.5	Mortars prepared with w/cm=0.4
PCaM	PCbM
 <p>Presence of net-like fissures, widthness of fissures <0.05mm located dominantly next to the edge of the specimen, Dotted spalling.</p>	 <p>Moderate spalling, severe spalling just along one edge.</p>
FA10aM	FA10bM
 <p>Light spalling over the entire test surface, light roughness of the one half of test surface and severe roughness of the other half.</p>	 <p>Very severe roughness, light spalling over the entire test surface.</p>
FA20aM	FA20bM
 <p>Light spalling over the entire test surface (light roughness) except in the central part and in two corners where it is more pronounced.</p>	 <p>Dotted spalling.</p>

The results of visual inspection indicated that the test specimens with lower water-to-binder ratio were less damaged, as well as those with 20% of fly ash as SCM, especially specimen FA20bM.

3.1.1 Bond strengths after 50 freeze-thaw cycles according to EN 13687-1

Mean bond strength values (f_{hm}) for dominant type of failure of test and etalon specimens, as well as photos of dollies and specimens after pull-off tests, are shown in Table 5. During the visual inspection, it was noticed that failures had occurred through the mortar layer (type B – cohesion failure in mortar layer), but also between mortar and adhesion layer (type B/Y - adhesion failure between mortar layer and adhesion layer). Therefore, loads at failure type B were accepted as valid, according to [14].

Table 5: Mean bond strength of test and etalon specimens and their photos after pull-off testing

Mean bond strength values of test specimens which were exposed to 50 freeze-thaw cycles		Mean bond strength values of etalon specimens	
PCaM $f_{hm} = 4.3 \text{ MPa (B)}$	PCbM $f_{hm} = 4.6 \text{ MPa (B)}$	PCaME $f_{hm} = 4.8 \text{ MPa (B)}$	PCbME $f_{hm} = 4.8 \text{ MPa (B)}$
			
FA10aM $f_{hm} = 4.8 \text{ MPa (B)}$	FA10bM $f_{hm} = 4.4 \text{ MPa (B/Y)}$	FA10aME $f_{hm} = 4.9 \text{ MPa (B)}$	FA10bME $f_{hm} = 5.6 \text{ MPa (B)}$
			
FA20aM $f_{hm} = 4.4 \text{ MPa (B)}$	FA20bM $f_{hm} = 5.4 \text{ MPa (B/Y)}$	FA20aME $f_{hm} = 4.2 \text{ MPa (B)}$	FA20bME $f_{hm} = 4.4 \text{ MPa (B/Y)}$
			

In the case when failure had occurred between adhesion layer and mortar layer (failure type B/Y), mean bond strength was also calculated, considering that its value is a lower than real tensile bond strength of mortar.

Considering the above, all types of applied mortars had mean bond strength higher than 2.00 MPa (Tab. 5, Fig. 4), and for that reason they fulfilled the requirement for structural repair mortars of class R4 in a term of thermal compatibility - Part 1: Freeze-thaw cycling with de-icing salt immersion [6] as well as requirements for Part 2: Thunder-shower cycling [16] and Part 4: Dry thermal cycling [17], in accordance with standard EN 1504-3 [3].

Change in bond strength of test specimens FA10aM and FA20aM relative to the bond strength of reference PCaM, after 50 freeze-thaw cycles, is shown in Figure 5. Due to the fact that all dominant types of PCaM, FA10aM and FA20aM failures belong to the same type (type B), the results can be directly compared. Specimens FA10aM and FA20aM had for 12% and 2% higher bond strength than reference PCaM, respectively.

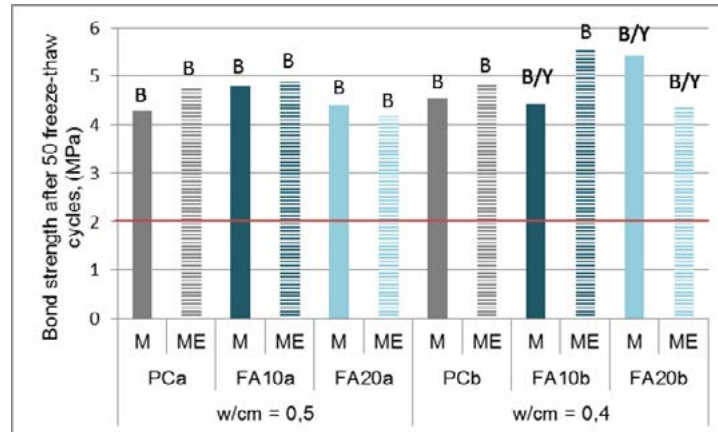


Figure 4: Bond strength of etalon specimens and the test specimens after 50 freeze-thaw cycles

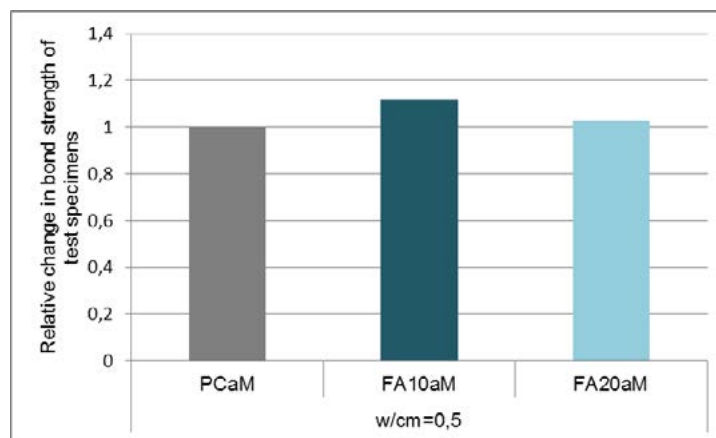


Figure 5: Relative change in bond strength of the test specimens (w/cm=0.5) after 50 freeze-thaw cycles

Considering that specimen PCbM had type B as dominant type of failure, while specimens FA10bM and FA20bM had type B/Y, the results can not be directly compared. But, taking that into account, change in bond strength of test specimens FA10bM and FA20bM relative to the bond strength of PCbM, after 50 freeze-thaw cycles, is shown in Figure 6 (FA10bM and FA20bM columns have red border colour).

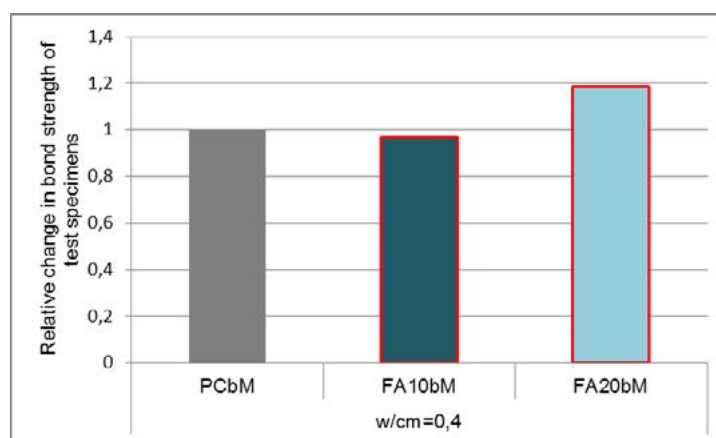


Figure 6: Relative change in bond strength of the test specimens (w/cm=0.4) after 50 freeze-thaw cycles

Even with dominant failures type B/Y, bond strength of specimen FA10bM was lower than reference PCbM just for 4%, while specimen FA20bM had for 17% higher bond strength than reference PCbM.

4 CONCLUSIONS

Based on the performed experimental research and the analysis of obtained results, in a term of thermal compatibility (freeze-thaw) according to EN 1504-3 [3], the following can be concluded:

- The obtained results of visual inspection, during and at the end of cycling, indicated that all mortars met the requirement for repair mortars in a term of thermal compatibility (freeze-thaw) according to [3];
- With mean bond strength values higher than 2.00 MPa, all tested mortars fulfilled the requirement for structural repair mortars of class R4 in a term of thermal compatibility Part 1: Freeze-thaw cycling, as well as for Part 2: Thunder-shower cycling and Part 4: Dry thermal cycling, in accordance with [3];
- Mortars with 20% of fly ash and with $w/cm=0.4$ had the lowest degree of damage and the highest mean bond strength value of all test specimens (mortars), and mortar with 10% of fly ash with $w/cm=0.5$ had the highest mean bond strength value among the mortars prepared with the same water-to-binder ratio.

Therefore, fly ash in an amount up to 20% can be used as SCM in repair mortars, in a term of thermal compatibility between mortar and concrete substrate, in accordance with EN 13687: Part 1 [6] as well as with Parts 2 [16] and 4 [17].

ACKNOWLEDGMENTS

Research in this paper is supported by the Ministry of Education, Science and Technological Development of the Republic of Serbia and realized within the project at Department of Civil Engineering and Geodesy, Faculty of Technical Sciences in Novi Sad: A comprehensive approach to improvement of interdisciplinary researches in construction education and science.

REFERENCES

- [1] Donatello, S. et al.: Durability of very high volume fly ash cement pastes and mortars in aggressive solutions, *Cement & Concrete Composites*, Vol.38, (2013), pp 12-20, ISSN 0958-9465
- [2] BS EN 1504-9:2008. *Products and systems for the protection and repair of concrete structures - Definitions, requirements, quality control and evaluation of conformity, Part 9: General principles for use of products and systems.*
- [3] BS EN 1504-3:2005. *Products and systems for the protection and repair of concrete structures - Definitions, requirements, quality control and evaluation of conformity, Part 3: Structural and non-structural repair.*
- [4] Flatt, R.J. et al.: Concrete: An eco material that needs to be improved, *Journal of the European Ceramic Society*, Vol. 32, (2012), pp. 2787–2798, ISSN 0955-2219
- [5] Nuccetelli, C. et al.: Alkali activated concrete with Serbian fly ash and its radiological impact, *Journal of Environmental Radioactivity*, Vol. 168, (2014), pp. 30-37, ISSN 0265-931X
- [6] BS EN 13687-1:2002. *Products and systems for the protection and repair of concrete structures – Test methods – Determination of thermal compatibility – Part 1: Freeze-thaw cycling with de-icing salt immersion.*
- [7] Lee, M-G. et al: A preliminary study of reactive powder concrete as a new repair material, *Construction and Building Materials*, Vol. 21, (2007), pp. 182–189, ISSN 0950-0618
- [8] ASTM C666 – 97. *Standard Test Method for Resistance of Concrete to Rapid Freezing and Thawing.*
- [9] Qian, Y. et al: Interfacial Tensile Bond between Substrate Concrete and Repairing Mortar under Freeze-Thaw Cycles, *Journal of Advanced Concrete Technology*, Vol. 14, (2016), pp. 421-432, ISSN 1347-3913
- [10] ASTM C666-03: 2008. *Standard test method for resistance of concrete to rapid freezing and thawing.*
- [11] SRPS EN 196-1: *Methods of testing cement – Part 1: Determination of strength.*
- [12] BS EN 1766:2000. *Products and systems for the protection and repair of concrete structures – Test methods – Reference concretes for testing.*
- [13] SRPS EN 206-1:2011. *Concrete – Part 1: Specification, performance, production and conformity.*
- [14] EN 1542:1999. *Products and systems for the protection and repair of concrete structures – Test methods – Measurement of bond strength by pull-off.*
- [15] BS EN 12190:1999. *Products and systems for the protection and repair of concrete structures – Test methods – Determination of compressive strength of repair mortar.*
- [16] BS EN 13687-2:2002. *Products and systems for the protection and repair of concrete structures – Test methods – Determination of thermal compatibility – Part 2: Thunder-shower cycling.*
- [17] BS EN 13687-4:2002. *Products and systems for the protection and repair of concrete structures – Test methods – Determination of thermal compatibility – Part 4: Dry thermal cycling.*

28

Michael Mrissa, Jan Vcelak , László Hajdu, Balázs Dávid, Miklós Krész, Jakub Sandak, Anna Sandak, Rok Kanduti, Monika Varkonji Sajn, Anja Jutraz, Katja Malovrh Rebec

Extending BIM for Air Quality Monitoring

Extending BIM for Air Quality Monitoring

M. Mrissa^{1,2}, J. Vcelak³, L. Hajdu^{1,2}, B. David^{1,2}, M. Kresz^{1,2}, J. Sandak^{1,2}, A. Sandak^{1,2}, R. Kanduti⁴, M. Varkonji Sajn⁵, A. Jutraz⁶, K. Malovrh Rebec⁷

¹ InnoRenew CoE
Livade 6, 6310 Izola, Slovenia
email: {firstname.surname}@innorenew.eu

² Univerza na Primorskem
Glagoljaška ulica 8, 6000 Koper - Capodistria, Slovenia
email: {firstname.surname}@upr.si

³ Czech Technical University in Prague, University Centre for Energy Efficient Buildings
Trinecka 1024, Bustehrad, 27343, Czech Republic
email: jan.vcelak@cvut.cz

⁴ Špica International
Pot k sejmišču 33, 1231 Ljubljana - Črnuče, Slovenia
email: Rok.Kanduti@spica.com

⁵ Unistarpro d.o.o.
Litostrojska Cesta 56, 1000 Ljubljana, Slovenia
email: monika.varkonji@unistarpro.si

⁶ Nacionalni Inštitut za Javno Zdravje
Trubarjeva cesta 2, 1000 Ljubljana, Slovenia
email: anja.jutraz@nijz.si

⁷ Zavod za Gradbeništvo Slovenije
Dimičeva ulica 12, 1000 Ljubljana
email: katja.malovrh@zag.si

SUMMARY: As we spend more than 90% of our time inside buildings, indoor environmental quality is a major concern for healthy living. Recent studies show that almost 80% of people in European countries and the United States suffer from SBS (Sick Building Syndrome), which affects physical health, productivity and psychological well-being. In this context, environmental quality monitoring provides stakeholders with crucial information about indoor living conditions, thus facilitating building management along its lifecycle, from design, construction and commissioning to usage, maintenance and end-of-life. However, currently available modelling tools for building management remain limited to static models and lack integration capacities to efficiently exploit environmental quality monitoring data. In order to overcome these limitations, we designed and implemented a generic software architecture that relies on accessible Building Information Model (BIM) attributes to add a dynamic layer that integrates environmental quality data coming from deployed sensors. Merging sensor data with BIM allows creation of a digital twin for the monitored building where live information about environmental quality enables evaluation through numerical simulation. Our solution allows accessing and displaying live sensor data, thus providing advanced functionality to the end-user and other systems in the building. In order to preserve genericity and separation of concerns, our solution stores sensor data in a separate database available through an application programming interface (API), which decouples BIM models from sensor data. Our proof-of-concept experiments were conducted with a cultural heritage building located in Bled, Slovenia. We demonstrated that it is possible to display live information regarding environmental quality (temperature, relative humidity, CO₂, particle matter, light) using Revit as an example, thus enabling end-users to follow the conditions of their living environment and take appropriate measures to improve its quality.

KEY WORDS: Building information model, Internet of Things, environmental quality monitoring, healthy living

1 INTRODUCTION

Conservation and renovation of cultural heritage buildings is a priority of the UNESCO Sustainable Development Goals (SDGs) as a part of the culture preservation program¹. It is as well a major concern for public and private owners. In this context, Information and Communication Technology (ICT) is ideal to provide stakeholders with crucial information about the building state and its environment and contribute to facilitating renovation processes.

However, current available tools for building monitoring and management remain particularly limited and lack integration capacities. On the one side, most popular software used for designing building (such as ArchiCAD, AutoCAD, Dynamo, Grasshopper, Maya, SketchUp, Revit, Rhino 3D, etc.) remain static, fragmented and barely compatible with each other. On the other side, Internet of Things (IoT) solutions, while they provide highly needed dynamic information about building conditions, are not integrated into existing modeling tools.

In this paper, we describe a solution to exploit data coming from building sensors via building modeling tools. We show how it is possible to use Building Information Model (BIM) attributes in order to provide the building modeling tool with specific information that allows accessing and displaying sensor data. We describe our solution to provide information about IoT sensors deployed in buildings so that modeling tools can access it and provide advanced functionality to the end user. The prototype software plug-in was created in Revit, but the same solution can be replicated in most state-of-the-art programs used by building designers. We focus on air quality monitoring, an essential aspect of healthy living and a major concern for building renovation. Our experiments have been conducted with a cultural heritage building located in Bled, Slovenia. We manage to display live information about air quality in a tool like Revit, therefore enabling stakeholders to follow air quality conditions before, during and after the renovation process. Our sensors measure temperature, relative humidity, pressure, CO₂, particulate matter, luminosity, volatile organic compound. Such information may enable taking adequate measures to improve air quality such as opening windows in case of high CO₂ level.

This paper is structured as follows: Section 2 highlights the need to integrate air quality information into the BIM to enable live monitoring of the building. Section 3 reviews most relevant work in the area and shows how air quality information is not yet integrated into BIM products. Section 4 presents our contribution to enable air quality information to be accessible to end users through BIM integration. Section 5 illustrates our proposal with a use case developed with a building from the Slovenian cultural heritage. Section 6 summarizes the results obtained and gives some guidelines for future work.

2 MOTIVATION

The use of BIM can be widely extended from (relatively sophisticated) designing tool for 3D structure and installations to variety of diverse aspects related to the building itself. Some of the state-of-the-art BIM additions can be used, for example, to simulate the indoor thermal, lightening and acoustic conditions which cumulatively affect the comfort and well-being of occupants. It supports different types of automated evaluation and analyses which are helpful for improving the building operations in terms of human comfort. It provides a 3D virtual environment with a workflow of integrated information through a software package capable to predict and decrease problems and errors [1]. The BIM as a digital representation of the building offers the unique possibility to combine diverse information related to the facility, including all phases of its life - from the concept to demolition and recycling. For that reason, it is feasible to consider it as a storage of the overall service-life performance data that can be automatically acquired by sensors or any IoT solutions (amongst others). The model of a building will contain therefore an additional layer, simplifying data access. This provides possibility for early warning of undesired building conditions that can automatically alert the building owner or users about the threat and recommended solutions. On the other hand, accessing well structured (time and location-wise) readings from sensors provides a unique possibility to validate simulation models already integrated with BIM. It is expected that further building modelling tools will develop in a close future. The same data would be highly useful for development of such models and further extension of the BIM usability.

¹ <https://en.unesco.org/courier/2017-april-june/culture-heart-sdgs>

BIM is recently used to document and manage cultural heritage structures. The Historic Building Information Modelling (HBIM) for the integration of contemporary technology and BIM approach in the field of cultural heritage documentation was introduced by [2]. HBIM can be implemented to enhance the performance of existing heritage buildings or plan for the conservation of unused facilities. The research reported here is a follow-up of the HBIM project conducted for the historic building Mrakova Domačia located in Bled (Slovenia). The old farmhouse was constructed in the eighteenth century and was abandoned for more the 40 years. The structure and interior were perfectly preserved and represent an authentic example of the ancient culture and habits in this Slovenian region. Just recently, the Local authorities in collaboration with Institute of Cultural Heritage of Slovenia decided to renovate the building and organize a modern exhibition place attracting visitors and tourists. The original HBIM model developed for the needs of this restoration included inventory of current building elements and their general conditions. It was found however, that several other aspects (than structure itself) are not represented as data or simulation models. Moreover, an effect of the restoration action on the building microclimate was difficult to predict, not to mention the reconstruction effects on human health. For that reason, monitoring of Indoor Air Quality (IAQ) was considered as an interesting addition to the HBIM-based model. In this context, the current IAQ state as well as its changes during and after restoration are assessed by the custom developed prototype sensor network, with all acquired data integrated with the HBIM model. As a result, the system allows an easy access to information about indoor pollutants and ambient air conditions that are highly useful to quantify an impact of the activities carried out in the building and during its future occupancy.

3 RELATED WORK

Due to industrial needs and building digitization, Building Information Modelling (BIM) [3] has become more and more important in the last decade. The main objective of the original idea is to support sharing, storing and managing information during the whole building lifecycle from the design phase to the operational period and to facilitate an interoperable communication channel in the architecture, engineering and construction (AEC) industry. More detailed description about the original model and an overview about methodologies can be found here [4,5]. The main advantage of the BIM model, which is regulated by the platform neutral Industry Foundation Classes (IFC) and Green Building XML (gbXML), is to be an open format specification that is not controlled by a single vendor or group of vendors in the field.

The BIM provides an efficient tool to describe the model and the essential properties of the building, however additional features, such as cost estimation, project management and IoT technology support are not available in the original format. It can be stated that with the expansion of the Building Information Modelling, the digital representation of the newly built structures is becoming a general practice in the field, but it is also important to exploit the original idea to create a commonly usable methodology to support existing and old buildings and extend the functionality of the original model to keep it ready to operate with latest technologies. Since the components of the building in the model are represented by objects, and the objects contain the different properties and attributes of the represented element, the structure of the model gives opportunity to extend the functionality effectively and use the existing digital representations to provide additional functionalities. In the literature, possible extension scenarios were introduced in [6].

3.1 Overview of BIM extensions

Researchers from different fields have demonstrated the extendibility of the original model. The different BIM extensions can be grouped by the application area of the extended model, and in the literature most research is focusing on the extensions that can be used in existing software applications. In most cases, building designers use CAD based software tools to create the 3D model of the building, such as Autodesk Revit or other CAD based software. An example of the extensions is the multidimensional model (nD) concept where the original model was expanded with dimensions where cost, accessibility, maintainability, sustainability, crime, energy, whole life costing, acoustics, and scheduling were included into the original model [7]. The n dimensional model also includes the life cycle assessment of the corresponding building. Other research papers are focusing on heat modelling and structural simulations in a case of fire or other disasters [8], where for example evacuation plans can be tested [9]. The following extension tries to evaluate the sustainability level and architectural designs using the Building Information Model [10]. These different BIM extensions are from several areas, and the original model is suitable to handle additional functionalities to provide a general and effective modelling methodology of our buildings.

IoT is the abbreviation of Internet of Things and it refers to the broad range of different devices and physical objects connected to each other and to the Internet in order to exchange and collect data. It includes the use of sensors,

actuators, communication equipment, data storage, computing devices, analytical and other software to achieve the desired behavior of connected devices or obtain the needed results. The following paper gives us a good overview about the IoT related extendibility of the original BIM model [11]. Nowadays, IoT solutions are becoming an important part of our life, and the integration of smart features, sensors, data processing and analysis of collected data into the BIM has become a key research area. It is also important to see that until now the model was used by researchers and the main contributors of the building industry, nevertheless IoT solutions give us an opportunity to bring the BIM closer to the end users, creating a widely used and general computer environment and support the area of smart buildings and system development. The usage of the IoT in BIM can be highly important if we are talking about the protection of cultural heritage. The different expansions of the model can be connected to movable objects in the building, HVAC vibrations or VOC measuring, energy monitoring and management, or harmful environmental effects. The following articles can give an overview about IoT and BIM integration in cultural heritage buildings [12,13,14].

3.2 Air quality monitoring

Air quality monitoring plays a major role if we are talking about human health in building environment. It is well known that air pollutants (e. g NO_x, CO, BTEX, PAH, PM₁₀, PM_{2.5}, PM₁, O₃, SO₂) can cause serious health problems. With the spread of IoT solutions, air quality monitoring has become a widely available and, in most cases, cheap solution to protect building users. In Europe, the World Health Organization (WHO) identified and recommended QA (Quality Assurance) and QC (Quality Control) activities to create a comparable methodology for Air Quality measurements. The following article gives us a good overview of sensor systems for air quality monitoring [15]. The installed sensor systems in public or private buildings are mostly low-cost sensors [16]. A good description about low-cost sensors can be found here [17]. The integration of air quality sensors into the BIM system is an important research area both from health and technological point of view.

From this perspective, and considering the state of the art, our research has for originality and main advantage to create an extended format which can be passed along different environments and encapsulate the information from the installed sensors in the building. The proposed methodology extends existing and commonly accepted IFC attributes, that results in direct integration of IoT solutions available for air quality assessment into the BIM modelling approach. It also presents the advantage to store sensor data on the cloud, therefore not overloading the data already present in BIM and allowing for runtime data access from the cloud storage.

4 CONTRIBUTION

Our contribution relies on the exploitation of BIM model attributes to enable access to sensor data. We designed an architecture that supports data collection and storage as well as its access through a Revit plugin that we developed. Our architecture presented in Fig. 1 shows the organization of our solution.

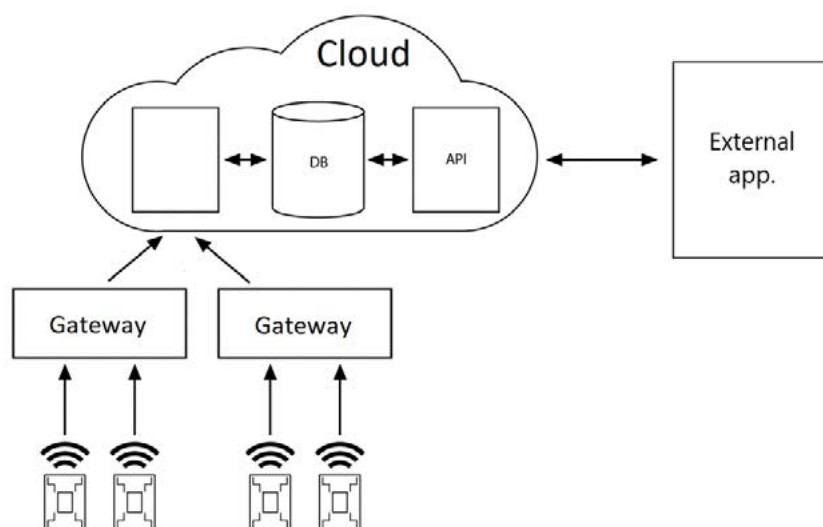


Figure 1. General architecture overview

Sensors connect to a gateway that forwards data to the cloud (we relied on the Microsoft Azure solution). Our cloud software receives data through its Application Programming Interface (API) and stores in a database that provides long term storage and makes data accessible to any external application such as Revit through another API. Our data model allows each organization to register buildings and store related sensor data. Management of building, sensors and data is realized through our developed Web interface or Revit plugin. Our plugin is visible in the Revit program above the ribbon “BIM.Sockets” and offers the following actions: “edit sensor”, “last record” and “report”.

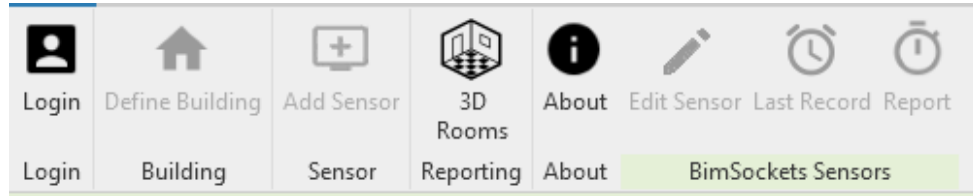


Figure 2. Revit plugin graphical interface

Our plugin communicates with our REST API hosted in Azure cloud. First users must authenticate, then select building from their list. Once a building is selected its parameters are written to Revit project information. The plugin saves building identification number and name, obtained from the API available online².

For displaying and storing data we created new BIM objects which represent sensors. To add a sensor, users are provided with a list of sensors, defined for a building. After selecting a sensor, the user must place it in a room, representing its physical location, on an object face. Selected sensor information is stored in the project. To ensure data transfer from Revit to other applications implementing BIM we decided to reuse common properties of objects, more specifically “Identity data”. Sensor identification number is written in the “Mark” property and its display name is stored in the “Comment” property. With this solution, exporting model for other programs also exports data added with our extension. Each sensor can only be added once per building, however multiple different sensors can be added in a building.

After successful deployment of sensors throughout building and connecting them to our platform, we can access their data through Revit. This can be accomplished with selecting desired sensor and selecting either “Last Record”, if we are looking for last reading transmitted from sensor, or “Report” where user select period and type of data aggregation. To test that data transfers from one BIM program to another, we exported our model to IFC format and imported it in free IFC viewer “BIM Vision”. After exporting all the required data transfer from Revit to IFC file. A major advantage of our solution is that only the information that allows the plugin to get access to data is stored in the BIM model, not the data itself, therefore keeping the BIM model as light as possible and allowing data updates without introducing any changes into the BIM. Fig. 3 shows measures displayed for a temperature sensor in Mrakova Domačia.

Time	Humidity	Illumination	Temperature
2019 Jun 01	39.88	19.23	26.28
2019 Jun 02	42.87	23.99	27.87
2019 Jun 03	47.24	23.66	27.13
2019 Jun 04	52.36	32.43	26.08
2019 Jun 05	54.82	23.61	25.88
2019 Jun 06	54.09	18.49	25.82
2019 Jun 07	53.19	20.39	25.78
2019 Jun 08	45.78	22.37	27.52
2019 Jun 09	44.79	21.81	28.79
2019 Jun 10	52.11	16.59	26.90
2019 Jun 11	57.86	15.63	26.25
2019 Jun 12	57.13	23.34	26.20
2019 Jun 13	55.45	24.68	26.15

Figure 3. Sensor measurements displayed with our Revit plugin

5 CONCLUSION

In this paper, we show an architecture to collect data sensor networks and enables their visualization in building modeling tools. We describe how we exploit specific attributes of the Building Information Model (BIM) in order to provide building modeling tools with specific information that allows accessing and displaying sensor data. Our prototype software plug-in was created in Revit, but our solution applies to most state-of-the-art programs used by building designers. We focus on air quality monitoring, an essential aspect of healthy living and a major concern for building renovation.

² <https://zoneiotapi.azurewebsites.net/docs/index.html>

Our experiments have been conducted with a cultural heritage building located in Bled, Slovenia. We show that it is possible to display live information about air quality (temperature, relative humidity, CO₂, particulate matter, volatile organic compound, pressure and luminosity) in a tool like Revit, therefore enabling stakeholders to follow air quality conditions before, during and after the renovation process.

Future work includes developing advanced recommendation mechanisms that can assist BIM users to design better buildings, to improve building performance and to spot weak points in building structure by exploiting sensor information. Such advance requires integrating AI algorithms into our plugin and further integration into BIM software.

ACKNOWLEDGMENTS

The authors gratefully acknowledge the European Commission for funding the InnoRenew CoE project (Grant Agreement 739574) under the Horizon2020 Widespread-Teaming program, the Republic of Slovenia (Investment funding of the Republic of Slovenia and the European Union of the European Regional Development Fund), and the Slovenian Research Agency ARRS for funding infrastructure program IO-0035.

REFERENCES

- [1] Taiwo, E.M., Yahya, K.B., Haron, Z.; Utilisation of building information modelling for indoor environmental quality assessment – A review. IOP Conf. Ser.: Earth Environ. Sci. 2019, 220 012051. doi:10.1088/1755-1315/220/1/012051
- [2] Murphy, M., McGovern E., Pavia, S.: Historic building information modelling (HBIM), Structural Survey Vol. 27 (2009) No 4., pp. 311 – 327
- [3] C.M. Eastman, P. Teicholz, R. Sacks, K. Liston BIM Handbook: A Guide to Building Information Modeling for Owners, Managers, Architects, Engineers, Contractors, and Fabricators John Wiley & Sons, Hoboken, NJ, USA (2008) ISBN: 978-0-470-54137-1
- [4] C. Cruz, Building information modeling, in: A Report of LAB, Le2i, Université de Bourgogne, 2008.
- [5] NIBS, National Building Information, Modeling Standards Part-1: Overview, Principles and Methodologies, US National Institute of Building Sciences Facilities Information Council, BIM Committee, 2007.
- [6] J. Zhang, A. Webster, M. Lawrence, M. Nepal, R. Pottinger, S. Staub-French, M. Tory Improving the usability of standard schemas Inform. Syst., 36 (2) (2011), pp. 209-221
- [7] A. Lee, S. Wu, G. Aouad, A. Lee, S. Wu (Eds.), nD Modelling: The Background in Constructing the Future: nD Modelling, Taylor and Francis (2006)
- [8] W. Tizani, M.J. Mawdesley Advances and challenges in computing in civil and building engineering Adv. Eng. Inform., 25 (2011), pp. 569-572
- [9] U. Ruppel, K. Schatz Designing a BIM-based serious game for fire safety evacuation simulations Adv. Eng. Inform., 25 (2011), pp. 600-611
- [10] T. Nguyen, T. Shehab, Z. Gao Evaluating sustainability of architectural designs using building information modeling Open Construct. Build. Technol. J., 4 (2010), pp. 1-8
- [11] Dave, Bhargav & Buda, Andrea & Nurminen, Antti & Främmling, Kary. (2018). A framework for integrating BIM and IoT through open standards. Automation in Construction. 95. 35-45. 10.1016/j.autcon.2018.07.022.
- [12] Changjiang Xiao, Nengcheng Chen, Dandan Li, You Lv, Jianya Gong (2017). "SCRMS: An RFID and Sensor Web-Enabled Smart Cultural Relics Management System"
- [13] Marulli, Fiammetta; Pareschi, Remo; Baldacci, Daniele (2016). "The Internet of Speaking Things and Its Applications to Cultural Heritage"
- [14] Borda, Ann; Bowen Jonathan P. (2017). "Smart Cities and Cultural Heritage – A Review of Developments and Future Opportunities"
- [15] Michele Penza, EuNetAir Consortium, COST Action TD1105: Overview of Sensor-systems for Air-quality Monitoring, Procedia Engineering, Volume 87, 2014, 1370-1377, ISSN 1877-7058
- [16] Aleixandre, M.; Gerboles, M. Review of small commercial sensors for indicative monitoring of ambient gas. *Chem. Eng. Trans.* **2012**, 30, 169–174.
- [17] Karagulian, Federico & Barbieri, Maurizio & Kotsev, Alexander & Spinelle, Laurent & Gerboles, Michel & Lagler, Friedrich & Redon, N. & Crunaire, Sabine & Borowiak, Annette. (2019). Review of the Performance of Low-Cost Sensors for Air Quality Monitoring. *Atmosphere*. 10.3390/atmos10090506.

29

Darko Nakov, Hatim Ejupi, Goran Markovski and Toni Arangjelovski

Fibre reinforcement – the key to sustainable reinforced concrete structures

FIBRE REINFORCEMENT – THE KEY TO SUSTAINABLE REINFORCED CONCRETE STRUCTURES

Darko Nakov¹, Hatim Ejupi², Goran Markovski³ and Toni Arangjelovski⁴

^{1,3,4} Prof. at University “Ss. Cyril and Methodius”, Faculty of Civil Engineering, Department of Concrete and Timber Structures, ² PhD candidate

Bul. Partizanski odredi 24, 1000 Skopje, Republic of North Macedonia

e-mail: nakov@gf.ukim.edu.mk

SUMMARY: One of the main reasons for strengthening, repair or even demolishing of concrete structures is the appearance of large deflections or cracks developed in the service life of the structures, caused by many different reasons. On the other hand, sustainability of concrete structures can be achieved if we avoid these actions by design of more durable structures. The addition of fibres to concrete is well known measure that can help in achieving this goal, proven by now on many short term tests. Since there is a scarcity of long-term tests dealing with fibre reinforced concrete, to find out the influence of different types of fibre reinforcement on the long-term deflections and long-term cracks of concrete structures, an experiment was carried out at the Faculty of Civil Engineering–Skopje. The experiment consists of 12 full scale reinforced concrete beams, all manufactured with concrete class C30/37, but reinforced with different types (steel, macro and micro polypropylene fibres and their combination) and amount of fibres (0, 0.38%, 0.39% and 0.76% from the volume) and additional longitudinal and transverse reinforcement. The results from the long-term tests showed up that even small amount of added fibre reinforcement have big influence on both deflections and cracks, thus ensuring more durable structures and reducing the costs for their possible repair or strengthening in future.

KEY WORDS: fibre reinforcement, sustainability, experiment, long-term deflections, long-term cracks.

1 INTRODUCTION

According to the World Commission on Environment and Development of the United Nations, sustainability means “meeting the needs of the present without compromising the ability of the future generations to meet their own needs”. Since concrete is the mostly used man made material, there is no doubt that reducing any amount of the current production will contribute in reducing the carbon footprint. Big amounts of greenhouse gas emissions (7-8% of the total GHG worldwide) are released during the process of production of 4.4 billion tons Portland cement annually. This is the reason why many researchers are dealing with partial replacement of cement with other materials as fly ash, silica fume, slag or other industrial by-products. Another way of reducing GHG emissions is by using recycled aggregates. However, all these types of improvements of the concrete mixes should be taken with great care and taking into account durability issues [1]. On the other hand, reducing the maintenance costs and the need of strengthening, repair and demolishing of the structures, and especially infrastructure, in their service life can be obtained with enhancing the durability performance.

Concrete buildings are usually designed for service life of 50 years, while concrete bridges for service life of 100 years, with an expectation that minimal maintenance will be required in that period. However, the situation in practice is different, and we are evidencing many structures, mainly bridges, with a need of some structural intervention due to occurred damages. Therefore, design of structures from the aspect of durability is essential for prolongation of their service life. The well-known measures for increasing durability usually are: increasing the cover to the reinforcement, usage of non-reactive aggregates, low alkali cements, curing of concrete etc. Another measure can be adding of discrete reinforcing fibres to the concrete matrices and in that way obtaining new material, called Fibre reinforced concrete.

Composite materials, reinforced with different types of fibres have been used since ancient times. Approximately 3500 years ago, straw was used to reinforce sun-baked bricks [2], and horsehair was used to reinforce masonry mortar.

The first widely commercial use of fibres was the use of asbestos fibres in a cement paste matrix in the year of 1898. Since the beginning of the previous century, at various intervals, short pieces of steel have been included within concrete in an attempt to improve its strength, ductility, durability and to overcome the typical characterization of brittleness of the cementitious materials. However, there was not much interest by research organizations or by the construction industry until the year of 1963, when Romualdi and Batson published the results of an investigation carried out on steel fibre reinforced concretes [3]. In the beginning, it was assumed that short pieces of steel or steel fibres enhance mostly the tensile strength of composites. In the year of 1964, Broms and Shah systematically studied the mechanical properties of the new material. Since then, intensive investigations began not only for the mechanical characteristics of the fibre reinforced concrete, but also for the determination of the influence of the fibres on the behaviour of different concrete and reinforced concrete elements. It comes out that the major contribution of the fibres is in enhancing the toughness and the durability of the elements.

One of the most promising materials nowadays is HFRC or Hybrid Fiber Reinforced Concrete. It contains two or more different fibre types (hybrid reinforcement) that are mixed so that the overall material is optimized to achieve synergy. The overall performance of the composite exceeds the performance induced by each of the fibres alone [2]. The synergies were classified by Banthia and Gupta into three groups, depending on the mechanisms involved [2]: 1. Hybrids based on fibre constitutive response, where one fibre is stronger and stiffer and provides strength, while the other is more ductile. 2. Hybrids based on fibre dimensions where one fibre is small and provides microcrack control at earlier stages of loading to arrest microcracks and enhance the first crack and strength, while the other fibre, which is bigger, provides the bridging mechanisms across macrocracks and induces toughness at high strains and crack openings. 3. Hybrids based on fibre function where one type of fibre induces strength or toughness in the hardened composite, while the second type of fibre provides fresh mix properties suitable for processing.

The fibres used in HFRC can be made either from one material, but with different geometries, or can be composed of different materials, such as polyethylene microfibers for microcrack control and deformed steel fibres for macrocrack bridging [2].

Up to now, there are only few published research studies dealing with long term behaviour of SFRC beams. Tan et al. in 1994 studied the behaviour of SFRC beams under sustained load as a one year study [4] and later the same research was continued as a ten year study of the deflections and crack widths under sustained load by Tan and Saha in 2005 [5]. Another research by Vasanelli et al. in 2012 [6] is dealing with the influence of long term sustained loading on the cracking behaviour and consequently on the structural durability. Due to the smaller carbon footprint of the polypropylene fibers, with the experimental program presented as follows, an attempt was made to replace all or one half of the steel fibres with polypropylene, and to compare all concrete types regarding deflections and cracks width.

2 EXPERIMENTAL PROGRAM

The experiment was carried out at the University “Ss. Cyril and Methodius”, Faculty of Civil Engineering-Skopje, Republic of North Macedonia. It involved testing of 12 full scale beams constructed from reinforced concrete and different types of fibre reinforced concrete with additional reinforcement. The beams had a cross section proportioned 15/28cm and a total length of $l=300\text{cm}$, Fig. 1. Together with each series of beams, control specimens were cast in order to test the compressive strength, flexural tensile strength, splitting tensile strength, elastic modulus and deformations due to creep and shrinkage. Some results are presented in [7], [8], [9] and [10]. In addition to the tests on mechanical and time-dependent properties of concrete, the used reinforcement was also tested.

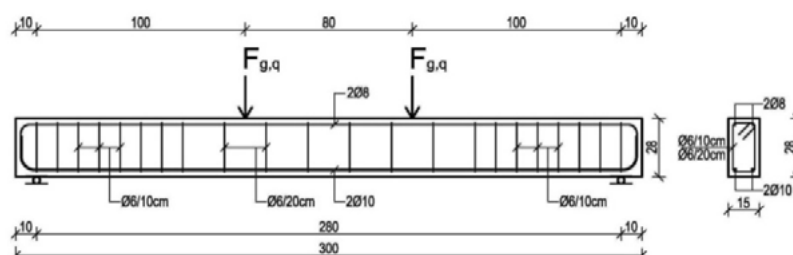


Figure 1: Geometry, reinforcement and loading scheme of full scale beams

All 12 beams were manufactured with concrete class C30/37. According to the used type of material, they were divided into three series, each containing 2 identical beams:

- Series A, Reinforced concrete (RC);
- Series B, Steel fibre reinforced concrete with 30 kg/m³ steel fibres and additional reinforcement (SFRC1);
- Series C, Steel fibre reinforced concrete with 60 kg/m³ steel fibres and additional reinforcement (SFRC2);
- Series D, Polypropylene fibre reinforced concrete with 3.46 kg/m³ macro polypropylene fibres and additional reinforcement (PPFRC).
- Series E, Hybrid polypropylene fibre reinforced concrete with 3.46 kg/m³ macro and 0.91 kg/m³ micro polypropylene fibres and additional reinforcement (HyPPFRC).
- Series F, Hybrid polypropylene steel fibre reinforced concrete with 30 kg/m³ steel fibres, 1.73 kg/m³ macro and 0.91 kg/m³ micro polypropylene fibres and additional reinforcement (HyPPSFRC).

The beams constructed of reinforced concrete were used for comparison with the beams constructed of fibre reinforced concrete. In each series, the plain reinforcement was kept the same. The longitudinal reinforcement was ribbed and of RA 400/500-2 quality, while the shear reinforcement was smooth, with GA 240/360 quality. Reinforcement 2Ø10, 2Ø8 and Ø6/10/20cm was used as tension, compression and shear reinforcement, respectively.

The used steel fibres were hooked-end HE1/50, produced of cold-drawn wire, manufactured by Arcelor Mittal, with a diameter of 1mm, length of 50mm and tensile strength of 1100 N/mm². The used macro polypropylene fibres were Durus, S400 monofilament fibre, manufactured by Adfil, with equivalent diameter of 0.9mm, length of 55mm, and tensile strength of 465N/mm². The used micro polypropylene fibres were Fibrin XT monofilament fibre, manufactured by Adfil, with equivalent diameter of 22µm, length of 13mm, and tensile strength of 380N/mm².

The mixture proportioning was done so that it was the same for the three types of concrete (Table 1).

Table 1: Mixture proportions for the three concrete types

Mixture proportions	(kg/m ³)
Cement CEM II/A-M 42.5N	410
Water	215
Water/Cement ratio, w/c	0.524
Aggregate:	
0-4 mm (river sand), 50%	875
4-8 mm (limestone), 20%	350
8-16 mm (limestone), 30%	525
Fibres:	
RC (no fibres)	0
SFRC1 (steel fibres, 0.38%)	30
SFRC2 (steel fibres, 0.76%)	60
PPFRC (macro polypropylene fibres, 0.38%)	3.46
HyPPFRC (macro, 0.38% + micro 0.1% polypropylene fibres)	3.46+0.91
HyPPSFRC (steel, 0.19% + macro, 0.19% + micro 0.1% polypropylene fibres)	15+1.73+0.91

The beams and control specimens were cured for 8 days and then they were transported to the Laboratory at the Faculty of Civil Engineering – Skopje, where they were kept under almost constant temperature with an average of 19.5°C and constant relative ambient humidity with an average of 60.2%, which was regulated with special humidifiers and dehumidifiers.

The beams from the six types of concrete have been pre-cracked with permanent and variable load "g + q", and afterwards a long term permanent load with intensity "g" has been applied at the age of concrete of 40 days, and held up to 230 days. The idea with the pre-cracking was to activate the fibers, since their effect is negligible in the elastic behavior. In that period the strains, deformations and crack widths have been measured.

Each day, the strains in the concrete (D1-D15), in the middle section of the beam through the thickness as well as on the top of the beam, were measured by a mechanical deflection meter, type Hugenberger, Switzerland, with a base of 250mm. The mechanical measurement of the deflections was done at 5 points through the length of the beam and 2 points over the supports by using deflection meters produced by Stopani, Italy. The crack widths were also measured in the above mentioned time period, in the region with constant moment, by use of a crack microscope - product of Controls,

Italy. The positions of the measurement points are presented in Figure 2.

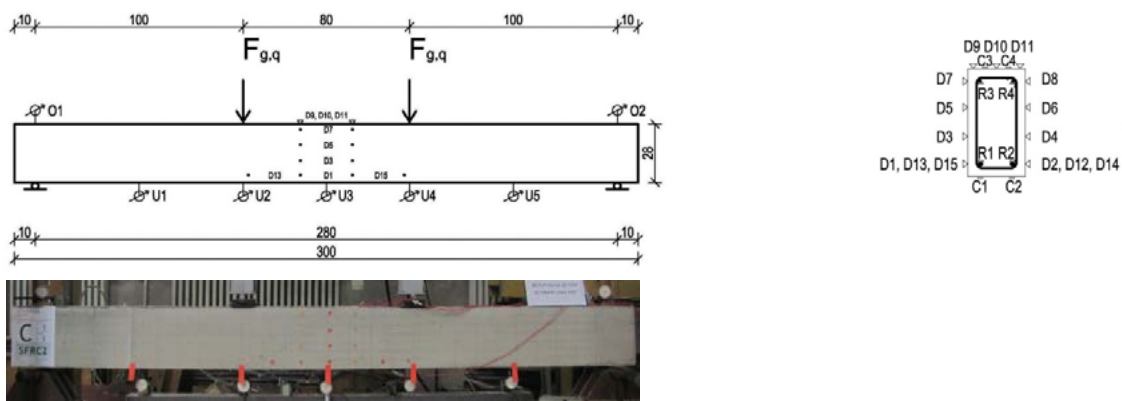


Figure 2: Positions of measurement points of full scale beams

The long term load, which consists of permanent sustained load “g”, after precracking of the beams with service load (permanent “g” plus variable load “q”), was applied by gravitation levers (Fig.3), which enabled an increase of the load for 13 times. The permanent load acts all the time, while the variable load was applied and removed after the precracking was done.

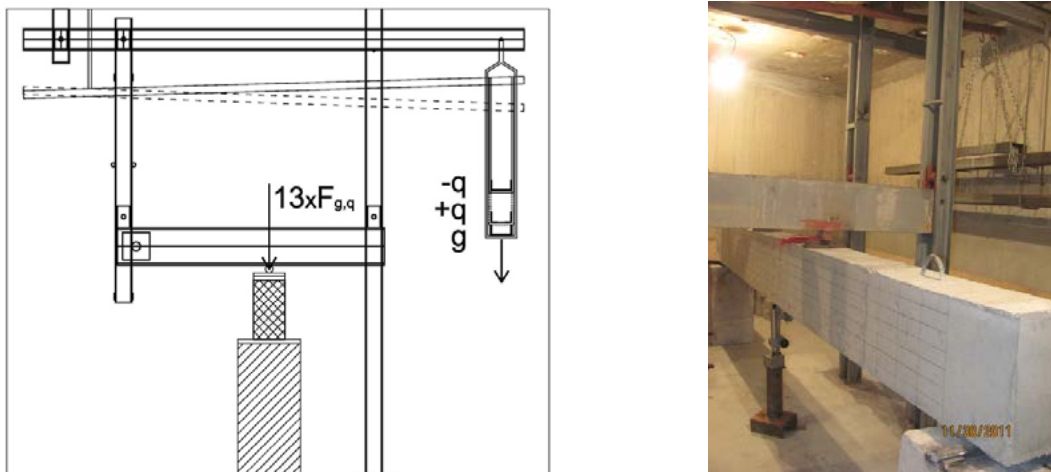


Figure 3: Gravitation lever

The bending moments are as follows: from self-weight of the beam, $M_{sw}=1\text{kNm}$, from permanent load “g”, $M_g=5.0\text{kNm}$, from variable load “q”, $M_q=3.1\text{kNm}$, from self-weight, permanent and variable load (precracking, service) $M_{sw+g+q}=9.1\text{kNm}$. The bending crack moment was $M_{cr}=6.1\text{kNm}$, while the ultimate bending moment $M_d=15.6\text{kNm}$. The intensity of the load was chosen so that the M_{cr} is bigger than M_{sw+g} and smaller than M_{sw+g+q} . The permanent load is 0.39 times the flexural strength, while the precracking load is 0.58 times the flexural strength of the beam without fibres.

3 SELECTED EXPERIMENTAL RESULTS

The results from the long term loading are presented in terms of time-dependent: deflections and cracks width.

3.1 Time-dependent deflections

All beams were first loaded with permanent load “g”. In order to induce cracks and activate the fibres, the beams were precracked with load “g+q” and then the load was returned to the level of permanent load which was acting in the period of 230 days. In Figure 4 and Figure 5, total and long term deflections in logarithmic scale are presented as an average value of two beams for each concrete type.

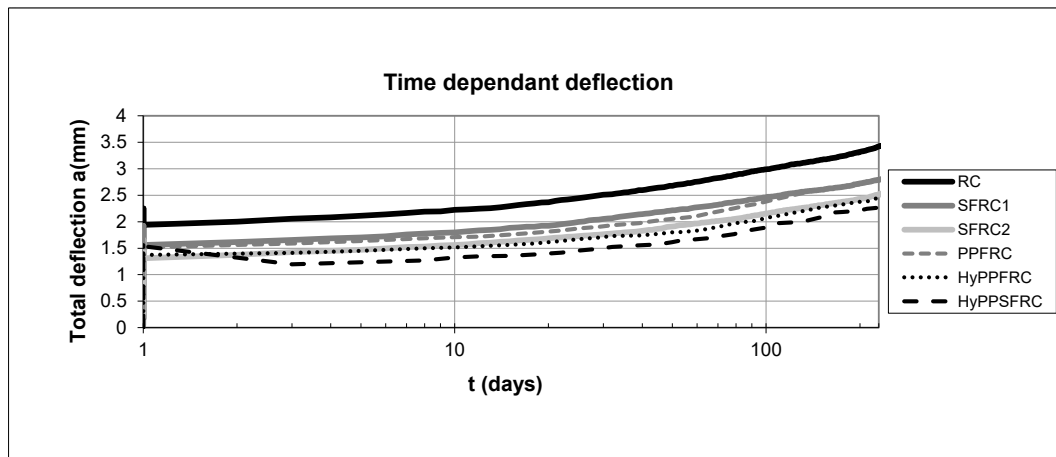


Figure 4: Total time-dependent deflections

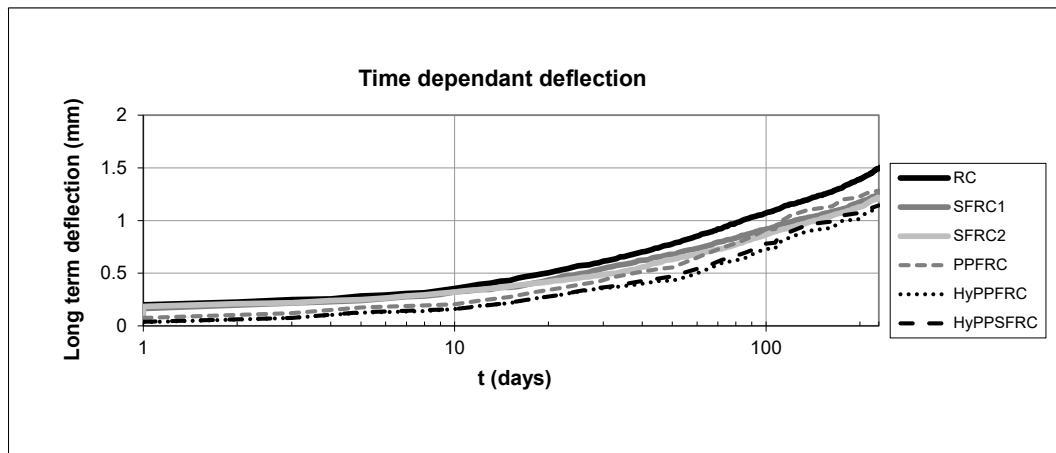


Figure 5: Long term deflections

From the figures can be noticed that the instantaneous, total and long term deflection decreased with the addition of fibres. Long term deflection, which is the total minus instantaneous deflection after precracking, at the level of permanent load “g”, for all concrete types decreased when compared to the ordinary reinforced concrete (RC) in the range from 13.3% to 24.7%. The decrease is as follows: 16.8% for SFRC1, 18.5% for SFRC2, 13.3% for PPFRC, 24.7% for HyPPFRC and 22.7% for HyPPSFRC. It can be noticed that in all concrete types deflections decreased with the addition of fibres, but the biggest decrease is at the hybrid fibre reinforced concrete types.

The values of the instantaneous and long-term deflections of the beams from all concrete types are presented in Table 2.

Table 2: Instantaneous and long-term deflections for all concrete types

Concrete type	RC	SFRC1	SFRC2	PPFRC	HyPPFRC	HyPPSFRC
Deflection(mm)						
a_0 (inst.) g	0.845	0.83	0.815	0.67	0.76	0.64
a (long-term) g	1.488	1.238	1.213	1.29	1.12	1.15

3.2 Time-dependent cracks width

Although all cracks that appeared during the application of the load or in the period of observing of 230 days, have been registered, the cracks width have been measured only in the middle third of the beams, i.e. in the part of the beams with constant bending moment. The time-dependent cracks widths for all concrete types are presented in Figure 6 and the final observed cracks widths are shown in Table 3.

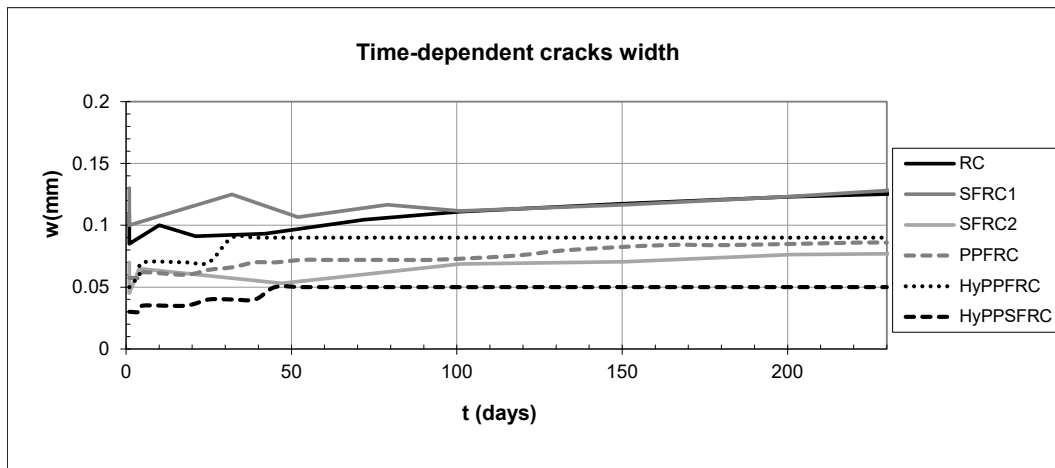


Figure 6: Time-dependent cracks width

Table 3: Final observed cracks width

Concrete type	RC	SFRC1	SFRC2	PPFRC	HyPPFRC	HyPPSFRC
Cracks width(mm)						
w (g)	0.13	0.13	0.077	0.086	0.09	0.05

As it was predicted, the cracks in all beams appeared between the level of permanent and service load. At the two reinforced concrete beams (RC), 4 and 6 cracks appeared from the precracking load. At the steel fibre reinforced concrete beams (SFRC1), 2 cracks appeared in each beam, while at the beams from SFRC2, 2 and 1 crack appeared. At the polypropylene fibre reinforced concrete beams (PPFRC), 4 and 5 cracks appeared. At the hybrid polypropylene fibre reinforced concrete beams (HyPPFRC), 2 cracks appeared in each beam. At the hybrid polypropylene steel fibre reinforced concrete beams (HyPPSFRC) 2 and 1 crack appeared.

After removal of the variable load “q”, the cracks width decreased and increased thereafter up to the moment of appearance of new cracks at some of the beams. The mentioned new cracks were with smaller crack width and therefore they decrease the average value of all crack widths. This can be also noticed from the Figure 6 in the first 100 days. After forming of all cracks there is only increase in their width.

From the Figure 6, can be noticed that the instantaneous cracks width at the moment of precracking and after precracking for SFRC1 are bigger than RC, while for SFRC2 and PPFRC are significantly smaller. However, total cracks width of RC and SFRC1 are the same, while the one of SFRC2 is reduced for 40.8% and the one of PPFRC is reduced for 33.8%. For the hybrid fibre reinforced concrete types, it can be noticed that after 50 days the cracks are stabilized since there is no increase in the cracks width. The total cracks width of HyPPFRC is reduced for 30.8%, while the one of HyPPSFRC is reduced for 61.5%.

However, having in mind the complexity of the process of cracking, the randomly oriented fibres in each type of fibre concrete and the low level of stress from the permanent load, which is about 20% from the concrete strength, can be concluded that the fibres significantly decrease the crack widths.

4 CONCLUSIONS

- Long term deflections of the beams subjected to sustained loads in the period of 230 days, for different fibre reinforced concrete types are reduced up to 25% when compared to ordinary concrete RC, with biggest decrease at the hybrid fibre reinforced concrete types.
- The final observed cracks width of the beams subjected to sustained loads in the period of 230 days, for different fibre reinforced concrete types are reduced up to 60% when compared to ordinary concrete RC, with biggest decrease at the hybrid fibre reinforced concrete type HyPPSFRC.

- From the presented results can be noticed that there is reduced ongoing of the fibre pull-out with time.
- The results presented in this paper indicate the positive influence of additional reinforcing of RC beams with different types of fibres on the long term deflections and cracks width and thus ensuring durability and sustainability of concrete structures.
- The reinforcing of the concrete mixes with fibres is mostly effective with certain combination of different types of fibres.

REFERENCES

- [1] Mackechnie, J. R. & Alexander, M. G.: Using durability to enhance concrete sustainability, *Journal of Green Building*, Volume 4, Number 3, (2009)
- [2] Bentur A.; Mindess S.: *Fibre Reinforced Cementitious Composites*, Second edition, Taylor and Francis, (2007)
- [3] Edgington J., Hannant D.J., Williams R.I.T., *Steel Fibre Reinforced Concrete*, Current Paper CP69/74, Building Research Establishment, Garston, Watford, (1974)
- [4] Tan K.H., Paramasivam P., Tan K.C., Long term deflections of Steel fiber-reinforced concrete beams, *ACI Structural Journal* (1994)
- [5] Tan K.H., Saha M.K., Ten-year study on Steel fiber-reinforced concrete beams under sustained loads, *ACI Structural Journal* (2005)
- [6] Vasanelli E., Micelli F., Aiello M.A., Plizzari G., Long term behaviour of fiber reinforced concrete beams in bending, BEFIB2012 – Fibre reinforced concrete, Guimaraes (2012)
- [7] Nakov D., Markovski G., Arangjelovski T. & Mark P., Creeping effect of SFRC elements under specific type of long term loading, RILEM Bookseries, Vol. 14, Pedro Serna et al: Creep behaviour in cracked sections of fibre reinforced concrete, Springer, (2017)
- [8] Nakov D., Markovski G. & Arangjelovski T., Influence of steel fibre reinforcement on the properties of concrete, 1st International Conference COMS, Zadar, (2017)
- [9] Nakov D., Markovski G., Arangjelovski T. & Mark P., Experimental and Analytical Analysis of Creep of Steel Fibre Reinforced Concrete, *Periodica Polytechnica Civil Engineering* 62(1), (2017)
- [10] Nakov D., Markovski G., Mark P. & Arangjelovski T., Analytical analysis of drying shrinkage of SFRC based on experimental results, Conference Fibre concrete 2015, Prague, (2015)

30

Mihael Ramšak

Appropriate sound insulation of facades as a measure to ensure acceptable acoustic comfort in residential buildings



APPROPRIATE SOUND INSULATION OF FACADES AS A MEASURE TO ENSURE ACCEPTABLE ACOUSTIC COMFORT IN RESIDENTIAL BUILDINGS

M. Ramšak¹

¹ Slovenian National Building and Civil Engineering Institute, Department of Building Physics,
Dimičeva ul. 12, 1000 Ljubljana
e-mail: mihael.ramsak@zag.si

SUMMARY: Wherever possible, the environment with residential buildings should be protected from the effects of noise sources by environmental noise reduction measures. If such measures cannot reduce the noise level in the environment to an acceptable level, acceptable acoustic comfort in the residential buildings shall be ensured by adequate sound insulation of the facades, which is the main topic of this paper. The paper outlines some of the criteria for providing good acoustic comfort in the residential buildings, on the basis of which the conditions and necessary measures for providing sufficient sound insulation of the facade elements are discussed. Since, in addition to the noise from the environment, the acoustic comfort in apartments is also affected by the noise from adjacent apartments in the building, the link between the sound insulation performance of facades and audibility of the speech noise from adjacent apartments is also discussed.

KEY WORDS: acoustic comfort, traffic noise, sound levels, sound insulation.

1 INTRODUCTION

One of the essential conditions for living comfort in residential buildings is acoustic comfort, which means providing such acoustic conditions in living spaces that will allow residents to sleep, rest, work and do other activities without interruption. This goal can be achieved by reducing the noise levels to such an extent that they do not exceed values which still provide adequate acoustic comfort. It can be done either by reducing the noise emission of the sound sources, by reducing the impact of sound propagation from the noise sources toward the living spaces of dwellings or by providing adequate sound insulation of dwellings. This contribution is focused on the protection of residential spaces against environmental noise by providing sufficient sound insulation performance of the facades.

It is well known that the sound insulation performance depends on the spectrum of noise which is to be reduced and that consequently the sound insulation performance of the façade is not the same for all environmental noise sources. In this respect the discussion in the following sections is focused on the sound insulation performance of the façade against the traffic noise which is recognized as a typical and the most relevant environmental noise source. Namely, recent research shows that more than 30% of EU citizens are exposed to road traffic noise levels above that viewed acceptable by the World Health Organisation (WHO).

The positive side of good sound insulation performance of the façade is the noise level reduction inside the building, but it should not be forgotten that this leads to an increase in sensitivity to noise from adjacent spaces in the building. In this respect the last part of this contribution is focused on a typical example of this kind, namely on the audibility of the speech from the adjacent apartments in the building.

2 MEASURES TO REDUCE THE IMPACT OF ENVIRONMENTAL NOISE SOURCES ON HOUSING

To reduce the impact of the environmental noise sources, such as: traffic, industry, etc., on the residents in the

residential buildings the following noise reduction measures are available:

- measures at the noise source,
- measures along the path of noise propagation and
- measures at the noise receiver.

In the case of traffic noise for example, typical noise reduction measure at the source is the use of the “quiet” road surfaces to reduce the tyre-road noise emission, which is the most important source of the traffic noise emission. To reduce the traffic noise propagation the noise barriers are used and to reduce the impact of the traffic noise on the indoor noise in residential buildings the improvement of the sound insulation performance of the façade is necessary.

For measures at the noise source and along the path of noise propagation the expression “active noise reduction measures” is usually used, while for the measures at the noise receiver by improving of the sound insulation performance of the façade, the expression “passive noise reduction measures” is usually used.

Closer to the noise source are the sound reduction measures implemented more effective they are, because the territory, protected by such measures, is larger in such cases. That is the reason why the active noise reduction measures have advantage compared to the passive noise reduction measures. Therefore, wherever possible, the environment in which residential buildings are located should be protected from the effects of noise sources primarily by the active noise reduction measures. But in spite of the advantage of the active noise reduction it is sometimes inevitable to use passive noise reduction measures by improving sound insulation performance of the façades. It is typically inevitable in the case of the sound insulation of upper flats of the high residential buildings near high-trafficked roads.

To ensure a good acoustic comfort in the building it is necessary to ensure that the level of the indoor noise due to the traffic should not be too high. At least in some Central European countries, including Slovenia, the mandatory limit indoor noise level is nowhere below 30 dBA at the moment, which is acceptable but it does not provide good acoustic comfort [2,3,4,5]. Namely, recent researches show that for a good acoustic comfort the limit noise level should not exceed 25 dBA [6,7].

3 SOUND INSULATION PERFORMANCE OF FACADES AND ITS INFLUENCE ON THE INDOOR NOISE LEVEL

The sound insulation performance of façade elements and façades is usually described by the sound reduction index R' [8]. It can be evaluated from:

$$R' = L_{outdoor,S} - L_{indoor} + 10 \cdot \log(S \cdot T / 0,16 \cdot V) - 3dB \quad (1)$$

where

- $L_{outdoor,S}$ is the average sound pressure level on the outside surface of the façade, including the reflected effects from the façade (dB),
- L_{indoor} is the average indoor sound pressure level in the receiving room (dB),
- S is the total area of the façade as seen from the inside (m^2),
- V is the volume of the receiving room (m^3)
- T is the reverberation time of the receiving room ($\approx 0,5s = T_0$ for furnished room).

The reverberation time is by definition the time, required for the sound level in the room to decrease for 60 dB after turning off the loudspeaker.

However, the recent findings show [9] that the standard level difference $D_{2m,nT}$ is a quantity which more appropriately reflects the human perceiving of the sound insulation performance of the façade than the sound reduction index. It can be evaluated from [8]:

$$D_{2m,nT} = L_{outdoor,2m} - L_{indoor} + 10 \cdot \log(T/T_0) \quad (2)$$

where

- $L_{outdoor,2m}$ is the average sound pressure level at 2m in front of the façade (dB),
 L_{indoor} is the average indoor sound pressure level in the receiving room (dB),
 T is the reverberation time of the receiving room ($\approx 0,5s$ for furnished room),
 T_0 is the reference reverberation time = 0,5s.

Both quantities R' and $D_{2m,nT}$ depend on the frequency of sound, so the sound insulation performance has to be determined for each frequency band within the relevant frequency region, usually between 100 Hz and 3150 Hz. Such a way of describing the sound insulation characteristics is obviously pretty cumbersome and that is why the procedure was established to evaluate the overall sound insulation performance with a single numbers R'_w (weighted sound reduction index) or $D_{2m,nT,w}$ (weighted standard level difference) [8].

The ultimate goal in expressing sound insulation performance is to determine the value that will represent the difference between the outdoor and indoor sound levels, accommodated to human perception. For that reason the spectral adaptation terms were introduced [8], C_{tr} for traffic noise and C for other types of noise, which have to be added to the single numbers R'_w or $D_{2m,nT,w}$ to get the abovementioned level difference:

$$R'_w + C_{tr} = R'_{Atr} \text{ and } R'_w + C = R'_A$$

$$D_{2m,nT,w} + C_{tr} = D_{2m,nT,Atr} \text{ and } D_{2m,nT,w} + C = D_{2m,nT,A}$$

As a typical practical example let us take $S = 4 \text{ m} \times 2,5 \text{ m} = 10 \text{ m}^2$ for a typical surface of the façade and $V = 3 \text{ m} \times 4 \text{ m} \times 2,5 \text{ m} = 30 \text{ m}^3$ for a typical room volume. Standard reverberation time of the room is 0,5 s (furnished room). The façade is presumed to be plain. In such a case R' and $D_{2m,nT}$ are approximately equal. For this typical example, we will hereafter express the sound insulation performance mainly by the weighted sound reduction indices R'_w , R'_{Atr} and R'_A .

Based on above mentioned assumptions the indoor sound pressure level, produced by the road traffic noise and accommodated to human perception of noise, is given by:

$$L_{indoor} \approx L_{outdoor,2m} - (R'_w + C_{tr}) \quad \text{dBA} \quad (3)$$

where

- L_{indoor} is the average indoor sound pressure level in the receiving room (dBA),
 $L_{outdoor,2m}$ is the average sound pressure level at 2m in front of the façade (dBA),
 $(R'_w + C_{tr}) = R'_{Atr,façade}$ is the weighted sound reduction index of façade, spectrally adapted to the traffic noise and accommodated to human perception of noise (dBA).

Based on equation (3) the required sound insulation performance of the façade for different outdoor traffic noise levels and for different indoor noise level limits is presented in Figure 1. The values of $R'_{Atr,façade}$ are calculated for the abovementioned characteristic dimensions and furnishing of the room. The outdoor noise levels in Figure 1 are the levels without reflection effects of sound from the façade (so called free-field noise levels, usually determined by the environmental noise modelling).

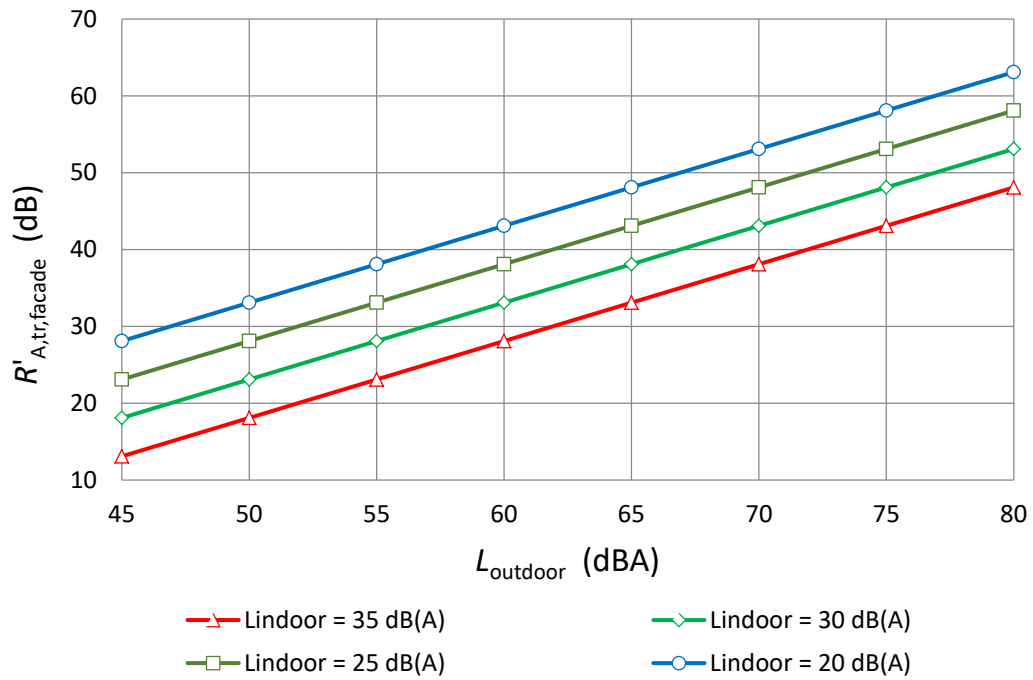


Figure 1: Required sound insulation performance of the façade for different outdoor noise levels and for different indoor noise level limits - calculation example for the characteristic dimensions and furnishing of the room

Overall sound insulation performance of the façade depends on the sound insulation performance of the wall and on the sound insulation performance of the glazed part of the façade. An example of sound insulation performance of the typical 10 m² large façade with the 1,4 m wide and 1,4 m high window is presented in Figure 2.

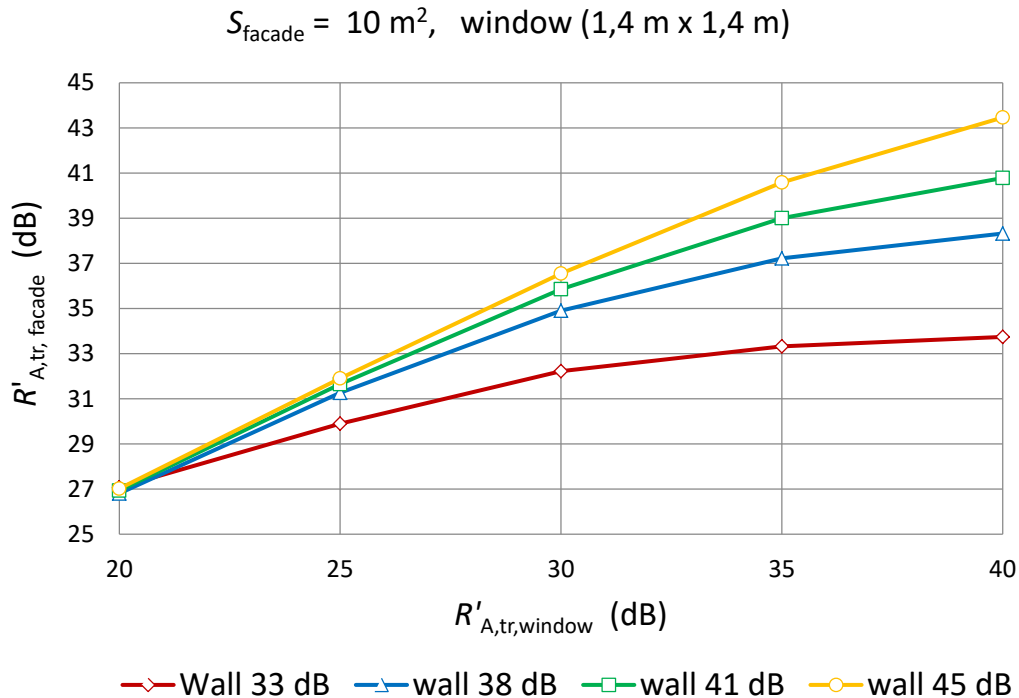


Figure 2: Sound insulation performance of the façade for different sound insulation performances of the window and of the wall - calculation example for the characteristic dimensions and furnishing of the room

Typical sound reduction index $R'_{Atr,window}$ of newly installed windows in Slovenia (not older than app. 10 years, with the triple glazing 4-12-4-12-4 or double glazing 4-16-8) is somewhat around 32 dB [10]. For a common case where the façade wall is masonry wall with the external thermal insulation lining (ETICS), the expected sound reduction index R'_{Atr} of the wall is around 45 dB [11]. In Figure 2 it can be seen that the combination of such a window with a typical façade wall with R'_{Atr} around 45 dB gives the overall sound reduction index of the façade $R'_{Atr,façade}$ around 38 dB. In Slovenia the prescribed indoor noise level limit in dwellings in the day time when the road traffic is the loudest is 35 dBA. Taking this into account it can be seen in Figure 1 that typical sound reduction index $R'_{Atr,façade}$ of the façade 38 dB is too low for the regions where the outdoor level exceeds 70 dBA, which means for the regions near high-trafficked roads. It is necessary to have in mind that the indoor noise limit 35 dBA does not provide a good acoustic comfort in dwellings so therefore the limit value should be lower. As a relevant indoor noise level for dwellings in a typical residential area the indoor level of maximum 25 dBA could be taken [6,7]. In such a case the typical sound insulation performance of the façade with the newly installed windows in Slovenia would be appropriate only for the regions where the outdoor noise level does not exceed 60 dBA which is a typical noise level for the regions near the roads with little traffic.

We presume now, as an example, that the sound reduction index of the window $R'_{Atr,window}$ would be 40 dB, which is a pretty high value for a window. From the graph in Figure 2 it can be seen that the overall sound reduction index of the façade $R'_{Atr,façade}$ would be approximately 43 dB in this case. The graph in Figure 1 further shows that for this value of the sound reduction index the limit outdoor noise (without reflections from the façade) should not exceed approximately 75 dBA for the case when the limit indoor noise level is taken to be 35 dBA. The noise level 75 dBA is typical for the regions near the high-trafficked roads. But in the case the indoor noise limit is lower, for example 25 dBA which is much more acceptable than 35 dBA, than the outdoor noise level should not exceed approximately 65 dBA which is a typical noise level for the regions near the roads with moderate traffic.

The above discussion shows that for providing a good acoustic comfort in dwellings the very good sound insulation performance of the façade is needed, especially in the regions near the high-trafficked roads. This is not so easy to achieve, especially due to the combined effect of the spectral characteristics of the road traffic noise and the unfavorable sound insulation characteristics of the masonry wall with the external thermal insulation lining (ETICS) in the low frequency region below app. 315 Hz [12]. All these lead to the rather low sound insulation performance of the façade wall with the typical sound reduction index R'_{Atr} around 45 dB. As already mentioned, to provide an acceptable acoustic comfort in dwellings the indoor noise should not exceed the noise level of around 25 dBA. It follows that such sound reduction index of the wall in combination with the sound reduction index of the window $R'_{Atr,window}$ (which rarely exceed the value of 45 dB) cannot provide sufficient sound insulation against the traffic noise in the noisy regions where the outdoor noise level exceed 70 dBA (Figure 1).

In addition to the abovementioned facts it is necessary to take into account that the sound insulation of the façade is of course provided only with the windows closed, which is not desirable from the point of view of living comfort. In addition, requiring the windows to stay closed requires different type of room ventilation, which may affect the sound insulation of facade. Therefore, caution should be exercised when installing ventilation devices (e.g. ventilation ducts in the facade) which, if not properly acoustically designed, can significantly impair the overall sound insulation of the facade. It is also important not to forget to mention that the sound insulation of the facade can also be significantly reduced due to the transmission of sound through improperly acoustically designed shutter boxes.

The conclusion is that primarily the whole area with residential buildings should be protected wherever it is possible. In that way a good acoustic comfort in the buildings is consequently also provided, without the restriction that windows have to be closed. Passive noise reduction measures with the adequate sound insulation performance of the façade should therefore be used only as an additional measure and only when they are inevitable (e.g. too high residential buildings located near high-traffic roads).

4 THE IMPACT OF INCREASING THE SOUND INSULATION OF A FAÇADE ON THE AUDIBILITY OF SPEECH FROM AN ADJACENT APARTMENTS

The environmental noise is of course not the only noise to which the people inside the residential building are exposed. They are also exposed to the noise produced inside the building, for example to the noise from adjacent apartments, like speech, TV, walking, moving of chairs etc., and to the noise of service equipment. In the case of poor

sound insulation of the facade, the influence of the outdoor noise on the indoor noise level mostly prevails compared to the effect of noise, generated by the noise sources inside the building. In such a case the environmental noise masks the impact of the noise sources in the building. But there is a completely different situation when the sound insulation of the facade is good. In such a case the sensitivity to noise generated by the noise sources inside the building becomes more highlighted, which means that it is necessary to provide better sound insulation against the noise of that sources [13,14,15]. Let us take as an example the audibility of speech from the adjacent apartment (Figure 3).

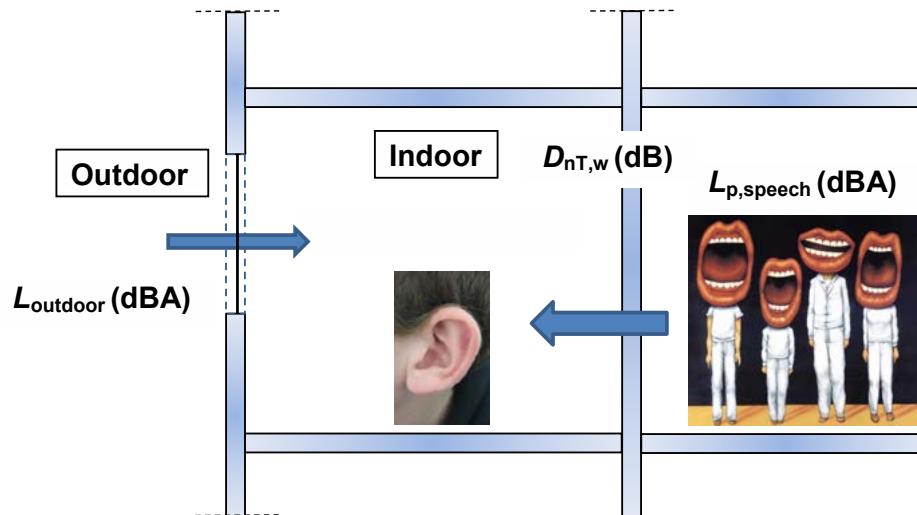


Figure 3: Audibility of speech in the adjacent room as a function of sound insulation performance $D_{nT,w}$ and the indoor noise level, produced by the environmental noise

Tables 1 and 2 show the speech audibility and intelligibility dependence on the sound insulation against adjacent room and on the indoor noise, produced by the environmental noise [15]. Sound insulation performance of the wall against adjacent room is described by the weighted standard level difference $D_{nT,w}$ in this case, like in the reference [15].

Table 1: Audibility of loud speech from adjacent room [15]

Sound insulation against adjacent room	Indoor noise, produced by the environmental noise			
	(dBA)			
	35	30	25	20
$D_{nT,w}$	Loud speech from adjacent room ($L_p = 75$ dBA) is			
(dB)				
62	not audible	not audible	not intelligible, barely audible	not intelligible
57	not audible	not intelligible, barely audible	not intelligible	still intelligible
52	not intelligible, barely audible	not intelligible	still intelligible	well intelligible
46	not intelligible	still intelligible	well intelligible	well intelligible

Table 2: Audibility of normal speech from adjacent room [15]

Sound insulation against adjacent room	Indoor noise, produced by the environmental noise			
	dBA			
	35	30	25	20
$D_{nT,w}$	Normal speech from adjacent room ($L_p = 68$ dBA) is			
dB				
62	Not audible	Not audible	Not audible	Not audible
57	Not audible	Not audible	Not audible	Not intelligible, barely audible
52	Not audible	Not audible	Not intelligible, barely audible	Not intelligible, but still audible
46	Not intelligible, barely audible	Not intelligible	Not intelligible, but still audible	Well intelligible

As mentioned before, for the geometry and standard reverberation time of a typical room it holds that $D_{nT,w} \approx R'_w$. The weighted sound reduction index for the wall between adjacent apartments, prescribed by the slovenian regulation [2], is 52 dB. In Tables 1 and 2, respectively, it can be seen that for this value in combination with the indoor noise limit 25 dBA the loud speech from the adjacent room is still intelligible, and the normal speech is barely audible and not intelligible. The value 52 dB is a minimum requirement and it is obviously not adequate for the good acoustic comfort. From Tables 1 and 2 it can also be seen that to provide a good acoustic comfort the value $D_{nT,w}$ should be at least 62 dB which usually entails radical construction measures to ensure such sound insulation performance which at the moment is still not a standard in the majority of european countries [16].

5 CONCLUSIONS

For protection against road traffic noise, active noise control measures at the source or on the path of noise propagation should be taken wherever possible. In such a way not just apartments are protected, but also the entire area in which residential buildings are located. Only in cases where these measures are not expected to be effective, e.g. in the cases of high-rise residential buildings near roads, the upper floors should be protected by passive measures by ensuring adequate sound insulation of the facades.

It turns out that, in order to provide adequate acoustic comfort in the building, it is necessary to provide relatively good sound insulation performance of the facade, especially near high-trafficked roads. By using the materials of the facade elements and facades which are common in newly built buildings and at adaptations of older buildings (eg ETICS) this is usually not guaranteed. In addition, care must be taken when using the ventilation systems in facades and by installation of shutter-boxes. If the sound insulation of these elements is inadequate, the sound insulation of the whole facade can be significantly degraded.

Last but not least it should be noted that by improving the sound insulation performance of the façade the sensitivity to noise, generated by the noise sources inside the building becomes more highlighted. For that reason good sound insulation performance of the façade shall always been linked to the good sound insulation performance of the internal partitions of the building. In the case of speech for example, the weighted standard level difference $D_{nT,w}$ of the partition should be at least 62 dB to ensure the good acoustic comfort in dwellings where the noise level is around 25 dBA. This usually entails radical construction measures to ensure such sound insulation performance which at the moment is still not the standard in the majority of european countries. It means that there is still a lot to do in this respect, with intention to raise the level of the noise control enough to ensure the desired acoustic comfort in dwellings.

REFERENCES

- [1] FEHRL Report 2006/02 Guidance manual for the implementation of low-noise road surface, 2006, Available from [http://doutoramento.schiu.com/referencias/outras/Sustainable%20road%20surfaces%20for%20traffic%20noise%20\(SILVIA\).pdf](http://doutoramento.schiu.com/referencias/outras/Sustainable%20road%20surfaces%20for%20traffic%20noise%20(SILVIA).pdf), Accessed 2020-02-04
- [2] Rules on the noise control in buildings (Official gazette No. 10/2012, Government of the Republic of Slovenia - Ministry of the Environment and Spatial planning) in conjunction with the Technical Guideline TSG-1-005:2012 Noise control in buildings,
- [3] Standard DIN 4109-1, Sound insulation in buildings-Part 1: Minimum requirements, 2018,
- [4] Standard ÖNORM B 8115-2, Sound insulation and room acoustics in buildings-Part 2: Requirements for the sound insulation, 2006,
- [5] Standard SIA 181, Sound insulation in buildings, SIA Zürich 2006,
- [6] Rasmussen, B. & Gerretsen, E.: Proposal for an Acoustic Classification Scheme for Housing, *COST Action TU0901-Towards a common framework in building acoustics throughout Europe*, COST office 2013, ISBN 978-84-616-7124-3, pp. 76-95
- [7] Gerretsen, E.: Classification of acoustic quality of dwellings-backgrounds of a renewed Dutch standard, Proceedings of Inter- noise 2001, pp. 2090-2095, ISBN 9080655430, The Hague, August 27-30,
- [8] Standard SIST EN ISO 12354-3 Building acoustics - Estimation of acoustic performance of buildings from the performance of elements-Part 3: Airborne sound insulation against outdoor sound, 2017,
- [9] Gerretsen, E. & Dunbavin, F.: Proposal of Harmonized Sound Insulation Descriptors, *COST Action TU0901-Towards a common framework in building acoustics throughout Europe*, COST office 2013, ISBN 978-84-616-7124-3, pp. 49-55
- [10] Façade sound insulation measurement results, Archive ZAG 2010-2019
- [11] Bauteildokumentation Schallschutz im Hochbau, Zusammenstellung gemessener Bauteile, ISBN 3-908483-55-7, SIA Zürich, 2005,
- [12] Nurzynski J.: The effect of additional thermal lining on the acoustic performance of a wall, 2008, Available from <https://pdfs.semanticscholar.org/2273/054faefee3ce8654fdf879b0221d6bb60de9.pdf>, Accessed: 2020-02-03
- [13] Kötz W.D. & Moll W.: Wie hoch sollte die Luftschalldämmung zwischen Wohnungen sein?, *Bauphysik* 10 (1988), H.3, pp.72-76,
- [14] Gösele K.: Zur Festlegung von Mindestanforderungen an den Luftschallschutz zwischen Wohnungen, *Bauphysik* 10 (1988), H.6, pp. 165-172,
- [15] Guideline VDI 4100: Sound insulation between rooms in buildings, Dwellings, Assessment and proposals for enhanced sound insulation between rooms, Verein Deutscher Ingenieure, Düsseldorf 2012,
- [16] Rasmussen, B. & Machimbarrena, M.: Existing Sound Insulation Performance Requirements and Classification Schemes For Housing Across Europe, *COST Action TU0901-Towards a common framework in building acoustics throughout Europe*, COST office 2013, ISBN 978-84-616-7124-3, pp.26-48.

31

Pavel Rovnaník, Cecílie Mizerová, Ivo Kusák and Pavel Schmid

Self-sensing properties of the slag geopolymer composite with graphite powder under flexure

SELF-SENSING PROPERTIES OF THE SLAG GEOPOLYMER COMPOSITE WITH GRAPHITE POWDER UNDER FLEXURE

Pavel Rovnaník, Cecílie Mizerová, Ivo Kusák and Pavel Schmid

Brno University of Technology, Faculty of Civil Engineering
Veveří 95, 602 00 Brno, Czech Republic
e-mail: rovnanik.p@vutbr.cz

SUMMARY: Development of smart materials is one of the great challenges for the sustainable building. New functionalities of common building materials can be achieved by the addition of conductive admixtures that reduce the electrical resistivity. Such composites gain the importance in the new field of applications that comprise self-sensing and self-heating materials or self-monitoring structures. This paper deals with the self-sensing properties of slag based geopolymer with graphite powder. The amount of graphite in the tested specimens was 3 and 10%, respectively. The self-sensing properties were tested under repeated flexural loading with constant amplitude in the configuration of three-point bending test. Both composites showed good sensing properties and reproducibility of the piezoresistive response to the flexural loading.

KEY WORDS: Slag; Geopolymer; Graphite; Piezoresistivity; Flexure.

1 INTRODUCTION

Electrically conducting cement-based composite materials have been extensively studied since the beginning of the new millennium [1, 2]. The studies are generally engaged in materials behaviour in various electric fields (DC, AC with various frequency) and determine a variety of material properties that are dependent on the change of the electrical resistivity. Aluminosilicate materials are considered good electrical insulators with the resistivity up to $10^9 \Omega \cdot m$ achieved for dry concrete [3]. In order to improve the electrical conductivity of these materials a conductive filler must be added to the basic mixture. Common conducting admixture are steel fibres or carbon fibres, graphite powder, steel slag, carbon nanotubes, carbon nanofibres, carbon black, or nickel powder [4–6]. Decrease in the electrical resistivity of the concrete results in new application possibilities such as development of self-sensing and self-heating composites, security composites eliminating electrical signal throughput or composites used for determining the weight of moving objects [7].

Alkali-activated slag used in current study is a clinker-free material which is considered an alternative to ordinary Portland cement concrete. This material is composed of granulated blast furnace slag and alkaline activator, which is usually alkaline hydroxide, carbonate or the most preferably silicate [1]. Alkali-activated slag is appreciated for its superior properties such as higher corrosion resistance against acid or sulphate attack [2, 8, 9] and also higher resistance to elevated temperatures [10–13].

Graphite is a carbon polymorph with a layered, planar structure. Individual layers of graphite are called graphene; within them the carbon atoms are arranged in a hexagonal lattice. These layers exhibit good conductivity along the planes, but its transversal conductivity is very low because the distance between graphene planes is 335.4 pm and the bond between them is only a weak van der Waals interaction. However, if the graphite is pressed perpendicular to the planes, these get closer to each other, which enables the easier migration of electrons between layers and leads to the enhancement of tunnelling conduction [14]. Graphite has already been used as a conductive functional filler in the fabrication of asphalt concrete with sensing properties. It dramatically decreased the electrical resistivity of this type of material and endowed it with self-sensing ability [15,16].

The present study aims to investigate the self-sensing properties of slag-based composite mortars with graphite powder as conductive admixtures under flexural loading. The results are compared to plain geopolymer mortar without graphite admixture treated under the same conditions.

2 MATERIALS AND METHODS

The mortars for the testing of the self-sensing properties were prepared from ground granulated blast furnace slag having the specific surface of 395 m²/kg and the mean particle size 17.8 μm. The solid sodium silicate SUSIL MP 2.0 (Vodní sklo, CZ) having the SiO₂/Na₂O ratio of 2.0 and content of 16.6% Na₂O was used as an activator. The fine quartz sand with a maximum grain size of 2.5 mm was used as an aggregate. In order to enhance the electrical conductivity of alkali-activated slag composite graphite powder was added. Its particle size distribution determined by laser granulometry is presented in Figure 1 and the average grain size was d₅₀ = 6.4 μm and d₉₀ = 13.0 μm. Triton X-100 (Sigma-Aldrich) was used as a dispersing agent for the graphite powder. It was added to the graphite suspension in the form of a 2% solution. In order to avoid the formation of large pores due to air entrapped during mixing, a 1% solution of the siloxane-based air-detraining agent (ADA) was used. The composition of tested mixtures is presented in Table 1.

Table 1: Composition of mixtures

Component	Slag (g)	SUSIL (g)	Sand (g)	Graphite (g)	Triton X-100 (ml)	ADA (ml)	Water (ml)
REF	2400	480	7200	-	-	-	1000
G3	2400	480	7200	72	40	28	970
G10	2400	480	7200	240	160	108	940

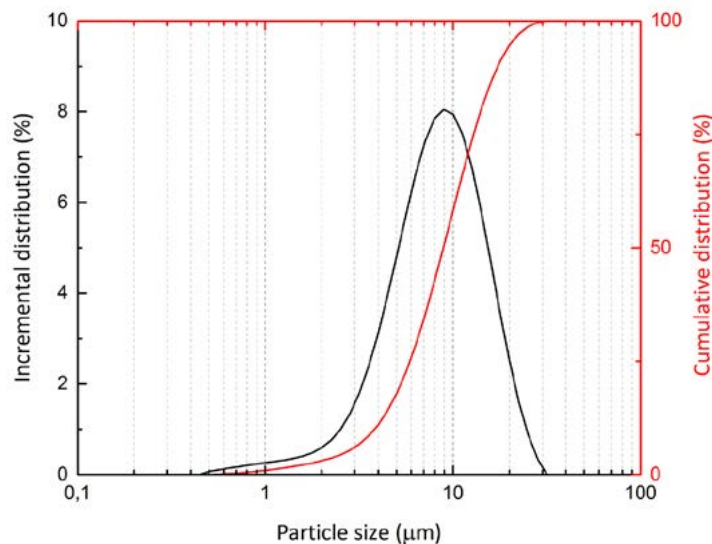


Figure 1: Particle size distribution of graphite powder obtained via laser granulometry

Alkali-activated slag was prepared according to the following procedure. Sodium silicate activator was suspended and partially dissolved in water. Then, slag and quartz aggregate were added and the mixture was stirred in a planetary mixer for about 5 min to prepare a fresh mortar. In case of composites with graphite, the graphite powder was firstly suspended in water together with Triton X-100 dispersant. Then, alkaline activator, slag and quartz sand were added and the mixture was stirred in the similar manner as the reference mixture. Finally, air-detraining agent was added in order to remove excess bubbles. Fresh mortars were cast in the prismatic moulds with dimensions 100 × 100 × 400 mm. Two specimens were prepared for each mixture. After setting the specimens were immersed in a water bath at 20 °C for 28 days. Before the measurement of sensing properties, the specimens were stored at ambient conditions until testing.

The specimens were provided with four self-adhesive copper tapes that were used as electrodes. In order to achieve better connectivity of copper tapes with slag composite, the graphite conductive paste was used as a transition layer. The distances between electrodes were 40 mm. The self-sensing properties were tested under three-point bending load with a 300 mm span using LabTest 6-1000.1.10 multi-purpose mechanical testing machine with displacement control. The measurement setup is depicted in Fig. 2. A sinusoidal signal generator Agilent 33220A and two multimeters Agilent 34410A were used to measure the electrical resistance. The frequency of AC source was 1 kHz and voltage of the sinusoidal generator was 5 V. The electrical current was calculated from the voltage measured on one of the voltmeters and the reference resistance R. The electrical resistance of the measured sample was computed from the electric current

flowing through the exact resistance R and the voltage that was measured separately on the test sample using Ohm's law and taking into account the internal resistance of the voltmeter. The longitudinal strain during loading was measured using strain gauge that was attached to the bottom tensile side of the specimen. Flexural strengths were calculated from the maximum loading force and compressive strength were measured on the far edge of each of the two residual pieces obtained from the flexural test.

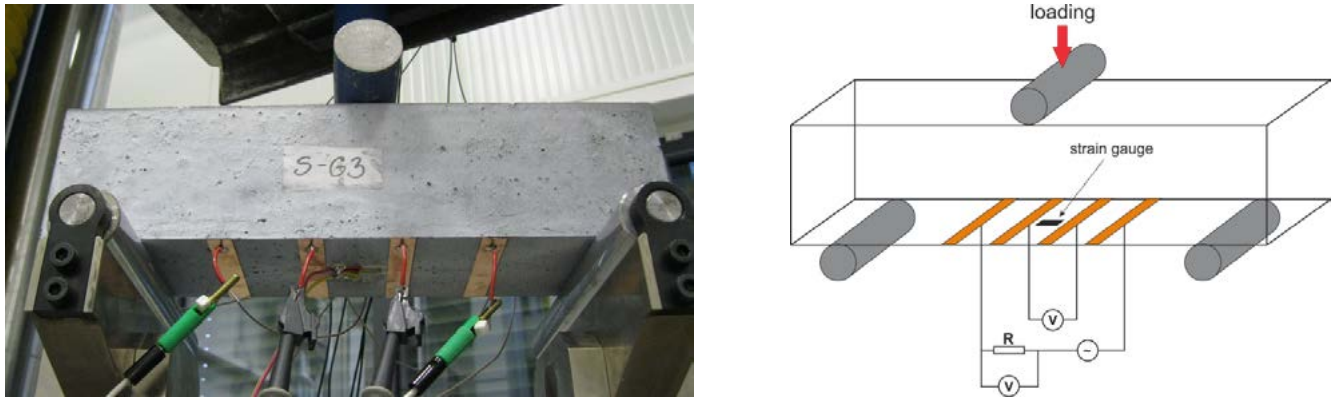


Figure 2: Placement of electrodes on the specimen surface during flexural testing and the experimental setup

3 RESULTS AND DISCUSSION

3.1 Mechanical properties

The basic mechanical properties, compressive and flexural strengths, were determined in order to evaluate the influence of the graphite powder on the mechanical performance of slag composites. Addition of graphite caused a slight deterioration of compressive strength only in the case of G10 mixture by 13% (Table 2). On the other hand, the flexural strengths of composites with graphite slightly increased but the absolute values remained quite low. These low values are generally caused by drying shrinkage of the slag geopolymer matrix forming some microcracks that can act as stress concentrators [17].

Table 2: Compressive and flexural strengths of AAS composites

Mixture	Compressive strength (MPa)	Flexural strength (MPa)
REF	58.9	2.90
G3	58.3	3.40
G10	51.4	3.08

3.2 Repeated loading

The self-sensing properties of building materials have their origin in the alteration of the conductive pathways inside composite materials, so the changes in resistivity, expressed as the fractional change in resistivity (FCR), are able to measure the sensing behaviour. The main advantage of the FCR parameter is that it is independent from loading conditions, and can be calculated as follows:

$$FCR (\%) = \frac{R - R_0}{R_0} \cdot 100, \tag{1}$$

where R is the electrical resistance and R_0 is the initial electrical resistance. The self-sensing properties of geopolymer composites were tested during repeated flexural loading in the three-point bending configuration. Totally 10 cycles were accomplished with the force amplitude between 0.07 and 1.50 kN, which corresponds to the flexural stress of 0.032–0.675 MPa. Fractional change in resistivity together with longitudinal strain of the composites during repeated loading are presented in Figs. 3–5. The strain increased during loading period and decreased during unloading which corresponds to

the tensile stress in the bottom part of the samples. The strain returned to approximately the same level at the end of each cycle and to zero at the end of the test, indicating elastic behaviour. The fractional change in resistivity generally decreased with increasing stress and increased again during unloading. However, there are some differences between tested composites depending on the graphite content. In the reference sample without any functional filler, the fractional change in resistivity slightly increased with each cycle, meaning that a kind of damage occurs though the strain measurement indicated elastic behaviour. There appeared also an additional negative peak on the resistivity curve during the unloading part of the cycle (Fig. 3). This extra peak was strong during the first cycle but it successively diminished with the increasing number of loading cycles. Similar extra peaks were previously observed during testing of concrete reinforced with carbon black and carbon fibres, but their origin have not been explained yet [18]. However, it is probably associated with the experimental setup rather than with the material itself. When the graphite had been added the additional signal disappeared although with G10 sample a weak and sharp peak can still be observed (Figs. 4 and 5). Nevertheless, the amplitude of the fractional change in resistivity is significantly higher for both graphite composites compared to the reference mixture.

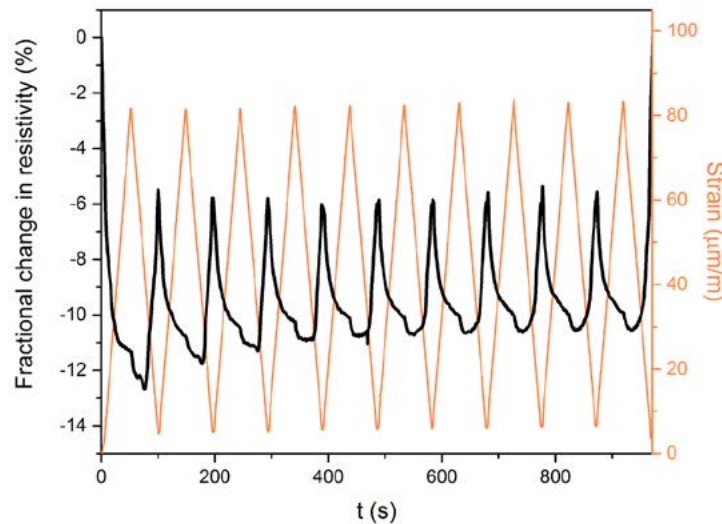


Figure 3: Fractional change in resistivity and longitudinal strain of reference sample during repeated flexural loading

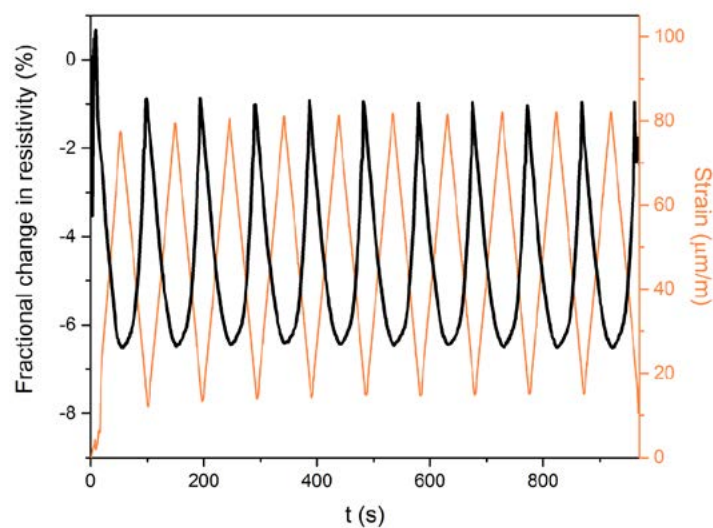


Figure 4: Fractional change in resistivity and longitudinal strain of G3 sample during repeated flexural loading

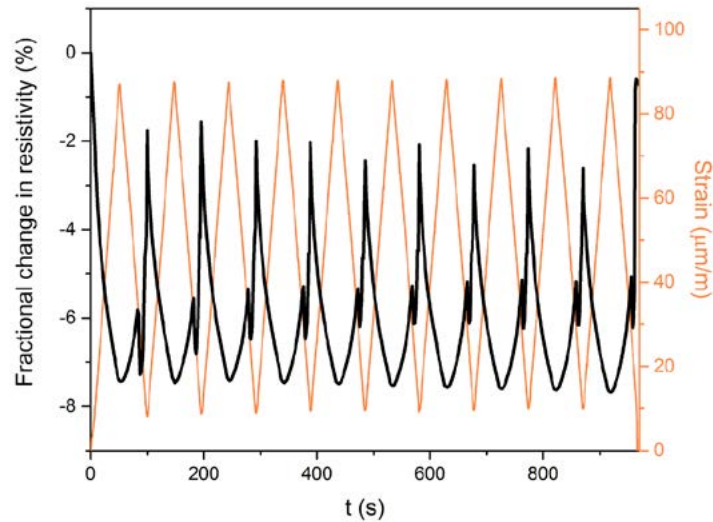


Figure 5: Fractional change in resistivity and longitudinal strain of G10 sample during repeated flexural loading

3.3 Loading until fracture

The self-sensing properties of geopolymer composites were also tested during monotonous loading until fracture. The applied loading rate was $5 \text{ N}\cdot\text{s}^{-1}$ and the maximum load decreased with increasing amount of functional filler. Figs. 6–8 show fractional change in resistivity together with longitudinal strain of tested samples during monotonous loading. Strain curves for REF and G3 samples are very similar. The strain increased linearly at lower loading stress and then increased abruptly just before complete failure. In the case of G10 sample, a sudden increase in strain near the point of failure did not appear because the strain gauge was destroyed couple of seconds before the fracture. The fractional change in resistivity decreased during flexural loading and increased abruptly when the beam cracked, and hence the conductive routes were destroyed. In the case of REF and G3 samples, a non-linear trend was observed. After initial drop in resistivity during the first 100 s, only very slow decline was achieved then up to failure point. Especially, with the reference mixture the change in resistivity was practically negligible (Fig. 6). This is even more obvious when we compare the curves of the fractional change in resistivity versus longitudinal strain for all three mixtures (Fig. 9). In the case of G10 composite, there is a gradual decrease in *FCR* up to the point of fracture. Therefore, despite the noticeable electrical response to the mechanical loading, the plain slag-based geopolymer is not suitable for the self-monitoring of structural elements under flexural load. Another aspect of the composite with graphite is that addition of graphite significantly decreased the longitudinal strain of the composite before the point of fracture (Fig. 9). This implies that graphite slightly improves the stiffness of the material in flexure, which is in accordance with previous mechanical fracture analysis [19].

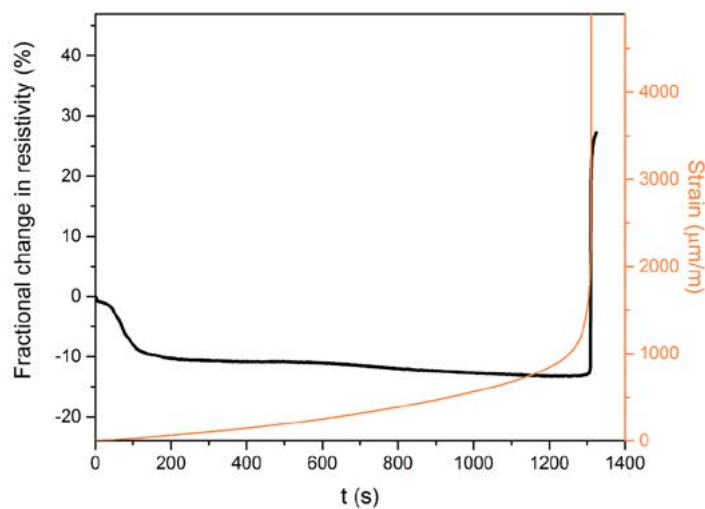


Figure 6: Fractional change in resistivity and longitudinal strain of reference sample during flexural loading until fracture

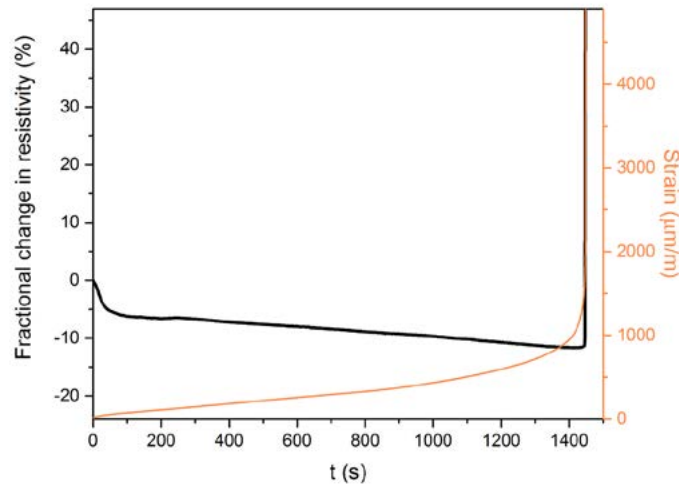


Figure 7: Fractional change in resistivity and longitudinal strain of G3 sample during flexural loading until fracture

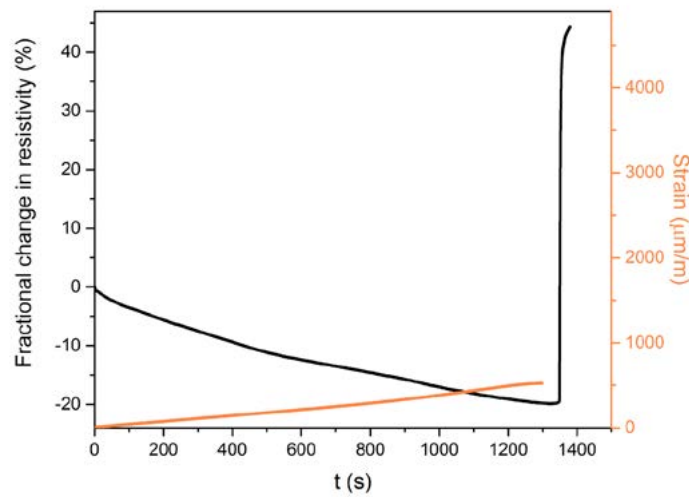


Figure 8: Fractional change in resistivity and longitudinal strain of G10 sample during flexural loading until fracture

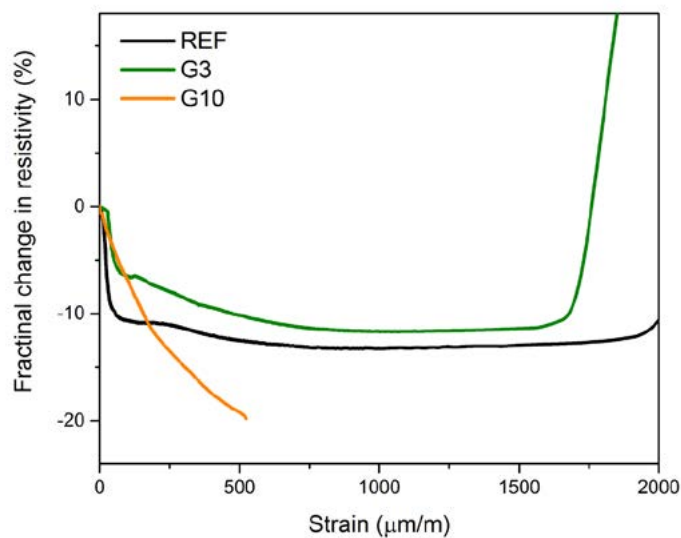


Figure 9: Comparison of trends in the fractional change in resistivity vs. longitudinal strain for three different slag composites

4 CONCLUSIONS

In this paper, self-sensing properties of slag-based composites with graphite powder as a conductive filler under flexural loading were investigated. The self-sensing properties were compared with plain composite without any conductive admixture as a reference material. Results of the mechanical testing showed that the addition of graphite powder up to 10% has almost no negative effect neither on the compressive nor flexural strength of the slag composite. All three tested mixtures exhibited self-sensing properties during both repeated and monotonous flexural loading. Although plain slag composite showed an electrical response to the mechanical loading, its sensitivity was lower than in the case of graphite-doped composites. The repeatability of the self-sensing measurement was very good and practically no fatigue damage during repeated loading was observed. REF and G3 samples showed lower electrical sensitivity when higher values of flexural force are applied. Especially, with the reference mixture the change in resistivity was almost negligible. As a conclusion, the measurement of the self-sensing properties of slag-based geopolymer composites revealed that addition of graphite up to 10% has a positive effect on its piezoresistive sensitivity and these composites are suitable for the self-monitoring of structural elements under flexural load.

ACKNOWLEDGMENTS

This outcome was elaborated with the financial support of Czech Science Foundation under the project No.19-11516S.

REFERENCES

- [1] Shi, C.; Roy, D.M. & Krivenko P.V.: *Alkali-activated Cements and Concretes*, Taylor & Francis, Oxon, UK, (2006)
- [2] Byfors, K. et al.: *ACI SP Proceedings*, 114 (1989) 1429
- [3] Monfore, G.E.: The electrical resistivity of concrete, *J. PCA Res. Dev. Lab.*, 10 (1968), pp. 35-48.
- [4] Hou, Z.; Li, Z.; Wang, J.: Electrical Conductivity of the Carbon Fiber Conductive Concrete, *J. Wuhan Univ. Technol.-Mater. Sci. Ed.*, 22 (2007), pp. 346-349.
- [5] Tian, X.; Hu, H.: Test and study on electrical property of conductive concrete, *Proc. Earth Planet. Sci.*, 5 (2012), pp. 83-87.
- [6] Han, B.; Ding, S.; Yu, X.: Intrinsic self-sensing concrete and structures: A review. *Measurement*, 59 (2015), pp. 110-128.
- [7] Han, B.; Yu, X.; Ou, J.: *Self-Sensing Concrete in Smart Structures*, Butterworth Heinemann, Oxford, UK, (2014)
- [8] Bakharev, T.; Sanjayan, J.G.; Cheng, Y.B.: Sulfate attack on alkali-activated slag concrete, *Cem. Concr. Res.*, 32 (2002), pp. 211-216.
- [9] Bakharev, T.; Sanjayan, J.G.; Cheng, Y.B.: Resistance of alkali-activated slag concrete to acid attack, *Cem. Concr. Res.*, 33 (2003), pp. 1607-1611.
- [10] Rovnanik, P.; Bayer, P.; Rovnaníková, P.: Characterization of alkali activated slag paste after exposure to high temperatures, *Constr. Build. Mat.*, 47 (2013), pp. 1479-1487.
- [11] Zuda, L. et al.: Thermal properties of alkali-activated aluminosilicate composite with lightweight aggregates at elevated temperatures, *Fire Mater.*, 35 (2011), pp. 231-244.
- [12] Guerrieri, M.; Sanjayan, J.; Collins, F.: Residual strength properties of sodium silicate alkali activated slag paste exposed to elevated temperatures, *Mater. Struct.*, 43 (2010), pp. 765-773.
- [13] Rashad, A.M. et al.: Chemical and mechanical stability of sodium sulfate activated slag after exposure to elevated temperature, *Cem. Concr. Res.*, 42 (2012), pp. 333-343.
- [14] Han, B.; Yu, X.; Kwon, E.: A self-sensing carbon nanotube/cement composite for traffic monitoring, *Nanotechnology*, 20 (2009), pp. 445501-445505.
- [15] Sun, S. et al.: Nano graphite platelets-enabled piezoresistive cementitious composites for structural health monitoring, *Constr. Build. Mater.*, 136 (2017), pp. 314-328.
- [16] Liu, X.; Wu, S.: Study on the graphite and carbon fiber modified asphalt concrete, *Constr. Build. Mater.*, 25 (2011), pp. 1807-1811.
- [17] Collins, F.G.; Sanjayan, J.G.: Microcracking and strength development of alkali-activated slag concrete, *Cem. Concr. Comp.*, 23 (2001), pp. 345-352.
- [18] Bontea, D.-M.; Chung, D.D.L.; Lee, G.C.: Damage in carbon fiber-reinforced concrete, monitored by electrical resistance measurement, *Cem. Concr. Res.*, 30 (2000), pp. 651-659.
- [19] Rovnaník, P.; Šimonová, H.; Topolář, L.; Keršner, Z.: Mechanical fracture properties of alkali-activated slag with graphite filler. In *Proceedings of the international conference Structural and Physical Aspects of Civil Engineering 2016*, Technical University of Košice, ISBN 978-80-553-2643-6, (2016) [CD].

32

Fidan Salihu, Meri Cvetkovska, Koce Todorov, Nikola Postolov and Riste Volčev

Inspection, assessment and repair of fire damaged concrete structure

INSPECTION, ASSESSMENT AND REPAIR OF FIRE DAMAGED CONCRETE STRUCTURE

Fidan Salihu¹, Meri Cvetkovska², Koce Todorov³, Nikola Postolov⁴ and Riste Volčev⁵

¹ Faculty of Civil Engineering and Architecture, University of Prishtina "Hasan Prishtina"
Prishtina, Kosovo
e-mail: fidan.salihu@uni-pr.edu

^{2,3,4,5} Faculty of Civil Engineering, Ss. Cyril and Methodius University in Skopje
Blvd Partizanski odredi 24, 1000 Skopje, North Macedonia
e-mail: cvetkovska@gf.ukim.edu.mk , todorov@gf.ukim.edu.mk , postolov@gf.ukim.edu.mk , volcev@gf.ukim.edu.mk

SUMMARY: Fire is a potential threat for any building and can seriously damage the structure. Structural response to fire is very complex and depends on used construction materials, type and geometrical characteristics of structural elements, duration and nature of fire, existing structural loads, structural and architectural details, etc. Proper design and successful repair of RC structure damaged in fire can only be provided if a detailed in-situ investigation, laboratory investigation and correct assessment of residual structural capacity is made. In December 2017, the basement of a building in Skopje was in fire. A part of the structure was in fire and the last three spans were completely burned. According to the damages recorded in situ, it was found out that fire caused severe damage to the reinforced concrete bearing structure. After the visual inspection, the residual concrete strength was defined by sclerometer and the results were compared with results obtained by the nonlinear transient heat transfer analysis of fire exposed elements. For the thermal analysis and for the nonlinear stress-strain analysis of the whole structure the program SAFIR was used and the results are presented in this paper. The results showed that during the fire action the strength and stiffness of structural elements were significantly reduced. Based on these results and the detailed in-situ investigation, an adequate repair of the damaged elements of the bearing structure was suggested and details are presented in this paper.

KEY WORDS: RC structure; fire; damages; assessment; thermal analysis, stress-strain analysis; repair method.

1 INTRODUCTION

In 2017 in the basement of a building in Skopje a fire broke out and affected one third of the basement area. The space in which the fire occurred is partially under the ground level. It is separated from the surrounding soil by 25 cm reinforced concrete wall on three sides and by 25 cm ceramic block wall from the rest of the basement (Figure 1). This part of the basement was used as a warehouse and contained high-calorie fuel (diapers). In the rest of the basement there was no burning material (garage in which in that moment there were no cars) which could be affected by the flames or by self-ignition due to high temperatures, so the fire did not spread to that part of the basement, which is evident from the fact that flames did not go out through the small windows on the east façade and did not cause the façade, made of extruded polystyrene, to be ignited. In the zone where the fire started, the windows planned by the project were not built. Due to the thermal insulation on the ceiling of the basement, made of extruded polystyrene, large amounts of smoke and heat were released. The smoke prevented the fire fighting brigade to react on time, so the fire was localized and brought under control after more than 8 hours of occurrence. Poor oxygen supply (low ventilation due to lack of windows) and high specific fire load (diaper storage) caused prolonged burning, followed by a slow rise in temperature, which reached high values after several hours of burning.

After the fire was extinguished, visual inspection was carried out and visible damages to most of the structural elements in the fire zone were registered. Out of the fire zone, the structure was not damaged. The structure was badly damaged and for the safety reasons it was suggested the concrete to be tested by a non-destructive method, by sclerometer, and the results to be compared with results obtained by the nonlinear transient heat transfer analysis conducted by the program SAFIR [1]. Based on the results of the visual inspection, the non-destructive testing of concrete and the conducted stress strain analysis, the residual load-bearing capacity of the structure was determined and adequate repair of damaged elements was suggested.

2 DESCRIPTION OF THE FIRE EXPOSED STRUCTURE

The construction of the residential building consists of four reinforced concrete frames in the y direction, at a distance of 4.0 + 6.0 + 4.8 m and five reinforced concrete frames in the x direction, at a distance of 4.83 + 4.55 + 4.55 + 4.83 m. (Figure 1). The Y1 frame is designed as reinforced concrete wall (P1) with a thickness of 25cm. The rest of the frames are made of reinforced concrete columns and beams. The beam are with dimensions of 25/50 cm or 30/50 respectively (beams in the middle frames Y2 and Y3). The columns are of different cross-sections. In the basement, in the fire zone, columns are 25/60 cm and 25/120 cm. The height of the underground level is 2.7 m. The floor over the basement is a reinforced concrete slab reinforced in two directions, with different spans (depending on the axial distances between the frames), with a thickness of 14 cm. The part of the building which is in contact with the surrounding soil is reinforced concrete wall with a thickness of 25 cm. All structural elements are designed with concrete MB30 and reinforcement RA 400 / 500-2.

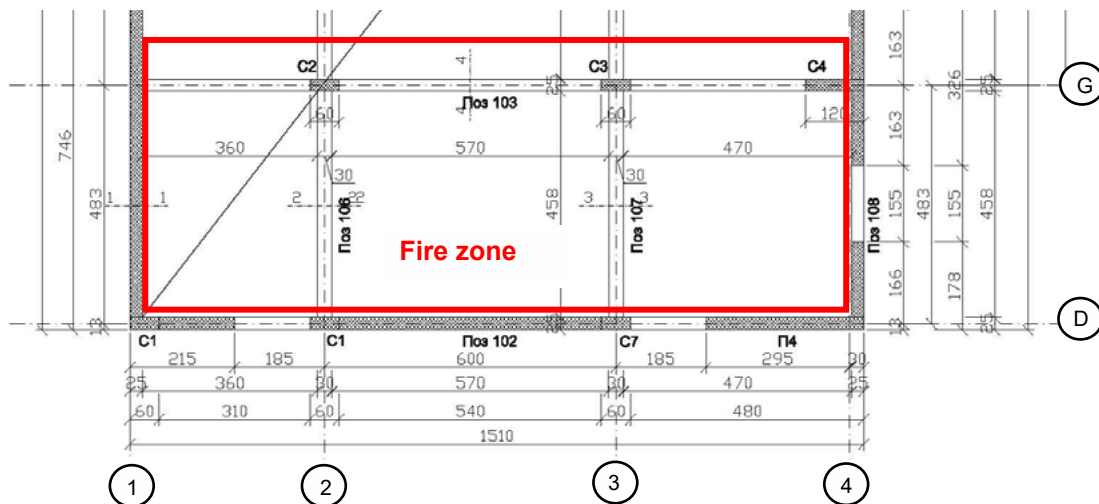


Figure 1: Disposition of the structural elements in fire zone

3 DESCRIPTION OF STRUCTURAL DAMAGES CAUSED BY FIRE

An on-site inspection of the fire exposed part of the structure was performed and the most important damages are presented on the following figures.

1. Spalling of the concrete and total collapse of the reinforced concrete slab in middle span (Figure 2) defined with system lines 2 and 3 in Y direction and G and D in X direction (Figure 1).
2. Falling off of the concrete cover of the RC slab (Figure 3) defined with system lines 1 and 2 in Y direction and G and D in X direction (Figure 1).
3. Falling off of the concrete cover and deformed reinforcement of RC walls (Figure 4) defined with system line 1 in Y direction and system line D in X direction (Figure 1).
4. Micro and macro cracks in RC beams and RC columns and falling off of concrete cover (Figure 5)



Figure 2: Spalling of concrete and collapse of RC slab defined



Figure 3: Falling off of concrete cover of RC slab defined with

with system lines 2 and 3 in Y, and G and D in X direction

system lines 1 and 2 in Y direction and G and D in X direction



Figure 4: Falling off of concrete cover of RC wall



Figure 5: Micro and macro cracks in RC beam

4 ASSESSMENT OF RESIDUAL BEARING CAPACITY OF FIRE EXPOSED STRUCTURE

When exposed to high temperature, concrete suffer significant degradation of compressive strength as well as other mechanical characteristics. The loss of mechanical properties is permanent, which means that during the cooling stage the concrete does not recover the strength and deformation characteristics. In case of hot rolled reinforcing bars the degradation process is reversible. Although the reinforcement loses the mechanical properties during the heating stage, during the cooling stage they are completely recovered, but the plastic deformations that occur in stage of temperature rise are irreversible. In order to determine the strength characteristics of the concrete after the action of fire, a non-destructive test was carried out using a Schmitt hammer (sclerometer). The test was carried out at a total of 14 measuring points (7 in the fire zone and 7 out of this zone) and a reduction of the compressive strength of concrete of about 25% was found only in the areas directly affected by the fire. Out of the fire zone the compressive strength was 40 Mpa, while in the fire zone it was 30 Mpa in average. This leads to the conclusion that, despite the long-term impact of fire (more than 8 hours), as a result of the low ventilation factor the temperature rise was slow and didn't rich more than 1000°C. This conclusion was supported by data on air temperatures, obtained by infrared camera. The measurements were carried out by firefighters.

The level of damage of the fire exposed structure, as well as its residual load bearing capacity, may be defined numerically, by parallel thermal and stress-strain analysis. The best results are achieved when the structure is analysed as a whole, but depending on the calculation options, the analysis may be conducted for a part of the structure that is directly exposed to fire, or for each structural element separately. From the aspect of defining the support conditions, the best results are achieved when the analysis are conducted for the whole structure, or eventually for part of it, in which case the surrounding cold elements which are not influenced by fire have to be included too.

For the nonlinear and transient thermal and stress-strain analysis of the fire exposed structure, the program SAFIR [1] was used. This program is specialized for structural fire analysis and is based on FEM. The analysis consists of two separate steps. The first step is the thermal analysis of the cross-sections of all fire exposed structural elements. The elements could be exposed to different nominal fire curves, as: standard fire ISO 834, parametric fire curve, other existing fire curves that define time-temperature relationship, or real fire that has to be previously defined. The second step is the stress-strain analysis of the structural elements or the whole structure and defines the structural response to high temperatures. The nonlinearity of the problem comes from: changes in material properties by high temperatures (mechanical and thermal), nonlinear temperature distribution in element's cross sections (no heat transfer is considered along the axis of the beams and columns) and the continuous change of the internal forces.

In this case the most damaged structural elements were defined and only one part of the whole structure was analysed. The most damaged RC frame, defined with system line "G", and the most affected RC slabs, defined with system lines G and D in X direction (Figure 1), were analysed. The input parameters, as: geometrical characteristics of

elements, physical and mechanical properties of construction materials and external loads were taken from the Main design. The geometry and support conditions are presented in Figures 6a and 6b, respectively.

The temperature field in the cross sections of the fire exposed elements depends on: intensity and duration of the fire (the fire model); position of the element in relation to the fire sector; element geometry; heat transfer coefficients (convection and radiation coefficients); thermal conductivity, specific heat and density of construction materials (concrete and steel).

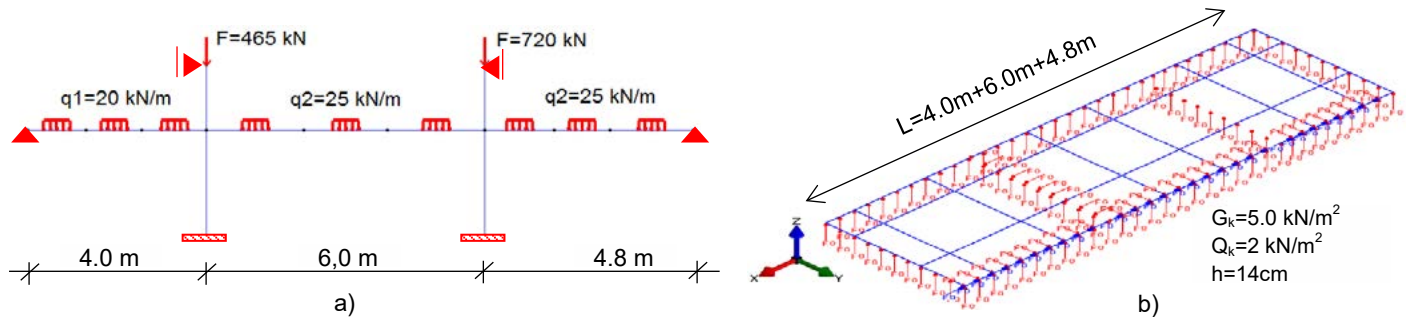


Figure 6: Geometry, support conditions and loads for analysed parts of the structure: a) RC frame, b) RC slabs

Based on the change in concrete colour and the depth to which it occurs, as well as the data from the fire-fighting brigade, it was determined that the fire lasted more than 8 hours. Because of the high fire load (stored diapers) and the low ventilation factor (windows preliminary planned were not built-in), high temperatures (almost 1000°C) were developed, but the temperature rise was very slow. This fact was important for defining the temperature-time curve, which refers to the fluid temperature in the fire compartment.

For the numerical analysis the ISO 834 standard fire curve was used although it didn't correspond to the real temperature-time curve and because of that, according to Eurocode 1 part 1-2 [2], the equivalent time of fire exposure was calculated. The temperature dependent material properties of steel and concrete were adopted as recommended in Eurocode 2, part 1-2 [3].

The thermal analysis results for the temperature fields in the cross sections of the beams and columns of the analysed RC frame are presented in Figure 7. These results are at the moment of failure of the RC frame, that numerically happened after 2.8 hours of fire action. The columns were exposed from all four sides and the beam was exposed only from three sides.

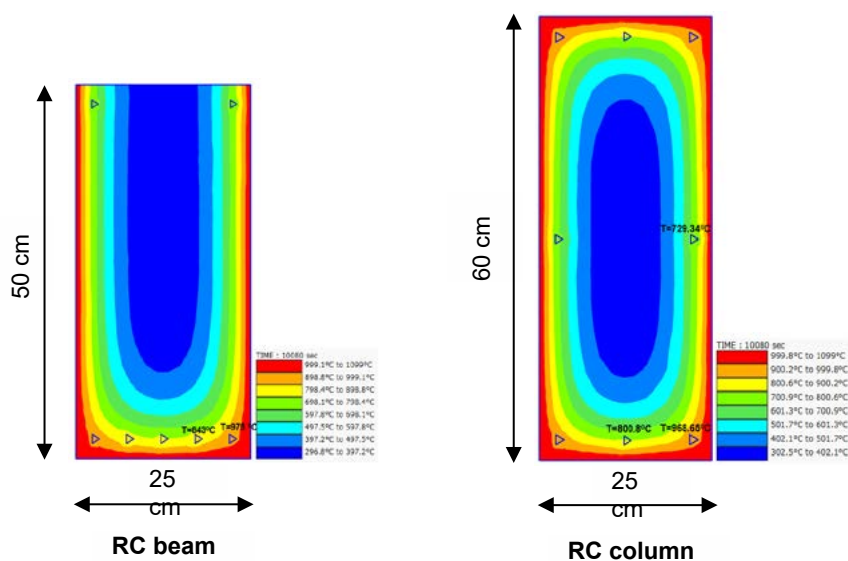


Figure 7: Temperature distribution in the cross sections of structural elements of most damaged RC frame, at the moment of numerically achieved failure, $t=2.8$ hours

As a result of the non-uniform temperature distribution in the cross section of the fire exposed elements and restrained

axial dilatation, the bending moments were redistributed [4] (Figure 8) and compressive axial force was induced (Figure 9a). The vertical displacements of the RC beam at the moment of failure ($t=2.8$ hours) are presented in Figure 9b. In practice the RC frame didn't collapse even after 8 hours of fire exposure. This is due to the low temperature rise and correspond to the equivalent time of standard fire exposure, which is 79 minutes and is less than the numerically achieved time of failure.

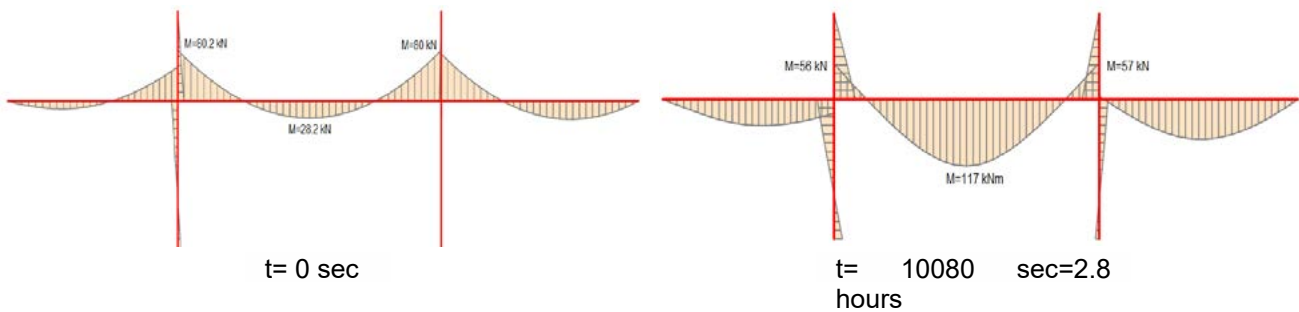


Figure 8: Redistribution of bending moments in the most damaged RC frame defined with system line "G", as a result of fire action

The RC slabs defined with system lines "G" and "D" (Figure 1) were analysed too. The two way slabs were constructed without top reinforcement in the middle part of the span. The most of the burning materials were under the slab in the middle span and as a result of the high temperatures spalling of concrete occurred, the reinforcement was directly exposed to fire and was transformed to catenary (Figure 2). The slab in the first and third span "survived" the fire. The slab defined with system lines "1" and "2" was visibly damaged, falling off of concrete cover occurred (Figure 3). According to the numerical analysis and considering the deflection criterion, failure occurred after 3 hours of ISO 834 fire action only in the last two spans. The membrane forces at moment $t=3$ hours are presented in Figure 11.

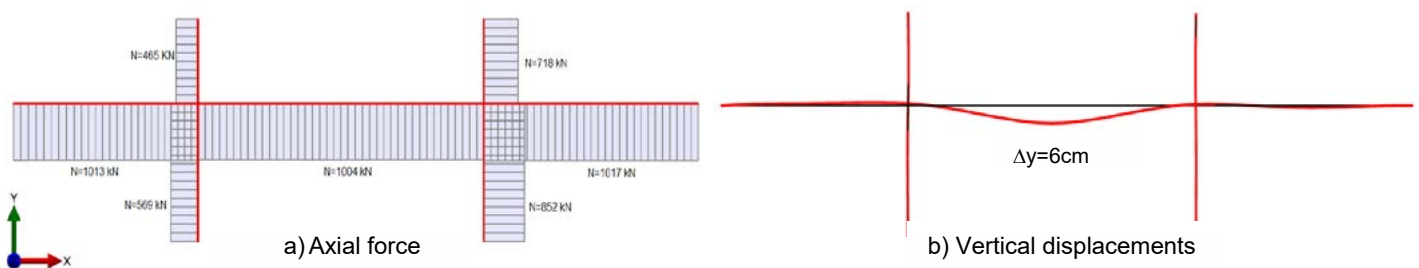


Figure 9: Axial forces and vertical displacements at the moment of numerically achieved failure

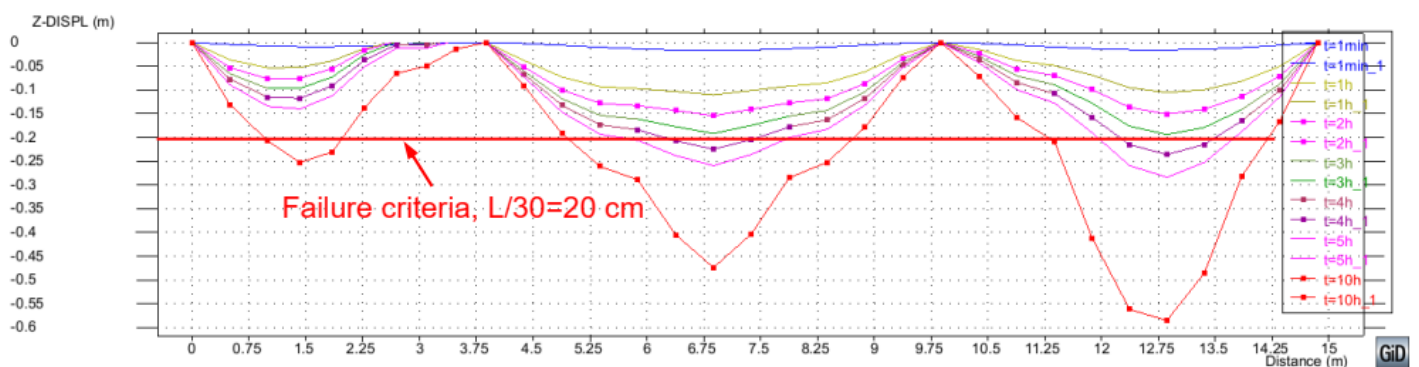


Figure 10: Numerically defined vertical displacements of the RC slabs in period of 10 hours of fire action

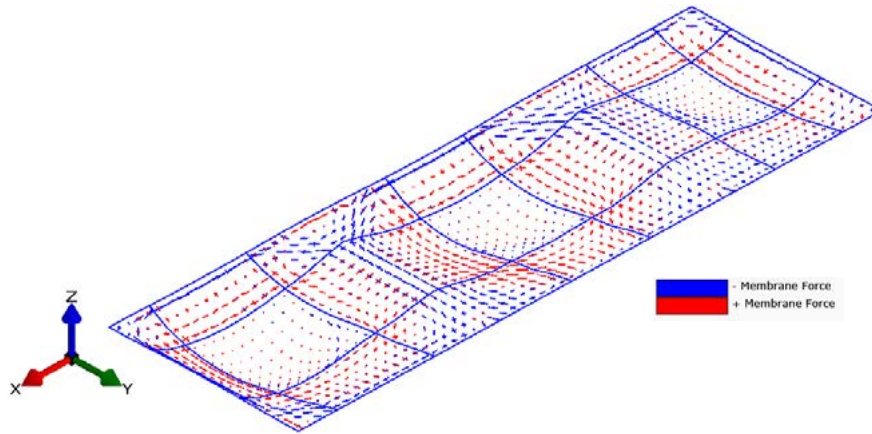


Figure 11: Membrane forces in the RC slabs at the moment of numerically achieved failure (t=3 hours)

5 STRENGTHENING AND REPAIR OF THE FIRE DAMAGED RC STRUCTURE

Based on the on-site recorded damages and numerically defined residual strength of the fire damaged RC structure, strengthening and repair measures were defined. The purpose of the suggested measures was restoring the initial mechanical resistance of the structure. According to the technological process, the suggested measures were divided into two groups: preparatory works and strengthening and repair measures. The preparatory works included:

- Demolishing of the collapsed reinforced concrete slab defined with the system lines 2 and 3 in Y direction and G and D in the X direction, respectively.
- Removal of the cement liner from the beams where the dimensions of the cross section should be increased.
- Removal of the cracked and crashed concrete from the surface layers of elements up to the level of unaffected concrete.

The purpose of the suggested strengthening and repair measures was to restore the load bearing capacity of the fired elements to their initial state, i.e. to the state prior to the occurrence of the fire. For this purpose demolition of the collapsed slab and construction of a completely new one was planned, as well as increase in cross section of the structural elements by adding new reinforcement and new concrete layer.

The thickness of the new slab defined by system lines 2 and 3 in the Y direction, and G and D in the X direction, was 14cm. The existing top reinforcement at the four sides of the slab was cleaned and used as main top reinforcement at the supports. In the transverse direction a new distribution bars $\varnothing 8/20\text{cm}$ were added. The bottom bars were cut at a distance of min. $50\varnothing$, measured from the inside of the beam, and used as anchors for the new reinforcing bars in both directions. The required new bottom reinforcement was determined according to the data from the original design documentation and was $\varnothing 8/15\text{cm}$ in both directions (Figure 12a).

The part of the slab defined with the system lines 1 and 2 in line Y, was planned to be repaired by scratching the degraded concrete (concrete cover layer with a thickness of 2 cm), setting up of anchors $\varnothing 10/45/45$, new bottom reinforcement $\varnothing 8/15\text{cm}$ in both directions and shotcreting new concrete layer with thickness 5 cm.

Columns C2 and C3 were repaired by increasing the cross-section dimensions and adding new reinforcement. The thickness of the new concrete layer was 12.5cm from each side. The new cross section dimensions are 50/85cm. The additional longitudinal reinforcement was RA16 $\varnothing 16$ and stirrups were $\varnothing 8/10\text{cm}$. Connection to the foundations was provided by anchors (Figure 12b).



Figure 12: Repair of: a) RC slab, b) RC column

Reinforced concrete walls were repaired by scratching the degraded concrete (the concrete cover with thickness of 2 cm), anchoring $\varnothing 10/45/45$, installment of new reinforcement $\varnothing 8/15\text{cm}$ in both directions and shotcreting of new concrete layer with thickness of 5cm (Figure 13).

The reinforced concrete beams in the fire zone, i.e. the beam defined with system line G in X direction, and beams defined with system lines 2 and 3 in Y direction, were repaired by increasing the cross section dimensions on three sides (laterally and from above). On lateral sides the new beams parallel to the existing ones were constructed. The parallel beams were 12.5cm width and were reinforced with $3\varnothing 14$ at the bottom and $2\varnothing 14$ at the top.

The cooperation with the existing beams was provided by side anchors $\varnothing 10/50$ cm, stirrups $\varnothing 8/10/20$ passing through the openings in the existing slab and additional reinforcing bars over the existing beams. In such a way the height of the beams was increased by 5 cm. The additional concrete layer was incorporated into the plane of the cement liner of the upper floor. The new dimensions of the RC beams are 50/55 cm (Figure 14).



Figure 13: Repair of RC walls



Figure 14: Repair of RC beams

6 EQUIVALENT TIME OF STANDARD FIRE EXPOSURE

In case of fire compartment with mainly cellulosic type of fire loads, the equivalent time of standard fire exposure is defined by:

$$t_{e,d} = (q_{f,d} \cdot k_b \cdot w_f) k_c$$

$q_{f,d}$ is the design fire load density according to EN 1991-1-2, annex E [2]. In case of diapers (a lot of paper material) the characteristic load value is $q_{f,k} = 1500 \text{ MJ/m}^2$. In the basement there was no active fire protection system, the fire risk was high and the final value of the design fire load density is: $q_{f,d} = 1500 \cdot 1.5 \cdot 1.0 = 2250 \text{ MJ/m}^2$

k_b is the conversion factor. Where no detailed assessment of the thermal properties of the enclosure is made, the conversion factor k_b may be taken as: $k_b = 0,07$

w_f is the ventilation factor. For small fire compartments [$A_f < 100 \text{ m}^2$] without openings in the roof, the factor w_f may be calculated as: $w_f = 0^{-1/2} \cdot A_f / A_t$. In this case there were no windows (the opening factor is almost 0) and the ventilation factor was less than 0.5.

k_c is the correction factor and is function of the material composing structural cross-sections. For RC structure $k_c = 1.0$

The equivalent time of standard fire exposure is: $t_{e,d} = 79 \text{ min}$. Numerically achieved fire resistance of structure is $t_{f,d} = 2.8 \text{ hours}$ and the criterion $t_{e,d} < t_{f,d}$ is fulfilled.

7 CONCLUSIONS

With the proposed strengthening and repair measures the load-bearing capacity of the structure was improved and the function of building was restored. The whole process lasted less than one month which was very important from aspect of providing living conditions in the building.

REFERENCES

- [1] SAFIR-Computer program, University of Liege, Belgium, 2014
- [2] European Committee for Standardization: *EN 1991-1-1, Eurocode 1: Actions on structures - Part 1-2: General actions - Actions on structures exposed to fire*, CEN, Brussels (2004)
- [3] European Committee for Standardization: *EN 1992-1-2, Eurocode 2 – Design of concrete structures - Part 1-2: General rules. Structural fire design*, CEN, Brussels (2004)
- [4] Cvetkovska, N.; Knezevic, M.; Qiang, X.; Chifliganec, C.; Lazarevska, M.; Trombeva Gavriloska, A.: Fire scenario influence on fire resistance of reinforced concrete frame structure, *Procedia Engineering-ELSEVIER*, Vol. 211, 2018, pp 28-35

33

Paulo Šćulac, Davor Grandić and Ivana Štimac Grandić

Degradation of tension stiffening due to corrosion – an experimental study on cracked specimens

DEGRADATION OF TENSION STIFFENING DUE TO CORROSION – AN EXPERIMENTAL STUDY ON CRACKED SPECIMENS

Paulo Šćulac, Davor Grandić and Ivana Štimac Grandić

University of Rijeka, Faculty of Civil Engineering
Radmile Matejčić 3, 51000 Rijeka, Croatia

e-mail: paulo.sculac@gradri.uniri.hr, davor.grandic@gradri.uniri.hr, istimac@gradri.uniri.hr

SUMMARY: In this work an experimental research will be presented in which reinforced concrete specimens were exposed to accelerated corrosion and tested in uniaxial tension in order to investigate the degradation of tension stiffening due to reinforcement corrosion. Before exposing the reinforced concrete specimens to accelerated corrosion in a cyclic corrosion test chamber cracks were introduced into the specimens. Testing was conducted on both corroded and controlling un-corroded specimens, and a relationship between the applied load and mean strain of the cracked specimens was established. The proposed test-setup is closer to the nature of a great number of reinforced concrete structures subjected mainly to bending, meaning that the cracks form in concrete members already at the beginning of the exploitation of the construction, i.e. well before the corrosion process has started.

KEY WORDS: reinforced concrete, accelerated corrosion, pitting, tension stiffening, deterioration, uniaxial tension

1 INTRODUCTION

Experiments on reinforced concrete specimens with corroded reinforcement loaded in uniaxial tension have been performed by many authors. Amleh and Mirza [1] carried out an experimental campaign using 14 specimens, 100 mm in diameter and 1000 mm long reinforced only with a 20 mm bar in the middle of the section. The specimens were first electrochemically corroded in a tank with 5 % sodium-chloride (NaCl) solution by using electric current (several levels of corrosion were achieved), and then loaded in uniaxial tension by applying force at both ends of the reinforcing bar protruding from the concrete specimen. Shimomura and Maruyama [2] demonstrated that corrosion reduces not only the reinforcing bar cross-sectional area but also the tension stiffening of the member with corroded reinforcement. Their experimental campaign consisted of 7 specimens and was similar to [1], with the main difference that the cross-section was square (100x100 mm). In [3] 10 specimens were prepared as in previous studies and tested in uniaxial tension, but here the specimens were laid and tested horizontally. Giordano with co-workers [4] investigated the effects of corrosion deterioration in an experimental campaign where the specimens were simultaneously subjected to loading (static or cyclic) and accelerated electrochemical corrosion. Prismatic specimens with 90x90 mm cross-section of 500 mm length and 14 mm bars were used. A power supply was connected to the bar (which acted like an anode) while 4 stainless steel plates were connected to the specimen sides, with the insertion of stainless steel wool, and acted like cathodes around the specimen. 3% of NaCl by weight of cement was also added in the concrete mix to ensure reinforcement depassivation. The concentration of corrosion was evident in the specimens subjected to cyclic loading [5]. Uniaxial tensile tests on 4 specimens with corroded reinforcement were also conducted by Kim and co-workers [6]. Corrosion was induced by electrochemical process using a pool containing NaCl solution with a copper plate inside placed on the top surface of the specimens, and electric current applied between the rebar and the copper plate. The location of the pool was either on the entire top surface, half, centre or only on the side, thus inducing irregular corrosion. Finally, Imperatore and her team [7] tested 2 full-scale 3 meters long tie specimens (150x150 mm with an embedded 16 mm bar) which were artificially corroded in a pool with NaCl solution.

As can be observed, in experiments carried out so far (except in [4]) the specimens are first corroded by an external current power supply and then subjected to uniaxial tension, i.e. specimens do not have cracks when the accelerated corrosion is induced. Disadvantage of the effect of corrosion on deterioration of RC elements obtained in this manner lies in the fact that (i) members in structures usually subjected to bending and/or axial force already have cracks

perpendicular to longitudinal reinforcement, and that (ii) galvanostatic accelerated corrosion (which causes mostly homogeneous reinforcement corrosion) does not represent the actual corrosion process under natural environment (localised corrosion) [8].

In this paper test setup and results of a preliminary series of RC ties will be presented: specimens were first subjected to uniaxial loading in order to induce cracks and afterwards exposed to accelerated corrosion. Corrosion was induced in an artificial climate environment, by exchanging wet (salt water) and dry (heating) cycles, simulating sufficiently representative the natural process of corrosion. After the corrosion process the specimens were again loaded in tension and a relationship between the applied load and mean strain of the cracked specimens was established.

This project is a continuation of a previously conducted comprehensive experimental research on reinforced concrete beam and slab specimens [9]. The specimens were simultaneously subjected to accelerated corrosion of reinforcement in an environmental chamber for 383 days, with wetting and drying cycles (representing natural chloride environment) and sustained loading (what caused cracks in concrete) for the whole duration of the experiment. Deflections and crack pattern was periodically monitored. During the experiment a high level of reinforcement corrosion was achieved (up to 8% and 3% of mass loss in beams and plates, respectively). The measured corrosion rates were much greater in cracked areas of beams and slabs, and a frequent appearance of localised corrosion was noticed in cracked areas and areas near cracks. This can be explained by an easier chloride ions penetration, but also oxygen and water, through cracks and further along the reinforcing bars due to deteriorated bond between steel and concrete near cracks.

2 EXPERIMENTAL SETUP

2.1 Specimen details

This experimental test setup aims to demonstrate how the existing cracks affect localised corrosion. The experimental campaign consisted of a preliminary series of tests on six specimens. Geometry and cross-section properties of the tie specimens are shown in Fig. 1. Length of the specimens was limited by corrosion test chamber dimensions. The concrete specimens are reinforced with a single hot-rolled ribbed bar of 8 mm in diameter running longitudinally through the centroid of the cross-section. Special attention was given to preventing corrosion at concrete ends, where the distance from outer surface to the bar is smaller than in the rest of the specimen. Before casting, at the specimen ends a rubber tube was inserted on the bar into the specimen for 5 cm; after casting it was removed while the resulting free space was filled with polyurethane sealant. Epoxy coating was also applied at the bar ends. The concrete compressive strength was measured on cubes (150 mm): mean compressive strength after 96 days was 38,8 MPa.

After casting, specimens were first cured for 7 days and then stored in laboratory conditions. The first tensile test was performed after 9,5 months. During this period shrinkage of concrete was periodically measured on 3 specimens using mechanical strain gauge with 250 mm gauge length: stainless steel marks were attached on two opposite sides of the specimen: on each side 4 steel marks at 250 mm distances (Fig. 2). Average shrinkage deformation measured after 9,5 months was $630 \cdot 10^{-6}$. As reported in [10] if shrinkage is not accounted for, initial member shortening can lead to reduction in tension stiffening. Procedures for subtracting the effect of shrinkage can be also found in [11, 12].

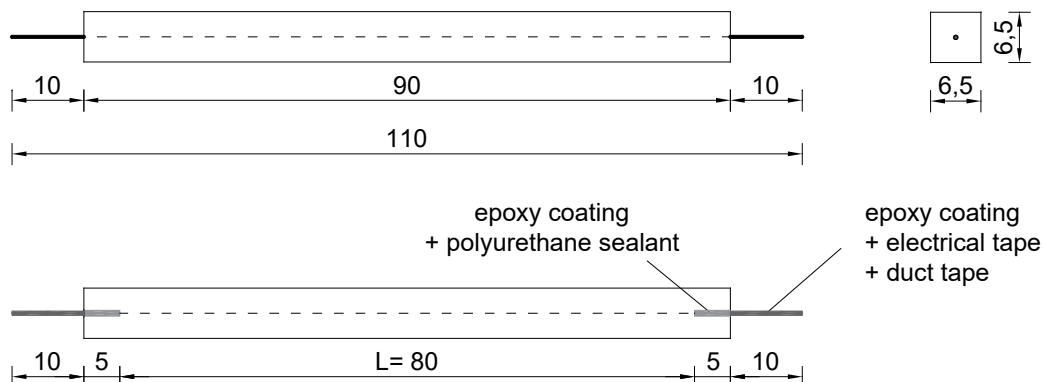


Figure 1: Test specimen details (dimensions in cm)



Figure 2: Measuring shrinkage deformation via stainless steel marks glued on specimens along the central axis

2.2 Testing procedure

The testing procedure is described in detail in Table 1. The tensile axial force was applied to the ends of the reinforcing bar protruding from each end of the concrete specimen and the specimen elongation measured. Testing was conducted on both corroded and controlling reinforced concrete specimens without corrosion. Before exposing the reinforced concrete specimens to accelerated corrosion, specimens were first loaded by a tensile force of 15,5 kN (310 MPa), what caused formation of cracks in the specimens: 4 or 5 cracks perpendicular to the member axis were observed (Fig. 4). Consequently, this cracks have significantly deteriorated the bond in the vicinity of the cracks. After unloading, the cracks were not completely closed (see also [13]): there was a residual crack width measured up to 0,1 mm.

Table 1: Testing procedure

Specimen	Phase 1	Phase 2	Phase 3	Note
A1	uniaxial tension			trial specimen
A2	uniaxial tension 15,5 kN, unloading	accelerated corrosion	uniaxial tension 15,5 kN, unloading	
A3	uniaxial tension 15,5 kN, unloading	accelerated corrosion	uniaxial tension 15,5 kN, unloading	
A4	uniaxial tension 15,5 kN, unloading	accelerated corrosion	uniaxial tension 15,5 kN, unloading	
A5	uniaxial tension up to 4% elongation (\approx 30 kN)			monotonic loading
A6	uniaxial tension 15,5 kN, unloading, uniaxial tension 30 kN			reverse loading

All tests were carried out in displacement control (universal testing machine *Zwick/Roell 600 kN*): load rate 0,00667 mm/s up to 15,5 kN for A2-A4; load rate 0,00667 mm/s up to 15,5 kN and 0,15 mm/s afterwards for A5; load rate 0,00667 mm/s up to 15,5 kN, unloading 0,5 mm/s and reloading 0,1 mm/s for A6. The applied force was measured by an external load cell, while the elongation of the specimen was recorded using 2 linear variable displacement transducers (LVDT), with original gauge length of 100 mm extended to 800 mm through specially made extensions, symmetrically placed on two opposite sides of the specimen. The experimental setup is shown in Fig. 3.

After unloading, specimens were exposed to reinforcement corrosion in a cyclic corrosion test chamber (*Ascott CCC1000ip*) by exchanging wet and dry cycles. An accelerated corrosion cycle is described in Table 2. The cycles were selected according to [9, 14]. In order to induce corrosion NaCl was melted into water (38 ‰ in relative to water mass) and sprayed onto the specimens. The corrosion process lasted for 1 year: actually 87 cycles were conducted; there were some random pauses in the beginning due to some unexpected damage of the equipment. After the corrosion process, specimens were taken out from the corrosion test chamber, and stored for 1 year in the laboratory (Fig 4.).

Table 2: An accelerated corrosion cycle in the cyclic corrosion test chamber

Day	Salt spray (38 ‰ NaCl)	Temperature, °C	Relative humidity, %	Phase description
1	(2 h on and 1 h off) X3 15 h off	30	n/a	spraying with salt water
2	off	30	70	wetting
3	off	up to 60 in 3 h 60 for 1h back to 30 in 20 h	20 20 n/a	heating and drying



Figure 3: Specimen prepared for testing with two LVDT-s mounted on opposite sides (left), uniaxial tension test setup (middle), cracks perpendicular to member axis formed during the tensile test (right)

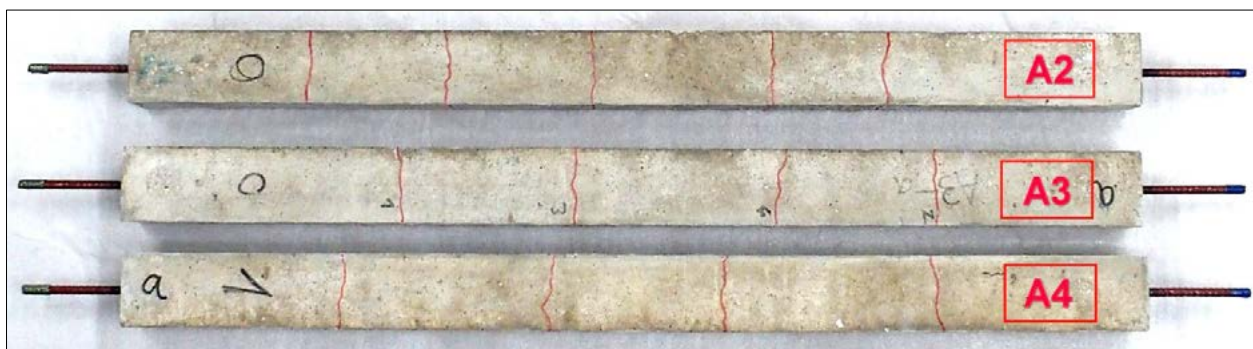


Figure 4: Test specimens after the accelerated corrosion process (crack pattern marked with red colour)

3 RESULTS

3.1 Uniaxial tensile test results

A relationship between the applied load and mean strain of the cracked specimens was established. Strain was obtained by dividing the average deformation of two LVDT-s by their gauge length. Fig. 5 shows the response of the specimens after the Phase 1 (applied load vs. average deformation diagram), compared with bare steel bar response. Due to the contribution of the intact concrete between the cracks the member is stiffer than the bare steel bar response (this is referred as tension stiffening). As may be noticed, the stiffness of the member decreases with each new crack.

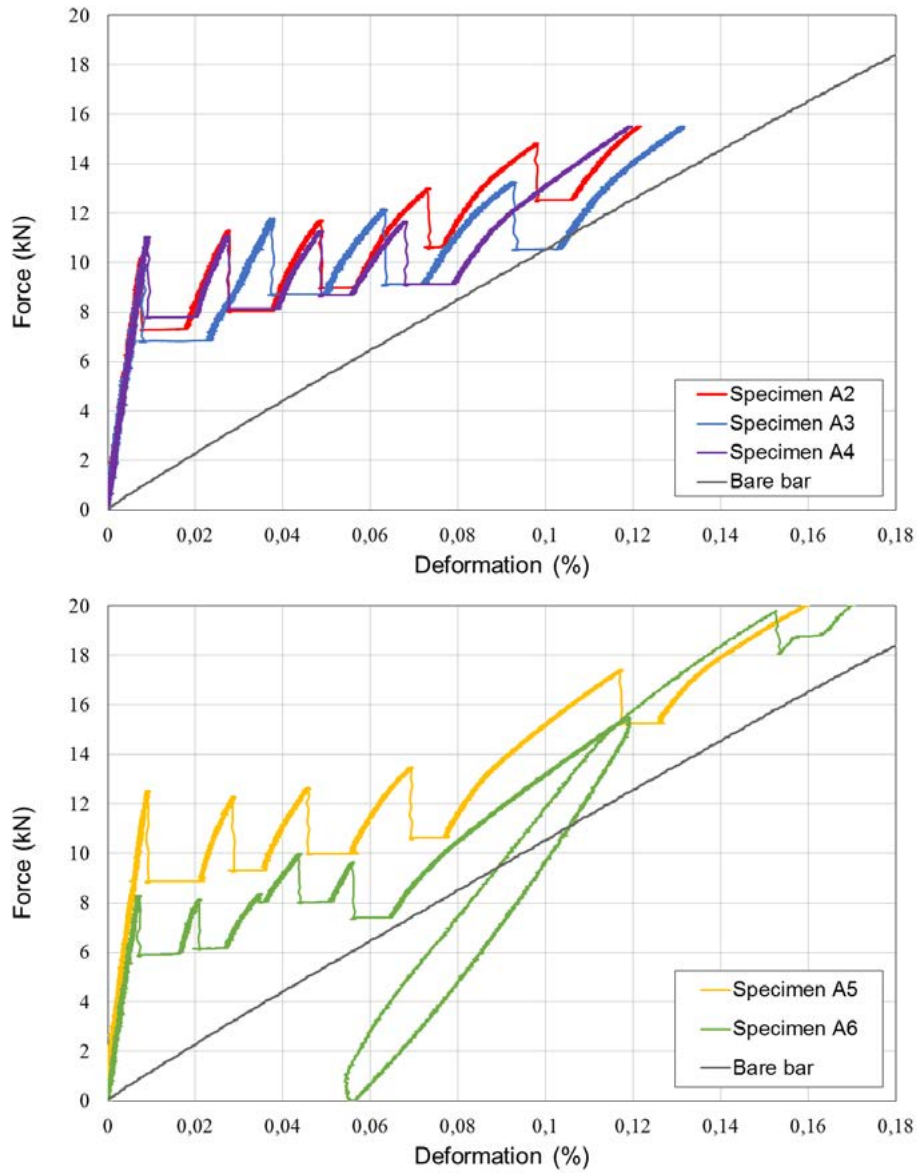


Figure 5: Uniaxial tension test: load - average strain diagram after Phase 1

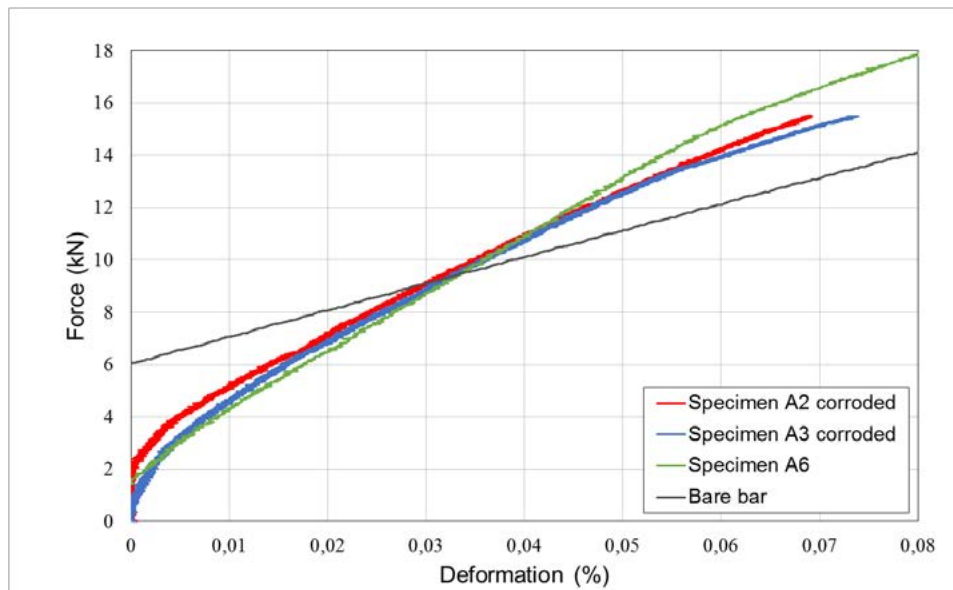


Figure 6: Uniaxial tension test: load - average strain diagram after corrosion (Phase 2)

Results of tensile test after corrosion are compared with control specimen A6 without corrosion on Fig. 6. Only results for two corroded specimens are shown (A2 and A3), since on specimen A4 one LVDT has not been recorded, so it was not possible to obtain the mean value. Both corroded specimens show very similar behaviour, and a decrease of tension stiffening may be noticed. This results indicate that tension stiffening is influenced by corrosion.

3.2 Testing of corroding bars

To establish the mass loss due to corrosion, after the tensile test the specimens were crashed with a hammer and reinforcement has been taken out (Fig. 7). Bars were cleaned according to ASTM G1-03 (2017) using 19% HCl for 2x15 min and only cloth and soft brushes.

Table 3 summarises mass losses due to corrosion. It can be noticed that mass loss was rather small - less than 2%. In case of uniform corrosion this wouldn't affect much the cross-section area reduction. However, as in this case the corrosion was localised at the vicinity of the cracks, the cross-section reduction was quite significant at some points. This may be clearly noticed on Fig. 8, which shows results of accelerated corrosion visible on the bars after cleaning. Bars were visually inspected: pits are of various size and irregular shape (rather shallow and wide than narrow and deep), in some cases undercutting.

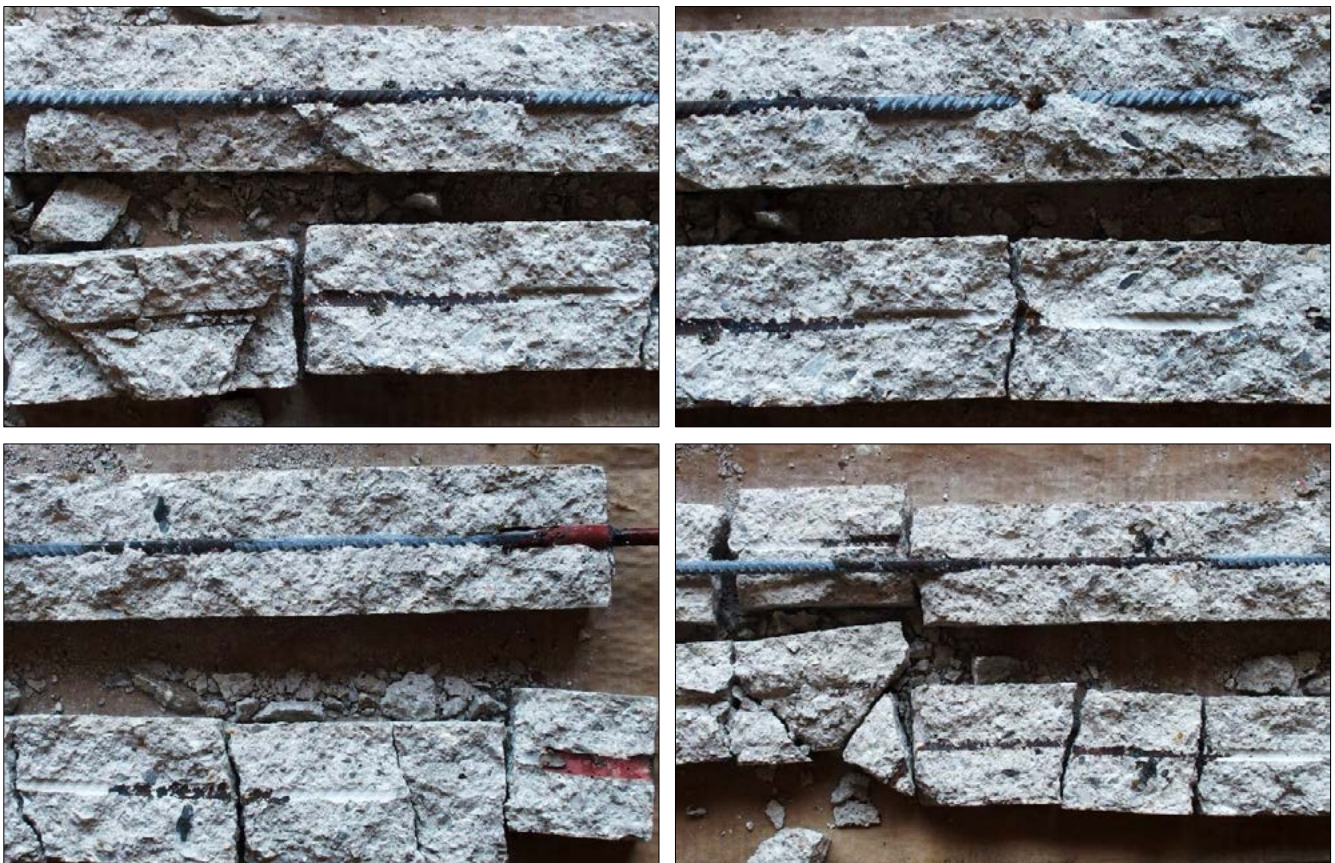


Figure 7: Extracting the corroded reinforcing bars from the specimens after the tensile test

Table 3: Mass loss due to corrosion

Reinforcement bar from specimen	Length, m	Mass, g	Mass loss*, g	Mass loss**, %
A2	1,10	430,54	5,23	1,65
A3	1,10	431,48	4,29	1,35
A4	1,095	427,77	6,01	1,89
Unit mass of un-corroded bar (mean value of 6 samples) equals to 396,15 g/m'				

* Obtained as: mass – (un-corroded bar unit mass x bar length)

**Obtained as: mass loss / (un-corroded bar unit mass x 0,8 m), since corrosion was only possible on the exposed part of the bar



Figure 8: Localised corrosion (top: bar from specimen A2, middle: bar from specimen A3, bottom: bar from specimen A4)

Corroded reinforcing bars were finally tested in uniaxial tension. Fig. 9 shows force vs. deformation diagram of both the corroded and un-corroded bars. Although the mass loss was rather small, the corroded bars have significantly changed their mechanical properties: (i) there is a significant loss of ductility: around 50% for specimens A2 & A3 and more than 70% for A4 comparable with un-corroded reinforcement; (ii) decrease in yield strength (what can be related to cross-section area loss); (iii) decrease in strength; (iv) decrease of initial stiffness (note the reduced slope of corroded bars in Fig. 9 right). On the basis of this experimental campaign it may be concluded that tensile stiffness of RC specimens is decreased both due to rebar stiffness loss and due to bond loss (affected to tension stiffening).

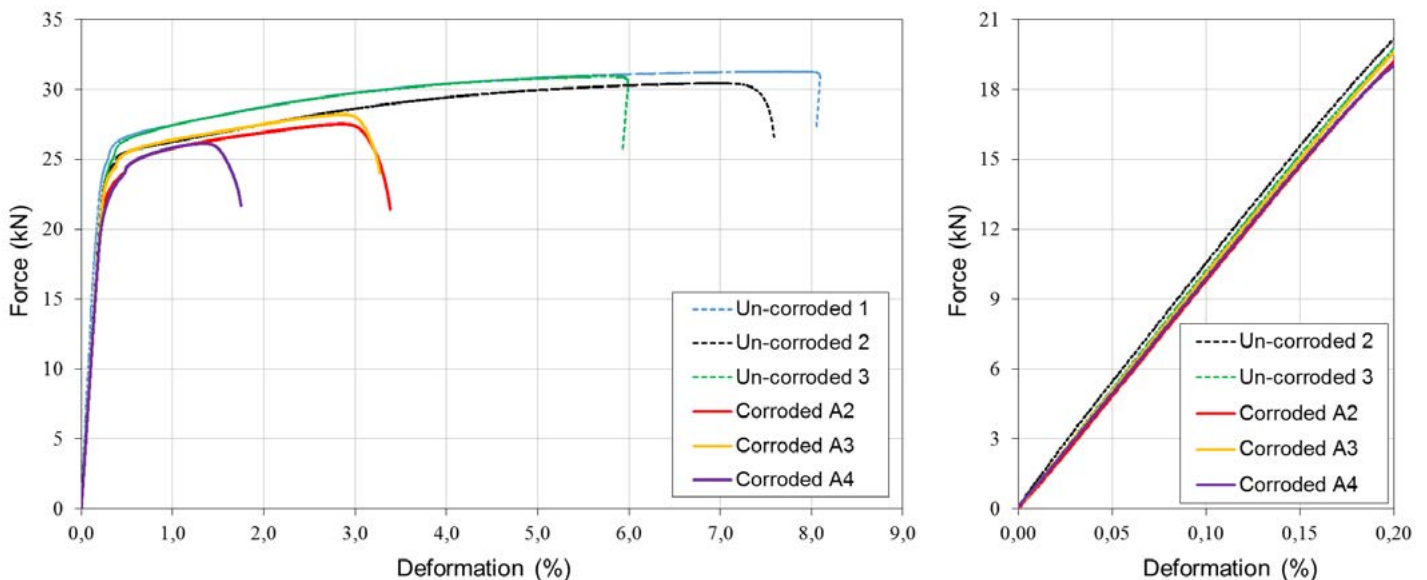


Figure 9: Force vs. deformation diagram for corroded and un-corroded bars, with enlarged initial part (right)

4 CONCLUSIONS

This experimental campaign aimed to confirm the effect of pre-existing cracks on localised corrosion initiation and development. In this test-setup corrosion has been induced in a test chamber using salt water and exchanging wet and dry cycles, what is similar to the corrosion process under natural environment.

The following conclusions may be summarized:

1) So far no such uniaxial tension RC tests have been conducted where specimens had been first loaded in order to induce cracks and then subjected to accelerated corrosion. As well, for the first time in tension specimens corrosion was induced in an artificial climate environment in a test chamber.

2) Although the bar mass loss is rather small (less than 2 %), at the vicinity of the cracks considerable localised corrosion has been observed, with significantly larger bar cross-section reduction than away from the cracks.

3) The preliminary results prove that tension stiffening effect has been reduced in corroded specimens.

4) This proposed experimental test-setup, where corrosion process has been coupled with cracks, is closer to the nature of a great number of RC structures. The focus of this preliminary 6 samples was on the test setup implementation. However, in order to propose a general degradation tension stiffening model that could better describe this process a more extensive experimental campaign has to be carried out including variations in: (i) bar diameters, (ii) concrete cross-sectional dimensions, (iii) concrete strengths and (iv) corrosion levels.

ACKNOWLEDGMENTS

This work has been supported in part by Ministry of Science, Education and Sports of the Republic of Croatia under the project Research Infrastructure for Campus-based Laboratories at the University of Rijeka, number RC.2.2.06-0001. Project has been co-funded from the European Fund for Regional Development (ERDF). The authors thank the University of Rijeka for supporting the publication of this paper through grant No. uniri-tehnic-18-127.

REFERENCES

- [1] Amleh, L.; Mirza, S.: Corrosion influence on bond between steel and concrete, *ACI Structural Journal*, Vol. 96 (1999), pp. 415-423.
- [2] Shimomura, T. & Maruyama, K.: Constitutive models for prediction of performance of deteriorated concrete structures, In *Second RILEM Workshop: Life prediction and aging management of concrete structures*, Paris, (2003), pp. 3 -12.
- [3] Shang, F. et al.: Three-dimensional nonlinear bond model incorporating transverse action in corroded RC members, *Journal of Advanced Concrete Technology*, Vol. 9 (2011) No. 1, pp. 89-102.
- [4] Giordano, L.; Mancini, G. & Tondolo, F.: Reinforced concrete members subjected to cyclic tension and corrosion, *Journal of Advanced concrete Technology*, Vol. 9 (2011) No. 3, pp. 277-285.
- [5] Mancini, G. et al.: Local reinforcing bar damage in r.c. members due to accelerated corrosion and loading, *Construction and Building Materials*, Vol. 69 (2014), pp. 116-123.
- [6] Kim, H.R. et al.: Evaluation of bond properties of reinforced concrete with corroded reinforcement by uniaxial tension testing, *International Journal of Concrete Structures and Materials*, Vol. 10 (2016) No. 3, pp. S43-S52
- [7] Imperatore, S.; Rinaldi, Z. & Spagnuolo, S.: Influence of corrosion on the experimental behaviour of R.C. ties, *Engineering Structures*, Vol. 198 (2019) 109458, pp. 1-11.
- [8] Yuan, Y.; Ji, Y. & Shah, S.P.: Comparison of two accelerated corrosion techniques for concrete structures, *ACI Structural Journal*, Vol. 104 (2007) No. 3, pp. 344-347.
- [9] Grandić, D. & Bjegović, D.: Reinforcement corrosion rate in cracked areas of RC-members subjected to sustained load. Proceedings of the Joint fib-RILEM Workshop held in Madrid - Modelling of corroding concrete structures, RILEM Bookseries vol. 5, Andrade, C.; Mancini, G. (Ed), pp. 65-83, ISBN 978-94-007-0677-4, Madrid, November 2010, Springer, (2011).
- [10] Bischoff, P.H.: Effects of shrinkage on tension stiffening and cracking in reinforced concrete, *Canadian Journal of Civil Engineering*, Vol. 28 (2001), pp. 363-374.
- [11] Kaklauskas, G. et al.: Tension-stiffening behaviour of reinforced concrete ties of various strength classes, Proceedings of Second International Conference on Performance-based and Life-cycle Structural Engineering (PLSE 2015), pp. 582-590, University of Queensland, Brisbane, Australia, (2015).
- [12] Zanuy, C.; de la Fuente, P. & Albajar, L.: Estimation of parameters defining negative tension stiffening, *Engineering Structures*, Vol. 32 (2010), pp. 3355-3362.
- [13] Chen, W.H.: Cracking damage assessment of reinforced concrete members, *Proceedings of the National Science Council, Republic of China. Part A*, Vol. 22 (6) (1998), pp. 765-774.
- [14] Li, C.Q.: Initiation of chloride-induced reinforcement corrosion in concrete structural members – experimentation, *ACI Structural Journal*, Vol. 98 (2001) No. 4, pp. 502-510.

34

Nina Štirmer, Jelena Šantek Bajto, Ivana Carević, Ivana Hržan

Mechanical properties of concrete containing wood biomass ash

MECHANICAL PROPERTIES OF CONCRETE CONTAINING WOOD BIOMASS ASH

Nina Štirmer¹, Jelena Šantek Bajto², Ivana Carević³, Ivana Hržan⁴

^{1,2,3,4} University of Zagreb, Faculty of Civil Engineering, Department of Materials
Kačićeva 26, 10 000 Zagreb, Croatia
e-mail: nina.stirmer@grad.unizg.hr, jelena.santek.bajto@grad.unizg.hr

SUMMARY: Renewable energy, together with environmentally-friendly materials, gives us an insight into a sustainable future – one where reliance on fossil fuels and greenhouse gas emissions are minimised. The leading source of renewable energy in the EU are biomass fuelled power plants. Among different types of biomass, wood has the widest application while holding the majority share with 59% of all renewable energy sources. Nevertheless, combustion of 1 tonne of wood biomass generates approximately 3% of wood biomass ash (WBA), resulting in large amounts of waste. WBA management is an issue in need for prompt solutions, to avert further endangerment of the environment as well as disposal costs. Using WBA as partial cement replacement in cement composites is considered to be a feasible application. However, the fluctuating chemical composition of WBAs somewhat differs from coal fly ash, already acknowledged as a supplementary cementitious material. Due to the aforementioned difference and lack of standards and guidelines for WBAs application in cement composites, its wider application is still limited. Therefore, the main goal of this research was to quantify the acceptable amount of fly WBAs in concrete, while considering the chemical composition of different fly WBAs. Three WBAs utilized in this research were collected from different power plants located in Croatia, that exploit untreated wood chips as fuel while applying different combustion technologies. Six concrete mixtures were prepared with ash content of 15% and 20%. The impact of each WBA on concrete properties was analysed based on the determined compressive strength and modulus of elasticity. Differences between particular WBAs have been reflected on the properties of concrete mixtures.

KEY WORDS: wood biomass, fly ash, compressive strength, modulus of elasticity.

1 INTRODUCTION

By accepting the European Green Deal in 2019, the European Union (EU) has committed to evolve into a climate-neutral global leader by the year 2050. Energy-intensive industries, including the cement industry which is one of the world's largest CO₂ emitters, are imperative for Europe's economy; hence the decarbonisation of this sector is fundamental [1]. According to the International Energy Agency reports [2], the cement industry should be inclined to enhance energy efficiency and application of alternative materials, using them as fuel and/or raw materials. Addressing these challenges have put supplementary cementitious materials (SCMs) in the spotlight. In order to ensure a thorough transformation of the European energy system, ambitious targets have been set for all Member States of the EU, which include implementing a minimum of 32% of renewable energy by 2030 [3]. In order to do so, Europe intends to phase-out coal-burning power plants by 2030, largely depending on the capacity of renewable energy sources to fill in the gap left by the coal downturn. A stable and continuous supply of energy needs to be enabled by different types of renewable energy such as solar, geothermal and hydrothermal energy, bioenergy, energy of the wind, etc. [3,4]. Exactly bioenergy and biomass could make a valuable contribution in establishing a low-carbon energy system, presuming that the biomass is produced and used in a sustainable manner [5,6]. The fact that wood biomass is considered to be a CO₂-neutral source of energy on account of releasing nearly equal amount of CO₂ by burning as it absorbs while growing, places it among the top biomass-source potentials for energy production in the EU with a majority share of 59% of all renewables [7–9]. Considering that around 3% of WBA is being generated during combustion of 1 t of the wood biomass, the expansion of wood biomass power plants is already resulting in sizeable amounts of wood biomass ash (WBA). While these numbers tend to be a strong indicator of the necessary strategic handling of WBA, current WBA management practice in Europe is based on disposing WBAs on landfills as well as using it as soil amendment/fertilizer, most times without any form of control, presenting a major environmental and economic problem [7,10–15].

By adopting the new "Circular Economy Package", along with the amending Directive 2018/851 on waste and the

Directive 2018/850 on the landfill of waste, the EU is resolutely advocating the minimization of waste landfilling [16,17]. Due to already present shortfall of disposal sites and rigorous EU landfilling directives, the costs of landfilling will undoubtedly rise in the future. Therefore, the “novel” concrete containing waste materials represents a possible application of WBA, at the same time resolving the problem of industrial waste along with reducing the cement quantities produced [18]. Although research studies reported until now have demonstrated that WBA can be used in the cement composites [10,19–22], there is still a necessity for a multidisciplinary and comprehensive approach to fully understand the chemical and microstructural characteristics of WBA and its impact on concrete properties.

The aim of this study was to determine how the addition of fly WBA to concrete mixtures by replacing a portion of cement affects the specified properties of concrete, relative to the reference portland cement concrete, principally its compressive strength and modulus of elasticity.

2 EXPERIMENTAL WORK

The experimental part of the research was designed to determine a suitable type and acceptable share of WBA used as a partial cement replacement, while considering the chemical composition of different fly WBAs. In total 7 concrete mixtures were prepared - 6 concrete mixtures by replacing cement with 15% and 20% of WBA and 1 reference mixture which did not contain WBA.

2.1 Materials

Concrete specimens were made by using crushed stone aggregate, Portland cement CEM I 42.5 R, water and fly wood biomass ash. Three fly WBAs utilized in this research were collected from different power plants located in Croatia, that exploit untreated wood chips as fuel while applying the following combustion technologies: grate combustor and grate and pulverized fuel combustor, Figure 1. Types of biomass fuel used in the concerned power plant are pure wood chips, residues from timber harvesting and waste from the timber industry, with the most common types of wood being beech, oak and hornbeam.

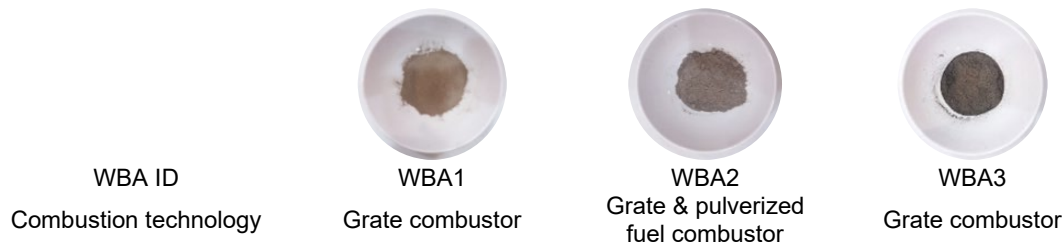


Figure 1: WBAs used in the experimental work

Chemical composition of the WBAs and cement applied in the concrete mixtures has been compared to criteria for coal fly ash according to standard EN 450-1:2013 Fly ash for concrete – Part 1: Definition, specifications and conformity criteria, Table 1.

Table 1: Chemical composition of the used WBAs and cement

Component [wt%]	WBA 1	WBA 2	WBA 3	Coal fly ash	EN 450-1 Criterion [23]	CEM I 42,5 R
pH value	13,15	13,45	12,87	12,50	-	12,86
SiO ₂	18,19	16,77	49,34	68,21	-	21,88
Al ₂ O ₃	3,14	2,53	12,42	29,00	-	4,94
Fe ₂ O ₃	2,10	1,71	4,78	7,09	-	3,15
CaO	57,93	43,68	18,58	6,67	< 10 mas. %	59,80
MgO	6,17	3,92	3,68	2,26	< 4 mas. %	2,01
Na ₂ O _{eq}	5,90	15,27	5,59	3,70	< 5 mas. %	1,67
SO ₃	1,70	6,58	1,17	0,77	< 3 mas. %	3,33
TiO ₂	0,13	0,10	1,21	0,92	-	0,23
P ₂ O ₅	1,97	2,09	1,40	1,29	< 5 mas. %	0,22
SiO ₂ + Al ₂ O ₃ + Fe ₂ O ₃	23,43	21,01	66,54	104,30	> 70 mas. %	29,97
Loss on ignition LOI (950 °C)	3,0	17,7	6,0	9,0	A: < 5 mas. % B: < 7 mas. %	3,6

					C: < 9 mas. %	
--	--	--	--	--	---------------	--

According to the results, properties of WBA differs significantly from the coal fly ash, traditionally well-known and widely used SCM. It is important to emphasize the high variability of WBAs chemical composition, depending on the raw material itself, along with the applied combustion technology [24–27]. The standard EN 450-1 covers only the application of fly ash obtained by co-incineration of wood biomass with fossil fuels. Therefore, the existing regulations for using fly ash in cement (EN 450-1) can be applied to WBA only as guidelines.

2.2 Mix design and methods

Concrete mixtures with 15% and 20% of WBA (labelled with mix ID M1-15/20, M2-15/20, M3-15/20) were prepared by replacing cement type CEM I 42.5 R. Along with them, a reference mixture (labelled with mix ID M0), which did not contain WBA, was made. All concrete mixtures were prepared with a maximum aggregate grain size $D_{max} = 16$ mm. The applied water / binder ratio ($w/b=0,5$) was uniform in all concrete mixtures (Table 2).

Table 2: Mix design

WBA ID	-	WBA1		WBA2		WBA3	
Mix ID	M0	M15 – WBA1	M20 – WBA1	M15 – WBA2	M20 – WBA2	M15 – WBA3	M20 – WBA3
WBA share [%]	0%	15%	20%	15%	20%	15%	20%
cement [kg]	380	323	304	323	304	323	304
WBA [kg]	0	57	76	57	76	57	76
aggregate [kg]	1825,95	1813,35	1815,66	1811,1	1806,12	1797,48	1788

The focus of this research was to determine the impact of WBA as cement replacement on concrete properties in fresh and hardened state. The mechanical properties in hardened state, i.e. compressive strength and modulus of elasticity were examined on specimen at the age of 7, 28 and 90 days. Cubed specimens (150 x 150 x 150 mm) and cylindrical specimens (ϕ 100 x 200 mm) were moulded immediately on completion of mixing. Three specimens per each mixture were prepared to be examined at the age of 7, 28 and 90 days: for each tested property, for each WBA type and particular share of WBA. The examined properties in fresh and hardened state are stated in Table 3.

Table 3: Test methods for concrete properties in fresh and hardened state

Examined properties & Method	
<i>Fresh state</i>	<i>Hardened state</i>
Testing fresh concrete – Part 6: Density (EN 12350-6:2019)	Testing hardened concrete – Part 3: Compressive strength of test specimens (EN 12390-3:2019)
Temperature measuring of fresh concrete (HRN U.M1.032:1981)	
Testing fresh concrete – Part 7: Air content – Pressure methods (EN 12350-7:2019)	Testing hardened concrete – Part 13: Determination of secant modulus of elasticity in compression (EN 12390-13:2013)
Testing fresh concrete – Part 2: Slump-test (EN 12350-2:2019)	

3 RESULTS ANALYSIS AND DISCUSSION

3.1 Fresh state results

Immediately upon completion of mixing, concrete properties in fresh state were determined. The comparison between the reference mixture without WBA, and the mixtures with 15% and 20% of WBA, are shown in Table 4.

Table 4: Fresh state results

Mix ID	M0	M15 – WBA1	M20 – WBA1	M15 – WBA2	M20 – WBA2	M15 – WBA3	M20 – WBA3
WBA share [%]	0%	15%	20%	15%	20%	15%	20%
Density [kg/m³]	2.500	2.470	2.480	2.490	2.500	2.510	2.450
Temperature [°C]	21,1	23,2	23,3	23,3	24,1	22,1	21,7
Air content [%]	1,2	1,3	1,4	1,5	1,5	1,2	1,6
Slump [mm]	60	60	50	10	10	60	70

As a result of density testing, significant influence of the WBA addition on the density of concrete in fresh state wasn't demonstrated. Even though the mixtures containing WBA have shown results comparable to the reference values, the presented results are somewhat lower. Accordingly, air content increased parallel to the decrease of concrete mixtures density.

Along with the density and air content testing, temperature of the concrete mixtures was observed. All 6 mixtures with different WBA content showed a slight increase of temperature up to approx. 3 °C compared to the reference mixture.

The presented results show that the addition of WBA can lead to a change in consistency of the concrete mixtures. When comparing mixtures containing 15% and 20% of WBA1 and mixtures containing 15% and 20% of WBA3 to the reference mixture M0, similar results were noted. While doing so, concrete mixtures with 20% of WBA1 had shown minor loss of workability with the increase of WBA quantity. The loss of workability was especially underlined in mixtures containing WBA2, where difficult moulding was encountered. Characterization of fly WBAs previously showed irregularly shaped and high porosity particles of higher specific surface, with high carbon and free CaO content, which can all be related to the increased water demand [24,25,28]. At the same time, the mixture containing 20% of WBA3 showed a slight improvement in consistency.

3.2 Hardened state results

The impact of each WBA on the mechanical properties of concrete was analysed based on the demonstrated compressive strength and modulus of elasticity. Differences between particular WBAs have been reflected on the properties of concrete mixtures.

Compressive strength testing was performed in accordance with EN 12390-3:2019 standard. The examination of compressive strength was conducted on specimen with WBA at different ages, followed by comparison to the reference values. Development of compressive strength through time, depending on the type and share of WBA, has been presented in Figure 2.

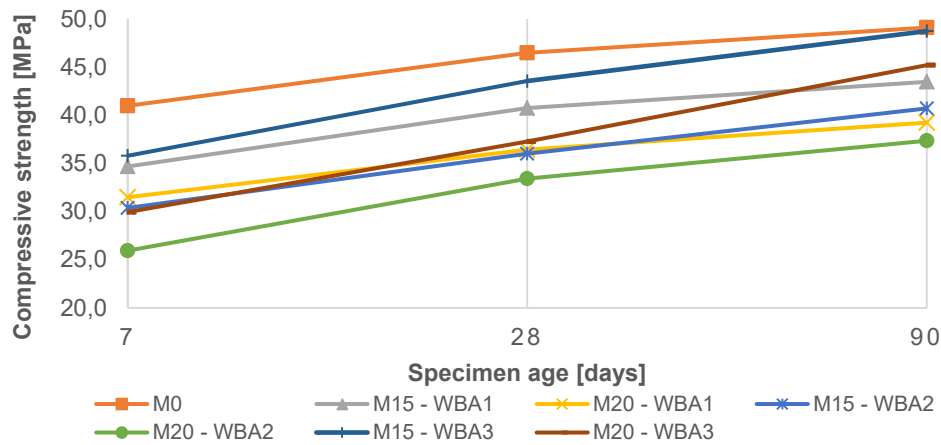


Figure 2: Compressive strength of concrete specimen at different ages

In accordance with the shown results determined on concrete specimen at different ages, a decrease in the obtained values of compressive strength is visible when compared to the reference mixture. Moreover, with an increase in the share of WBA replacing cement compressive strength is reduced. Related findings were also discussed by other researchers [29–32]. Comparing the results obtained after 28 days, the compressive strength ratios are similar to those obtained after 7 days. Based on the values after 90 days it can be concluded that the replacement of cement with WBA reduces compressive strength. When comparing all three types of ash, the lowest values were observed on the concrete specimens made with WBA2, while replacing cement with 15% of WBA3 resulted in nearly the same compressive strength as the reference mixture.

Modulus of elasticity testing was performed in accordance with EN 12390-13:2013 standard. The examination of modulus of elasticity was conducted on specimen with WBA at different ages, followed by comparison to the reference values. Development of modulus of elasticity through time, depending on the type and share of WBA, has been presented in Figure 3.

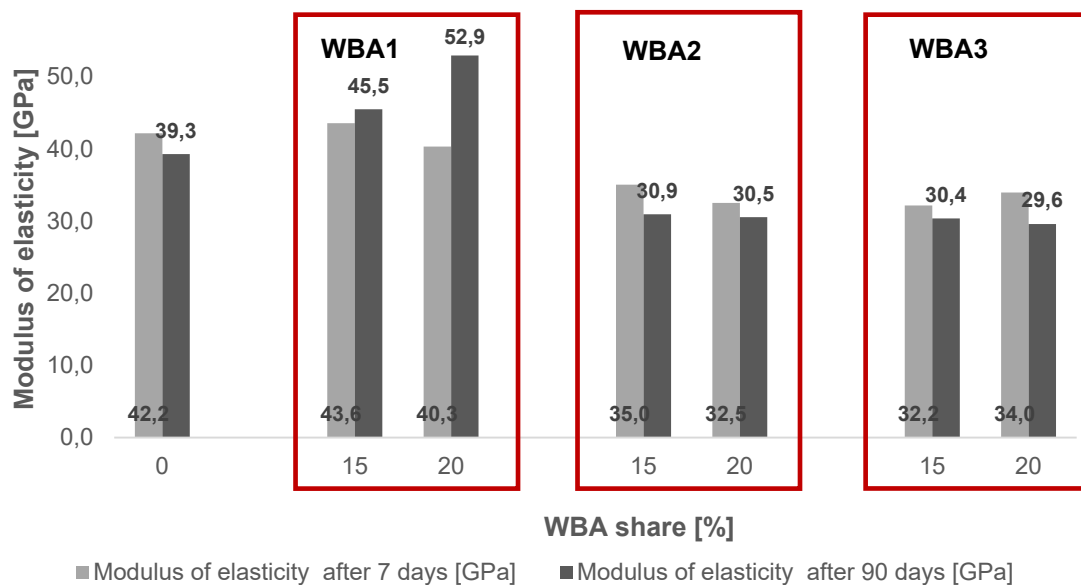


Figure 3: Modulus of elasticity of concrete specimens at different ages

The results obtained by the examination of modulus of elasticity after 7 days show that by replacing part of the cement with WBA generally reduces the values of the modulus of elasticity. Only the mixture with 15% of WBA1 presented an increase in the early values of the modulus of elasticity, in addition to the highest values reached. It can be observed that specimens made with WBA2 and WBA3 achieved similar results after 90 days but still lower than the reference values. This 90-day drop amounts up to 22% for samples made with 20% of WBA2 and 18% for samples made with 20% of

WBA3.

4 CONCLUSIONS

Seeing that the chemical composition of WBA differs from that of coal ash and does not meet the existing regulation for use of fly ash in concrete (EN 450-1), additional research is needed to determine the potential and adequacy of WBA as cement replacement. However, certain conclusion can be established and used as a reference for future experimental work based on the performed research:

- Partial cement replacement with WBA does not significantly affect, i.e. reduce the density of fresh concrete;
- The temperature values of concrete mixtures with WBA are increased compared to the temperature of the reference mixture;
- Air content in concrete mixtures with WBA raised with the increased share of WBA, correlating with the reduction of density of concrete mixtures containing WBA;
- As a result of consistency testing, all cement mixtures had shown the same behavioural trend of increased water need, proportionally increasing with the quantity of WBA. Reduced workability, caused by replacement of cement with WBA, is highly dependent on WBA type;
- Using WBA as a partial cement replacement reduces the compressive strength of concrete;
- By adding WBA to concrete as cement replacement, the modulus of elasticity decreases. A higher proportion of cement replacement results in a greater reduction of modulus of elasticity.

All of the examined properties are also highly dependent on the WBA used.

ACKNOWLEDGMENTS

This research was performed within research project „Transformation of Wood Biomass Ash into Resilient Construction Composites – TAREC²” (IP-06-2016) and “Young Researchers' Career Development Project – Training of Doctoral Students” (DOK-01-2018), funded by the Croatian Science Foundation.

REFERENCES

- [1] Sugawara, E., Nikaido, H., The European Green Deal, 58 (2019) 7250–7. <https://doi.org/10.1128/AAC.03728-14>.
- [2] International Energy Agency, Technology Roadmap - Low-Carbon Transition in the Cement Industry, (2018) 66. www.wbcsdcement.org.
- [3] DIRECTIVE (EU) 2018/2001 OF THE EUROPEAN PARLIAMENT AND OF THE COUNCIL of 11 December 2018 on the promotion of the use of energy from renewable sources (recast), Off. J. Eur. Union. Volume 61 (2018) L 328/82-209. <https://eur-lex.europa.eu/legal-content/EN/TXT/HTML/?uri=CELEX:32018L2001&from=hr>.
- [4] Agora Energiewende, European Energy Transition 2030: The Big Picture, (2019).
- [5] Bioeconomy, T.E.C.K.C. for, Brief on biomass for energy in the European Union, (2016) 1–8. <https://doi.org/10.2760/546943>.
- [6] Agrela, F., Cabrera, M., Alshaaer, M. et al., Biomass fly ash and biomass bottom ash 2, in: New Trends Eco-Efficient Recycl. Concr., 2019: pp. 23–58. <https://doi.org/10.1016/B978-0-08-102480-5.00002-6>.
- [7] Agrela, F., Cabrera, M., Alshaaer, M. et al., Biomass fly ash and biomass bottom ash 2, 2019. <https://doi.org/10.1016/B978-0-08-102480-5.00002-6>.
- [8] Vassilev, S. V., Baxter, D., Andersen, L.K. et al., An overview of the composition and application of biomass ash., Fuel. 105 (2012) 19–39. <https://doi.org/10.1016/j.fuel.2012.10.001>.
- [9] The European Commission's Knowledge Center for Bioeconomy, Brief on biomass for energy in the European Union, (2016) 1–8. <https://doi.org/10.2760/546943>.
- [10] Ukrainczyk, N., Vrbos, N., Koenders, E.A.B., Reuse of Woody Biomass Ash Waste in Cementitious Materials, Chem. Biochem. Eng. Q. (2016). <https://doi.org/10.15255/CABEQ.2015.2231>.
- [11] Cheah, C.B., Ramli, M., The implementation of wood waste ash as a partial cement replacement material in the

- production of structural grade concrete and mortar: An overview, *Resour. Conserv. Recycl.* 55 (2011) 669–685. <https://doi.org/10.1016/j.resconrec.2011.02.002>.
- [12] Maresca, A., Hyks, J., Astrup, T.F., Recirculation of biomass ashes onto forest soils: ash composition, mineralogy and leaching properties, *Waste Manag.* 70 (2017) 127–138. <https://doi.org/10.1016/j.wasman.2017.09.008>.
- [13] Freire, M., Lopes, H., Tarelho, L.A.C., Critical aspects of biomass ashes utilization in soils: Composition, leachability, PAH and PCDD/F, *Waste Manag.* 46 (2015) 304–315. <https://doi.org/10.1016/j.wasman.2015.08.036>.
- [14] Pesonen, J., Kuokkanen, T., Rautio, P. et al., Bioavailability of nutrients and harmful elements in ash fertilizers: Effect of granulation, *Biomass and Bioenergy.* 100 (2017) 92–97. <https://doi.org/10.1016/j.biombioe.2017.03.019>.
- [15] Bioenergy, I.E.A., Combustion, B., Options for increased use of ash from biomass combustion and co-firing, (n.d.).
- [16] Directive (EU) 2018/851 of the European Parliament and of the Council of 30 May 2018 amending Directive 2008/98/EC on waste, *Off. J. Eur. Union.* (2018) 109–140. <https://doi.org/10.1023/A:1009932427938>.
- [17] Directive of the European Parliament and of the Council of 30 May 2018 amending Directive 1999/31/EC on the landfill of waste, *Off. J. Eur. Union.* 2018 (2018) 100–108. <https://eur-lex.europa.eu/legal-content/EN/TXT/PDF/?uri=CELEX:32018L0850&from=EN>.
- [18] Teixeira, E.R., Camões, A., Branco, F.G., Valorisation of wood fly ash on concrete, *Resour. Conserv. Recycl.* 145 (2019) 292–310. <https://doi.org/10.1016/j.resconrec.2019.02.028>.
- [19] Wang, S., Miller, A., Llamazos, E. et al., Biomass fly ash in concrete: Mixture proportioning and mechanical properties, *Fuel.* 87 (2008) 365–371. <https://doi.org/10.1016/j.fuel.2007.05.026>.
- [20] Rajamma, R., Ball, R.J., Tarelho, L.A.C. et al., Characterisation and use of biomass fly ash in cement-based materials, *J. Hazard. Mater.* 172 (2009) 1049–1060. <https://doi.org/10.1016/j.jhazmat.2009.07.109>.
- [21] Chowdhury, S., Mishra, M., Suganya, O., The incorporation of wood waste ash as a partial cement replacement material for making structural grade concrete: An overview, *Ain Shams Eng. J.* 6 (2015) 429–437. <https://doi.org/10.1016/j.asej.2014.11.005>.
- [22] Ottosen, L.M., Hansen, E.Ø., Jensen, P.E. et al., Wood ash used as partly sand and/or cement replacement in mortar, *Int. J. Sustain. Dev. Plan.* 11 (2016) 781–791. <https://doi.org/10.2495/SDP-V11-N5-781-791>.
- [23] Fly ash for concrete - Part 1: Definition, specifications and conformity criteria (EN 450-1:2013), 2013.
- [24] Carević, I., Serdar, M., Štirmer, N. et al., Preliminary screening of wood biomass ashes for partial resources replacements in cementitious materials, *J. Clean. Prod.* 229 (2019) 1045–1064. <https://doi.org/10.1016/j.jclepro.2019.04.321>.
- [25] Cheah, C.B., Ramli, M., The implementation of wood waste ash as a partial cement replacement material in the production of structural grade concrete and mortar: An overview, *Resour. Conserv. Recycl.* 55 (2011) 669–685. <https://doi.org/10.1016/j.resconrec.2011.02.002>.
- [26] Siddique, R., Cachim, P., Waste and Supplementary Cementitious Materials in Concrete, 2018.
- [27] Sigvardsen, N.M., Kirkelund, G.M., Jensen, P.E. et al., Impact of production parameters on physiochemical characteristics of wood ash.pdf, *Resour. Conserv. Recycl.* 145 (2019) 230–240. <https://doi.org/https://doi.org/10.1016/j.resconrec.2019.02.034>.
- [28] Rissanen, J., Ohenoja, K., Kinnunen, P. et al., Milling of peat-wood fly ash: Effect on water demand of mortar and rheology of cement paste, *Constr. Build. Mater.* 180 (2018) 143–153. <https://doi.org/10.1016/j.conbuildmat.2018.05.014>.
- [29] Ghorpade, V.G., Effect of wood waste ash on the strength characteristics of concrete, *Nat. Environ. Pollut. Technol.* 11 (2012) 121–124.
- [30] Subbaramaiah, G., Sudarsana Rao, H., Ghorpade, V.G., Effect of Addition And Partial Replacement Of Cement By Wood Waste Ash On Strength Properties Of Structural Grade Concrete, *IJSET-International J. Innov. Sci. Eng. Technol.* 2 (2015) 736–743. www.ijset.com.
- [31] J.Geetanjali, J., Reethesh, C.M., Jyothi Swaroop, A. et al., a Brief Study on the Strength Properties of Concrete By Partial Replacement of Cement With Wood Ash and Natural Sand With 100% Crushed Stone Sand, *Int. J. Res. Eng. Technol.* 06 (2017) 1–7. <https://doi.org/10.15623/ijret.2017.0614001>.
- [32] Chowdhury, S., Maniar, A., Suganya, O.M., Strength development in concrete with wood ash blended cement and use of soft computing models to predict strength parameters, *J. Adv. Res.* 6 (2014) 907–913. <https://doi.org/10.1016/j.jare.2014.08.006>.

35

**Gordana G. Tanasijević, John L. Provis, Vedran N. Carević, Ivan S. Ignjatović
and Miroslav M. Komljenović**

Effect of accelerated carbonation on the efficiency of immobilization of CS in the alkali-activated blast furnace slag

EFFECT OF ACCELERATED CARBONATION ON THE EFFICIENCY OF IMMOBILIZATION OF Cs IN THE ALKALI-ACTIVATED BLAST FURNACE SLAG

Gordana G. Tanasijević¹, John L. Provis², Vedran N. Carević³, Ivan S. Ignjatović³, and Miroslav M. Komljenović¹

¹Institute for Multidisciplinary Research, University of Belgrade, Kneza Višeslava 1, 11030 Belgrade, Serbia
e-mail: gordana@imsi.rs; miroslav.komljenovic@imsi.rs

²Department of Materials Science and Engineering, University of Sheffield, Mappin St, Sheffield S1 3JD, UK
e-mail: j.provis@sheffield.ac.uk

³Faculty of Civil Engineering, University of Belgrade, Bul. Kralja Aleksandra 73, 11000 Belgrade, Serbia
e-mail: vedran@imk.grf.bg.ac.rs; ivani@imk.grf.bg.ac.rs

SUMMARY: In this paper the effect of accelerated carbonation process on the effectiveness of immobilization of cesium (simulated radioactive and toxic waste) in the alkali-activated blast furnace slag (AABFS) matrix was studied. Blast furnace slag (BFS) was contaminated with 2% and 5% Cs (with respect to the dry BFS mass) and alkali-activated with sodium silicate solution, while the AABFS samples were cured sealed in plastic envelopes for 24 h at 95°C. First series of AABFS samples were exposed to accelerated carbonation (open curing), while the second (reference) series of AABFS samples left to aging (also sealed) at room temperature until testing. Thereafter AABFS samples were subjected to a short-term (five-day) leaching tests according to the ANSI/ANS-16.1-2003 standard. The strength of AABFS mortars were tested according to the SRPS EN 196-1 standard, while the carbonation was confirmed by phenolphthalein test and SEM analysis. The diffusion coefficient (D) and non-dimensional leachability index (L) of cesium leached from AABFS were calculated according to the ANSI/ANS-16.1–2003 standard. A correlation between the accelerated carbonation process and the effectiveness of immobilization of cesium in AABFS was established.

Keywords: Carbonation; Immobilization; Cesium; Simulated radioactive waste; Alkali-activated binders; Blast furnace slag.

1 INTRODUCTION

Alkali-activated binders (AABs), as a promising alternative to traditional Portland cement binders in the concept of sustainable development, have drawn significant public attention around the world in the past several decades. AABs have not only been frequently studied by the researchers but also applied in various industries, including the construction industry. Among various possible applications, the immobilization of hazardous, toxic, and nuclear wastes with AABs presents quite an interesting option, which might contribute significantly to the environmental protection [1].

Blast furnace slag (BFS) is a by-product from pig iron production and it is frequently used as supplementary cementitious material in cement and concrete industry. On the other hand, alkali-activated blast furnace slag (AABFS) seem to be a better option than traditional Portland cement binders for immobilization of hazardous, toxic, and nuclear wastes due to better physical and mechanical properties of AABFS, as well as better resistance to different corrosive environments [2].

Cesium is considered as one of the most difficult radionuclide to immobilize due to its weak bonding and high mobility within many common binder matrices. Generally, strength and leaching testing are considered to provide the most significant information regarding the efficiency of toxic and radioactive waste immobilization, and so are widely used to determine the influence of immobilized species on the properties of AABs [3].

In this paper, the impact of accelerated carbonation process on leaching and strength of AABFS doped with 2% and 5% cesium (i.e., a solidified simulated radioactive waste) was investigated. A short-term (5 days) leaching procedure was performed according to the ANSI/ANS-16.1-2003 standard [4].

2 EXPERIMENTAL

2.1 Materials

In this work, ground granulated blast furnace slag (BFS) from pig iron production at the facility “Železara Smederevo” (Serbia) was used as a solid precursor for the synthesis of AABFS. Sodium silicate solution was used as an alkali activator, while cesium chloride was used as the Cs source. This paper is a continuation of our previously published work [3] and more details regarding the properties of all materials used and experimental procedures are given there.

2.2 Paste preparation

The AABFS pastes were prepared by mixing ground granulated BFS, sodium silicate solution, and water or cesium chloride solution (in the case of AABFS doped with Cs). The amount of Na₂O was 4% in all cases, and the doping level of Cs was either 2.0% or 5.0% with respect to the total mass of BFS. The mix proportions of AABFS pastes, as well as their setting times according to the EN 196-3 standard [5] are given in Table 1. The AABFS paste was mixed for two minutes, then cast into a cylindrical plastic mold (ø 60 × 10 mm), after which the air bubbles were removed using a vibrating table. The AABFS pastes were cured covered with plastic sheet for 24 h at 95 °C, and then either rapidly carbonated in a chamber at room temperature or cured covered also at room temperature until testing. For SEM analysis, selected fragments of the AABFS paste samples were immersed in isopropyl alcohol for 24 h and then dried at 50 °C for 2 h. Prior to the SEM analysis the samples were Au-coated.

Table 1: AABFS paste composition and setting time

Sample	BFS mass (g)	Sodium silicate mass (g)	Added water mass (g)	CsCl mass (g)	Water/binder ratio	Setting time (min)	
						Initial	Final
AABFS	675	162.15	60	0.0	0.205 ± 0.05	15	30
AABFS + 2% Cs				17.1		40	60
AABFS + 5% Cs				42.75		60	80

2.3 Mortar preparation

Mortars of AABFS were prepared by adding the activator solution of specified concentration to water (containing CsCl for doped samples) and then mixing this solution with the BFS and standard sand (BFS/sand ratio was 1:3) in accordance with the EN 196–1 standard [6]. Mortars were homogenized in an automatic mixer for 3 min and cast into triplicate mortar prisms (40 × 40 × 160 mm) on a vibrating table. The AABFS mortars were cured under the same conditions as the AABFS pastes.

2.4 Accelerated carbonation

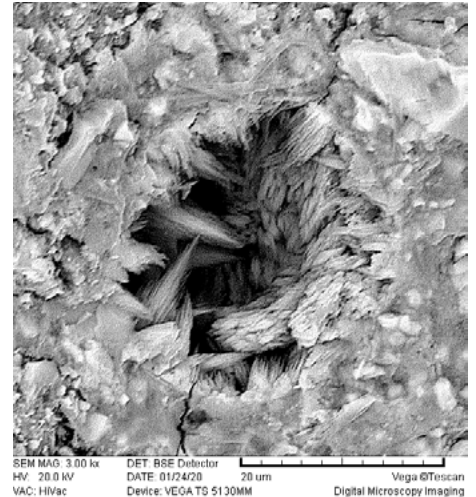
AABFS paste and mortar samples were subjected to the accelerated carbonation according to the EN 13295: 2004 standard [7] in the carbonation chamber (type MEMMERT ICH 260C, Figure 1). Prior to exposure to high CO₂ concentration, the samples were pre-conditioned in the laboratory for a period of 14 days at 21 ± 2°C and 60 ± 10% relative humidity, until they reached a constant mass. Thereafter, the samples were placed in a carbonation chamber, and exposed to the CO₂ concentration of 1.0%, also at RH 60 ± 10% and 21 ± 2°C, for a period of 56 days. After 56 days of open curing in a chamber, samples were broken using three point bending test method. The carbonation depth was examined by phenolphthalein test on a cross section of mortar prisms, while the formation of carbonate phases in the pores of AABFS matrix was confirmed by the SEM analysis (Figure 2).



Figure 1: Accelerated carbonation chamber



Figure 2: Carbonation identification (phenolphthalein test – left, SEM analysis – right)



2.5 Mortar strength

The strengths of all AABFS mortars were determined according to the EN 196-1 (2008) standard [6], using a Compression testing machine (Matest, Italy).

2.6 Leaching tests

Leaching of different elements (Si, Al, Ca, Mg, Na, K, Fe, and Cs) from hardened (both reference and rapidly carbonated) AABFS pastes was determined according to the ANSI/ANS-16.1-2003 standard procedure. This test is a semi-dynamic leach experiment that consists of submerging a monolithic sample with a fixed geometry, into deionized water at a fixed liquid-volume to solid-geometric surface area ratio, and replacing all of the leachate at given time intervals. The standard leaching test was performed without any stirring within a period of 5 days, where the leachate was completely replaced by fresh leachant after cumulative leach times of 2, 7, 24, 48, 72, 96, and 120 hours. An inductively coupled plasma optical emission spectrometer (ICP–OES, Avio 200, Perkin Elmer, USA) was used to determine the concentrations of leached elements present in the leachate.

3 RESULTS AND DISCUSSION

3.1 Mortar strength

The results of AABFS mortar compressive strength testing are given in Table 2.

Table 2: Mortar strength of AABFS after 90 days (with and without Cs added)

Sample type	AABFS	AABFS + 2% Cs	AABFS + 5% Cs
	Compressive strength and standard deviations (MPa)		
Reference (closed cured)	68.4 ± 2.6	74.1 ± 1.1	73.8 ± 2.8
56 days of accelerated carbonation	81.6 ± 1.3	93.6 ± 2.4	91.5 ± 2.2
	Relative compressive strength (<i>with respect to its counterpart</i>)		
Reference (closed cured)	1.00	1.00	1.00
56 days of accelerated carbonation	1.19	1.26	1.24

The AABFS mortar reference samples achieved compressive strengths of almost 70 MPa after 90 days of closed curing, including initial 24 hours of reaction at 95°C. Doping AABFS with 2% or 5% Cs resulted in a slight increase (5-6 MPa) in mortar compressive strength, probably due to promotion of the dissolution of BFS or some structural reorganization of AABFS gels [3].

After 56 days of accelerated carbonation the compressive strength of AABFS mortars significantly increased (19-26%), regardless of the level of Cs doping (Table 2). It is obvious that the solution present in the pores of AABFS matrix was significantly carbonated in this process (Figure 2), which resulted in likely reduction of matrix porosity and obvious increase in AABFS mortar strength at the same time.

3.2 Leaching

The incremental leach fractions of alkali metal cations (Cs, Na, and K), as well as the AABFS matrix main building blocks (Ca, Si, and Al), present in the leachate over the period of 120 hours are given in Figures 3 and 4, respectively. The concentrations of Mg and Fe present in the leachate were below the detection limit throughout the whole period of testing, and therefore are not shown.

Significant amounts of leached Na, Si, and K were noticed in the case of the reference AABFS (non-doped with Cs and non-carbonated), while their concentration reached its peak after the first 24 hours of testing (Figures 3c, 3e, and 4c). The fast increase of Na, K, and Si concentrations after the first 24 hours of testing was probably due to the leaching of non-bound or loosely bound ions present in the pore solution at or close to the surface of specimens, which is also known as the surface wash-off phenomenon [8]. Between 48 and 120 hours of testing the migration of ions through the AABFS matrix was diffusion controlled, which resulted in lower leaching rates. Generally, the concentration of alkali metal cations (Na, and K) and Si in the leachates was much higher than the concentration of Ca and Al, which means that C-S-H and/or C-A-S-H gels, usually present in the matured AABFS, are highly resistant to water leaching. The excess of sodium silicate (alkali activator) present in the AABFS was probably the main reason of high concentration of Na and Si present in the leachate, while K originated from BFS itself.

The concentration of Cs leached from the reference (non-carbonated) AABFS samples doped with either 2% Cs or 5% Cs also reached its peak after the first 24 hours of testing (Figure 3a). Similar leaching patterns were also present when other elements of interest were tested (Figures 3c, 3e, and 4c). As in the case of Na, K, and Si leaching, the fast increase of Cs concentrations after the first 24 hours of testing was probably due to the leaching of non-bound or loosely bound Cs ions present in the pore solution at or close to the surface of specimens. As already explained, between 48 and 120 hours of testing the migration of ions through the AABFS matrix was diffusion controlled, which resulted in lower leaching rates. Generally, higher addition of Cs promoted not only leaching of Cs, but of Na and Si as well (Figures 3c and 4c).

After accelerated carbonation (Figures 3b,d,f, and 4b,d,f) the leaching patterns of elements tested were more or less similar to the reference AABFS samples. However, the concentration of leached elements was somewhat lower, particularly in the case of Cs, Ca, and Si, confirming that accelerated carbonation increased their resistance to leaching, probably due to reduced AABFS matrix porosity. Indirect evidence for this assumption is significant increase in the strength of AABFS mortars.

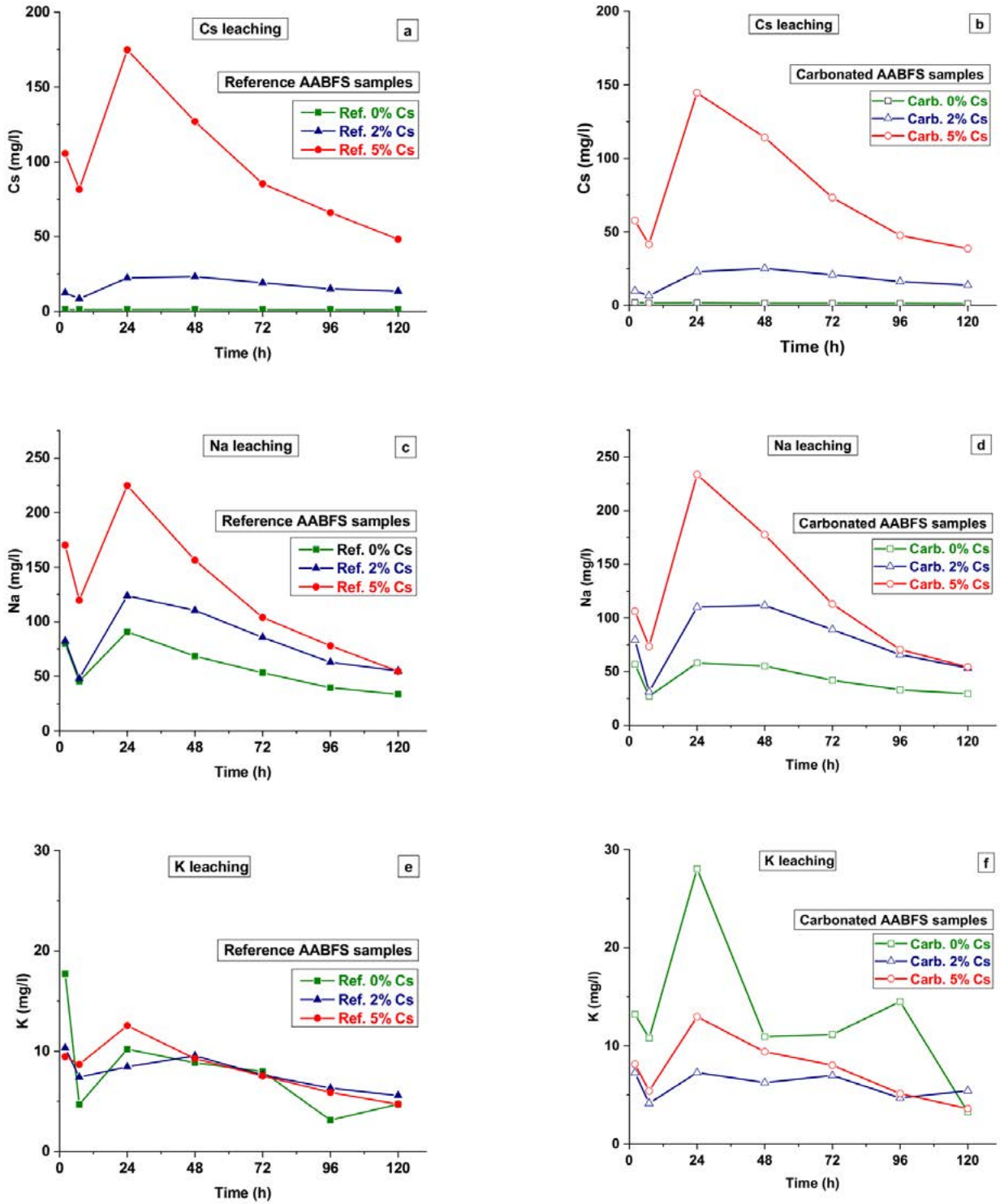


Figure 3: Incremental leaching of Cs, Na, and K from the AABFS matrices up to 120 hours, with and without Cs addition (reference samples - left, carbonated samples – right; analytical uncertainty in each point is approximately 1%)

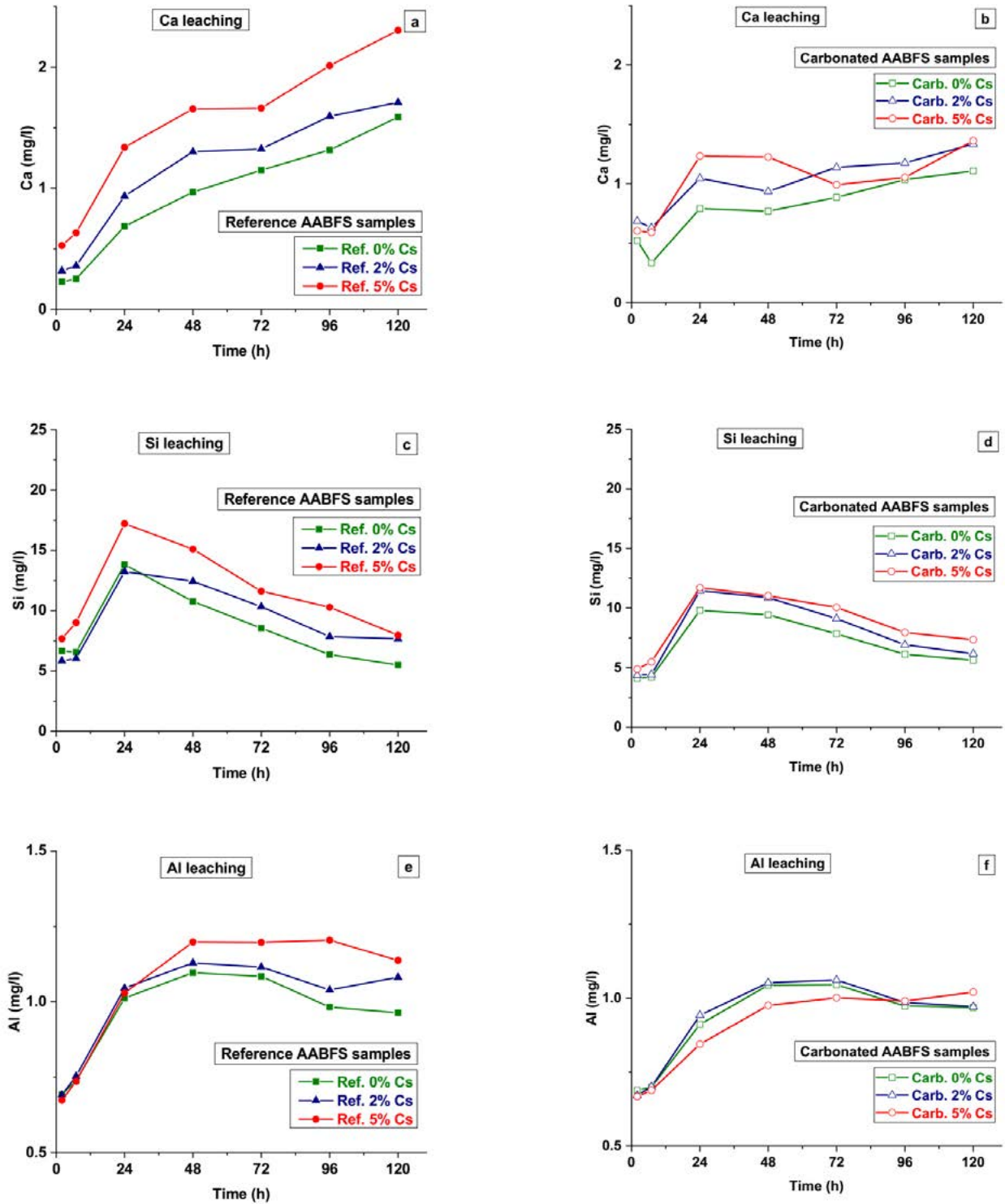


Figure 4: Incremental leaching of Ca, Si, and Al from the AABFS matrices up to 120 hours, with and without Cs addition (reference samples - left, carbonated samples – right; analytical uncertainty in each point is approximately 1%)

3.3 Diffusion coefficient (D) and leachability index (L) of cesium leached from AABFS

The diffusion coefficient (D) and non-dimensional leachability index (L) of cesium leached from AABFS were calculated according to the ANSI/ANS-16.1–2003 standard [4], and given in Figures 5 and 6, respectively.

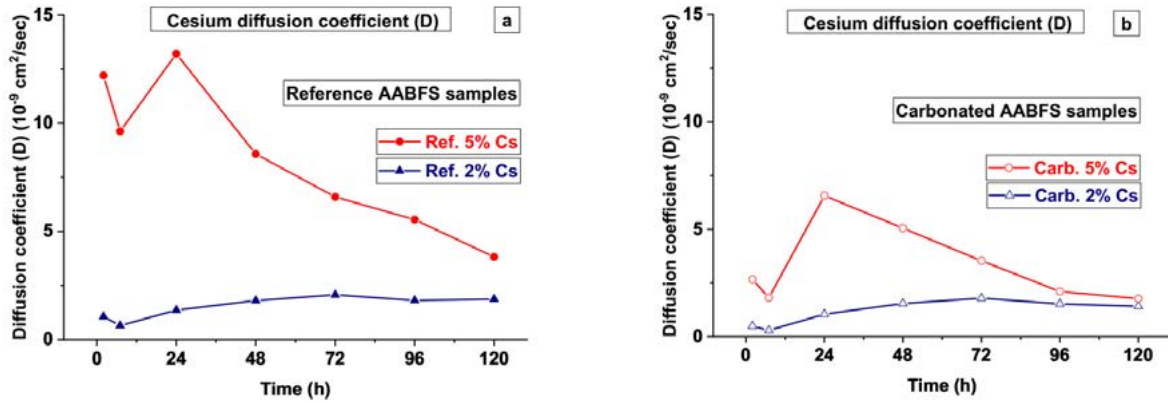


Figure 5: Diffusion coefficient (D) of cesium leached from AABFS versus time (AABFS doped with 2% and 5% Cs; a) reference samples and b) carbonated samples)

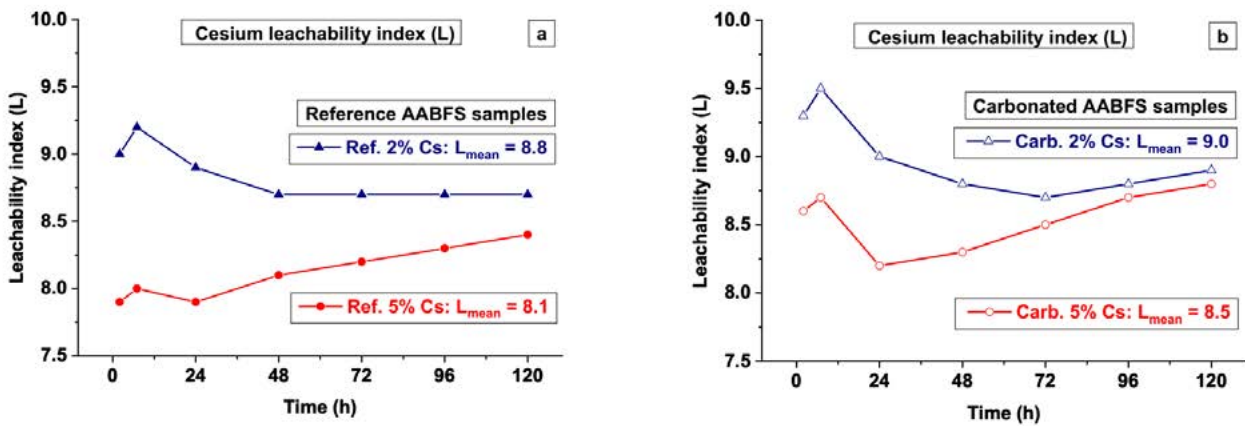


Figure 6: Non-dimensional leachability index (L) of cesium leached from AABFS versus time (AABFS doped with 2% and 5% Cs; a) reference samples and b) carbonated samples)

The leachability index (L) is a parameter that characterizes the leaching resistance of an element of interest. It can be used to estimate the applicability of a certain material or matrix for safe immobilization of hazardous waste, whereby a value of 6 is considered as the threshold for a given matrix to be accepted as adequate for the immobilization of radioactive wastes [9]. As already presented in our previous research [3], the mean leachability index of cesium leached from AABFS doped with 2% and 5% Cs after initial 1 day of closed curing at 95°C exceeded the minimum required value of 6 (Table 3).

Table 3: Mean leachability index (L) of cesium immobilized in AABFS

Addition of Cs	AABFS + Cs		
	After 1 day of closed curing at 95°C [3]	After 1 day of closed curing at 95°C and up to 90 days of closed curing at 21 ± 2°C	After 1 day of closed curing at 95°C and up to 90 days of open curing at 21 ± 2°C (56 days of carbonation)
	Reference samples		Carbonated samples
2%	7.8	8.8	9.0
5%	7.0	8.1	8.5

After prolonged (up to 90 days) curing, the leachability index further increased, exceeding the value of 8 in all cases and even reaching the value of 9 in the case of carbonated AABFS doped with 2% Cs. Therefore, AABFS synthesized under the experimental conditions used in this study can be considered as a potentially efficient matrix for immobilizing cesium from radioactive wastes.

4. CONCLUSIONS

In this paper, the impact of accelerated carbonation process on leaching resistance and strength of AABFS doped with 2% and 5% cesium (i.e., a solidified simulated radioactive waste) was investigated. Accelerated carbonation together with the prolonged curing had positive impact on the effectiveness of immobilization of cesium in AABFS identified by an increase in Leachability index. AABFS synthesized under the experimental conditions used in this study can be considered as a potentially efficient matrix for immobilizing cesium from radioactive wastes.

ACKNOWLEDGEMENTS

This research was financially supported by the NATO SPS programme (project G5402) and the Ministry of Education, Science and Technological Development of the Republic of Serbia (project TR 34026).

REFERENCES

- [1] Bernal, S.A. et al.: Other Potential Applications for Alkali-Activated Materials. Chapter 12 in *Alkali Activated Materials: State-of-the-Art Report, RILEM TC 224-AAM*, J.L. Provis, J.S.J van Deventer (Eds.), Springer, ISBN: 978-94-007-7672-2 (eBook), Dordrecht, Heidelberg, New York, London, (2014) pp. 339-381
- [2] Shi, C., Krivenko, P.V. & Roy, D.M.: *Alkali-Activated Cements and Concretes*, Taylor & Francis, ISBN: 978-0-415-70004-7, Abingdon, UK, (2006)
- [3] Komljenović, M. et al.: Immobilization of cesium with alkali-activated blast furnace slag, *Journal of Hazardous Materials*, 388 (2020) 121765, ISSN: 0304-3894. Available from <https://doi.org/10.1016/j.jhazmat.2019.121765>
- [4] ANSI/ANS-16.1-2003 (R2017), Measurement of the leachability of solidified low-level radioactive wastes by a short-term test procedure, American Nuclear Society
- [5] EN 196-3: 2008, Methods of testing cement Part 3: Determination of setting times and soundness
- [6] EN 196-1: 2008, Methods of testing cement – part 1: determination of strength
- [7] EN 13295: 2004 - Products and systems for the protection and repair of concrete structures - Test methods - Determination of resistance to carbonation
- [8] Abdel Rahman, R.O., Zaki, A.A.: Assessment of the leaching characteristics of incineration ashes in cement matrix, *Chemical Engineering Journal*, 155 (2009) pp. 698–708, ISSN: 1385-8947
- [9] Abdel Rahman, R.O., Zaki, A.A. & El-Kamash, A.M.: Modeling the long-term leaching behavior of ¹³⁷Cs, ⁶⁰Co, and ^{152,154}Eu radionuclides from cement–clay matrices, *Journal of Hazardous Materials*, 145 (2007) pp. 372–380, ISSN: 0304-3894

36

Priscilla Teck, Ruben Snellings, Jan Elsen

Characterization of the reaction degree of slag in a cement by neural networks based electron microscopy image analysis

CHARACTERIZATION OF THE REACTION DEGREE OF SLAG IN A CEMENT BY NEURAL NETWORKS BASED ELECTRON MICROSCOPY IMAGE ANALYSIS

Priscilla Teck^{1,2}, Ruben Snellings¹, Jan Elsen²

¹ VITO, Sustainable Materials,
Boeretang 200, 2400 Mol, Belgium
e-mail: priscilla.teck@vito.be, ruben.snellings@vito.be

² KULeuven, Geology,
Celestijnenlaan 200 E, 3001 Heverlee, Belgium
e-mail: jan.elsen@kuleuven.be

SUMMARY: Ground granulated blast furnace slag is often used as a supplementary cementitious material in cement to improve the durability of the cement and reduce CO₂ emissions. The performance of the slag containing cement depends on the degree of reaction of the slag, which makes measurement of the reaction degree essential. Commonly used methods are XRD, selective dissolution and electron microscopy image analysis. RILEM round robin results have shown that XRD-PONKCS required further protocol development and selective dissolution tended to underestimate the degree of reaction. Electron microscopy seemed to give more consistent results, however, image analysis using BSE images + EDX mappings is time consuming and resolution dependent. Developing an image analysis algorithm that correctly segments the electron microscopy images can take a long time, involving many cycles of trial and error and is user dependent. In our study, we compare classical “manual” image analysis to artificial intelligence assisted image analysis using artificial neural networks for determining the reaction degree of slag in cement. Artificial neural networks are a type of machine learning model that will independently attempt to find the optimal way to segment an image based on a limited number of example segmentations (training cases). In addition to using color information to segment, these networks can also recognize phases based on shapes and textures. Therefore, they have a large potential to enhance image analysis. We use a real hydrated cement containing GGBFS and show that the reaction degree of GGBFS obtained by a neural networks based model is similar to “manual” image analysis and XRD PONCKS. Furthermore, the neural network model proved to require less development effort and contains less systematic errors than the “manual” image analysis making it a promising technique to use in the future.

KEY WORDS: reaction degree slag, cement, image analysis, neural networks, microscopy

1 INTRODUCTION

Supplementary cementitious materials (SCMs) are often used to reduce the CO₂ emissions of cement production. By adding SCMs, the performance and durability of the cement must not be compromised, therefore high quality materials are necessary [1]. Small amounts of materials (up to 15%) can be added to a cement without significant performance loss, even if these materials are largely inert [2]. When adding more material (beyond 30% is desired to have a real impact on CO₂ reduction), material reactivity is of major importance. Parameters that control reactivity for SCMs are only partially understood, even for widely used blast furnace cements [3][4]. Furthermore, despite that several different techniques that are available, measuring reactivity by quantification of the degree of reaction of SCMs in cements stays difficult. RILEM round robin tests on quantifying the reaction degree of slag and fly ash in blended cement have shown that the precision is rather low and at best $\pm 5\%$. They showed selective dissolution results are quite scattered and tend to underestimate the degree of reaction. Analysis of portlandite consumption significantly underestimates the degree of reaction and XRD PONKCS results were scattered. Most consistent results were obtained using electron microscopy [5].

However, preparation of samples for microscopy and measurement time can be time consuming. Furthermore, access to microscopes can be limited and analysis protocols are often not very robust [6]. Therefore, the use of microscopy image analysis for quantitative analysis of SCM reaction degree is limited.

There are different possibilities when it comes to quantitatively analyzing microscopy images. One classical method for analyzing such images is a point counting procedure, this involves a human operator counting up to 3000 points per sample and distinguishing between the different phases in the cement. This is a very time-consuming method prone to human bias. Another option is to develop a segmentation procedure using thresholding, filters and other image processing tools. This approach is less prone to human error and less time consuming. However, development of a robust procedure that can accurately analyze large amounts of images is time consuming and resource intensive (requiring expertise in both software development, image analysis and material characterization). Additionally, the procedures are often very case specific and therefore, might not work on other datasets, even of similar materials measured by different microscopes. Therefore this type of image analysis is still prone to systematic errors [7]. More advanced systems like mineral liberation analysis (MLA) are able to combine energy dispersive X-ray spectroscopy (EDX) information with back scattered electron (BSE) images. This system shows a range of advantages including systematic computer-automated analysis and increased through-put reducing human error and improving statistical representatively [8]. However, MLA requires specific software which is not always available, analysis is to some extent a black box model, segmentation is as well based on thresholding combinations and requires standard reference materials which are not always available [8]. Therefore, MLA is also prone to systematic errors.

Another promising option is the use of deep learning for image analysis. In recent years, significant progress has been made, using artificial neural networks for the segmentation of microscopy images, mainly in the field of medical image analysis [9]. Several models for microscopy image segmentation have been proposed. The most well-known one being the U-net which was developed in 2015 by Ronneberger, Fischer & Brox [10]. Artificial neural networks function based on supervised learning, i.e., based on a limited number of examples, they attempt to find the underlying structure in the data and can learn to segment images. Therefore, these networks are suitable when a large amount of data must be analyzed.

In this study we will use a cement containing 40% ground granulated blast furnace slag (GGBFS). The aim is to characterize the reactivity of the GGBFS at different reaction conditions using microscopy image analysis. An image analysis procedure applying thresholding and an artificial neural network based segmentation approach will be developed. Performance of both methods will be compared in terms of accuracy, reproducibility, development effort etc. Results will be validated with XRD PONKCS.

2 MATERIALS AND SAMPLE PREPARATION

2.1 Sample composition

The cement is composed of 50% Portland cement clinker, 40% GGBFS, and 10% limestone filler. Composition of each of the components as obtained by XRF analysis can be found in Table 1. Paste samples were prepared according to [11] at curing temperatures of 5, 20 and 40 °C and using water/binder ratios of 0.4, 0.5 and 0.6. Table 2 lists the different cement pastes, 6 samples were prepared at curing temperature 20 °C and water/binder ratio 0.5, they were left curing for different periods of time (1, 2, 7, 28, 90, 180 days). At other water/binder ratios and curing temperatures, one sample was made and cured for 28 days. Samples were stored in plastic tubes (12 mL) immersed in water at the correct curing temperature. After the respective curing time, a slice of 2-3 mm thickness was cut and immersed in 100mL isopropanol to stop the hydration reaction. Slices were left there for 1 week and the isopropanol was refreshed every 1-3 days [11].

Table 1: XRF results [wt.%] and densities [g/cm³] of the raw components.

	CEM I 52.5 R	GGBFS	Limestone filler
SiO ₂	20.35	35.21	0.85
Al ₂ O ₃	5.46	11.27	0.15
TiO ₂	0.28	1.07	0.01
MnO	0.04	0.21	0.06
Fe ₂ O ₃	2.4	0.26	0.16
CaO	62.33	41.64	54.54
MgO	1.49	5.96	0.91
K ₂ O	0.89	0.64	0.04
Na ₂ O	0.20	0.22	0.01
SO ₃	3.68	-	0.01
P ₂ O ₅	0.12	0.01	0.01
LOI	1.87	(+0.16)	43.32
Total	99.11	96.49	100.07
Density	3.12	2.89	2.72

Table 2: Curing temperatures and water/binder ratios (W/B) of the different samples. At water/binder 0.5 and Temperature = 20 °C, 6 samples were prepared and left for different curing times (1, 2, 7, 28, 90, 180 days), while for other W/B ratios and curing temperatures, one sample was made and cured for 28 days.

Temperature	W/B = 0.4	W/B = 0.5	W/B = 0.6
5 °C	X ₂₈	X ₂₈	X ₂₈
20 °C	X ₂₈	X ₁ X ₂ X ₇ X ₂₈ X ₉₀ X ₁₈₀	X ₂₈
40 °C	X ₂₈	X ₂₈	X ₂₈

2.2 Preparation of polished sections

From each cement paste sample, a polished section was prepared. Samples were impregnated under vacuum using an epofix resin. To guarantee that the resin impregnates the surface of the cement, the sample was slightly lifted and pressed onto the bottom of the sample holder using a spatula. This also ensured that sample is positioned perfectly flat in the sample holder. After 24 hours of hardening, the polished section was removed from the mould and carefully polished using a water-free lubricant and abrasive. Samples were polished at 9 µm until 2/3 of the sample is uncovered while attention was made not to polish too deep and uncover non-impregnated sample. Then, samples were polished for 2-10 minutes at 3 µm and 1 µm until all scratches were removed.

3 DATA ACQUISITION AND ANALYSIS METHODOLOGY

3.1 Data acquisition SEM

Image data were acquired using a FEI FEG Nova NanoSEM 450 equipped with a Bruker XFlash 5030 detector. An electron acceleration voltage of 20 kV and a working distance of 8 mm were used. For each of the 14 samples, 25 mappings of size 341*512 pixels were acquired in BSE and EDX mode using a 500x magnification. A total of 350 BSE images and EDX mappings was acquired. EDX mappings containing Mg, Al, Si and Ca were combined with BSE images and converted to a color image. Figure 1 shows an example of a BSE image and a combined BSE-EDX color image.

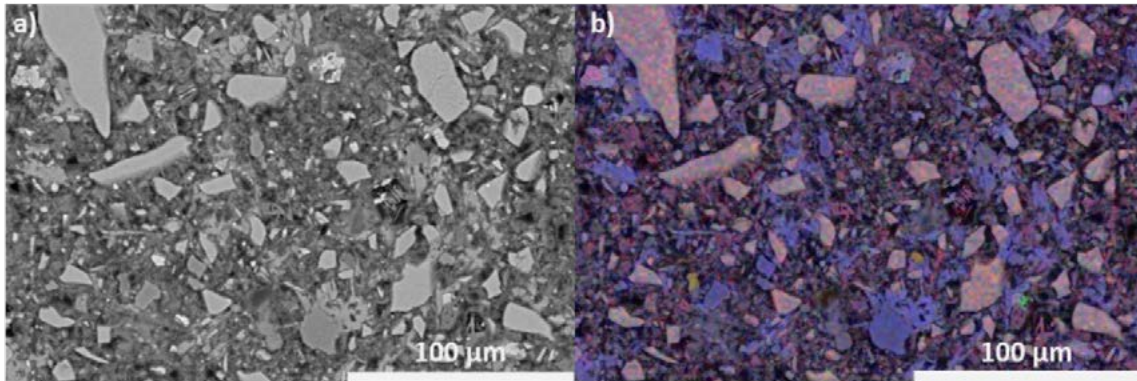


Figure 1: a) BSE image of the cement at 500x b) combined BSE+EDX image of cement at 500x. Slag particles are characterized by their homogeneous light grey color and distinct borders. In the combined BSE-EDX image, they appear light pinkish.

Two methods were used to analyze the images and to extract the reaction degree of slag: 1) Classical image segmentation using thresholds and 2) image segmentation using a neural network approach. Both methods are compared and the reaction degree values obtained by image analysis are compared to XRD PONCKS analysis results for validation.

3.2 Image segmentation algorithm applying thresholds

First, a segmentation algorithm using thresholds combining BSE image and EDX mappings was developed. Using only BSE images proved insufficient due to overlap between grey values of the slag and clinker phases. Elements that were used from the EDX mapping were Mg, Si, Ca and Al. A segmented mask is shown in Figure 2. This procedure was developed in Python using the Hyperspy library [12][13]. Steps for segmenting the images are as follows:

- Equalize BSE image
- Apply a threshold that selects the brightest phases
- Remove noise by removing patches of pixel size 1 and fill holes in particles
- Calculate the average value for each element of the EDX mappings for each selected particle
- Apply K-means algorithm on these values and select the cluster that consists of slag particles
- Apply segmentation to images and calculate reaction degree

Equalizing will stretch the histogram to make sure pixel values range from 0 to 255, this also increases contrast. Applying a threshold results in binary images where mainly slag and clinker are selected (white) and everything else becomes background (black). Slag and clinker are selected together because their pixels value range overlap in the histogram. Main challenge is then to distinguish between slag particles and clinker. Noise is removed by removing the smallest selected patches and since particles are solid, holes within particles are filled. Since the signal to noise ratio of the EDX element mappings is quite low, for each particle selected on the BSE image, the average value of the EDX mapping is calculated, this reduces influence of noise on the data. Distinguishing slag from clinker based on these values may be prone by operator bias, therefore, differentiating between the phases is done by a clustering algorithm, in this case the K-means algorithm. One of the clusters contains the slag material, these particles are selected and the percentage of pixels in the image that is selected as slag can be calculated. Based on this value, and together with the water to binder ratio, the reaction degree of slag is determined.

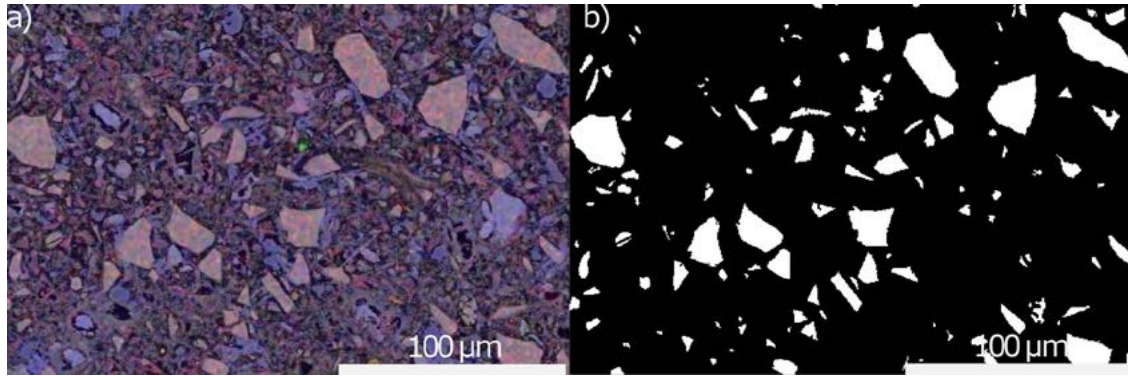


Figure 2: combined BSE-EDX image and resulting mask after segmentation by thresholding algorithm. Slag particles are selected in white.

3.3 Image segmentation using convolutional neural networks (CNN)

CNNs are machine learning models which make use of layers that all apply different convolutions (filters) to images and pass the result on to the next layer. In the last (fully connected) layer, the model produces a list of probabilities of the object belonging to a certain class. The layers contain weight matrices, these are sequentially applied to the input to propagate, and, eventually generate the output image. The weights are adapted during training by minimizing a loss function (i.e. the parameters of each layer are tuned). Therefore, the manual definition of thresholds or filter steps is not required, they are calculated during the training phase. This way, the model will learn to classify objects into different categories [14]. Once a model is trained, it can be used to classify objects, often with an accuracy comparable to humans. CNN training (model calibration/fitting) is performed by supervised learning, i.e. the network is presented a number of example images which it will use to adapt its weights and thereby finding the underlying structure of the data necessary for classification.

The type/architecture of CNN used is the U-net [10]. This is an architecture that was designed specifically for image segmentation of microscopy images in the field of biomedicine. It applies both downsampling and upsampling steps that create the U-shape of the network which is shown in Figure 3 [10]. Attempts were made using more recently developed segmentation models like the Mask-RCNN [15] and Segnet [16], however, a U-net was found best suitable for this task. It is much faster to train than the Mask-RCNN and is better at correctly positioning the borders of grains.

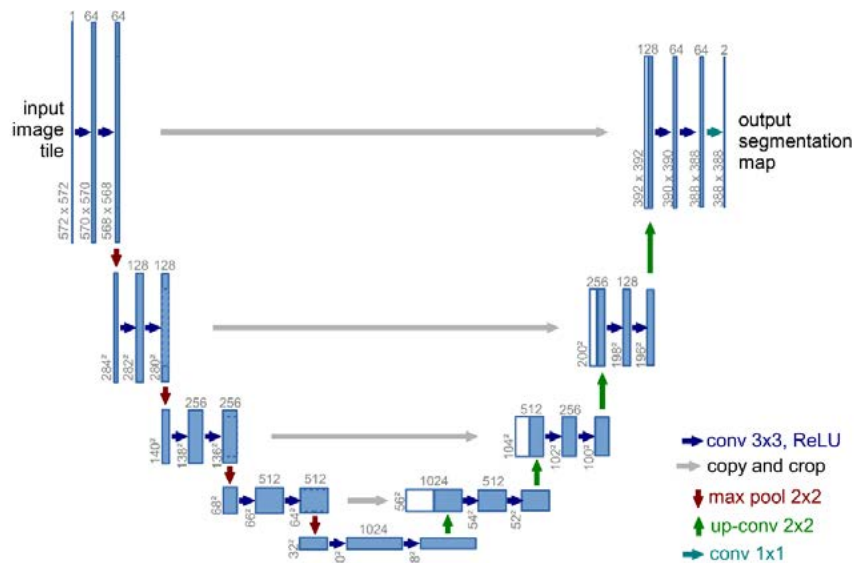


Figure 3 U-net architecture: The image is downsampled by applying convolutions, extracting the features. In the second part, the image is upsampled, using spatial information from the downsampling path in order to preserve spatial information. The output is a binary mask with the same size as the original image [10].

One of the most common problems training neural networks is overfitting. This occurs when the model works well on the training data while it is not able to correctly process unseen data, a common cause is too little training data. An element that makes the U-net very suitable for this task is that it was developed to work on a very limited data set using extensive data augmentation to overcome this. Since the data set used here is quite limited, increasing the amount of training data by data augmentation is required to prevent overfitting. The transformations carried out on both image and mask are: horizontal flip, vertical flip, shear, rotation, shift, zoom, adapt brightness. Data augmentation transformations are applied randomly and multiple times per image.

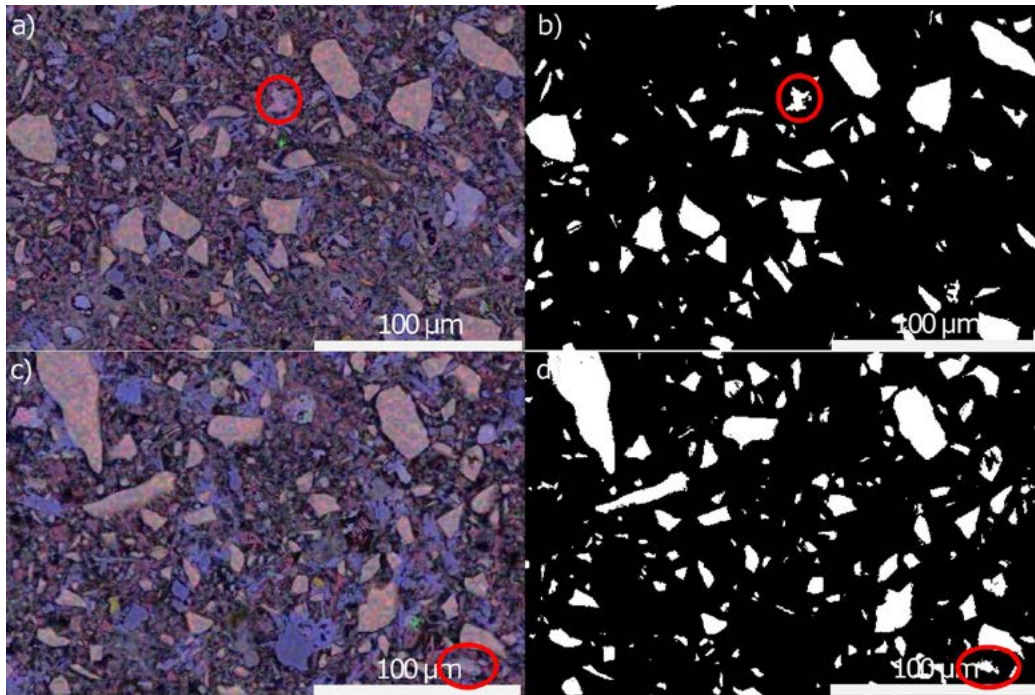


Figure 4: a) and b) are training images obtained by the segmentation algorithm, in red, a small error is selected. c) is a test image and d) is the output of the neural network model which also shows small errors.

From the total of 350 images, 70 representative images were chosen for training and ground truth masks were created. In a first attempt, the masks generated with the segmentation algorithm (as previously explained) were chosen as ground truth data for training. However, this algorithm still resulted in small errors and incorrectly segmented patches when it comes to the binary masked image. After training the neural network using the training data, the masks generated by the neural network contained errors very similar to the ones in the training set. Figure 4 shows an image of BSE-EDX image segmented using the segmentation algorithm with thresholds and the output of the neural network model that was trained on these data, both contain small errors. Therefore, preference was given for creating masks on the one hand by filtering and thresholding the image and on the other hand by manually adapting the image masks to remove errors. This results in 70 images of which the mask is nearly perfect. Figure 5 shows an example of a manually adapted image mask compared to the output of the thresholding algorithm. 50 images were chosen for training, 10 for validation and 10 for testing.

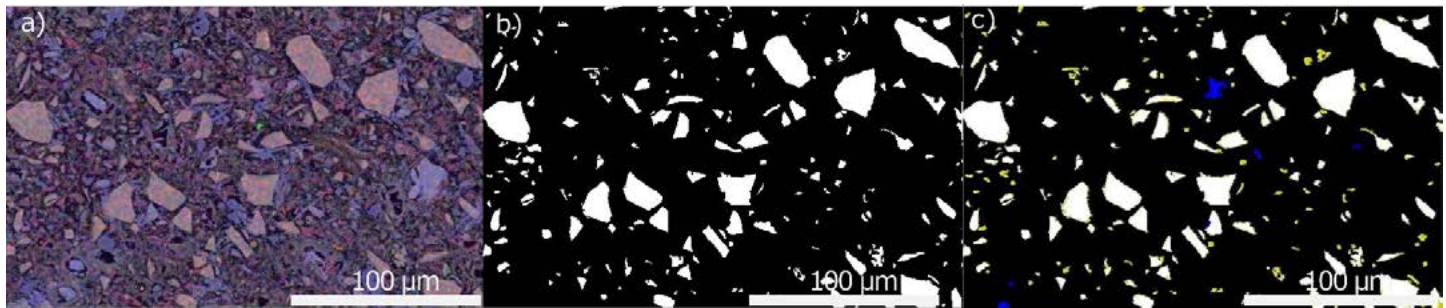


Figure 5: a) BSE-EDX image, b) mask manually adapted without errors, c) difference with manual segmentation algorithm: yellow patches were added, blue patches were removed.

The model was trained on RGB images containing the combined information of BSE + EDX. Training was carried out for 500 epochs which took around 1hour15min on one NVIDIA GeForce RTX 2080 Ti GPU. The model with best training and validation performance was chosen for testing. Based on the percentage of GGBFS left in the cement and the water/binder ratio, the reaction degree could be calculated.

3.4 XRD data acquisition and analysis by Rietveld-PONKCS phase quantification

XRD measurements were made on powdered samples using a Malvern-Panalytical Empyrean diffractometer. The diffractometer was equipped with a CoK α X-ray tube which was operated at 40 kV and 45 mA. Measurements were carried out in Bragg-Brentano configuration over an angular range of 5 to 90 $^{\circ}2\theta$. The step size used was 0.013 $^{\circ}2\theta$. A 2D solid state PIXcel3D detector with 255 channels covering an active length of 3.35 $^{\circ}2\theta$ was used to record the diffracted X-ray intensity signal. The equivalent counting time per step was 50 s, corresponding to a total measurement duration of about 22 min. XRD data were analyzed using Rietveld refinement to quantify the crystalline phase composition. In order to quantify the degree of reaction of the slag, a PONKCS phase [17] for the slag was integrated into the quantitative phase analysis following the procedure in [18]. The quantification results were recalculated to the initial clinker content to enable comparison across samples.

4 RESULTS AND DISCUSSION

Figure 6 shows the differences in segmented output between the two image segmentation methods. Average total difference between test set and ground truth for the manual segmentation model is 1.4 %. For the U-net model 2.9 %. Difference in percentage of GGBFS is, in both cases, 0.4 %. Main differences in segmentation are along the borders of grains and the identification of the smallest patches. In the images segmented by the U-net model, the clinker phase is hardly ever selected while this does occur using the thresholding algorithm. In terms of development effort: training the artificial neural network can be fast and flexible, in this case, training took 1 hour 15 minutes on our GPU. The most time consuming part is the generation of training data. This takes up to a couple of days for 70 images to manually adapt each individual image until no more errors are present. Using data augmentation, sufficient images were generated for training. Once trained, the model could segment all 350 different images in less than 30 seconds. Developing a segmentation algorithm using thresholds that works on all 350 images took more than a week and can only segment images of one sample at a time since some parameters have to be tuned based on image properties of the individual images.

Therefore, with regard to development effort, the artificial neural network approach scores better. Accuracy of both methods is similar, however, when looking visually at the output, the neural network is better at distinguishing between GGBFS and Portland clinker grains. Using a thresholding algorithm, it can be very hard to exclude the same particles without creating side effects which cannot be avoided due to the rigidity of thresholds. The U-net model can, apart from the grey level, take into account parameters like shape, size, texture etc. The major disadvantage is that it is a black box model and that it is very hard to check which features are used and their relative share to obtain the result.

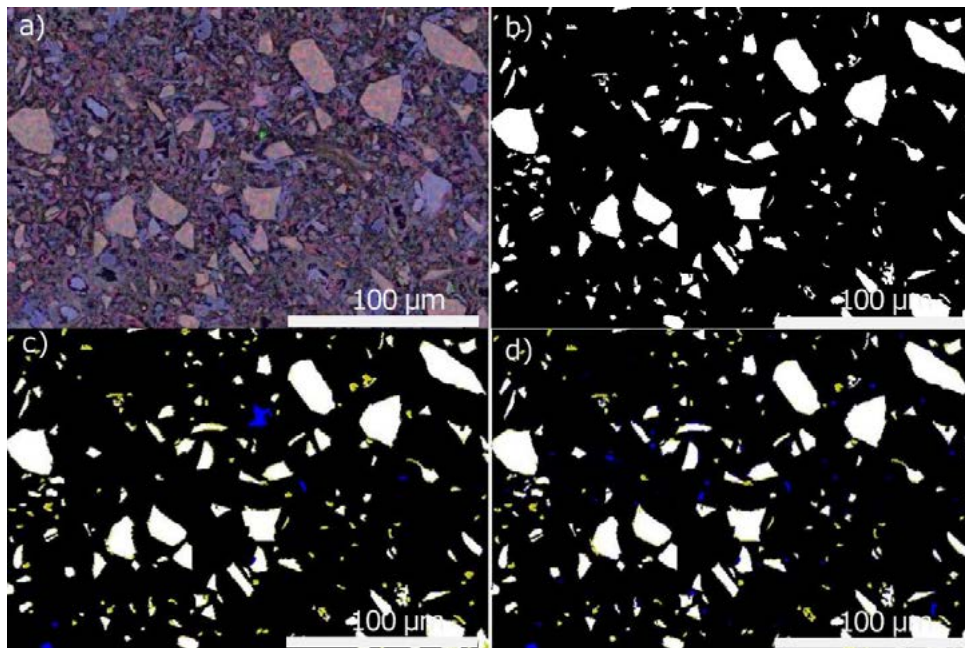


Figure 6: a) BSE-EDX image, b) ground truth mask, c) difference ground truth mask and output thresholding algorithm, d) difference ground truth mask and output U-net model. Yellow patches are selected as slag in the ground truth mask, however, are not selected as such in output thresholding/U-net. Blue patches are not selected as slag in the corrected mask, however, they are selected in the output of the thresholding/U-net.

Figure 7 shows the reaction degree calculated for the various reaction conditions calculated using the different techniques. These results generally agree. The only exception occurs at day one, due to the limited amount of GGBFS that has reacted, a lot of small particles are still present that could not be identified at 500x magnification. This results in an overestimation of the reaction degree. Using additional BSE-EDX data acquired at 1000x magnification resulted in a reaction degree of 15 % for both segmentation methods. When looking at the reaction degree at different reaction times, it is initially limited (10-20 %) at day one but steadily increases with hydration age up to 60-70 % at 180 days. At 28 days, there is clearly an effect of temperature, reaction degree is much higher in samples that were cured at 20 °C and 40 °C compared to 5 °C. The water/binder ratio seems to have little effect in this stage.

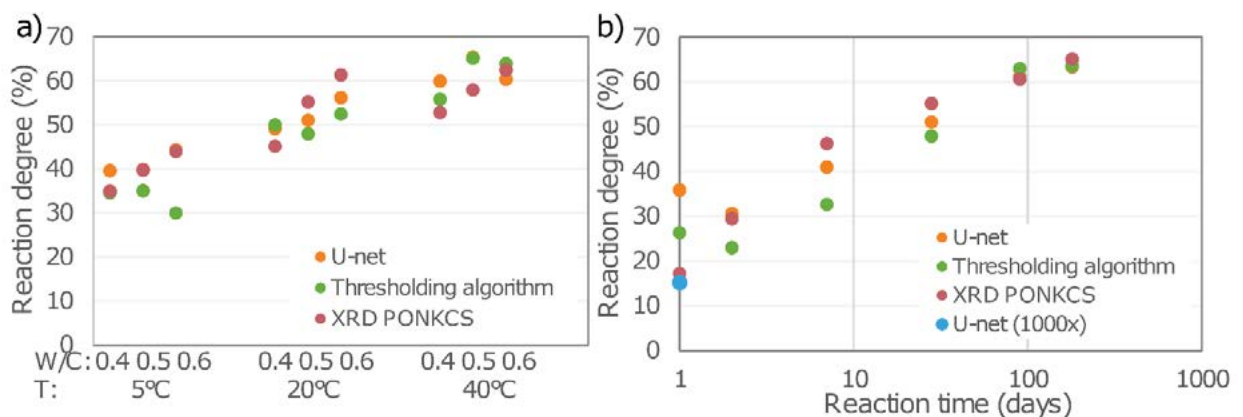


Figure 7: a) Reaction degree of GGBFS at different temperatures of curing and different water/binder ratio's at 28 days of age. b) Development of GGBFS degree of reaction as function of age (1,2,7,28,90,180 days, water/binder = 0.5, T = 20°C). Image data acquired at 500x magnification except when explicitly mentioned.

5 CONCLUSION

In this work, we tried to calculate the reaction degree of GGBFS using an artificial neural network for image segmentation of BSE-EDX images. The image segmentation model that was found most suitable for this task is the U-net. Visual inspection of the segmented images showed that slag particles could be identified accurately and that the amount of incorrectly selected patches was limited. Errors mainly occurred when trying to identify the smallest patches and the borders of the grains. Accuracy was similar to the segmentation algorithm. With regard to development effort, developing a segmentation algorithm takes a long time, with a lot of trial and error and, in the end, it is still prone to systematic errors, e.g. selecting clinkers particles as well as GGBFS particles. However, each step of the procedure can be controlled. Development of the procedure using the U-net requires less effort. The most time consuming part is the acquisition of good training data. When the training data contains errors, the segmented output of the trained model will contain very similar errors, therefore, acquisition of good training data is essential. Furthermore, the model generalizes well compared to the segmentation algorithm. It can accurately segment all 350 images at once, while using the segmentation algorithm, some parameters have to be tuned for each sample. The main disadvantage of the artificial neural network is that the model is a black box, it is very hard to examine which features the artificial neural network uses to update its weights. When calculating the degree of reaction of GGBFS, the results of the reaction degree calculated from the images segmented by the U-net, the segmentation algorithm and XRD are in agreement. This shows that, using artificial neural networks for image segmentation can measure the degree of reaction of SCMs with a similar level of accuracy as other commonly used methods. Next steps will be to use higher resolution images for training and attempts will be made using only BSE images. Furthermore, we will look whether this approach can be used for analyzing different systems containing other phase compositions.

REFERENCES

- [1] Provis, J. L.; Bernal, S. A.: Geopolymers and related alkali-activated materials. *Annual Review of Materials Research*, 44, (2014) pp. 299-327.
- [2] Snellings, R.: Assessing, understanding and unlocking supplementary cementitious materials. *RILEM Technical Letters*, 1, (2016) pp. 50-55.
- [3] Juenger, M. et al.: Supplementary Cementitious Materials for Concrete: Characterization Needs. *MRS Online Proceedings Library Archive* 1488 (2012).
- [4] Snellings, R.; Mertens, G. & Elsen, J.: Supplementary Cementitious Materials. *Reviews In Mineralogy & Geochemistry*, 74, (2012) pp. 211-278.
- [5] Durdziński, P. et al.: Outcomes of the RILEM round robin on degree of reaction of slag and fly ash in blended cements. *Materials and Structures*, 50, (2017) No. 2, p. 135.
- [6] Kocaba, V.; Gallucci, E. & Scrivener, K. L.: Methods for determination of degree of reaction of slag in blended cement pastes. *Cement and Concrete Research*, 42, (2012) No.3, pp. 511-525.
- [7] Deschner, F. et al.: Quantification of fly ash in hydrated, blended Portland cement pastes by backscattered electron imaging. *Journal of microscopy*, 251, (2013) No.2, pp. 188-204.
- [8] Sylvester, P.: Use of the Mineral Liberation Analyzer (MLA) for mineralogical studies of sediments and sedimentary rocks. *Mineralogical Association of Canada Short Course Series*. 42, (2012) pp. 1-16.
- [9] Litjens, G. et al.: A survey on deep learning in medical image analysis. *Medical image analysis*, 42, (2017) pp. 60-88.
- [10] Ronneberger, O.; Fischer, P. & Brox, T.: U-net: Convolutional networks for biomedical image segmentation. *In International Conference on Medical image computing and computer-assisted intervention*, (2015) pp. 234-241. Springer, Cham.
- [11] Scrivener, K.; Snellings, R. & Lothenbach, B.: A practical guide to microstructural analysis of cementitious materials (Vol. 540). Boca Raton: Crc Press. (2016).
- [12] Guido, R.: Python reference manual, (1995).
- [13] de la Peña, F. et al.: Electron microscopy (big and small) data analysis with the open source software package HyperSpy. *Microscopy and Microanalysis* 23, no. S1 (2017): pp. 214-215.
- [14] Krizhevsky, A.; Sutskever, I. & Hinton, G. E. Imagenet classification with deep convolutional neural networks. *Advances in Neural Information Processing Systems*, 25, (2012) pp.1106–1114.
- [15] He, K. et al.: Mask r-cnn. *In Proceedings of the IEEE international conference on computer vision* (2017) pp. 2961-2969.
- [16] Badrinarayanan, V.; Kendall, A. & Cipolla, R. Segnet: A deep convolutional encoder-decoder architecture for image segmentation. *IEEE transactions on pattern analysis and machine intelligence*, 39, (2017) No.12, pp. 2481-2495.
- [17] Scarlett, N.; Madsen, I.C.: Quantification of phases with partial or no known crystal structures, *Powder Diffr.* 21, (2006) pp. 278–284.
- [18] Snellings R.; Salze A. & Scrivener K.L.: Use of X-ray diffraction to quantify amorphous supplementary cementitious materials in anhydrous and hydrated blended cements, *Cement and Concrete Research*, 64, (2014) pp. 89–98.

37

Dejan Vasić and Marina Davidović

BIM application in civil engineering projects



BIM APPLICATION IN CIVIL ENGINEERING PROJECTS

Dejan Vasić¹ and Marina Davidović²

^{1,2}University of Novi Sad, Faculty of Technical Sciences, Department of Civil Engineering and Geodesy

Dositej Obradović Square 6, 21000 Novi Sad, Republic of Serbia

e-mail: marina.davidovic@uns.ac.rs

SUMMARY: BIM, abbreviation from “Building Information Modeling” is a relatively new concept in the technical disciplines. Scientists, engineers and designers consider this technology as future in all stages of design. In traditional design, there are two-dimensional elements, while BIM also implies a third dimension. However, the BIM model of an object is not just a 3D model, it is also a model that contains numerous kinds of data and information that can be used and manipulated throughout the whole life cycle. This paper gives an overview of BIM technology and modeling based on captured data. The obtained point cloud, as input data is obtained by laser scanning. Two case studies are presented - creating a 3D smart home model and 12 km long rail.

KEY WORDS: BIM, laser scanning, point cloud, house, rail

1 INTRODUCTION

Complex architectural works, modern construction techniques and the management of the entire construction site is inconceivable without the modern technical solutions. One of the technologies that emerge in project management and construction is BIM. BIM is similar to the concept of PLM (Product Lifecycle Management) because, in addition to physical characteristics of an object, it also deals with: cost management, project management and simultaneous work on different aspects of object usage [1].

Most modern companies use BIM to manage and coordinate projects in three dimensions. With the help of 3D models and their inspection, many construction issues and dilemmas are solved very successfully. The benefits of BIM usage are numerous, from project running and managing, detecting possible errors to the visual identity of the building itself. This could also prevent problems during construction work [2].

The aim of this paper is to present the basic characteristics of BIM "for as-built models", as it is not about design but about surveying existing data. BIM level of details and software are described and then realized project is presented - from data capturing to the 3D smart model creation.

2 BIM

The BIM application begins with the production of high-quality 3D terrain bases such as digital terrain models and digital surface models. Then, it proceeds with modelling based on relevant information about the project, design and object location. This leads to the development of an intelligent 3D model whose elements are linked dynamically, not only by points, surface and planes but also by a rich set of shared data. All of these steps depend largely on the quality of the collected data, and according to model level of development, there is a division into groups, presented below.

2.1. BIM level of development

Level of Development (LOD) is the degree to which the element's geometry and attached information has been thought through – the degree to which project team members may rely on the information when using the model. There are LOD from 100 to 500 presented in Figure 1 below [URL1].

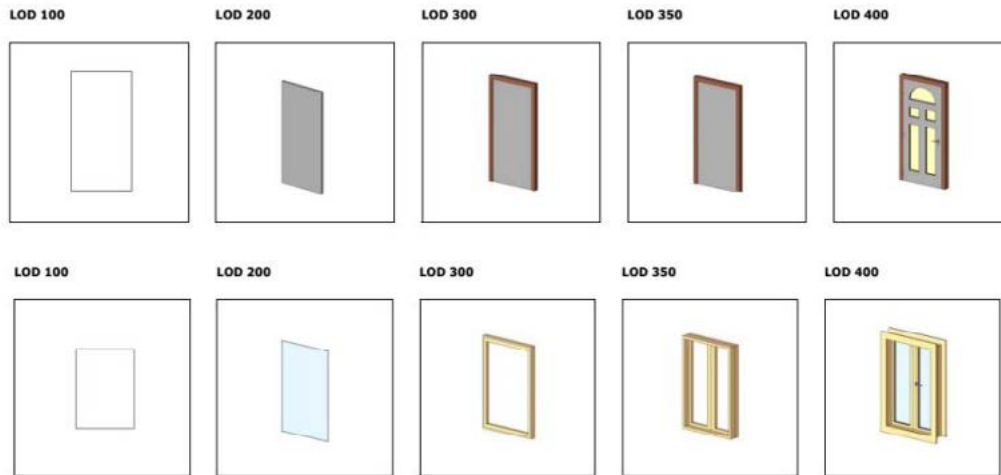


Figure 1: BIM levels of detail for windows and doors LOD 100-LOD 400 [URL1]

As it can be seen from the Figure 1, this LOD division is depending of the level of details, where LOD 100 model have just some core elements, presented with symbol. LOD 200 assembly with approximate quantities, size, shape, location, and orientation. LOD 300 presents an upgrade on LOD 200, having more details about and some details around object. LOD 350 interfaces with other building systems where non-graphic information may also be attached to the model element. LOD 400 model element is graphically represented within the model as a specific system, object or assembly in terms of size, shape, location, quantity, and orientation with detailing, fabrication, assembly, and installation information. LOD 500 presents an upgrade of LOD 400 model, having more specific and tiny details.

2.2. BIM software

BIM Software is mostly used by individuals, businesses and government agencies involved in the planning, design, construction, management and maintenance of various elements such as: buildings, rivers and canals, power and gas facilities with associated network, factories, roads, bridges, tunnels and many other infrastructure facilities [3].

AutoCAD Civil 3D is an Autodesk BIM solution for civil engineering. Software used for object design, ie. in building construction is numerous. Some of the more popular ones are Revit, Tekla, AlarmCAD, ArchiCad, AutoCad AEC, Applications, AutoSPRINK, Bentley Building, CADPipe, Design Master Software, FireAcad, GenerativeComponents.

The Revit software is specifically designed for BIM, to empower architectural and construction professionals to bring the idea to construction with an approach based on coordinated and consistent modelling. This includes the functionality of all Revit disciplines (architecture, engineering, energy, installations, construction) into one single interface [1].

Some of the most popular BIM software solutions for pipe, installation and metal modeling structures are Revit, InfiPoints and EdgeWise.

3. PROJECTS REALIZED WITH BIM TECHNOLOGY

Quality management requires a quality inventory of the entire construction site and coordination of machines in the construction process. Surveying can offer assistance in this process. The role of surveying engineering in the BIM creation is to provide information about the physical and functional characteristics of the site and present it in digital format. Whether it is a field project, a monitoring project for the implementation of planning documents, or the BIM creation of an existing object, modern spatial data acquisition technologies enable detailed and high-quality digital representations of real objects [1].

This chapter presents two projects that are realized thanks to the data obtained by modern surveying methods.

3.1. BIM model of house

This paper part gives a detailed insight into house modelling. The input data was point cloud, obtained by terrestrial laser scanning. The used scanner is Trimble FX. Initial preparing of point cloud included matching and reduction of points number in order to make easier further manipulation.

The modelling is conducted in several stages. At first, the basic building elements are modelled: walls, floors, poles and roof. Afterwards, doors and windows, fences and other details are modelled. It is preferable to use the Section Box tool because it provides a limited view for a specific area of interest. During the individual elements modelling, it is enough to model one with precise dimensions, colour, material and other required characteristics, and save it as a so-called "family". Afterwards, in the main project that element is imported to the appropriate position the required number of times [4].

Figure 2 shows the matched point cloud and the created BIM model based on it. Regarding above explained LOD levels, this house presents LOD 300 model.

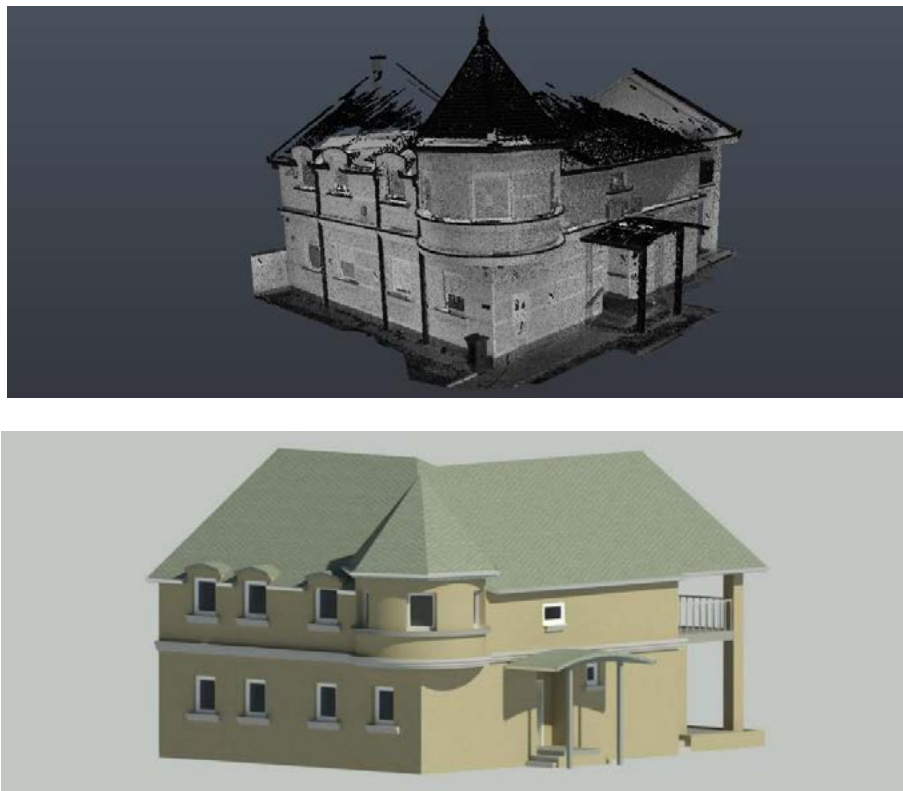


Figure 2. From point cloud to BIM model-object

When the modeling of the exterior object was completed, the modeling of the interior began. In addition to basic floor maps, BIM includes many other details. On the basis of point cloud and photographs of the building, desks, chairs, computers and other office furniture, as well as elements in toilets, corridors etc. were modeled. Particular elements were formed, and then placed on right position. This process was repeated for all other elements within the home. Figure 3 shows the floor maps of this BIM model [4].

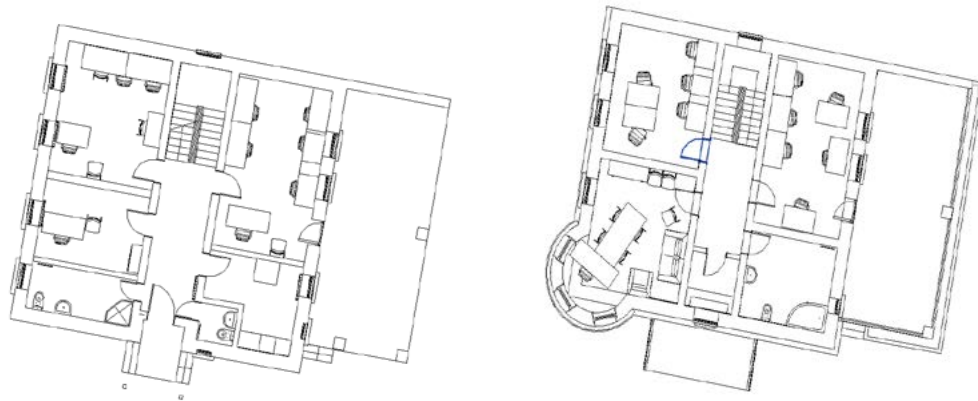


Figure 3: Detailed floor maps- 1st and 2nd floor

3.2. BIM model of rail

The other project presented in this paper is scanning and then modelling of the rail in Austria. The surveying is accomplished by mounting scanner on train, and 12 km of railway and its environment is covered. The laser scanner that was used is Trimble MX8. After initial adjustments and processing of the point cloud, modeling was conducted (Figure 4).



Figure 4. From point cloud to BIM model-rail

At first, an axis was made from the trajectories obtained from the point cloud. That axis is duplicated and moved in the way that directions of rails are obtained. Between the rails, beams are modelled and situated. The beam modelling process is performed by utilizing the characteristics of Deutsche Bahn manual. That is a specification for all German and Austrian rails, consisting of different types with different measures. One beam with all its details, such as screws and additional small elements is modelled according to that specification. Afterwards, it is just multiplied at a certain distance,

measured from the point cloud, and checked in the manual. Figure 5 presents the point cloud rail beams and its model [2].

Then entire railroad is attached to the ground model, which is previously obtained from the point cloud in MicroStation software.

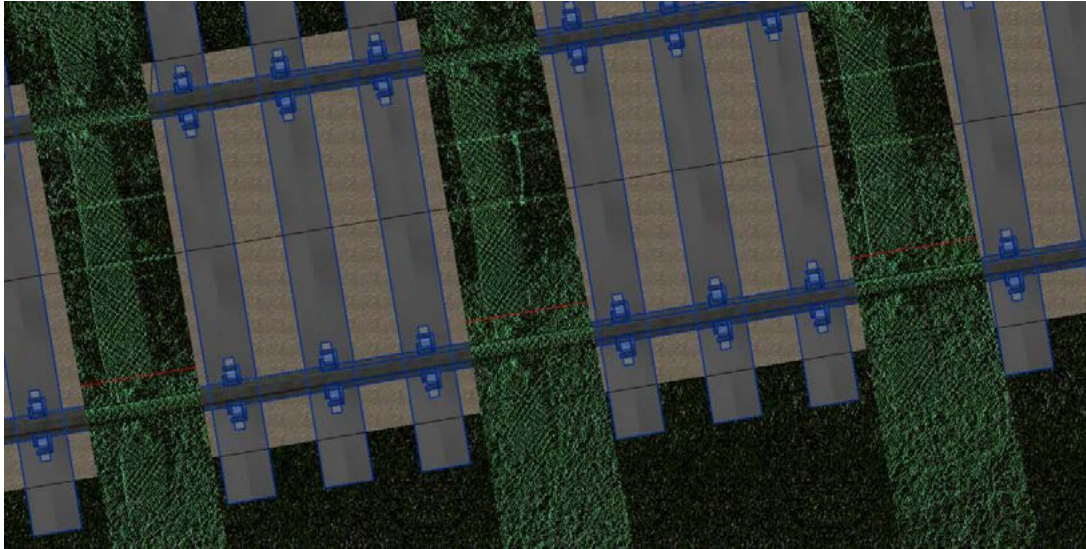


Figure 5: Point cloud and BIM model of rail beam

After that, details surrounding the railway, such as houses, buildings, stations and ramps were modelled. Figure 6 shows one part of rendered BIM model- railway and its environment. The level of detail is equal to LOD 250. This model provided plenty of views and renders, such as wire-frame model, intensity model, classifications by height and other characteristics. Also, this 3D smart model is varying, ie. some dimensions or materials could be changed, and that will affect the calculations and further processes [2].





Figure 6 - Rendered BIM model of the rail and environment

4 CONCLUSION

Although the roots of BIM technology are related to architecture, the principles of working on an accurate 3D digital model apply to almost all infrastructure projects that surveyors participate on daily basis. As explained in this paper, the basis of a BIM system is a 3D model of an object that, in addition to the visual representation, contains many other information, such as geodetic coordinates, quantities of materials and elements, properties of the element (thermal conductivity, mass or strength), structural elements of the object, prices and many other required information. BIM also enables so-called as-built models, i.e. models of the existing state of facilities, which we presented in our paper [4].

In the next phase of creating BIM for an existing object, the database needs to be supplemented with significant information about facility. In the case of roads, this could also be a construction control as it provides an insight into the thickness of the road layers as well as the registration of supporting lines and installations. Information relevant to the database could include contractors and the work costs, the year of construction, manufacturers of individual facility parts, information on maintenance and consumption and many others. Information relevant to the pipes could be related to the profiles, materials, volume, pressure in the pipe etc. This would complete the creation process and enable changes of this technology in further exploitation of the object [1].

With laser scanning and BIM, surveyors can embrace and expand its significant role in major construction projects. At any place where the redevelopment of existing facilities is planned, architects and civil engineers will need information on the existing condition in order to begin the redevelopment process. Ensuring the rapid collection of accurate data on often complex and abandoned structures is the job of surveyors. Surveying experts are the ones who will have to deal with often complex objects and provide reliable data on their real state and create 3D models suitable for further development of the BIM process, ie. designing models of the existing state [5].

Note: Project presented in paper is published with kind permission of the contributor. The original data were provided by DataDEV company, Novi Sad, Republic of Serbia.

REFERENCES

[1] Sabadoš, I., Ninkov, T., Petković, M., Batilović, M., Antonić, N.: BIM i geodezija, Zbornik radova građevinskog fakulteta, vol. 30, pp. 149-161, 2016

[2] Vasić, D., Davidović, M., Batilović, M.: Mobile Mapping System: Suitability for Building Information Modeling of Railway, FIG Working week, Amsterdam, 2020

[3] Azhar, S., Nadeem, A., Y. N. Mok, J., H. Y. Leung, B.: „Building Information Modeling (BIM): A New Paradigm for Visual Interactive Modeling and Simulation for Construction Projects“, Proceedings of First International Conference on Construction in Developing Countries, “Advancing and Integrating Construction Education, Research & Practice”, Pakistan, Karachi, pp. 435-446, 2008

[4] Davidović, M., Vasić, D.: BIM tehnologija kao novi koncept u geodeziji, Izgradnja, 2020

[5] Bečirević, D., Babić, L., Cigrovski, I.: Od podataka laserskog skeniranja do BIM modela postojećeg stanja, Ekscentar, vol. 17, pp. 87-92, 2014

[URL1] <https://www.a2kstore.com/levels-of-development-levels-of-detail-lod-explained>

38

Dejan Vasić, Mehmed Batilović, Marina Davidović and Tatjana Kuzmić

Application of terrestrial laser scanning methodology in façade reconstruction and rehabilitation projects



APPLICATION OF TERRESTRIAL LASER SCANNING METHODOLOGY IN FAÇADE RECONSTRUCTION AND REHABILITATION PROJECTS

Dejan Vasić¹, Mehmed Batilović², Marina Davidović³ and Tatjana Kuzmić⁴

^{1,2,3,4} University of Novi Sad, Faculty of Technical Sciences, Department of Civil Engineering and Geodesy

Dositej Obradović Square 6, 21000 Novi Sad, Republic of Serbia

e-mail: coms2020@zag.si

SUMMARY: In recent years, the need for spatial data and products that can be obtained by processing them has been increasing. As a result, there is a tendency to collect data as quickly as possible, which led to the development of new methods, as well as to the improvement of the quality of the final products. In addition to saving time, tendency is also to collect data of more accuracy, higher density, extraction of as diverse information as possible based on the collected data, etc. Moreover, high demand exists in developing the devices and platforms by which raw spatial data is collected. Specifically, their features are getting better, the devices are getting smaller and more compact, and ultimately, cheaper, making them significantly more affordable and attractive to users. Terrestrial laser scanning enables quick and easy collection of spatial geometric data. By using laser scanner, the area of interest is surveyed with high frequency. Based on the collected data, the position of each point in the 3D local coordinate system is determined. In addition, it is possible to perform georeferencing of spatial data, i.e. defining them in the state coordinate system. The paper gives a brief overview of terrestrial laser scanning technology, methodology of data collection and processing for the needs of digitization of facades with a high level of detail.

KEY WORDS: terrestrial laser scanning, façade, point cloud, reconstruction, rehabilitation

1 INTRODUCTION

In geodesy, as in many other scientific disciplines, it has come to an intense development of technologies, methods and processes. This development not only contributes to faster data collection and easier processing, but also to the collection of much more meaningful and comprehensive data, which was previously unthinkable. Data can be stored, subsequently further reviewed and processed. This is precisely the case with laser scanning technology and facade scanning. Laser scanning technology has marked a major milestone in modern geodetic surveying technologies and spatial data acquisition. Scanning the facades with this technology produces a point cloud of the building's or object's facade that gives a very high level of detail to its true digital representation. The resulting point cloud can be used to digitize the characteristic edges and elements of the facade - decorations, windows, doors, etc. Documentation of buildings has proven to be a valuable tool for a variety of civil engineering issues including: protection and preservation, restoration and conservation, monitoring and management, identification and interpretation of buildings, sites and cultural landscapes [1].

Numerous scientific papers deal with the analysis and improvement of the application of laser scanning technology in the facade documentation. Paper [2] presents the study of a preserved mansion house of cultural significance, using TLS techniques for facade documentation. Multiple scans were registered using artificial targets and appropriate software to form a single contiguous 3D model. Further process resulted in a model that offers measurement possibilities valuable to future plans and designs for preservation and restoration. The objective of paper [3] is to find the potential of the terrestrial laser scanning technique to detect the deterioration on the surfaces of the building facades and to quantitatively measure the dimensions of the damaged areas. The paper is focusing on detecting the bowing of marble cladding and the surface delamination of brick facades. The results show that the terrestrial laser scanning technique gives a reasonable method

for this purpose. Paper [4] deals with facade scanning of The City Hall of Novi Sad using Leica Scan Station scanner. A GPS receiver was used to measure coordinates of three different points on the facade, so that the scans may be georeferenced later in the process. At the end of scanning process there were three point clouds which represented front, the west and east parts of the City Hall's facade. Refined point clouds were exported in DXF and 3DS formats and visualized in Leica Virtual Explorer Architect.

2 MODERN GEODETIC TECHNOLOGIES

Spatial data collection in the field of engineering geodesy is carried out today by conventional methods, most frequently with the required accuracy. The development of new technologies, devices and processing methods imposes new ways of measurement and collecting 3D data about terrain and objects. New methods are not only more efficient but they provide an incomparably higher level of detail than conventional methods, and they often have an advantage over them [5]. Laser scanning is one of these modern technologies that has lately been very popular in the surveying community.

2.1 Terrestrial Laser Scanning

Laser scanning is a technology that has been widely used in recent years for collecting spatial data. What makes it attractive for using is fast and relatively easy way of collecting data with large density and high quality. In spite of conventional geodetic methods of collecting data, where most of the time is spent on collecting data, in laser scanning significantly larger amount of time is left for data analysis and interpretation. The lack of laser scanning method is that huge amounts of data are generated while surveying, so the appropriate resources to handle these data and their processing are needed [6].

Terrestrial laser scanning enables quick and easy collection of spatial geometric data on buildings, machines, objects, etc. A laser sensor within a terrestrial laser scanner emits pulses of laser light traveling through space and reflecting obstacles, i.e. surfaces of buildings, objects and the like. For each laser reflected pulse, a length S' and two orthogonal angles w_1 and w_2 are recorded (Figure 1). Based on this data and the intensity of the reflected signal, the position of each point in the 3D local coordinate system is determined. The intensity of the reflected wave is significant for visualization, especially with complex and dense point clouds [7]. The main output data of the surveying with laser scanner are dense sets of points, where their density depends on the device, and with the advancement of technology, the density increases [8].

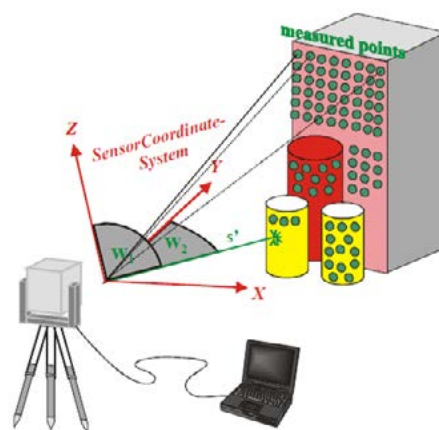


Figure 1: Terrestrial laser scanning [7]

With the terrestrial laser scanning method, the scanning is performed from multiple locations, i.e. from multiple scans. At the first station, the scanner collects spatial data within its field of view, and after that the scanner moves to the next point from which the second part of the object is scanned. The process can be repeated until the complete subject is recorded. Between these individual point clouds, i.e. scans there must be an overlap to allow the scans to be matched.

3 THE APPLICATION OF TERRESTRIAL LASER SCANNING TECHNOLOGY FOR FAÇADES SCANNING

The data obtained by laser scanning of a particular area contains useful information and they are considered as very valuable data source. Compared to traditional surveying methods, laser scanning is more applicable on different terrains and faster in terms of surveying process and post-processing as well [9].

For the case study in this paper, house located in Germany is used and it is surveyed by terrestrial laser scanning technology. The initial step after surveying process is point cloud matching and every other post-processing step largely depends on the quality of matching step. The prepared point cloud for further processing is shown in Figure 2.



Figure 2: Point cloud of the house

After initial steps, the process of extraction is carried out. The software package used for this purpose is Micro Station. This is a CAD software platform for two and three dimensional design and drafting, used in the architectural and engineering industries.

At the beginning, the narrow vertical profile, i.e. section is set up, so the view is appropriate for digitizing. The simple tools, as lines and polygons are used, and with displayed point cloud, the edges of windows, doors and roof with all other details are drawn. Later, hatches could be used for improving the presentation of exterior - for example, roof is hatched, and the part that is separating the floors as well. After facade extraction of one side, the other three sides of house are extracted in the same way, so the final product is whole exterior of the house digitized. Figure 3 shows one side of carried out facade extraction.

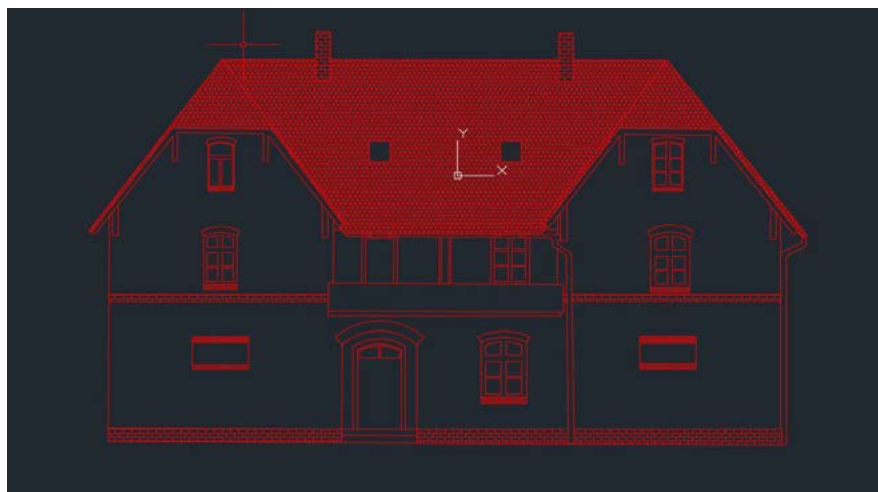


Figure 3: Digitized exterior from obtained point cloud

Different elements of house can be separated by different layers, after which any attributes can be assigned, as well. For example, the windows can be separated in one specific layer, and then area, dimensions, position and other data can be assigned as layer attributes. After separating different elements in different layers, and presenting them with different colours, by using MicroStation tools, wireframe model of the house is created (shown in Figure 4).

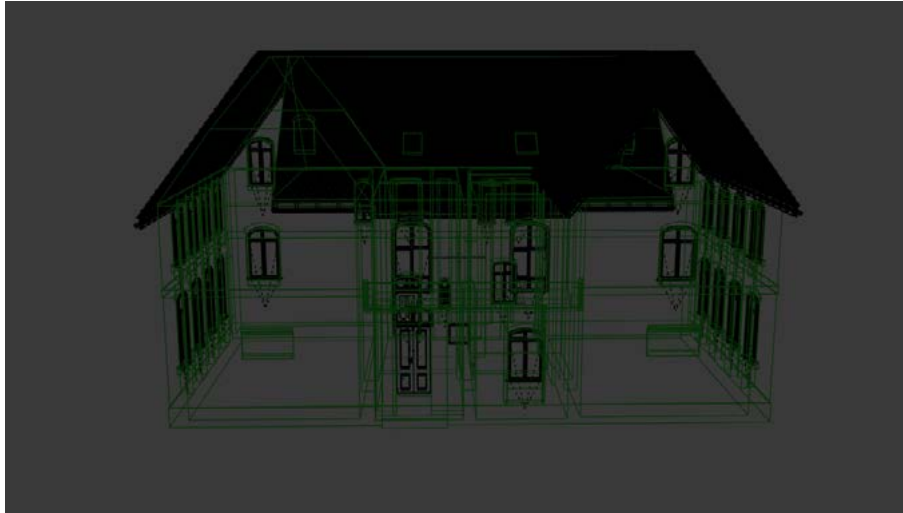


Figure 4: Wireframe model of the house

The purpose of above presented project is digitalization of exterior of the house. This method can also be very useful for different types of rehabilitation and reconstruction projects. For example, after extraction process of elements of interest, the elaborate of facades can be compared with previous, and any changes could easily be detected.

Using the appropriate software, it is very quick and easy to create drawings such as floor plans, longitudinal and cross-sections and facade drawings that architects and designers need for documentation of the building condition. Based on these drafts, facility renovation projects can be planned as well. Thanks to the high precision and high level of detail of 3D scanner measurements, it is possible to create a reconstruction plan for both the original shape of the facade and the ornaments on the facade. Another great advantage of this approach is the ability to generate accurate cost estimates, which allows the investor to realistically plan costs. Also, 3D modelling of the entire interior of the building provides the possibility of using modern software for calculations of statics and loads on different parts of the building, which allows faster and more accurate identification of critical points. In addition, the digital display of the building makes it very easy to detect and document damage, cracks and other potential hazards, thanks to the high resolution and level of detail of the laser scanning technology.

4 CONCLUSION

The laser scanning method is applicable to a growing number of areas, and consequently, increasing attention is paid to the further development of this method and improving its accuracy [9].

By using traditional geodetic methods, the process of facade extraction would be impossible, especially with above presented quality of final product. With terrestrial scanner, in less time is possible to obtain a significantly larger amount of data, representation of a larger part of the terrain, higher level of detail and the possibility of subsequent additional analysis and processing of the collected data.

The point cloud provides very different manipulation possibilities, and there are a lot of software that enables it. In this paper the MicroStation is used, and it is presented how detailed facade extraction can be carried out. The wireframe model of the house in Germany is also created. But, there are even more possibilities that software packages in

integration with modern technologies can offer. One of them is BIM creation. BIM, or Building Information Model is a process for creating and managing information on a construction project across the project lifecycle. One of the key outputs of this process is the 3D smart model, the digital description of every aspect of the built asset, including facades, of course. So further work can be directed to BIM modelling discovering all possibilities it offers.

ACKNOWLEDGMENTS

The authors gratefully acknowledge the funding provided by the Ministry of Education, Science and Technological Development of Republic of Serbia under project "Development of a decision support system for integrated water resources management in the basin", number TR37018. In addition, this research has partially been supported also by the Faculty of Technical Sciences, Department of Civil Engineering and Geodesy under project „A comprehensive approach to improvement of interdisciplinary researches in construction education and science“.

REFERENCES

- [1] N.A. Haddad, N.A.: From ground surveying to 3D laser scanner: A review of techniques used for spatial documentation of historic sites, *Journal of King Saud University–Engineering Sciences*, Vol. (23), No. 2, pp. 109-118, 2011
- [2] Karagianni, A.: Terrestrial Laser Scanning in Building Documentation, *Civil Engineering and Architecture*, Vol. (5), No. 6, pp. 215-221, 2017
- [3] F. Al-Neshawy, F., Piironen, J., Peltola, S., Puttonen, J.: The potential of the terrestrial laser scanning for geometrical building facades inspection, *Journal of Structural Mechanics*, Vol. (42), No. 4, pp. 235-245, 2009
- [4] Pajić, V., Jovanović, D., Govedarica, M.: Modeling city hall's facade using laser scanning technology, *Pregled NCD*, Vol. (15), pp. 59-63, 2009
- [5] Vasić, D.: Model geodetskog premera savremenim akvizicionim tehnologijama, PhD dissertation, Novi Sad, 2017
- [6] Kuzmić, T., Ninkov, T., Bulatović, V., Vasić, D., Davidović, M.: Modern geodetic methods with application in the environmental management and its protection, 7th International Symposium on Environmental and Material Flow Management – EMFM 2017, pp. 59-70, 2017
- [7] Staiger, R.: Terrestrial Laser Scanning Technology, Systems and Applications, *Proc. 2nd FIG Reg. Conf.*, pp. 1-10, 2003
- [8] Vasić, D., Batilović, M., Kuzmić, T., Davidović, M.: The importance of Mobile laser scanning in the collection of road infrastructure data, *FIG Commission 3 Workshop and Annual Meeting*, Napoli, pp. 1-13, 2018
- [9] Vasić, D., Batilović, M., Davidović, M., Kuzmić, T.: Modern Methods of Processing and Extracting Data from Point Cloud, *FIG Working Week 2019 Hanoi, Vietnam*, April 22–26, 2019

39

Luka Zevnik, Maurizio Bellotto

Industrialization of an alkali-activated slag binder: solving the issues of early strength and superplasticizer efficiency

INDUSTRIALIZATION OF AN ALKALI-ACTIVATED SLAG BINDER: SOLVING THE ISSUES OF EARLY STRENGTH AND SUPERPLASTICIZER EFFICIENCY

Luka Zevnik², Maurizio Bellotto²

¹ LZ Concrete, Leonardo d.o.o., Slovenia
email: l.zevnik@gmail.com

² Department of Chemistry, Materials and Chemical Engineering, Polytechnic of Milano, Milano, Italy
email: mauriziopietro.bellotto@polimi.it

SUMMARY: The production of alkali activated binders as dry-premixed powders which hydrate and harden on mixing with water effectively widens up the ease and scope of application of such systems. However some issues must be tackled for enabling a wide scale commercial use of such binders. The most relevant are assuring an adequate early strength, providing efficient superplasticizers and providing compatibility with the EN-197 prescriptions. We show a practical example of an industrial solution.

Activation by sodium carbonate alone gives a slow setting and hardening, and several options have been proposed in the past to accelerate it. We have chosen hydrated lime or clinker as the accelerating addition, to use the calcite precipitation equilibrium as the sink for carbonate ions in solution. The best performances in terms of early setting and strength development are obtained for equimolar additions of hydrated lime and sodium carbonate. When using clinker as the accelerating addition, it is possible to formulate a CEM III/C by allowing clinker ≥ 5 wt% and sodium carbonate ≤ 5 wt%.

A drawback of these systems is the lack of efficacy of conventional superplasticizers, with sugars and lignosulfonates behaving the best but showing only limited effect. This lack of efficiency can be related to the much lower Ca^{2+} concentration in the pore solution compared to Portland cement. To overcome this limitation we have tried sodium sulfate as an activator with Ordinary Portland Cement CEM I as the accelerating addition. We have also prepared similar blends with bypass condensation kiln dust as a replacement for sodium sulfate. Bypass condensation kiln dust is a mixture of potassium and sodium chlorides and sulphates. These systems are reactive and show excellent behavior with all conventional superplasticizers. Similarly to the above, CEM III/C cements can be formulated by allowing clinker ≥ 5 wt% and the activator ≤ 5 wt%.

With such a system (called EConcrete) we have batched a concrete to cast an industrial flooring. The maximum aggregate size was 16 mm, with a water/binder ratio of 0.45. The compressive strength was 5 MPa at 1 day, 35 MPa at 7 days and 45 MPa at 28 days. The slab was 100 m² and was cast without shrinkage cuts, and yet no cracking has appeared after more than 1 year. Notwithstanding the high level of chlorides in the kiln bypass dust, no reinforcement corrosion has been noticed, and a very low chloride permeability has been measured on the manufact.

KEY WORDS: One-part alkali activated slag binder; hydration mechanism; pore solution evolution before setting; rheological behavior; superplasticizer efficiency

1 INTRODUCTION

First data about the possibility of producing a binder material from granulated blast-furnace slag and caustic soda in combination with slaked lime go back to 1895 [1]. Later, in the 1930s, H. Kühl reported studies on the setting behavior of mixtures of ground slag and a solution of caustic potash [2]. R. Feret reported on the necessity to study slags as a cement component [3]. In 1940, A. Purdon reported on the results of first extensive laboratory studies on cements without OPC clinker, consisting of slag and caustic alkalis produced with a base and an alkaline salt [4]. 'Purdocement' was developed by Arthur Oscar Purdon, one of the pioneers in the research of alkali-activated slag cements [5,6]. This development was technically related to the advanced techniques used in the steel production for the fast cooling of blast furnace slag realized at that time. Several buildings were erected within the period 1952–1959 using concrete with Purdocement.

Later, in 1957, a Soviet Union scientist Victor Glukhovskiy [7] was the first to discover the possibility of making binding materials using low-calcium or calcium-free aluminosilicates (clays) and solutions of alkali metals. He called these binders "soil cements" and "soil silicates" in order to reflect their similarity to natural minerals. Depending on the composition of their constituent materials, the Alkaline Activated Cements (AACs) were divided into two groups: alkaline ($\text{Me}_2\text{O}-\text{Me}_2\text{O}_3-\text{SiO}_2-\text{H}_2\text{O}$) and alkaline-alkaline earth ($\text{Me}_2\text{O}-\text{MeO}-\text{Me}_2\text{O}_3-\text{SiO}_2-\text{H}_2\text{O}$). As a result, a variety of AACs have been formulated from metallurgical slags, clays, aluminosilicate rocks, fuel ashes and other constituents. Extensive research and development of AACs and AAC-based concretes started since those times. In particular, Trief cements (NaCl and NaOH activated GGBS, wet ground and added to concrete as a slurry) [8], F-cements (sodium carbonate and sodium hydroxide activated GGBS including NSF as a superplasticizer) from Scandinavian countries [9] and alkali-activated blended cements are more recent examples.

1.1 Mechanisms of setting and hardening of alkali activated slag cements

Alkali activated slag cements may be defined "High-calcium alkali-activated cements", to distinguish them from geopolymers which are "Low-calcium alkali-activated cements". Alkali-activated Portland and alkali-activated slag cements are representatives of this alkali-activated cement model. Contents of SiO_2+CaO are over 70 mass%, and content of Al_2O_3 is less than 20 mass%. The main reaction product in this case is a C-S-H, which is formed at early stages of hydration. The alkaline N-A-S-H as well as C-N-A-S-H, as a result of the slower crystallization process in these cements, occur at the later stages. Moreover, high pH-values of the medium in which the hydration process takes place tend to block a transfer of the Ca-ions into solution, this is an explanation of the absence of $\text{Ca}(\text{OH})_2$ and the fact that the basicity of the resulting calcium silicate hydrate, as a rule, exceeds 1 [10]. The low $[\text{Ca}^{2+}]$ in solution significantly affects also the rheological fresh-state properties of these systems.

The important characteristics of these systems is that they can be formulated as "one-part" binders, that is binders which set and harden by mixing with water and do not require the use of highly caustic solutions. This solution was already practiced by Purdon in the early '50s.

Blast-furnace slag mixed with water sets very slowly. Therefore, slag was formerly often combined with lime, in a 0.25/1 lime/slag ratio. Later, slag was also mixed with Portland clinker to improve its properties. In comparison to Portland cement (PC), all these cements were still slow hardening [9]. Purdon developed a slag cement with high early strength. He discovered that blast-furnace slag can be activated more intensely by adding caustic alkalis such as NaOH or KOH [6] than by adding lime or Portland clinker. Caustic alkalis can be added directly to the cement or NaOH can be formed at the moment of cement wetting. This is done by adding chemicals, such as Na_2CO_3 and $\text{Ca}(\text{OH})_2$, to the cement to form NaOH. Also other chemicals such as Na_2SO_4 could be used as a substitute for Na_2CO_3 [11].

'Le Purdociment' produced two types of cement, cement type 'P' containing a small amount of Portland Cement and cement 'C', which contained a small amount of lime. In both cements Na_2SO_4 was used (Table 1).

Table 1: Probable compositions of Purdocement (mass wt%) (annual report 'Le Purdociment', 1955)

	Slag	Portland Cement	Ca(OH) ₂	Na ₂ SO ₄
Type P	91	5	/	4
Type C	91	/	5	4

These compositions are actually quite close to those of EConcrete. Today like in the '50s the key point is to adapt the material to the current industrial practices, which today require not only fast setting and high mechanical strength, but also compatibility with the chemical admixtures.

Examples of buildings realized with "Purdociment" in Brussels in the late '50s are reported below. Apart from damages caused by carbonation visible in some instances, the strength of the material is still higher than the design strength.

1.2 Records of buildings made with alkali-activated slag cements

Use of Purdociment:



Fig. 1: Left: Corner of Breydel street No 9 and Avenue Oudergem No 15; Righth: Royal building (left southern part, right eastern side building)



Fig. 2: Left: King Victor Square No 12 and 13; Righth: Factory 'Delle' in Ukkel

Other more recent examples are [12]:



Fig 3: Illustration of the alkali-activated slag demonstration project: (a) effect drawing of Jianke Chongqing; (b) illustration of the construction section; (c) side view of the structure made with alkali-activated slag concrete

This material was done using an alkaline solution, blend of sodium silicate and sodium hydroxide.

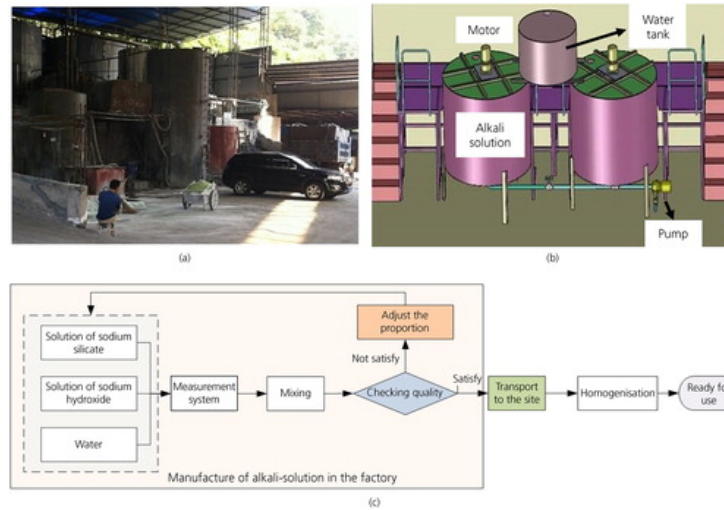


Fig. 4: Alkali solution manufacture process and the field storing set-up: (a) alkali solution manufacturing factory; (b) field storing and homogenisation set-up; (c) alkali solution manufacturing process

1.3 Corrosion resistance of alkali activated binders

Alkali activated binders are particularly resistant to corrosion, even in high chloride environments. In addition chloride penetration is highly reduced at high slag loadings, as shown in Figure 5, reprinted from [13].

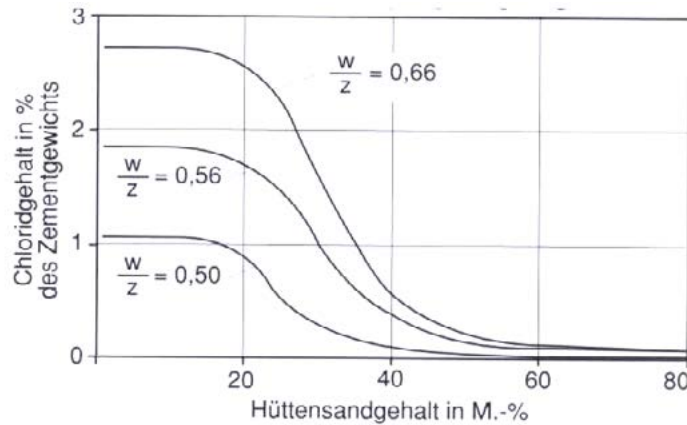


Fig. 5: Chloride penetration vs. slag content in cement.

1.4 Goals of this study

The main goal of this study is to demonstrate an industrial application with alkali-activated binder – casting a concrete slab of 100m² (12,5x8m). For using regular concrete technology (mixing plant, transport, casting) we have to develop the formulation without liquid activator. To achieve adequate early compressive strength and limit the drying shrinkage problems the alkali-activated binder should have work efficiently with commercially available PCE superplasticizer. For regular industrial use of alkali-activated materials, the formulation should have been compatible with EN-197. With achieving these goals, we would show that use of greener binders in every-day practice is not a far future, and thus encourage the scientific community to realize the scientific achievements in industrial concrete practice.

2 MATERIALS AND METHODS

2.1 Blast furnace slag

The blast furnace slag used in this study has been supplied by ECOCEM France SAS. The composition of this material is highly constant batch over batch. Its main characteristics are summarized below:

- composition: Al₂O₃ 10.70%
MgO 7.41%
- chemical modulus [(CaO+MgO)/SiO₂] 1.33
- granular distribution: D₅₀ 11.37 μm
D₉₀ 31.96 μm
D₁₀ 2.27 μm
- amorphous fraction (by X-ray diffraction) ≥ 95%
- activity index (by isoperibolic calorimetry at 6d) = 41%

2.2 Sodium carbonate and sodium sulphate

Na₂CO₃ and Na₂SO₄ were supplied by Sigma-Aldrich (Merck) as anhydrous reagent grade products.

2.3 Hydrated lime

Ventilated hydrated lime was supplied as CL90-S according to EN 459-1:2010.

2.4 Limestone flour

Limestone flour comes from the cutting into slabs of the blocks of marble extracted from the Apuan Alps in Italy. The product was supplied by Cages Srlu after wet micronizing the raw material. Its characteristics are summarized below:

- composition: CaCO₃ 97.43%
MgCO₃ 2.13%
- brightness (% ISO) 93.50
- granular distribution: D₅₀ 1.59 μm
D₉₀ 4.00 μm
D₁₀ 0.58 μm

2.5 Kiln dust

The kiln dust was supplied by the cement factory Salanit Anhovo d.d.. It originates from the condensation of the volatiles spilled from the clinkering zone of the kiln. Its major element composition is as follows:

SiO ₂	0.74 %	Al ₂ O ₃	0.19 %
Fe ₂ O ₃	0.21 %	CaO	4.39 %
MgO	0.06 %	Na ₂ O	15.67 %
K ₂ O	33.45 %	SO ₃	15.49 %
Cl	28.79 %		

It is constituted by the following mineralogical phases: apthitalite [K₃Na(SO₄)₂], sodium chloride, potassium chloride, anhydrite [CaSO₄], C₂S, quartz, ye'elimite [C₄A₃Ŝ], lime [CaO] and portlandite [Ca(OH)₂].

2.6 Superplasticizer

The PCE superplasticizer XP4 was supplied by formulator Leonardo d.o.o. The XP4 was certified according to EN 934-2.

2.7 Analytical methods

The various formulations have been characterized by calorimetry, both isothermal (TAM Air – TA Instruments) and isoperibolic (semi-adiabatic). The isoperibolic calorimeter was calibrated by measuring the thermal exchange coefficient and the sample heat capacity.

The phase composition has been measured by X-ray diffraction (XRD) using a Panalytical X'Pert Pro diffractometer with Co radiation equipped with X'Celerator detector, adopting a Bragg-Brentano geometry, with a 2θ range of 5-84°, step size of 0.017° and a time per step of 100s. The semi-quantitative analysis was performed by the internal standard method by adding ZnO and the data were analysed by the Rietveld method. In such a way it was also possible to estimate the amount of amorphous and/or undetected phases.

The interstitial solution was extracted before setting by centrifugation at the desired curing time, acidified with 0.1M HCl and analysed by ICP-AES.

The mechanical strength of the hardened paste was measured on 15x15x60 mm³ prisms cast in Teflon formworks. Both indirect tensile strength and compressive strength were measured, each measurement being repeated for 3 times.

The fresh and hardened concrete properties, shown in section 3.3. were done in accordance with standards using by concrete plants.

3 RESULTS AND DISCUSSION

3.1 Activation by Na₂CO₃

3.1.1 Activation by Na₂CO₃ and Ca(OH)₂

The combined use of Na₂CO₃ and Ca(OH)₂ fulfils two requirements: on one hand it allows the attainment of a higher pH than the use of Na₂CO₃ alone, by the reaction



thus accelerating slag dissolution. On the other hand it consumes the carbonate ions in solution, thus allowing the Ca²⁺ concentration to increase through slag dissolution, triggering the precipitation of C-(N)-A-S-H type gel and thus causing setting, as discussed in [9]. Indeed C-S-H precipitation needs a threshold Ca²⁺ concentration of about 1 mM to precipitate, as reported in Fig.6 from [14,15]

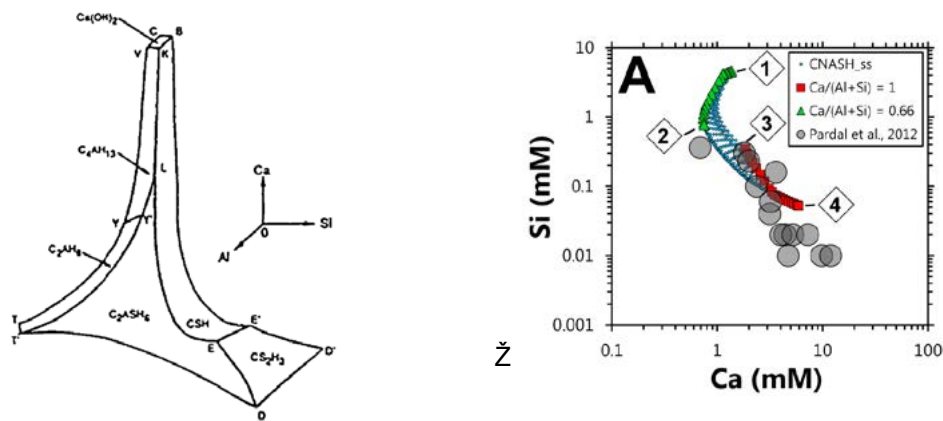


Fig. 6: Phase diagram in CaO–Al₂O₃–SiO₂–H₂O system

As shown in Fig.7 the optimal ratio between Na₂CO₃ and Ca(OH)₂ is equimolar: for higher Na₂CO₃ content hydration is retarded, while for higher Ca(OH)₂ the long-term hydration degree is reduced. The calorimetric data have been measured on paste with water/solid ratio (w/s) of 0.3.

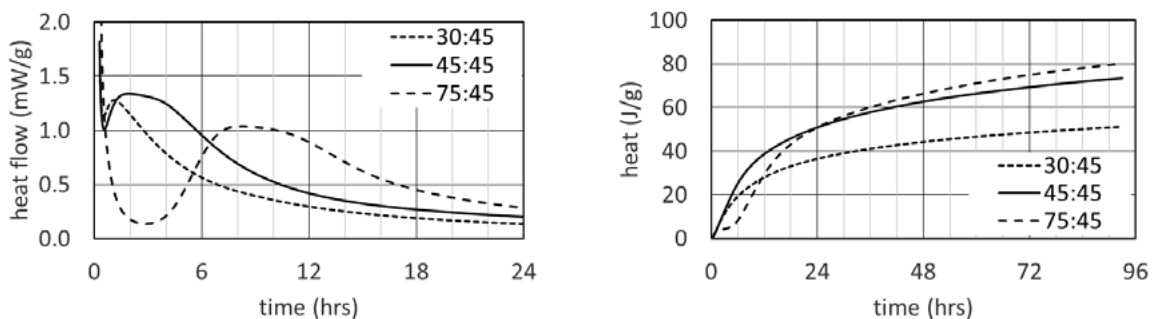


Fig. 7: Isothermal calorimetry of alkali activated slag. The samples are named following the Na₂CO₃:Ca(OH)₂ content, as mmoles per 100 grams of binder. Heat flux (left) and cumulative heat (right).

The retardation due to the excess of Na_2CO_3 can be attributed to the longer persistence of CO_3^{2-} in solution maintaining a low Ca^{2+} concentration and preventing C-(N)-A-S-H precipitation, while the limited extent of hydration in excess of $\text{Ca}(\text{OH})_2$ can be attributed to the higher Ca^{2+} concentration in solution, decreasing the undersaturation of slag and limiting its dissolution.

Such a fine balance of the effects of the solution ionic concentrations causes a strong influence of w/s on the hydration rate, as shown in Fig.8 (left). On increasing w/s the maximum heat flux strongly decreases. Isoperibolic calorimetry has been measured on paste on a binder constituted by slag, 5% Na_2CO_3 and 3.5% $\text{Ca}(\text{OH})_2$, corresponding to 45 mmoles of each per 100 g of binder.

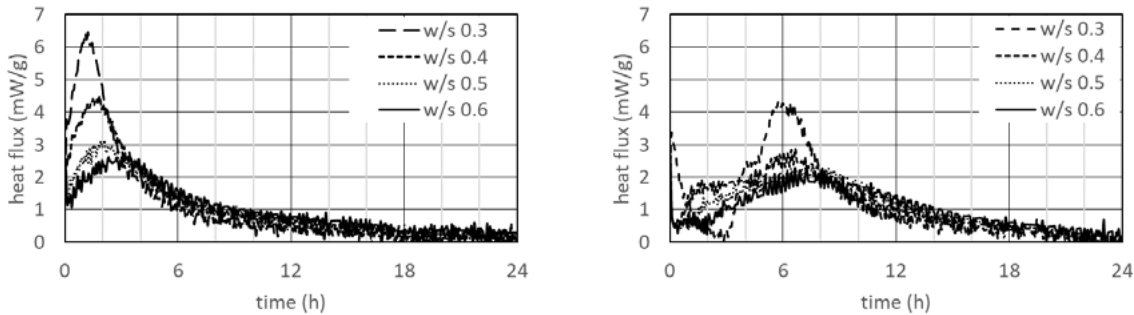


Fig. 8: Isoperibolic calorimetry of slag activated with Na_2CO_3 and $\text{Ca}(\text{OH})_2$ (left), or clinker (right) at different w/s.

3.1.2 Activation by Na_2CO_3 and clinker

When substituting $\text{Ca}(\text{OH})_2$ with clinker the activation mechanism is similar to what discussed previously. The slower availability of Ca^{2+} in solution retards the attainment of the maximum heat flux, as shown in Fig.3b. Moreover, the sensitivity to w/s decreases since Ca^{2+} is continuously available through the hydration of clinker. Isoperibolic calorimetry has been measured on paste on a binder constituted by slag, 5% Na_2CO_3 and 6% ground clinker, without gypsum addition. Such a system complies to the compositional requirements of CEM III/C.

3.1.3 Activation by Na_2CO_3 and limestone flour

Limestone flour can be used as a source for Ca^{2+} in solution instead of $\text{Ca}(\text{OH})_2$ or clinker. Of course, in such a case hydration will be slower, but the acceleration compared to the use of an inert SiO_2 powder is significant as shown in Fig.9. Isoperibolic calorimetry has been measured on paste on a binder constituted by slag and limestone flour in equal amounts (47.5% each) and 5% Na_2CO_3 .

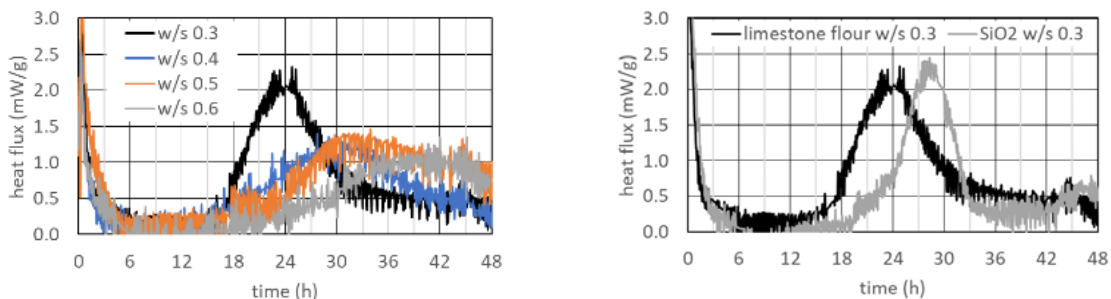


Fig. 9. Isoperibolic calorimetry of slag activated with Na_2CO_3 and limestone flour at different w/s (left), and comparison between limestone flour and SiO_2 filler at w/s 0.3 (right).

3.1.4 Phase composition and interstitial solution

The phase composition of the three above system dealt with, hydrated with w/s 0.5, is reported in Table 2.

Table 2: Evolution of the phase composition during hydration.

phase (%)	Na ₂ CO ₃ + Ca(OH) ₂			Na ₂ CO ₃ + clinker			Na ₂ CO ₃ + limestone flour		
	2d	7d	28d	2d	7d	28d	2d	7d	28d
C ₂ S	–	–	–	1.1	n.d.	1.0	–	–	–
C ₃ S	–	–	–	4.9	n.d.	2.6	–	–	–
C ₃ A	–	–	–	0.1	n.d.	0	–	–	–
calcite	12.3	13.2	14.5	11.4	n.d.	11.1	46.3	45.3	43.8
vaterite	0	2.3	1.5	–	n.d.	–	0.3	0.7	0.5
aragonite	–	–	–	–	n.d.	–	0	0	0.2
quartz	–	–	–	–	n.d.	–	0.0	0.0	0.1
hydrotalcite	0.3	0	0	2.9	n.d.	1.6	–	–	–
hem carbonate	4.2	4.3	5.9	2.7	n.d.	4.0	1.0	1.1	1.4
strätlingite	0	1.8	2.6	6.3	n.d.	6.7	–	–	–
amorphous	83.2	78.4	75.5	70.6	n.d.	73.0	52.4	52.9	54.0

Abundant calcium carbonate precipitates in the blends containing Ca(OH)₂ and clinker. In the mix with limestone flour calcite decreases with curing time, supporting the evidence of its reactivity. AFm phases (hydrotalcite, hem carbonate and strätlingite) are formed, their quantities increasing with curing time. Strätlingite points to a high Si/Ca ratio in solution. The amorphous component, possibly associated to C-S-H precipitation, increases with time.

The composition of the interstitial solution before setting is shown in Table 3. Ca²⁺ concentration increases initially until the beginning of the heat flux peak, further supporting the proposed mechanism of C-(N)-A-S-H precipitation. Concurrently the aluminates concentration decreases.

Table 3: Evolution of the ionic composition of the interstitial solution before setting.

sample: Na ₂ CO ₃ +	w/s	curing time (h)	Ca (mmol)	Mg (mmol)	Al (mmol)	Na (mol)
Ca(OH) ₂	0.3	0	0.19	0.00	9.55	2.60
Ca(OH) ₂	0.6	0	0.02	–	6.01	1.39
Ca(OH) ₂	0.6	1	0.19	0.01	1.63	0.90
Ca(OH) ₂	0.6	3	0.08	0.04	0.98	0.73
clinker	0.3	0	0.35	0.03	6.91	2.82
clinker	0.6	0	0.04	–	0.07	1.33
clinker	0.6	2	0.56	0.01	0.07	0.96
clinker	0.6	4	0.57	0.04	7.35	1.27
limestone flour	0.6	6	0.33	0.01	0.69	0.98
limestone flour	0.6	30	0.37	0.00	1.12	0.87

3.1.5 Mechanical strength

The mechanical strength of the above formulations is reported in Table 4. Performances decrease substantially on increasing w/s, and the formulation with limestone flour shows interesting high strength also at short curing times.

Table 4. Mechanical strength.

sample: Na ₂ CO ₃ +	w/s	curing (days)	density (g/cm ³)	splitting (MPa)	compression (MPa)
Ca(OH) ₂	0.3	2	2.019(3)	3.2(5)	26(3)
		7	2.008(4)	4.8(6)	33(2)
		28	2.021(3)	5.2(5)	44(3)
	0.5	2	1.793(3)	1.2(2)	10.0(2)
		7	1.789(5)	2.03(5)	12.8(6)
		28	1.780(5)	2.5(1)	19(2)
clinker	0.3	1	2.035(7)	2.6(3)	23.7(3)
		7	2.040(1)	4.2(2)	42(1)
		28	2.023(7)	4.0(4)	51(3)
	0.5	1	1.798(9)	0.97(7)	7(2)
		7	1.782(4)	2.34(9)	20(1)
		28	1.79(2)	2.6(3)	22.5(8)
limestone flour	0.3	2	1.904(6)	1.8(3)	26(1)
		7	1.990(6)	2.5(5)	40.1(8)
		28	1.970(9)	2.9(6)	49(3)
	0.5	2	1.782(3)	1.0(1)	11.4(4)
		7	1.63(2)	1.8(2)	14(1)
		28	1.63(1)	2.2(3)	18.4(4)

3.2 Activation by Na₂SO₄ or kiln dust

Activation with Na₂SO₄ alone gives low mechanical properties and requires the addition of a provider of alkalinity to enhance performances and speed up slag dissolution kinetics. The activation by Na₂SO₄ is not controlled by alkalinity, but by the different precipitation equilibria which are established in the system. We have used CEM I 52,5 R as the provider of alkalinity, designing the formulations in order to have them compliant to the compositional requirements of CEM III/C. For activation with both Na₂SO₄ and kiln dust two blends have been designed: one with 6% CEM I and 2% activator and the other with 15% CEM I and 5% activator, the rest being slag: 92% and 80% respectively.

The isoperibolic calorimetric measurements are shown in Fig.10. The pastes have been mixed with w/s 0.5 or with w/s 0.3 with the addition of 0.2 wt% of a powdered PCE superplasticizer. The superplasticized paste was very fluid, even more fluid than the paste with w/s 0.5 and no superplasticizer, showing an excellent efficiency of the superplasticizer.

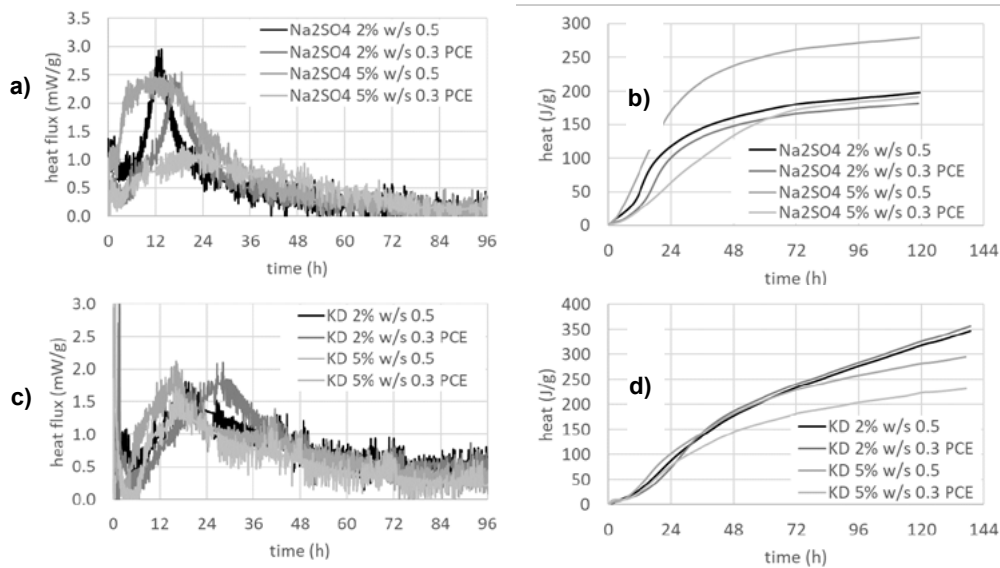


Fig. 10. Isoperibolic calorimetry of slag activated with Na₂SO₄ and CEM I – (a) and (b) – and with kiln dust and CEM I –(c) and (d). Heat flux – (a) and (c) – and cumulative heat – (b) and (d).

The presence of superplasticizer does not retard significantly hydration in the formulations with 6% CEM I and 2% activator, while the cumulative heat of hydration in the presence of superplasticizer is lower for the formulations with 15% CEM I and 5% activator. Tentatively this can be attributed to the influence of PCE on CEM I hydration, which is more significant the higher the cement content in the formulation.

The phases which form upon hydration are ettringite and calcium carbonate, both calcite and vaterite. Portlandite is also present, more abundant for the formulations with 15% CEM I. Hydrocalumite is present in the formulations with kiln dust.

3.3 Industrialization of AASB: casting of 100m² slab

For the large-scale application we have used an AASB with the following composition, called EConcrete binder:

Table 5: EConcrete composition

GGBS	85%
Clinker	10%
Kiln dust	5%

The project was performed at Nikotrans Begrad concrete plant (Kranj, Slovenia) on November 11, 2018. Information about the project is shown in Table 6.

Table 6.: EConcrete industrial project: casting of industrial pavement

area	12x8 m ²
thickness	15 cm
concrete volume	15 m ³ (2x7,5 m ³)
reinforcement	two metallic soldered nets
location	Praše, Kranj, Slovenia
datum	nov 2018
temperature at casting	5-8°C
temperature at curing (7 days)	-2-8°C



Tabele 7: EONcrete slab composition, fresh and hardened properties

EONcrete binder	360 kg/m ³
Sand (Sava river) 0-4 mm	1030 kg/m ³
Sand (Sava river) 4-8 mm	200 kg/m ³
gravel(Sava river) 8-16 mm	400 kg/m ³
Gravel (Sava river) 16-32 mm	280 kg/m ³
water-to-binder ratio	0.50
superplasticizer	0.7% (25% solid content)
slump	150 mm
air entrapment	1,9%
bleeding	NO
Pumping	excellent
setting time (initial/final)	8.5/9.3 hours
compressive strength 1d	4.0 Mpa
compressive strength 2d	13.5 Mpa
compressive strength 3d	20.0 Mpa
compressive strength 7d	30.5 Mpa
compressive strength 28d	42.0 Mpa
compressive strength 90d	43.0 Mpa
Compressive strength 480d	65.0 MPa

3.3.1 Corrosion resistance of EONcrete slab

The activation system of EONcrete is composed of waste material from cement production, called kiln dust. One of the main components of this material is also the Cl⁻, as already shown in the Section 2. Therefore we have measured the leaching of chlorides from the sample, to show that chlorides and almost completely reacted during the hydration and are thus harmless to the steel corrosion. The samples for measuring Cl⁻ in the EONcrete were done according to EN 1744-3:2002 and measure according to EN 196-2:2013. Preparation of the samples and the analytics were done in Salonit Anhovo laboratories. The results are written in Tabele 8.

Tabele 8: The leaching of Cl⁻ in EONcrete samples

Curing time (days)	Cl ⁻ (ppm) (mg/kg s.c.)
0 (fresh concrete)	15000*
28	142
480	16

*calculated from the composition

In the Figure 11 the steel rebar and EONcrete interface show no signs of corrosion (age of 480 days).



Fig 11. Steel rebar in a cylinder sample taken from the casted slab.

3.3.2 Shrinkage of EConcrete slab



Fig. 13. No cracks around the column (age of 480 days). No special reinforcement around the column.

4 CONCLUSION

Alkali activated blast furnace slag is formulated with solid activators, to produce a binder which sets and hardens upon the addition of water. Sodium carbonate and sodium sulphate are used as the activators, and kiln dust has also been used as a substitute for Na_2SO_4 . All of the activators require an accelerator in order to deliver the rapid setting and hardening which is customary to Portland cement. In the case of Na_2CO_3 activation, the accelerators used are $\text{Ca}(\text{OH})_2$ or clinker. For Na_2SO_4 activation, CEM I has been used as an accelerator. Hydration is controlled by the chemistry of the interstitial solution, and the adsorption of superplasticizers as well. While the available PCE superplasticizers are not effective with the Na_2CO_3 activated formulations, the systems activated with Na_2SO_4 or kiln dust show an excellent behaviour in association with PCE superplasticizers. The slab casted in nov 2018 shows excellent shrinkage behaviour, no corrosion and impressive compressive strength.

REFERENCES

- [1] Whiting, J.: Manufacture of cement. US Patent No 544706, (1895).
- [2] Kühn, H.: Chemistry of cement, in German, Band III, Verlag Technik, Berlin, 1958.
- [3] Feret, R.: Slags for the manufacture of cement, Rev. Mater. Constr. Tr. Publications, 1 – 145, (1939).
- [4] Purdon, A.: The action of alkalis on blast furnace slag, J. Soc. Chem Ind., 59, 191 – 202, (1940).
- [5] Shi C, Krivenko PV, Roy DM (2006) Alkali-activated cements and concretes. Taylor and Francis, Abingdon
- [6] Torgal FP, Gomes JP, Jalali S (2008) Some considerations about the durability of historic mortars. In: Proceedings of the historical mortars conference, 24–26 September 2008, Lisbon
- [7] Glukhovskiy, V.D., Pashkov, I.A., Yavorskiy, G.A.: New building material, in Russian, Bulletin of Technical Information, GlavKievStroy, Kiev, 1957.
- [8] British Patents 673 866, 1949; 674913, 1950.
- [9] Forss B., (1983), Experiences from use of F-cement – a binder base on alkali-activated blastfurnace slag. In G.M. Idorn, Steen Rostan (eds.), Alkalis in Concrete, Danish Concrete Association, Copenhagen, Denmark, pp. 101-104.
- [10] Glasser, F.P.: The roles of alkalis in controlling phase development in calcium aluminosilicate binders. In:

Proceedings of the 1st Int. Conf. "Alkaline cements and concretes". Krivenko P. (ed.), 485 – 492, Kiev, 1994.

[11] Purdon A.O., 1940 The action of alkalis on blast furnace slag. Journal of the Society of Chemical Industry 59:191–202.

[12] Yang K, Yang C, Zhang J et al. (2018) First structural use of site-cast, alkali-activated slag concrete in China. Proceedings of the Institution of Civil Engineers – Structures and Buildings 171(10): 800–809

[13] Ground Granulated Blast Furnace Slag (GGBS) as a concrete additive - Current situation and scenarios for its use in Germany - 23.03.2007 - Vdz_1 101 0005\VDZ_Gespräche Hüttensand als Zusatzstoff_Mc Sachstandsbericht Beiträge Gesamt Sachstandsbericht_GGBS_Schlussfassung_060731_rev1 070323.doc last processed by: Dr. Christoph Müller, Verein Deutscher Zementwerke, Düsseldorf

[14] Dron, R., 1974, Experimental and theoretical study of the CaO–Al₂O₃–SiO₂–H₂O system (Supplementary paper). 6th International Congress on the Chemistry of Cement held in Moscow in 1974, Moscow, USSR, 2(1):208–211.

[15] Myers R.J., 2015. Thermodynamic Modelling of CaO-Al₂O₃-SiO₂-H₂O-Based Cements, PhD thesis, Department of Materials Science & Engineering The University of Sheffield

40

Lea Žibret, Martina Cvetković, Maruša Borštnar, Mojca Lončnar, Andrej Ipavec and Sabina Dolenc

Use of steel slag for the synthesis of belite sulfoaluminate clinker

USE OF STEEL SLAG FOR THE SYNTHESIS OF BELITE-SULFOALUMINATE CLINKER

L. Žibret¹, M. Cvetković¹, M. Borštnar¹, M. Lončnar², A. Ipavec³ and S. Dolenc¹

¹ Slovenian National Building and Civil Engineering Institute, Department of Materials, Laboratory for Cements, Mortars and Ceramics
Dimičeva ulica 12, SI-1000 Ljubljana, Slovenia, EU
e-mail: lea.zibret@zag.si, martina_cvetkovic@yahoo.com, marusa.borstnar@zag.si, sabina.dolenc@zag.si

² SIJ Acroni d.o.o.
Cesta Borisa Kidriča 44, SI-4270 Jesenice, Slovenia, EU
e-mail: mojca.loncnar@acroni.si

³ Salanit Anhovo d.d.
Anhovo 1, SI-5210 Deskle, Slovenia, EU
e-mail: andrej.ipavec@salonit.si

SUMMARY: Belite-sulfoaluminate (BCSA) cements are low-carbon mineral binders, which require low energy consumption and allow the incorporation of various secondary raw materials in the clinker raw meal. In this study two types of unprocessed steel slags, coming from stainless steel production, were incorporated in the BCSA clinkers. The clinker phase composition, clinker reactivity, and the compressive strength of the cement were studied to evaluate the possible use of the slag in BCSA clinkers. The cement clinkers were synthesized by using natural raw materials, white titanogypsum, mill scale, as well as two different steel slags: (i) EAF S slag, which is a by-product of melting the recycled steel scrap in an electric arc furnace, and (ii) ladle slag as a by-product of the processes of secondary metallurgy, in various quantities. Raw mixtures with two different targeted phase compositions varying in belite, calcium sulfoaluminate and ferrite phases were sintered at 1250 °C. Clinker phases were determined by Rietveld quantitative phase analysis, while their distribution, morphology and incorporation of foreign ions in the phases were studied by SEM/EDS analysis. The clinker reactivity was determined by isothermal calorimetry. BCSA cements were prepared by adding titanogypsum. The compressive strength of the cement pastes was determined after 7 days of hydration. The presence of a predicted major clinker phases was confirmed by Rietveld analysis, however periclase was also detected. Microscopy revealed subhedral grains of belite and euhedral grains of calcium sulfoaluminate phases, while ferrite occurred as an interstitial phase. The results showed differences in the microstructure and reactivity of the clinker and cement, which can be attributed to varying amounts of ettringite due to different slag types.

KEY WORDS: belite-sulfoaluminate cement, cement clinker, steel slags, clinker microstructure, cement reactivity

1 INTRODUCTION

Today one of the main issues is a reduction of the carbon footprint, which is being implemented in various fields. In construction materials it can be solved by development of new low-carbon mineral binders, like belite-sulfoaluminate (BCSA) cements, also known as belite-ye'elinite-ferrite (BYF) cements [1-3]. One of the main issues for the production of such cement is to obtain a sufficient source of aluminium [2]. Since the natural source of Al, bauxite, is too expensive and also geographically-limited, many studies are focused on its replacement by Al-rich secondary raw materials [4-6]. However, steel slag can also be incorporated in BCSA clinkers [7].

This study is focused on the use of two types of steel slags for the production BCSA clinker – electric arc furnace slag from stainless steel production (EAF S) and ladle slag as a by-product of the processes of secondary metallurgy. BCSA clinkers of the two targeted compositions were prepared and phase composition was determined for clinkers, using two different raw mixtures. Further microstructural investigations, clinker reactivity and compressive strength after 7 days of curing were performed for clinkers, sintered at 1250 °C.

2 MATERIALS

The four clinkers having two nominal phase compositions: 65 wt% C₂S, 20 wt% C₄A₃S̄, 10 wt% C₄AF or 50 wt% C₂S, 35 wt% C₄A₃S̄, 10 wt% C₄AF (Table 1), were prepared with proportion of limestone, flysch, white titanogypsum and with either EAF S slag, which is generated during stainless-steel production in an electric arc furnace or ladle slag as a by-product of the processes of secondary metallurgy (AOD and VOD reactor) for an aluminium source. Sampling of slag generated during the production of selected stainless-steel grades, two coming from austenitic stainless CrNi steel and one from austenitic stainless CrNiMo steel were made. Two representative samples were prepared by mixing the sampled slag from three equivalent parts. Unprocessed slag was used. However, the metal phases were removed by sieving and magnets before grinding the slag for the chemical analysis and synthesis of the clinkers in the laboratory.

Bauxite, calcite powder and mill scale were also used for correction. Materials were proportioned by adapting the Bogue method [8]. Raw mix proportioning is given in table 3. The chemical composition of raw materials is given in Table 2. It was determined by wet chemistry methods according to EN 196-2 [9] and X-ray fluorescence spectroscopy (XRF).

Table 1: Targeted phase composition of prepared clinkers (wt%).

	C ₂ S	C ₄ A ₃ S̄	C ₄ AF	Total
KEOP-1	65	20	10	95
KEOP-2	50	35	10	95
KVOD/AOD-1	65	20	10	95
KVOD/AOD-2	50	35	10	95

Table 2: Chemical composition of raw materials (wt%).

	Limestone	Titanogypsum	Bauxite	Flysch	Calcite	Mill scale	EAF S slag	Ladle slag
LOI 950°C	41.41	21.35	0.15	24.65	42.80	0.00	0.00	0.00
*SiO ₂	4.76	0.13	5.88	32.02	n.a.	1.08	24.62	24.43
*Al ₂ O ₃	0.86	1.16	87.69	7.74	n.a.	0.20	7.18	6.79
*Fe ₂ O ₃	0.51	0.04	1.89	3.49	n.a.	95.75	2.03	1.75
*CaO	51.51	32.62	0.06	28.83	56.06	0.19	48.06	53.70
*MgO	0.90	0.04	0.52	1.69	n.a.	0.29	10.30	9.40
*SO ₃	0.09	45.39	0.17	0.07	n.a.	0.01	b.d.l.	b.d.l.
**Na ₂ O	0.81	0.26	0.08	0.54	n.a.	0.67	b.d.l.	b.d.l.
**K ₂ O	0.14	0.01	0.39	1.33	n.a.	0.02	b.d.l.	b.d.l.
**TiO ₂	0.04	0.72	3.81	0.38	n.a.	0.01	0.99	0.63
**Cr ₂ O ₃	0.02	0.02	0.07	0.02	n.a.	0.08	2.68	1.05
**MnO	0.04	0.01	0.01	0.07	n.a.	0.60	1.70	0.72
**NiO	b.d.l.	b.d.l.	b.d.l.	0.01	n.a.	0.12	0.05	0.05

* - EN 196-2 [9]; ** - XRF; b.d.l. – below the limit of detection; n.a. – not analyzed

Table 3: Raw mix design (wt%).

Raw mix	Limestone	Titanogypsum	Bauxite	Flysch	Calcite	Mill scale	EAF S slag	Ladle slag
KEOP-1	37.6	4.1	5.6	33.1	3.6	0.7	15.3	-
KEOP-2	39.8	7.4	13.3	22.7	3.4	1.0	12.4	-
KVOD/AOD-1	35.6	4.2	5.6	33.3	3.4	0.7	-	17.2
KVOD/AOD-2	36.0	7.6	13.7	19.8	3.2	1.1	-	18.6

All raw materials were homogenized and ground to pass through a 200 μm sieve. Raw mixtures (200 g) were homogenized for 3 h in 200 ml of isopropanol. Pressed pellets were prepared using a HPM 25/5 press at 10.6 kN. For each pellet 15 g of material was used. The clinker mixtures were subjected to a uniform heating regime: a heating rate of 10 $^{\circ}\text{C}/\text{min}$, holding time 1 hour at a sintering temperature of 1250 $^{\circ}\text{C}$, and natural cooling in a closed furnace. Furthermore, after sintering all the clinkers were ground to a particle size below 125 μm and the cement was prepared by adding 20.3 wt% of white titanogypsum. The amount of gypsum needed was calculated according to [8].

3 METHODS

The phase composition of the clinkers was determined using an X-ray diffraction in a PANalytical Empyrean X-ray diffractometer equipped with $\text{CuK}\alpha$ radiation with $\lambda = 1.54 \text{ \AA}$. The samples were milled to a particle size of less than 63 μm . The ground powder was manually back-loaded into a circular sample holder (diameter 16 mm) to mitigate the preferred orientation effect for XRD data collection. The data were collected at 45 kV and a current of 40 mA, over the 2θ range from 4° to 70° , at a scan rate of $0.026^{\circ} 2\theta/\text{min}$. The obtained data were analysed using X'PertHighScore Plus diffraction software from PANalytical, using PAN-ICSD V3.4 powder diffraction files. All Rietveld refinements were done using X'Pert High Score Plus diffraction software from PANalytical, using the structures for the phases from ICDD PDF-4+ 2016 RDB powder diffraction files. The following codes have been used: β C_2S (04 007 2687), γ C_2S (04 010 9508), $\text{C}_4\text{A}_3\text{S}$ orthorhombic (04 011 1786), $\text{C}_4\text{A}_3\text{S}$ cubic (04 009 7268), C_4AF (04 006 8923, 98 026 1869), M (01 071 1176). The amorphous phase was not considered.

The cross-sections of the selected clinker samples (KEOP-1, KVOD/AOD-1) were examined using a JEOL IT5500 Scanning Electron Microscope (SEM) equipped with an Energy Dispersive X-ray spectrometer (EDS), at an accelerating voltage of 20 kV, and a working distance of 10 mm.

The reactivity of clinkers from the selected phase composition for two types of slags (KEOP-1, KVOD/AOD-1) was assessed by isothermal conduction calorimetry using a TAM Air calorimeter (TA Instruments). The mixtures (w/c 0.4) were hand mixed for 5 min and then placed into the calorimeter. However, external mixing could lead to the loss of some very early hydration data [11]. The heat evolution was evaluated for 3 days at 20 $^{\circ}\text{C}$.

For the determination of the compressive strength of the selected cements of high belite phase composition, incorporating EAF S and ladle slag (KEOP-1, KVOD/AOD-1), cement pastes with a water/cement (w/c) ratio of 0.4 were cast into prismatic moulds, $10 \times 10 \times 25 \text{ mm}$. The samples of the cement pastes were demoulded 24 h after casting, and cured until testing in sealed plastic bags under laboratory conditions at $T (21 \pm 2) ^{\circ}\text{C}$ and 95% RH until testing. The compressive strength was determined after 7 days on three specimens per mixture using ToniNORM, Toni-Technic by Zwick testing machine with a loading rate of 0.04 kN/s.

4 RESULTS AND DISCUSSION

4.1 X-ray powder diffraction

XRD pattern for main clinker phases is shown on Figure 1 and the results of quantitative XRD analysis (Rietveld refinement) are given in Table 4. Besides targeted main clinker phases (Table 1) periclase (M) was detected.

Table 4. Phase composition of the clinkers, obtained by X-ray powder diffraction (wt%).

	β - C_2S	γ - C_2S	$\text{C}_4\text{A}_3\text{S}$ cub.	$\text{C}_4\text{A}_3\text{S}$ ortor.	C_4AF	M
KEOP-1	65.9	0.2	8.5	12.9	9,7	2,8
KEOP-2	52.6	0.0	17.1	19.8	8,5	2,1
KVOD/AOD-1	66.0	1.5	7.6	11.2	10,3	3,3
KVOD/AOD-2	49.6	0.2	13.2	23.7	10,0	3,4

If we compare the samples according to the type of slag used, clinkers of high belite phase composition that contained EAF S (KEOP-1) slag had higher $C_4A_3\dot{S}$ content than ladle slag clinkers of the same targeted phase composition (KVOD/AOD-1). However, for the low belite phase composition the difference in $C_4A_3\dot{S}$ content due to slag type was not evident. On the other hand, C_2S content does not significantly change due to the type of slag incorporated in the clinker (Table 4). C_4AF content is close to the targeted phase composition in all the samples. Clinkers with ladle slag have more C_4AF than clinkers with EAF slag, although the difference is not very convincing. Periclase according to the added type of slag does not show significant differences (Table 4).

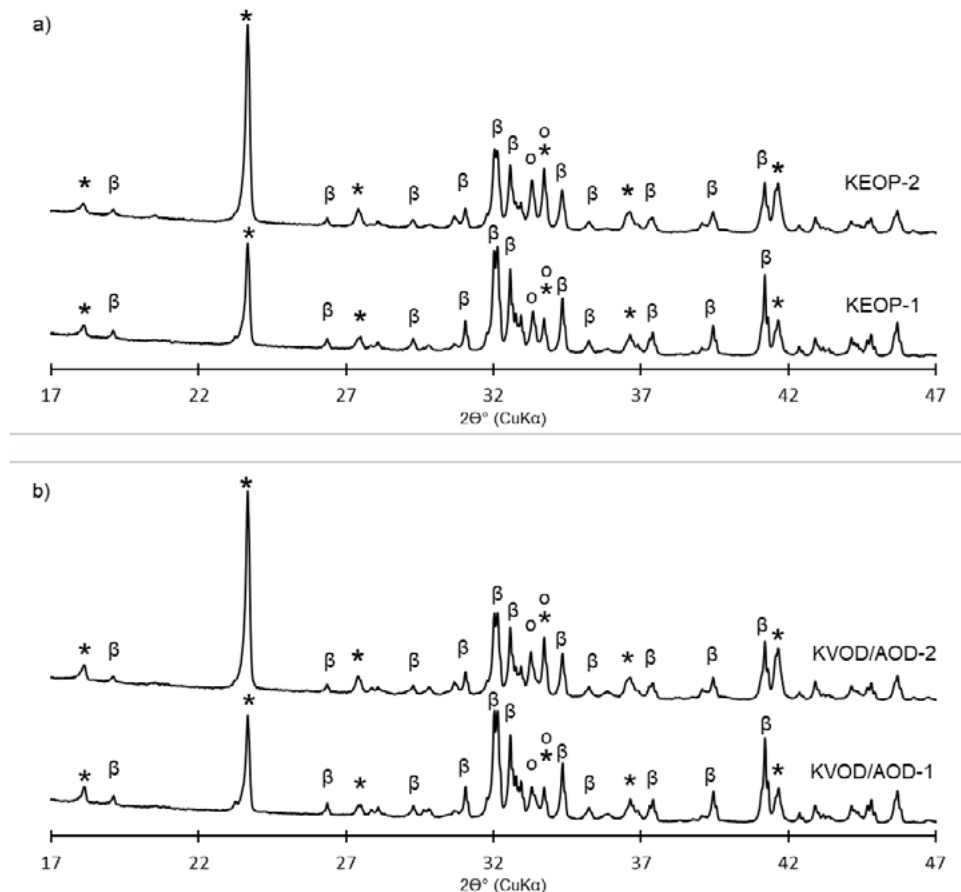


Figure 1: XRD pattern of clinkers with EAF S slag (a) and ladle slag (b). Legend for the targeted clinker phases: * - $C_4A_3\dot{S}$; β - C_2S ; o - C_4AF .

4.2 SEM/EDS

SEM/EDS analysis was performed on the selected phase composition (samples KEOP-1 and KVOD/AOD-1). It was carried out in order to check the presence of major and minor phases determined by XRD and to observe the potential microstructural differences regarding the type of slag used. The SEM/BSE images show a similar microstructure for clinkers with EAF S slag (Figure 2a, c) and in clinkers with ladle slag (Figure 1b, d). Belite is presented by subhedral rounded medium grey grains, while calcium sulfoaluminate has a dark grey euhedral hexagonal or quadrilateral crystal cross-sections. The ferrite phase formed an interstitial phase between the calcium sulfoaluminate and belite. Dark euhedral grains of periclase are also evident, which can be attributed to high magnesium content in both slag samples (around 10 wt%). Grain size of the calcium sulfoaluminate, belite and periclase was larger in the clinker with ladle slag (KVOD/AOD-1), where the grain diameter average was 6.7 μm for belite, 4.2 μm for calcium sulfoaluminate and 3.2 μm for periclase. In the clinker with EAF S slag, the grain size average was 5.5 μm for belite, 3.9 μm for calcium sulfoaluminate and 2.2 μm for periclase.

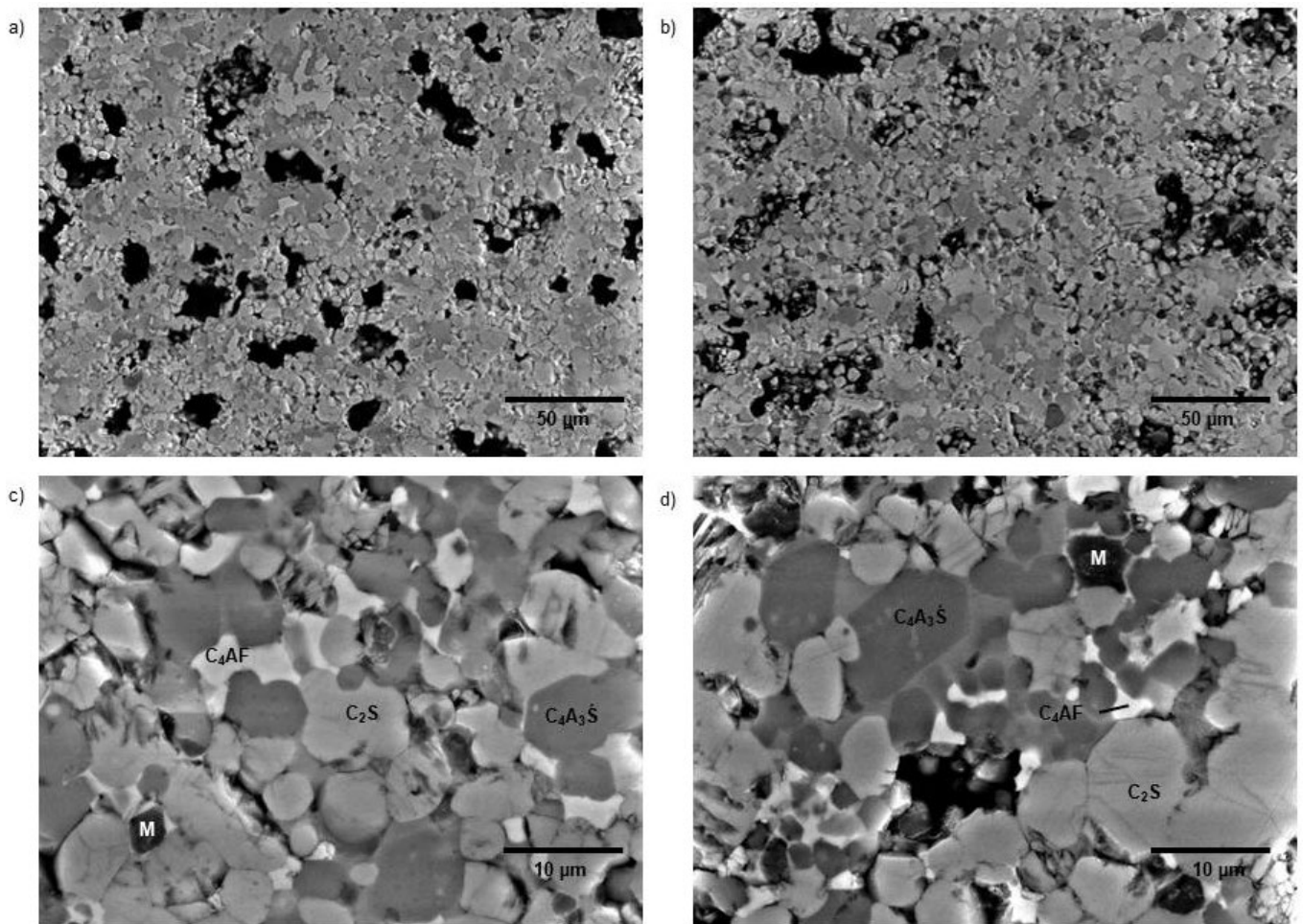


Figure 2: SEM/BSE microphotographs of clinkers KEOP-1 (left) and KVOD/AOD-1 (right).

EDS analysis of the main clinker phases was performed for clinkers of the selected phase composition with EAF S and ladle slag (Figure 2). In clinkers with EAF S slag belite, as well as Ca and Si, it includes the following elements, written in descending order: Al, Mg, Fe, S, K, Na and Ti. In clinkers with the ladle slag the same elements were detected in belite phase, but in a slightly different quantitative order: Al, Fe, Mg, S, Ti, K and Na. Calcium sulfoaluminate in both samples, as well as Ca, Al and S, consisted of Si, Fe, Cr, Mg, K, Na and Ti, while ferrite in both samples, as well as Ca, Al and Fe, it includes Si, Ti, Mn, Mg, S, Cr, K and Na (elements are written in descending order). In periclase, as well as Mg, there was Ca, Si, Al, Fe, Ni, S, K, Ti and Na.

Among the slag derived trace elements, Cr is embedded in calcium sulfoaluminate, Mn and Cr in ferrite and Ni in periclase. The maximum quantities of Ti, which was derived from bauxite, can be found in the ferrite phase (Figure 3).

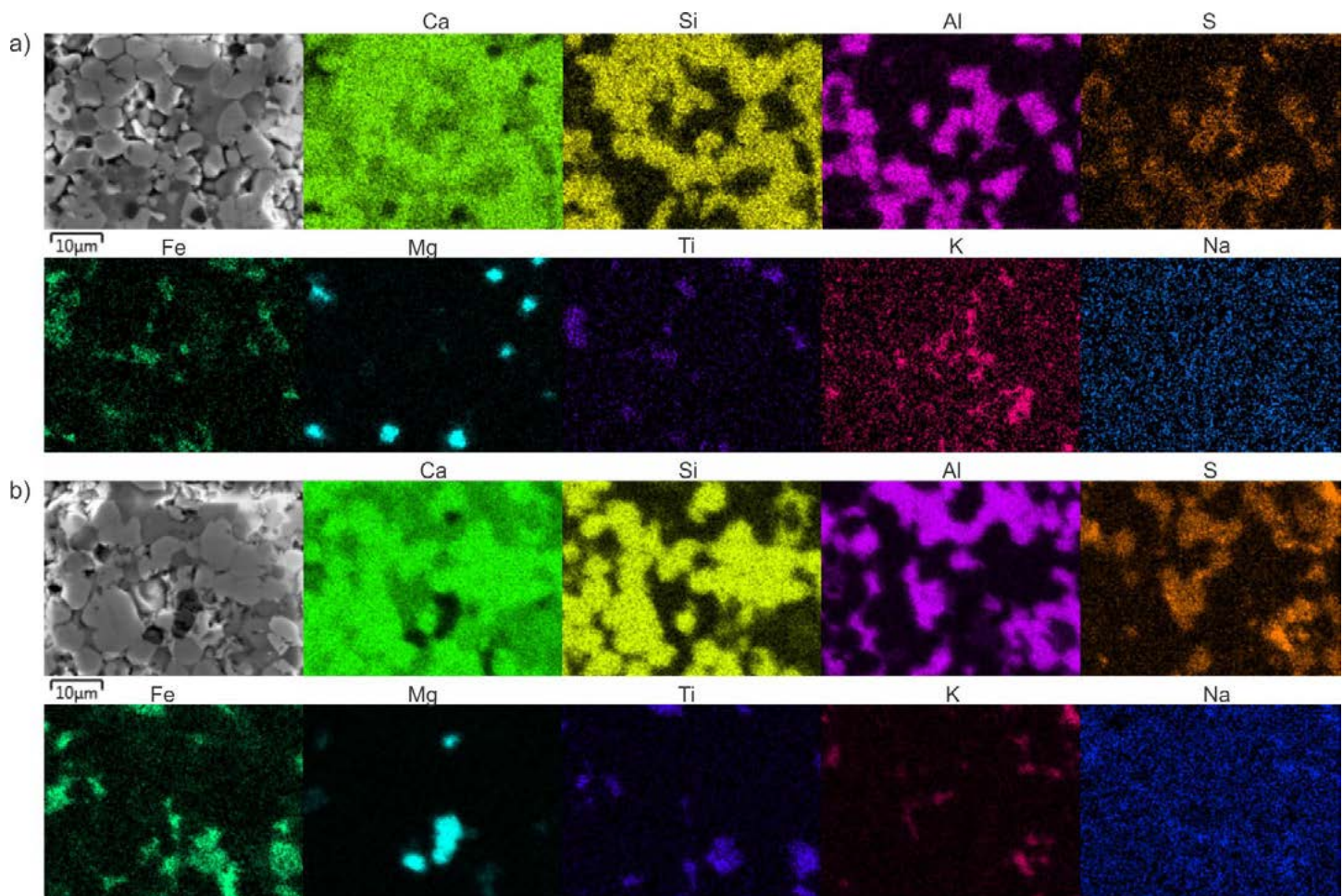


Figure 3: Elemental maps of Ca, Si, Al, S, Fe, Mg, Ti, K and Na for clinkers KEOP-1 (a) and KVOD/AOD-1 (b).

SEM/EDS analysis results in the main part coincided with the results of the XRD analysis. All the main phases whose presence was determined by X-ray powder diffraction were also clearly visible in the SEM/EDS microphotographs of clinkers (belite, ferrite and calcium sulfoaluminat). Among the minor phases, only periclase was clearly evident by SEM/EDS analysis, while other minor phases were not found.

4.3 Isothermal calorimetry

Isothermal calorimetry was performed on clinkers of the selected phase composition with the incorporation of EAF S or ladle slag. There was a significant difference in the calorimetric curves between clinkers with EAF S and ladle slag (Figure 4a, b). The clinker with EAF S slag had one peak during the main hydration phase, which appeared at 18.4 h, with released heat flow of 0.8 mW/g (Figure 4a). Hydration of the clinker with ladle slag starts earlier and has a more complex hydration evolution with two main peaks. The first appears at 6.6 h with a released heat flow of 1.2 mW/g while the second peak appears at 15.9 h with a released heat flow of 1.2 mW/g. According to the literature, the first peak during the main hydration phase can be attributed to ettringite crystallization, while the second peak during the main hydration phase most probably reflects the formation of the monosulfate phase after the complete sulfate depletion in the presence of water [10-14]. Therefore, due to the crystallization of the monosulfate, a reduced amount of ettringite can be expected in the clinker with ladle slag. The difference in the reaction pattern is evident also from the cumulative heat curves (Figure 4b), where the total heat of hydration after 72 h for the EAF S slag clinker is 103.4 J/g and for the ladle slag clinker it is 112.2 J/g.

Differences in the calorimetric pattern of hydration between the EAF S slag clinker and the ladle slag clinker could be attributed to the following factors: (i) increased calcium sulfoaluminat content in the EAF S slag clinker, which may result in more ettringite formation; (ii) increased grain size in the ladle slag clinker, which may decrease clinker reactivity; (iii) variations regarding minor elements, incorporated in main clinker phases.

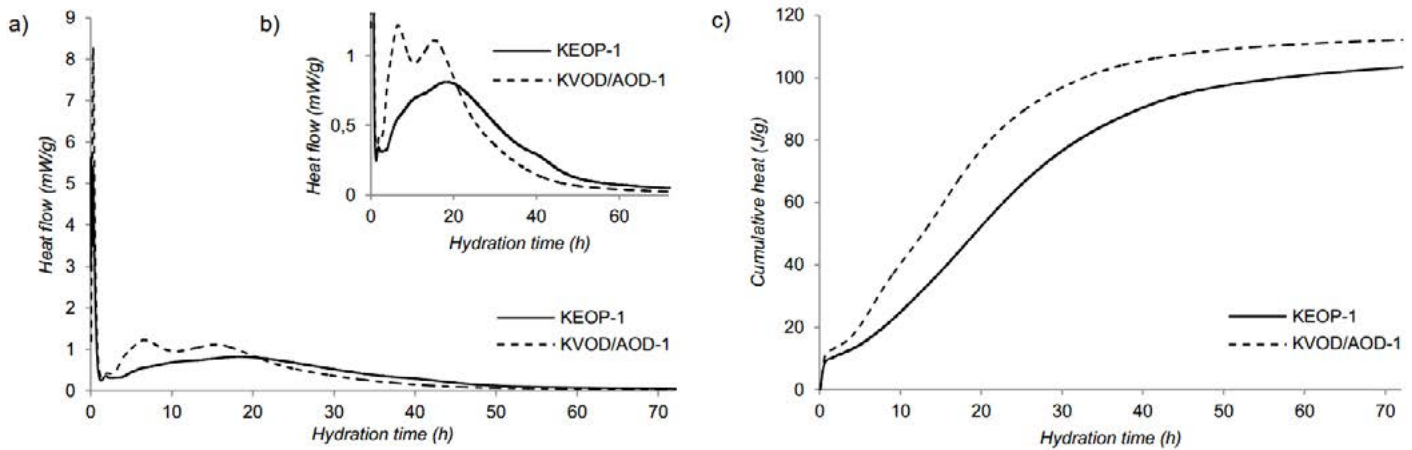


Figure 4: Isothermal conduction calorimetry for clinkers KEOP-1 with addition of EAF S slag and KVOD/AOD-1 with ladle slag: a) heat flow evolution, b) calorimetric curves at main hydration phase and c) cumulative heat evolution.

4.4 Compressive strength

After 7 days of curing clinkers with EOP S slag, it developed a compressive strength of 28.1 N/mm², while the clinkers with ladle slag developed a compressive strength of only 22.8 N/mm² (Table 5). The lower compressive strength of the clinker with ladle slag can be explained by the reduced amount of ettringite, which leads to a lower volume of hydrates and thus to a lower compressive strength [10].

Table 5: Compressive strength of cement pastes after 7 days of curing.

Sample	KEOP-1	KVOD/AOD-1
Compressive strength (N/mm ²)	28.1	22.8

5 CONCLUSIONS

The present work focused on evaluating the effect of raw material (different slag types: EAF S slag from stainless steel production and ladle slag as a by-product of the processes of secondary metallurgy) on belite-sulfoaluminate clinker microstructure, reactivity and compressive strength of cement pastes after 7 days of hydration.

In BCSA clinkers with EAF S slag and in BCSA clinkers with ladle slag the main clinker phases were generally developed due to the targeted phase composition. However, in clinkers with EAF S slag more calcium sulfoaluminate phase was formed than in clinkers with the same targeted phase composition with ladle slag. A decrease in the ferrite content was detected in all the samples. Among minor phases periclase was documented by XRD and SEM/BSE analysis.

Both clinkers with both types of slags had a similar microstructure, composed of rounded subhedral belite grains and angular euhedral calcium sulfoaluminate, and periclase grains and ferrite as an interstitial phase. The main clinker phases in the ladle slag clinker had a larger grain size than the main clinker phases in the EAF S clinker, which could contribute to the reduction of ladle slag clinker reactivity.

The hydration curve of the clinker with ladle slag points to a faster formation of ettringite than the clinker with EAF S slag, which was followed by monosulfate precipitation. On the other hand, the clinker with EAF S slag had a slower hydration reaction, most probably due to ettringite formation. Consequently, the clinker with EAF S slag had a higher compressive strength than the clinker with ladle slag.

The differences of the hydration pattern due to the type of slag, incorporated in BCSA clinker, could be attributed to the variation of the chemical composition of both slags, consequently influencing the phase composition, clinker microstructure, its reactivity and the compressive strength of the cement pastes. However, further investigations will be focused on the processed slags (mineral product after metal extraction) with a more constant chemical composition.

ACKNOWLEDGMENTS

Project No. C3330-17-529035 "Raziskovalci-2.0-ZAG-529035" was granted by the Ministry of Education, Science and Sport of the Republic of Slovenia. The investment is co-financed by the Republic of Slovenia, Ministry of Education, Science and Sport and the European Regional Development Fund.

REFERENCES

- [1] Gartner, E.: Industrially interesting approaches to "low CO₂" cements, *Cement and Concrete Research*, 2004, Vol. 34 No. 9, pp. 1489-1498.
- [2] Gartner, E. & Sui, T.; Alternative cement clinkers, *Cement and Concrete Research*, 2018, Vol. 114, pp. 27-39.
- [3] Damtoft, J.S. et al.: Sustainable development and climate change initiatives, *Cement and Concrete Research*, 2008, Vol. 38 No. 9, pp. 115-127.
- [4] Ma, B. et al.: Synthesis and characterization of high belite sulfoaluminate cement through rich alumina fly ash and desulfurization gypsum, *Ceramic Silikáty*, 2013, Vol. 57 No.1, pp. 7-13.
- [5] Wang, W. et al.: Ex Experimental investigation and modelling of sulfoaluminate cement preparation using desulfurization gypsum and red mud, *Industrial & Engineering Chemistry Research*, 2013, Vol. 52, pp. 1261-1226.
- [6] Kramar, S. et al.: Use of fly ash and phosphogypsum for the synthesis of belite-sulfoaluminate clinker, *Materiales de Construcción*, 2019, Vol. 69, No. 333, pp. 1-12.
- [7] Iacobescu, R.I. et al.: Synthesis, characterization and properties of calcium ferroaluminate belite cements produced with electric arc furnace steel slag as raw material, *Cement and Concrete Composites*, 2013, Vol. 44, pp. 1-8.
- [8] Chen, I.A. & Juenger, M.C.G.: Synthesis and hydration of calcium sulfoaluminate-belite cements with varied phase compositions, *Journal of Materials Science*, 2011, Vol. 46, pp. 2568-2577.
- [9] EN 196-2. Methods of testing cement – Part 2, Chemical analysis of cement, Slovenian Institute for Standardization (SIST) and European Committee for standardization (CEN), 2013, p. 78.
- [10] Ben Haha et al.: Advances in understanding ye'elinite-rich cements, *Cement and Concrete Research*, 2019, Vol. 123, pp. 1-20.
- [11] Winnefeld, F. & Lothenbach, B.: Hydration of calcium sulfoaluminate cements – experimental findings and thermodynamic modelling, *Cement and Concrete Research*, 2010, Vol. 40, pp. 1239-1247.
- [12] Bullerjahn, F. et al.: Hydration reactions and stages of clinker composed mainly of stoichiometric ye'elinite,, *Cement and Concrete Research*, 2019, Vol. 116, pp. 120-133.
- [13] Rungchet, A. et al.: Hydration and Physico-mechanical Properties of Blended Calcium Sulfoaluminate-belite Cement Made of Industrial By-products, *KMUTNB International Journal of Applied Science and Technology*, 2016, Vol. 9, No. 4, pp. 279-287.
- [14] Winnefeld, F. et al.: Using gypsum to control hydration kinetics of CSA cements, *Construction and Building Materials*, 2017, Vol. 155, pp. 154-163.